ROLE OF PROTEIN-PROTEIN INTERACTIONS IN METABOLISM: GENETICS, STRUCTURE, FUNCTION

EDITED BY: Amit V. Pandey, Colin J. Henderson, Yuji Ishii, Michel Kranendonk, Wayne L. Backes and Ulrich M. Zanger

PUBLISHED IN: Frontiers in Pharmacology

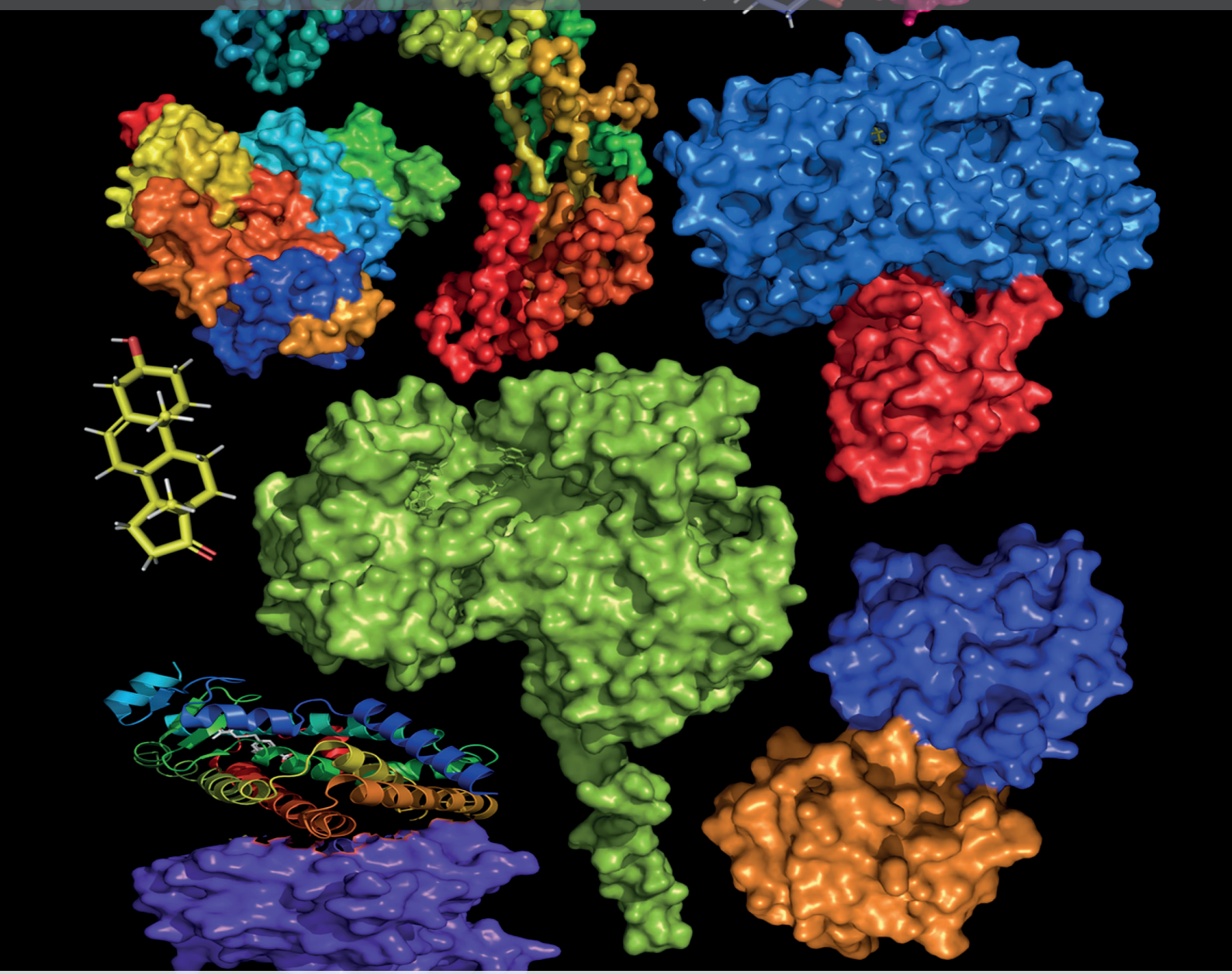

frontiers Research Topics

frontiers

ISSN 1664-8714
ISBN 978-2-88945-385-6
DOI 10.3389/978-2-88945-385-6

About Frontiers

Frontiers is more than just an open-access publisher of scholarly articles: it is a pioneering approach to the world of academia, radically improving the way scholarly research is managed. The grand vision of Frontiers is a world where all people have an equal opportunity to seek, share and generate knowledge. Frontiers provides immediate and permanent online open access to all its publications, but this alone is not enough to realize our grand goals.

Frontiers Journal Series

The Frontiers Journal Series is a multi-tier and interdisciplinary set of open-access, online journals, promising a paradigm shift from the current review, selection and dissemination processes in academic publishing. All Frontiers journals are driven by researchers for researchers; therefore, they constitute a service to the scholarly community. At the same time, the Frontiers Journal Series operates on a revolutionary invention, the tiered publishing system, initially addressing specific communities of scholars, and gradually climbing up to broader public understanding, thus serving the interests of the lay society, too.

Dedication to Quality

Each Frontiers article is a landmark of the highest quality, thanks to genuinely collaborative interactions between authors and review editors, who include some of the world's best academicians. Research must be certified by peers before entering a stream of knowledge that may eventually reach the public - and shape society; therefore, Frontiers only applies the most rigorous and unbiased reviews.
Frontiers revolutionizes research publishing by freely delivering the most outstanding research, evaluated with no bias from both the academic and social point of view.
By applying the most advanced information technologies, Frontiers is catapulting scholarly publishing into a new generation.

What are Frontiers Research Topics?

Frontiers Research Topics are very popular trademarks of the Frontiers Journals Series: they are collections of at least ten articles, all centered on a particular subject. With their unique mix of varied contributions from Original Research to Review Articles, Frontiers Research Topics unify the most influential researchers, the latest key findings and historical advances in a hot research area! Find out more on how to host your own Frontiers Research Topic or contribute to one as an author by contacting the Frontiers Editorial Office: **researchtopics@frontiersin.org**

ROLE OF PROTEIN-PROTEIN INTERACTIONS IN METABOLISM: GENETICS, STRUCTURE, FUNCTION

Topic Editors:
Amit V. Pandey, University Children's Hospital Bern, Switzerland and University of Bern, Switzerland
Colin J. Henderson, University of Dundee, United Kingdom
Yuji Ishii, Kyushu University, Japan
Michel Kranendonk, Universidade Nova de Lisboa, Portugal
Wayne L. Backes, Louisiana State University Health Sciences Center – New Orleans, United States
Ulrich M. Zanger, Dr. Margarete Fischer-Bosch-Institute of Clinical Pharmacology, Germany and Eberhard-Karls-University, Germany

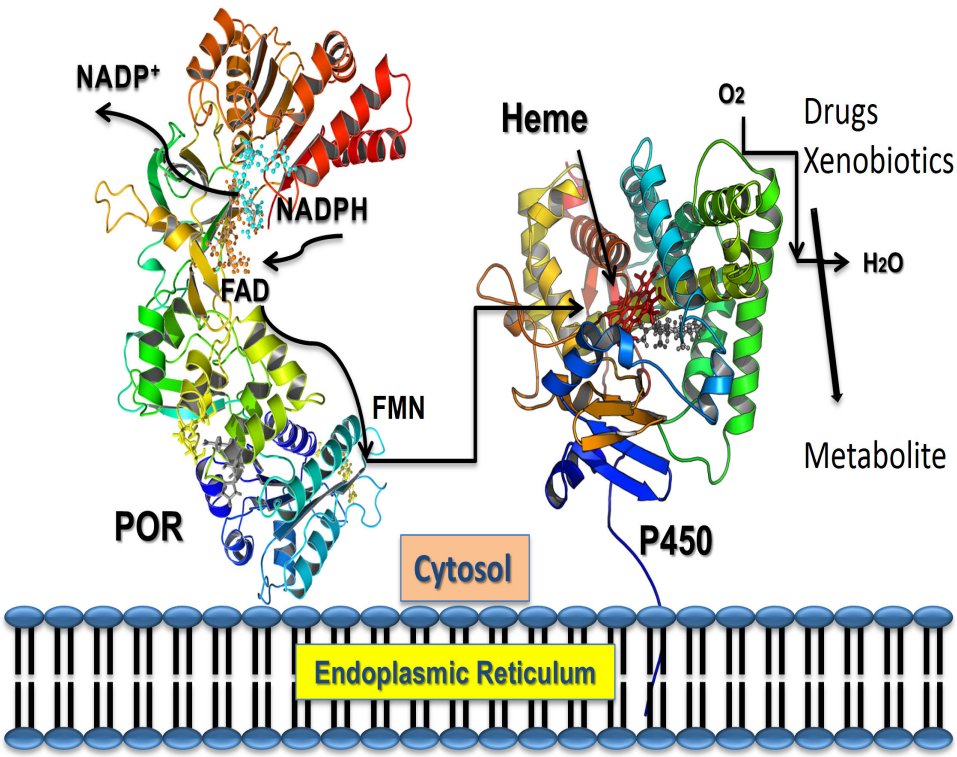

The POR located into the endoplasmic reticulum, interacts with the cytochrome P450s and other redox partners for metabolic reactions. Taken from: Pandey AV and Sproll P (2014) Pharmacogenomics of human P450 oxidoreductase. *Front. Pharmacol.* 5:103. doi: 10.3389/fphar.2014.00103.

Cover image: Structural models of P450 oxidoreductase (POR), Cytochrome P450s, adrenodoxin, UDP-Glucuronosyltransferase 2B7, PPAR gamma, cholesterol and androstenedione, highlighting the role of protein-protein interactions in metabolism. Cover image created by Amit V. Pandey.

Genetic variations may change the structure and function of individual proteins as well as affect their interactions with other proteins and thereby impact metabolic processes dependent on protein-protein interactions. For example, cytochrome P450 proteins, which metabolize a vast array of drugs, steroids and other xenobiotics, are dependent on interactions with redox and allosteric partner proteins for their localization, stability, (catalytic) function and metabolic diversity (reactions). Genetic variations may impact such interactions by changing the splicing and/or amino acid sequence which in turn may impact protein topology, localization, post translational modifications and three dimensional structure. More generally, research on single gene defects and their role in disease, as well as recent large scale sequencing studies suggest that a large number of genetic variations may contribute to disease not only by affecting gene function or expression but also by modulating complex protein interaction networks.

The aim of this research topic is to bring together researchers working in the area of drug, steroid and xenobiotic metabolism who are studying protein-protein interactions, to describe their recent advances in the field. We are aiming for a comprehensive analysis of the subject from different approaches including genetics, proteomics, transcriptomics, structural biology, biochemistry and pharmacology. Of particular interest are papers dealing with translational research describing the role of novel genetic variations altering protein-protein interaction. Authors may submit original articles, reviews and opinion or hypothesis papers dealing with the role of protein-protein interactions in health and disease.

Potential topics include, but are not limited to:

- Role of protein-protein interactions in xenobiotic metabolism by cytochrome P450s and other drug metabolism enzymes.
- Role of classical and novel interaction partners for cytochrome P450-dependent metabolism which may include interactions with redox partners, interactions with other P450 enzymes to form P450 dimers/multimers, P450-UGT interactions and proteins involved in posttranslational modification of P450s.
- Effect of genetic variations (mutations and polymorphisms) on metabolism affected by protein-protein interactions.
- Structural implications of mutations and polymorphisms on protein-protein interactions.
- Functional characterization of protein-protein interactions.
- Analysis of protein-protein interaction networks in health and disease.
- Regulatory mechanisms governing metabolic processes based on protein-protein interactions.
- Experimental approaches for identification of new protein-protein interactions including changes caused by mutations and polymorphisms.

Citation: Pandey, A. V., Henderson, C. J., Ishii, Y., Kranendonk, M., Backes, W. L., Zanger, U. M., eds. (2018). Role of Protein-Protein Interactions in Metabolism: Genetics, Structure, Function. Lausanne: Frontiers Media. doi: 10.3389/978-2-88945-385-6

Table of Contents

Biochemistry, Biophysics and Biotechnological Implications

frontiers in Pharmacology

EDITORIAL
published: 27 November 2017
doi: 10.3389/fphar.2017.00881

Editorial: Role of Protein-Protein Interactions in Metabolism: Genetics, Structure, Function

Amit V. Pandey[1, 2], Colin J. Henderson[3], Yuji Ishii[4], Michel Kranendonk[5], Wayne L. Backes[6] and Ulrich M. Zanger[7, 8]*

[1] Pediatric Endocrinology, Diabetology and Metabolism, University Children's Hospital Bern, Bern, Switzerland, [2] Department of Biomedical Research, University of Bern, Bern, Switzerland, [3] Division of Cancer Research, Jacqui Wood Cancer Centre, School of Medicine, University of Dundee, Dundee, United Kingdom, [4] Laboratory of Molecular Life Sciences, Graduate School of Pharmaceutical Sciences, Kyushu University, Fukuoka, Japan, [5] Center for Toxicogenomics and Human Health (ToxOmics), Genetics, Oncology and Human Toxicology, Universidade Nova de Lisboa, Lisbon, Portugal, [6] Department of Pharmacology and Experimental Therapeutics, Louisiana State University Health Sciences Center New Orleans, New Orleans, LA, United States, [7] Department of Molecular and Cell Biology, Dr. Margarete Fischer-Bosch-Institute of Clinical Pharmacology, Stuttgart, Germany, [8] Eberhard Karls University of Tübingen, Tübingen, Germany

Keywords: cytochrome P450, POR, UGT, PXR, drug metabolism

Editorial on the Research Topic

Role of Protein-Protein Interactions in Metabolism: Genetics, Structure, Function

This editorial describes the articles published under our research topic "Role of protein-protein interactions in metabolism: Genetics, structure, function." Our aim was to bring together researchers working on drug, steroid, and xenobiotic metabolism with interest in protein-protein interaction for presenting their latest findings and share their opinions on recent advances in the field. Recent advances in genetics (Meyer, 2004) and structural biology have greatly enhanced our understanding of molecular details of diversity and differences behind control of metabolic processes. The topic attracted a wide range of manuscripts using genetics, proteomics, biochemical, and structural biological approaches in study of protein-protein interactions.

In six original articles, four reviews, and one mini-review, leading experts in the field described different approaches and use of advanced technologies in the study of protein-protein interactions related to metabolic processes.

In a review of human UDP-glucuronosyltransfares (UGTs) Fujiwara et al. discussed the current understanding of the structure and function of UGTs in relation to protein-protein interactions and oligomerization and summarized their own as well as other related studies on interactions of UGTs with other proteins (Fujiwara et al., 2010). Nakamura et al. described the modification of UGT2B3 by creation of an N-glycosylation site to alter its sensitivity toward CYP3A1. It has been known for some time that CYP3A4 can change the activities of UGTs in isoform specific manner (Ishii et al., 2014). Rouleau et al. used a proteomics approach to study the protein-protein interactions of human UGT1As with other proteins including UGTs, transporters, and dehydrogenases. Role of UGTs in gene regulation as well as metabolic regulation by interactions with other proteins has become an emerging area of interest (Audet-Delage et al., 2017).

Pavek provided a review of pregnane X receptor (PXR) interactions with other nuclear receptors and its role in gene regulation (Rulcova et al., 2010). Ryu et al. have reviewed the interactions of cytochrome P450 proteins (Omura, 2010; Zanger and Schwab, 2013) with the membrane associated progesterone receptors (MAPR). Many MAPRs share similarities to cytochrome b5 and therefore are evolutionary adapted for interactions with cytochrome P450s (Xie et al., 2011).

OPEN ACCESS

Edited and reviewed by:
Marcelo Rizzatti Luizon, Universidade Federal de Minas Gerais, Brazil

****Correspondence:***
Amit V. Pandey
amit@pandeylab.org

Specialty section:
This article was submitted to Pharmacogenetics and Pharmacogenomics, a section of the journal Frontiers in Pharmacology

Received: *06 November 2017*
Accepted: *14 November 2017*
Published: *27 November 2017*

Citation:
Pandey AV, Henderson CJ, Ishii Y, Kranendonk M, Backes WL and Zanger UM (2017) Editorial: Role of Protein-Protein Interactions in Metabolism: Genetics, Structure, Function. Front. Pharmacol. 8:881. doi: 10.3389/fphar.2017.00881

Udhane et al. explored the role of genetic variations in human NADPH cytochrome P450 oxidoreductase (POR) found in apparently normal human population, in the metabolism of drugs and steroid hormones. Human POR (Pandey and Flück, 2013) is a diflavin reductase containing both the flavin mononucleotide (FMN) and flavin adenine dinucleotide (FAD) co-factors in separate domains that are linked by a hinge segment and interacts with cytochrome P450 proteins (Zanger and Schwab, 2013) and other redox partners (Pandey and Flück, 2013; Riddick et al., 2013). Using CYP19A1 (aromatase) (Pandey et al., 2007) for steroid metabolism and CYP3A4 for drug metabolism (Flück et al., 2010), Udhane et al. found variable effects of POR genetic variants in the FMN binding and hinge regions of POR on the activities of CYP11A1 and CYP3A4. Režen et al. studied the polymorphisms of *CYP51A1* (Lewinska et al., 2013) for impact on interactions with POR. Using computational models Režen et al. predicted that *CYP51A1* variants R277L and D152G have lower binding affinity for POR.

A thorough review of the biophysical techniques used in study of Cytochrome P450 proteins as well their interactions with other proteins involved in xenobiotic metabolism was provided by Lampe. By examining the X-ray crystal structures of P450 enzymes, Reed and Backes were able to identify potential contact points for the formation of P450-P450 complexes when interacting in membranes. This information allows for the predictions of how P450 system proteins are organized in the endoplasmic reticulum as well as the functional consequences of these interactions (Davydov et al., 2013).

Campelo et al. performed a study on the salt-induced changes of the dynamics properties of human POR (also described as CPR, CYPOR) by changing specific amino acids of the hinge segment which were postulated to play a critical role in electron transfer to its redox partners. Striking changes in the salt-profile of cytochrome c reduction by POR were observed with several of mutations created by Campelo et al. These results demonstrated that both electrostatics and flexibility of the hinge segment in POR are critical. Knowledge on the molecular mechanism of POR's gated electron transfer is of importance for the understanding the crucial role POR's for the activity of its redox-partners. Such knowledge may shed light on the impact of specific human polymorphic variants of POR (Sim et al., 2009) in specific pathologies but may also find biotechnological applications, such as P450 mediated metabolite production (Bernhardt and Urlacher, 2014). Degregorio et al. applied a chimeric approach for finding the optimal redox conditions to support cytochrome P450s reactions. A chimeric protein consisting of the reductase domain of bacterium *Bacillus megaterium* BM3 and a modified CYP3A4 was created to achieve a P450 containing its own reductase domain for a stable and efficient electron transfer during catalytic reactions. By using different linkers in between reductase and P450, Degregorio et al. could achieve 2 to 3-fold maximum velocity and coupling efficiency compared to use of separate P450 and redox partner proteins (Munro et al., 1996).

In conclusion, this research topic illustrated the up-to-date status of the field by leading scientists and provided a current state of the art on the importance of protein-protein interactions in metabolism and their role in a range of human diseases as well as biotechnological applications of the findings obtained from basic studies. We hope that the information gained from publication of this research topic will stimulate research on the role of protein-protein interactions in metabolism and facilitate further advances in the field.

AUTHOR CONTRIBUTIONS

All authors listed have made a substantial, direct and intellectual contribution to the work, and approved it for publication.

FUNDING

AP was funded by grants from the Swiss National Science Foundation (31003A-134926), Bern University Research Foundation and Department of Clinical Biomedical Research, University of Bern, Switzerland. YI was supported by Grants-in-Aid for Scientific Research (B)[#25293039] from the Japanese Society for the Promotion of Science. MK was funded by a joint ANR/FCT program; France: ANR-13-ISV5-0001 (DODYCOEL), and Portuguese national funds, through the Fundação para a Ciência e a Tecnologia (Project FCT-ANR/BEX-BCM/0002/2013). WB was supported by the National Institutes of Health (USA) Grants ES004344 and ES013648 from NIEHS, USPHS. UZ was supported by grants from the Robert Bosch Foundation, Stuttgart, Germany.

ACKNOWLEDGMENTS

The Editors acknowledge valuable contributions from all the authors and thank the Review Editors and external Reviewers who provided their critical reviews and expertise. We appreciated the professional support from the Frontiers in Pharmacology editorial office and production team for their help during the publication process.

REFERENCES

Audet-Delage, Y., Rouleau, M., Rouleau, M., Roberge, J., Miard, S., Picard, F., et al. (2017). Cross-talk between alternatively spliced ugt1a isoforms and colon cancer cell metabolism. *Mol. Pharmacol.* 91, 167–177. doi: 10.1124/mol.116.106161

Bernhardt, R., and Urlacher, V.B. (2014). Cytochromes P450 as promising catalysts for biotechnological application: chances and limitations. *Appl. Microbiol. Biotechnol.* 98, 6185–6203. doi: 10.1007/s00253-014-5767-7

Davydov, D. R., Davydova, N. Y., Sineva, E. V., Kufareva, I., and Halpert, J. R. (2013). Pivotal role of P450–P450 interactions in CYP3A4 allostery: the case of α-naphthoflavone. *Biochem. J.* 453, 219–230. doi: 10.1042/bj20130398

Flück, C.E., Mullis, P.E., and Pandey, A.V. (2010). Reduction in hepatic drug metabolizing CYP3A4 activities caused by P450 oxidoreductase mutations identified in patients with disordered steroid metabolism. *Biochem. Biophys. Res. Commun.* 401, 149–153. doi: 10.1016/j.bbrc.2010.09.035

Fujiwara, R., Nakajima, M., Oda, S., Yamanaka, H., Ikushiro, S., Sakaki, T., et al. (2010). Interactions between human UDP-glucuronosyltransferase (UGT) 2B7 and UGT1A enzymes. *J. Pharm. Sci.* 99, 442–454. doi: 10.1002/jps.21830

Ishii, Y., Koba, H., Kinoshita, K., Oizaki, T., Iwamoto, Y., Takeda, S., et al. (2014). Alteration of the function of the UDP-glucuronosyltransferase 1A subfamily by cytochrome P450 3A4: different susceptibility for UGT isoforms and UGT1A1/7 variants. *Drug Metabol. Dispos.* 42, 229–238. doi: 10.1124/dmd.113.054833

Lewinska, M., Zelenko, U., Merzel, F., Golic Grdadolnik, S., Murray, J.C., and Rozman, D. (2013). Polymorphisms of CYP51A1 from cholesterol synthesis: associations with birth weight and maternal lipid levels and impact on CYP51 protein structure. *PLoS ONE* 8:e82554. doi: 10.1371/journal.pone.0082554

Meyer, U.A. (2004). Pharmacogenetics – five decades of therapeutic lessons from genetic diversity. *Nat. Rev. Genet.* 5:669. doi: 10.1038/nrg1428

Munro, A. W., Daff, S., Coggins, J. R., Lindsay, J. G., and Chapman, S. K. (1996). Probing electron transfer in flavocytochrome P-450 BM3 and its component domains. *Eur. J. Biochem.* 239, 403–409. doi: 10.1111/j.1432-1033.1996.0403u.x

Omura, T. (2010). Structural diversity of cytochrome P450 enzyme system. *J. Biochem.* 147, 297–306. doi: 10.1093/jb/mvq001

Pandey, A. V., and Flück, C.E. (2013). NADPH P450 oxidoreductase: structure, function, and pathology of diseases. *Pharmacol. Ther.* 138, 229–254. doi: 10.1016/j.pharmthera.2013.01.01

Pandey, A. V., Kempná, P., Hofer, G., Mullis, P. E., and Flück, C. E. (2007). Modulation of human CYP19A1 activity by mutant NADPH P450 oxidoreductase. *Mol. Endocrinol.* 21, 2579–2595. doi: 10.1210/me.2007-0245

Riddick, D. S., Ding, X., Wolf, C. R., Porter, T. D., Pandey, A. V., Zhang, Q. Y., et al. (2013). NADPH-cytochrome P450 oxidoreductase: roles inphysiology, pharmacology, and toxicology. *Drug Metab. Dispos.* 41, 12–23. doi: 10.1124/dmd.112.048991

Rulcova, A., Prokopova, I., Krausova, L., Bitman, M., Vrzal, R., Dvorak, Z., et al. (2010). Stereoselective interactions of warfarin enantiomers with the pregnane X nuclear receptor in gene regulation of major drug-metabolizing cytochrome P450 enzymes. *J. Thromb. Haemost.* 8, 2708–2717. doi: 10.1111/j.1538-7836.2010.04036.x

Sim, S. C., Miller, W. L., Zhong, X. B., Arlt, W., Ogata, T., Ding, X., et al. (2009). Nomenclature for alleles of the cytochrome P450 oxidoreductase gene. *Pharmacogenet. Genomics* 19, 565–566. doi: 10.1097/FPC.0b013e32832af5b7

Xie, Y., Bruce, A., He, L., Wei, F., Tao, L., and Tang, D. (2011). CYB5D2 enhances HeLa cells survival of etoposide-induced cytotoxicity. *Biochem. Cell Biol.* 89, 341–350. doi: 10.1139/o11-004

Zanger, U. M., and Schwab, M. (2013). Cytochrome P450 enzymes in drug metabolism: regulation of gene expression, enzyme activities, and impact of genetic variation. *Pharmacol. Ther.* 138, 103–141. doi: 10.1016/j.pharmthera.2012.12.007

Conflict of Interest Statement: The authors declare that the research was conducted in the absence of any commercial or financial relationships that could be construed as a potential conflict of interest.

frontiers in Pharmacology

REVIEW
published: 24 October 2016
doi: 10.3389/fphar.2016.00388

Structure and Protein–Protein Interactions of Human UDP-Glucuronosyltransferases

Ryoichi Fujiwara[1], Tsuyoshi Yokoi[2] and Miki Nakajima[3]*

[1] Department of Pharmaceutics, School of Pharmacy, Kitasato University, Tokyo, Japan, [2] Department of Drug Safety Sciences, Division of Clinical Pharmacology, Nagoya University Graduate School of Medicine, Nagoya, Japan, [3] Drug Metabolism and Toxicology, Faculty of Pharmaceutical Sciences, Kanazawa University, Kanazawa, Japan

Mammalian UDP-glucuronosyltransferases (UGTs) catalyze the transfer of glucuronic acid from UDP-glucuronic acid to various xenobiotics and endobiotics. Since UGTs comprise rate-limiting enzymes for metabolism of various compounds, co-administration of UGT-inhibiting drugs and genetic deficiency of *UGT* genes can cause an increased blood concentration of these compounds. During the last few decades, extensive efforts have been made to advance the understanding of gene structure, function, substrate specificity, and inhibition/induction properties of UGTs. However, molecular mechanisms and physiological importance of the oligomerization and protein–protein interactions of UGTs are still largely unknown. While three-dimensional structures of human UGTs can be useful to reveal the details of oligomerization and protein–protein interactions of UGTs, little is known about the protein structures of human UGTs due to the difficulty in solving crystal structures of membrane-bound proteins. Meanwhile, soluble forms of plant and bacterial UGTs as well as a partial domain of human UGT2B7 have been crystallized and enabled us to predict three-dimensional structures of human UGTs using a homology-modeling technique. The homology-modeled structures of human UGTs do not only provide the detailed information about substrate binding or substrate specificity in human UGTs, but also contribute with unique knowledge on oligomerization and protein–protein interactions of UGTs. Furthermore, various *in vitro* approaches indicate that UGT-mediated glucuronidation is involved in cell death, apoptosis, and oxidative stress as well. In the present review article, recent understandings of UGT protein structures as well as physiological importance of the oligomerization and protein–protein interactions of human UGTs are discussed.

Keywords: UDP-glucuronosyltransferase (UGT), protein–protein interactions, glucuronidation, glucuronides, drug-metabolizing enzymes

OPEN ACCESS

Edited by:
Yuji Ishii,
Kyushu University, Japan

Reviewed by:
Karl Walter Bock,
University of Tübingen, Germany
Ben Lewis,
Flinders University, Australia

****Correspondence:***
Ryoichi Fujiwara
fujiwarar@pharm.kitasato-u.ac.jp

Specialty section:
This article was submitted to Pharmacogenetics and Pharmacogenomics, a section of the journal Frontiers in Pharmacology

Received: *15 August 2016*
Accepted: *05 October 2016*
Published: *24 October 2016*

Citation:
Fujiwara R, Yokoi T and Nakajima M (2016) Structure and Protein–Protein Interactions of Human UDP-Glucuronosyltransferases. Front. Pharmacol. 7:388. doi: 10.3389/fphar.2016.00388

INTRODUCTION

Humans are exposed on a daily basis to xenobiotics that may potentially be toxic or pharmacologically active. Xenobiotics are often hydrophobic and therefore may accumulate in the body. To facilitate the excretion of xenobiotics, detoxifying enzymes metabolize them mostly in the liver to increase their hydrophilicity. Since such xenobiotic-metabolizing enzymes play an important role in the metabolism of clinically used drugs, they are also called drug-metabolizing enzymes. Phase I drug-metabolizing enzymes, such as cytochrome P450s (CYPs) and

esterases, catalyze oxidation, reduction, and hydrolysis of xenobiotics (Satoh and Hosokawa, 1998; Nebert and Russell, 2002). The formed metabolites, as well as parental compounds, are further metabolized by phase II drug-metabolizing enzymes, such as UDP-glucuronosyltransferases (UGTs), sulfotransferases, and glutathione *S*-transferases (Jancova et al., 2010; Miners et al., 2010). Among these, UGTs have been reported with the highest contribution to drug metabolism (Williams et al., 2004).

UDP-glucuronosyltransferases-mediated glucuronidation can be a rate-limiting step in the clearance of endogenous and exogenous substances. Therefore, inhibition of UGTs by co-administered drugs or genetic deficiency in the *UGT* gene can increase blood concentrations of their substrates *in vivo*, whereas induction of UGT genes would result in a decrease of blood concentrations of their substrates (Lankisch et al., 2009; Hirashima et al., 2016). Three-dimensional crystal structures are useful to facilitate the understanding of protein structures that determine substrate- and/or inhibitor-binding. Due to the difficulty in obtaining the crystal structure of membrane proteins, entire three-dimensional structures of human UGTs have not been determined except for a partial domain of human UGT (Miley et al., 2007). On the other hand, entire crystal structures of soluble forms of plant and bacterial UGTs have previously been reported (Mulichak et al., 2003; Shi et al., 2014). These solved structures were used as templates of homology modeling of human UGTs (Fujiwara et al., 2009a). Although amino acid similarities are not high between mammalian and plant/bacterial UGTs, the modeled human UGT structures are comparable to plant and bacterial UGTs, suggesting that the structures of plant/bacterial UGTs may aid in the structural clarification of human UGTs.

UDP-glucuronosyltransferases enzymes comprise a superfamily. One of the most unique and important properties of UGTs is that they form homo- and hetero-oligomers such as dimers, trimers, and tetramers (Finel and Kurkela, 2008). Tukey and Tephly (1981) were the first to report that rat UGTs functioned in an oligomeric form. Subsequently, various *in vitro* techniques such as cross-linking and fluorescence resonance energy transfer (FRET) imaging demonstrated the oligomerization of UGT proteins (Ikushiro et al., 1997; Operaña and Tukey, 2007). Interestingly, accumulating evidence indicates that UGT–UGT interactions affect their enzymatic activities (Ishii et al., 2001; Fujiwara et al., 2007a,b). Analyses using the homology-modeled UGT structures further revealed the region responsible for the oligomerization of UGTs (Lewis et al., 2011). Moreover, specific antibodies against UGTs immunoprecipitated not only UGTs but also CYPs in human liver microsomes, indicating that UGTs appeared to interact with other microsomal proteins (Fujiwara and Itoh, 2014). Indeed, recently developed techniques such as mass spectrometry analysis of immunoprecipitates revealed that UGTs may interact with a variety of microsomal proteins including epoxide hydrolase 1, carboxylesterase 1, alcohol dehydrogenases, and glutathione *S*-transferases (Fujiwara and Itoh, 2014).

In this review article, recent advances in the knowledge on the three-dimensional structure, protein interactions of human UGTs, and physiological roles of UGTs are introduced along with early and recent analytical tools that demonstrate the presence of UGT oligomers.

UDP-GLUCURONOSYLTRANSFERASE (UGT)

Human UGT Families and Their Function

UDP-Glucuronosyltransferase (UGT, EC 2.4.1.17), which belongs to a large glycosyltransferase (GT) 1 family of GTs (EC 2.4.1.-; GT), is a family of membrane-bound proteins that catalyze a transfer of glucuronic acid from UDP-glucuronic acid to various endogenous and exogenous substances (**Figure 1**) (Mackenzie et al., 2005). UGTs are specifically expressed in the ER and most the UGTs are localized in the luminal side of the ER-membrane, which is rich in UDP-glucuronic acid. In humans, the *UGT* gene superfamily contains *UGT1* and *UGT2*.

The single human *UGT1* gene, located on chromosome 2q37.1, contains multiple exon 1s and common exons 2–5, spanning approximately 200 kbp. Individual UGT1 isoforms, UGT1A1, UGT1A3, UGT1A4, UGT1A5, UGT1A6, UGT1A7, UGT1A8, UGT1A9, and UGT1A10, are generated by exon sharing of the *UGT1* gene (**Figure 2A**). Importantly, Dr. Girard et al. (2007) discovered that there are two types of exon 5, exons 5a and 5b, which encodes a shorter amino acid sequence. Compared to 50–55 kDa proteins encoded by exons 1–4 and 5a (UGT1A_i1), which is a main variant, the proteins encoded by exons 1–4 and 5b (UGT1A_i2) are smaller (45 kDa) and generally exhibit lower enzymatic activities.

Human *UGT2* genes, including *UGT2A* and *UGT2B*, are located on chromosome 4q13.2. UGT2A1 and UGT2A2 are generated by exon sharing of unique exon 1s and common exons 2–6 of the *UGT2A* gene in the same manner as UGT1A proteins, whereas a single gene encodes UGT2A3. UGT2B family proteins, UGT2B4, UGT2B7, UGT2B10, UGT2B11, UGT2B15, UGT2B17, and UGT2B28, are encoded by each unique gene in a cluster (**Figure 2B**). Transcriptional diversity has been reported in the *UGT2B7* locus. Original six exons as well as extra three exon 1s and two exon 6s of the *UGT2B7* gene can produce up to 22 transcript variants which encode 7 types of UGT2B7 proteins (UGT2B7_i1 to _i7) (Ménard et al., 2011). Similar to UGT1A_i1, UGT2B7_i1 exhibits the highest enzyme activity compared to UGT2B7_i2 to _i7 proteins. Recently conducted targeted RNA next-generation sequencing revealed that transcriptional diversity, such as new internal exons and exon skipping, could be observed in other *UGT2B* genes (Tourancheau et al., 2016). The expression and enzyme activities of such alternative UGT2Bs need to be determined in the future.

Tissue Distribution of UGTs

In humans, all of 9 UGT1 and 10 UGT2 isoforms are expressed in a tissue-specific manner. In the liver, which is the most important tissue in metabolism of xenobiotics, UGT1A1, UGT1A3, UGT1A4, UGT1A6, UGT1A9, UGT2B4, UGT2B7, UGT2B10, UGT2B15, and UGT2B17 are expressed (Nakamura et al., 2008; Izukawa et al., 2009). UGT1A8 and UGT1A10 are mainly expressed in the small intestine, colon, and bladder.

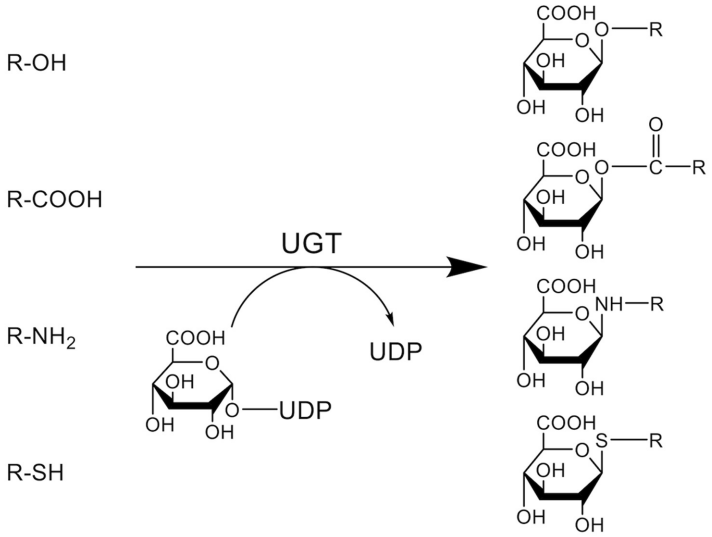

FIGURE 1 | Conjugation reaction catalyzed by UDP-glucuronosyltransferases (UGTs). UGTs catalyze the transfer of glucuronic acid from UDP-glucuronic acid to an oxygen, nitrogen, or sulfur atom of their substrates. (R = substrate).

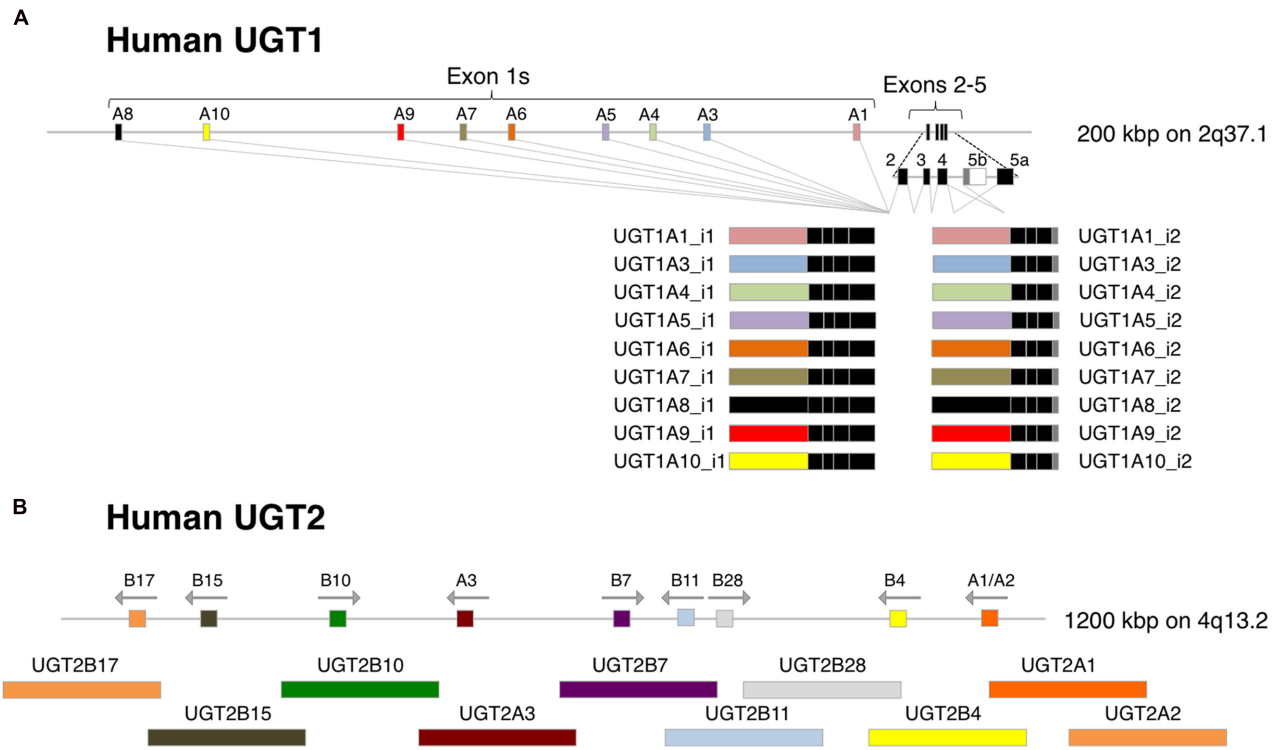

FIGURE 2 | Gene structures of human *UGT1* and *UGT2*. (A) Human *UGT1* gene contains multiple exon 1s and common exons 2–5, and each UGT1 isoform are generated by exon sharing of the gene. Exon 5a produces UGT1A_i1 proteins, while exon 5b produced smaller UGT1A_i2 proteins. **(B)** UGT2A1 and UGT2A2 are generated by exon sharing of unique exon 1s and common exons 2–6 of the *UGT2A* gene in the same manner as UGT1A proteins. UGT2A3 and UGT2B family proteins are encoded by each unique gene in a cluster.

UGT1A7 has been characterized as an isoform that is specifically expressed in the stomach (Strassburg et al., 1997). In the kidneys, UGT1A9 and UGT2B7 are highly and other UGTs such as UGT1A4, UGT1A6, and UGT2B11 are moderately expressed. The expression of UGT2B28 is limited to the bladder, where various UGT1 and UGT2 members are also expressed. UGT2A1 and UGT2A2 are expressed in nasal tissue, whereas UGT2A3 is expressed mainly in liver and small intestine, and slightly in lung and nasal tissues (Sneitz et al., 2009). Since UGT2A family isoforms glucuronidate endogenous substances rather than drugs, it has been believed that they have certain physiological role in those organs, although more investigation is required.

Substrate Specificity of UGTs

UDP-glucuronosyltransferases catalyze the transfer of glucuronic acid from UDP-glucuronic acid to an oxygen, nitrogen, or sulfur atom in their substrates (**Figure 1**). UGT1A1 glucuronidates relatively bulky molecules such as bilirubin, SN-38, and etoposide, as well as planar or smaller molecules such as estradiol, 1-naphthol, and 4-methylumbelliferone (Bosma et al., 1994; Watanabe et al., 2003; Mano et al., 2004). While these smaller compounds can be glucuronidated by several other UGT1 and UGT2 family proteins, bilirubin is solely glucuronidated by UGT1A1 (Bosma et al., 1994). UGT1A4 has been recognized as one of the UGT isoforms that can glucuronidate tertiary amines (e.g., nicotine, imipramine, trifluoperazine, and lamotrigine) (Kuehl and Murphy, 2003; Smith et al., 2003; Rowland et al., 2006). A recent study demonstrated that clearances of nicotine, amitriptyline, imipramine, and diphenhydramine by UGT2B10-mediated *N*-glucuronidation were significantly higher than those by UGT1A3 and UGT1A4, indicating that UGT2B10 plays an important role in *N*-glucuronidation of certain amine-containing compounds (Kato et al., 2013). As UGT1A6 was originally characterized as a phenol-glucuronidating enzyme, it mainly glucuronidates small phenolic substances such as 4-nitrophenol, 1-naphthol, and 4-methylumbelliferone (Hanioka et al., 2001). 5-Hydroxytriptamine, also called serotonin, has been recognized as a specific substrate of UGT1A6 (Krishnaswamy et al., 2003). UGT1A9 metabolizes a wide variety of substances such as mycophenolic acid, scopoletin, and entacapone (Kurkela et al., 2003; Bernard and Guillemette, 2004). Propofol has been used as a selective substrate of UGT1A9 in the livers, although it can also be glucuronidated by UGT1A7, UGT1A8, and UGT1A10 in the gastrointestine (Court, 2005). UGT2B isoforms are especially important in the glucuronidation of endogenous compounds such as androsterone, testosterone, and dihydrotestosterone. Zidovudine and morphine are specifically metabolized by UGT2B7 (Barbier et al., 2000). It has been shown that UGT2B15 is the major enzyme responsible for sipoglitazar glucuronidation in humans, while multiple UGT1A and UGT2B members slightly glucuronidate sipoglitazar (Nishihara et al., 2013). UGT2B17, which has more than 95% homology with UGT2B15, can glucuronidate a wide variety of exogenous and endogenous compounds, including coumarins, anthraquinones, flavonoids, and androgens (Turgeon et al., 2003). Therefore, each UGT isoform exhibits broad but distinct substrate specificities.

Significance of Extrahepatic UGTs

Because bilirubin is solely glucuronidated by UGT1A1, genetic deficiency in the *UGT1A1* gene can result in an onset of severe hyperbilirubinemia (>20 mg/dL serum bilirubin) in humans (Beutler et al., 1998). Knockout of *Ugt1a1* in mice causes very severe hyperbilirubinemia (>15 mg/dL serum bilirubin), which is lethal within 11 days of birth due to the development of kernicterus (Nguyen et al., 2008). Since UGT1A1 is highly expressed in the liver, it was previously commonly believed that hepatic UGT1A1 mainly contribute to the bilirubin glucuronidation. However, a recent study demonstrated that liver-specific knockout of the *Ugt1* gene, including *Ugt1a1*, resulted in a mild increase of serum bilirubin (2 mg/dL serum bilirubin; Chen et al., 2013). Furthermore, increased expressions of intestinal UGT1A1 lead to decreased serum bilirubin levels (from 12 to 2 mg/dL) in 14-day-old humanized *UGT1* mice, indicating that intestinal UGT1A1 also plays an important role in bilirubin metabolism (Fujiwara et al., 2010b, 2012). UGT1A1 expressed in the skin and brain might also be responsible for bilirubin metabolism in neonates although to a lesser extent (Sumida et al., 2013; Kutsuno et al., 2015). In addition to UGT1A1, substantial expression of UGT1A8 and UGT1A10 mRNA are also observed in the small intestine (Nakamura et al., 2008). Since recombinant UGT1A1, UGT1A8, and UGT1A10 glucuronidate raloxifene *in vitro*, these enzymes might be responsible for the extremely poor oral bioavailability of raloxifene (Mizuma, 2009). However, it should be noted that the UGT1A8 protein was barely detected in human small intestine in a targeted peptide-based quantification study (Sato et al., 2014). Therefore, the role of UGT1A8 in intestinal glucuronidation *in vivo* needs to be carefully investigated in the future. These data support a concept that in addition to hepatic UGTs, extrahepatic UGTs also play a dominant role in glucuronidation of endogenous and exogenous compounds (Fujiwara et al., 2015).

THREE-DIMENSIONAL STRUCTURE OF HUMAN UGTs

Structure of Glycosyltransferase 1 Family Protein

Due to difficulties in crystallizing membrane-bound protein, X-ray crystal structures of membrane-bound human UGTs have not been determined. As mentioned above, human UGTs belong to a large glycosyltransferase (GT) 1 family. Because plant and bacterial GT1 family proteins are soluble forms, several X-ray crystal structures of plant and bacterial GTs have successfully been determined. In 2003, a 2.8-Å crystal structure of TDP-*epi*-vancosaminyltransferase (GtfA), which is one of the GT1 family proteins that transfer 4-*epi*-vancosamine from TDP-*epi*-vancosamine to its substrate, in *Amycolatopsis orientalis* was solved (Mulichak et al., 2003). The crystal structure (PDB ID: 1PN3) revealed that GtfA adopts a GT-B fold that consists of two separate Rossmann domains with a connecting linker and a catalytic cleft. In addition, other GT1 family proteins such as plant UDP-glucose

flavanoid 3-*O* glucosyltransferase (2C1X) and multifunctional triterpene/flavonoid glycosyltransferase UGT71G1 (2ACV) also have the GT-B fold (Shao et al., 2005; Offen et al., 2006). These findings lead us to hypothesize that human UGTs would also be GT-B fold enzymes.

Predicted Structure of Human UGTs

Human UGT1 and UGT2 family members consist of approximately 530 amino acids. One of the unique properties of UGTs is that they sometimes recognize overlapping but specific substrates, while they commonly recognize a co-substrate UDP-glucuronic acid (Mackenzie et al., 2005). Because UGT1 family proteins are generated by exon sharing of the single *UGT1* gene (**Figure 2A**), their C-terminal amino acid sequences encoded by the common exons 2–5 are identical. Although UGT2 family proteins are encoded by their individual genes (**Figure 2B**), the C-terminal amino acid sequences exhibit extremely high amino acid similarity. In contrast, the N-terminal amino acid sequences of UGT1 and UGT2 family members exhibit relatively lower amino acid similarity. For example, the sequence homology is 24–49% between N-terminal regions of UGT1 family enzymes (Mackenzie et al., 1997). Point mutation analyses demonstrated that mutations in the N- and C-terminal halves dramatically decreased the affinities toward substrates and UDP-glucuronic acid, respectively (Xiong et al., 2006; Patana et al., 2007; Fujiwara et al., 2009b; Kerdpin et al., 2009). These mutagenesis studies support an assumption that human UGTs have two domains, the highly conserved C-terminal halves responsible for the UDP-glucuronic acid binding and the unique N-terminal halves responsible for the substrate binding. A 1.8-Å resolution apo crystal structure of the C-terminal half of human UGT2B7 (2O6L), which is a solely available X-ray crystal structure of human UGTs, confirmed that the C-terminal domain contained a preserved nucleotide-sugar binding site (Miley et al., 2007).

Homology-Modeled Structure of Human UGTs

Three-dimensional structures of unsolved proteins can be modeled by homology-modeling. Locuson and Tracy (2007) conducted homology modeling of human UGT1A1 using the crystallized structure of plant UGT71G1 (2ACV) as a template. The length of the amino acid sequence of human UGT1A1 (533 amino acids) is relatively longer than that of plant UGT71G1 (463 amino acids). The amino acid similarity between UGT1A1 and UGT71G1 is 34%, but it was sufficient to obtain a reliable homology-model. The overall three-dimensional structure of UGT1A1 showed two Rossmann fold-like domains (Locuson and Tracy, 2007). Banerjee et al. (2008) modeled a three-dimensional structure of human UGT1A10 using UDP-galactose 4-epimerase (1XEL) from *Escherichia coli* as a template structure (Banerjee et al., 2008). The modeled structures of substrate- and UDP sugar-binding pockets were overlapped well with those of the template structure. The structural analysis indicated that lysine residues at 314 and 404 (K314 and K404) would play a critical role in the UDP-glucuronic acid binding of UGT1A10. They confirmed, by *in vitro* mutagenesis analysis, the importance of K314 and K404 in the UDP-glucuronic acid binding. Therefore, the homology-modeled structures of human UGTs are relatively reliable, even though the amino acid similarities are not high between human and plant/bacteria UGTs. Similar homology-modeling approaches have been carried out by many research groups to simulate the three dimensional structures of human UGTs (**Table 1**). Structural similarity of C-terminal domains was very high between the modeled structures and the crystallized structure of the C-terminal half of human UGT2B7 (2O6L), supporting the reliability of the homology-modeling technique (**Figure 3**).

Among the 19 functional human UGT proteins, UGT1A9 exhibits several unique properties. In 2007, we demonstrated that UGT1A9 was uniquely stable against heat treatment, while the other human UGTs lost their enzymatic activities when incubated at higher temperature (Fujiwara et al., 2007b). Importantly, 13 amino acid residues were found to be specific to UGT1A9 among 9 UGT1A isoforms. To examine the role of these residues in the thermal stability of UGT1A9, we conducted molecular dynamics simulation of homology-modeled structures of UGT1A9 as well as UGT1A8 as a reference at higher and lower temperatures. The *in silico* simulation revealed that the UGT1A9-specific residues were collectively involved in the thermal stability of UGT1A9 (Fujiwara et al., 2009b). *In vitro* mutagenesis analysis confirmed that the UGT1A9-specific residues, Arg42, Lys91, Ala92, Tyr106, Gly111, Tyr113, Asp115, Asn152, Leu173, Leu219, His221, Arg222, and Glu241, contributed to protein stability. Since the results of *in silico* and *in vitro* analyses were consistent, it is considered that the homology-modeled structure of human UGT1A9 (**Figure 3**) was relatively reliable.

DIMERIZATION AND OLIGOMERIZATION OF UGTs

The first evidence to demonstrate the oligomerization of mammalian UGTs was reported by Tukey and Tephly (1981). Shortly after the publication, Matern et al. (1982) demonstrated oligomeric UGTs in . Subsequently, a number of research groups showed that mammalian UGTs including human UGTs formed homo- and hetero-oligomers such as dimers, trimers, and tetramers. In this section, earlier and recent analytical tools used to show the oligomeric UGTs are summarized.

Gel Permeation Chromatography

Tukey and Tephly (1981) purified two different UGT isoforms, which mediate estrone and *p*-nitrophenol glucuronidations, respectively, from rabbit liver microsomes by DEAE-cellulose chromatography and affinity chromatography on UDP-hexanolamine Sepharose-4B. Both enzymes exhibited molecular weights of 57 kDa in the SDS-PAGE analysis. Interestingly, a gel filtration study of the purified UGT isoforms by an Ultragel AcA 34 column revealed that both UGTs had apparent molecular weights of 230 kDa (Tukey and Tephly, 1981), which is approximately 4 times larger than the size of monomeric UGTs. This was the first report demonstrating that mammalian UGTs could be present as tetramers.

TABLE 1 | Homology modeled human UDP-glucuronosyltransferases (UGTs) and their template structures.

Modeled UGT	Template	Template PDB ID	Reference
UGT1A1	*Medicago truncatula* triterpene UDP-glucosyl transferase (UGT71G1)	2ACV	Locuson and Tracy, 2007
UGT1A1	*Medicago truncatula* triterpene UDP-glucosyl transferase (UGT71G1)	2ACV	Li and Wu, 2007
UGT1A1	*Arabidopsis thaliana* hydroquinone glucosyltransferase (UGT72B1)	2VCE	Laakkonen and Finel, 2010
	Amycolatopsis orientalis UDP-glycosyltransferase (GtfB)	1IIR	
	Streptomyces antibioticus oleandomycin glycosyltransferase	2IYA	
	Homo sapiens UGT2B7 (C-terminal domain)	2O6L	
UGT1A1	*Arabidopsis thaliana* hydroquinone glucosyltransferase (UGT72B1)	2VCE	Song et al., 2015
	Streptomyces antibioticus oleandomycin glycosyltransferase	2IYA	
	Vitis vinifera UDP-glucose flavonoid 3-*o*-glycosyltransferase (VvGTI)	2C1X	
UGT1A3	*Medicago truncatula* multifunctional (iso)flavonoid glycosyltransferase (UGT85H2)	2PQ6	Song et al., 2015
	Vitis vinifera UDP-glucose flavonoid 3-*o*-glycosyltransferase (VvGTI)	2C1X	
	Medicago truncatula Flavonoid 3-*o*-glucosyltransferase (UGT78G1)	3HBF	
UGT1A3	*Streptomyces antibioticus* oleandomycin glycosyltransferase	2IYA	Yao et al., 2015; Liu X. et al., 2016
	Vitis vinifera UDP-glucose flavonoid 3-*o* glycosyltransferase (VvGTI)	2C1X	
	Arabidopsis thaliana hydroquinone glucosyltransferase (UGT72B1)	2VCE	
UGT1A3	*Vitis vinifera* UDP-glucose flavonoid 3-*o* glycosyltransferase (VvGTI)	2C1Z	Schirris et al., 2015
UGT1A8 and UGT1A9	*Amycolatopsis orientalis* TDP-epi-vancosaminyltransferase (GtfA)	1PN3	Fujiwara et al., 2009a
UGT1A9	*Vitis vinifera* UDP-glucose flavonoid 3-*o*-glycosyltransferase (VvGTI)	2C1Z	Wu et al., 2012
UGT1A9	*Vitis vinifera* UDP-glucose flavonoid 3-*o*-glycosyltransferase (VvGTI)	2C1Z	Li et al., 2016
	Homo sapiens UGT2B7 (C-terminal domain)	2O6L	
UGT1A9 and UGT1A10	*Streptomyces antibioticus* oleandomycin glycosyltransferase	2IYA	Tripathi et al., 2016
	Streptomyces fradiae C-glycosyltransferase (UrdGT2)	2P6P	
	Medicago truncatula triterpene UDP-glucosyl transferase (UGT71G1)	2ACV	
	Homo sapiens UGT2B7 (C-terminal domain)	2O6L	
UGT1A10	*Escherichia coli* UDP-galactose 4-epimerase	1XEL	Banerjee et al., 2008
UGT2B7	*Vitis vinifera* UDP-glucose flavonoid 3-*o*-glycosyltransferase (VvGTI)	2C1X, 2C1Z, 2C9Z	Lewis et al., 2011; Chau et al., 2014
	Medicago truncatula triterpene UDP-glucosyl transferase (UGT71G1)	2ACV, 2ACW	
	Homo sapiens UGT2B7 (C-terminal domain)	2O6L	
UGT2B7	*Streptomyces antibioticus* oleandomycin glycosyltransferase	2IYA	Zhang et al., 2016
	Medicago truncatula multifunctional (iso)flavonoid glycosyltransferase (UGT85H2)	2PQ6	
C-terminal domains of UGT1, UGT2A1/2A2, UGT2A3, UGT2B4, UGT2B10, UGT2B11, UGT2B15, UGT2B17, UGT2B28	*Homo sapiens* UGT2B7 (C-terminal domain)	2O6L	Nair et al., 2015

Matern et al. (1982) similarly purified UGTs that catalyze chenodeoxycholic acid and testosterone glucuronidations from rat liver microsomes by a series of purification steps such as polyethylene glycol fractionation, DEAE-Sepharose CL-6B chromatography, UDP-hexanolamine-Sepharose 4B chromatography, and Bio-Gel A-1.5 m chromatography. While the molecular weight of subunit was determined to be 54 kDa in the SDS-PAGE analysis, the apparent molecular weight of the enzyme was calculated to be 316 kDa in a polyacrylamide gradient slab gel electrophoresis (Matern et al., 1982). The data indicated that rat UGTs were also present as tetrameric or even larger oligomeric forms.

Radiation Inactivation

Radiation inactivation is an analytical tool to determine molecular weights of membrane-bound enzymes *in situ* (Kempner and Schlegel, 1979). Enzymes are inactivated when they are irradiated with ionizing radiation. The extent of radiation-induced inactivation of the enzymes is directly associated with the radiation dose and the molecular weight of the concerned enzymes. Peters et al. (1984) determined the molecular weights of rat UGTs by radiation-inactivation of SDS-treated lyophilized liver microsomes using a calibrated ^{60}Co source. The radiation-inactivation analysis revealed that bilirubin mono-glucuronidation was catalyzed by a 41.5 kDa protein, while bilirubin di-glucuronidation was catalyzed by a 175 kDa protein. It was further demonstrated that proteins with molecular weight of 142 and 159 kDa catalyzed glucuronidations of testosterone and phenolphthalein, respectively (Peters et al., 1984). Similarly, the radiation inactivation analysis by Gschaidmeier and Bock (1994) revealed that molecular weights of UGTs catalyzing the glucuronidations of 1-naphthol, 6-hydroxychrysene, 3,6-dihydroxybenzo[*a*]pyrene, and 3,6-dihydroxychrysene were 91–218 kDa. The series of radiation

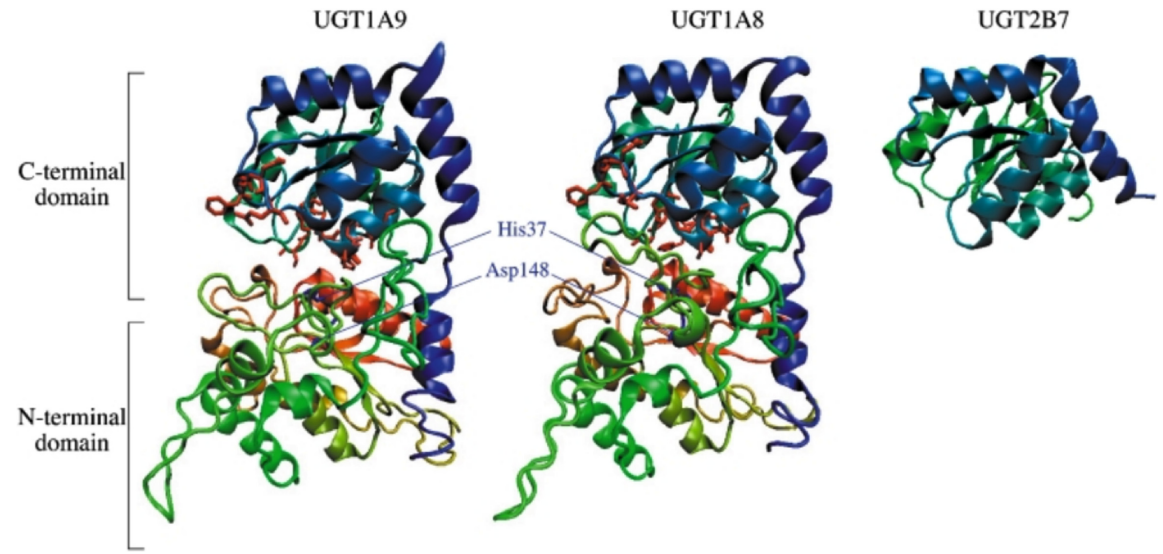

FIGURE 3 | Homology-modeled structures of human UGT1A9 and UGT1A8. Three-dimensional structures of human UGT1A9 and UGT1A8 were homology-modeled using *Amycolatopsis orientalis* GtfA (PDB ID: 1PN3) as template structures. The structures of UGT1A9 and UGT1A8 contain two Rossmann fold-like domains in the N-terminus and C-terminus. The structures are colored from red at the N-terminal to blue at the C-terminal. Amino acid residues that are predicted to interact with UDPGA and to be important for the catalysis are shown by red and blue licorice, respectively. The X-ray crystal structure of the C-terminal domain of UGT2B7 was retrieved from the Protein Data Bank (PDB ID: 2O6L). Adapted from Drug Metabolism and Pharmacokinetics (Fujiwara et al., 2009a).

inactivation analyses clearly demonstrated that mammalian UGTs were functional as oligomeric proteins that are composed of two to four subunits.

Cross-Linking

In intact cells, most of proteins are interacting with other protein(s) (Jeong et al., 2001). Upon the denaturing process in the SDS-PAGE analysis, such protein interactions via disulfide binding, hydrogen binding, and hydrophobic or salt-bridge interactions are disrupted, so that the proteins are separated according to their molecular weight. Cross-linkers are reagents that can introduce covalent chemical bonds between specific amino acids of proteins. Thus, proteins treated with cross-linkers can be observed as bands with higher molecular weights rather than their monomeric forms on SDS-PAGE followed by immunoblotting. Ikushiro et al. (1997) used 1,6-bis(maleimido)hexane (BMH), which is a homobifunctional cross-linker that reacts with sulfhydryl-groups of proteins. When rat liver microsomes that were incubated with BMH and were applied to the SDS-PAGE followed by the immunoblotting analysis using anti UGT1 or UGT2B1 antibodies, multiple bands with molecular masses of 50–60 kDa as well as of 120–130 kDa were observed (Ikushiro et al., 1997). They concluded that sulfhydryl group(s) of rat UGTs are located on the outside of the proteins and play a critical role in the formation of UGT dimers. Ghosh et al. (2001) used the disulfide cross-linker BMH and an amino group cross-linker dimethyl 3,3′-dithiobispropionimidate (DTBP) to demonstrate homo-oligomers of human UGT1A1, finding that both BMH and DTBT produced bands corresponding to homo-dimers of UGT1A1 on the SDS-PAGE analysis. The density of the bands was apparently reduced when UGT1A1-expressed cells were incubated with DTBP at pH 9.0, indicating that homodimerization of human UGT1A1 can be disrupted at alkaline pH.

Affinity Purification and Immunoprecipitations

Immunopurification and immunoprecipitation are classical methods to identify proteins interacting with a target protein. When rat liver microsomes were solubilized in buffer containing 1% Emulgen 913 and were applied to a UGT1 antibody-conjugated Sepharose 4B column, not only UGT1 isozymes but also unidentified 50-kDa protein(s) were co-eluted by eluting solution containing UGT1A-peptides (Ikushiro et al., 1997). Amino acid sequencing of the 50-kDa proteins and immunoblotting studies further revealed that the protein interacting with UGT1A was UGT2B1. Although the method used in a study by Kurkela et al. (2003) was Ni-column which is not immunopurification, they purified homo-oligomer of UGT1A9 that consisted of His- and hemagglutinin (HA)-tagged UGT1A9.

Fremont et al. (2005) conducted immunoprecipitation assays to examine protein–protein interactions between UGT1A1, UGT1A6, and UGT2B7 in human liver microsomes. When solubilized microsomes were incubated with UGT1A1-, UGT1A6-, and UGT2B7-specific antibodies, not only the antigenic proteins but also other UGT isozymes were co-immunoprecipitated. In 2007, we established cell lines that are individually or simultaneously expressing human UGT1A6 and UGT1A9 (Fujiwara et al., 2007b). A human UGT1A6-specific antibody co-immunoprecipitated UGT1A9, as well

as UGT1A6, in the UGT1A6-UGT1A9 double expression cells, although it did not immunoprecipitate UGT1A9 in the UGT1A9-expressed cells. When cyan fluorescent protein (CFP)- and HA-tagged UGT1A1s were simultaneously expressed in COS cells, anti-HA beads immunoprecipitated both CFP- and HA-tagged UGT1A1s (Operaña and Tukey, 2007). Taken together, immunoaffinity purification and immunoprecipitation assays are typical but still powerful tools to demonstrate homo- and hetero-oligomerization of UGTs. Immunoprecipitation assays by Bellemare et al. (2010) further revealed that inactive UGT1A_i2 proteins form not only homo-oligomers (i2-i2) but also hetero-oligomers with UGT1A_i1 proteins (i1-i2).

Fluorescence Resonance Energy Transfer (FRET)

To examine UGT–UGT interactions in intact cells, Operaña and Tukey (2007) conducted a FRET analysis using cyan and yellow fluorescent proteins (CFP and YFP)-tagged recombinant human UGTs expressed in COS cells. When correction for donor and acceptor bleed through was performed and FRET signal was analyzed, it was revealed that the two fusion UGT proteins resided within ångströms from each other. Their FRET analysis demonstrated homo-oligomerization of all UGT1A isoforms as well as hetero-oligomerization of UGT1A1 with the other UGT1A isoforms. The FRET analysis conducted by a different research group indicated that not only UGT1As, but also human UGT2B7 formed homo-oligomers in SF9 cells (Yuan et al., 2015; Liu Y.Q. et al., 2016).

REGIONS AND AMINO ACID RESIDUES RESPONSIBLE FOR OLIGOMERIZATION OF UGTs

Importance of N-terminal Domain

To examine the region responsible for the oligomerization of UGTs, Meech and Mackenzie (1997) constructed a couple of chimeric rat UGT2B1 proteins fused with ecdysteroid glucosyltransferase (EGT), which does not oligomerize. While intact UGT2B1 formed dimers, the dimerization was not observed when the C-terminal half of UGT2B1 was fused with the N-terminal half of EGT. In 2001, two-hybrid analysis by Ghosh et al. (2001) showed that UGT1A1s that were mutated or partially deleted in their N-terminal region (L175E, C233Y, or del152-180) abolished the ability to form homo-oligomers, while UGT1A1 with partial truncation of the C-terminal (K530X) still formed homo-oligomers (Ghosh et al., 2001). These data indicated that the N-terminal domains are involved in oligomerization of mammalian UGTs.

Hydrophobic Amino Acids on the Surface of Modeled UGT2B7

Hydrophobic amino acid residues on the surface of proteins can mediate protein–protein interactions by introducing proline brackets and π−π interactions. To identify such hydrophobic amino acid residues of UGTs, Lewis et al. (2011) obtained a three-dimensional structure of human UGT2B7 by homology modeling (**Table 1**). In the homology-modeled structure of human UGT2B7, a cluster of highly hydrophobic amino acid residues on a B′-C loop (amino acid residues 183–200) was located on the protein surface (Lewis et al., 2011). Thus, not only *in vitro* studies, but *in silico* structural analyses also supported the involvement of the N-terminal region of UGTs in oligomerization.

PROTEIN–PROTEIN INTERACTIONS OF UGTS WITH OTHER PROTEINS

Protein Interactions with CYPs

Cytochrome P450s are phase I drug-metabolizing enzymes that are expressed in the ER membrane. To investigate the possible protein-interactions between UGTs and CYPs, Taura et al. (2000) applied solubilized rat liver microsomes to a CYP1A1-conjugated Sepharose 4B column. It was found that multiple UGT isoforms were co-eluted in a fraction where CYP1A1 was eluted. Rat UGTs were detected in immunoprecipitates when solubilized rat liver microsomes were reacted with specific antibodies against CYP3A2, CYP2B2, CYP2C11, and CYP1A2 (Ishii et al., 2007). Antibodies against human UGT2B7 and CYP3A4 immunoprecipitated not only their antigenic proteins but also CYP3A4 and UGT2B7, respectively, in solubilized human liver microsomes (Fremont et al., 2005; Takeda et al., 2005, 2009). These data indicate that mammalian UGTs interact with CYPs in liver microsomes. It remains to be determined whether such UGT-CYP interactions can still be observed in a reconstituted system.

Protein Interactions with Microsomal Proteins

Immunoprecipitation assay with human UGT2B7 antibody was conducted using solubilized human liver microsomes. The obtained immunoprecipitate was digested with trypsin, and the resulting peptides were analyzed by LC-MS/MS to identify proteins interacting with UGT2B7 in human liver microsomes (Fujiwara and Itoh, 2014). The extensive peptide analysis showed that the peptide sequences of UGT2B7, epoxide hydrolase 1, carboxylesterase 1, alcohol dehydrogenases, and glutathione *S*-transferases, as well as CYPs, were included in the immunoprecipitates. It was confirmed that such peptide sequences were not detected in immunoprecipitates obtained with a control rabbit IgG antibody. Therefore, UGT2B7 might be able to form a metabolosome, which is a functional unit of metabolism (Mori et al., 2011) in liver microsomes.

Protein Interactions with Cytoplasmic Proteins

In contrast to normal UGT1A proteins (UGT1A_i1) that are expressed in the luminal side of the ER membrane, a

portion of UGT1A_i2 is cytoplasmic (Lévesque et al., 2007). Immunoprecipitates of solubilized human intestine and kidney homogenates with anti-UGT1A_i2 antibody were applied to a global peptide analysis (Rouleau et al., 2014). It was found that cytoplasmic catalase and peroxiredoxin 1 were co-immunoprecipitated with UGT1A_i2 proteins in both tissues, indicating that the truncated UGT1A isoform 2 is interacting with those cytoplasmic proteins. Since such protein–protein interactions were not observed when anti-UGT1A_i1 antibody was used, the interactions with cytoplasmic proteins would be specific to UGT1A_i2 proteins.

PHYSIOLOGICAL SIGNIFICANCE OF OLIGOMERIZATION AND PROTEIN–PROTEIN INTERACTIONS OF UGTs

Impact of UGT–UGT Interactions on the UGT-Mediated Glucuronidations

To investigate the effect of UGT–UGT interactions on the UGT activities, Ishii et al. (2001, 2004) cloned guinea pig UGT2B21 and UGT2B22 and examined morphine 6-*O*-glucuronidation in COS-7 cells expressing these UGTs. While UGT2B21 glucuronidates morphine, UGT2B22 does not have such ability to glucuronidate morphine. Morphine 6-glucuronide formation was 4.5-fold higher in COS-7 cells co-transfected with UGT2B21 and UGT2B22 compared to that in the cells transfected with UGT2B21 alone, indicating that protein–protein interactions between UGT2B21 and UGT2B22 upregulated the UGT activities (Ishii et al., 2001, 2004). This observation led us to investigate the impact of UGT–UGT interactions on the enzyme activities in humans (Fujiwara et al., 2007b; Nakajima et al., 2007). When we established stable expression systems of double human UGT1As in HEK293 cells, the S_{50} value of UGT1A1-mediated bilirubin glucuronidation was decreased by twofold by the co-expressions of UGT1A4 or UGT1A6 (Fujiwara et al., 2007a). A similar decrease of the S_{50} value was observed in the UGT1A1-mediated estradiol 3-*O*-glucuronidation in a co-expression system of UGT1A1 and UGT2B7 in HEK293 cells (Fujiwara et al., 2010a). These data showed that substrate-binding affinity of UGT1A1 toward bilirubin and estradiol was increased when UGT1A1 was co-expressed with UGT1A4, UGT1A6, and UGT2B7. Meanwhile, co-expression of UGT1A9 decreased the V_{max} value of UGT1A1-mediated estradiol 3-*O*-glucuronidation without affecting the S_{50} value (Fujiwara et al., 2007b). Kurkela et al. (2004) demonstrated that the rate of UGT1A9-catalyzed scopoletin glucuronidation was significantly decreased by co-expression of UGT1A4. Thus, UGT–UGT-interactions can modulate the catalytic rate of glucuronidation as well as the affinity of substrates toward UGTs. Importantly, the effects are dependent on interacting UGT isoforms and compounds used as substrates.

Interestingly, even though sorafenib is mainly metabolized by UGT1A9, it was demonstrated that the AUC of sorafenib was twice higher in patients with UGT1A1 variants or with hyperbilirubinemia (Peer et al., 2012). This finding indicates that UGT1A1 might control the enzyme activity of UGT1A9 *in vivo* by interacting with UGT1A9.

Although UGT1A_i2 proteins carry a potential UDP-glucuronic acid binding-site, they do not show substantial glucuronidation activity. As described above, the inactive UGT1A_i2 proteins form hetero-oligomers with functional UGT1A_i1 proteins. It was shown that glucuronide formation mediated by UGT1A_i1 proteins was significantly suppressed when UGT1A_i2 was co-expressed with UGT1A_i1 (Bellemare et al., 2010). The expression level and the ratio of UGT1A_i1 and _i2 are different in each tissue (Girard et al., 2007), suggesting that UGT1A_i2 can be a factor suppressing the glucuronidation in certain tissues. Interestingly, such suppression of UGT1 activity can also be caused by a truncated mutant of UGT1A1 (Gln331Stop; C to T at nucleotide 991), possibly by forming oligomers (Koiwai et al., 1996).

Impact of UGT-CYP Interactions on the UGT Activities

While a K_m value of morphine 3-glucuronide formation was 0.38 mM in UGT2B7-expressing COS-1 cells, a much higher K_m value (3.7 mM) was observed in UGT2B7 and CYP3A4 co-expressing cells (Takeda et al., 2005). In contrast, co-expression of CYP1A2 or CYP2C9 did not affect the kinetic parameters of UGT2B7-catalyzed morphine 3-glucuronide formations. In addition, co-expression of CYP3A4 increased a K_m value of UGT1A6-mediated serotonin glucuronidation by ∼fourfold, whereas it barely affected K_m values of UGT1A1-mediated 4-MU, SN-38-, or estradiol 3-*O*-glucuronidations as well as UGT1A7-mediated 4-MU, SN-38-, and 4-hydroxybiphenyl-glucuronidations (Ishii et al., 2014). Meanwhile, co-expression of CYP3A4 increased V_{max} values of UGT1A1-mediated 4-MU, SN-38-, and estradiol 3-*O*-glucuronidations, UGT1A6-mediated serotonin glucuronidation, and UGT1A7-mediated 4-MU, SN-38-, and 4-hydroxybiphenyl-glucuronidations, although it did not affect the UGT2B7-mediated morphine 3-glucuronidation (Takeda et al., 2005; Ishii et al., 2014). Therefore, CYP isoforms differently affect UGT-mediated glucuronidations and the effects are depending on UGT isoforms as well as their substrates.

Effect UGTs on Other Physiological Functions

Interestingly, a more than 40-fold interindividual variability in UGT1A6-catalyzed serotonin glucuronidation was observed among individual human liver microsomes (Krishnaswamy et al., 2003, 2005). Such variability could not be explained even when the activities were normalized with the UGT1A6 content and its genetic polymorphisms, indicating that there might be some unidentified factor that is capable of modulating the UGT1A6 activity. Since CYP isoforms can modulate UGT activities in different ways, interindividual variability in the CYP expression and function might be one of the causes of these wide interindividual variabilities in UGT1A6-catalyzed serotonin glucuronidation.

Miyauchi et al. (2015) investigated the effect of UGT2B7 on CYP3A4 activities by establishing a co-expression system of UGT2B7 and CYP3A4. They found that co-expression of UGT2B7 significantly decreased the V_{max} value of CYP3A4 activity without affecting a K_m value using luciferin-6′-pentafluorobenzyl ether as a substrate. Similarly, co-expression of UGT2B7 decreased the CYP3A4-mediated testosterone 6β-hydroxylation at a single substrate concentration (Miyauchi et al., 2015). These observations indicated that UGTs might suppress the enzyme activities of CYPs.

In a recent study by Liu M. et al. (2016), it was demonstrated that silencing of UGT1A expressions led to inhibitions of actinomycin D- and etoposide-induced p53 expressions in human colon HT29 and LS180 cells. Tissue-specific deletion of the *Ugt1* locus in intestinal crypt stem cells not only reduced p53 activation, but also compromised apoptosis. It was further demonstrated that reduced expression of UGT1A in intestine caused greater size and number of tumors in the colon cancer models (Liu M. et al., 2016).

When UGT1A_i2 was knocked-down in colorectal carcinoma-derived HT115 cells, expressions of a number of genes were up- or down-regulated (Rouleau et al., 2014). Among those genes, hemoglobin-alpha was significantly induced by the knockdown of UGT1A_i2. The function of hemoglobin-alpha proteins has been linked to cellular antioxidant potential (Widmer et al., 2010). Furthermore, it was found that knocked-down of UGT1A_i2 reduced a chemical-induced ROS formation in HT115 cells and significantly induced superoxide dismutase 1, an antioxidative gene. Although the underlying mechanism of induction of hemoglobin-alpha by knockdown of UGT1A_i2 is still unknown, the observation clearly indicates that UGT1A_i2 proteins are involved in the regulation of oxidative stress in cells. Taking all these findings together, it appears that UGTs are multifunctional proteins that controls metabolism, cell death and development of tumors, and oxidative stress.

CRITIQUE AND FUTURE RESEARCH DIRECTIONS

Protein Structure of UGTs

Various three-dimensional structures of human UGTs have been simulated by homology modeling (**Table 1**) and they are relatively acceptable as mentioned above. However, due to the extremely low amino acid similarity and different length of the amino acid sequence between human UGTs and template plant and bacterial UGTs, the reliability of the modeled human UGT protein structures is still an open question. Indeed, it is generally believed that the identity of amino acid sequence with the template needs to be more than 70% to obtain reliable structure. Furthermore, there is a significant structural difference between human and plant/bacterial UGTs that human UGTs are membrane proteins while plant and bacterial UGTs are not. To obtain a completely reliable modeled structure of human UGTs, an X-ray crystal structure of human UGTs needs to be successfully solved. Importantly, as mammalian UGTs abolish their enzyme activities when they are solubilized, a solubilized and crystallized structure of human UGTs might be an enzymatically inactive form. The instability of the protein structure of human UGTs can also be an obstacle in crystallizing them. Interestingly, UGT1A9 solely exhibited its enzymatic activity in the presence of 0.2% Triton X-100, although activities of other UGT1A and 2B isoforms were abolished by the detergent treatment (Kurkela et al., 2003). Human UGT1A9 is uniquely stable against a heat treatment as well (Fujiwara et al., 2009a), indicating that the protein structure of UGT1A9 must be more stable than the structures of other UGT isoforms. Therefore, human UGT1A9 is a promising human UGT isoform that has a potential to be crystallized as an active form.

Oligomerization of UGTs *In vivo*

Gel filtration and radiation inactivation analyses, where the liver microsomes were mixed with detergents, showed that monomeric UGTs catalyzed glucuronidation of certain compounds. It is well known that detergents can disrupt oligomerization of proteins; therefore, the monomeric UGTs might have been artificially generated from disruption of UGT oligomers. While SDS-PAGE shows the molecular weight of individual subunits of proteins under the reduced and denatured condition, oligomerization can be preserved in native-PAGE analysis. Our native-PAGE analysis of recombinant human UGTs expressed in HEK293 cells showed that most of UGTs were present as monomers, whereas some of them were still forming oligomers (**Figure 4**) (Fujiwara et al., 2007a). However, again, such monomers could have been a result from disruption of oligomeric UGTs due to a fact that the native-PAGE experiment required 1% Triton X-100 and 0.2% SDS to slightly solubilize the cell homogenates. Therefore, it is unclear whether UGTs dominantly exist as oligomer or monomer in intact cells.

Fluorescence resonance energy transfer is an analytical tool to demonstrate oligomerization of proteins in intact cells. Interestingly, FRET efficiency, which is a marker for co-localization and interaction, was 90% in COS cells expressing CFP- and YFP-tagged UGT1A7s (Operaña and Tukey, 2007), indicating that most of UGT1A7 was interacting with each other to form oligomers in intact cells. Meanwhile, the FRET efficiency was lower in certain UGT1A isoforms such as UGT1A3 and UGT1A9. These observations indicate that UGTs would exist as both monomeric and oligomeric forms in intact cells with variable extent depending on UGT isoforms. A limitation of the FRET analysis is that tagged UGT proteins, not intact proteins, were used. Therefore, determination of the extent of monomeric/oligomeric forms of intact UGT *in cellulo* is a future issue.

Availability and Application of *Ugt1* and *Ugt2* Knockout Mice

Various data indicate that UGTs can be multifunctional proteins that are involved in cellular metabolism, apoptosis, carcinogenesis, and oxidative stress as well as glucuronidation.

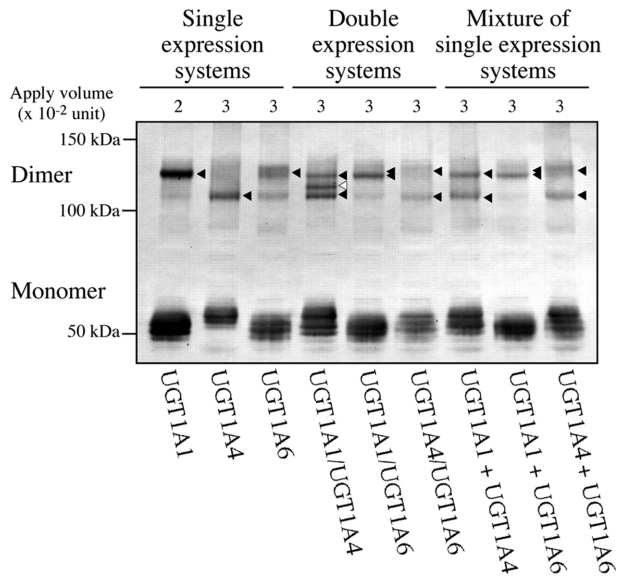

FIGURE 4 | Native PAGE analyses of UGT1A isoforms in single or double expression systems. Single or multiple UGT1A isoforms were stably expressed in HEK293 cells. Total cell homogenates were solubilized with 1% Triton X-100 and 0.2% SDS, and then were subjected to a native gel. Immunoblotting was conducted with rabbit anti-human UGT1A antibody. The bands with closed and open arrowheads indicate homo- and hetero-dimers, respectively. Hetero-dimer was detected in the double expression system of UGT1A1 and UGT1A4, while such oligomer was not observed when single expression systems of UGT1A1 and UGT1A4 were mixed. Adapted from Drug Metabolism and Disposition (Fujiwara et al., 2007a).

However, these unique properties of UGTs have not been fully validated by *in vivo* data. *Ugt1*- and *Ugt2*-knockout animals are promising *in vivo* models for investigating the roles of UGTs in such cellular metabolism, apoptosis, carcinogenesis, and oxidative stress. With extensive efforts by Drs. Tukey and Koller and their colleagues, *Ugt1*- and *Ugt2*-knockout mice were previously developed in 2008 and 2015, respectively (Nguyen et al., 2008; Fay et al., 2015). While *Ugt2* knockout mice can be used for the phenotype analysis, *Ugt1* knockout mice are lethal within 11 days after birth due to development of a bilirubin-induced irreversible brain damage, kernicterus. To conduct phenotype analyses in *Ugt1* knockout mice, therefore, we need to first avoid the lethality of the mice. Inhibitors of bilirubin production and inducers of bilirubin clearance might have potentials to rescue the lethality of the *Ugt1* knockout mice.

Possible Role of UGTs in Transport of UGT Substrates and Metabolites

Transporters responsible for the uptake of the co-substrate UDP-glucuronic acid from cytosol to the luminal side of ER membrane have been identified (Muraoka et al., 2001). Although studies suggested that there are proteins that are involved in the efflux of hydrophilic glucuronide across the ER membrane (Bánhegyi et al., 1996; Csala et al., 2004), such transporter(s) has not been identified. As shown in **Figure 5**, it was originally hypothesized that oligomerization and/or protein–protein interactions of UGTs have a role in transporting glucuronides across the ER membrane (Lin and Wong, 2002; Ishii et al., 2005); however, such evidence has not yet been obtained. Even in the immunoprecipitates of liver microsomes with anti-UGT2B7 antibody, no peptide sequences of transporters was observed (Fujiwara and Itoh, 2014). Further studies are required to fully understand the detailed information on the

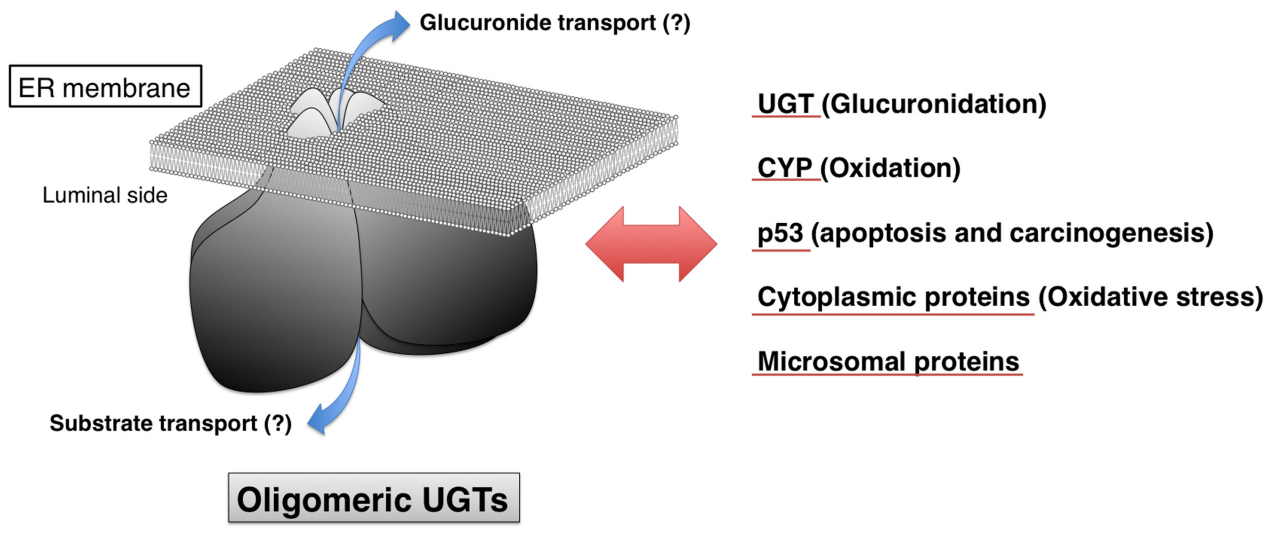

FIGURE 5 | Proposed model of oligomeric human UGTs. Human UGTs form homo- and hetero-oligomers in ER membrane. As indicated with blue arrows, oligomerization of UGTs might be involved in the transport of substrates and glucuronides across the ER membrane. Protein–protein interactions of human UGT with other microsomal and cytoplasmic proteins such as UGT, CYP, and p53 can make a great impact on glucuronidation, oxidation, apoptosis, carcinogenesis, and oxidative stress.

transport of UGT substrates and their metabolites across the ER membrane.

CONCLUSION

In addition to enzyme inhibition and induction, oligomerization is a predominant factor regulating the function of UGTs. UGTs are multifunctional proteins that are involved not only in glucuronidation, but also in cellular metabolism, apoptosis, carcinogenesis, and oxidative stress in the human body (**Figure 5**). Global protein interactions of UGTs with other microsomal or cytoplasmic proteins might be a contributing factor to a wide interindividual variability in UGT-catalyzed glucuronidations.

AUTHOR CONTRIBUTIONS

All authors listed, have made substantial, direct and intellectual contribution to the work, and approved it for publication.

ACKNOWLEDGMENT

This work was partly supported by the Naito Foundation (RF).

REFERENCES

Banerjee, R., Pennington, M. W., Garza, A., and Owens, I. S. (2008). Mapping the UDP-glucuronic acid binding site in UDP-glucuronosyltransferase-1A10 by homology-based modeling: confirmation with biochemical evidence. *Biochemistry* 47, 7385–7392. doi: 10.1021/bi8006127

Bánhegyi, G., Braun, L., Marcolongo, P., Csala, M., Fulceri, R., Mandl, J., et al. (1996). Evidence for an UDP-glucuronic acid/phenol glucuronide antiport in rat liver microsomal vesicles. *Biochem. J.* 315, 171–176. doi: 10.1042/bj3150171

Barbier, O., Turgeon, D., Girard, C., Green, M. D., Tephly, T. R., Hum, D. W., et al. (2000). 3′-azido-3′-deoxythimidine (AZT) is glucuronidated by human UDP-glucuronosyltransferase 2B7 (UGT2B7). *Drug Metab. Dispos.* 28, 497–502.

Bellemare, J., Rouleau, M., Harvey, M., and Guillemette, C. (2010). Modulation of the human glucuronosyltransferase UGT1A pathway by splice isoform polypeptides is mediated through protein-protein interactions. *J. Biol. Chem.* 285, 3600–3607. doi: 10.1074/jbc.M109.083139

Bernard, O., and Guillemette, C. (2004). The main role of UGT1A9 in the hepatic metabolism of mycophenolic acid and the effects of naturally occurring variants. *Drug Metab. Dispos.* 32, 775–778. doi: 10.1124/dmd.32.8.775

Beutler, E., Gelbart, T., and Demina, A. (1998). Racial variability in the UDP-glucuronosyltransferase 1 (UGT1A1) promoter: a balanced polymorphism for regulation of bilirubin metabolism? *Proc. Natl. Acad. Sci. U.S.A.* 95, 8170–8174. doi: 10.1073/pnas.95.14.8170

Bosma, P. J., Seppen, J., Goldhoorn, B., Bakker, C., Elferink, R. O., Chowdhury, J. R., et al. (1994). Bilirubin UDP-glucuronosyltransferase 1 is the only relevant bilirubin glucuronidating isoform in man. *J. Biol. Chem.* 269, 17960–17964.

Chau, N., Elliot, D. J., Lewis, B. C., Burns, K., Johnston, M. R., Mackenzie, P. I., et al. (2014). Morphine glucuronidation and glucosidation represent complementary metabolic pathways that are both catalyzed by UDP-glucuronosyltransferase 2B7: kinetic, inhibition, and molecular modeling studies. *J. Pharmacol. Exp. Ther.* 349, 126–137. doi: 10.1124/jpet.113.212258

Chen, S., Yueh, M. F., Bigo, C., Barbier, O., Wang, K., Karin, M., et al. (2013). Intestinal glucuronidation protects against chemotherapy-induced toxicity by irinotecan (CPT-11). *Proc. Natl. Acad. Sci. U.S.A.* 110, 19143–19148. doi: 10.1073/pnas.1319123110

Court, M. H. (2005). Isoform-selective probe substrates for in vitro studies of human UDP-glucuronosyltransferases. *Methods Enzymol.* 400, 104–116. doi: 10.1016/S0076-6879(05)00007-8

Csala, M., Staines, A. G., Bánhegyi, G., Mandl, J., Coughtrie, M. W., and Burchell, B. (2004). Evidence for multiple glucuronide transporters in rat liver microsomes. *Biochem. Pharmacol.* 68, 1353–1362. doi: 10.1016/j.bcp.2004.05.055

Fay, M. J., Nguyen, M. T., Snouwaert, J. N., Dye, R., Grant, D. J., Bodnar, W. M., et al. (2015). Xenobiotic metabolism in mice lacking the UDP-glucuronosyltransferase 2 family. *Drug Metab. Dispos.* 43, 1838–1846. doi: 10.1124/dmd.115.065482

Finel, M., and Kurkela, M. (2008). The UDP-glucuronosyltransferases as oligomeric enzymes. *Curr. Drug Metab.* 9, 70–76. doi: 10.2174/138920008783331158

Fremont, J. J., Wang, R. W., and King, C. D. (2005). Coimmunoprecipitation of UDP-glucuronosyltransferase isoforms and cytochrome P450 3A4. *Mol. Pharmacol.* 67, 260–262. doi: 10.1124/mol.104.006361

Fujiwara, R., Chen, S., Karin, M., and Tukey, R. H. (2012). Reduced expression of UGT1A1 in intestines of humanized UGT1 mice via inactivation of NF-κB leads to hyperbilirubinemia. *Gastroenterology* 142, 109–118. doi: 10.1053/j.gastro.2011.09.045

Fujiwara, R., and Itoh, T. (2014). Extensive protein-protein interactions involving UDP-glucuronosyltransferase (UGT) 2B7 in human liver microsomes. *Drug Metab. Pharmacokinet.* 29, 259–265. doi: 10.2133/dmpk.DMPK-13-RG-096

Fujiwara, R., Maruo, Y., Chen, S., and Tukey, R. H. (2015). Role of extrahepatic UDP-glucuronosyltransferase 1A1: advances in understanding breast milk-induced neonatal hyperbilirubinemia. *Toxicol. Appl. Pharmacol.* 289, 124–132. doi: 10.1016/j.taap.2015.08.018

Fujiwara, R., Nakajima, M., Oda, S., Yamanaka, H., Ikushiro, S. I., Sakaki, T., et al. (2010a). Interactions between human UDP-glucuronosyltransferase (UGT) 2B7 and UGT1A enzymes. *J. Pharm. Sci.* 99, 442–454. doi: 10.1002/jps.21830

Fujiwara, R., Nakajima, M., Yamamoto, T., Nagao, H., and Yokoi, T. (2009a). In silico and in vitro approaches to elucidate the thermal stability of human UDP-glucuronosyltransferase (UGT) 1A9. *Drug Metab. Pharmacokinet.* 24, 235–244. doi: 10.2133/dmpk.24.235

Fujiwara, R., Nakajima, M., Yamanaka, H., Katoh, M., and Yokoi, T. (2007a). Interactions between human UGT1A1, UGT1A4, and UGT1A6 affect their enzymatic activities. *Drug Metab. Dispos.* 35, 1781–1787. doi: 10.1124/dmd.107.016402

Fujiwara, R., Nakajima, M., Yamanaka, H., Nakamura, A., Katoh, M., Ikushiro, S., et al. (2007b). Effects of coexpression of UGT1A9 on enzymatic activities of human UGT1A isoforms. *Drug Metab. Dispos.* 35, 747–757.

Fujiwara, R., Nakajima, M., Yamanaka, H., and Yokoi, T. (2009b). Key amino acid residues responsible for the differences in substrate specificity of human UDP-glucuronosyltransferase (UGT) 1A9 and UGT1A8. *Drug Metab. Dispos.* 37, 41–46. doi: 10.1124/dmd.108.022913

Fujiwara, R., Nguyen, N., Chen, S., and Tukey, R. H. (2010b). Developmental hyperbilirubinemia and CNS toxicity in mice humanized with the UDP glucuronosyltransferase 1 (UGT1) locus. *Proc. Natl. Acad. Sci. U.S.A.* 107, 5024–5029. doi: 10.1073/pnas.0913290107

Ghosh, S. S., Sappal, B. S., Kalpana, G. V., Lee, S. W., Chowdhury, J. R., and Chowdhury, N. R. (2001). Homodimerization of human bilirubin-uridine-diphosphoglucuronate glucuronosyltransferase-1 (UGT1A1) and its functional implications. *J. Biol. Chem.* 276, 42108–42115. doi: 10.1074/jbc.M106742200

Girard, H., Lévesque, E., Bellemare, J., Journault, K., Caillier, B., and Guillemette, C. (2007). Genetic diversity at the UGT1 locus is amplified by a novel 3′ alternative splicing mechanism leading to nine additional UGT1A proteins that act as regulators of glucuronidation activity. *Pharmacogenet. Genomics* 17, 1077–1089. doi: 10.1097/FPC.0b013e3282f1f118

Gschaidmeier, H., and Bock, K. W. (1994). Radiation inactivation analysis of microsomal UDP-glucuronosyltransferases catalysing mono-and diglucuronide formation of 3, 6-dihydroxybenzo (a) pyrene and

3, 6-dihydroxychrysene. *Biochem. Pharmacol.* 48, 1545–1549. doi: 10.1016/0006-2952(94)90198-8

Hanioka, N., Jinno, H., Tanaka-Kagawa, T., Nishimura, T., and Ando, M. (2001). Determination of UDP-glucuronosyltransferase UGT1A6 activity in human and rat liver microsomes by HPLC with UV detection. *J. Pharm. Biomed. Anal.* 25, 65–75. doi: 10.1016/S0731-7085(00)00491-X

Hirashima, R., Michimae, H., Takemoto, H., Sasaki, A., Kobayashi, Y., Itoh, T., et al. (2016). Induction of the UDP-glucuronosyltransferase 1A1 during the perinatal period can cause neurodevelopmental toxicity. *Mol. Pharmacol.* 90, 265–274. doi: 10.1124/mol.116.104174

Ikushiro, S., Emi, Y., and Iyanagi, T. (1997). Protein-protein interactions between UDP-glucuronosyltransferase isozymes in rat hepatic microsomes. *Biochemistry* 36, 7154–7161. doi: 10.1021/bi9702344

Ishii, Y., Iwanaga, M., Nishimura, Y., Takeda, S., Ikushiro, S. I., Nagata, K., et al. (2007). Protein-protein interactions between rat hepatic cytochromes P450 (P450s) and UDP-glucuronosyltransferases (UGTs): evidence for the functionally active UGT in P450-UGT complex. *Drug Metab. Pharmacokinet.* 22, 367–376. doi: 10.2133/dmpk.22.367

Ishii, Y., Koba, H., Kinoshita, K., Oizaki, T., Iwamoto, Y., Takeda, S., et al. (2014). Alteration of the function of the UDP-glucuronosyltransferase 1A subfamily by cytochrome P450 3A4: different susceptibility for UGT isoforms and UGT1A1/7 variants. *Drug Metab. Dispos.* 42, 229–238. doi: 10.1124/dmd.113.054833

Ishii, Y., Miyoshi, A., Maji, D., Yamada, H., and Oguri, K. (2004). Simultaneous expression of guinea pig UDP-glucuronosyltransferase 2B21 (UGT2B21) and 2B22 in COS-7 cells enhances UGT2B21-catalyzed chloramphenicol glucuronidation. *Drug Metab. Dispos.* 32, 1057–1060. doi: 10.1124/dmd.32.10

Ishii, Y., Miyoshi, A., Watanabe, R., Tsuruda, K., Tsuda, M., Yamaguchi-Nagamatsu, Y., et al. (2001). Simultaneous expression of guinea pig UDP-glucuronosyltransferase 2B21 and 2B22 in COS-7 cells enhances UDP-glucuronosyltransferase 2B21-catalyzed morphine-6-glucuronide formation. *Mol. Pharmacol.* 60, 1040–1048.

Ishii, Y., Takeda, S., Yamada, H., and Oguri, K. (2005). Functional protein-protein interaction of drug metabolizing enzymes. *Front. Biosci.* 10:887–895. doi: 10.2741/1583

Izukawa, T., Nakajima, M., Fujiwara, R., Yamanaka, H., Fukami, T., Takamiya, M., et al. (2009). Quantitative analysis of UDP-glucuronosyltransferase (UGT) 1A and UGT2B expression levels in human livers. *Drug Metab. Dispos.* 37, 1759–1768. doi: 10.1124/dmd.109.027227

Jancova, P., Anzenbacher, P., and Anzenbacherova, E. (2010). Phase II drug metabolizing enzymes. *Biomed. Pap. Med. Fac. Univ. Palacky Olomouc. Czech. Repub.* 154, 103–116. doi: 10.5507/bp.2010.017

Jeong, H., Mason, S. P., Barabási, A. L., and Oltvai, Z. N. (2001). Lethality and centrality in protein networks. *Nature* 411, 41–42. doi: 10.1038/35075138

Kato, Y., Izukawa, T., Oda, S., Fukami, T., Finel, M., Yokoi, T., et al. (2013). Human UDP-glucuronosyltransferase (UGT) 2B10 in drug N-glucuronidation: substrate screening and comparison with UGT1A3 and UGT1A4. *Drug Metab. Dispos.* 41, 1389–1397. doi: 10.1124/dmd.113.051565

Kempner, E. S., and Schlegel, W. (1979). Size determination of enzymes by radiation inactivation. *Anal. Biochem.* 92, 2–10. doi: 10.1016/0003-2697(79)90617-1

Kerdpin, O., Mackenzie, P. I., Bowalgaha, K., Finel, M., and Miners, J. O. (2009). Influence of N-terminal domain histidine and proline residues on the substrate selectivities of human UDP-glucuronosyltransferase 1A1, 1A6, 1A9, 2B7, and 2B10. *Drug Metab. Dispos.* 37, 1948–1955. doi: 10.1124/dmd.109.028225

Koiwai, O., Aono, S., Adachi, Y., Kamisako, T., Yasui, Y., Nishizawa, M., et al. (1996). Crigler-Najjar syndrome type II is inherited both as a dominant and as a recessive trait. *Hum. Mol. Genet.* 5, 645–647. doi: 10.1093/hmg/5.5.645

Krishnaswamy, S., Duan, S. X., von Moltke, L. L., and Greenblatt, D. J. (2003). Validation of serotonin (5-hydroxtryptamine) as an in vitro substrate probe for human UDP-glucuronosyltransferase (UGT) 1A6. *Drug Metab. Dispos.* 31, 133–139. doi: 10.1124/dmd.31.1.133

Krishnaswamy, S., Hao, Q., Al-Rohaimi, A., Hesse, L. M., von Moltke, L. L., and Greenblatt, D. J. (2005). UDP glucuronosyltransferase (UGT) 1A6 pharmacogenetics: II. Functional impact of the three most common nonsynonymous UGT1A6 polymorphisms (S7A, T181A, and R184S). *J. Pharmacol. Exp. Ther.* 313, 1340–1346. doi: 10.1124/jpet.104.081968

Kuehl, G. E., and Murphy, S. E. (2003). N-glucuronidation of nicotine and cotinine by human liver microsomes and heterologously expressed UDP-glucuronosyltransferases. *Drug Metab. Dispos.* 31, 1361–1368. doi: 10.1124/dmd.31.11.1361

Kurkela, M., García-Horsman, J. A., Luukkanen, L., Mörsky, S., Taskinen, J., Baumann, M., et al. (2003). Expression and characterization of recombinant human UDP-glucuronosyltransferases (UGTs) UGT1A9. *UGT*1A9 is more resistant to detergent inhibition than other UGTs and was purified as an active dimeric enzyme. *J. Biol. Chem.* 278, 3536–3544. doi: 10.1074/jbc.M206136200

Kurkela, M., Hirvonen, J., Kostiainen, R., and Finel, M. (2004). The interactions between the N-terminal and C-terminal domains of the human UDP-glucuronosyltransferases are partly isoform-specific, and may involve both monomers. *Biochem. Pharmacol.* 68, 2443–2450. doi: 10.1016/j.bcp.2004.08.019

Kutsuno, Y., Hirashima, R., Sakamoto, M., Ushikubo, H., Michimae, H., Itoh, T., et al. (2015). Expression of UDP-glucuronosyltransferase 1 (UGT1) and glucuronidation activity toward endogenous substances in humanized UGT1 mouse brain. *Drug Metab. Dispos.* 43, 1071–1076. doi: 10.1124/dmd.115.063719

Laakkonen, L., and Finel, M. (2010). A molecular model of the human UDP-glucuronosyltransferase 1A1, its membrane orientation, and the interactions between different parts of the enzyme. *Mol. Pharmacol.* 77, 931–939. doi: 10.1124/mol.109.063289

Lankisch, T. O., Behrens, G., Ehmer, U., Möbius, U., Rockstroh, J., Wehmeier, M., et al. (2009). Gilbert's syndrome and hyperbilirubinemia in protease inhibitor therapy–an extended haplotype of genetic variants increases risk in indinavir treatment. *J. Hepatol.* 50, 1010–1018. doi: 10.1016/S0168-8278(09)61009-6

Lévesque, E., Girard, H., Journault, K., Lépine, J., and Guillemette, C. (2007). Regulation of the UGT1A1 bilirubin-conjugating pathway: role of a new splicing event at the UGT1A locus. *Hepatology* 45, 128–138. doi: 10.1002/hep.21464

Lewis, B. C., Mackenzie, P. I., and Miners, J. O. (2011). Homodimerization of UDP-glucuronosyltransferase 2B7 (UGT2B7) and identification of a putative dimerization domain by protein homology modeling. *Biochem. Pharmacol.* 82, 2016–2023. doi: 10.1016/j.bcp.2011.09.007

Li, C., and Wu, Q. (2007). Adaptive evolution of multiple-variable exons and structural diversity of drug-metabolizing enzymes. *BMC Evol. Biol.* 7:69. doi: 10.1186/1471-2148-7-1

Li, L., Huang, X. J., Peng, J. L., Zheng, M. Y., Zhong, D. F., Zhang, C. F., et al. (2016). Wedelolactone metabolism in rats through regioselective glucuronidation catalyzed by uridine diphosphate-glucuronosyltransferases 1As (UGT1As). *Phytomedicine* 23, 340–349. doi: 10.1016/j.phymed.2016.01.007

Lin, J. H., and Wong, B. K. (2002). Complexities of glucuronidation affecting in vitro in vivo extrapolation. *Curr. Drug Metab.* 3, 623–646. doi: 10.2174/1389200023336992

Liu, M., Chen, S., Yueh, M. F., Wang, G., Hao, H., and Tukey, R. H. (2016). Reduction of p53 by knockdown of the UGT1 locus in colon epithelial cells causes an increase in tumorigenesis. *Cell Mol. Gastroenterol. Hepatol.* 2, 63–76. doi: 10.1016/j.jcmgh.2015.08.008

Liu, X., Cao, Y. F., Ran, R. X., Dong, P. P., Gonzalez, F. J., Wu, X., et al. (2016). New insights into the risk of phthalates: Inhibition of UDP-glucuronosyltransferases. *Chemosphere* 144, 1966–1972. doi: 10.1016/j.chemosphere.2015.10.076

Liu, Y. Q., Yuan, L. M., Gao, Z. Z., Xiao, Y. S., Sun, H. Y., Yu, L. S., et al. (2016). Dimerization of human uridine diphosphate glucuronosyltransferase allozymes 1A1 and 1A9 alters their quercetin glucuronidation activities. *Sci Rep* 6:23763. doi: 10.1038/srep23763

Locuson, C. W., and Tracy, T. S. (2007). Comparative modelling of the human UDP-glucuronosyltransferases: insights into structure and mechanism. *Xenobiotica* 37, 155–168. doi: 10.1080/00498250601129109

Mackenzie, P. I., Bock, K. W., Burchell, B., Guillemette, C., Ikushiro, S. I., Iyanagi, T., et al. (2005). Nomenclature update for the mammalian UDP glycosyltransferase (UGT) gene superfamily. *Pharmacogenet. Genomics* 15, 677–685. doi: 10.1097/01.fpc.0000173483.13689.56

Mackenzie, P. I., Owens, I. S., Burchell, B., Bock, K. W., Bairoch, A., Belanger, A., et al. (1997). The UDP glycosyltransferase gene superfamily: recommended nomenclature update based on evolutionary divergence. *Pharmacogenet Genomics* 7, 255–269. doi: 10.1097/00008571-199708000-00001

Mano, Y., Usui, T., and Kamimura, H. (2004). Effects of β-estradiol and propofol on the 4-methylumbelliferone glucuronidation in recombinant human UGT

isozymes 1A1, 1A8 and 1A9. *Biopharm. Drug Dispos.* 25, 339–344. doi: 10.1002/bdd.418

Matern, H., Matern, S., and Gerok, W. (1982). Isolation and characterization of rat liver microsomal UDP-glucuronosyltransferase activity toward chenodeoxycholic acid and testosterone as a single form of enzyme. *J. Biol. Chem.* 257, 7422–7429.

Meech, R., and Mackenzie, P. I. (1997). UDP-glucuronosyltransferase, the role of the amino terminus in dimerization. *J. Biol. Chem.* 272, 26913–26917. doi: 10.1074/jbc.272.43.26913

Ménard, V., Eap, O., Roberge, J., Harvey, M., Levesque, E., and Guillemette, C. (2011). Transcriptional diversity at the UGT2B7 locus is dictated by extensive pre-mRNA splicing mechanisms that give rise to multiple mRNA splice variants. *Pharmacogenet. Genomics* 21, 631–641. doi: 10.1097/FPC.0b013e3283498147

Miley, M. J., Zielinska, A. K., Keenan, J. E., Bratton, S. M., Radominska-Pandya, A., and Redinbo, M. R. (2007). Crystal structure of the cofactor-binding domain of the human phase II drug-metabolism enzyme UDP-glucuronosyltransferase 2B7. *J. Mol. Biol.* 369, 498–511. doi: 10.1016/j.jmb.2007.03.066

Miners, J. O., Mackenzie, P. I., and Knights, K. M. (2010). The prediction of drug-glucuronidation parameters in humans: UDP-glucuronosyltransferase enzyme-selective substrate and inhibitor probes for reaction phenotyping and in vitro–in vivo extrapolation of drug clearance and drug-drug interaction potential. *Drug Metab. Rev.* 42, 196–208. doi: 10.3109/03602530903210716

Miyauchi, Y., Nagata, K., Yamazoe, Y., Mackenzie, P. I., Yamada, H., and Ishii, Y. (2015). Suppression of cytochrome P450 3A4 function by UDP-glucuronosyltransferase 2B7 through a protein-protein interaction: cooperative roles of the cytosolic carboxyl-terminal domain and the luminal anchoring region. *Mol. Pharmacol.* 88, 800–812. doi: 10.1124/mol.115.098582

Mizuma, T. (2009). Intestinal glucuronidation metabolism may have a greater impact on oral bioavailability than hepatic glucuronidation metabolism in humans: a study with raloxifene, substrate for UGT1A1, 1A8, 1A9, and 1A10. *Int. J. Pharm.* 378, 140–141. doi: 10.1016/j.ijpharm.2009.05.044

Mori, Y., Kiyonaka, S., and Kanai, Y. (2011). Transportsomes and channelsomes: are they functional units for physiological responses? *Channels* 5, 387–390. doi: 10.4161/chan.5.5.16466

Mulichak, A. M., Losey, H. C., Lu, W., Wawrzak, Z., Walsh, C. T., and Garavito, R. M. (2003). Structure of the TDP-epi-vancosaminyltransferase GtfA from the chloroeremomycin biosynthetic pathway. *Proc. Natl. Acad. Sci. U.S.A.* 100, 9238–9243. doi: 10.1073/pnas.1233577100

Muraoka, M., Kawakita, M., and Ishida, N. (2001). Molecular characterization of human UDP-glucuronic acid/UDP-N-acetylgalactosamine transporter, a novel nucleotide sugar transporter with dual substrate specificity. *FEBS Lett.* 495, 87–93. doi: 10.1016/S0014-5793(01)02358-4

Nair, P. C., Meech, R., Mackenzie, P. I., McKinnon, R. A., and Miners, J. O. (2015). Insights into the UDP-sugar selectivities of human UDP-glycosyltransferases (UGT): a molecular modeling perspective. *Drug Metab. Rev.* 47, 335–345. doi: 10.3109/03602532.2015.1071835

Nakajima, M., Yamanaka, H., Fujiwara, R., Katoh, M., and Yokoi, T. (2007). Stereoselective glucuronidation of 5-(4′-hydroxyphenyl)-5-phenylhydantoin by human UDP-glucuronosyltransferase (UGT) 1A1, UGT1A9, and UGT2B15: effects of UGT-UGT interactions. *Drug Metab. Dispos.* 35, 1679–1686. doi: 10.1124/dmd.107.015909

Nakamura, A., Nakajima, M., Yamanaka, H., Fujiwara, R., and Yokoi, T. (2008). Expression of UGT1A and UGT2B mRNA in human normal tissues and various cell lines. *Drug Metab. Dispos.* 36, 1461–1464. doi: 10.1124/dmd.108.021428

Nebert, D. W., and Russell, D. W. (2002). Clinical importance of the cytochromes P450. *Lancet* 360, 1155–1162. doi: 10.1016/S0140-6736(02)11203-7

Nguyen, N., Bonzo, J. A., Chen, S., Chouinard, S., Kelner, M. J., Hardiman, G., et al. (2008). Disruption of the ugt1 locus in mice resembles human Crigler-Najjar type I disease. *J. Biol. Chem.* 283, 7901–7911. doi: 10.1074/jbc.M709244200

Nishihara, M., Hiura, Y., Kawaguchi, N., Takahashi, J., and Asahi, S. (2013). UDP-glucuronosyltransferase 2B15 (UGT2B15) is the major enzyme responsible for spoglitazar glucuronidation in humans: Retrospective identification of the UGT isoform by in vitro analysis and the effect of UGT2B15* 2 mutation. *Drug Metab. Pharmacokinet.* 28, 475–484. doi: 10.2133/dmpk.DMPK-13-RG-004

Offen, W., Martinez-Fleites, C., Yang, M., Kiat-Lim, E., Davis, B. G., Tarling, C. A., et al. (2006). Structure of a flavonoid glucosyltransferase reveals the basis for plant natural product modification. *EMBO J.* 25, 1396–1405. doi: 10.1038/sj.emboj.7600970

Operaña, T. N., and Tukey, R. H. (2007). Oligomerization of the UDP-glucuronosyltransferase 1A proteins: homo- and heterodimerization analysis by fluorescence resonance energy transfer and co-immunoprecipitation. *J. Biol. Chem.* 282, 4821–4829. doi: 10.1074/jbc.M609417200

Patana, A. S., Kurkela, M., Goldman, A., and Finel, M. (2007). The human UDP-glucuronosyltransferase: identification of key residues within the nucleotide-sugar binding site. *Mol. Pharmacol.* 72, 604–611. doi: 10.1124/mol.107.036871

Peer, C. J., Sissung, T. M., Kim, A., Jain, L., Woo, S., Gardner, E. R., et al. (2012). Sorafenib is an inhibitor of UGT1A1 but is metabolized by UGT1A9: implications of genetic variants on pharmacokinetics and hyperbilirubinemia. *Clin. Cancer Res.* 18, 2099–2107. doi: 10.1158/1078-0432.CCR-11-2484

Peters, W. H., Jansen, P. L., and Nauta, H. (1984). The molecular weights of UDP-glucuronyltransferase determined with radiation-inactivation analysis. A molecular model of bilirubin UDP-glucuronyltransferase. *J. Biol. Chem.* 259, 11701–11705.

Rouleau, M., Roberge, J., Bellemare, J., and Guillemette, C. (2014). Dual roles for splice variants of the glucuronidation pathway as regulators of cellular metabolism. *Mol. Pharmacol.* 85, 29–36. doi: 10.1124/mol.113.089227

Rowland, A., Elliot, D. J., Williams, J. A., Mackenzie, P. I., Dickinson, R. G., and Miners, J. O. (2006). In vitro characterization of lamotrigine N2-glucuronidation and the lamotrigine-valproic acid interaction. *Drug Metab. Dispos.* 34, 1055–1062.

Sato, Y., Nagata, M., Tetsuka, K., Tamura, K., Miyashita, A., Kawamura, A., et al. (2014). Optimized methods for targeted peptide-based quantification of human uridine 5′-diphosphate-glucuronosyltransferases in biological specimens using liquid chromatography–tandem mass spectrometry. *Drug Metab. Dispos.* 42, 885–889. doi: 10.1124/dmd.113.056291

Satoh, T., and Hosokawa, M. (1998). The mammalian carboxylesterases: from molecules to functions. *Annu. Rev. Pharmacol. Toxicol.* 38, 257–288. doi: 10.1146/annurev.pharmtox.38.1.257

Schirris, T. J., Ritschel, T., Bilos, A., Smeitink, J. A., and Russel, F. G. (2015). Statin lactonization by uridine 5′-diphospho-glucuronosyltransferases (UGTs). *Mol. Pharm.* 12, 4048–4055. doi: 10.1021/acs.molpharmaceut.5b00474

Shao, H., He, X., Achnine, L., Blount, J. W., Dixon, R. A., and Wang, X. (2005). Crystal structures of a multifunctional triterpene/flavonoid glycosyltransferase from *Medicago truncatula*. *Plant Cell* 17, 3141–3154. doi: 10.1105/tpc.105.035055

Shi, W. W., Jiang, Y. L., Zhu, F., Yang, Y. H., Shao, Q. Y., Yang, H. B., et al. (2014). Structure of a novel O-linked N-acetyl-D-glucosamine (O-GlcNAc) transferase, GtfA, reveals insights into the glycosylation of pneumococcal serine-rich repeat adhesins. *J. Biol. Chem.* 289, 20898–20907. doi: 10.1074/jbc.M114.581934

Smith, P. A., Sorich, M. J., McKinnon, R. A., and Miners, J. O. (2003). Pharmacophore and quantitative structure-activity relationship modeling: complementary approaches for the rationalization and prediction of UDP-glucuronosyltransferase 1A4 substrate selectivity. *J. Med. Chem.* 46, 1617–1626. doi: 10.1021/jm020397c

Sneitz, N., Court, M. H., Zhang, X., Laajanen, K., Yee, K. K., Dalton, P., et al. (2009). Human UDP-glucuronosyltransferase UGT2A2: cDNA construction, expression, and functional characterization in comparison with UGT2A1 and UGT2A3. *Pharmacogenet. Genomics* 19, 923–934. doi: 10.1097/FPC.0b013e3283330767

Song, J. H., Cui, L., An, L. B., Li, W. T., Fang, Z. Z., Zhang, Y. Y., et al. (2015). Inhibition of UDP-glucuronosyltransferases (UGTs) activity by constituents of *Schisandra chinensis*. *Phytother. Res.* 29, 1658–1664. doi: 10.1002/ptr.5395

Strassburg, C. P., Oldhafer, K., Manns, M. P., and Tukey, R. H. (1997). Differential expression of the UGT1A locus in human liver, biliary, and gastric tissue: identification of UGT1A7 and UGT1A10 transcripts in extrahepatic tissue. *Mol. Pharmacol.* 52, 212–220.

Sumida, K., Kawana, M., Kouno, E., Itoh, T., Takano, S., Narawa, T., et al. (2013). Importance of UDP-glucuronosyltransferase 1A1 expression in skin and its induction by UVB in neonatal hyperbilirubinemia. *Mol. Pharmacol.* 84, 679–686. doi: 10.1124/mol.113.088112

Takeda, S., Ishii, Y., Iwanaga, M., Mackenzie, P. I., Nagata, K., Yamazoe, Y., et al. (2005). Modulation of UDP-glucuronosyltransferase function by

cytochrome P450: evidence for the alteration of UGT2B7-catalyzed glucuronidation of morphine by CYP3A4. *Mol. Pharmacol.* 67, 665–672. doi: 10.1124/mol.104.007641

Takeda, S., Ishii, Y., Iwanaga, M., Nurrochmad, A., Ito, Y., Mackenzie, P. I., et al. (2009). Interaction of cytochrome P450 3A4 and UDP-glucuronosyltransferase 2B7: evidence for protein-protein association and possible involvement of CYP3A4 J-helix in the interaction. *Mol. Pharmacol.* 75, 956–964. doi: 10.1124/mol.108.052001

Taura, K. I., Yamada, H., Hagino, Y., Ishii, Y., Mori, M. A., and Oguri, K. (2000). Interaction between cytochrome P450 and other drug-metabolizing enzymes: evidence for an association of CYP1A1 with microsomal epoxide hydrolase and UDP-glucuronosyltransferase. *Biochem. Biophys. Res. Commun.* 273, 1048–1052. doi: 10.1006/bbrc.2000.3076

Tourancheau, A., Margaillan, G., Rouleau, M., Gilbert, I., Villeneuve, L., Lévesque, E., et al. (2016). Unravelling the transcriptomic landscape of the major phase II UDP-glucuronosyltransferase drug metabolizing pathway using targeted RNA sequencing. *Pharm. J.* 16, 60–70. doi: 10.1038/tpj.2015.20

Tripathi, S. P., Prajapati, R., Verma, N., and Sangamwar, A. T. (2016). Predicting substrate selectivity between UGT1A9 and UGT1A10 using molecular modelling and molecular dynamics approach. *Mol. Simul.* 42, 270–288. doi: 10.1080/08927022.2015.1044451

Tukey, R. H., and Tephly, T. R. (1981). Purification of properties of rabbit liver estrone and p-nitrophenol UDP-glucuronyltransferases. *Arch. Biochem. Biophys.* 209, 565–578. doi: 10.1016/0003-9861(81)90314-3

Turgeon, D., Carrier, J. S., Chouinard, S., and Bélanger, A. (2003). Glucuronidation activity of the UGT2B17 enzyme toward xenobiotics. *Drug Metab. Dispos.* 31, 670–676. doi: 10.1124/dmd.31.5.670

Watanabe, Y., Nakajima, M., Ohashi, N., Kume, T., and Yokoi, T. (2003). Glucuronidation of etoposide in human liver microsomes is specifically catalyzed by UDP-glucuronosyltransferase 1A1. *Drug Metab. Dispos.* 31, 589–595. doi: 10.1124/dmd.31.5.589

Widmer, C. C., Pereira, C. P., Gehrig, P., Vallelian, F., Schoedon, G., Buehler, P. W., et al. (2010). Hemoglobin can attenuate hydrogen peroxide–induced oxidative stress by acting as an antioxidative peroxidase. *Antioxid. Redox. Signal.* 12, 185–198. doi: 10.1089/ars.2009.2826

Williams, J. A., Hyland, R., Jones, B. C., Smith, D. A., Hurst, S., Goosen, T. C., et al. (2004). Drug-drug interactions for UDP-glucuronosyltransferase substrates: a pharmacokinetic explanation for typically observed low exposure (AUCi/AUC) ratios. *Drug Metab. Dispos.* 32, 1201–1208. doi: 10.1124/dmd.104.000794

Wu, B., Wang, X., Zhang, S., and Hu, M. (2012). Accurate prediction of glucuronidation of structurally diverse phenolics by human UGT1A9 using combined experimental and in silico approaches. *Pharm. Res.* 29, 1544–1561. doi: 10.1007/s11095-012-0666-z

Xiong, Y., Bernardi, D., Bratton, S., Ward, M. D., Battaglia, E., Finel, M., et al. (2006). Phenylalanine 90 and 93 are localized within the phenol binding site of human UDP-glucuronosyltransferase 1A10 as determined by photoaffinity labeling, mass spectrometry, and site-directed mutagenesis. *Biochemistry* 45, 2322–2332. doi: 10.1021/bi0519001

Yao, Z., Liu, Y. Z., Ma, A. L., Wang, S. F., Lu, D., Hu, C. M., et al. (2015). Chiral inhibition of rivaroxaban derivatives towards UDP-glucuronosyltransferase (UGT) isoforms. *Chirality* 27, 936–943. doi: 10.1002/chir.22505

Yuan, L., Qian, S., Xiao, Y., Sun, H., and Zeng, S. (2015). Homo-and hetero-dimerization of human UDP-glucuronosyltransferase 2B7 (UGT2B7) wild type and its allelic variants affect zidovudine glucuronidation activity. *Biochem. Pharmacol.* 95, 58–70. doi: 10.1016/j.bcp.2015.03.002

Zhang, Q., Cao, Y. F., Ran, R. X., Li, R. S., Wu, X., Dong, P. P., et al. (2016). Strong specific inhibition of UDP-glucuronosyltransferase 2B7 by atractylenolide I and III. *Phytother. Res.* 30, 25–30. doi: 10.1002/ptr.5496

Conflict of Interest Statement: The authors declare that the research was conducted in the absence of any commercial or financial relationships that could be construed as a potential conflict of interest.

frontiers in Pharmacology

ORIGINAL RESEARCH
published: 14 November 2016
doi: 10.3389/fphar.2016.00427

Introduction of an *N*-Glycosylation Site into UDP-Glucuronosyltransferase 2B3 Alters Its Sensitivity to Cytochrome P450 3A1-Dependent Modulation

*Tatsuro Nakamura[1], Naho Yamaguchi[1], Yuu Miyauchi[1], Tomoki Takeda[1], Yasushi Yamazoe[2], Kiyoshi Nagata[3], Peter I. Mackenzie[4], Hideyuki Yamada[1†] and Yuji Ishii[1]**

[1] Laboratory of Molecular Life Sciences, Graduate School of Pharmaceutical Sciences, Kyushu University, Fukuoka, Japan, [2] The Cabinet Office, Government of Japan, Tokyo, Japan, [3] Department of Environmental Health Science, Tohoku Medical and Pharmaceutical University, Sendai, Japan, [4] Department of Clinical Pharmacology, Flinders University, Adelaide, SA, Australia

OPEN ACCESS

Edited by:
Vita Dolzan,
University of Ljubljana, Slovenia

Reviewed by:
Todd D. Porter,
University of Kentucky, USA
Pieter Swart,
Stellenbosch University, South Africa

***Correspondence:**
Yuji Ishii
ishii@phar.kyushu-u.ac.jp

†deceased

Specialty section:
This article was submitted to Pharmacogenetics and Pharmacogenomics, a section of the journal Frontiers in Pharmacology

Received: *28 September 2016*
Accepted: *26 October 2016*
Published: *14 November 2016*

Citation:
Nakamura T, Yamaguchi N, Miyauchi Y, Takeda T, Yamazoe Y, Nagata K, Mackenzie PI, Yamada H and Ishii Y (2016) Introduction of an N-Glycosylation Site into UDP-Glucuronosyltransferase 2B3 Alters Its Sensitivity to Cytochrome P450 3A1-Dependent Modulation. Front. Pharmacol. 7:427. doi: 10.3389/fphar.2016.00427

Our previous studies have demonstrated functional protein–protein interactions between cytochrome P450 (CYP) 3A and UDP-glucuronosyltransferase (UGT). However, the role of carbohydrate chains of UGTs in the interaction with CYP is not well understood. To address this issue, we examined whether CYP3A1 modulates the function of UGT2B3 which lacks potential glycosylation sites. We also examined whether the introduction of *N*-glycosylation to UGT2B3 affects CYP3A-dependent modulation of UGT function. To introduce a potential glycosylation site into UGT2B3, Ser 316 of UGT2B3 was substituted with Asn by site-directed mutagenesis. A baculovirus-Sf-9 cell system for expressing CYP3A1 and UGT2B3/UGT2B3(S316N) was established using a Bac-to-Bac system. Glycosylation of UGT2B3(S316N) was demonstrated in this expression system. The microsomal activity of recombinant UGT was determined using 4-methylumbelliferone as a substrate. The effect of CYP3A1 co-expression on UGT function was examined by comparing the kinetic profiles between single (UGT alone) and double expression (UGT plus CYP) systems. The kinetics of the two expression systems fitted a Michaelis–Menten equation. When the 4-MU concentration was varied, co-expression of CYP3A1 lowered the V_{max} of UGT2B3-mediated conjugation. Conversely, for UGT2B3(S316N), the V_{max} in the dual expression system was higher than that in the single expression system. The data obtained demonstrate that the introduction of *N*-glycosylation to UGT2B3 alters its sensitivity to CYP3A1-dependent modulation while CYP3A1 enhanced UGT2B3(S316N) activity, and wild-type UGT2B3 was suppressed by CYP3A1. These data suggest that *N*-glycosylation of UGT is one of the determinants regulating the interaction between CYP3A and UGT.

Keywords: UDP-glucuronosyltransferase, UGT, cytochrome P450, P450, CYP, protein–protein interaction

INTRODUCTION

The potential for drug metabolism varies from one individual to another. Therefore, drug metabolism capacity is a factor determining whether a drug produces pharmacological or adverse effects. Drug metabolism is classified into phase 1 and phase 2 reactions. The major reaction of phase 1 is oxidation in which cytochrome P450 (CYP) plays a key role (Guengerich and Rendic, 2010). Of all the enzymes including phase 2, UDP-glucuronosyltransferase (UGT) is mediating conjugation with glucuronic acid supplied from a cofactor (UDP-glucuronic acid, UDPGA) (Rowland et al., 2013). CYP and UGT are bound to the endoplasmic reticulum membrane, and their catalytic domains are localized in the cytosolic and luminal sides, respectively (Shepherd et al., 1989; Yamazaki et al., 1993). These enzymes have long been considered to work separately. However, we have shown that several UGTs can be trapped by a CYP1A1-immobilized affinity column (Taura et al., 2000). Moreover, our previous studies have shown that interaction between CYP3A4 and UGT2B7 alters the regio-selectivity of UGT2B7-catalyzed morphine glucuronidation (Takeda et al., 2005, 2009). Furthermore, CYP3A4 alters the function of UGT1A subfamily isoforms in an isoform and allelic variant specific fashion (Ishii et al., 2014). Rat UGTs are efficiently co-immunoprecipitated with anti-CYP3A antibody and the CYP3A-UGT complex is catalytically active for 4-methylumbelliferone glucuronidation (Ishii et al., 2007). Although the mechanisms of the interaction between CYP3A and UGT have not been clarified, the J-helix region of CYP3A4 is a candidate region involved in the interaction with UGT2B7 (Takeda et al., 2009). The domain(s) of UGT2B7 involved in the interaction with CYP3A4 has also been reported (Miyauchi et al., 2015). It is suggested that the hydrophobic regions at both the carboxyl terminal and luminal anchoring segment of UGT2B7 are crucial. However, further details about the interaction remain to be clarified.

Many UGTs have consensus sequences for *N*-glycosylation (Mackenzie, 1990a,b; Barbier et al., 2000; Nakajima et al., 2010; Nagaoka et al., 2012). The sequence can be generalized as NX(S/T), where X is any amino acid except proline, and approximately 70-90% of this sequence is glycosylated at its asparagine (N) residue (Gavel and von Heijne, 1990). Earlier studies have reported that *N*-glycosylation affects the enzyme activity of UGTs (Mackenzie, 1990a,b; Barbier et al., 2000; Nakajima et al., 2010; Nagaoka et al., 2012). We have reported that CYP3A4 interacts with UGT1A1, 1A6, 1A7, and 2B7 (Takeda et al., 2005; Ishii et al., 2014). All of these UGT isoforms possess potential *N*-glycosylation sites. However, the role of *N*-glycosylation of UGT in the interaction with CYP3A is unknown. Although the inhibition of *N*-glycosylation reduces UGT1A9 activity, deglycosylation of the mature form (*N*-glycosylated form) did not affect its catalytic properties (Nakajima et al., 2010). Thus, *N*-glycosylation has been suggested to be important for the protein folding of UGT. However, multiple mutations of the three *N*-glycosylation sites on UGT2B7 have different effects on substrate specificities (Nagaoka et al., 2012). Because of the important roles of *N*-glycosylation in UGT folding and function, we hypothesized that the *N*-glycosylation of UGT affects the interaction between CYP3A and UGT. To address this issue, we focused on rat UGT2B3 (Mackenzie, 1987) which does not possess potential glycosylation sites. We examined whether CYP3A1 modulates UGT2B3 and whether the introduction of *N*-glycosylation to UGT2B3 affects the CYP3A-dependent modulation of the UGT function.

MATERIALS AND METHODS

Materials

4-Methylumbelliferone (4-MU) and alamethicin were purchased from Sigma−Aldrich (St. Louis, MO, USA). UDP-Glucuronic acid (UDPGA) trisodium salt and 4-MU-β-D-glucuronide were obtained from Nakalai Tesque (Kyoto, Japan). Endoglycosidase H (EndoH) was purchased from New England Biolabos (Beverly, MA, USA). All other reagents were of the highest grade commercially available.

Animals

Animal experiments in this study were conducted following the approval of the Ethics Committee for Animal Experiments of Kyushu University. Male Wistar rats (7 weeks-old) were obtained from Charles River Japan (Tokyo, Japan) and were maintained for one week with free access to water and a suitable diet under a 7 a.m. to 7 p.m. light/dark cycle. For isolation of total RNA, liver tissue was quickly cut into small fragments, immediately immersed in liquid nitrogen, and stored at −80°C until required.

Expression System

Baculovirus for expressing CYP3A1 and UGT2B3 in Sf-9 cells was prepared using a Bac-to-Bac system (Invitrogen). CYP3A1 cDNA was subcloned from P91023(B) (Nagata et al., 1999) into pFastBac1 vector at an *Eco*RI site. The sequencing reaction was carried out using a Big Dye® Terminator v3.1 Cycle Sequencing Kit (Life Technologies). Then, cDNA sequences were confirmed by an ABI 3130xl Genetic Analyzer. CYP3A1 has two synonymous and one non-synonymous nucleotide substitutions: C1035G, G1074A, and T1055A, respectively, when compared with the database (Gonzalez et al., 1985; GenBank accession M10161). T1055A causes an amino acid substitution, M352K, and this CYP3A1 is known to be catalytically active (Nagata et al., 1999). It was used as the CYP3A1 in this study.

UGT2B3 cDNA was amplified from the total RNA of Wistar rat liver by a reverse transcription-polymerase chain reaction (RT-PCR), and cloned into pFastBac1. Isolation of total RNA and the RT-reaction were carried out by a method previously reported (Mutoh et al., 2006). To amplify the cDNA, nested PCR with two primer sets was used. The primer set for the first round PCR was UGT2B3(-20,-1)F1, 5′- TAA GGA TTT TGA TTT TTA AG-3′ and UGT2B3(1647,1628)R1, 5′-CAT AAA T TA GAA TGA GGC TG-3′. The primer set for the second round PCR was PstI-UGT2B3(-5,15)F2, 5′-AAC TGC AGT TAA GAT GCC TGG GAA GTG G-3′, and PstI-UGT2B3(1615, 1596)R2, 5′-AAC TGC AGT GTA GTG CAT TGT AA ATG AG-3′ with restriction sites (*Pst*I) underlined. The PCR was carried out with LA-Taq DNA polymerase (TaKaRa Bio, Kyoto) using

the manufacturer's recommended protocol with the following components: 1xLA-Taq buffer, 2 mM $MgCl_2$, 2.5 mM each dNTP, the primers F1 and R1 (5 μM each) and the cDNA in 100 μL (first round PCR). The amplification was carried out using the PROGRAM TEMP CONTROL SYSTEM PC-800 (ASTEC, Fukuoka, Japan) with 94°C, 4 min-(94°C, 1 min, 50°C, 1 min, 72°C, 2 min)×30 cycles-72°C, 20 min −4°C, ∞. The second round PCR was carried out as above but using primers F2 and R2. The resulting PCR products were restricted with PstI and cloned into pFastBac1. The sequence was confirmed by DNA sequencing as described above. UGT2B3 has a non-synonymous nucleotide substitution, T1498A, which causes a single amino-acid change, S500T. We used this as a wild-type UGT2B3 in this study.

Escherichia coli DH10Bac was transformed either with pFastBac1 plasmid carrying UGT2B3 or CYP3A1 cDNA to prepare recombinant bacmid DNA. Production and amplification of recombinant baculovirus and expression of recombinant proteins in Sf-9 cells were carried out according to the method described previously (Ishii et al., 2014).

The Introduction of a Potential *N*-Glycosylation Site into UGT2B3

UGT2B3 exhibits 83% identity to UGT2B2 (Mackenzie, 1986) in amino acid sequences. The Asn 316 of UGT2B2 is a potential site for glycosylation. Therefore, the Ser 316 of UGT2B3 was replaced with Asn by site-directed mutagenesis (SDM), and an expression system for the UGT2B3(S316N) mutant was constructed in a similar way as described above. The primers for the SDM were designed by Quick Change Primer Design (Agilent Technology). The primers used were UGT2B3(931, 964)(947G→A)SDM-F, 5′-GGG TCA ATG GTC AGC AAC ATG ACA GAA GAA AAG G-3′ and UGT2B3(964, 931)(947C→T)SDM-R, 5′-CCT TTT CTT CTG TCA TGT TGC TGA CCA TTG ACC C-3′. The procedures were carried out according to the manufacturer's recommendations. The introduction of the mutation at the appropriate position and the absence of other unwanted mutations were confirmed by DNA sequencing.

Kinetic Analysis

The kinetic analysis was performed using 100 μg microsomal protein. The amount of microsomal protein used was unified by adding control baculosomes. The activity of UGT2B3-catalyzed glucuronidation was determined by high-performance liquid chromatography (HPLC) with 4-MU as a substrate (Hanioka et al., 2001). The microsomes and alamethicin were mixed and preincubated for 30 min on ice. The assay was started by adding UDPGA and incubation was performed for 60 min at 37°C. The reaction was stopped with 100 μL 1 M trichloroacetic acid (TCA). After chilling on ice for 30 min, the incubation mixture was centrifuged (15,000 rpm, 4°C, 10 min). The supernatant containing the 4-MU glucuronide formed was analyzed by HPLC with a fluorescence detector (Ex 315 nm, Em 375 nm).

Data Analysis

The kinetics fitted a Michaelis−Menten equation, and the kinetic parameters were calculated using GraphPad Prism software (GraphPad Software Inc., San Diego, CA, USA). The statistical difference in kinetic parameters between UGT2B3 single expression and UGT2B3-CYP3A1 dual expression was evaluated by repeating the extra sum-of-squares *F* test.

Immunoblotting

Proteins were determined by the method of Lowry et al. (1951) with bovine serum albumin as a standard. SDS-polyacrylamide gel electrophoresis (SDS-PAGE) was performed according to Laemmli (1970). Proteins separated by SDS-PAGE were electroblotted to a polyviniliden difluoride membrane. UGT2B3 and UGT2B3(S316N) were detected by a goat anti-mouse low-pI form UGT antibody (Mackenzie et al., 1984). CYP3A1 was detected by rabbit anti-CYP3A2 antibody (Nagata et al., 1990). Immunochemical detection was conducted either with horseradish peroxidase (HRP)-conjugated secondary antibodies, HRP-rabbit anti-goat IgG (MP Biomedicals, Santa Ana, CA, USA), or HRP-donkey anti-rabbit IgG (GE Healthcare, Piscataway, NJ, USA). These were diluted 10,000- and 40,000-fold before use, respectively. Clarity Western ECL Substrate (Bio-Rad, Hercules, CA, USA) was used as the substrate of HRP, and the chemiluminescence emitted was analyzed by a ChemiDoc MP System (Bio-Rad).

His-Tag Pull-Down Assay

Introduction of hemagglutinin (HA)-tag at the carboxyl terminus of UGT2B3 was carried out by a two-step PCR. At the first step, primer HA(21,1)-UGT2B3(1590,1573)R, 5′-ATC TGG AAC ATC GTA TGG GTA CTC ATT CTT CAT TTT CTT-3′ and primer F2 were used. The PCR reaction was basically the same as that above except that pFastBac1-UGT2B3 was the template. In the second step, PstI-TCA-HA(27,1)R, 5′-AAC TGC AGT CAA GGG TAA TCT GGA ACA TCG TAT GGG TA-3′ and primer F2 were used (Underline, *Pst*I site). In the second step, the PCR products of the first step were used as a template. The PCR products were restricted with PstI and cloned into pFastBac1. To construct HA-tagged UGT2B3(S316N), an SDM described above was carried out with pFastBac1-UGT2B3-HA. To construct hexa-histidine $(His)_6$-tagged CYP3A1, PCR was carried out with the following primers: NotI-CYP3A1 (-4,16)F, 5′-ATA AGA ATG CGG CCG CAG GGA TGG ACC TGC TTT CAG-3′ and XhoI-CYP3A1-Histag(1510,1494)R, 5′-CCG CTC GAG TCA GTG ATG GTG ATG GTG ATG TGA TCC AGT TAT GAT TTC A-3′ (Underlines: *Not*I and *Xho*I sites, respectively). The PCR products were purified and restricted with *Not*I and *Xho*I and then subcloned into pFastBac1 restricted with the same enzymes. Their recombinant baculovirus was prepared as described above. Sf-9 cells were transfected with the recombinant virus for either CYP3A1-$(His)_6$ and/or UGT2B3-HA/UGT2B3(S316N). The resulting microsomes were solubilized with sodium cholate and the pulled down assays were carried out as described previously (Miyauchi et al., 2015).

Modeling of the Structure of the UGTs

The models were constructed using Phyre[2] (Protein Homology/Analogy Recognition Engine V 2.0) web server,

http://www.sbg.bio.ic.ac.uk/phyre2/html/ (Kelley et al., 2015) with UGT2B7 (amino acid residue from 285 to 450) as a template (Miley et al., 2007). Although the program is designed for prediction using multiple templates, only UGT2B7 was selected as a template in this case.

RESULTS

Expression of UGT2B3 and the Glycosylation Mutant, UGT2B3(S316N)

UGT2B3 was expressed in Sf-9 cells, and the protein band in the 50−60 kDa molecular mass range that was immunoreactive toward anti-mouse low pI form UGT antibody and was absent in control microsomes was judged to be UGT2B3 (**Figure 1A**). To introduce an *N*-glycosylated sugar chain to UGT2B3, we referred to UGT2B2 (Mackenzie, 1986) which has a potential *N*-glycosylation site and exhibits high similarity to UGT2B3 in primary sequence. Then, the Ser316 of UGT2B3 was substituted to Asn to establish an expression system for UGT2B3(S316N). The immune-reactive band with higher molecular mass and absent in control microsomes was judged to be UGT2B3(S316N)(**Figure 1A**). Thus, the molecular mass was increased by the introduction of a potential glycosylation site suggesting newly introduced *N*-glycosylation. This was also supported by a reduction in size after EndoH-treatment (**Figure 1A**).

Effect of Co-Expression of CYP3A1 on UGT2B3- and UGT2B3(S316N)-Catalyzed Glucuronidation

CYP3A1 was co-expressed in Sf-9 cells with UGT2B3 or UGT2B3(S316N). Sf-9 cells, the microsomes of which express UGT2B3 or UGT2B3(S316N) having a comparable band intensity to that in the single expression system, were selected and subjected to further investigation of their enzymatic properties (**Figures 1B–E**). The amount of UGT2B3 and microsomal protein used for the assay was also unified between the single and dual expression systems. For this, we rendered the protein level uniform with baculosomes obtained from Sf-9 cells infected with control baculovirus. When CYP3A1 was expressed together with UGT2B3, the V_{max} of UGT2B3-catalyzed 4-MU glucuronidation was significantly decreased (**Figure 2**; **Table 1**). The kinetic profiles for both the single and double expression could be fitted to a Michaelis−Menten equation. When the 4-MU concentration was varied, the V_{max} was reduced significantly while the K_m was comparable (**Table 1**). Furthermore, the same was also true for the kinetics by varying the UDPGA concentration (**Figure 3**; **Table 1**). The V_{max} was lowered by CYP3A1 cotransfection while the K_m for UDPGA was comparable. Therefore, CYP3A1 suppressed the activity of UGT2B3 which lacks potential glycosylation sites. However, when CYP3A1 was expressed together with UGT2B3(S316N), the V_{max} of UGT2B3(S316N)-catalyzed 4-MU glucuronidation was significantly increased (**Figure 3**; **Table 2**). The kinetic profiles for both single and double expression could be fitted to a Michaelis−Menten equation. When the 4-MU concentration was varied, the V_{max} was increased significantly while the K_m was comparable (**Table 2**). Both the V_{max} and

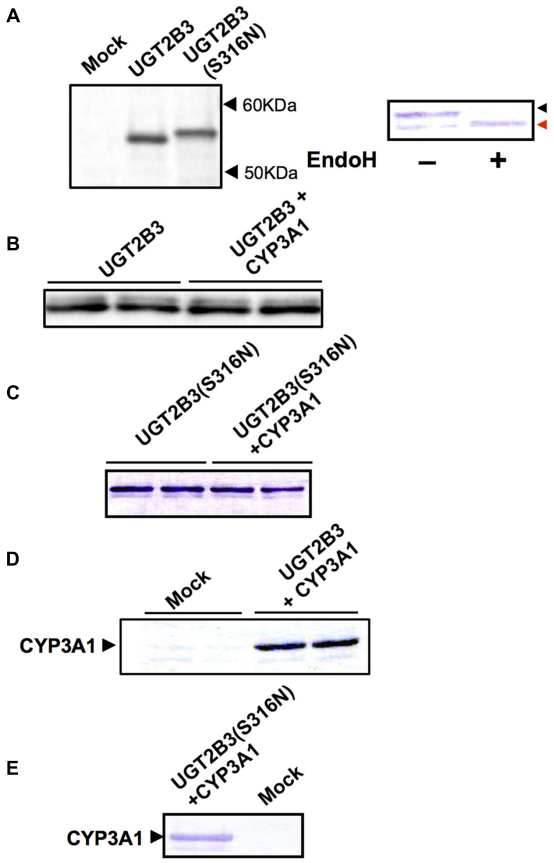

FIGURE 1 | Immunoblots of the expression of UGT2B3, UGT2B3(S316N), and CYP3A1 in Sf-9 cells. To obtain microsomes simultaneously expressing CYP3A1 and UGT2B3/UGT2B3(S316N), Sf-9 cells were transfected with recombinant baculovirus for CYP3A1 and UGT2B3/UGT2B3(S316N). The lanes labeled "UGT2B3" and "UGT2B3(S316N)" show microsomal samples of single transfected cells. The lanes labeled "UGT2B3+CYP3A1" and "UGT2B3(S316N)+CYP3A1" show double transfected cells. Baculosomes (5 μg protein) from UGT2B3 single-expressing Sf-9 cells were electrophoresed (SDS-PAGE). For baculosomes of CYP3A1-UGT2B3 co-expression systems, protein amounts equivalent to UGT2B3 for the single-expressing system were used. Similarly, baculosomes (3 μg protein) from UGT2B3(S316N) single-expressing Sf-9 cells were electrophoresed. For baculosomes of CYP3A1-UGT2B3(S316N) co-expression systems, protein amounts equivalent to UGT2B3(S316N) for the single-expressing system were used. Mock represents the baculosomes (10 μg protein) from Sf-9 cells infected with baculovirus without passenger DNA which served as controls. The proteins in the gel were electrically transferred to a polyvinilidene difluoride membrane, and blotted with goat anti-mouse low p*I* form UGT **(A–C)** and rabbit anti-CYP3A2 **(D,E)**, antibodies, respectively. In right panel of **(A)**, baculosomes (25 μg protein) from UGT2B3(S316N)-expressing Sf-9 cells were treated with Endoglycosidase H (EndoH, 500 U) at 37°C for 17 h. Four microgram protein of the digest was subjected to immunoblotting with goat anti-mouse low p*I* form UGT antibody as a primary antibody. Black and red arrow heads represent original and deglycosylated UGT2B3(S316N), respectively.

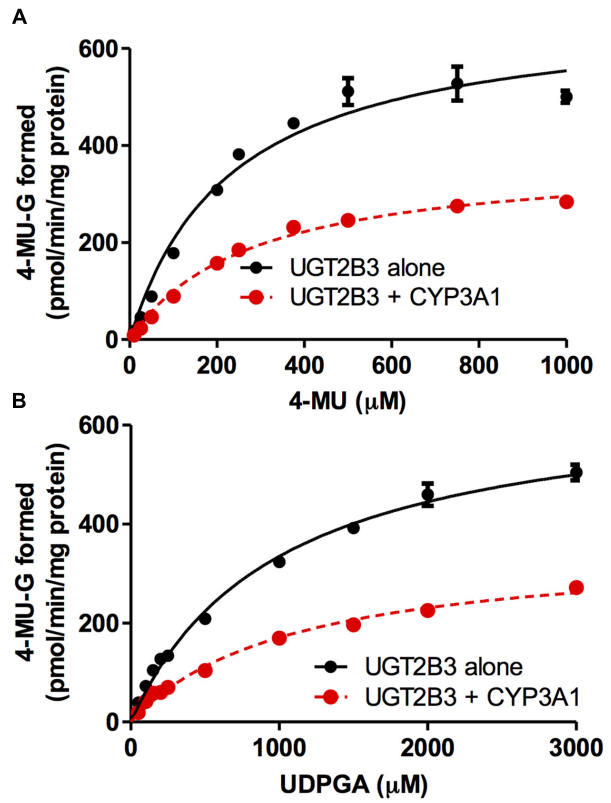

FIGURE 2 | Michaelis–Menten plots of 4-MU glucuronidation catalyzed by UGT2B3 in the absence and presence of CYP3A1 co-expression. The plots of UGT2B3 single- and UGT2B3-CYP3A1-dual are shown. The kinetics obtained by varying the 4-MU concentration **(A)** and UDPGA concentration **(B)** are shown. In **(A)**, the 4-MU concentration was varied over the range 10–1000 μM while the UDPGA concentration was fixed at 2 mM. In **(B)**, the UDPGA concentration was varied over the range 50 μM–3 mM while the 4-MU concentration was fixed at 1 mM. The total amount of protein added to the assay mixture was standardized at 100 μg. For this, when necessary, control baculosomes were added to the reaction mixture. Kinetic parameters were calculated by fitting the curve to a Michaelis–Menten equation, and they are listed in **Table 1**.

K_m of UGT2B3(S316N)-catalyzed 4-MU glucuronidation was significantly increased by varying the UDPGA concentration (**Figure 3**; **Table 2**). In sharp contrast to the wild-type UGT2B3, co-expression of CYP3A1 increased UGT2B3(S316N) activity.

Effect of EndoH-Treatment on the Activity of UGT2B3(S316N)

The glucuronidation activities of microsomes expressing UGT alone, UGT2B3(S316N), and UGT and CYP, UGT2B3(S316N)-CYP3A1, were compared with or without EndoH-treatment (**Figure 4**). The 4-MU glucuronidation activity in UGT2B3(S316N)-CYP3A1 was significantly higher than the UGT2B3(S316N) single expression even after treatment with EndoH. The deglycosylation did not affect the activity of UGT2B3(S316N).

TABLE 1 | Kinetic parameters for 4-MU glucuronide formation catalyzed by Sf-9 microsomes expressing UGT2B3 alone and UGT2B3 + CYP3A1: kinetics by varying 4-MU or UDPGA concentration.

	K_m (μM)	V_{max} (pmol/min/mg protein)	CLint (μg/min/mg protein)
By varying 4-MU concentration			
UGT2B3	231 ± 31	682 ± 33	2.95
UGT2B3+CYP3A1	278 ± 20	377 ± 11*	1.36
By varying UDPGA concentration			
UGT2B3	982 ± 70	664 ± 20	0.676
UGT2B3+CYP3A1	1088 ± 103	356 ± 14*	0.327

*Data were fitted to a Michaelis–Menten equation (**Figure 2**). Results are the estimated value ± SE. *Significantly different from UGT2B3 single expression ($p < 0.0001$).*

Protein–Protein Interaction of CYP3A1 and UGT2B3/UGT2B3(S316N)

$(His)_6$-tagged CYP3A1 was constructed and, the baculovirus encoding it subsequently co-transfected with either UGT2B3 or UGT2B3(S316N) which were tagged with HA. A band immunoreactive to an anti-HA antibody was observed in the precipitates (**Figure 5**). However, there was no pull down when they were expressed singly. Therefore, both HA-tagged UGT2B3 and UGT2B3(S316N) were pulled down by $(His)_6$-tagged CYP3A1 which suggests that CYP3A1 interacts with not only UGT2B3 but also UGT2B3(S316N).

Prediction of the Structure of the Carboxyl Terminal Domain of Wild-Type UGT2B3 and a Glycosylated Mutant UGT2B3(S316N)

The structures of part of the carboxyl terminal domain of UGT2B3 and UGT2B3(S316N) were predicted by *Phyre*[2] with UGT2B7 as template (**Figure 6**). For comparison, the structure of UGT2B3 which has Asn at 316 as a potential *N*-glycosylation site was also predicted. For reference, the prediction was also carried out for the UGT2B7 and UGT2B2 with UGT2B7 as a template. In UGT2B7, Asn 315 is the corresponding residue. Overall, it seems that the predicted structures are very similar to each other. The structure around residue 316 or 315 (for UGT2B7), a β-strand structure was observed except for UGT2B3. Although the prediction does not include the effect of the glycosylation chain, it is assumed that substitution of Ser 316 for Asn altered the partial structure of UGT2B3.

DISCUSSION

The effect of CYP3A1 on UGT2B3 which lacks a potential glycosylation site was studied. Since it is evident that CYP3A1 modulates UGT2B3 activity, *N*-glycosylation is not essential for CYP3A1 to modulate this UGT. Furthermore, this study demonstrates that the introduction of *N*-glycosylation to UGT2B3 alters UGT sensitivity to a functional protein–protein interaction with CYP3A: wild-type UGT2B3 which lacks

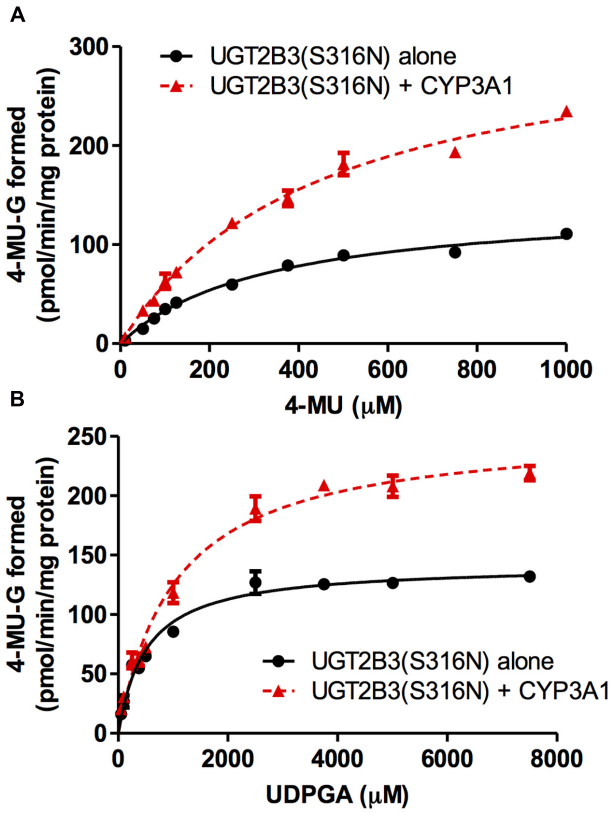

FIGURE 3 | Michaelis–Menten plots of 4-MU glucuronidation catalyzed by UGT2B3(S316N) in the absence and presence of CYP3A1 co-expression. The plots for UGT2B3(S316N) single- and UGT2B3(S316N)-CYP3A1-dual are shown. The kinetics obtained by varying the 4-MU concentration **(A)** and UDPGA concentration **(B)** are shown. In **(A)**, the 4-MU concentration was varied over the range 10–1000 μM while the UDPGA concentration was fixed at 2 mM. In **(B)**, the UDPGA concentration was varied over the range 50 μM–7.5 mM while the 4-MU concentration was fixed at 1 mM. The total amount of protein added to the assay mixture was standardized at 100 μg. For this, when necessary, control baculosomes were added to the reaction mixture. The kinetic parameters were calculated by fitting the curve to a Michaelis–Menten equation, and they are listed in **Table 2**.

TABLE 2 | Kinetic parameters for 4-MU glucuronide formation catalyzed by Sf-9 microsomes expressing UGT2B3(S316N) alone and UGT2B3(S316N) + CYP3A1: kinetics by varying 4-MU or UDPGA concentration.

	K_m (μM)	V_{max} (pmol/min/mg protein)	CLint (μg/min/mg protein)
By varying 4-MU concentration			
UGT2B3(S316N)	330 ± 33	143 ± 6	0.433
UGT2B3(S316N)+CYP3A1	444 ± 43	329 ± 43*	0.740
By varying UDPGA concentration			
UGT2B3(S316N)	513 ± 51	142 ± 4	0.277
UGT2B3(S316N)+CYP3A1	1040 ± 100*	256 ± 8*	0.245

*Data were fitted to a Michaelis–Menten equation (**Figure 3**). Results are the estimated value ± SE. *Significantly different from UGT2B3(S316N) single expression ($p < 0.0001$).*

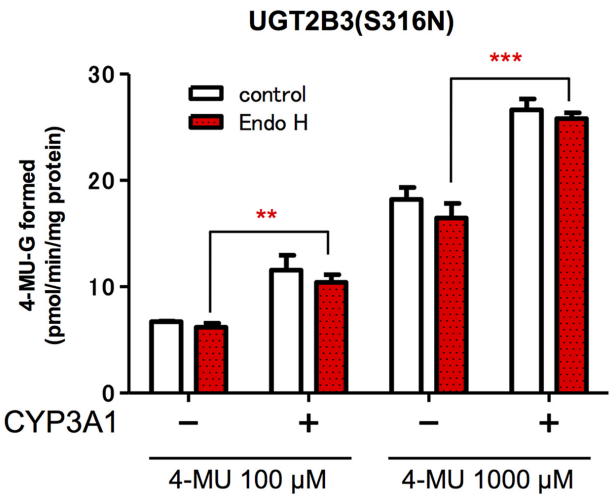

FIGURE 4 | Effect of EndoH-treatment on the glucuronidation catalyzed by UGT2B3(S316N). Baculosomes (20 μg protein) from UGT2B3(S316N) single- and UGT2B3(S316N)-CYP3A1 dual-expressing Sf-9 cells were treated with Endoglycosidase H (EndoH, 250 U) at 37°C for 1 h. The UGT activity was assayed with 100 or 1000 μM 4-MU and UDPGA fixed at 3 mM. Significantly different from UGT2B3(S316N) single expression (**$p < 0.001$; ***$p < 0.0001$).

N-glycosylation sites is suppressed by CYP3A1, whereas this P450 increases UGT2B3(S316N) activity. These results suggest that although the *N*-glycosylation of UGT is not essential for modulation by CYP3A, the *N*-sugar chain linked to UGT is one of the factors regulating this interaction between CYP3A and UGT. In this study, we focused on the effect of CYP3A1 on UGT function. To allow a comparison, we carried out several transfection experiments to obtain microsomes for UGT single and CYP3A1-UGT dual microsomes with a comparable UGT level and the results shown in **Tables 1** and **2** allow an examination of the effect of CYP3A1 on each UGT. Although the activity of UGT2B3 and UGT2B3(S316N) cannot be simply compared between **Tables 1** and **2,** it seems that the introduction of *N*-glycosylation to UGT2B3 at this position reduces the glucuronidation activity. Based on this, it is likely that CYP3A1 increases the function of the glycosylated mutant UGT2B3(S316N) to approach that of the wild type. In general, the methods that involve introduction of mutation(s) to the potential glycosyation site to inhibit glycosylation are a well-known strategy to investigate the role of glycosylation on enzyme function. In some enzymes, the activity was increased by reducing the glycosylation site, while in some other enzymes, the activity was decreased (Skropeta, 2009). *N*-Glycosylation is involved in the protein folding of UGT1A9 and important for catalytic function (Nakajima et al., 2010). However, deglycosylation of the mature UGT1A9 did not affect its function. In the case of UGT2B3(S316N), *N*-glycosylation resulted in positive modulation by CYP3A1 (**Figure 4**). However, the increase in UGT activity was consistent even after EndoH-treatment (**Figure 4**). Therefore, it is suggested that the engineered glycosylated chain of UGT2B3(S316N) is no longer required after

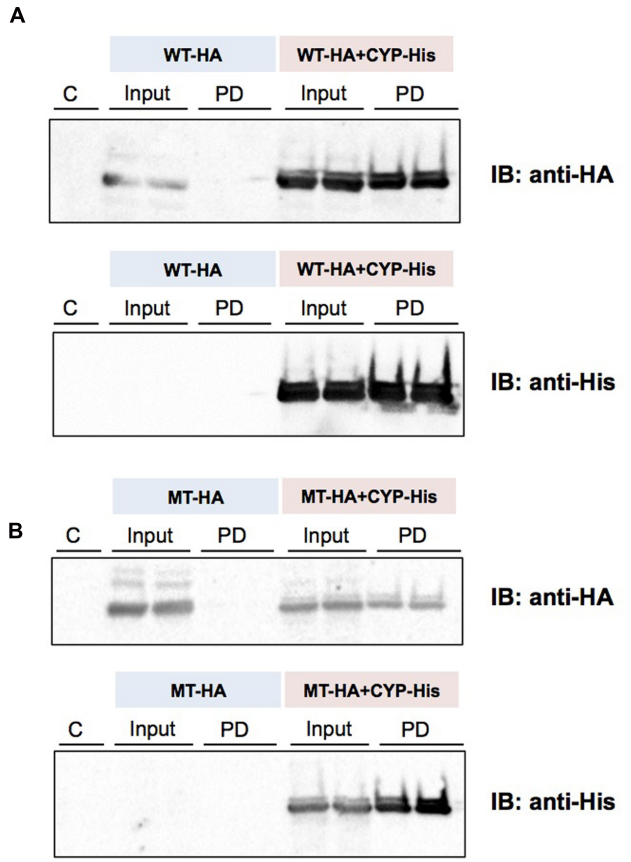

FIGURE 5 | Detection of an interaction between CYP3A1 and UGT2B3/UGT2B3(S316N) by His-tag pull-down assay. UGT2B3-HA and UGT2B3(S316N)-HA were expressed in the presence and absence of coexpressed His-CYP3A1. The pull-down assay was performed according to methods previously published (Miyauchi et al., 2015) with slight modification. Microsomes (2 mg protein/mL) were solubilized with sodium cholate. Then the solubilized microsomes were used in each assay. His-CYP3A1 and proteins trapped by this P450 were eluted with buffer containing imidazole at a high concentration. Each protein was detected by immunoblotting with a specific antibody: rabbit anti-HA or rabbit anti-His. Solubilized microsomes and His-CYP3A1–trapped samples are indicated as Input (30% of the input) and PD (pull down), respectively. In **(A)**, HA-tagged wild-type UGT2B3 (WT-HA) was used. In **(B)**, HA-tagged UGT2B3(S316N) (MT-HA) was used. WT-HA+CYP-His and MT-HA+CYP-His indicate microsomes coexpressing UGT2B3-HA or UGT2B3(S316N)-HA with His-CYP3A1, respectively. Duplicate assays were carried out. For each pull-down sample, one half of the precipitate was subjected to SDS-PAGE for detection with either HA or His while the lanes shown by "C" represent a negative control sample obtained by the same procedures but using solubilized control microsomes as an input, with microsomes prepared from Sf-9 cells transfected with control baculovirus alone. Details are described in the Section "Materials and Methods".

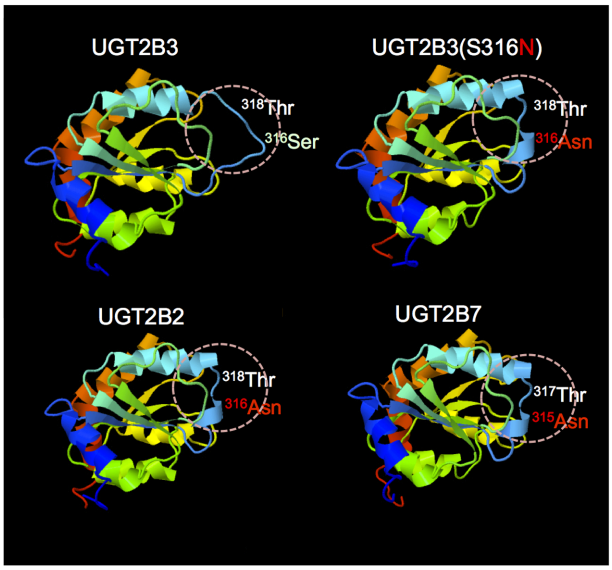

FIGURE 6 | Comparison of the predicted structure of UGT2B3 wild-type, UGT2B3(S316N), UGT2B2, and UGT2B7: the region spanning from 285 to 450. The models were constructed using the Phyre2 web server (Kelley et al., 2015) with the UGT2B7 (amino acid residue from 285 to 450) as a template. Template: UGT2B7, Miley et al. (2007) (DOI: 10.2210/pdb2o6l/pdb).

maturation and fixing the conformation of UGT2B3(S316N). This was also true for UGT2B3(S316N) without co-expression of CYP3A1. Taken together, these findings suggest that the complex formation with CYP3A1 affects the conformation of UGT2B3(S316N). Although the kinetics were not studied when examining the effect of deglycosylation, the activity was consistent at both low and high substrate concentrations. It is assumed that deglycosylation did not alter the affinity to the substrate. Since glycosylation of UGT has been shown to be important during synthesis of the enzyme but not once the mature enzyme is formed (Nakajima et al., 2010), it is assumed that the CYP3A1-dependent modulation of UGT2B3(S316N) that we observed is due to the interaction of CYP3A4 with the secondary structure of UGT2B3(S316N) during the process of formation of the mature UGT enzyme. However, whether glycosylation or merely the presence of the Asn at that site is sufficient to alter structure and function, remains to be clarified in a future study. Nevertheless, our current study suggests that the introduction of a potential glycosylation site to UGT2B3 alters its CYP3A1-dependent modulation.

UGT2B7 is known to interact with CYP3A4 (Takeda et al., 2005, 2009; Miyauchi et al., 2015). Furthermore, the crystal structure of the cofactor-binding domain of UGT2B7 (from residues 285 to 450) has been determined (Miley et al., 2007). So far, that is the sole example of a crystal structure of mammalian UGTs. Concerning the structural differences between UGT2B3 and UGT2B3(S316N), the structures of the corresponding region were predicted by *Phyre*^{2} with UGT2B7 as a template (**Figure 6**). The results were very similar except around the 316th residue. So, on the basis of the prediction, the substitution of Ser at the 316th residue of UGT2B3 by Asn converted the random coil to a β-strand structure (**Figure 6**). It is reasonable to suppose that the combination of the structural difference and the *N*-glycosylation in UGT2B3(S316N) resulted in a different susceptibility to modulation by CYP3A1.

This study suggests that *N*-glycosylation of UGT is one of the determinants of the functional interaction between CYP3A and UGT. UGT function is known to be affected by *N*-glycosylation (Mackenzie, 1990a,b; Barbier et al., 2000; Nakajima et al., 2010; Nagaoka et al., 2012). Many UGTs have *N*-glycosylation at more than two positions (Barbier et al., 2000; Nagaoka et al., 2012). Therefore, the role of *N*-glycosylation of the other UGTs is very important for functional protein−protein interactions with CYP3A. Further studies are necessary to determine the importance of *N*-glycosylation of UGTs in the UGT-CYP interactions.

AUTHOR CONTRIBUTIONS

Participated in research design: TN, NY, YM, TT, YY, KN, PM, HY, and YI. Conducted experiments: TN, NY, and YI. Contributed new reagents or analytical tools: TN and NH. Performed data analysis: TN, NY, and YI. Wrote or contributed the writing of the manuscript: TN, NY, YM, and YI.

FUNDING

This study was supported in part by Grants-in-Aid for Scientific Research (B)[#25293039] from the Japanese Society for the Promotion of Science to YI.

ACKNOWLEDGMENT

The authors thank the Research Support Center, Research Center for Human Disease Modeling, Graduate School of Medical Sciences, Kyushu University, for technical support.

REFERENCES

Barbier, O., Girard, C., Breton, R., Bélanger, A., and Hum, D. W. (2000). N-glycosylation and residue 96 are involved in the functional properties of UDP-glucuronosyltransferase enzymes. *Biochemistry* 39, 11540–11552. doi: 10.1021/bi000779p

Gavel, Y., and von Heijne, G. (1990). Sequence differences between glycosylated and non-glycosylated Asn-X-Thr/Ser acceptor sites: implications for protein engineering. *Protein Eng.* 3, 433–442. doi: 10.1093/protein/3.5.433

Gonzalez, F. J., Nebert, D. W., Hardwick, J. P., and Kasper, C. B. (1985). Complete cDNA and protein sequence of a pregnenolone 16 alpha-carbonitrile-induced cytochrome P-450. A representative of a new gene family. *J. Biol. Chem.* 260, 7435–7441.

Guengerich, F. P., and Rendic, S. (2010). Update information on drug metabolism systems–2009, part I. *Curr. Drug Metab.* 11, 1–3. doi: 10.2174/138920010791110908

Hanioka, N., Jinno, H., Nishimura, T., Ando, M., Ozawa, S., and Sawada, J. (2001). High-performance liquid chromatographic assay for glucuronidation activity of 7-ethyl-10-hydroxycamptothecin (SN-38), the active metabolite of irinotecan (CPT-11), in human liver microsomes. *Biomed. Chromatogr.* 15, 328–333. doi: 10.1002/bmc.76

Ishii, Y., Iwanaga, M., Nishimura, Y., Takeda, S., Ikushiro, S., Nagata, K., et al. (2007). Protein-protein interactions between rat hepatic cytochromes P450 (P450s) and UDP-glucuronosyltransferases (UGTs): evidence for the functionally active UGT in P450-UGT complex. *Drug Metab. Pharmacokinet.* 22, 367–376. doi: 10.2133/dmpk.22.367

Ishii, Y., Koba, H., Kinoshita, K., Oizaki, T., Iwamoto, Y., Takeda, S., et al. (2014). Alteration of the function of the UDP-glucuronosyltransferase 1A subfamily by cytochrome P450 3A4: different susceptibility for UGT isoforms and UGT1A1/7 variants. *Drug Metab. Dispos.* 42, 229–238. doi: 10.1124/dmd.113.054833

Kelley, L. A., Mezulis, S., Yates, C. M., Wass, M. N., and Sternberg, M. J. (2015). The Phyre2 web portal for protein modeling, prediction and analysis. *Nat. Protoc.* 10, 845–858. doi: 10.1038/nprot.2015.053

Laemmli, U. K. (1970). Cleavage of structural proteins during the assembly of the head of bacteriophage T4. *Nature* 227, 680–685. doi: 10.1038/227680a0

Lowry, O. H., Rosebrough, N. J., Farr, A. L., and Randall, R. J. (1951). Protein measurement with the folin phenol reagent. *J. Biol. Chem.* 193, 265–275.

Mackenzie, P. I. (1986). Rat liver UDP-glucuronosyltransferase. cDNA sequence and expression of a form glucuronidating 3-hydroxyandrogens. *J. Biol. Chem.* 261, 14112–14117.

Mackenzie, P. I. (1987). Rat liver UDP-glucuronosyltransferase. Identification of cDNAs encoding two enzymes which glucuronidate testosterone, dihydrotestosterone, and beta-estradiol. *J. Biol. Chem.* 262, 9744–9749.

Mackenzie, P. I. (1990a). Expression of chimeric cDNAs in cell culture defines a region of UDP glucuronosyltransferase involved in substrate selection. *J. Biol. Chem.* 265, 3432–3435.

Mackenzie, P. I. (1990b). The effect of N-linked glycosylation on the substrate preferences of UDP glucuronosyltransferases. *Biochem. Biophys. Res. Commun.* 166, 1293–1299. doi: 10.1016/0006-291X(90)91006-E

Mackenzie, P. I., Hjelmeland, L. M., and Owens, I. S. (1984). Purification and immunochemical characterization of a low-pI form of UDP glucuronosyltransferase from mouse liver. *Arch. Biochem. Biophys.* 231, 487–497. doi: 10.1016/0003-9861(84)90412-0

Miley, M. J., Zielinska, A. K., Keenan, J. E., Bratton, S. M., Radominska-Pandya, A., and Redinbo, M. R. (2007). Crystal structure of the cofactor-binding domain of the human phase II drug-metabolism enzyme UDP-glucuronosyltransferase 2B7. *J. Mol. Biol.* 369, 498–511. doi: 10.1016/j.jmb.2007.03.066

Miyauchi, Y., Nagata, K., Yamazoe, Y., Mackenzie, P. I., Yamada, H., and Ishii, Y. (2015). Suppression of Cytochrome P450 3A4 function by UDP-Glucuronosyltransferase 2B7 through a protein-protein interaction: cooperative roles of the cytosolic carboxyl-terminal domain and the luminal anchoring region. *Mol. Pharmacol.* 88, 800–812. doi: 10.1124/mol.115.098582

Mutoh, J., Taketoh, J., Okamura, K., Kagawa, T., Ishida, T., Ishii, Y., et al. (2006). Fetal pituitary gonadotropin as an initial target of dioxin in its impairment of cholesterol transportation and steroidogenesis in rats. *Endocrinology* 147, 927–936. doi: 10.1210/en.2005-1125

Nagata, K., Gonzalez, F. J., Yamazoe, Y., and Kato, R. (1990) Purification and characterization of four catalytically active testosterone 6 beta-hydroxylase P-450s from rat liver microsomes: comparison of a novel form with three structurally and functionally related forms. *J. Biochem.* 107, 718–725.

Nagaoka, K., Hanioka, N., Ikushiro, S., Yamano, S., and Narimatsu, S. (2012). The effects of N-glycosylation on the glucuronidation of zidovudine and morphine by UGT2B7 expressed in HEK293 cells. *Drug Metab. Pharmacokinet.* 27, 388–397. doi: 10.2133/dmpk.DMPK-11-RG-135

Nagata, K., Ogino, M., Shimada, M., Miyata, M., Gonzalez, F. J., and Yamazoe, Y. (1999). Structure and expression of the rat CYP3A1 gene: isolation of the gene (P450/6betaB) and characterization of the recombinant protein. *Arch. Biochem. Biophys.* 362, 242–253. doi: 10.1006/abbi.1998.1030

Nakajima, M., Koga, T., Sakai, H., Yamanaka, H., Fujiwara, R., and Yokoi, T. (2010). N-Glycosylation plays a role in protein folding of human UGT1A9. *Biochem. Pharmacol.* 79, 1165–1172. doi: 10.1016/j.bcp.2009.11.020

Rowland, A., Miners, J. O., and Mackenzie, P. I. (2013). The UDP-glucuronosyltransferases: their role in drug metabolism and detoxification. *Int. J. Biochem. Cell Biol.* 45, 1121–1132. doi: 10.1016/j.biocel.2013.02.019

Shepherd, S. R., Baird, S. J., Hallinan, T., and Burchell, B. (1989). An investigation of the transverse topology of bilirubin UDP-glucuronosyltransferase in rat hepatic endoplasmic reticulum. *Biochem. J.* 259, 617–620. doi: 10.1042/bj2590617

Skropeta, D. (2009). The effect of individual N-glycans on enzyme activity. *Bioorg. Med. Chem.* 17, 2645–2653. doi: 10.1016/j.bmc.2009.02.037

Takeda, S., Ishii, Y., Iwanaga, M., Mackenzie, P. I., Nagata, K., Yamazoe, Y., et al. (2005). Modulation of UDP-glucuronosyltransferase function by cytochrome P450: evidence for the alteration of UGT2B7-catalyzed glucuronidation of morphine by CYP3A4. *Mol. Pharmacol.* 67, 665–672. doi: 10.1124/mol.104.007641

Takeda, S., Ishii, Y., Iwanaga, M., Nurrochmad, A., Ito, Y., Mackenzie, P. I., et al. (2009). Interaction of cytochrome P450 3A4 and UDP-glucuronosyltransferase 2B7: evidence for protein-protein association and possible involvement of CYP3A4 J-helix in the interaction. *Mol. Pharmacol.* 75, 956–964. doi: 10.1124/mol.108.052001

Taura, K., Yamada, H., Hagino, Y., Ishii, Y., Mori, M., and Oguri, K. (2000). Interaction between cytochrome P450 and other drug-metabolizing enzymes: evidence for an association of CYP1A1 with microsomal epoxide hydrolase and UDP-glucuronosyltransferase. *Biochem. Biophys. Res. Commun.* 273, 1048–1052. doi: 10.1006/bbrc.2000.3076

Yamazaki, S., Sato, K., Suhara, K., Sakaguchi, M., Mihara, K., and Omura, T. (1993). Importance of the proline-rich region following signal-anchor sequence in the formation of correct conformation of microsomal cytochrome P-450s. *J. Biochem.* 114, 652–657.

Conflict of Interest Statement: The authors declare that the research was conducted in the absence of any commercial or financial relationships that could be construed as a potential conflict of interest.

frontiers in Pharmacology

ORIGINAL RESEARCH
published: 03 February 2017
doi: 10.3389/fphar.2017.00023

Endogenous Protein Interactome of Human UDP-Glucuronosyltransferases Exposed by Untargeted Proteomics

*Michèle Rouleau, Yannick Audet-Delage, Sylvie Desjardins, Mélanie Rouleau, Camille Girard-Bock and Chantal Guillemette **

Pharmacogenomics Laboratory, Canada Research Chair in Pharmacogenomics, Faculty of Pharmacy, Centre Hospitalier Universitaire de Québec Research Center, Laval University, Québec, QC, Canada

The conjugative metabolism mediated by UDP-glucuronosyltransferase enzymes (UGTs) significantly influences the bioavailability and biological responses of endogenous molecule substrates and xenobiotics including drugs. UGTs participate in the regulation of cellular homeostasis by limiting stress induced by toxic molecules, and by controlling hormonal signaling networks. Glucuronidation is highly regulated at genomic, transcriptional, post-transcriptional and post-translational levels. However, the UGT protein interaction network, which is likely to influence glucuronidation, has received little attention. We investigated the endogenous protein interactome of human UGT1A enzymes in main drug metabolizing non-malignant tissues where UGT expression is most prevalent, using an unbiased proteomics approach. Mass spectrometry analysis of affinity-purified UGT1A enzymes and associated protein complexes in liver, kidney and intestine tissues revealed an intricate interactome linking UGT1A enzymes to multiple metabolic pathways. Several proteins of pharmacological importance such as transferases (including UGT2 enzymes), transporters and dehydrogenases were identified, upholding a potential coordinated cellular response to small lipophilic molecules and drugs. Furthermore, a significant cluster of functionally related enzymes involved in fatty acid β-oxidation, as well as in the glycolysis and glycogenolysis pathways were enriched in UGT1A enzymes complexes. Several partnerships were confirmed by co-immunoprecipitations and co-localization by confocal microscopy. An enhanced accumulation of lipid droplets in a kidney cell model overexpressing the UGT1A9 enzyme supported the presence of a functional interplay. Our work provides unprecedented evidence for a functional interaction between glucuronidation and bioenergetic metabolism.

Keywords: UGT, proteomics, protein-protein interaction, affinity purification, mass spectrometry, metabolism, human tissues

OPEN ACCESS

Edited by:
Yuji Ishii,
Kyushu University, Japan

Reviewed by:
Ben Lewis,
Flinders University, Australia
Shinichi Ikushiro,
Toyama Prefectural University, Japan

****Correspondence:***
Chantal Guillemette
chantal.guillemette@crchudequebec.ulaval.ca

Specialty section:
This article was submitted to Pharmacogenetics and Pharmacogenomics, a section of the journal Frontiers in Pharmacology

Received: *01 December 2016*
Accepted: *12 January 2017*
Published: *03 February 2017*

Citation:
Rouleau M, Audet-Delage Y, Desjardins S, Rouleau M, Girard-Bock C and Guillemette C (2017) Endogenous Protein Interactome of Human UDP-Glucuronosyltransferases Exposed by Untargeted Proteomics. Front. Pharmacol. 8:23. doi: 10.3389/fphar.2017.00023

Abbreviations: AP, affinity purification; UGT, UDP-glucuronosyltransferases; IP, immunoprecipitation; PPIs, protein-protein interactions; UDP-GlcA, Uridine diphospho-glucuronic acid; ER, endoplasmic reticulum; MS, mass spectrometry.

INTRODUCTION

UDP-glucuronosyltransferases (UGTs) are well known for their crucial role in the regulation of cellular homeostasis, by limiting stress induced by toxic drugs, other xenobiotics and endogenous lipophilic molecules, and by controlling the hormonal signaling network (Rowland et al., 2013; Guillemette et al., 2014). UGTs coordinate the transfer of the sugar moiety of their co-substrate UDP-glucuronic acid (UDP-GlcA) to amino, hydroxyl and thiol groups on a variety of lipophilic molecules, thereby reducing their bioactivity and facilitating their excretion. In humans, nine UGT1A and ten UGT2 enzymes constitute the main glucuronidating enzymes. UGTs are found in nearly all tissues, each UGT displaying a distinct profile of tissue expression, and are most abundant in the liver, kidney and gastrointestinal tract, where drug metabolism is highly active. These membrane-bound enzymes localized in the endoplasmic reticulum (ER) share between 55 and 97% sequence identity, thus displaying substrate specificity and some overlapping substrate preferences (Rowland et al., 2013; Guillemette et al., 2014; Tourancheau et al., 2016). For instance, the alternative first exons of the single *UGT1* gene produce the nine UGT1A enzymes with distinct N-terminal substrate binding domains but common C-terminal UDP-GlcA-binding and transmembrane domains. The seven UGT2B enzymes and UGT2A3 are encoded by eight distinct genes, whereas UGT2A1 and UGT2A2 originate from a single gene by a UGT1A-like, alternative exon 1 strategy. However, similar to UGT1As, substrate binding domains of UGT2 enzymes are more divergent than their C-terminal domains.

Genetic variations, epigenetic regulation, as well as post-transcriptional and translational modifications, all contribute to the modulation of UGT conjugation activity, thereby influencing an individual's response to pharmacologic molecules and the bioactivity of endogenous molecules (Guillemette et al., 2010, 2014; Ramírez et al., 2010; Hu et al., 2014; Dluzen and Lazarus, 2015). For instance, genetic lesions at the *UGT1* locus that impair UGT1A1 expression or activity result in transient or fatal hyperbilirubinemia, characterizing Gilbert and Crigler-Najjar syndromes, respectively (Costa, 2006).

Several lines of evidence support protein-protein interactions (PPIs) among UGTs and with other enzymes of pharmacological importance (Taura et al., 2000; Fremont et al., 2005; Takeda et al., 2005a,b, 2009; Ishii et al., 2007, 2014; Operaña and Tukey, 2007). These interactions may also significantly influence UGT enzymatic activity (Bellemare et al., 2010b; Ménard et al., 2013; Ishii et al., 2014; Fujiwara et al., 2016). In addition, interactions of UGT proteins with some anti-oxidant enzymes that have been recently uncovered have raised the interesting concept of alternative functions of UGTs in cells (Rouleau et al., 2014). However, most studies have been conducted in cell-based systems with overexpression of tagged UGTs and little evidence in human tissues supports the extent of this mechanism and its physiological significance.

PPIs are essential to cell functions including responses to extracellular and intracellular stimuli, protein subcellular distribution, enzymatic activity, and stability. Understanding molecular interaction networks in specific biological contexts is therefore highly informative of protein functions. We aimed to gain insight on the endogenous protein interaction network of UGT1A enzymes by applying an unbiased proteomics approach in main drug metabolizing human tissues. In doing so, we provide support to a potential coordinated cellular response to small lipophilic molecules and drugs. Importantly, a potential functional interplay between UGT1A enzymes and those of bioenergetic pathways also emerges from this exhaustive endogenous interaction network.

MATERIALS AND METHODS

UGT1A Enzyme Antibodies

The anti-UGT1A rabbit polyclonal antibody (#9348) that specifically recognizes UGT1A enzymes, and not the alternative UGT1A variant isoforms 2, has been described (Bellemare et al., 2011). Purification was performed using the biotinylated immunogenic peptide (K_{520}KGRVKKAHKSKTH_{533}; Genscript, Piscataway, NJ, USA) and streptavidin magnetic beads (Genscript) per the manufacturer's instructions. Antibodies (3 ml) were incubated O/N at 4°C with peptide-streptavidin beads, and then washed with PBS to remove unbound immunoglobulins. UGT1A-specific antibodies were eluted using glycine (0.125 M, pH 2.9), and rapidly buffered with Tris pH 8.0. Purified antibodies were subsequently concentrated using a centrifugal filter unit (cut off 3 kDa; Millipore (Fisher Scientific), Ottawa, ON) to a final volume of 1 ml.

Affinity Purification of Endogenous UGT1A Enzymes and Their Interacting Partners in Human Tissues and a UGT1A Expressing Cellular Model

Human liver, kidney and intestine S9 fractions comprised of ER and associated membranes as well as cytosolic cellular content (Xenotech LLC, Lenexa, KS, USA) were from 50, 4, and 13 donors, respectively. This study was reviewed by the local ethics committee and was exempt given that anonymized human tissues were from a commercial source. Human colon cancer HT-29 cells (ATCC, Manassas, VA, USA) were grown in DMEM supplemented with 10% fetal bovine serum (Wisent, St-Bruno, QC, Canada), 50 mg/ml streptomycin, 100 IU/ml penicillin, at 37°C in a humidified incubator with 5% CO_2 as recommended by ATCC. Immunoprecipitations (IP) were conducted according to standard procedures (Savas et al., 2011; Ruan et al., 2012), with at least three independent replicates per sample source. For each sample, 1 mg protein was lysed in 1 ml lysis buffer A [final concentration: 50 mM Tris-HCl pH 7.4, 150 mM NaCl, 0.3% deoxycholic acid, 1% Igepal CA-630 (Sigma-Aldrich), 1 mM EDTA, complete protease inhibitor (Roche, Laval, QC, Canada)] for 45 min on ice. This buffer included deoxycholate to enhance membrane solubilization and stringency of immunoprecipitation conditions. Lysates were then homogenized by pipetting up and down through fine needles (18G followed by 20G) 10–20 times on ice. Lysates were cleared of debris by centrifugation for 15 min at 13,000 g. UGT1A enzymes were immunoprecipitated from cleared lysates with 4 μg of purified anti-UGT1A for 1 h

at 4°C with end-over-end agitation. After addition of protein G–coated magnetic beads (200 µl Dynabeads, Life Technologies, Burlington, ON), lysates were incubated O/N at 4°C. Beads were washed three times with 1 ml lysis buffer A and subsequently processed for mass spectrometry (MS) analysis, as described below. Control IPs were conducted in similar conditions using 4 µg normal rabbit IgGs (Sigma-Aldrich) per protein sample. The inclusion of 150 mM NaCl and 0.3% deoxycholate ensured stringent wash conditions.

Liquid Chromatography-MS/MS Identification of UGT1A Interacting Partners

Protein complexes bound to magnetic beads were washed 5 times with 20 mM ammonium bicarbonate (1 ml). Tryptic digestion and desalting was performed as described (Rouleau et al., 2016). Briefly, bead-bound proteins were digested in 10 µg/µl trypsin for 5 hrs at 37°C. The tryptic digest was recovered, dried, and resuspended in 30 µl sample buffer (3% acetonitrile, 0.1% trifluoroacetic acid, 0.5% acetic acid). Peptides were desalted on a C18 Empore filter (ThermoFisher Scientific), dried out, resuspended in 10 µl 0.1% formic acid and analyzed using high-performance liquid chromatography-coupled MS/MS on a LTQ linear ion trap-mass spectrometer equipped with a nanoelectrospray ion source (Thermo Electron, San Jose, CA, USA) or on a triple-quadrupole time-of-flight mass spectrometer (TripleTOF 5600, AB Sciex, Concord, ON) as described (Rouleau et al., 2014). Data files were submitted for simultaneous searches using Protein Pilot version 4 software (AB Sciex) utilizing the Paragon and Progroup algorithms (Shilov). The RAW or MGF file created by Protein Pilot was used to search with Mascot (Matrix Science, London, UK; version 2.4.1). Mascot was set up to search against the human protein database (Uniref May 2012; 204083 entries) supplemented with a complete human UGT protein sequence database comprised of common UGT coding variations and protein sequences of newly discovered alternatively spliced UGT isoforms (assembled in-house November 2013; 882 entries). Mascot analysis was conducted using the following settings: tryptic peptides, fragment and parent ion tolerance of 0.100 Da, deamidation of asparagine and glutamine and oxidation of methionine specified as variable modifications, deisotoping was not performed, two missed cleavage were allowed. Mass spectra were also searched in a reversed database (decoy) to evaluate the false discovery rate (FDR). On-beads digestion and MS analyses were performed by the proteomics platform of the CHU de Québec Research Center. The MS proteomics data have been deposited to the ProteomeXchange Consortium (http://proteomecentral.proteomexchange.org) via the PRIDE partner repository with the dataset identifier PXD000295.

Identification of proteins in Scaffold (version 4.6.1; Proteome Software, Portland, OR) was carried out using two sets of criteria: (1) for UGT proteins, 95% peptide and protein probability, and 1 unique peptide were used, considering the high level of sequence identity among the proteins in this family. For the same reason of high sequence identity, each identified peptide was manually assigned to the proper UGT protein or to the common UGT sequence (**Supplementary Table 1**). (2) For UGT1A interacting proteins, specificity threshold was set to 95% peptide and protein probability and a minimum of 2 unique peptides. Proteins that contained similar peptides and could not be differentiated based on MS/MS analysis alone were grouped to satisfy the principles of parsimony. Detailed proteomics datasets are provided in **Supplementary Tables 4–7**.

Confidence scores of each UGT1A-protein interaction were determined using the computational tools provided online at http://crapome.org (Choi et al., 2011). Spectral counts for each identified protein were normalized to the length of the protein and total number of spectra in the experiment. Two empirical scores (FC-A and more stringent FC-B) and one probability score (SAINT) (Mellacheruvu et al., 2013) were then calculated based on normalized spectral counts of identified proteins in UGT1A immunoprecipitation samples compared to our matching control immunoprecipitation samples (CRAPome Workflow 3). Confidence score calculations were conducted separately for each tissue, with the following *analysis options*: FC-A: Default parameters; FC-B: *User* controls, *stringent* background estimation, *geometric* combining replicates; SAINT: *User* Controls, *Average - best 2* Combining replicates, *10* Virtual controls and *default* SAINT options. Confidence scores for all UGT1A interaction partners are given in **Supplementary Table 2**.

Bioinformatics Tools and Data Analysis

The common external contaminants keratins and trypsin were manually removed from the lists of interacting proteins prior to pathway enrichment analysis. UGT1A interacting partners were classified according to KEGG pathways (update November 12, 2016) using ClueGO and CluePedia Apps (v2.3.2) in Cytoscape 3.4 (Bindea et al., 2009, 2013). Enrichment was determined based on a two-sided hypergeometric statistical test and a Bonferroni step down correction method. Only enriched pathways with $P < 0.05$ and a Kappa score threshold of 0.4 were considered. The following optional criteria were also used for the search: minimum # genes = 4, minimum 2% genes. The UGT1A interactome was generated using Cytoscape basic tools. Because protein annotations based on tools such as KEGG and Gene Ontology are partial, the UGT1A interactome was subsequently manually extended to include significant UGT1A interactors that were absent in the original output but involved in enriched pathways, per their Uniprot entries (www.uniprot.org) and literature mining. Details are included in the legend of **Figure 3**.

Validation of Protein-Protein Interactions by Co-IP and Immunofluorescence (IF)

HEK293 cells stably expressing the human enzyme UGT1A9-myc/his (a pool of cells) were used (Bellemare et al., 2010a). Expression and glucuronidation activity of the tagged UGT1A9 in this model have been described and were similar to the untagged enzyme (Bellemare et al., 2010a). In the current study, only the myc tag served for UGT1A9 detection and the his tag was not exploited. Cells were transfected with

Lipofectamine 2000 (Life Technologies) to transiently express tagged protein partners. HA-ACOT8 and FLAG-SH3KBP1 were kindly provided by Dr Ming-Derg Lai (National Cheng Kung University, Taiwan; Hung et al., 2014) and Dr Mark McNiven (Mayo Clinic, Rochester, MN; Schroeder et al., 2010) respectively. The PHKA2-myc-FLAG expression construct was purchased from OriGene (Rockville, MD, USA).

Co-IP: HEK293 cells (3×10^5 cells plated in 10 cm dishes) were harvested 40 h post-transfection. Cells were washed three times with PBS, lysed in 800 µl lysis buffer B (50 mM Tris-HCl pH 7.4, 150 mM NaCl, 1% Igepal, 1 mM DTT, complete protease inhibitor) for 1 h at 4°C and subsequently homogenized and centrifuged as described above. Immunoprecipitation with purified anti-UGT1A antibodies (2 µg) or control rabbit IgG (2 µg) and 50 µl Protein-G magnetic beads was as above. Protein complexes were washed three times in lysis buffer B and eluted in Laemmli sample buffer by heating at 95°C for 5 min. Eluates were subjected to SDS-PAGE, and the presence of interacting partners was revealed by immunoblotting using anti-tag antibodies specified in figures and legends: anti-myc (clone 4A6, EMD Millipore, Etobicoke, ON, Canada; 1:5000), anti-FLAG (clone M2, Sigma-Aldrich, St-Louis, MO, USA; 1:20 000) and anti-HA (Y-11, Santa Cruz Biotechnologies, Dallas, TX, USA; 1:500).

IF: HEK293 cells (2×10^5 cells per well of 6-well plates) grown on coverslips were harvested 36 h post-transfection and processed for IF, as described (Rouleau et al., 2016). ACOT8 was detected with anti-HA (1:500), SH3KBP1 with anti-FLAG (1:1500), UGT1A9-myc/his with anti-myc (1:200) or purified anti-UGT1A (1:500), and with secondary goat anti-rabbit, goat anti-mouse or donkey anti-mouse respectively, conjugated to either AlexaFluor 488 or 594 (1:1000; Invitrogen). Immunofluorescence images were acquired on a LSM510 META NLO laser scanning confocal microscope (Zeiss, Toronto, ON, Canada). Zen 2009 software version 5.5 SP1 (Zeiss) was used for image acquisitions.

Quantification of Lipid Droplets

HEK293 cells grown on coverslips were fixed in 3.7% formaldehyde (Sigma) for 30 min at RT. Cells were then gently washed three times with PBS and incubated for 10 min in 0.4 µg/mL Nile Red (Sigma). After being rinsed three times, coverslips were mounted on glass slides using Fluoromount (Sigma) as a mounting medium. Images were acquired on a Wave FX-Borealis (Quorum Technologies, Guelph, ON, Canada) - Leica DMI 6000B (Clemex Technologies inc., Longueil, QC, Canada) confocal microscope, with a 491 nm laser and 536 nm filter. Z-stacks were acquired every 0.15 µm. Stacks were analyzed using ImageJ (v1.51f; U.S. National Institutes of Health, Bethesda, MD, USA) and the 3-D Object Counter plugin (Bolte and Cordelieres, 2006). Results are derived from 3 independent experiments and more than 140 cells per experiment were analyzed for each condition. Fluorescence images were acquired on an LSM 510 microscope as above.

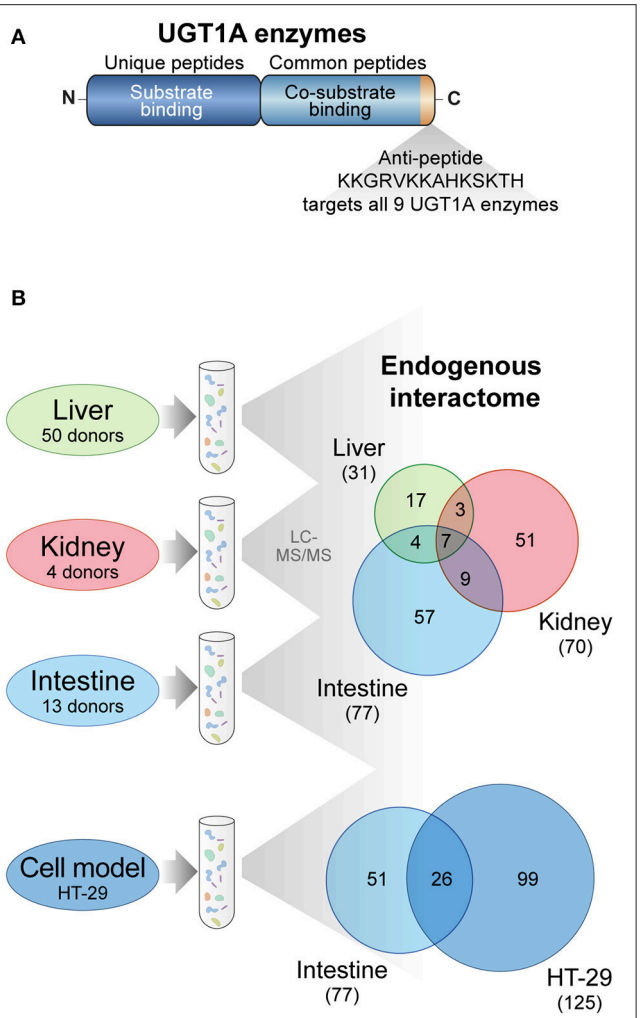

FIGURE 1 | UGT1A interaction network investigated by untargeted proteomics. (A) The nine UGT1A enzymes are distinguished by the amino acid sequence of their substrate binding domain (unique peptides) whereas they share identical C-terminal co-substrate and transmembrane domains (common peptides). The anti-UGT1A antibody used in this study was raised against a C-terminal peptide common to all nine UGT1A enzymes but does not recognize the main spliced alternative isoforms 2 or UGT1A_i2s. **(B)** Experimental approach to establish endogenous UGT1A protein interactomes in drug metabolizing tissues and in the colon cancer cell model HT-29. Immunoprecipitation of UGT1A enzymes was conducted with the anti-UGT1A antibody. The numbers of common and unique UGT1A protein partners identified by mass spectrometry and above confidence threshold are represented in the Venn diagrams. Datasets were established on a minimum of two biological replicates. A Venn diagram for the 4 matrices is presented in **Supplementary Figure 2**. A list of proteins in each group is provided in **Supplementary Table 3**.

RESULTS

Endogenous UGT1A Enzymes Associate with Several Other Metabolic Proteins in Non-malignant Human Tissues

The endogenous interactome of human UGT1A enzymes was established in three major metabolic tissues, namely liver, kidney

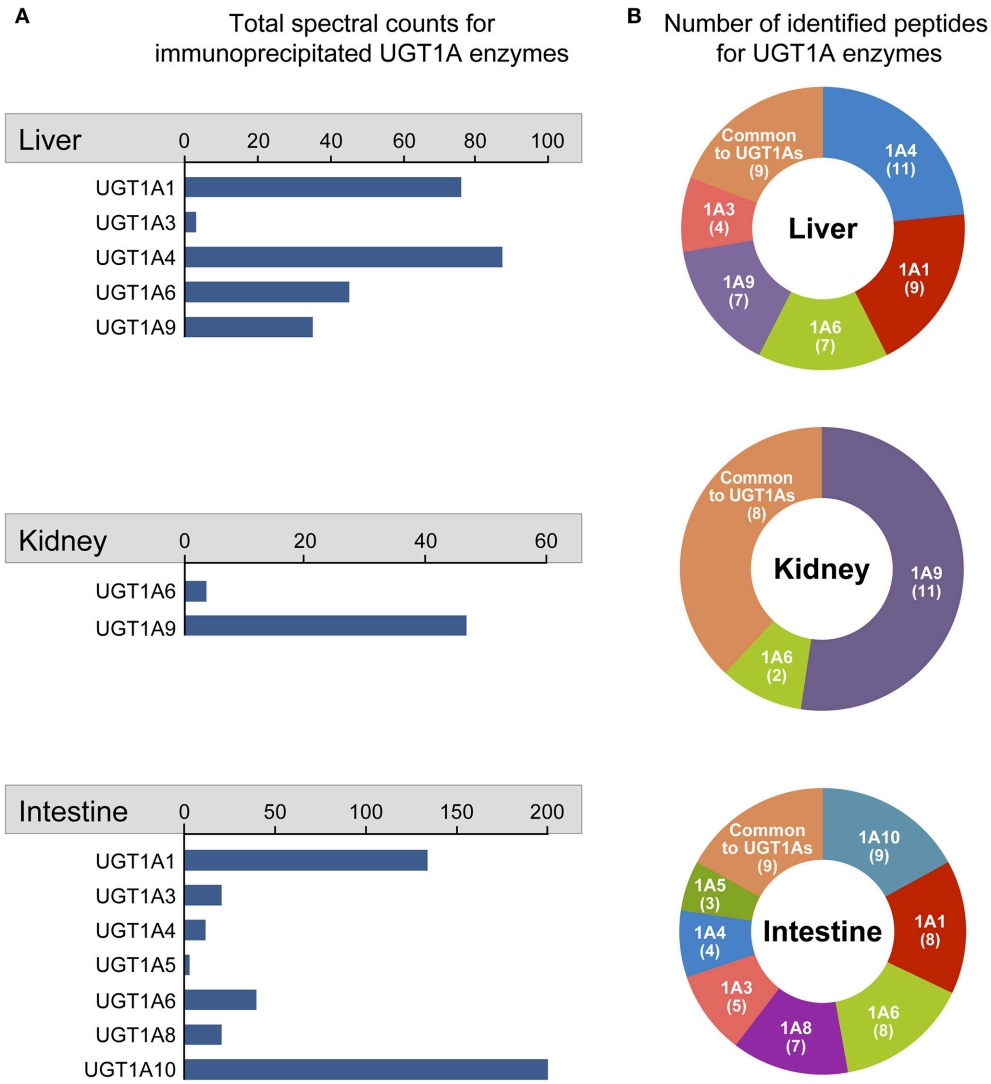

FIGURE 2 | Quantitative overview of UGT1A enzymes immunoprecipitated from each tissue. Identification of immunoprecipitated UGT1A enzymes was based on the detection of peptides unique to specified UGT1A enzymes. **(A)** The quantitative assessment of each immunoprecipitated UGT1A is given by the total number of spectral counts for peptides unique to each UGT1A identified by mass spectrometry. Total spectral counts for peptides common to all UGT1A enzymes (Liver: 465; Kidney: 67; Intestine: 1561) were not considered in the quantitative assessment of specific UGT1As. **(B)** For each tissue, the number of peptides unique to each UGT1A identified by MS/MS analysis is represented in ring charts. Detailed quantification and unique/common UGT1A peptides identified are presented in **Supplementary Table 1**.

and intestine from pools of 4–50 donors, using S9 tissue fractions comprised of ER and associated membranes as well as cytosolic cellular content (**Figure 1**). IPs were conducted with an antibody specific to the C-terminal region common to the nine human UGT1A enzymes, thereby allowing affinity purification of all UGT1A enzymes expressed in studied tissues (**Figure 1A**). This antibody was shown by western blotting to lack affinity for alternatively spliced UGT1A isoform 2 proteins derived from the same human *UGT1* gene locus (Bellemare et al., 2011). The experimental approach to establish the endogenous UGT1A enzymes interactome using the anti-UGT1A enzymes antibody is presented in **Figure 1B**.

Multiple UGT1A enzymes were immunopurified from each tissue in line with their documented expression profile (**Figure 2**). The list of specific UGT1A enzymes immunoprecipitated from each tissue was established based on their unique N-terminal peptide sequences, whereas multiple additional peptides corresponding to the common C-terminal half of the UGT1A proteins and thereby common to all UGT1A enzymes were also observed (**Figure 2B**, **Supplementary Figure 1**; **Supplementary Table 1**).

Spectral counts for unique peptides provided a quantitative appreciation of immunoprecipitated UGT1A (**Figure 2A**). UGT1A1 and UGT1A4 were the most abundant UGT1As

TABLE 1 | Top 10 UGT1A interaction partners[a] for each tissue based on confidence score.

Liver				Kidney				Intestine			
Protein name[b]	Coverage (%)[c]	Total spectral counts[d]	FC_B score	Protein name[b]	Coverage (%)[c]	Total spectral counts[d]	FC_B score	Protein name[b]	Coverage (%)[c]	Total spectral counts[d]	FC_B score
PHKB	36	193	28.55	TOP2B	16	53	5.93	ATP5A1	13	8	4.91
PHKA2	34	180	26.62	PFKL	24	35	4.68	UGT2A3	24	61	4.63
PHKG2	40	68	10.49	TRA2B	24	36	4.21	**GBF1**	12	60	4.60
PRDX2	47	55	7.62	ATP5A1	33	32	4.10	**SLC25A5**	35	54	4.37
UGT2B7	19	31	5.53	**PRDX2**	41	50	3.60	RALGAPB	13	51	4.26
PRDX1	35	25	3.42	**PRDX1**	44	39	3.08	**PRDX2**	24	46	4.06
ECH1	28	17	2.61	HSPA8	30	21	2.70	**PRDX1**	31	45	4.01
SLC25A5	17	9	2.20	SLC34A2	16	17	2.66	RALGAPA2	6	29	3.28
GBF1	4	9	2.15	ACCA2	43	21	2.30	**ECH1**	30	21	2.84
UGT2B4	11	12	1.98	ASS1	42	21	2.22	PDIA3	5	3	2.82

[a] *Excluding common IP protein contaminants (structural, ribosomal and RNA-binding proteins).*
[b] *Proteins in bold were identified in the 3 tissues.*
[c] *Total coverage calculated with peptides identified in all replicates (n = 4, 3 and 2 for the liver, kidney and intestine, respectively).*
[d] *Total spectral counts of all replicates.*

in hepatic IPs, whereas UGT1A1 and UGT1A10 were predominantly immunopurified from the intestine and UGT1A9 from the kidney (**Figure 2A**, **Supplementary Table 1**). UGT1A9 ($n = 51$ spectra) was far more abundant than UGT1A6 ($n = 2$ spectra) in the kidney whereas UGT1A10 ($n = 194$ spectra) predominated over most other UGT1A in the intestine, although all UGT1A enzymes were identified besides UGT1A7 and UGT1A9. These metrics indicated that an exhaustive immunoprecipitation of UGT1As from each tissue was achieved.

UGT1A Interaction Network and Functional Annotation

A total of 9 independent AP-MS datasets (4 liver, 3 kidney, and 2 intestine replicates of control and UGT1A AP-MS) efficiently immunoprecipitated UGT1A enzymes and associated proteins. Mass spectra were assigned to specific proteins using Mascot and Scaffold software. A list of UGT1A-interacting proteins was created based on the analysis of total spectral counts assigned to each identified protein in each replicate to obtain empirical (FC-B) and probability (SAINT) confidence scores (**Supplementary Table 2**). Using a FC-B score threshold of 1.42, we reported a total of 148 proteins forming endogenous interactions with UGT1A enzymes in the three surveyed human tissues (31 in the liver, 70 in the kidney and 77 in the intestine) (**Figure 1B**, **Supplementary Table 2**). This FC-B threshold was selected based on the validated protein partner having the lowest probability score, corresponding to PHKA2 in the intestine (see below). This approach was chosen because of the inherent difficulty to obtain similar replicate datasets with AP-MS from tissues, especially in intestine, a variability highly penalized in the SAINT scoring algorithm (**Supplementary Figure 2**). To further strengthen the UGT1A interactome in the gastrointestinal tract, we also conducted three more replicate AP-MS experiments of endogenous UGT1A enzymes with the human colon cancer cell line HT-29, expressing high levels of UGT1As. The intestinal UGT expression profile is well represented in HT-29 cells, with UGT1A1, UGT1A6, UGT1A8, and UGT1A10 immunoprecipitated in similar proportions (**Supplementary Table 1**). Using the FC-B threshold used for tissues (1.42), 125 interaction partners were selected for further analysis. Of those, 44 proteins were common with those immunoprecipitated in non-malignant tissue samples, including 26 common with the intestine dataset (**Figure 1B**, **Supplementary Figure 3**). UGT1A protein partners with highest significance scores are given in **Table 1** whereas a complete list of immunoprecipitated protein partners is provided in **Supplementary Table 2**.

To portray the global functions enriched in the UGT1A interactome, the UGT1A protein partners from the three surveyed tissues were classified per the KEGG pathway database. Structural proteins such as tubulins, myosins, actin, as well as multiple ribosomal protein subunits (RPL/RPS proteins) and other RNA-binding proteins involved in mRNA splicing (e.g., heterogeneous ribonucleotide proteins (hnRNPs) and serine/arginine-rich splicing factors (SRSF) proteins) were significant classes of proteins immunoprecipitated with UGT1As. However, because these proteins are frequently non-specifically enriched in AP-MS experiments (Mellacheruvu et al., 2013), the specificity of interactions with UGT1A will require validation and will not be discussed further.

The interactome of UGT1A enzymes is characterized by numerous metabolic proteins playing roles in detoxification and bioenergetic pathways (**Figure 3**). They include the UGT2 glucuronosyltransferases UGT2A3, UGT2B4, UGT2B7, and UGT2B17, the glutathione S-transferase GSTA1, glycine N-acyltransferase GLYAT, the alcohol dehydrogenase ALDH2 and the antioxidant enzymes PRDX1 and PRDX2 (full protein names are provided in **Table 2**). Given their functions in line with high scoring proteins, ADH1B and PRDX3 were also included in the final interactome, having confidence interaction scores just below threshold (FC-B = 1.37; **Supplementary Figure 2**).

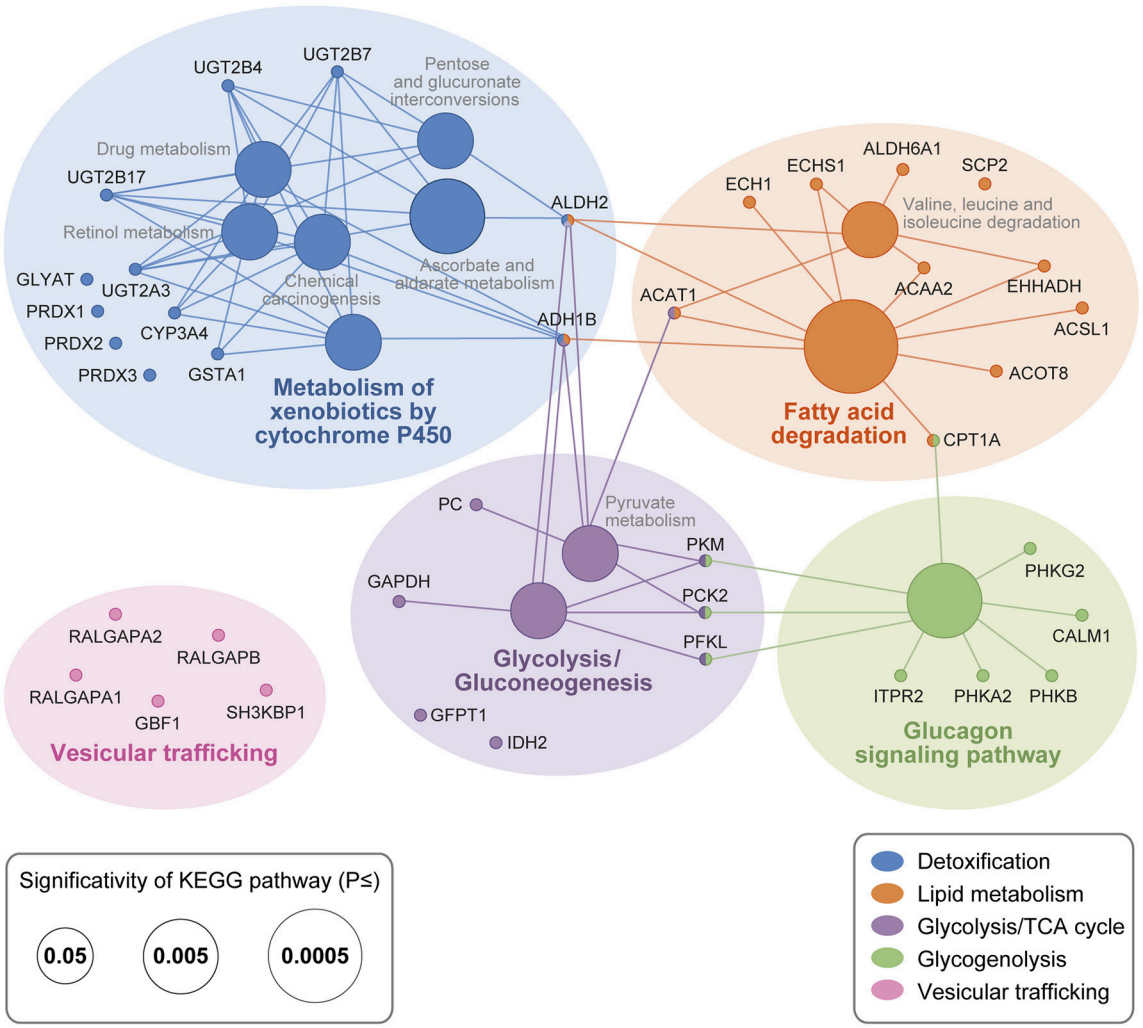

FIGURE 3 | UGT1A interaction network in drug metabolizing tissues. UGT1A interacting proteins were classified according to KEGG pathways with ClueGO/CluePedia (Bindea et al., 2009, 2013). Node size is representative of pathway enrichment significance. Interactome was enhanced with significant interaction partners not part of KEGG pathways that are functionally related based on Uniprot and literature. These proteins are not linked to nodes but are grouped according to global functions. Structural proteins, ribosomal protein subunits and other RNA-binding proteins involved in mRNA splicing are not shown but were significantly enriched in UGT1A IPs. Full protein names are provided in **Table 2**. Complete lists of UGT1A interacting proteins are provided in **Supplementary Table 2**.

Similarly, the cytochrome P450 CYP3A4 was included because also observed in liver tissue with a single high confidence peptide and a previously observed interaction partner (Fremont et al., 2005; Ishii et al., 2014). Enzymes of the lipid metabolism pathway were also significantly represented and most particularly several peroxisomal and mitochondrial proteins involved in fatty acid β-oxidation, namely ACOT8, ECH1, CPT1A, and ACAA2. To encompass all potential protein partners involved in lipid metabolism, a pathway that was functionally validated at a later stage (see below), relevant but slightly lower scoring proteins were incorporated in the final interactome, namely SCP2, ACSL1, EHHADH, ACAT1, and ECHS1 (FC-B = 1.38–1.19; **Supplementary Figure 2**). Finally, the glycolysis/pyruvate and glycogenolysis metabolic pathways were also significantly enriched, given the high number of immunoprecipitated UGT1A partners in these pathways. Several other protein partners, including transporters (SLC25A5, SLC25A13, and SLC34A2) and proteins participating in vesicular trafficking (RALGAPA1, RALGAPA2, RALGAPB, and GBF1) were also immunoprecipitated from tissues and may represent important partners (**Table 1**, **Figure 3**). The interaction network of UGT1A enzymes established in the HT-29 cell model was consistent with that built from tissues, with enrichments in xenobiotic and bioenergetics metabolic pathways. Several transporters, anti-oxidant, lipid metabolism, glycolytic/glycogen metabolic enzymes and vesicular trafficking proteins were all significantly identified in AP-MS on cells, as in tissues (**Supplementary Table 2**), further supporting the significance of the endogenous interactome of UGT1A enzymes.

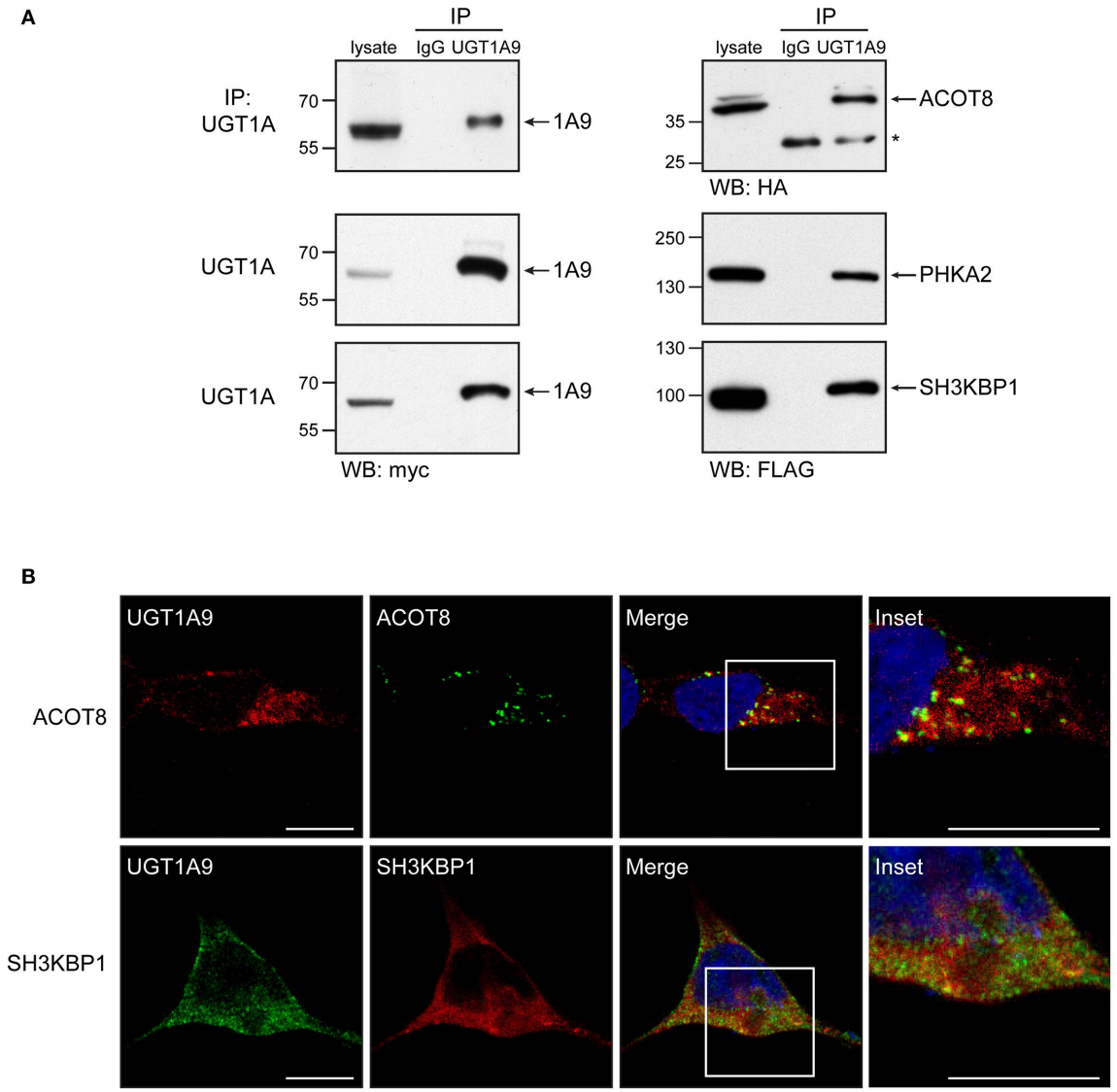

FIGURE 4 | Validation of selected protein interactions by immunoprecipitation and immunofluorescence in a UGT negative kidney cell model. **(A)** Immunoprecipitation (IP) of UGT1A9, with purified anti-UGT1A antibodies, was conducted in HEK293-UGT1A9_myc/his transiently transfected with the indicated protein partner. UGT1A9 was immunodetected with anti-myc, whereas protein partners were detected with anti-tag antibodies as specified below immunoblots. Control IPs were conducted with normal rabbit immunoglobulins (IgG). Lysates (IP input) are shown as references. Protein bands denoted by the asterisk are the rabbit IgGs used in IPs. **(B)** Co-localization of UGT1A9 and the protein partners ACOT8 and SH3KBP1/CIN85 assessed by immunofluorescence in HEK293-UGT1A9_myc/his transiently expressing specified partners. Confocal microscope images are representative of three independent experiments. Partial co-localization is detected by yellow labeling in merged images. Insets present enlargements of boxed regions in merged images. Bar = 20 μm.

Experimental Validation of Selected UGT1A Partners

Using the non-malignant kidney model cell line HEK293 (a UGT negative model) stably expressing a myc/his-tagged UGT1A9 enzyme, selected partnerships with enzymes of bioenergetic cellular pathways were confirmed by a co-IP/immunodetection approach. The peroxisomal acyl-coenzyme A thioesterase ACOT8, involved in fatty acid β-oxidation, and the cytosolic phosphorylase b kinase regulatory subunit A2 (PHKA2), involved in glycogen degradation, were selected based on their significant enrichment in more than one tissue (ACOT8 in kidney, intestine and HT-29; PHKA2 in all 4 matrices). The cytosolic SH3 domain-containing kinase-binding protein 1, also known as cbl-interacting protein of 85 kDa (SH3KBP1/CIN85), an adaptor protein regulating membrane trafficking and receptor signaling, was also chosen as a representative protein partner of the vesicular trafficking pathway, given its identification in the kidney and HT-29 datasets. After transient expression of selected partners as tagged proteins in the kidney cell model stably expressing UGT1A9, each of the candidate partners

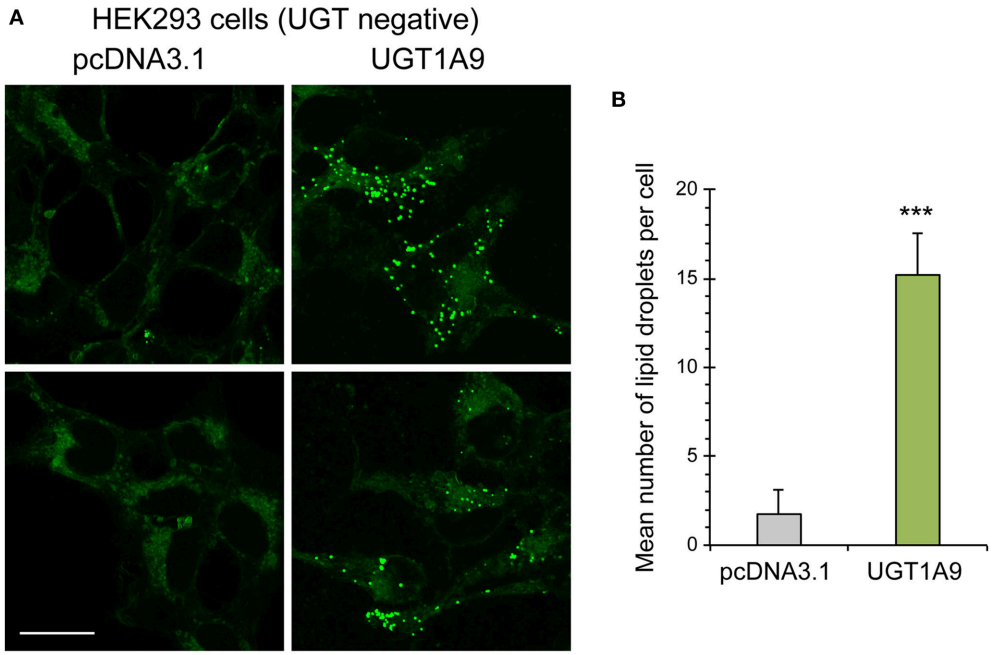

FIGURE 5 | Accumulation of cellular lipid droplets in UGT1A9 expressing HEK293 cells. (A) Representative images of lipid droplets (green fluorescence) stained with Nile Red in HEK293-UGT1A9_myc-his or control HEK cells (stably transfected with the empty pcDNA3.1 vector—UGT negative cells). Bar = 20 μm. **(B)** Average number of lipid droplets per cell stably expressing UGT1A9 or control HEK cells. Lipid droplets per cell were counted in at least 140 cells per condition and averaged ($n = 3$ independent experiments).

was specifically enriched by an IP of UGT1A (**Figure 4A**). Likelihood of a physical interaction of ACOT8 and CIN85 with UGT1A enzymes was further supported by their partial co-localization with UGT1A9 detected by IF and confocal microscopy (**Figure 4B**).

Influence of UGT1A on Cellular Lipid Droplets

Pathway enrichment analysis identified several proteins involved in lipid metabolism and suggested a possible functional implication of UGT1A enzymes in this pathway. This was explored by measuring levels of lipid droplet in HEK293 cells stably expressing or not the UGT1A9 enzyme. Lipid droplets, cytoplasmic organelles that constitute a store of neutral lipids such as triacylglycerides, were labeled with Nile Red and counted. This analysis revealed that the number of lipid droplets per cell was significantly higher in UGT1A9-expressing cells relative to control cells (by 7.5-fold, $P < 0.001$), whereas average size and staining intensity of lipid droplets were similar between UGT negative and UGT1A9-expressing HEK293 cells (**Figure 5**).

DISCUSSION

Defining protein interaction networks is a key step toward a better understanding of functional crosstalk among cellular pathways. In the current work, we established the endogenous interactome of key metabolic UGT1A enzymes in three relevant human tissues. Data suggest an interplay between UGT1A enzymes regulating the glucuronidation pathway and enzymes involved in multiple cellular energetic pathways, most notably with lipid and glucose/glycogen metabolism. This interactome considerably expands what was known about UGT1A protein interactions in the literature (reviewed by Ishii et al., 2010; Fujiwara et al., 2016) and public databases (3 interactions among UGT1A enzymes reported in STRING database (http://string-db.org/), none in the iRefWEB database (http://wodaklab.org/iRefWeb/), accessed November 9, 2016).

One of our study's strength relies on the use of an unbiased approach targeting endogenous proteins in non-malignant human tissues, as opposed to most studies that used the overexpression of an exogenous tagged protein expressed in a cellular model (Taura et al., 2000; Takeda et al., 2005a,b, 2009; Fujiwara et al., 2007a,b, 2010; Kurkela et al., 2007). In addition, profiles of immunoprecipitated UGT1A enzymes replicated well their known tissue distribution, and spectral peptide counting further reflected the relative abundance of these UGT1A enzymes previously established by mass spectrometry-based multiple reaction monitoring and RNA-sequencing (Fallon et al., 2013a,b; Sato et al., 2014; Margaillan et al., 2015a,b; Tourancheau et al., 2016). Of note, our data support the notion that both UGT1A8 and UGT1A10 enzymes are expressed in the intestine, as peptides unique to each UGT were detected (**Figure 2**; **Supplementary Table 1**) (Strassburg et al., 2000; Sato et al., 2014; Fujiwara et al., 2016; Troberg et al., 2016). Moreover, two peptides specific to the UGT1A5 enzyme sequence were

TABLE 2 | Complete names of most significant UGT1A protein partners[a].

Protein Names[b]	
Abbreviation	**Complete names**
ACAA2	3-ketoacyl-CoA thiolase, mitochondrial
ACAT1/SOAT1	Sterol O-acyltransferase 1
ACOT8	Acyl-coenzyme A thioesterase 8
ACSL1	Long-chain-fatty-acid–CoA ligase 1
ADH1B	Alcohol dehydrogenase 1B
ALDH2	Aldehyde dehydrogenase, mitochondrial
ALDH6A1	Methylmalonate-semialdehyde dehydrogenase [acylating], mitochondrial
ASS1	Argininosuccinate synthase
ATP5A1	ATP synthase subunit alpha, mitochondrial
CALM1	Calmodulin
CPT1A	Carnitine O-palmitoyltransferase 1, liver isoform
CYP3A4	Cytochrome P450 3A4
ECH1	Delta(3,5)-Delta(2,4)-dienoyl-CoA isomerase, mitochondrial
ECHS1	Enoyl-CoA hydratase, mitochondrial
EHHADH	Peroxisomal bifunctional enzyme
GAPDH	Glyceraldehyde-3-phosphate dehydrogenase
GBF1	Golgi-specific brefeldin A-resistance guanine nucleotide exchange factor 1
GLYAT	Glycine N-acyltransferase
GSTA1	Glutathione S-transferase A1
HSPA8	Heat shock cognate 71 kDa protein
IDH2	Isocitrate dehydrogenase [NADP], mitochondrial
ITPR2	Inositol 1,4,5-trisphosphate receptor type 2
PC	Pyruvate carboxylase, mitochondrial
PCK2	Phosphoenolpyruvate carboxykinase [GTP], mitochondrial
PDIA3	Protein disulfide-isomerase A3
PFKL	ATP-dependent 6-phosphofructokinase, liver type
PHKA2	Phosphorylase b kinase regulatory subunit alpha, liver isoform
PHKB	Phosphorylase b kinase regulatory subunit beta
PHKG2	Phosphorylase b kinase gamma catalytic chain, liver/testis isoform
PKM	Pyruvate kinase
PRDX1	Peroxiredoxin-1
PRDX2	Peroxiredoxin-2
PRDX3	Peroxiredoxin-3
RALGAPA1	Ral GTPase-activating protein subunit alpha-1
RALGAPA2	Ral GTPase-activating protein subunit alpha-2
RALGAPB	Ral GTPase-activating protein subunit beta
SCP2	Non-specific lipid-transfer protein
SH3KBP1	SH3 domain-containing kinase-binding protein 1
SLC25A13	Calcium-binding mitochondrial carrier protein Aralar2
SLC25A5	ADP/ATP translocase 2
SLC34A2	Sodium-dependent phosphate transport protein 2B
TOP2B	DNA topoisomerase 2-beta
TRA2B	Transformer-2 protein homolog beta

[a] *Complete list of immunoprecipitated proteins is provided in* ***Supplementary Table 2****.*
[b] *Protein names are according to Uniprot (www.uniprot.org; accessed December 21, 2016).*

detected in the intestine, albeit at low levels (1 spectrum for each peptide) relative to other expressed UGT1As, providing evidence for its intestinal expression at the protein level (**Supplementary Figure 4**).

We provide unprecedented data on protein-protein interactions within the UGT family, namely between UGT1A and UGT2A3 enzymes and/or UGT2B family members. UGT1A-UGT2 interactions were observed in the liver (UGT2B4 and UGT2B7), in the kidney (UGT2B7) and in the intestine (UGT2B7, UGT2B17, and UGT2A3), and reflect the expression profiles of these UGT2 enzymes (Harbourt et al., 2012; Fallon et al., 2013a,b; Sato et al., 2014; Margaillan et al., 2015a,b; Tourancheau et al., 2016). Our current study offers a representative view of the endogenous UGT1A enzyme interactome in relevant drug metabolizing tissues. Findings are consistent with the interactions between several UGT1A enzymes and UGT2B7 detected in microsomes from liver tissues (Fremont et al., 2005; Fujiwara and Itoh, 2014) and when overexpressed in heterologous cell model systems as tagged proteins (Kurkela et al., 2007; Operaña and Tukey, 2007; Fujiwara et al., 2010; Ishii et al., 2010, 2014; Liu et al., 2016). In addition, other transferases and anti-oxidant PRDX1, PRDX2 and PRDX3 enzymes were also found associated with UGT1A enzymes. The interaction network is also in line with a model favoring detoxifying enzymes acting in a "metabolosome," i.e. a complex of xenobiotic-metabolizing enzymes and associated transport proteins regulating drug and xenobiotics inactivation and elimination (Taura et al., 2000; Takeda et al., 2005a,b, 2009; Akizawa et al., 2008; Mori et al., 2011; Fujiwara and Itoh, 2014; Ishii et al., 2014; Rouleau et al., 2014; Fujiwara et al., 2016).

The significant number of peroxisomal and mitochondrial enzymes regulating fatty acid β-oxidation identified in protein complexes with UGT1A enzymes hinted toward a potential involvement of UGT1A in regulating lipid metabolism. The higher number of lipid droplets, a reservoir of neutral lipids (such as fatty acids, sterol esters and phospholipids) (Thiam et al., 2013), in the UGT negative kidney cell model HEK293 overexpressing UGT1A9 lends support to this hypothesis. This observation is reminiscent of higher levels of lipid bodies induced by the overexpression of the peroxisomal ACOT8 protein, a confirmed UGT1A protein partner (Ishizuka et al., 2004). A modulation of lipid storage levels by overexpression of the UGT2B7 enzyme was also recently uncovered in breast and pancreatic cancer cell line models (Dates et al., 2015). This potential functional link between UGTs and lipid metabolism is intriguing and may be independent of the glucuronidation of some bioactive lipids previously reported (Turgeon et al., 2003). The underlying mechanism(s) of increased lipid droplets and the potential involvement of protein complexes comprised of UGT1A enzymes thus remain to be addressed and are aspects that fall beyond the scope of this study.

While UGT1A are ER-resident enzymes, their presence in other subcellular compartments such as the mitochondria is suggested by their co-localization with markers of several organelles (Rouleau et al., 2016). An intimate connection between ER, mitochondria, peroxisomes, and lipid droplets is also well recognized (Currie et al., 2013; Schrader et al., 2015). This is consistent with the significant number of peroxisomal and mitochondrial proteins interacting with UGT1A enzymes. Indeed, peroxisomes and lipid droplets are ER-derived substructures, whereas interactions between the ER and mitochondria at the so-called mitochondria-associated ER

membranes are gaining recognition as important sites of ER-mitochondria crosstalk where regulation of calcium signaling, lipid transport and tricarboxylic acid cycle take place (Hayashi et al., 2009; Tabak et al., 2013; Lodhi and Semenkovich, 2014; Pol et al., 2014).

The UGT1A interaction network exposes multiple links with enzymes of bioenergetic pathways. Besides lipids, glycogen catabolism as well as glycolytic and tricarboxylic acid cycle pathways may be influenced by the interactions of UGT1A with several subunits of the phosphorylase b and glycolytic/TCA cycle enzymes. It could be envisioned that UGT1A enzymes participate in the regulation of metabolite levels to prevent the toxic impact of excess concentrations of basic constituents, a hypothesis that remains to be addressed. Interestingly, mice with a disrupted *UGT1* gene locus (*UGT1*$^{-/-}$ mice) are short-lived, dying within 1 week of birth. Whereas hyperbilirubinemia induced by UGT1A1 deficiency appears largely responsible for early death, highly perturbed hepatic expression of genes involved in general cellular metabolic function, and notably those of starch, sugar and fatty acid metabolism was also observed in *UGT1*$^{-/-}$ mice, also supporting a contribution of UGT1A enzymes in those metabolic pathways (Nguyen et al., 2008). Rodent cell models from UGT1A-deficient mice or Gunn rats may constitute valuable models to investigate the interplay between UGT1A enzymes and global metabolic pathways.

One of the limitations of this study is that it examines complexes in which UGT1A enzymes reside and it does not provide information on direct interactions of UGT1A with proteins. Approaches such as proximity ligation and fluorescence resonance energy transfer are necessary to move forward with a better understanding of direct protein interactions and the domains involved. It is well documented that UGTs, like numerous metabolic enzymes, homo- and hetero-oligomerize with other UGTs (Fujiwara et al., 2007a; Kurkela et al., 2007; Operaña and Tukey, 2007; Bellemare et al., 2010b). It is therefore conceivable that UGT1A enzymes influence the activity of other metabolic enzymes by direct interactions that could alter the stoichiometry or composition of metabolic protein complexes. In turn, interactions of UGT1A enzymes with other metabolic enzymes may influence the glucuronidation pathway and thus contribute to the variable conjugation rates of individuals. This notion is supported by the altered activity of several UGT1A enzymes by CYP3A4 demonstrated in a cell-based system (Ishii et al., 2014). As well, the antagonistic or stimulatory functions of interactions among UGT1A and UGT2 enzymes, or with alternatively spliced isoforms, are consistent with a potential mode of regulation of UGTs by PPI (Fujiwara et al., 2007a; Bellemare et al., 2010b; Bushey and Lazarus, 2012; Rouleau et al., 2014, 2016; Audet-Delage et al., 2017).

In summary, we established an effective affinity purification method coupled to mass spectrometry for the enrichment and identification of protein complexes interacting with endogenous UGT1A enzymes. We successfully applied this approach to UGT1A enzymes expressed in drug metabolizing tissues and a UGT positive cell model to uncover an interaction map linking glucuronidation enzymes to other metabolic proteins involved in detoxification, as well as in the regulation of bioenergetic molecules (lipids and carbohydrates). Our data also support physical and functional interactions between ER and other subcellular compartments. The crosstalk among cellular metabolic functions exposed in this work warrants future investigations to address the impact of UGT1A-protein interactions on detoxification functions of UGT1A enzymes and of UGT1A enzymes on global metabolic cellular functions.

AUTHOR CONTRIBUTIONS

Conceptualization: CG; Methodology, MiR, MéR, YAD, CG; Investigation, MéR, YAD, CGB, SD; Formal Analysis, MiR, MéR, YAD, CGB, SD, CG. Writing—Review and Editing, All authors; Visualization, MiR, YAD, CG; Supervision, MiR, CG; Funding Acquisition, CG.

ACKNOWLEDGMENTS

The authors would like to thank Dr. MD Lai (National Cheng Kung University, Taiwan) and Dr. MA McNiven (Mayo Clinic, Rochester, USA) for the gift of reagents, Mario Harvey, Lyne Villeneuve and Joannie Roberge for technical assistance, Sylvie Bourassa at the Proteomics Platform of CHU de Québec Research Center for mass spectrometry analysis, and France Couture for artwork. This work was supported by the Natural Sciences and Engineering Research Council of Canada (342176-2012). YAD received a Ph.D. studentship award from the Fonds de Recherche Québec-Santé, MéR received a Canadian Institutes for Health Research Frederick Banting and Charles Best Graduate Scholarship award, CGB received a studentship from the Fonds de l'Enseignement et de la Recherche of the Faculty of Pharmacy of Laval University. CG holds a Tier I Canada Research Chair in Pharmacogenomics.

SUPPLEMENTARY MATERIAL

The Supplementary Material for this article can be found online at: http://journal.frontiersin.org/article/10.3389/fphar.2017.00023/full#supplementary-material

Supplementary Figure S1 | MS identification of human UGT1A in drug metabolizing tissues.

Supplementary Figure S2 | Confidence interaction scores SAINT vs. FC_B for interaction partners of UGT1A enzymes.

Supplementary Figure S3 | Overlap of UGT1A enzymes interacting proteins identified in each non-malignant human tissue and in the gastrointestinal cancer model cell line HT-29.

Supplementary Figure S4 | Identification of UGT1A5 enzyme expression in the intestine.

Supplementary Table S1 | UGT1A enzymes affinity purified from human tissue S9 fractions.

Supplementary Table S2 | LC-MS/MS identification of interacting proteins in human tissue S9 fractions.

Supplementary Table S3 | List of proteins in each group of the Venn diagrams (Figure 1B and Supplementary Figure 2).

Supplementary Table S4 | Liver proteomics data.

Supplementary Table S5 | Kidney proteomics data.

Supplementary Table S6 | Intestine proteomics data.

Supplementary Table S7 | HT-29 proteomics data.

REFERENCES

Akizawa, E., Koiwai, K., Hayano, T., Maezawa, S., Matsushita, T., and Koiwai, O. (2008). Direct binding of ligandin to uridine 5'-diphosphate glucuronosyltransferase 1A1. *Hepatol. Res.* 38, 402–409. doi: 10.1111/j.1872-034X.2007.00285.x

Audet-Delage, Y., Rouleau, M., Rouleau, M., Roberge, J., Miard, S., Picard, F., et al. (2017). Cross-talk between alternatively spliced UGT1A isoforms and colon cancer cell metabolism. *Mol. Pharmacol.* 91, 1–10. doi: 10.1124/mol.116.106161

Bellemare, J., Rouleau, M., Girard, H., Harvey, M., and Guillemette, C. (2010a). Alternatively spliced products of the UGT1A gene interact with the enzymatically active proteins to inhibit glucuronosyltransferase activity *in vitro*. *Drug Metab. Dispos.* 38, 1785–1789. doi: 10.1124/dmd.110.034835

Bellemare, J., Rouleau, M., Harvey, M., and Guillemette, C. (2010b). Modulation of the human glucuronosyltransferase UGT1A pathway by splice isoform polypeptides is mediated through protein-protein interactions. *J. Biol. Chem.* 285, 3600–3607. doi: 10.1074/jbc.M109.083139

Bellemare, J., Rouleau, M., Harvey, M., Popa, I., Pelletier, G., Tetu, B., et al. (2011). Immunohistochemical expression of conjugating UGT1A-derived isoforms in normal and tumoral drug-metabolizing tissues in humans. *J. Pathol.* 223, 425–435. doi: 10.1002/path.2805

Bindea, G., Galon, J., and Mlecnik, B. (2013). CluePedia Cytoscape plugin: pathway insights using integrated experimental and *in silico* data. *Bioinformatics* 29, 661–663. doi: 10.1093/bioinformatics/btt019

Bindea, G., Mlecnik, B., Hackl, H., Charoentong, P., Tosolini, M., Kirilovsky, A., et al. (2009). ClueGO: a Cytoscape plug-in to decipher functionally grouped gene ontology and pathway annotation networks. *Bioinformatics* 25, 1091–1093. doi: 10.1093/bioinformatics/btp101

Bolte, S., and Cordelieres, F. P. (2006). A guided tour into subcellular colocalization analysis in light microscopy. *J. Microsc.* 224, 213–232. doi: 10.1111/j.1365-2818.2006.01706.x

Bushey, R. T., and Lazarus, P. (2012). Identification and functional characterization of a novel UDP-glucuronosyltransferase 2A1 splice variant: potential importance in tobacco-related cancer susceptibility. *J. Pharmacol. Exp. Ther.* 343, 712–724. doi: 10.1124/jpet.112.198770

Choi, H., Larsen, B., Lin, Z. Y., Breitkreutz, A., Mellacheruvu, D., Fermin, D., et al. (2011). SAINT: probabilistic scoring of affinity purification-mass spectrometry data. *Nat. Methods* 8, 70–73. doi: 10.1038/nmeth.1541

Costa, E. (2006). Hematologically important mutations: bilirubin UDP-glucuronosyltransferase gene mutations in Gilbert and Crigler-Najjar syndromes. *Blood Cells Mol. Dis.* 36, 77–80. doi: 10.1016/j.bcmd.2005.10.006

Currie, E., Schulze, A., Zechner, R., Walther, T. C., and Farese, R. V. Jr. (2013). Cellular fatty acid metabolism and cancer. *Cell Metab.* 18, 153–161. doi: 10.1016/j.cmet.2013.05.017

Dates, C. R., Fahmi, T., Pyrek, S. J., Yao-Borengasser, A., Borowa-Mazgaj, B., Bratton, S. M., et al. (2015). Human UDP-Glucuronosyltransferases: effects of altered expression in breast and pancreatic cancer cell lines. *Cancer Biol. Ther.* 16, 714–723. doi: 10.1080/15384047.2015.1026480

Dluzen, D. F., and Lazarus, P. (2015). MicroRNA regulation of the major drug-metabolizing enzymes and related transcription factors. *Drug Metab. Rev.* 47, 320–334. doi: 10.3109/03602532.2015.1076438

Fallon, J. K., Neubert, H., Goosen, T. C., and Smith, P. C. (2013a). Targeted precise quantification of 12 human recombinant uridine-diphosphate glucuronosyl transferase 1A and 2B isoforms using nano-ultra-high-performance liquid chromatography/tandem mass spectrometry with selected reaction monitoring. *Drug Metab. Dispos.* 41, 2076–2080. doi: 10.1124/dmd.113.053801

Fallon, J. K., Neubert, H., Hyland, R., Goosen, T. C., and Smith, P. C. (2013b). Targeted quantitative proteomics for the analysis of 14 UGT1As and -2Bs in human liver using NanoUPLC-MS/MS with selected reaction monitoring. *J. Proteome Res.* 12, 4402–4413. doi: 10.1021/pr4004213

Fremont, J. J., Wang, R. W., and King, C. D. (2005). Coimmunoprecipitation of UDP-glucuronosyltransferase isoforms and cytochrome P450 3A4. *Mol. Pharmacol.* 67, 260–262. doi: 10.1124/mol.104.006361

Fujiwara, R., and Itoh, T. (2014). Extensive protein-protein interactions involving UDP-glucuronosyltransferase (UGT) 2B7 in human liver microsomes. *Drug Metab. Pharmacokinet.* 29, 259–265. doi: 10.2133/dmpk.DMPK-13-RG-096

Fujiwara, R., Nakajima, M., Oda, S., Yamanaka, H., Ikushiro, S., Sakaki, T., et al. (2010). Interactions between human UDP-glucuronosyltransferase (UGT) 2B7 and UGT1A enzymes. *J. Pharm. Sci.* 99, 442–454. doi: 10.1002/jps.21830

Fujiwara, R., Nakajima, M., Yamanaka, H., Katoh, M., and Yokoi, T. (2007a). Interactions between human UGT1A1, UGT1A4, and UGT1A6 affect their enzymatic activities. *Drug Metab. Dispos.* 35, 1781–1787. doi: 10.1124/dmd.107.016402

Fujiwara, R., Nakajima, M., Yamanaka, H., Nakamura, A., Katoh, M., Ikushiro, S., et al. (2007b). Effects of coexpression of UGT1A9 on enzymatic activities of human UGT1A isoforms. *Drug Metab. Dispos.* 35, 747–757. doi: 10.1124/dmd.106.014191

Fujiwara, R., Yokoi, T., and Nakajima, M. (2016). Structure and protein-protein interactions of human UDP-glucuronosyltransferases. *Front. Pharmacol.* 7:388. doi: 10.3389/fphar.2016.00388

Guillemette, C., Levesque, E., Harvey, M., Bellemare, J., and Menard, V. (2010). UGT genomic diversity: beyond gene duplication. *Drug Metab. Rev.* 42, 24–44. doi: 10.3109/03602530903210682

Guillemette, C., Levesque, E., and Rouleau, M. (2014). Pharmacogenomics of human uridine diphospho-glucuronosyltransferases and clinical implications. *Clin. Pharmacol. Ther.* 96, 324–339. doi: 10.1038/clpt.2014.126

Harbourt, D. E., Fallon, J. K., Ito, S., Baba, T., Ritter, J. K., Glish, G. L., et al. (2012). Quantification of human uridine-diphosphate glucuronosyl transferase 1A isoforms in liver, intestine, and kidney using nanobore liquid chromatography-tandem mass spectrometry. *Anal. Chem.* 84, 98–105. doi: 10.1021/ac201704a

Hayashi, T., Rizzuto, R., Hajnoczky, G., and Su, T. P. (2009). MAM: more than just a housekeeper. *Trends Cell Biol.* 19, 81–88. doi: 10.1016/j.tcb.2008.12.002

Hu, D. G., Meech, R., McKinnon, R. A., and Mackenzie, P. I. (2014). Transcriptional regulation of human UDP-glucuronosyltransferase genes. *Drug Metab. Rev.* 46, 421–458. doi: 10.3109/03602532.2014.973037

Hung, Y. H., Chan, Y. S., Chang, Y. S., Lee, K. T., Hsu, H. P., Yen, M. C., et al. (2014). Fatty acid metabolic enzyme acyl-CoA thioesterase 8 promotes the development of hepatocellular carcinoma. *Oncol. Rep.* 31, 2797–2803. doi: 10.3892/or.2014.3155

Ishii, Y., Iwanaga, M., Nishimura, Y., Takeda, S., Ikushiro, S., Nagata, K., et al. (2007). Protein-protein interactions between rat hepatic cytochromes P450 (P450s) and UDP-glucuronosyltransferases (UGTs): evidence for the functionally active UGT in P450-UGT complex. *Drug Metab. Pharmacokinet.* 22, 367–376. doi: 10.2133/dmpk.22.367

Ishii, Y., Koba, H., Kinoshita, K., Oizaki, T., Iwamoto, Y., Takeda, S., et al. (2014). Alteration of the function of the UDP-glucuronosyltransferase 1A subfamily by cytochrome P450 3A4: different susceptibility for UGT isoforms and UGT1A1/7 variants. *Drug Metab. Dispos.* 42, 229–238. doi: 10.1124/dmd.113.054833

Ishii, Y., Takeda, S., and Yamada, H. (2010). Modulation of UDP-glucuronosyltransferase activity by protein-protein association. *Drug Metab. Rev.* 42, 145–158. doi: 10.3109/03602530903208579

Ishizuka, M., Toyama, Y., Watanabe, H., Fujiki, Y., Takeuchi, A., Yamasaki, S., et al. (2004). Overexpression of human acyl-CoA thioesterase upregulates peroxisome biogenesis. *Exp. Cell Res.* 297, 127–141. doi: 10.1016/j.yexcr.2004.02.029

Kurkela, M., Patana, A. S., Mackenzie, P. I., Court, M. H., Tate, C. G., Hirvonen, J., et al. (2007). Interactions with other human UDP-glucuronosyltransferases attenuate the consequences of the Y485D mutation on the activity and substrate affinity of UGT1A6. *Pharmacogenet. Genomics* 17, 115–126. doi: 10.1097/FPC.0b013e328011b598

Liu, Y. Q., Yuan, L. M., Gao, Z. Z., Xiao, Y. S., Sun, H. Y., Yu, L. S., et al. (2016). Dimerization of human uridine diphosphate glucuronosyltransferase allozymes 1A1 and 1A9 alters their quercetin glucuronidation activities. *Sci. Rep.* 6:23763. doi: 10.1038/srep23763

Lodhi, I. J., and Semenkovich, C. F. (2014). Peroxisomes: a nexus for lipid metabolism and cellular signaling. *Cell Metab.* 19, 380–392. doi: 10.1016/j.cmet.2014.01.002

Margaillan, G., Rouleau, M., Fallon, J. K., Caron, P., Villeneuve, L., Turcotte, V., et al. (2015a). Quantitative profiling of human renal UDP-glucuronosyltransferases and glucuronidation activity: a comparison of normal and tumoral kidney tissues. *Drug Metab. Dispos.* 43, 611–619. doi: 10.1124/dmd.114.062877

Margaillan, G., Rouleau, M., Klein, K., Fallon, J. K., Caron, P., Villeneuve, L., et al. (2015b). Multiplexed targeted quantitative proteomics predicts hepatic glucuronidation potential. *Drug Metab. Dispos.* 43, 1331–1335. doi: 10.1124/dmd.115.065391

Mellacheruvu, D., Wright, Z., Couzens, A. L., Lambert, J. P., St-Denis, N. A., Li, T., et al. (2013). The CRAPome: a contaminant repository for affinity purification-mass spectrometry data. *Nat. Methods* 10, 730–736. doi: 10.1038/nmeth.2557

Ménard, V., Collin, P., Margaillan, G., and Guillemette, C. (2013). Modulation of the UGT2B7 enzyme activity by C-terminally truncated proteins derived from alternative splicing. *Drug Metab. Dispos.* 41, 2197–2205. doi: 10.1124/dmd.113.053876

Mori, Y., Kiyonaka, S., and Kanai, Y. (2011). Transportsomes and channelsomes: are they functional units for physiological responses? *Channels* 5, 387–390. doi: 10.4161/chan.5.5.16466

Nguyen, N., Bonzo, J. A., Chen, S., Chouinard, S., Kelner, M. J., Hardiman, G., et al. (2008). Disruption of the ugt1 locus in mice resembles human Crigler-Najjar type I disease. *J. Biol. Chem.* 283, 7901–7911. doi: 10.1074/jbc.M709244200

Operaña, T. N., and Tukey, R. H. (2007). Oligomerization of the UDP-glucuronosyltransferase 1A proteins: homo- and heterodimerization analysis by fluorescence resonance energy transfer and co-immunoprecipitation. *J. Biol. Chem.* 282, 4821–4829. doi: 10.1074/jbc.M609417200

Pol, A., Gross, S. P., and Parton, R. G. (2014). Review: biogenesis of the multifunctional lipid droplet: lipids, proteins, and sites. *J. Cell Biol.* 204, 635–646. doi: 10.1083/jcb.201311051

Ramírez, J., Ratain, M. J., and Innocenti, F. (2010). Uridine 5′-diphospho-glucuronosyltransferase genetic polymorphisms and response to cancer chemotherapy. *Future Oncol.* 6, 563–585. doi: 10.2217/fon.10.17

Rouleau, M., Roberge, J., Bellemare, J., and Guillemette, C. (2014). Dual roles for splice variants of the glucuronidation pathway as regulators of cellular metabolism. *Mol. Pharmacol.* 85, 29–36. doi: 10.1124/mol.113.089227

Rouleau, M., Tourancheau, A., Girard-Bock, C., Villeneuve, L., Vaucher, J., Duperre, A. M., et al. (2016). Divergent expression and metabolic functions of human glucuronosyltransferases through alternative splicing. *Cell Rep.* 17, 114–124. doi: 10.1016/j.celrep.2016.08.077

Rowland, A., Miners, J. O., and Mackenzie, P. I. (2013). The UDP-glucuronosyltransferases: their role in drug metabolism and detoxification. *Int. J. Biochem. Cell Biol.* 45, 1121–1132. doi: 10.1016/j.biocel.2013.02.019

Ruan, H. B., Han, X., Li, M. D., Singh, J. P., Qian, K., Azarhoush, S., et al. (2012). O-GlcNAc transferase/host cell factor C1 complex regulates gluconeogenesis by modulating PGC-1alpha stability. *Cell Metab.* 16, 226–237. doi: 10.1016/j.cmet.2012.07.006

Sato, Y., Nagata, M., Tetsuka, K., Tamura, K., Miyashita, A., Kawamura, A., et al. (2014). Optimized methods for targeted peptide-based quantification of human uridine 5'-diphosphate-glucuronosyltransferases in biological specimens using liquid chromatography-tandem mass spectrometry. *Drug Metab. Dispos.* 42, 885–889. doi: 10.1124/dmd.113.056291

Savas, J. N., Stein, B. D., Wu, C. C., and Yates, J. R. III. (2011). Mass spectrometry accelerates membrane protein analysis. *Trends Biochem. Sci.* 36, 388–396. doi: 10.1016/j.tibs.2011.04.005

Schrader, M., Godinho, L. F., Costello, J. L., and Islinger, M. (2015). The different facets of organelle interplay-an overview of organelle interactions. *Front Cell Dev Biol* 3:56. doi: 10.3389/fcell.2015.00056

Schroeder, B., Weller, S. G., Chen, J., Billadeau, D., and McNiven, M. A. (2010). A Dyn2-CIN85 complex mediates degradative traffic of the EGFR by regulation of late endosomal budding. *EMBO J.* 29, 3039–3053. doi: 10.1038/emboj.2010.190

Strassburg, C. P., Kneip, S., Topp, J., Obermayer-Straub, P., Barut, A., Tukey, R. H., et al. (2000). Polymorphic gene regulation and interindividual variation of UDP-glucuronosyltransferase activity in human small intestine. *J. Biol. Chem.* 275, 36164–36171. doi: 10.1074/jbc.M002180200

Tabak, H. F., Braakman, I., and van der Zand, A. (2013). Peroxisome formation and maintenance are dependent on the endoplasmic reticulum. *Annu. Rev. Biochem.* 82, 723–744. doi: 10.1146/annurev-biochem-081111-125123

Takeda, S., Ishii, Y., Iwanaga, M., Mackenzie, P. I., Nagata, K., Yamazoe, Y., et al. (2005a). Modulation of UDP-glucuronosyltransferase function by cytochrome P450: evidence for the alteration of UGT2B7-catalyzed glucuronidation of morphine by CYP3A4. *Mol. Pharmacol.* 67, 665–672. doi: 10.1124/mol.104.007641

Takeda, S., Ishii, Y., Iwanaga, M., Nurrochmad, A., Ito, Y., Mackenzie, P. I., et al. (2009). Interaction of cytochrome P450 3A4 and UDP-glucuronosyltransferase 2B7: evidence for protein-protein association and possible involvement of CYP3A4 J-helix in the interaction. *Mol. Pharmacol.* 75, 956–964. doi: 10.1124/mol.108.052001

Takeda, S., Ishii, Y., Mackenzie, P. I., Nagata, K., Yamazoe, Y., Oguri, K., et al. (2005b). Modulation of UDP-glucuronosyltransferase 2B7 function by cytochrome P450s *in vitro*: differential effects of CYP1A2, CYP2C9 and CYP3A4. *Biol. Pharm. Bull.* 28, 2026–2027. doi: 10.1248/bpb.28.2026

Taura, K. I., Yamada, H., Hagino, Y., Ishii, Y., Mori, M. A., and Oguri, K. (2000). Interaction between cytochrome P450 and other drug-metabolizing enzymes: evidence for an association of CYP1A1 with microsomal epoxide hydrolase and UDP-glucuronosyltransferase. *Biochem. Biophys. Res. Commun.* 273, 1048–1052. doi: 10.1006/bbrc.2000.3076

Thiam, A. R., Farese, R. V. Jr., and Walther, T. C. (2013). The biophysics and cell biology of lipid droplets. *Nat. Rev. Mol. Cell Biol.* 14, 775–786. doi: 10.1038/nrm3699

Tourancheau, A., Margaillan, G., Rouleau, M., Gilbert, I., Villeneuve, L., Levesque, E., et al. (2016). Unravelling the transcriptomic landscape of the major phase II UDP-glucuronosyltransferase drug metabolizing pathway using targeted RNA sequencing. *Pharmacogenomics J.* 16, 60–70. doi: 10.1038/tpj.2015.20

Troberg, J., Jarvinen, E., Ge, G. B., Yang, L., and Finel, M. (2016). UGT1A10 is a high activity and important extrahepatic enzyme: why has its role in intestinal glucuronidation been frequently underestimated? *Mol. Pharm.* doi: 10.1021/acs.molpharmaceut.6b00852. [Epub ahead of print].

Turgeon, D., Chouinard, S., Belanger, P., Picard, S., Labbe, J. F., Borgeat, P., et al. (2003). Glucuronidation of arachidonic and linoleic acid metabolites by human UDP-glucuronosyltransferases. *J. Lipid Res.* 44, 1182–1191. doi: 10.1194/jlr.M300010-JLR200

Conflict of Interest Statement: The authors declare that the research was conducted in the absence of any commercial or financial relationships that could be construed as a potential conflict of interest.

frontiers in Pharmacology

REVIEW
published: 25 November 2016
doi: 10.3389/fphar.2016.00456

Pregnane X Receptor (PXR)-Mediated Gene Repression and Cross-Talk of PXR with Other Nuclear Receptors via Coactivator Interactions

*Petr Pavek**

Department of Pharmacology and Toxicology and Centre for Drug Development, Faculty of Pharmacy in Hradec Kralove, Charles University in Prague, Hradec Kralove, Czechia

Pregnane X receptor is a ligand-activated nuclear receptor (NR) that mainly controls inducible expression of xenobiotics handling genes including biotransformation enzymes and drug transporters. Nowadays it is clear that PXR is also involved in regulation of intermediate metabolism through *trans*-activation and *trans*-repression of genes controlling glucose, lipid, cholesterol, bile acid, and bilirubin homeostasis. In these processes PXR cross-talks with other NRs. Accumulating evidence suggests that the cross-talk is often mediated by competing for common coactivators or by disruption of coactivation and activity of other transcription factors by the ligand-activated PXR. In this respect mainly PXR-CAR and PXR-HNF4α interference have been reported and several cytochrome P450 enzymes (such as CYP7A1 and CYP8B1), phase II enzymes (SULT1E1, Gsta2, Ugt1a1), drug and endobiotic transporters (OCT1, Mrp2, Mrp3, Oatp1a, and Oatp4) as well as intermediate metabolism enzymes (PEPCK1 and G6Pase) have been shown as down-regulated genes after PXR activation. In this review, I summarize our current knowledge of PXR-mediated repression and coactivation interference in PXR-controlled gene expression regulation.

Keywords: PXR, nuclear receptor, gene regulation, metabolism, cross-talk

OPEN ACCESS

Edited by:
Ulrich M. Zanger, Dr. Margarete Fischer-Bosch-Institute of Clinical Pharmacology, Germany

Reviewed by:
Ramiro Jover, University of Valencia, Spain
Yuji Ishii, Kyushu University, Japan

***Correspondence:**
Petr Pavek
petr.pavek@faf.cuni.cz

Specialty section:
This article was submitted to Pharmacogenetics and Pharmacogenomics, a section of the journal Frontiers in Pharmacology

Received: *29 August 2016*
Accepted: *14 November 2016*
Published: *25 November 2016*

Citation:
Pavek P (2016) Pregnane X Receptor (PXR)-Mediated Gene Repression and Cross-Talk of PXR with Other Nuclear Receptors via Coactivator Interactions. Front. Pharmacol. 7:456. doi: 10.3389/fphar.2016.00456

INTRODUCTION

Pregnane X receptor (PXR) is now accepted as a master transcription factor of xenobiotic- and drug-inducible expression of key genes that encode members of the phase I and phase II metabolic enzymes and drug transporters. Moreover, accumulating evidence suggests that PXR plays an integral role also in endobiotic metabolism by regulating important genes implicated in glucose,

Abbreviations: CAR, constitutive androstane receptor; ChiP, Chromatin immunoprecipitation assay; CREB, cAMP-response element-binding protein; CYP450, cytochrome P450; CYP3A4, cytochrome P4503A4, CYP7A1, cholesterol 7α-hydroxylase; DR-1, direct repeat separated by one nucleotide; FoxA2, forkhead factor 2; FOXO1, forkhead box protein O1; FXR, farnesoid X receptor; HNF4α, hepatocyte nuclear factor 4α; Hmgcs2, mitochondrial 3-hydroxy-3-methylglutarate-CoA synthase 2; GST; glutathione *S*-transferase; M2H, mammalian two hybrid assay; NR, nuclear receptor; OCT1, organic cation transporter 1; PGC-1alpha, PPARgamma coactivator 1α; PXR, pregnane X receptor; PGC-1α, peroxisome proliferator-activated receptor gamma, coactivator 1 α (PPARGC1A); RXRα, Retinoid X Receptor Alpha; SGK2, serum/glucocorticoid regulated kinase 2; SLC22A1, solute carrier family of transporter A 1; SRC-1, steroid receptor coactivator; SREBP-1, Sterol regulatory element binding protein 1.

lipid, and bile acid metabolism. In addition, it was documented that PXR both induces as well as suppresses expression of numerous hepatic transcripts. The latest report shows that PXR up-regulates 164 genes, but down-regulates expression of 334 genes in primary human hepatocytes (Kandel et al., 2016). In this review I summarize well-documented examples of PXR-mediated *trans*-repression and coactivation interference in the PXR-mediated transactivation.

Pregnane X Receptor

Nuclear receptors (NRs) form a super-family of transcription factors implicated in various physiological functions, from development, detoxification to homeostasis. Many NRs are ligand-activated transcription factors sharing a common evolutionary history and similar sequence features at the protein level, mainly in their DNA-binding domain (DBD), and to a lesser extent in ligand binding domains (LBD). PXR (or NR subfamily 1, group I, member 2, NR1I2), together with CAR (NR1I3), and vitamin D receptors (VDR, NR1I1), form a group I of the subfamily 1 of NRs (Moore et al., 2006; di Masi et al., 2009; Smutny et al., 2013).

Mouse PXR (mPXR) was first identified in 1998 by using an expressed sequence tag to screen a mouse liver library. It was found to be activated by derivatives of dexamethasone and pregnenolone (Kliewer et al., 1998). At the same time, the human steroid X receptor was cloned (Blumberg et al., 1998) and established to be the human homologue of mPXR involved in CYP450 3A4 regulation (CYP3A4) (Bertilsson et al., 1998; Lehmann et al., 1998).

Human PXR (hPXR) is the product of the *NR1I2* gene, which is located on chromosome 3, locus 3q11–q13.3. The *NR1I2* gene comprises 10 exons separated by nine intronic regions (Hustert et al., 2001; Zhang et al., 2001). PXR, like any other member in the NR super-family, is composed of the DBD, the H region, and the C-terminal LBD. PXR-DBD is involved in receptor dimerization and in the binding of specific DNA sequences. H region (or Hinge region) is a flexible domain that connects the DBD with the LBD. PXR heterodimerizes with RXRα to form a transcriptionally active complex (Blumberg et al., 1998; Lehmann et al., 1998).

The flexible ligand-binding pocket of PXR-LBD enables binding of a wide range of structurally unrelated endogenous and exogenous ligands. Watkins et al. (2001) first showed the crystal structure of the ligand-binding domain both alone and in complex with the PXR ligand SR12813. The PXR-LBD structure consists of a three-layered α-helical sandwich (α1–α3/α4–α5–α8–α9/α7–α10) and five-stranded antiparallel β-sheets (β1, β10, β2, β3, and β4). Interestingly, PXR-LBD contains an insert of approximately 60 residues which is unique within members of the NR super-family. This is the main reason for the larger cavity as well as the wider substrate diversity of PXR ligands. The *apo*-PXR binding cavity volume is approximately 1150 $Å^3$; in the presence of ligands it can extend to 1290–1540 $Å^3$ (Chrencik et al., 2005). Thus, the binding cavity volume is substantially larger than that of many other NRs. The ligand pockets of PXR, CAR as well as VDR are lined by mostly hydrophobic residues. The cavity of PXR is lined by 28 amino acids, of which eight have polar or charged side chains (Watkins et al., 2001; di Masi et al., 2009). The PXR-LBD ends with a short helix (αAF) which is critical for the structural organization of the AF-2 (the activation function 2) region to recruit transcriptional coregulators. In NR LBDs, the AF-2 region binds the Leu-Xxx-Xxx-Leu-Leu (LXXLL) motifs of transcriptional coactivators, and the Ile/Leu-Xxx-Xxx-Ile/Val-Ile motifs of corepressors (Lazar, 2003; Rosenfeld et al., 2006). The coactivator recruitment appears to play a central role in fixing ligands in the correct arrangement in the large PXR cavity after a coreppresor release.

Pregnane X receptor is primarily expressed in the liver, intestine, and to a lesser extend in the kidney. Expression of PXR/Pxr mRNA in other tissues including lung, stomach, peripheral blood monocytes, uterus, ovary, breast, adrenal gland, bone marrow, and some regions of the brain is minor (see the comprehensive review by Pavek and Dvorak, 2008). Mouse liver immunostaining suggests that mPXR is mainly located in the cytosol of untreated liver cells. Similar to CAR/mCar, mPxr forms a protein complex with cytoplasmic CAR retention protein (CCRP) and the heat shock protein 90 (hsp90), which retains the cytosolic localization of PXR. Upon ligand binding to mPxr, the Pxr dissociates from the multi-protein complex and translocates to the nucleus in primary mouse hepatocytes to activate gene transcription (Kawana et al., 2003; Squires et al., 2004). In contrast, nuclear localization of human PXR has been reported in mammalian tumor derived cell lines (Saradhi et al., 2005).

Pregnane X receptor was originally characterized as the key transcription factor that activates hepatic genes encoding drug-metabolizing enzymes and drug efflux transporters (Kliewer et al., 2002). PXR protects the body from harmful foreign toxicants or endogenous toxic substances by an autoregulation mechanism. PXR ligands activate a number of genes involved in their metabolism that in feedback manner contribute to their clearance. PXR has a wide spectrum of ligands belonging to drugs (such as antibiotic rifampicin, anticancer drugs tamoxifen and taxol, antihypertensive drug nifedipine, antifungal drug clotrimazole, or herbal antidepressant hyperforin), endogenous ligands (including steroids such as lithocholic acid) or products of gut microflora (di Masi et al., 2009; Smutny et al., 2013; Venkatesh et al., 2014).

Nowadays, it is clear that the xenobiotic-sensing PXR pathway regulates also energy metabolism, and reciprocally, the energy homeostasis affects drug metabolism. In the review, I focus on the PXR-mediated regulation of phosphoenolpyruvate carboxykinase (PEPCK) and glucose-6-phosphatase (G6Pase), two rate-limiting enzymes of hepatic gluconeogenesis; Hmgcs2, the key enzyme involved in ketogenesis; the active form of SREBP-1, which regulates genes required for sterol biosynthesis, fatty acid and lipid production and glucose metabolism; and lastly CYP7A1 and CYP8B1 enzymes critically involved in bile acid synthesis. PXR or its rodent orthologues have also been shown to be involved in heme, bilirubin and thyroxin clearance, in bone homeostasis and vitamin D metabolism. In addition, PXR activation is known to suppress the activity of NF-κB, which is the key regulator of inflammation and

In all NRs, m and h denote mouse and human, respectively.

immune response (Xie et al., 2003; Zhou et al., 2009; Gao and Xie, 2012; Wang et al., 2012). These effects of PXR activation are, however, beyond the scope of the present review.

PXR Coactivation

Coactivators and corepressors have been found critical for the function of DNA-binding transcription factors (TFs). Coactivator and corepressor proteins are components of multisubunit coregulator complexes involved in transcriptional gene regulation machinery (for a comprehensive review on coactivator/corepressors see Rosenfeld et al., 2006; Oladimeji et al., 2016).

PXR-LBD AF-2 region binds the LXXLL motifs of transcriptional coactivators as was shown with a 25 amino acid residue fragment of the human SRC-1. The motif forms hydrophobic contacts with the surface of hPXR in a groove composed of α3, α4, and AF-2 region. From the LBD side, PXR ligands are in direct contacts with αAF of AF-2 region (Xue et al., 2007). Both the SR12813 ligand and SRC-1 coactivator peptide in the crystal model stabilize the LBD of PXR. A charge clamp involving PXR residues Lys259 and Glu427 stabilizes the weak helix dipole at the C- and N-terminus of the LXXLL motif (Watkins et al., 2003; Xue et al., 2007).

SRC-1 was the first coactivator identified for hPXR (Kliewer et al., 1998; Lehmann et al., 1998). The members of the SRC family contain several conserved structural domains: a N-terminal basic helix-loop-helix-Per/ARNT/Sim (bHLH-PAS) domain, a central NR interaction domain (RID) with three LXXLL motifs, and two activation domains (AD1 and AD2) at the C-terminus. Once recruited to the target gene promoters by ligand-activated NRs, SRCs trigger the/an assembly of a multi-protein coactivator complex by further recruiting secondary coactivators and histone modifying enzymes to activation domains 1 and 2 (AD-1 and AD-2) such as CBP/p300, coactivator associated arginine methyltransferase 1 (CARM1) and protein arginine methyltransferase 1 (PRMT1). The formed transcriptional complex remodels transcriptionally inactive chromatin within the target gene and attracts components of the RNA polymerase II transcriptional complex. The AD-1 domain binds p300 and CBP, both of which are potent histone acetyltransferases (HATs) that remodel chromatin to allow accessibility for the transcription preinitiation complex. The AD-2 domain recruit protein arginine *N*-methyltransferase (PRMT) family members, such as CARM1 and PRMT1, which methylate residues of histone proteins and other chromatin-associated proteins (Szwarc et al., 2014; Wang et al., 2016).

The paradigm of NR action is that ligand binding enhances the receptor's affinity for coactivator proteins, while decreasing its affinity for corepressors such as the silencing mediator of retinoid and thyroid receptors (SMRT, NR corepressor 2, NCoR2) and of the NR corepressor (NCoR, *NCOR1*), allowing further binding of the coactivators. Coactivators often have an intrinsic HAT activity, which weakens the association of histones to DNA, and therefore promotes gene transcription. On contrary, corepressors recruit histone deacetylases (HDACs), which strengthen the association of histones to DNA, and therefore repress gene transcription.

The mechanism of ligand-dependent activation of PXR significantly differs from that seen in many other NRs. Coactivation by SRC-1 stimulated after PXR activation has not been confirmed in some rigorous biophysical studies (Navaratnarajah et al., 2012). It was also demonstrated that PXR and SRC-1 interact in the absence of a PXR ligand, and further, that the interaction is strengthened by rifampicin (Saini et al., 2005; Li and Chiang, 2006; Rulcova et al., 2010; Krausova et al., 2011; Hyrsova et al., 2016). Moreover, no ligand activated release, or even stronger interaction with SMRTα has been reported for PXR (Takeshita et al., 2002; Mani et al., 2005; Li et al., 2009; Navaratnarajah et al., 2012; Hirooka-Masui et al., 2013). Nevertheless, also contradictory results have been published regarding SMRT and NCoR interaction with PXR (Ding and Staudinger, 2005b; Johnson et al., 2006). SMRT (or its overexpression) has been documented as the repressor of PXR-mediated transactivation (Takeshita et al., 2002; Mani et al., 2005; Johnson et al., 2006; Hirooka-Masui et al., 2013). In addition, repressed PXR by SMRT has been reported to inhibit the activation of *CYP24A1* gene by vitamin D receptor (Konno et al., 2009).

Recently, Masuyama et al. (2000) also found that PXR interacts with SRC-1 and NR interacting protein 1 (NRIP1, RIP140) in a ligand dependent manner. These data indicate that different ligands may specifically change the conformation of PXR-LBD resulting in different interaction with coactivators.

The interactions of co-factors with TFs are governed by post-translational modifications. Phosphorylation plays an important role in the regulation of NRs functions, enabling integration of different cellular and extracellular stimuli in their functions. PXR is phosphorylated by protein kinase A (PKA), resulting in strengthened interaction with SRC-1 and PBP coactivators (Ding and Staudinger, 2005a). In contrast, the activity of PXR can be repressed by the activation of protein kinase C (PKC) isoforms which alters the phosphorylation status of PXR and represses PXR-SRC-1 interaction, but strengthens PXR-NCoR interaction (Ding and Staudinger, 2005b). Therefore, the phosphorylation status of PXR can modulate coactivator/corepressor recruitment which could reflect the ligand-independent activation of PXR.

NR CROSSTALK BASED ON COACTIVATORS PROTEIN–PROTEIN INTERACTIONS

As other NRs, PXR needs coactivators and corepressors for its transcriptional activity and for tuning of the tissue-, ligand-, and promoter (gene)-specific transactivation (Smutny et al., 2013). Coactivators and corepressors are common for the most of NRs and TFs. In addition, some NRs share the same response elements in transactivation of their target genes. This is the most strikingly evident in case of the *CYP3A4* gene, when PXR, CAR, and VDR share four different response elements in proximal promoter and two enhancer elements in gene- and tissue-specific

manner (Pavek et al., 2010). This is the mechanistic molecular base for so called **cross-talk of NRs** in positive and negative transcriptional regulation, in forming negative feedback loops and in hierarchy of NRs in regulatory networks (Pascussi et al., 2008).

Recently, the competition for common coactivators emerged as an important process in the NR-mediated gene regulation. Competition for the common coactivators PGC-1α or GRIP-1 has been recently reported as a putative mechanism of crosstalk between CAR and the estrogen receptor (Min et al., 2002), HNF4α and PXR (Bhalla et al., 2004; Li and Chiang, 2005), and HNF4α and CAR (Miao et al., 2006). Competition for the common Src-1 coactivator has been reported for Pxr-Car crosstalk (Saini et al., 2005), as well as for Lxr and the retinoid-related orphan receptor α (Rorα) interaction (Wada et al., 2008); and considered as the underlying mechanisms in cases of Car-Lxrα/LXRα interaction (Zhai et al., 2010).

Competition For Coactivators and Cross-Talk in PXR-Mediated Regulation of Intermediary Metabolism

Pregnane X Receptor has been shown to regulate glucose and lipid homeostasis during fasting and modifies the risk of hyperglycemia, diabetes, obesity, dyslipidemia, and hepatosteatosis. Key transcription factors and their cofactors in glucose and lipid homeostasis have been described to crosstalk with PXR regulation.

CREB

In response to fasting and/or starvation, the liver increases the production of glucose by stimulating both gluconeogenesis and glycogenolysis. In the process glucagon up-regulates the transcription of the hepatic genes that encode rate-limiting enzymes of glucose homeostasis, such as the glucose-6-phosphatase catalytic subunit (**G6Pase**), or **PEPCK1** (phosphoenolpyruvate carboxykinase 1, PCK1). Glucagon stimulates PKA (cAMP-dependent protein kinase) that phosphorylates the CREB [CRE (cAMP response element)-binding protein]. The phosphorylation of CREB leads to the recruitment of HATs CBP/p300, binding of CREB to CREB response elements (CREs), and the activation of the CRE-bearing genes, such as those for *G6Pase* and *PEPCK1*, as well as PGC-1α. The coactivators linked to CREB transactivation (as well as FOXO1) include CBP/p300, CREB regulated transcription coactivator 2 (CRTC2), PGC-1α, and protein arginine methyltransferases (PRMTs) (Oh et al., 2013).

It has been reported that rifampicin-activated PXR represses the transcription of the *G6Pase* gene by inhibiting the DNA-binding ability of CREB to its response element CRE and that direct interaction of PXR with CREB is involved (see **Figure 1**) (Kodama et al., 2007).

In opposite to suppressive effects of PXR/mPxr activation on gluconeogenic genes via CREB signaling, human-specific induction of ***PEPCK*** and ***G6Pase*** genes have been described recently in rifampicin-treated HepG2 cells stably expressing human PXR. In these observations, serum- and glucocorticoid-regulated kinase 2 (SGK2) has been found as an essential factor for the PXR-induced *G6Pase* gene up-regulation. Non-phosphorylated SGK2 has been found to co-activate PXR-mediated *trans*-activation of gluconeogenic genes in human liver cells, thereby enhancing gluconeogenesis and glucose production (Gotoh and Negishi, 2014, 2015). In the mechanism the activated PXR scaffolds both the protein phosphatase 2C (PP2C) and SGK2 in order to stimulate PP2C to dephosphorylate SGK2. Dephosphorylated SGK2 co-activates PXR in the *trans*-activation of these genes (see **Figure 2**). At the same time, the ligand-activated PXR stimulates expression of the *SGK2* gene (Gotoh and Negishi, 2014). This finding of PXR-induced gluconeogenesis is consistent with the clinical observation that rifampicin can increase blood glucose level in humans (Hakkola et al., 2016; Rysa et al., 2013) even though the effect was attributed to the hepatic glucose transporter 2 (Glut2) mRNA down-regulation in subsequent experiments in rats (Rysa et al., 2013).

FOXO1

The forkhead box O transcription factor FOXO1 is regarded as a master regulator of energy metabolism in numerous organs including the liver, pancreas, adipose tissue and skeletal muscle. FOXO1 regulates the transcriptional cascades controlling glucose and lipid metabolism. FOXO1 is an activator of gluconeogenic genes, such as ***PEPCK1***, ***G6P***, and ***insulin-like growth factor-binding protein 1*** (***Igfbp1***) via promoting the function of PGC-1α during fasting. Insulin inhibits FOXO1 activity leading to the repression of these genes. These gluconeogenic genes contain an insulin response sequence (IRS), which FOXO1 directly binds to, and activates them in the absence of insulin. Insulin triggers the phosphorylation of FOXO1 through the phosphatidylinositol 3-kinase (PI3K)-Akt pathway. Phosphorylation inactivates FOXO1 by decreasing its binding affinity to IRS of its target genes, which results in translocation of FOXO1 from the nucleus (see reviews by Kousteni, 2012; Oh et al., 2013).

It has been shown that Foxo1 coactivates mouse Pxr (mPxr) in an insulin-PI3K-Akt-signaling dependent manner in the same way as CAR (Kodama et al., 2004). Foxo1 stimulates the Pxr-mediated transactivation of the ***CYP3A4*** gene reporter construct. Insulin as well as the constitutively active Akt abolished the coactivation of mPxr by mouse Foxo1 in CYP3A4 luciferase reporter construct activation in HepG2 cells (**Figure 3A**). At the same time PCN-activated Pxr inhibited the mouse Foxo1 binding to the IRS of human *IGFBP1* gene in EMSA assays. Based on the given data, Foxo1 and PXR were proposed to reciprocally coregulate their target genes (**Figure 3B**) (Kodama et al., 2004).

FoxA2

FoxA2, a winged-helix/forkhead transcription factor, is the key regulatory factor for the normal development of endoderm-derived organs, such as the liver, pancreas, lungs, and prostate. FoxA2 is also important factor in the glucose and lipid metabolism control. FoxA2 activates gluconeogenic genes such

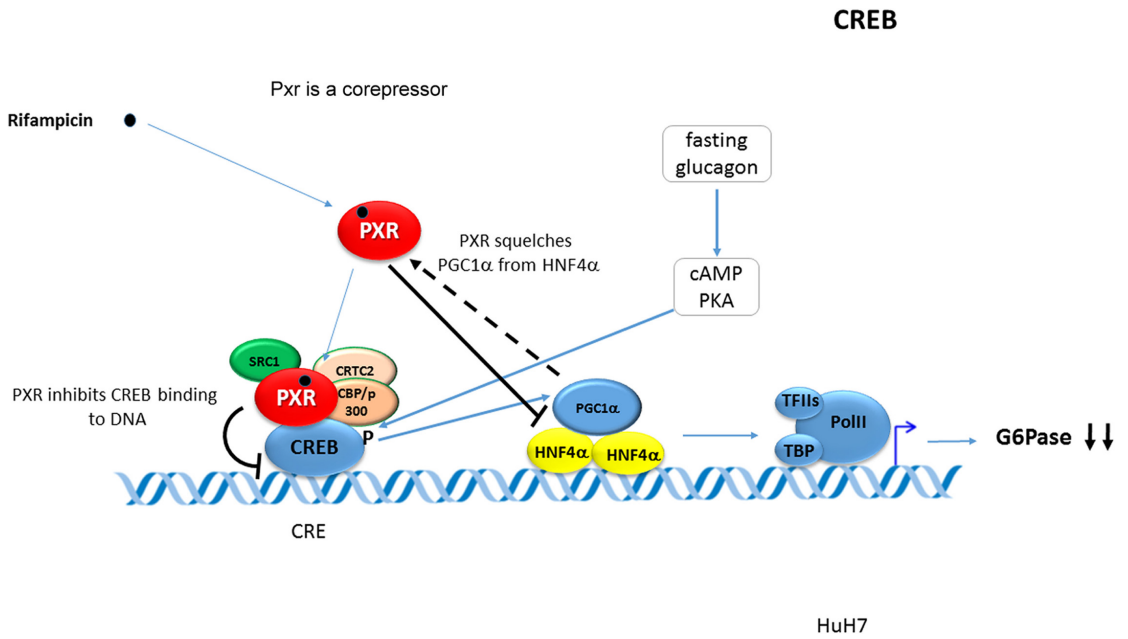

FIGURE 1 | Pregnane X Receptor represses the transcription of the G6Pase. PXR represses the transcription of the *G6Pase* gene by inhibiting the DNA-binding ability of CREB to its response element CRE. PXR directly interacts with CREB. The figure has been drawn based on data by Kodama et al. (2007). Black bold arrows indicate effects of activated PXR on the *G6Pase* gene expression. Blue arrows indicate stimulation or activation. Dashed arrow indicates squelching (competition for a common coactivator). CRE -CREB response element.

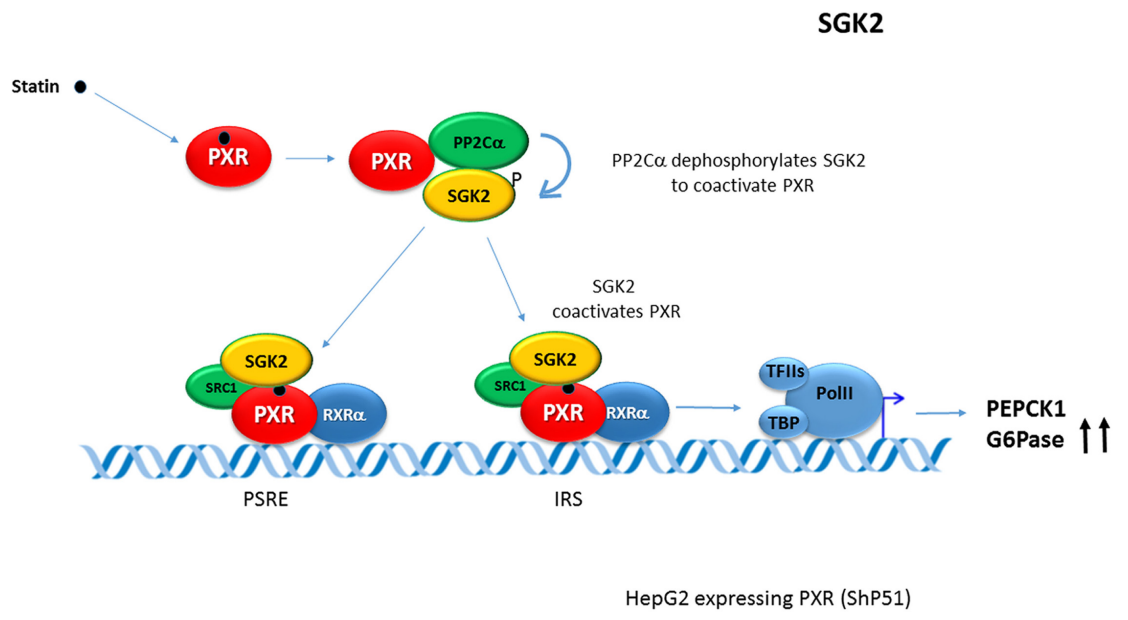

FIGURE 2 | Human-specific induction of PEPCK and G6Pase genes by PXR. In the model, serum- and glucocorticoid-regulated kinase 2 (SGK2) has been found as an essential factor for PXR-induced glucose 6-phosphatase (G6Pase) up-regulation. Non-phosphorylated SGK2 co-activates PXR-mediated *trans*-activation of gluconeogenic genes in human liver cells, thereby enhancing gluconeogenesis and glucose production (Gotoh and Negishi, 2014, 2015). In the mechanism, activated PXR scaffolds the protein phosphatase 2C (PP2C) and SGK2 to stimulate PP2C to dephosphorylate SGK2. Dephosphorylated SGK2 co-activates PXR in the *trans*-activation of these *PEPCK1* and *G6Pase* genes. At the same time, ligand-activated PXR transactivates the expression of SGK2 (Gotoh and Negishi, 2014). Blue arrows indicate the effect of the activated PXR on tested genes expression. PSRE, PXR-SGK2 response elements; IRS, insulin response sequence (IRS).

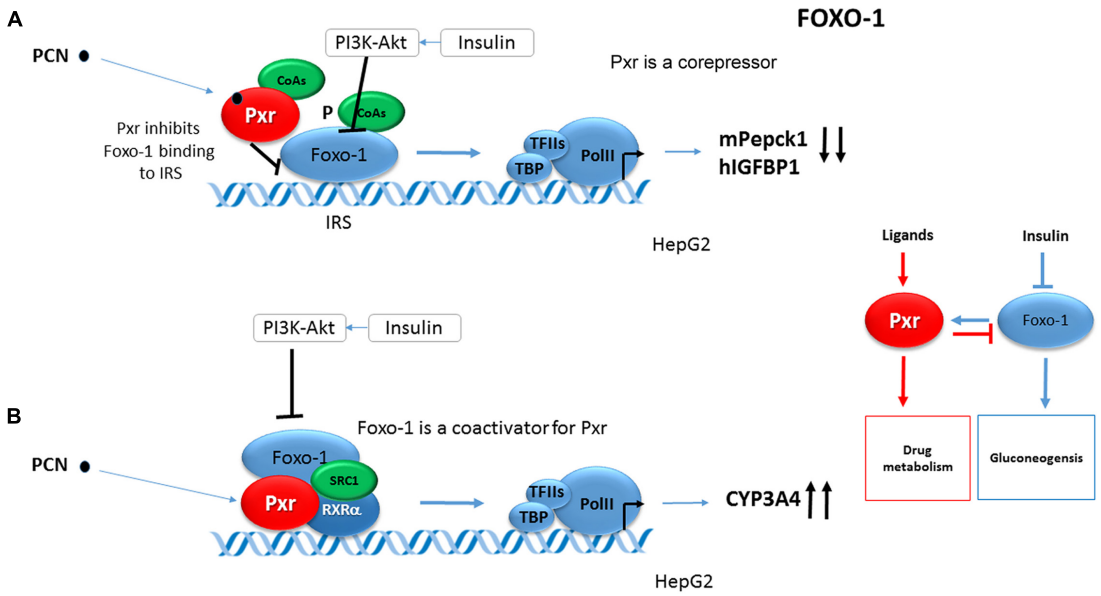

FIGURE 3 | Reciprocal crosstalk of Pxr and Foxo1. (A) Foxo1 coactivates PXR in an insulin-PI3K-Akt-signaling dependent manner (Kodama et al., 2004). Foxo1 stimulates Pxr-mediated transactivation of *CYP3A4* gene reporter construct. Insulin as well as the constitutively active Akt abolishes the coactivation of mPxr by mouse Foxo1 in *CYP3A4* gene luciferase reporter construct activation in HepG2 cells. **(B)** PCN-activated mPxr inhibits mFoxo1 binding to IRS of human *IGFBP1* gene in EMSA assay (Kodama et al., 2004). Black bold arrows indicate effects of activated Pxr on gene expression. PCN, pregnenolone 16α-carbonitrile, a rodent specific ligand of Pxr

as ***Pepck*** and ***G6p*** genes, as well as ***Cpt1a*** and ***Hmgcs2***. These enzymes are activated to increase the supply of glucose or ketone-bodies in fasting mouse liver (Wolfrum et al., 2004; Friedman and Kaestner, 2006).

Pregnane X Receptor cross-talks with the FoxA2 to repress the transcription of the *Cpt1a* and *Hmgcs2* genes. mPXR was found to directly bind to the DBD of FoxA2 to inhibit its binding to the FoxA2 response elements in *Cpt1a* and *Hmgcs2* genes promoters (Nakamura et al., 2007) (see **Figure 4**).

SREBP-1

Sterol regulatory element binding protein 1 is a lipogenic transcription factor of the basic helix-loop-helix family. Srebps are a group of transcription factors which activate an array of genes involved in the synthesis of cholesterol and triglycerides. Whereas Srebp-2 is mainly involved in cholesterol biosynthesis, Srebp-1a and Srebp1c, two isoforms encoded from different promoters, mainly activate genes involved in fatty acid and triglyceride synthesis. SREBP-1 binds to sterol regulatory elements (SREs) in promoters of lipogenic genes and induces fatty acid and triglyceride synthesis (Bakan and Laplante, 2012; Guo et al., 2014).

It was observed that SREBP-1 attenuates drug-mediated induction of hepatic CYPs. The activation of SREBP-1 by insulin or low cholesterol levels in mouse liver and primary human hepatocytes inhibits the transcriptional effects of PXR (as well as of CAR) by SREBP-1 binding to and competing with coactivators such as SRC-1 (Roth et al., 2008b). Conversely, PXR transcriptionally activates Insig-1 by binding to an enhancer sequence of the *Insig-1* gene. Insig-1 in turn reduces the nuclear protein level of the active Srebp-1 (Roth et al., 2008a) (**Figure 5**).

COMPETITION FOR COACTIVATORS AND CROSS-TALK IN PXR-MEDIATED REGULATION OF CYP450 ENZYMES INVOLVED IN CHOLESTEROL/BILE ACID METABOLISM AND IN DETOXIFICATION MECHANISMS

Pregnane X Receptor is an important factor in controlling both cholesterol and bile acid synthesis, as well as in xenobiotic and endobiotic metabolism, respectively. CYP7A1, CYP8A1, and CYP3A4 genes and their animal orthologs are major target genes of the activated PXR/Pxr in these processes.

PGC-1α

PPARgamma coactivator 1α is a key metabolic regulator of liver energy metabolism in fasting adaption and it was originally identified as a peroxisome proliferator-activated receptor-γ-interacting coactivator in brown adipose tissue. Numerous studies showed that PGC-1α is a versatile coactivator for numerous NRs implicated together in diverse biological functions including lipid and glucose metabolisms. In the liver PGC-1α has been shown to increase the HNF-4α-mediated transactivation of ***CYP7A1*** and together with FOXO1 and

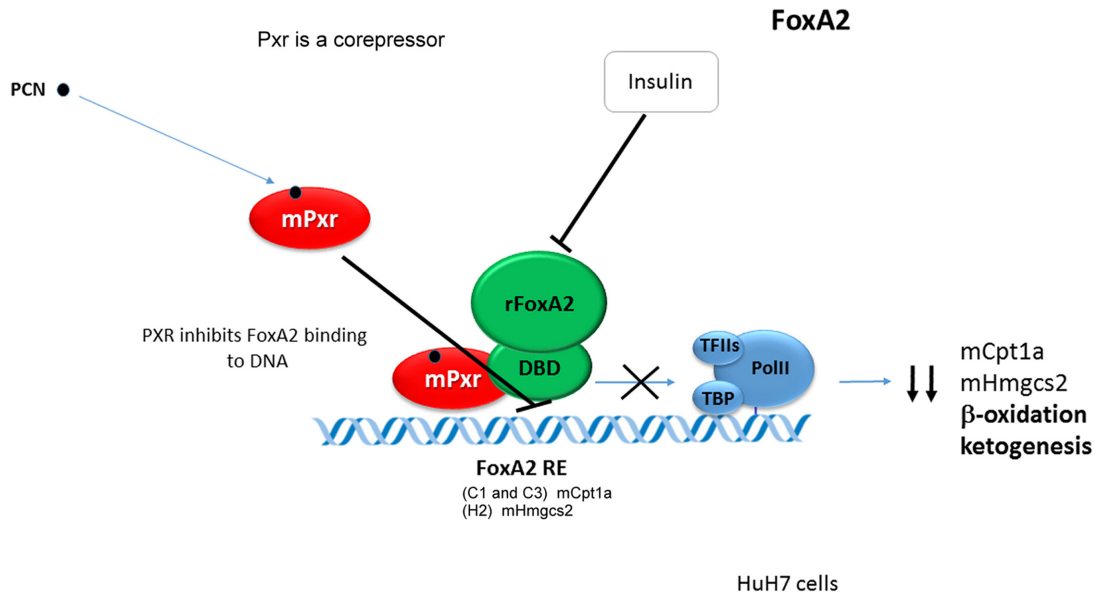

FIGURE 4 | Pregnane X Receptor cross-talks with the FoxA2 to repress the transcription of the Cpt1a and Hmgcs2 genes. Mouse Pxr directly bounds to with the DBD of FoxA2 to inhibit its binding to the FoxA2 response elements and to repress *Cpt1a* and *Hmgcs2* genes transactivation (Nakamura et al., 2007). Black bold arrows indicate effects of activated Pxr on gene expression.

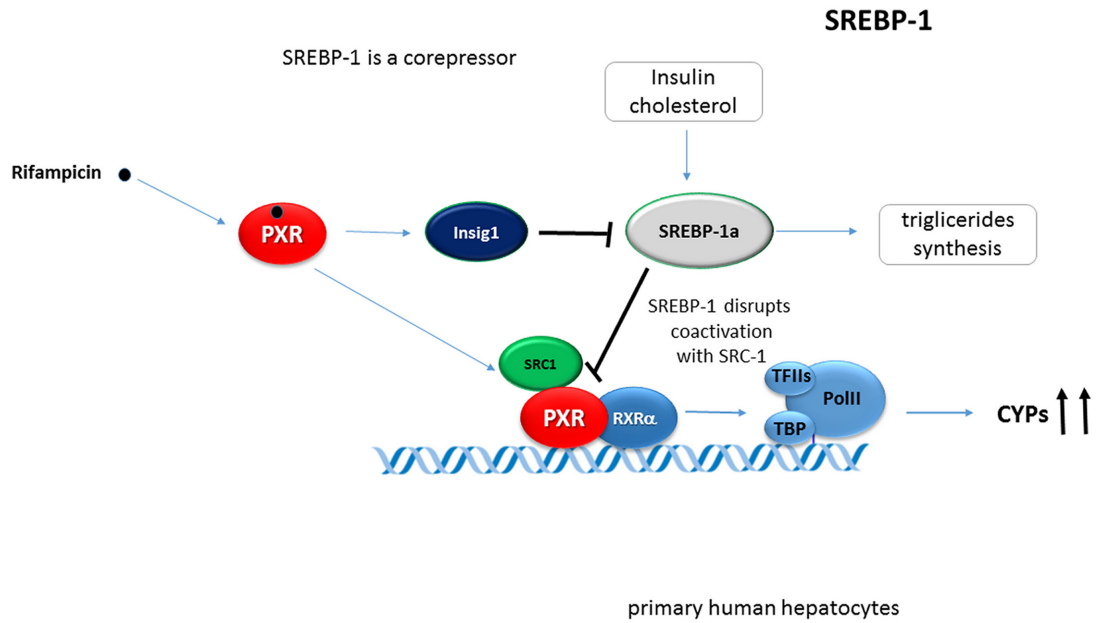

FIGURE 5 | SREBP-1 inhibits PXR-mediated transactivation of hepatic CYPs. Activation of SREBP-1 by insulin in mouse liver and primary human hepatocytes inhibits the transcriptional effect of PXR due to SREBP-1 competing with coactivators such as SRC-1 (Roth et al., 2008b). PXR transcriptionally activates Insig-1 by binding to an enhancer sequence of the *Insig-1* gene reducing nuclear protein levels of the active form of Srebp-1. SREBP1a strongly interacts with PXR. Black bold arrows indicate the effect of activated PXR on genes expression.

HNF4α controls the fasting-induced hepatic gluconeogenesis via ***PEPCK1*** and ***G6Pase*** genes. In addition, PGC-1α is involved in fatty-acid β-oxidation, ketogenesis and heme biosynthesis. In extrahepatic tissues, it controls adaptive thermogenesis, homocysteine metabolism, mitochondrial biogenesis, peripheral circadian clock, fiber-type switching in skeletal muscle and in heart development. The basal hepatic expression of PGC-1α is relatively low in fed conditions, but its expression is

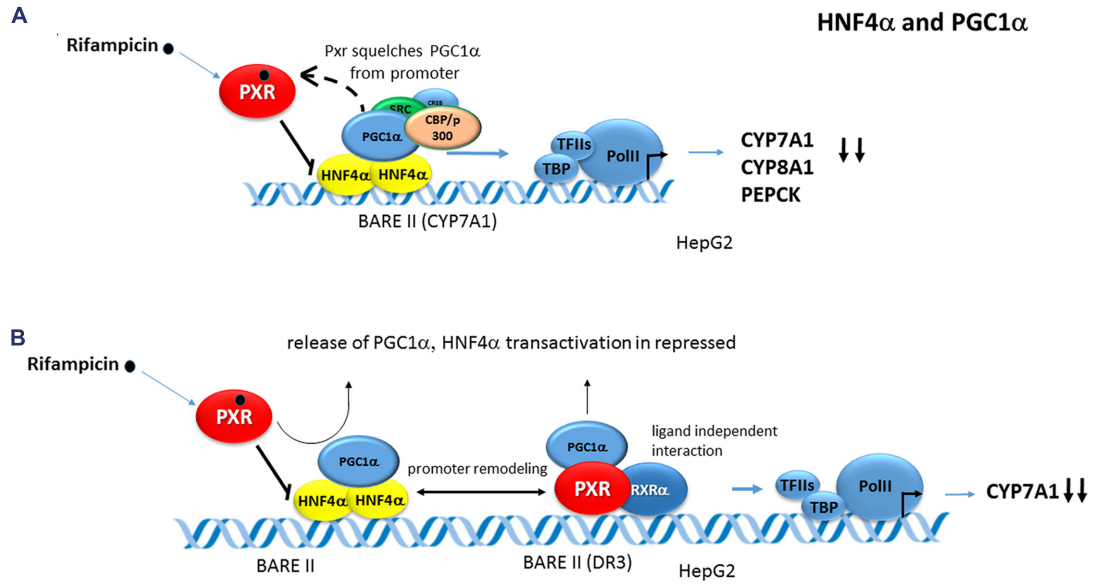

FIGURE 6 | Crosstalk of PXR with HNF4α in CYP7A1 and CYP8A1 regulation. (A) Rifampicin did not inhibit HNF4α binding to the native promoters of *CYP7A1* and *CYP8B1* (and *PEPCK1)* genes but stimulates dissociation of PGC-1α from HNF4α by competing for binding PGC-1α to HNF4α. This leads to attenuation of HNF4α-mediated transactivation and down-regulation of the genes (Bhalla et al., 2004). **(B)** In another model, activated PXR triggers interaction of PXR with HNF4α in the context of promoter resulting in chromatin remodeling and release of PGC-1α. This again results in HNF4α-controlled expression attenuation (Li and Chiang, 2005). Black bold arrows indicate the inhibitory effects of activated PXR on genes expression. Dashed arrow indicates squelching (competition for a common coactivator).

readily upregulated by fasting, glucagon and diabetes, mainly through an altered insulin–glucagon balance. PGC-1α cannot bind to DNA itself but functions as a coactivator via its LXXLL motif by interacting with a number of NRs and TFs, such as peroxisome proliferator-activated receptor alpha (PPARα), FOXO1, hepatocyte nuclear factor 4 alpha (HNF4α), mineralocorticoid (MR), glucocorticoid (GR), liver X receptors (LXR), the CAR, vitamin D receptor (VDR), or PXR. In addition, PGC-1α has a strong transcriptional activation domain at the N terminus, which interacts with several HAT complexes including CBP/p300 (Handschin, 2009; Liu and Lin, 2011).

Rifampicin, a prototype ligand for human PXR, is known to reduce hepatic bile acid levels in patients with cholestasis. Therefore, a functional cross-talk between PXR and HNF-4α, a key hepatic regulator of genes involved in bile acid synthesis including the cholesterol 7-alpha hydroxylase (***CYP7A1***) and sterol 12-alpha hydroxylase (***CYP8B1***) genes, has been studied. It was shown that PXR interacts with the coactivator PGC-1α through its C-terminal ligand binding domain in a rifampicin-dependent manner and that PGC-1α coactivates PXR transactivation (Bhalla et al., 2004; Li and Chiang, 2005, 2006; Hyrsova et al., 2016). Consistently, endogenous Pgc-1α from mouse liver extracts was found to bind to PXR, and recombinant PGC-1α directly interacts with PXR. In addition, rifampicin-dependent interaction of PXR with PGC-1α was shown in cells by co-immunoprecipitation and by intranuclear localization studies using confocal microscopy (Bhalla et al., 2004). Nevertheless, also conflicting results have been reported as regards significant rifampicin-mediated stimulation of PXR interaction with PGC-1α. No evidence of interaction was observed in GST pull-down assay and only a weak effect was seen in the mammalian two hybrid (M2H) assay (Li and Chiang, 2006).

PGC-1α at the same time coactivates and enhances the transcriptional activity of HNF-4α in the regulation of several liver-specific genes, including *CYP7A1*, *CYP8A1*, *SHP*, *OCT1 (SLC22A1)*, and *PEPCK1* (Bhalla et al., 2004; Li and Chiang, 2005, 2006; Hyrsova et al., 2016). This PGC-1α coactivation of HNF4α was reported to be suppressed by PXR ligands in an SHP-independent manner. In the case of ***CYP7A1*** and ***CYP8A1*** genes, rifampicin treatment did not inhibit HNF-4α binding to native promoters of these genes but resulted in dissociation of PGC-1α from HNF4α-formed transcription complex and subsequent gene repression (Bhalla et al., 2004). Most interestingly, the same effect was also observed in the *PEPCK1* regulation. The authors therefore proposed that PXR could be inhibitory in the process by competing for PGC-1α binding to HNF4α that dominantly controls the high hepatic expression of *CYP7A1, CYP8A1*, and *PEPCK* genes (Bhalla et al., 2004) (see also chapter HNF4α, **Figure 6A**).

A slightly different model of PXR-HNF4α crosstalk in *CYP7A1* gene repression has been proposed by Li and Chiang (Li and Chiang, 2005). In their experiments employing M2H assay and ChiP, rifampicin enhanced PXR interaction with HNF4α in the context of *CYP7A1* gene promoter, but reduced PGC-1α interaction with HNF4α resulting in overall *CYP7A1* repression (see also chapter HNF4α, **Figure 6B**).

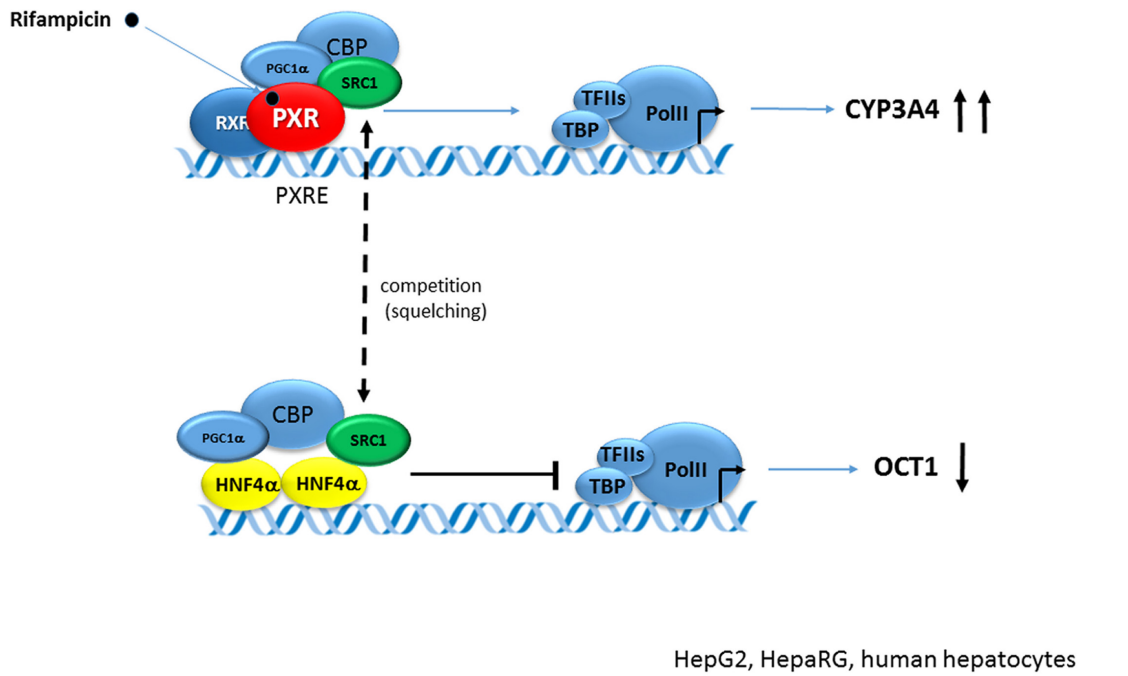

FIGURE 7 | Crosstalk of PXR and HN4α in OCT1 gene repression. Activated PXR competes and deplete ("squelches") the SRC-1 coactivator from HNF4-mediated transactivation of *OCT1* (*SLC22A1*) gene. OCT1 is dominantly regulated by HNF4α in the liver (Hyrsova et al., 2016). Dashed arrow indicates the squelching (competition for common coactivator). Black bold arrows indicate the effects of activated PXR on genes expression

In a recent study, we examined the suppressive effect of activated PXR on **OCT1** (SLC22A1) expression. OCT1 is one of the most tightly controlled genes with HNF4α transactivation. We rather observed competition for SRC-1 than PGC-1α coactivator in PXR-HNF4α interaction, thereby suggesting a gene(promoter)-specific crosstalk of PXR-HNF4α in the case of *OCT1* gene regulation (Hyrsova et al., 2016) (**Figure 7**).

HNF4α

Hepatocyte nuclear factor 4α is a master transcriptional activator for a large number of genes in hepatocytes and pancreatic cells. HNF4α belongs to the "orphan" NRs (it is classified as NR2A1), although fatty-acid CoA thioesters have been proposed as its ligands. Mutations in this gene have been associated with the monogenic autosomal dominant non-insulin-dependent diabetes mellitus type I (MODY 1, maturity onset diabetes of the young). HNF4α also belongs among the so called liver-enriched transcription factors controlling liver physiology, differentiation and drug-metabolism enzymes expression (Jover et al., 2009). By using a combination of ChiPs and promoter microarrays, 910 genes in hepatocytes and 758 genes in pancreatic islets were regulated by HNF4α in regulatory circuits together with HNF1α and HNF6 transcription factors (Odom et al., 2004). HNF4α is essential for cholesterol and glucose/energy metabolism because it is a key factor for the basal hepatic expression of *CYP7A1*, *CYP8B1*, *G6Pase*, and *PEPCK* genes, respectively.

These genes all contain functional HNF4α-binding sites in their promoter, and mutation of these sites substantially disrupt promoter activation. HNF4α binds as a homodimer mainly to DR1 response elements. Such DR1 motifs have been found in the bile acid responsive element (BARE) II region at −148 to −129 in the human *CYP7A1* gene promoter and at +198 to +227 of the human *CYP8B1* gene promoter. The promoter of human PEPCK gene also contains a functional HNF4α-binding site at −431 to −418 (Watt et al., 2003; Crestani et al., 2004).

Hepatocyte nuclear factor 4α augments the PXR/Pxr-mediated transactivation of the human ***CYP3A4*** and mouse ***Cyp3a11*** genes (Tirona et al., 2003; Li and Chiang, 2006). This enhancement was proposed through *cis*-acting HNF4α-binding sites in the proximal promoter and at the far upstream enhancer region for the *CYP3A4* gene (Tirona et al., 2003; Matsumura et al., 2004; Pavek et al., 2010) even though an HNF4α-RE independent mechanism has also been proposed (Li and Chiang, 2006). Rifampicin strongly stimulates PXR and HNF4α interaction in *CYP3A4* gene transactivation, which is further augmented by PGC-1α and SRC-1 coactivators, but inhibited by Small heterodimer partner (SHP, NR0B2) (Tirona et al., 2003; Li and Chiang, 2006). ChiPs revealed that the rifampicin-activated PXR recruits HNF4α and SRC-1 (but not PGC-1α) to the *CYP3A4* gene chromatin. In *CYP3A4* transactivation, SHP, PXR, and HNF4α have been proposed to interact and compete for binding to each other

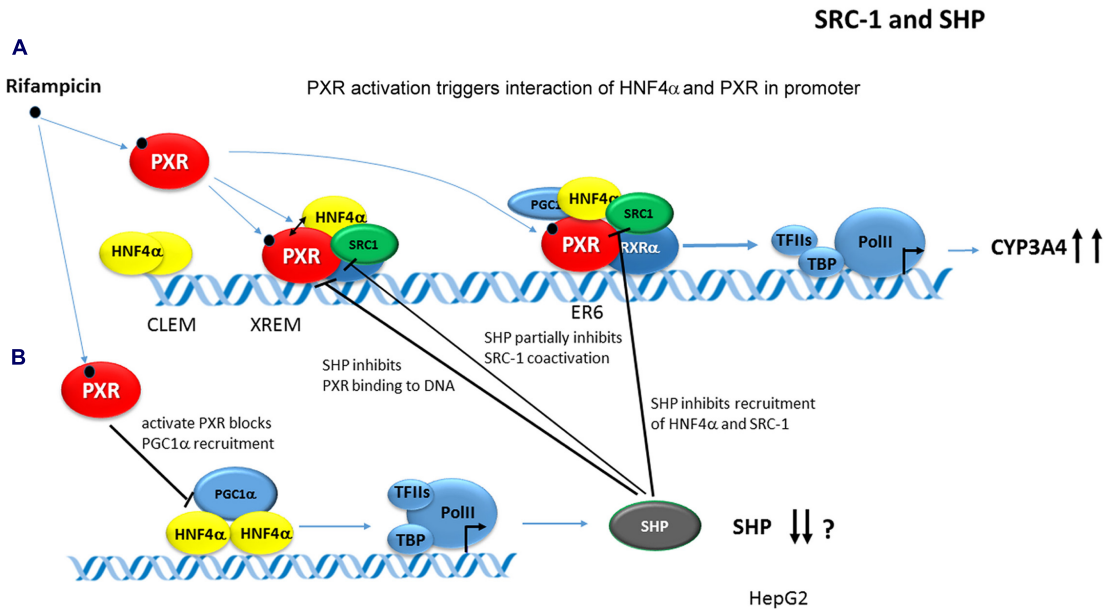

FIGURE 8 | Model of PXR-mediated transactivation of CYP3A4 gene. In the model, PXR ligands stimulate PXR/Pxr binding to DNA and interaction of PXR with HNF4α. PXR-HNF4α-SRC-1 complex transactivates *CYP3A4* gene promoter **(A)**. PXR at the same time trans-represses *SHP* gene expression. SHP interferes with PXR-HNF4α-SRC-1 coactivation and with PXR-DNA interaction **(B)** (Ourlin et al., 2003; Li and Chiang, 2006).

(Li and Chiang, 2006). Concomitantly, PXR has been proposed to inhibit SHP promoter activity and to repress *SHP* gene transcription by disrupting PGC-1α coactivation of HNF4α (Li and Chiang, 2006) (**Figure 8**).

In the case of ***CYP7A1*** gene promoter, HNF4α directly binds with PXR and both NRs are strongly co-activated by PGC-1α (Li and Chiang, 2005, 2006). With respect to PXR-mediated *CYP7A1* gene repression, two theories regarding the mechanism have been postulated based on the PXR-HNF4α-PGC-1α crosstalk. Bhalla et al. (2004; Dr. Jongsook Kim Kemper's group) proposed that PXR competes for the binding of PGC-1α with HNF4α in *CYP7A1* gene regulation and squelches PGC-1α from HNF4α/DNA complex (**Figure 6A**). The group of Dr. Chiang proposed that the activation of PXR by rifampicin promotes PXR interaction with HNF4α in the *CYP7A1* gene promoter, but blocks PGC-1α interaction mainly with HNF4α and to a lesser extend with PXR. This results in the inhibition of *CYP7A1* gene expression dominantly transactivated by HNF4α-PGC-1α (Li and Chiang, 2005) (**Figure 6B**). The latter authors also argue that "squelching" of the common coactivator PGC-1α is an unlikely mechanism since PGC-1α mostly interacts with PXR in a ligand-independent manner.

Pregnane X Receptor activation by rifampicin was also found to repress the estrogen sulfotransferase 1E1 (***SULT1E1***) gene. Mechanistic studies showed that activated PXR displaces HNF4α bound to the PXR-responsive enhancer of *SULT1E1* gene resulting in promoter remodeling, histone 3 deacetylation and repressed expression (Kodama et al., 2011).

SRC-1

Steroid receptor coactivator 1 is a well-known coactivator with the conserved N-terminal basic helix—loop—helix-Per/ARNT/Sim (bHLH-PAS) domain, a central NR interaction domain (RID) with three LXXLL motifs, and two activation domains (AD1 and AD2) at the C-terminus. SRC-1 interacts with many NRs including PXR, LXRα, CAR, FXR, HNF4α, GR etc. It was shown that PXR and SRC-1 interact in the absence of a PXR ligand and the interaction is strengthened by rifampicin (Saini et al., 2005; Li and Chiang, 2006; Rulcova et al., 2010; Krausova et al., 2011; Hyrsova et al., 2016), although SRC-1 was proposed to bind to PXR much weaker that PGC-1α (Li and Chiang, 2005).

Interesting results have been obtained with *Pxr*-null, *Car*-null and double-KO mice. In *Pxr*-null mice, *Car* target genes *Mrp2*, *Mrp3*, *Ugt1a1*, *Oatp4*, and *Gsta2* were up-regulated. A detailed investigation has shown that unliganded Pxr may attract coactivators such as Src-1 from Car to dominate over Car and to control the constitutive activity of Car in detoxification enzymes regulation (Saini et al., 2005). Based on this, the ligand-free Pxr can suppress both the constitutive and ligand-induced activity of Car by competing for common coactivator Src-1 in a target gene specific manner. This finding also highlights a regulatory hierarchy of Pxr/Car (PXR/CAR) cross-talk in the regulation of common target detoxifying enzymes (Saini et al., 2005).

The antidiabetic drug metformin was reported to suppress PXR-regulated transactivation of *CYP3A4* gene (Krausova et al., 2011). Metformin did not affect PXR expression, instead it disturbed PXR interaction with SRC-1 (Krausova et al., 2011).

Since there is some analogy with the regulation of PXR and PGC-1α interaction by metformin-induced SIRT1, we can speculate that SIRT1 can play a role in the process (Hakkola et al., 2016).

SHP

The small (or short) heterodimer partner (SHP) is a NR (NR subfamily 0, group B, member 2) encoded by the *NR0B2* gene in humans. SHP is unusual as a NR in that it lacks a DNA binding domain. No endogenous ligand has been found, therefore SHP belongs to the "orphan" subfamily. SHP executes its regulatory function through protein–protein interactions as a coreppresor of numerous NRs (including PXR, CAR, LXRs, PPARs, HNF4α, LRH-1, GR, TRβ, RARα, FXR, ERs, ERRs etc.), TFs (such as FOXO1, C/EBPα, NF-κB etc.) or kinases (such as C-jun or Smad3) (Zhang et al., 2011). SHP represses the transcriptional activities of its target proteins by utilizing two functional LXXLL-related motifs in the LBD domain. The binding of SHP to TFs/NRs either competes or dissociates coactivators on the AF-1/2 domains from the receptors. SHP is thus involved in bile acid, cholesterol, triglyceride, glucose, and drug metabolism. SHP mainly plays important role in the negative regulation of the conversion of cholesterol to bile acids via FXR, as well in regulating the expression of genes playing roles in bile acid transport (BSEP, NTCP), lipid metabolism (SREBP1C), and gluconeogenesis (PEPCK, G6Pase) (Zhang et al., 2011; Zou et al., 2015).

It was shown that SHP inhibits PXR-mediated transactivation of the *CYP3A4* gene by interfering with PXR binding to promoter response elements (Ourlin et al., 2003; Pavek et al., 2012; Smutny et al., 2014). However, this finding has been questioned by Li and Chiang (Li and Chiang, 2006). Instead, they proposed that HNF4α and SHP compete for binding to PXR in *CYP3A4* gene transactivation after rifampicin treatment. In addition, SHP partially blocks PXR-SRC-1 (but not PXR-PGC-1α) interaction in *CYP3A4* gene regulation (Li and Chiang, 2006). Interestingly, rifampicin strongly enhanced PXR−SHP interaction in M2H and GST pull-down assays (Li and Chiang, 2006). In addition, it was shown that the activated PXR *trans*-represses SHP expression, which is dominantly controlled by HNF4α-PGC-1α regulation, by blocking PGC-1α recruitment to *SHP* gene promotor chromatin (Li and Chiang, 2006). By this mechanism, PXR may concomitantly inhibit SHP gene transcription and maximizes the PXR-mediated induction of the *CYP3A4* gene in human livers (Li and Chiang, 2006) (see **Figure 8**).

SIRT1

SIRT1 (silent mating type information regulation 2 homolog 1) also named as NAD^+-dependent deacetylase sirtuin-1, is a protein that is encoded by the SIRT1 gene in humans. SIRT1 is a deacetylase protein which is both catalytically activated by increased NAD^+ level and also transcriptionally induced during fasting. SIRT1, a mammalian ortholog of the yeast Sir2 protein, belongs into the class III of HDAC that has been reported to deacetylate many target proteins including some NRs, either activating or repressing their functions. Sirtuin 1 is a key metabolic/energy sensor and mediates homeostatic responses to caloric restriction. Accumulating evidence indicates that Sirtuin 1 is a master regulator that controls hepatic lipid metabolism. During fasting conditions, SIRT1 deacetylates and alters the expression and the activities of key transcriptional regulators involved in hepatic lipogenesis, β-oxidation, and cholesterol/bile acid metabolism (Moore et al., 2012; Kemper et al., 2013). In addition, SIRT1 deacetylates PGC-1α and thus enhances its ability to coactivate gluconeogenic genes (Rodgers et al., 2005).

SIRT1 is one of two major regulators of hepatic energy homeostasis (together with PGC-1α) involved in PXR signaling. SIRT1 binds and deacetylates PXR after the ligand-dependent activation of PXR (Biswas et al., 2011; Buler et al., 2011). Interestingly, Buler et al. (2011) found PGC-1α-mediated regulation of PXR expression. SIRT1 was also shown to interfere with PCN-induced Pxr coactivation by Pgc-1α in *Cyp3a11* gene transactivation (**Figure 9**). Thus SIRT1 and PGC-1α fasting-activated pathways differentially affect PXR/Pxr-mediated function.

RXRα

Pregnane X Receptor heterodimerizes with the NR retinoid X receptor α (RXRα, NR2B1), encoded by the *RXRA* gene (Blumberg et al., 1998; Kliewer et al., 1998). Similarly, other NRs such as CAR, FXR, LXR, and PPARs form heterodimers with hetero-oligomeric partner RXRα. Therefore, it is logical to suppose crosstalk due to the competition for the common heteropartner. However, no NR−NR interactions have been reported at the level of RXR crosstalk between these receptors in the literature. It was shown that ligand-activated LXRα transactivates *CYP3A4* gene expression but suppresses the PXR-dependent transcription of *CYP3A4* through known PXR-responsive elements dNR1 and eNR3A4. However, the amount of RXRα was not found as the limiting factor in *CYP3A4* transcription after simultaneous activation of PXR and LXRα (Watanabe et al., 2013). We can thus speculate that there is sufficiently high amount of RXRα in hepatocytes to sustain parallel heterodimerization with several activated NRs. We should also take into account that PXR forms functional homodimer, which again suggests that RXRα amount may not be a limiting factor for PXR activity (Noble et al., 2006).

Some retinoids and rexinoids, ligands of RXRα, significantly induce the PXR/RXR-mediated transactivation (Wang et al., 2006; Pettersson et al., 2008). Interestingly, rexinoids can antagonize PXR activation by rifampicin due to the reduced binding of PXR/RXR to PXR response elements. In addition, rexinoids, bexarotene (LGD1069), and LG100268 can stimulate protein degradation of both PXR and RXR (Pettersson et al., 2008). Therefore, ligand-dependent PXR-RXR interactions may have an effect on PXR target genes expression.

NF-κB

Proinflammatory stimuli down-regulate CYP expression and drug-metabolizing activities in the liver.

NF-κB is the key regulator of inflammation and immune responses. The NF-κB family comprises five members, namely p65 or Rel A, Rel B, c-Rel, p50, and p52. NF-κB normally resides in the cytoplasm bound to the protein inhibitor of NF-κB (IκB).

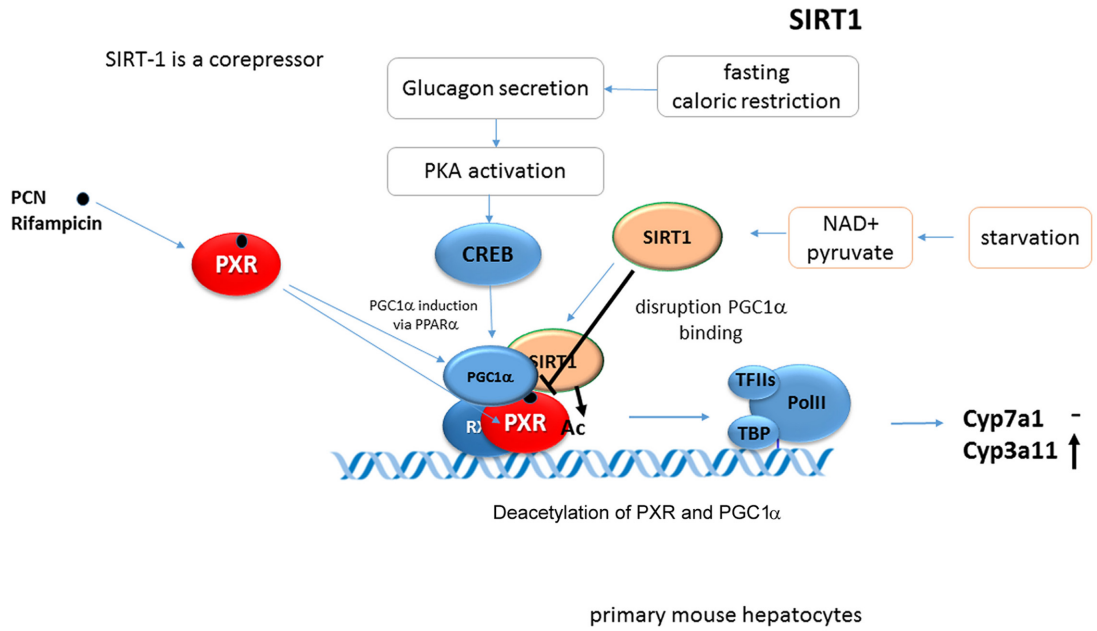

FIGURE 9 | SIRT1 represses Pxr-PGC-1α coactivation in Cyp3a11 gene regulation. SIRT1 binds to PXR and deacetylate PXR after its ligand-dependent activation. Sirt1 interferes with Pxr-Pgc-1α coactivation in *Cyp3a11* gene regulation (Biswas et al., 2011; Buler et al., 2011).

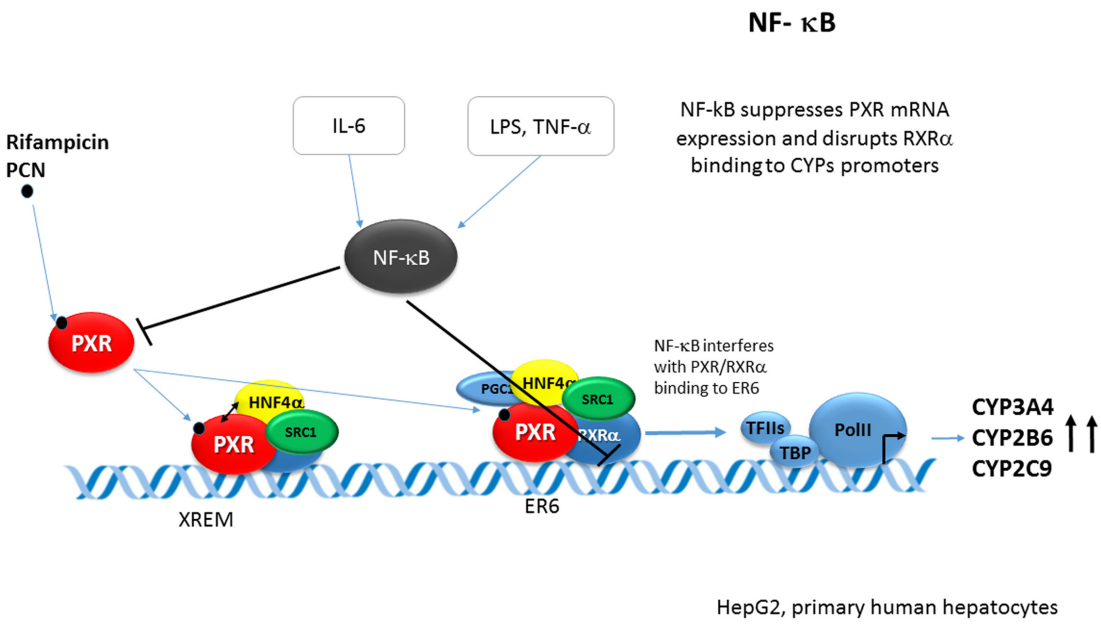

FIGURE 10 | Crosstalk of NF-κB p65 and PXR-RXRα in PXR-mediated CYPs regulation. Proinflammatory cytokine interleukin 6 (IL-6) down-regulates PXR mRNA in primary human hepatocytes. In addition, activation of NF-κB by either LPS or TNF-α leads to PXR suppression through interaction of NF-κB p65 and the PXR-RXRα heterodimer. NF-κB p65 directly binds to RXRα DBD and thus disrupts the association of the PXR/RXRα complex with the PXR responsive sequence ER6 of the *CYP3A4* gene (Pascussi et al., 2000; Gu et al., 2006).

Activating signals, such as pro-inflammatory cytokines lead to phosphorylation and degradation of IκB, thus allowing NF-κB to translocate to the nucleus. In the nucleus, NF-κB directly regulates the transactivation and expression of its target genes.

Signaling mediated by lipopolysaccharide (LPS) and cytokines, such as IL-1 and TNFα, leads to the activation of NF-κB. Activated NF-κB was shown to repress PXR activation and the PXR-mediated induction of several CYPs. Pascussi et al.

first have shown that the proinflammatory cytokine interleukin 6 (IL-6) down-regulates PXR mRNA in primary human hepatocytes and inhibits the rifampicin-mediated induction of the PXR target CYPs genes such as *CYP2B6, CYP2C8/9,* and *CYP3A4*. However, PXR activity itself was not affected by the IL-6 in reporter assays (Pascussi et al., 2000).

Gu et al. (2006) reported that the activation of NF-κB by either LPS or TNF-α leads to PXR suppression through the interaction of NF-κB p65 and PXR-RXRα heterodimer. NF-κB p65 disrupted the association of the PXR/RXRα complex with the PXR responsive sequences ER6 in electrophoretic mobility shift and ChiPs. This interference has been explained by the direct binding of NF-κB p65 to the RXRα DBD in the GST pull-down assay (**Figure 10**).

Zhou et al. (2006) further corroborated the NF-κB-PXR crosstalk and reported that NF-κB activation inhibits hPXR activation, and that inhibition of NF-κB potentiates PXR activation. In addition, they showed that NF-κB target genes are up-regulated and small bowel inflammation is significantly increased in $Pxr^{-/-}$ mice.

In addition to NF-κB signaling, both protein kinase C and A (PKC and PKA) signaling is involved in repressing *CYP3A* gene expression by affecting the PXR activity during inflammation. Mechanistically, posttranslational modifications of PXR by the kinase signaling are involved. I refer to other reviews for more details (Smutny et al., 2013; Oladimeji et al., 2016).

Thus, the reciprocal crosstalk between PXR and NF-κB is the proposed mechanism for the anti-inflammatory function of PXR and down-regulation of PXR target CYPs during inflammation.

DISCUSSION AND CONCLUSION

In the review, I comprehensively summarize our current knowledge about the molecular mechanisms of: (i) competition for coactivator binding to PXR, (ii) coactivation of PXR by other transcription factors or NRs leading to NRs cross-talk, (iii) signaling and posttranslational modification of PXR that impairs its coactivation and (iv) *trans*-repression of TFs and NRs by PXR. All these processes form the NR-signaling network that enables at the same time sensing to caloric restriction or to toxic injury. Some of the mechanisms confirm our view on the hierarchy of xenobiotic and endobiotic metabolism regulation and propose novel targets for drug development. However, considering the number of NRs, coactivators, corepressors and signaling pathways that orchestrate transcriptome and proteome regulation, it is clear that we have discovered only a minor part of the network.

Pregnane X Receptor plays both positive and negative roles in regulating numerous genes involved in homeostasis and detoxification. Indeed, the latest report shows that PXR down-regulates expression of twice as many genes than it induces in primary human hepatocytes (Kandel et al., 2016). According to current knowledge, *SULT1E1*, *SHP*, *HNF4α*, *OCT1*, and *FOXO1* genes are the only candidates that have been reported as repressed genes of activated PXR in detailed mechanistic studies (Li and Chiang, 2006; Zhou et al., 2006; Kodama et al., 2011; Kodama et al., 2015). In the case of these genes, however, protein−protein interactions of coactivators with NRs or TFs take place and no direct *trans*-repression via a *cis*-acting PXR repression element has been reported so far.

Therefore, a better understanding of the coactivator/corepressor relationships in PXR-mediated gene regulation may help us do delineate the regulation of other genes repressed by activated PXR in PXR expressing tissues.

AUTHOR CONTRIBUTIONS

The author confirms being the sole contributor of this work and approved it for publication.

FUNDING

This work was funded by the Czech Scientific Agency (GACR 303/12/G163 to PP).

REFERENCES

Bakan, I., and Laplante, M. (2012). Connecting mTORC1 signaling to SREBP-1 activation. *Curr. Opin. Lipidol.* 23, 226–234. doi: 10.1097/MOL.0b013e328352dd03

Bertilsson, G., Heidrich, J., Svensson, K., Asman, M., Jendeberg, L., Sydow-Backman, M., et al. (1998). Identification of a human nuclear receptor defines a new signaling pathway for CYP3A induction. *Proc. Natl. Acad. Sci. U.S.A.* 95, 12208–12213. doi: 10.1073/pnas.95.21.12208

Bhalla, S., Ozalp, C., Fang, S., Xiang, L., and Kemper, J. K. (2004). Ligand-activated pregnane X receptor interferes with HNF-4 signaling by targeting a common coactivator PGC-1alpha. Functional implications in hepatic cholesterol and glucose metabolism. *J. Biol. Chem.* 279, 45139–45147. doi: 10.1074/jbc.M405423200

Biswas, A., Pasquel, D., Tyagi, R. K., and Mani, S. (2011). Acetylation of pregnane X receptor protein determines selective function independent of ligand activation. *Biochem. Biophys. Res. Commun.* 406, 371–376. doi: 10.1016/j.bbrc.2011.02.048

Blumberg, B., Sabbagh, W. Jr., Juguilon, H., Bolado, J. Jr., van Meter, C. M., Ong, E. S., et al. (1998). SXR, a novel steroid and xenobiotic-sensing nuclear receptor. *Genes Dev.* 12, 3195–3205. doi: 10.1101/gad.12.20.3195

Buler, M., Aatsinki, S. M., Skoumal, R., and Hakkola, J. (2011). Energy sensing factors PGC-1alpha and SIRT1 modulate PXR expression and function. *Biochem. Pharmacol.* 82, 2008–2015. doi: 10.1016/j.bcp.2011.09.006

Chrencik, J. E., Orans, J., Moore, L. B., Xue, Y., Peng, L., Collins, J. L., et al. (2005). Structural disorder in the complex of human pregnane X receptor and the macrolide antibiotic rifampicin. *Mol. Endocrinol.* 19, 1125–1134. doi: 10.1210/me.2004-0346

Crestani, M., De Fabiani, E., Caruso, D., Mitro, N., Gilardi, F., Vigil Chacon, A. B., et al. (2004). LXR (liver X receptor) and HNF-4 (hepatocyte nuclear factor-4): key regulators in reverse cholesterol transport. *Biochem. Soc. Trans.* 32, 92–96. doi: 10.1042/bst0320092

di Masi, A., De Marinis, E., Ascenzi, P., and Marino, M. (2009). Nuclear receptors CAR and PXR: molecular, functional, and biomedical aspects. *Mol. Aspects Med.* 30, 297–343. doi: 10.1016/j.mam.2009.04.002

Ding, X., and Staudinger, J. L. (2005a). Induction of drug metabolism by forskolin: the role of the pregnane X receptor and the protein kinase a signal transduction pathway. *J. Pharmacol. Exp. Ther.* 312, 849–856. doi: 10.1124/jpet.104.076331

Ding, X., and Staudinger, J. L. (2005b). Repression of PXR-mediated induction of hepatic CYP3A gene expression by protein kinase C. *Biochem. Pharmacol.* 69, 867–873. doi: 10.1016/j.bcp.2004.11.025

Friedman, J. R., and Kaestner, K. H. (2006). The foxa family of transcription factors in development and metabolism. *Cell Mol. Life Sci.* 63, 2317–2328. doi: 10.1007/s00018-006-6095-6

Gao, J., and Xie, W. (2012). Targeting xenobiotic receptors PXR and CAR for metabolic diseases. *Trends Pharmacol. Sci.* 33, 552–558. doi: 10.1016/j.tips.2012.07.003

Gotoh, S., and Negishi, M. (2014). Serum- and glucocorticoid-regulated kinase 2 determines drug-activated pregnane X receptor to induce gluconeogenesis in human liver cells. *J. Pharmacol. Exp. Ther.* 348, 131–140. doi: 10.1124/jpet.113.209379

Gotoh, S., and Negishi, M. (2015). Statin-activated nuclear receptor PXR promotes SGK2 dephosphorylation by scaffolding PP2C to induce hepatic gluconeogenesis. *Sci. Rep.* 5:14076. doi: 10.1038/srep14076

Gu, X., Ke, S., Liu, D., Sheng, T., Thomas, P. E., Rabson, A. B., et al. (2006). Role of NF-kappaB in regulation of PXR-mediated gene expression: a mechanism for the suppression of cytochrome P-450 3A4 by proinflammatory agents. *J. Biol. Chem.* 281, 17882–17889. doi: 10.1074/jbc.M601302200

Guo, D., Bell, E. H., Mischel, P., and Chakravarti, A. (2014). Targeting SREBP-1-driven lipid metabolism to treat cancer. *Curr. Pharm. Des.* 20, 2619–2626. doi: 10.2174/13816128113199990486

Hakkola, J., Rysa, J., and Hukkanen, J. (2016). Regulation of hepatic energy metabolism by the nuclear receptor PXR. *Biochim. Biophys. Acta* 1859, 1072–1082. doi: 10.1016/j.bbagrm.2016.03.012

Handschin, C. (2009). The biology of PGC-1alpha and its therapeutic potential. *Trends Pharmacol. Sci.* 30, 322–329. doi: 10.1016/j.tips.2009.03.006

Hirooka-Masui, K., Lesmana, R., Iwasaki, T., Xu, M., Hayasaka, K., Haraguchi, M., et al. (2013). Interaction of silencing mediator for retinoid and thyroid receptors with steroid and xenobiotic receptor on multidrug resistance 1 promoter. *Life Sci.* 92, 911–915. doi: 10.1016/j.lfs.2013.03.007

Hustert, E., Zibat, A., Presecan-Siedel, E., Eiselt, R., Mueller, R., Fuss, C., et al. (2001). Natural protein variants of pregnane X receptor with altered transactivation activity toward CYP3A4. *Drug Metab. Dispos.* 29, 1454–1459.

Hyrsova, L., Smutny, T., Carazo, A., Moravcik, S., Mandikova, J., Trejtnar, F., et al. (2016). The pregnane X receptor down-regulates organic cation transporter 1 (SLC22A1) in human hepatocytes by competing for ("squelching") SRC-1 coactivator. *Br. J. Pharmacol.* 173, 1703–1715. doi: 10.1111/bph.13472

Johnson, D. R., Li, C. W., Chen, L. Y., Ghosh, J. C., and Chen, J. D. (2006). Regulation and binding of pregnane X receptor by nuclear receptor corepressor silencing mediator of retinoid and thyroid hormone receptors (SMRT). *Mol. Pharmacol.* 69, 99–108.

Jover, R., Moya, M., and Gomez-Lechon, M. J. (2009). Transcriptional regulation of cytochrome p450 genes by the nuclear receptor hepatocyte nuclear factor 4-alpha. *Curr. Drug Metab.* 10, 508–519. doi: 10.2174/138920009788898000

Kandel, B. A., Thomas, M., Winter, S., Damm, G., Seehofer, D., Burk, O., et al. (2016). Genomewide comparison of the inducible transcriptomes of nuclear receptors CAR, PXR and PPARalpha in primary human hepatocytes. *Biochim. Biophys. Acta* 1859, 1218–1227. doi: 10.1016/j.bbagrm.2016.03.007

Kawana, K., Ikuta, T., Kobayashi, Y., Gotoh, O., Takeda, K., and Kawajiri, K. (2003). Molecular mechanism of nuclear translocation of an orphan nuclear receptor. *SXR. Mol. Pharmacol.* 63, 524–531. doi: 10.1124/mol.63.3.524

Kemper, J. K., Choi, S. E., and Kim, D. H. (2013). Sirtuin 1 deacetylase: a key regulator of hepatic lipid metabolism. *Vitam. Horm.* 91, 385–404. doi: 10.1016/B978-0-12-407766-9.00016-X

Kliewer, S. A., Goodwin, B., and Willson, T. M. (2002). The nuclear pregnane X receptor: a key regulator of xenobiotic metabolism. *Endocr. Rev.* 23, 687–702. doi: 10.1210/er.2001-0038

Kliewer, S. A., Moore, J. T., Wade, L., Staudinger, J. L., Watson, M. A., Jones, S. A., et al. (1998). An orphan nuclear receptor activated by pregnanes defines a novel steroid signaling pathway. *Cell* 92, 73–82. doi: 10.1016/S0092-8674(00)80900-9

Kodama, S., Hosseinpour, F., Goldstein, J. A., and Negishi, M. (2011). Liganded pregnane X receptor represses the human sulfotransferase SULT1E1 promoter through disrupting its chromatin structure. *Nucleic Acids Res.* 39, 8392–8403. doi: 10.1093/nar/gkr458

Kodama, S., Koike, C., Negishi, M., and Yamamoto, Y. (2004). Nuclear receptors CAR and PXR cross talk with FOXO1 to regulate genes that encode drug-metabolizing and gluconeogenic enzymes. *Mol. Cell. Biol.* 24, 7931–7940. doi: 10.1128/MCB.24.18.7931-7940.2004

Kodama, S., Moore, R., Yamamoto, Y., and Negishi, M. (2007). Human nuclear pregnane X receptor cross-talk with CREB to repress cAMP activation of the glucose-6-phosphatase gene. *Biochem. J.* 407, 373–381. doi: 10.1042/BJ20070481

Kodama, S., Yamazaki, Y., and Negishi, M. (2015). Pregnane X receptor represses HNF4alpha gene to Induce Insulin-Like Growth Factor-Binding Protein IGFBP1 that alters morphology of and migrates HepG2 cells. *Mol. Pharmacol.* 88, 746–757. doi: 10.1124/mol.115.099341

Konno, Y., Kodama, S., Moore, R., Kamiya, N., and Negishi, M. (2009). Nuclear xenobiotic receptor pregnane X receptor locks corepressor silencing mediator for retinoid and thyroid hormone receptors (SMRT) onto the CYP24A1 promoter to attenuate vitamin D3 activation. *Mol. Pharmacol.* 75, 265–271. doi: 10.1124/mol.108.051904

Kousteni, S. (2012). FoxO1, the transcriptional chief of staff of energy metabolism. *Bone* 50, 437–443. doi: 10.1016/j.bone.2011.06.034

Krausova, L., Stejskalova, L., Wang, H., Vrzal, R., Dvorak, Z., Mani, S., et al. (2011). Metformin suppresses pregnane X receptor (PXR)-regulated transactivation of CYP3A4 gene. *Biochem. Pharmacol.* 82, 1771–1780. doi: 10.1016/j.bcp.2011.08.023

Lazar, M. A. (2003). Nuclear receptor corepressors. *Nucl. Recept. Signal.* 1, e001. doi: 10.1621/nrs.01001

Lehmann, J. M., McKee, D. D., Watson, M. A., Willson, T. M., Moore, J. T., and Kliewer, S. A. (1998). The human orphan nuclear receptor PXR is activated by compounds that regulate CYP3A4 gene expression and cause drug interactions. *J. Clin. Invest.* 102, 1016–1023. doi: 10.1172/JCI3703

Li, C. W., Dinh, G. K., and Chen, J. D. (2009). Preferential physical and functional interaction of pregnane X receptor with the SMRTalpha isoform. *Mol. Pharmacol.* 75, 363–373. doi: 10.1124/mol.108.047845

Li, T., and Chiang, J. Y. (2005). Mechanism of rifampicin and pregnane X receptor inhibition of human cholesterol 7 alpha-hydroxylase gene transcription. *Am. J. Physiol. Gastrointest. Liver Physiol.* 288, G74–G84. doi: 10.1152/ajpgi.00258.2004

Li, T., and Chiang, J. Y. (2006). Rifampicin induction of CYP3A4 requires pregnane X receptor cross talk with hepatocyte nuclear factor 4alpha and coactivators, and suppression of small heterodimer partner gene expression. *Drug Metab. Dispos.* 34, 756–764. doi: 10.1124/dmd.105.007575

Liu, C., and Lin, J. D. (2011). PGC-1 coactivators in the control of energy metabolism. *Acta Biochim. Biophys Sin. (Shanghai)* 43, 248–257. doi: 10.1093/abbs/gmr007

Mani, S., Huang, H., Sundarababu, S., Liu, W., Kalpana, G., Smith, A. B., et al. (2005). Activation of the steroid and xenobiotic receptor (human pregnane X receptor) by nontaxane microtubule-stabilizing agents. *Clin. Cancer Res.* 11, 6359–6369. doi: 10.1158/1078-0432.CCR-05-0252

Masuyama, H., Hiramatsu, Y., Kunitomi, M., Kudo, T., and MacDonald, P. N. (2000). Endocrine disrupting chemicals, phthalic acid and nonylphenol, activate Pregnane X receptor-mediated transcription. *Mol. Endocrinol.* 14, 421–428. doi: 10.1210/mend.14.3.0424

Matsumura, K., Saito, T., Takahashi, Y., Ozeki, T., Kiyotani, K., Fujieda, M., et al. (2004). Identification of a novel polymorphic enhancer of the human CYP3A4 gene. *Mol. Pharmacol.* 65, 326–334. doi: 10.1124/mol.65.2.326

Miao, J., Fang, S., Bae, Y., and Kemper, J. K. (2006). Functional inhibitory cross-talk between constitutive androstane receptor and hepatic nuclear factor-4 in hepatic lipid/glucose metabolism is mediated by competition for binding to the DR1 motif and to the common coactivators. GRIP-1 and PGC-1alpha. *J. Biol. Chem.* 281, 14537–14546. doi: 10.1074/jbc.M510713200

Min, G., Kim, H., Bae, Y., Petz, L., and Kemper, J. K. (2002). Inhibitory cross-talk between estrogen receptor (ER) and constitutively activated androstane receptor (CAR). CAR inhibits ER-mediated signaling pathway by squelching p160 coactivators. *J. Biol. Chem.* 277, 34626–34633. doi: 10.1074/jbc.M205239200

Moore, D. D., Kato, S., Xie, W., Mangelsdorf, D. J., Schmidt, D. R., Xiao, R., et al. (2006). International Union of Pharmacology. LXII. The NR1H and NR1I

receptors: constitutive androstane receptor, pregnene X receptor, farnesoid X receptor alpha, farnesoid X receptor beta, liver X receptor alpha, liver X receptor beta, and vitamin D receptor. *Pharmacol. Rev.* 58, 742–759. doi: 10.1124/pr.58.4.6

Moore, R. L., Dai, Y., and Faller, D. V. (2012). Sirtuin 1 (SIRT1) and steroid hormone receptor activity in cancer. *J. Endocrinol.* 213, 37–48. doi: 10.1530/JOE-11-0217

Nakamura, K., Moore, R., Negishi, M., and Sueyoshi, T. (2007). Nuclear pregnane X receptor cross-talk with FoxA2 to mediate drug-induced regulation of lipid metabolism in fasting mouse liver. *J. Biol. Chem.* 282, 9768–9776. doi: 10.1074/jbc.M610072200

Navaratnarajah, P., Steele, B. L., Redinbo, M. R., and Thompson, N. L. (2012). Rifampicin-independent interactions between the pregnane X receptor ligand binding domain and peptide fragments of coactivator and corepressor proteins. *Biochemistry* 51, 19–31. doi: 10.1021/bi2011674

Noble, S. M., Carnahan, V. E., Moore, L. B., Luntz, T., Wang, H., Ittoop, O. R., et al. (2006). Human PXR forms a tryptophan zipper-mediated homodimer. *Biochemistry* 45, 8579–8589. doi: 10.1021/bi0602821

Odom, D. T., Zizlsperger, N., Gordon, D. B., Bell, G. W., Rinaldi, N. J., Murray, H. L., et al. (2004). Control of pancreas and liver gene expression by HNF transcription factors. *Science* 303, 1378–1381. doi: 10.1126/science.1089769

Oh, K. J., Han, H. S., Kim, M. J., and Koo, S. H. (2013). CREB and FoxO1: two transcription factors for the regulation of hepatic gluconeogenesis. *BMB Rep.* 46, 567–574. doi: 10.5483/BMBRep.2013.46.12.248

Oladimeji, P., Cui, H., Zhang, C., and Chen, T. (2016). Regulation of PXR and CAR by protein-protein interaction and signaling crosstalk. *Exp. Opin. Drug Metab. Toxicol.* 12, 997–1010. doi: 10.1080/17425255.2016.1201069

Ourlin, J. C., Lasserre, F., Pineau, T., Fabre, J. M., Sa-Cunha, A., Maurel, P., et al. (2003). The small heterodimer partner interacts with the pregnane X receptor and represses its transcriptional activity. *Mol. Endocrinol.* 17, 1693–1703. doi: 10.1210/me.2002-0383

Pascussi, J. M., Gerbal-Chaloin, S., Duret, C., Daujat-Chavanieu, M., Vilarem, M. J., and Maurel, P. (2008). The tangle of nuclear receptors that controls xenobiotic metabolism and transport: crosstalk and consequences. *Annu. Rev. Pharmacol. Toxicol.* 48, 1–32. doi: 10.1146/annurev.pharmtox.47.120505.105349

Pascussi, J. M., Gerbal-Chaloin, S., Pichard-Garcia, L., Daujat, M., Fabre, J. M., Maurel, P., et al. (2000). Interleukin-6 negatively regulates the expression of pregnane X receptor and constitutively activated receptor in primary human hepatocytes. *Biochem. Biophys. Res. Commun.* 274, 707–713. doi: 10.1006/bbrc.2000.3219

Pavek, P., and Dvorak, Z. (2008). Xenobiotic-induced transcriptional regulation of xenobiotic metabolizing enzymes of the cytochrome P450 superfamily in human extrahepatic tissues. *Curr. Drug Metab.* 9, 129–143. doi: 10.2174/138920008783571774

Pavek, P., Pospechova, K., Svecova, L., Syrova, Z., Stejskalova, L., Blazkova, J., et al. (2010). Intestinal cell-specific vitamin D receptor (VDR)-mediated transcriptional regulation of CYP3A4 gene. *Biochem. Pharmacol.* 79, 277–287. doi: 10.1016/j.bcp.2009.08.017

Pavek, P., Stejskalova, L., Krausova, L., Bitman, M., Vrzal, R., and Dvorak, Z. (2012). Rifampicin does not significantly affect the expression of small heterodimer partner in primary human hepatocytes. *Front. Pharmacol.* 3:1. doi: 10.3389/fphar.2012.00001

Pettersson, F., Hanna, N., Lagodich, M., Dupere-Richer, D., Couture, M. C., Choi, C., et al. (2008). Rexinoids modulate steroid and xenobiotic receptor activity by increasing its protein turnover in a calpain-dependent manner. *J. Biol. Chem.* 283, 21945–21952. doi: 10.1074/jbc.M710358200

Rodgers, J. T., Lerin, C., Haas, W., Gygi, S. P., Spiegelman, B. M., and Puigserver, P. (2005). Nutrient control of glucose homeostasis through a complex of PGC-1alpha and SIRT1. *Nature* 434, 113–118. doi: 10.1038/nature03354

Rosenfeld, M. G., Lunyak, V. V., and Glass, C. K. (2006). Sensors and signals: a coactivator/corepressor/epigenetic code for integrating signal-dependent programs of transcriptional response. *Genes Dev.* 20, 1405–1428. doi: 10.1101/gad.1424806

Roth, A., Looser, R., Kaufmann, M., Blattler, S. M., Rencurel, F., Huang, W., et al. (2008a). Regulatory cross-talk between drug metabolism and lipid homeostasis: constitutive androstane receptor and pregnane X receptor increase Insig-1 expression. *Mol. Pharmacol.* 73, 1282–1289. doi: 10.1124/mol.107.041012

Roth, A., Looser, R., Kaufmann, M., and Meyer, U. A. (2008b). Sterol regulatory element binding protein 1 interacts with pregnane X receptor and constitutive androstane receptor and represses their target genes. *Pharmacogenet Genomics* 18, 325–337. doi: 10.1097/FPC.0b013e3282f706e0

Rulcova, A., Prokopova, I., Krausova, L., Bitman, M., Vrzal, R., Dvorak, Z., et al. (2010). Stereoselective interactions of warfarin enantiomers with the pregnane X nuclear receptor in gene regulation of major drug-metabolizing cytochrome P450 enzymes. *J. Thromb. Haemost.* 8, 2708–2717. doi: 10.1111/j.1538-7836.2010.04036.x

Rysa, J., Buler, M., Savolainen, M. J., Ruskoaho, H., Hakkola, J., and Hukkanen, J. (2013). Pregnane X receptor agonists impair postprandial glucose tolerance. *Clin. Pharmacol. Ther.* 93, 556–563. doi: 10.1038/clpt.2013.48

Saini, S. P., Mu, Y., Gong, H., Toma, D., Uppal, H., Ren, S., et al. (2005). Dual role of orphan nuclear receptor pregnane X receptor in bilirubin detoxification in mice. *Hepatology* 41, 497–505. doi: 10.1002/hep.20570

Saradhi, M., Sengupta, A., Mukhopadhyay, G., and Tyagi, R. K. (2005). Pregnane and Xenobiotic Receptor (PXR/SXR) resides predominantly in the nuclear compartment of the interphase cell and associates with the condensed chromosomes during mitosis. *Biochim. Biophys. Acta* 1746, 85–94. doi: 10.1016/j.bbamcr.2005.10.004

Smutny, T., Bitman, M., Urban, M., Dubecka, M., Vrzal, R., Dvorak, Z., et al. (2014). U0126, a mitogen-activated protein kinase kinase 1 and 2 (MEK1 and 2) inhibitor, selectively up-regulates main isoforms of CYP3A subfamily via a pregnane X receptor (PXR) in HepG2 cells. *Arch. Toxicol.* 88, 2243–2259. doi: 10.1007/s00204-014-1254-2

Smutny, T., Mani, S., and Pavek, P. (2013). Post-translational and post-transcriptional modifications of pregnane X receptor (PXR) in regulation of the cytochrome P450 superfamily. *Curr. Drug Metab.* 14, 1059–1069. doi: 10.2174/138920021466613121153307

Squires, E. J., Sueyoshi, T., and Negishi, M. (2004). Cytoplasmic localization of pregnane X receptor and ligand-dependent nuclear translocation in mouse liver. *J. Biol. Chem.* 279, 49307–49314. doi: 10.1074/jbc.M407281200

Szwarc, M. M., Kommagani, R., Lessey, B. A., and Lydon, J. P. (2014). The p160/steroid receptor coactivator family: potent arbiters of uterine physiology and dysfunction. *Biol. Reprod.* 91, 122. doi: 10.1095/biolreprod.114.125021

Takeshita, A., Taguchi, M., Koibuchi, N., and Ozawa, Y. (2002). Putative role of the orphan nuclear receptor SXR (steroid and xenobiotic receptor) in the mechanism of CYP3A4 inhibition by xenobiotics. *J. Biol. Chem.* 277, 32453–32458. doi: 10.1074/jbc.M111245200

Tirona, R. G., Lee, W., Leake, B. F., Lan, L. B., Cline, C. B., Lamba, V., et al. (2003). The orphan nuclear receptor HNF4alpha determines PXR- and CAR-mediated xenobiotic induction of CYP3A4. *Nat. Med.* 9, 220–224. doi: 10.1038/nm815

Venkatesh, M., Mukherjee, S., Wang, H., Li, H., Sun, K., Benechet, A. P., et al. (2014). Symbiotic bacterial metabolites regulate gastrointestinal barrier function via the xenobiotic sensor PXR and Toll-like receptor 4. *Immunity* 41, 296–310. doi: 10.1016/j.immuni.2014.06.014

Wada, T., Kang, H. S., Jetten, A. M., and Xie, W. (2008). The emerging role of nuclear receptor RORalpha and its crosstalk with LXR in xeno- and endobiotic gene regulation. *Exp. Biol. Med.* 233, 1191–1201. doi: 10.3181/0802-MR-50

Wang, K., Mendy, A. J., Dai, G., Luo, H. R., He, L., and Wan, Y. J. (2006). Retinoids activate the RXR/SXR-mediated pathway and induce the endogenous CYP3A4 activity in Huh7 human hepatoma cells. *Toxicol. Sci.* 92, 51–60. doi: 10.1093/toxsci/kfj207

Wang, L., Lonard, D. M., and O'Malley, B. W. (2016). The role of steroid receptor coactivators in hormone dependent cancers and their potential as therapeutic targets. *Horm. Cancer* 7, 229–235. doi: 10.1007/s12672-016-0261-6

Wang, Y. M., Ong, S. S., Chai, S. C., and Chen, T. (2012). Role of CAR and PXR in xenobiotic sensing and metabolism. *Exp. Opin. Drug Metab. Toxicol.* 8, 803–817. doi: 10.1517/17425255.2012.685237

Watanabe, K., Sakurai, K., Tsuchiya, Y., Yamazoe, Y., and Yoshinari, K. (2013). Dual roles of nuclear receptor liver X receptor alpha (LXRalpha) in the CYP3A4 expression in human hepatocytes as a positive and negative regulator. *Biochem. Pharmacol.* 86, 428–436. doi: 10.1016/j.bcp.2013.05.016

Watkins, R. E., Davis-Searles, P. R., Lambert, M. H., and Redinbo, M. R. (2003). Coactivator binding promotes the specific interaction between ligand and the pregnane X receptor. *J. Mol. Biol.* 331, 815–828. doi: 10.1016/S0022-2836(03)00795-2

Watkins, R. E., Wisely, G. B., Moore, L. B., Collins, J. L., Lambert, M. H., Williams, S. P., et al. (2001). The human nuclear xenobiotic receptor PXR: structural determinants of directed promiscuity. *Science* 292, 2329–2333. doi: 10.1126/science.1060762

Watt, A. J., Garrison, W. D., and Duncan, S. A. (2003). HNF4: a central regulator of hepatocyte differentiation and function. *Hepatology* 37, 1249–1253. doi: 10.1053/jhep.2003.50273

Wolfrum, C., Asilmaz, E., Luca, E., Friedman, J. M., and Stoffel, M. (2004). Foxa2 regulates lipid metabolism and ketogenesis in the liver during fasting and in diabetes. *Nature* 432, 1027–1032. doi: 10.1038/nature03047

Xie, W., Yeuh, M. F., Radominska-Pandya, A., Saini, S. P., Negishi, Y., Bottroff, B. S., et al. (2003). Control of steroid, heme, and carcinogen metabolism by nuclear pregnane X receptor and constitutive androstane receptor. *Proc. Natl. Acad. Sci. U.S.A.* 100, 4150–4155. doi: 10.1073/pnas.0438010100

Xue, Y., Moore, L. B., Orans, J., Peng, L., Bencharit, S., Kliewer, S. A., et al. (2007). Crystal structure of the pregnane X receptor-estradiol complex provides insights into endobiotic recognition. *Mol. Endocrinol.* 21, 1028–1038. doi: 10.1210/me.2006-0323

Zhai, Y., Wada, T., Zhang, B., Khadem, S., Ren, S., Kuruba, R., et al. (2010). A functional cross-talk between liver X receptor-alpha and constitutive androstane receptor links lipogenesis and xenobiotic responses. *Mol. Pharmacol.* 78, 666–674. doi: 10.1124/mol.110.064618

Zhang, J., Kuehl, P., Green, E. D., Touchman, J. W., Watkins, P. B., Daly, A., et al. (2001). The human pregnane X receptor: genomic structure and identification and functional characterization of natural allelic variants. *Pharmacogenetics* 11, 555–572. doi: 10.1097/00008571-200110000-00003

Zhang, Y., Hagedorn, C. H., and Wang, L. (2011). Role of nuclear receptor SHP in metabolism and cancer. *Biochim. Biophys. Acta* 1812, 893–908. doi: 10.1016/j.bbadis.2010.10.006

Zhou, C., Tabb, M. M., Nelson, E. L., Grun, F., Verma, S., Sadatrafiei, A., et al. (2006). Mutual repression between steroid and xenobiotic receptor and NF-kappaB signaling pathways links xenobiotic metabolism and inflammation. *J. Clin. Invest.* 116, 2280–2289. doi: 10.1172/JCI26283

Zhou, C., Verma, S., and Blumberg, B. (2009). The steroid and xenobiotic receptor (SXR), beyond xenobiotic metabolism. *Nucl. Recept. Signal.* 7, e001. doi: 10.1621/nrs.07001

Zou, A., Lehn, S., Magee, N., and Zhang, Y. (2015). New insights into orphan nuclear receptor SHP in liver cancer. *Nucl. Receptor Res.* 2:101162. doi: 10.11131/2015/101162

Conflict of Interest Statement: The author declares that the research was conducted in the absence of any commercial or financial relationships that could be construed as a potential conflict of interest.

frontiers in Pharmacology

MINI REVIEW
published: 27 March 2017
doi: 10.3389/fphar.2017.00159

Membrane Associated Progesterone Receptors: Promiscuous Proteins with Pleiotropic Functions – Focus on Interactions with Cytochromes P450

*Chang S. Ryu[1,2], Kathrin Klein[1,2] and Ulrich M. Zanger[1,2]**

[1] Department of Molecular and Cell Biology, Dr. Margarete Fischer-Bosch-Institute of Clinical Pharmacology, Stuttgart, Germany, [2] Eberhard-Karls-University, Tübingen, Germany

Membrane-associated progesterone receptors (MAPR) are a group of four rather small, partially homologous proteins, which share a similar non-covalent heme-binding domain that is related to cytochrome b5, a well-known functional interaction partner of microsomal cytochrome P450 (CYP) monooxygenase systems. Apart from their structural similarities the four proteins progesterone membrane component 1 (PGRMC1, also referred to as IZA, sigma-2 receptor, Dap1), PGRMC2, neudesin (NENF) and neuferricin (CYB5D2) display surprisingly divergent and multifunctional physiological properties related to cholesterol/steroid biosynthesis, drug metabolism and response, iron homeostasis, heme trafficking, energy metabolism, autophagy, apoptosis, cell cycle regulation, cell migration, neural functions, and tumorigenesis and cancer progression. The purpose of this mini-review is to briefly summarize the structural and functional properties of MAPRs with particular focus on their interactions with the CYP system. For PGRMC1, originally identified as a non-canonical progesterone-binding protein that mediates some immediate non-genomic actions of progesterone, available evidence indicates mainly activating interactions with steroidogenic CYPs including CYP11A1, CYP21A2, CYP17, CYP19, CYP51A1, and CYP61A1, while interactions with drug metabolizing CYPs including CYP2C2, CYP2C8, CYP2C9, CYP2E1, and CYP3A4 were either ineffective or slightly inhibitory. For the other MAPRs the evidence is so far less conclusive. We also point out that experimental limitations question some of the previous conclusions. Use of appropriate model systems should help to further clarify the true impact of these proteins on CYP-mediated metabolic pathways.

Keywords: cytochrome P450, membrane-associated progesterone receptor, neudesin, neuferricin, PGRMC1, PGRMC2, protein-protein interaction

OPEN ACCESS

Edited by:
Andrea Gaedigk, Children's Mercy Hospital, USA

Reviewed by:
Hans Neubauer, University of Düsseldorf, Germany
Ilpo Huhtaniemi, Imperial College London, UK

****Correspondence:***
Ulrich M. Zanger
uli.zanger@ikp-stuttgart.de

Specialty section:
This article was submitted to Pharmacogenetics and Pharmacogenomics, a section of the journal Frontiers in Pharmacology

Received: *12 January 2017*
Accepted: *13 March 2017*
Published: *27 March 2017*

Citation:
Ryu CS, Klein K and Zanger UM (2017) Membrane Associated Progesterone Receptors: Promiscuous Proteins with Pleiotropic Functions – Focus on Interactions with Cytochromes P450. Front. Pharmacol. 8:159. doi: 10.3389/fphar.2017.00159

INTRODUCTION

Inter- and intraindividual variability in the expression and activity of drug metabolizing enzymes, transporters and their regulators is a major determinant of drug response, both in terms of drug efficacy and adverse events. The cytochrome P450 enzymes, a superfamily of microsomal and mitochondrial hemoproteins (CYP), are particularly variable between and within subjects (Zanger and Schwab, 2013). Despite half a century of pharmacogenetic research, much of the

interindividual variation remains unexplained (Meyer, 2004; Lauschke and Ingelman-Sundberg, 2015). This "dark variation" may be explained by so far unidentified or unexplored genes that influence drug metabolism at the level of protein-protein interactions (PPI). The multiple monooxygenase functions of microsomal CYP enzymes strictly depend on PPI with the single microsomal flavoprotein NADPH:cytochrome P450 oxidoreductase (POR) to allow electron transfer from NADPH to the heme iron (Pandey and Fluck, 2013; Kandel and Lampe, 2014). Since POR is present in the endoplasmic reticulum (ER) at sub-stoichiometric amounts compared to CYP, it has been proposed that their interactions involve transient oligomeric complexes (Backes and Kelley, 2003). In contrast to POR, the small hemoprotein cytochrome b5 (CYB5), which is located together with CYB5-reductase and the other components on the cytoplasmic side of the ER, is not an obligatory electron donor for CYPs but acts as modulator of enzyme activity in CYP- and sometimes substrate-dependent way (Henderson et al., 2015). For a long time, POR and CYB5 were the only proteins known to functionally interact with CYPs during the microsomal monooxygenase reaction. Only in recent years new PPI candidates for cytochromes P450 have been considered (see other articles in this Research Topic).

A particularly intriguing group of proteins are the so-called "membrane-associated progesterone receptor" (MAPR) proteins. The term emphasizes their common ability to bind progesterone and to elicit rapid steroidal effects independent of the classical steroid hormone receptors (Wehling, 1997; Mifsud and Bateman, 2002). Following the initial purification of a high-affinity progesterone-binding protein (later termed progesterone receptor membrane component 1, PGRMC1) from porcine liver membranes and cDNA cloning (Meyer et al., 1996; Gerdes et al., 1998), MAPRs were recognized as evolutionarily conserved, distant homologs of CYB5, that can principally interact with CYPs and modulate their functions (Min et al., 2004; Hughes et al., 2007).

The purpose of this review is to provide an overview and critical assessment of the studies elucidating potential interactions of MAPRs with CYPs. Apart from this, MAPRs interact with an increasing number of different proteins and are involved in a wide variety of cellular functions including cholesterol and steroid homeostasis, cell cycle regulation, cell migration, neurogenesis, autophagy, heme homeostasis and more that are only briefly mentioned but not the focus of this review. Readers interested in these aspects are referred to excellent reviews by others (Losel et al., 2008; Ahmed et al., 2012; Kimura et al., 2012; Neubauer et al., 2013; Cahill et al., 2016; Hasegawa et al., 2016).

MOLECULAR, BIOCHEMICAL AND CELLULAR PROPERTIES OF MAPRs

The four MAPR proteins PGRMC1, PGRMC2, neuferricin and neudesin share a homologous CYB5-like heme/steroid-binding domain but lack homology with the classical nuclear or membrane-bound steroid receptors (Mifsud and Bateman, 2002; Min et al., 2005; Kimura et al., 2012). Recent crystallographic analyses confirmed the hemoprotein nature of PGRMC1 with a special five-coordinated heme iron involving Tyr113, as opposed to the six-coordinated heme with two axial histidines in CYB5 (Min et al., 2005; Kaluka et al., 2015; Kabe et al., 2016). Interestingly, this difference allows human PGRMC1 to form stable homodimers through hydrophobic heme-heme stacking interactions, explaining earlier observations of dimeric complexes (Min et al., 2004; Kabe et al., 2016). Since the heme-binding residues are conserved among MAPRs, these proteins may all share the ability of heme-dependent homo- and/or heterodimerization (Peluso et al., 2014). Although PGRMC1 had originally been defined as a component of a progesterone-binding protein complex with affinities in the nM range (Meyer et al., 1996), it remained questionable whether progesterone actually binds directly to PGRMC1 itself. A recent study provided first qualitative spectroscopic evidence that this is indeed the case, while it is still not proven for other MAPRs (Kaluka et al., 2015).

PRGMC1

PRGMC1 is predominantly expressed in mammalian liver and kidney but also found in steroidogenic and reproductive tissues, brain, breast, heart, lung, skeletal muscle, pancreas, and other organs (Gerdes et al., 1998; Kimura et al., 2012). Typically it is colocalized with CYPs in the smooth ER, but it has also been localized in the nucleus, cytoplasm, plasma membrane, and mitochondria (Kimura et al., 2012; Piel et al., 2016). Expression is inducible by carcinogens, including dioxin (Selmin et al., 1996), and increased in breast and other tumors, where it contributes to cancer progression (Neubauer et al., 2008; Ruan et al., 2017). Reported physiological functions affected by PGRMC1 include cholesterol/steroid biosynthesis and metabolism (see below), iron homeostasis and heme trafficking by regulating hepcidin expression and ferrochelatase activity (Craven et al., 2007; Li et al., 2016; Piel et al., 2016), promotion of autophagy through interaction with MAP1LC3B (Mir et al., 2013), regulation of cell cycle, proliferation, and cell death (Peluso et al., 2014), maintenance of female reproductive functions in PGRMC1 conditional knock-out mice (McCallum et al., 2016), cell migration and invasion (Sueldo et al., 2015), amyloid beta binding and synaptotoxicity in a mouse model of Alzheimer's disease (Izzo et al., 2014), and others (Losel et al., 2008; Ahmed et al., 2012; Neubauer et al., 2013; Cahill et al., 2016; Hasegawa et al., 2016). A growing number of studies supports furthermore a role of PGRMC1 in drug response and as potential drug target, e.g., by increasing susceptibility to tyrosine kinase inhibitors (Ahmed et al., 2010), decreasing doxorubicin cytotoxicity (Lin et al., 2015), or mediating atypical antipsychotic drug-induced lipid disturbances (Cai et al., 2015). Importantly, in 2011 PGRMC1 was identified as the elusive sigma 2 receptor (S2R), an intracellular orphan receptor that binds to many drugs and that is abundant in liver and kidney (Xu et al., 2011; Ahmed et al., 2012).

PGRMC2

PGRMC2 harbors a structurally similar CYB5 domain as PGRMC1, while there are differences in the N-terminal transmembrane domain (Cahill, 2007). Human PGRMC2

protein is 247 amino acids in length. Despite its structural similarities to PGRMC1, PGRMC2 has been less well studied (Wendler and Wehling, 2013; Hasegawa et al., 2016). Expression appears to be ubiquitous with similar intracellular localization (Chen et al., 2010; Intlekofer and Petersen, 2011). In SKOV-3 ovarian cancer cells no differences between PGRMC1 and 2 in regard to cell viability or response to cisplatin and progesterone were found, but only PGRMC2 inhibited cell migration (Albrecht et al., 2012). PGRMC2 was also implicated in cell cycle regulation (Peluso et al., 2014).

Neudesin

Neudesin was originally identified as a mouse secreted protein with neurotrophic activity and termed neuron-derived neurotrophic factor (NENF) (Kimura et al., 2005). In adult mice, neudesin was expressed preferentially in the CNS spinal cord but also in several peripheral tissues (Kimura et al., 2005, 2012). NMR studies suggested a similar structure with a potential heme-binding pocket (Han et al., 2012). The physiological roles of neudesin as a secreted protein appear to be significantly different from PGRMC1/2, including particularly neurotrophic activity that required heme binding and was mediated through mitogen-activated protein (MAP) and phosphatidylinositol 3-kinase (PI-3K) pathways (Kimura et al., 2005). Several neurological functions have been studied in knockout mice as summarized elsewhere (Ohta et al., 2015). Extracellular/secreted neudesin may be involved in carcinogen resistance and tumor cell immortalization, although specific receptors remain unknown (Ohta et al., 2015).

Neuferricin

Neuferricin (CYP5D2) was discovered *via* a homology-based search of the CYB5-like heme/steroid-binding domain of neudesin, alternatively termed cytochrome B5 Domain Containing 2 (CYB5D2) (Kimura et al., 2010). Neuferricin is also widely expressed in several tissues including the CNS, heart, adrenal glands, and kidneys. Human neuferricin is 264 amino acids in length and includes a cleavable signal sequence at its N terminus followed by a heme-binding domain that may involve aspartic acid (D86) instead of tyrosine in heme binding (Bruce and Rybak, 2014). CYB5D2 can be detected as secreted hemoprotein in some cell lines but also colocalized with POR in the ER (Xie et al., 2011; Bruce and Rybak, 2014). Ectopic CYB5D2 expression inhibited cell proliferation and anchorage-independent colony growth of HeLa cells (Bruce and Rybak, 2014).

SPECIFIC INVOLVEMENT OF MAPRS IN CYP FUNCTIONS

The available evidence suggesting that MAPR proteins can interact with the microsomal CYP-monooxygenase system to modulate its function is based on different species from yeast to human, various experimental systems, and relates to CYP enzymes catalyzing steroidogenic or xenobiotic reactions (**Table 1**). The levels of interactions may include not only physical PPIs but also indirect influences via heme transfer, heme and iron homeostasis, and transcriptional regulation (**Figure 1**).

PGRMC1

First indications for a link between PGRMC1 and CYP function came from two independent studies. Identification of the adrenal "inner zone antigen" (IZA) as a MAPR member (Raza et al., 2001), its localization in both steroidogenic and steroid metabolizing tissues and the fact that an anti-IZA monoclonal antibody decreased certain adrenal steroidhydroxylase activities led the authors to suggest a function in steroid hormone biosynthesis and/or metabolism (Min et al., 2004). By coexpressing IZA/PGRMC1 with CYP21A2, CYP11B1 or CYP17 in COS-7 cells they found differential effects, namely enhancement of progesterone 21-hydroxylation, no effect on progesterone 11β- or 17α-hydroxylation, and activation of the CYP17-catalyzed 17–20 lyase reaction (Min et al., 2004, 2005). About at the same time a search for novel yeast genes involved in DNA damage response led to the identification of *Dap1* (Hand et al., 2003). Steroid analyses of *Saccharomyces cerevisiae* yeast cells lacking *Dap1* revealed decreased levels of ergosterol but increased levels of its intermediates, suggesting a partial defect in sterol synthesis by lanosterol-14-demethylase, the highly conserved yeast-essential Erg11/CYP51 (Hand et al., 2003). Genetic follow-up studies supported a model in which heme binding by Dap1 is required to activate Erg11/CYP51, although a Dap1-Erg11 complex could not be directly detected by immunoprecipitation experiments (Mallory et al., 2005).

Further evidence for a role of Dap1/PGRMC1 in CYP function was provided by Hughes et al. (2007) working with *Schizosaccharomyces pombe*. After confirming that fission yeast Dap1 is also a hemoprotein and directly binds to and activates enzymatic activities of CYP51A1 (Erg11) and CYP61A1 (Erg5), they investigated whether PGRMC1 is required for cholesterol synthesis in mammals (Hughes et al., 2007). RNA interference-mediated knock-down of hPGRMC1 in HEK293 cells resulted in lanosterol accumulation, indicating that PGRMC1 was required for the demethylation of lanosterol by the Erg11 homolog, CYP51A1. Using a coexpression/coimmunoprecipitation approach PGRMC1 was shown to form a stable complex with CYP51A1 (Hughes et al., 2007). The authors applied the latter experiment also to CYP7A1, CYP21A2, and CYP3A4, demonstrating physically stable PGRMC1-CYP complexes in all cases. PGRMC1 was later shown to also activate CYP19 aromatase (Ahmed et al., 2012). Collectively these studies strongly suggest the ability of PGRMC1 to form functional PPIs with steroidogenic and possibly other CYPs. Interestingly, the documented functional influence of PGRMC1 on various steroidogenic CYPs appeared to be generally positive.

The above mentioned ability of PGRMC1 to complex with CYP3A4 first indicated the possibility that PGRMC1 may also interact with drug metabolizing P450s (Hughes et al., 2007). Although the authors emphasized the apparent existence of stoichiometric and physically stable complexes, it should be kept in mind that the experimental conditions of overexpressing tagged and manipulated proteins were quite artificial and that it

TABLE 1 | Functional interactions between membrane-associated progesterone receptors (MAPR) proteins and cytochrome P450 system.

MAPR	CYP	System	Enzymatic activity	Direction of influence	Reference
IZA/PGRMC1 (rat)	CYP21A2 (rat)	Inhibition by anti-IZA monoclonal antibody	Progesterone 21-hydroxylase	Activation	Laird et al., 1988
IZA/PGRMC1 (rat)	CYP21A2 (rat)	COS-7 cell coexpression	Progesterone 21-hydroxylase	Activation	Min et al., 2004
IZA/PGRMC1 (rat)	CYP17 (guinea pig)	COS-7 cell coexpression	Progesterone 17α-hydroxylase	Little or no influence	Min et al., 2005
IZA/PGRMC1 (rat)	CYP17 (guinea pig)	COS-7 cell coexpression	17α-Hydroxyprogesterone 17–20 lyase	Activation	Min et al., 2005
IZA/PGRMC1 (rat)	CYP11B1 (rat)	COS-7 cell coexpression	Progesterone 11β-hydroxylase	Little or no influence	Min et al., 2004
PGRMC1 (human)	CYP19A1 (human)	CYP19-engineered MCF-7 human breast cancer cells RNAi knockdown	Androst-4-ene-3,17-dione conversion	Activation	Ahmed et al., 2012
Dap1/PGRMC1 (*S. cerevisiae*)	CYP51A1 (*S. cerevisiae*)	*S. cerevisiae* genetics	Lanosterol-14-demethylase	Activation	Hand et al., 2003 Mallory et al., 2005
Dap1/PGRMC1 (*S. pombe*)	CYP51A1 (*S. pombe*)	*S. pombe* strain lacking DAP1	Lanosterol-14-demethylase	Activation	Hughes et al., 2007
Dap1/PGRMC1 (*S. pombe*)	CYP61A1 (*S. pombe*)	*S. pombe* strain lacking DAP1	Lanosterol-22-desaturase	Activation	Hughes et al., 2007
PGRMC1 (rabbit)	CYP2C2 (rabbit)	HEK293, HepG2 cell coexpression	Luciferin 6′ methyl ether *O*-demethylation	Inhibition	Szczesna-Skorupa and Kemper, 2011
PGRMC1 (human)	CYP2C8 (human)	HEK293, HepG2 cell coexpression	Luciferin 6′ methyl ether *O*-demethylation	Inhibition	Szczesna-Skorupa and Kemper, 2011
PGRMC1 (human)	CYP3A4 (human)	HEK293, HepG2 cell coexpression	Luciferin 6′ pentafluorobenzyl ether depentafluorobenzylation	Inhibition	Szczesna-Skorupa and Kemper, 2011
PGRMC1 (human)	CYP2C9 (human)	HepG2 coexpression, human hepatocytes RNAi knockdown	*S*-Warfarin 7-hydroxylase and diclofenac 4′-hydroxylase	Inhibition	Oda et al., 2011
PGRMC1 (human)	CYP3A4 (human)	HepG2 coexpression, human hepatocytes RNAi knockdown	Testosterone 6β-hydroxylase and midazolam 1′-hydroxylase	Inhibition	Oda et al., 2011
PGRMC1 (human)	CYP2E1 (human)	HepG2 coexpression, human hepatocytes RNAi knockdown	Chlorzoxazone 6-hydroxylase and 7-ethoxycoumarin *O*-deethylase	No influence	Oda et al., 2011
PGRMC2 (human)	CYP3A4 (human)	Human liver genetic association	Atorvastatin 2-hydroxylase	Inhibition	Klein et al., 2012
CYB5D2 (human)	CYP3A4 (human)	Hela cell expression and RNAi knockdown	Luciferin 6′ pentafluorobenzyl ether depentafluorobenzylation	Activation	Bruce and Rybak, 2014

is unknown, whether PGRMC1 abundance in the ER is sufficient for the formation of 1:1 complexes at higher concentrations.

Two studies have investigated the question whether PGRMC1 affects drug metabolizing CYPs functionally. Szczesna-Skorupa and Kemper, using cotransfection and coimmunoprecipitation of FLAG-tagged PGRMC1 with variously tagged rabbit CYP2C2 and human CYP2C8 and CYP3A4 in HEK293 cells could show efficient binding of PGRMC1 to all three CYPs, for CYP2C2 mainly mediated by the cytoplasmic domain (Szczesna-Skorupa and Kemper, 2011). The effect of PGRMC1 on enzymatic activity was tested by siRNA-mediated downregulation of endogenous PGRMC1, and by coexpression with functional CYP plasmids in HEK293 and HepG2 hepatoma cells (**Table 1**). Surprisingly, the results were quite opposite to those of steroidogenic CYPs, as CYP activities were either unchanged or slightly increased in PGRMC1-deficient cells, but decreased in presence of exogenously expressed PGRMC1. Interestingly, the inhibitory effect could be partially and CYP isoform-dependently reversed by increased expression of POR, also shown to directly interact with PGRMC1. The authors concluded that in contrast to steroidogenic CYPs, PGRMC1 is not required by drug metabolizing CYPs for enzymatic activity and that the CYP differential effects may be explained by the intricate PPI affinities in triple CYP-POR-PGRMC1 systems (Szczesna-Skorupa and Kemper, 2011).

Oda et al. (2011) found differential effects of PGRMC1 cotransfection with CYP2C9, CYP2E1, and CYP3A4 in HepG2 cells. While CYP3A4 had increased K_m and decreased V_{max} with two different substrates (testosterone and midazolam), CYP2C9 K_m was unchanged but V_{max} also decreased, and CYP2E1 activity (chlorzoxazone, 7-ethoxycoumarin) remained unchanged. The authors also confirmed direct interactions of PGRMC1 with all three CYPs (Oda et al., 2011).

More recently, Kabe et al. (2016) in their structural study investigated the relevance of heme-mediated dimerization on functional interactions with human CYPs. By incubation of FLAG-tagged PGRMC1 with microsomes from insect-cells expressing POR, CYB5, and either CYP1A2 or CYP3A4, they showed by immunoprecipitation that only wild-type PGRMC1 but not the Y113F mutant interacted with the present CYP. The interaction with CYP1A2 was furthermore blocked by incubation with a CO-generating reagent, indicating that

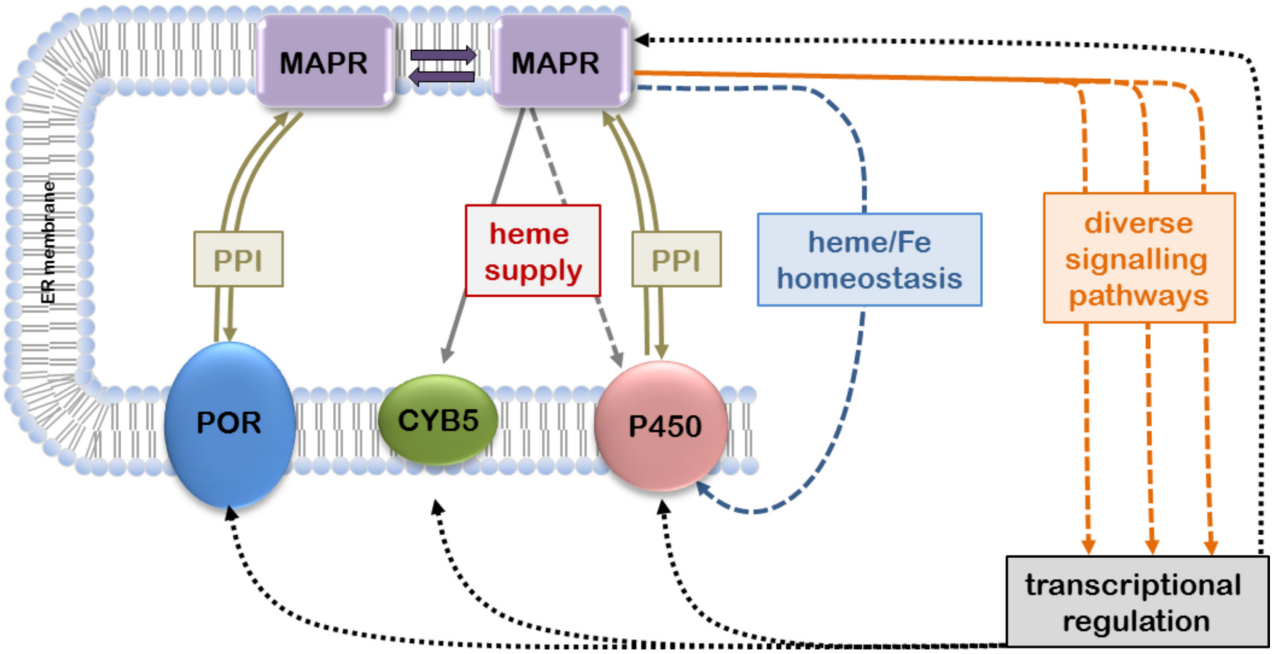

FIGURE 1 | Confirmed and hypothetical interactions of membrane-associated progesterone receptors (MAPRs) with microsomal cytochrome P450 (CYP) system. MAPR proteins located in the endoplasmic reticulum (ER) membrane can directly interact with each other to form homo- and heterodimers; MAPR monomers and dimers may participate in PPIs with P450 oxidoreductase (POR), cytochrome b5 (CYB5) and/or CYPs. Transfer of heme to CYB5 and possibly CYPs as well as involvement in iron/heme homeostasis may influence heme integration and thus CYP function. Furthermore, MAPRs participate in diverse signaling pathways that may affect transcriptional regulation of CYP gene expression (double arrows, confirmed protein-protein interactions; solid arrows, confirmed influence; dashed arrows, hypothetical influence).

PGRMC1 dimerization is necessary for the interaction. To test whether CYP-mediated enzymatic functions are affected they used HCT116 human colon cancer cells stably expressing control or PGRMC1 shRNA to reduce endogenous PGRMC1 expression and incubated them with doxorubicin. PGRMC1 knock-down suppressed the conversion of doxorubicin to doxorubicinol, and increased cell sensitivity to doxorubicinol. This effect was partially reversed by coexpression of the wild-type PGRMC1 but not of the Y113F mutant. Assuming that CYP2D6 and CYP3A4 are the relevant enzymes for doxorubicinol-formation in HCT116 cells, the authors concluded that interaction of CYPs with the PGRMC1 dimer was a crucial component of CYP activity (Kabe et al., 2016). However, this conclusion is severely flawed because the metabolic step from doxorubicin to doxorubicinol is not a hydroxylation but in fact a 2-electron reduction of a ketogroup to an aliphatic alcohol. This reduction is not catalyzed by CYPs 2D6 and 3A4 as indicated in the paper, but mainly by cytosolic carbonyl reductase 1 (Kassner et al., 2008). Furthermore the use of HCT116 cells with very low CYP3A4 expression seems inappropriate for CYP metabolism studies (Habano et al., 2011). We therefore believe that this and other previously reported functional and cellular effects of PGRMC1 on doxorubicin-metabolism or cytotoxicity (e.g., Friel et al., 2015; Lin et al., 2015) are not due to interactions with CYPs but must have other reasons.

Finally the recent study by Piel et al. (2016) should be mentioned here again as it demonstrated a role of PGRMC1 in heme homeostasis and its ability to directly transfer heme to CYB5 *in vitro*. The authors suggest that PGRMC1 may be a heme chaperone or sensor, and this could of course have additional direct or indirect implications for CYP function (**Figure 1**).

PGRMC2

Despite its high similarity to PGRMC1 much less is known about PGRMC2 (Wendler and Wehling, 2013). The first observation indicating a role in CYP function was made in a pharmacogenetic screen in human livers, where an intronic PGRMC2 polymorphism (rs3733260) was significantly associated with lower levels of mRNA expression, protein and enzyme activity (Klein et al., 2012). Although the directionality of this influence was the same as that observed for PGRMC1 and CYP3A4, it should be noted that the data are correlative in nature and would also be compatible with gene regulatory mechanisms (**Figure 1**). Stable physical interactions of PGRMC2 were demonstrated in human embryonic kidney cells for CYP1A2 and CYP3A4, suggesting similar interaction potential as for PGRMC1 (Albrecht et al., 2012). It should thus be interesting to investigate the potential of PGRMC2 to modulate CYP function and/or expression in a valid system.

Neudesin and Neuferricin

To our knowledge, only one study (Bruce and Rybak, 2014) directly addressed the potential interaction of these proteins with CYPs. The authors showed that neuferricin is colocalized

with POR in HeLa cells. Neuferricin knockdown reduced endogenous CYP51A1 (lanosterol demethylase) protein levels, which lead to increased sensitivity toward mevalonate, an intermediate of the cholesterol synthesis pathway. This suggested a stabilizing role of neuferricin for CYP51A1, as previously described for PGRMC1 and Dap1 (Hughes et al., 2007). Data further indicated that neuferricin knockdown also decreased the fraction of endogenous CYP3A4 activity that was enhanced by overexpressed POR, indicating activation of CYP3A4 by neuferricin, in contrast to the inhibitory effects of PGRMC1 (see above). However, it should be pointed out that the neuferricin data consists of a single point measurement carried out in a cell model that is not usually applied for drug metabolism studies, leaving it unclear whether the conclusion can be generalized. The same argument applies to the studies on HeLa cell exposure to chemotherapeutic agents such as paclitaxel, cisplatin, and doxorubicin, which resulted in increased sensitivities in CYB5D2 deficient cells (Bruce and Rybak, 2014). Since the expression levels of drug metabolizing CYPs are very low in HeLa cells, the construction of a link between CYB5D2 and function of drug metabolizing CYPs based on these data is in our opinion questionable.

CONCLUSION AND FUTURE PERSPECTIVES

Direct physical interactions of MAPRs, especially of mammalian PGRMC1 or yeast Dap1, with various cytochromes P450 are strongly supported by experimental data. However, data are still limited and in our view use of inappropriate model systems questions some conclusions on functional interactions with CYPs. Open questions that remain to be studied are, for example: which direct MAPR-CYP interactions are possible in binary, ternary, and higher order complexes and how do they affect function; how could MAPRs indirectly influence CYP function, e.g., by regulating heme supply and protein stability; are there MAPR signaling pathways that affect transcriptional regulation of CYPs and possibly other drug metabolizing enzymes, etc. It is of eminent importance that valid experimental systems, which express the CYP system at physiological levels, e.g., primary hepatocytes or genetically modified mice, are used in future studies.

AUTHOR CONTRIBUTIONS

All authors listed have made substantial, direct and intellectual contribution to the work, and approved it for publication.

FUNDING

Supported by the National Research Foundation of Korea, Ministry of Education (Basic Science Research Program grant No. 2015R1A6A3A03015840 to CR), the Alexander von Humboldt Foundation (Postdoctoral Research Fellowship to CR), and by the Robert Bosch Foundation, Stuttgart, Germany.

REFERENCES

Ahmed, I. S., Rohe, H. J., Twist, K. E., and Craven, R. J. (2010). Pgrmc1 (Progesterone receptor membrane component 1) associates with epidermal growth factor receptor and regulates erlotinib sensitivity. *J. Biol. Chem.* 285, 24775–24782. doi: 10.1074/jbc.M110.134585

Ahmed, I. S. A., Chamberlain, C., and Craven, R. J. (2012). S2R(Pgrmc1): the cytochrome-related sigma-2 receptor that regulates lipid and drug metabolism and hormone signaling. *Expert Opin. Drug Metab. Toxicol.* 8, 361–370. doi: 10.1517/17425255.2012.658367

Albrecht, C., Huck, V., Wehling, M., and Wendler, A. (2012). In vitro inhibition of SKOV-3 cell migration as a distinctive feature of progesterone receptor membrane component type 2 versus type 1. *Steroids* 77, 1543–1550. doi: 10.1016/j.steroids.2012.09.006

Backes, W. L., and Kelley, R. W. (2003). Organization of multiple cytochrome P450s with NADPH-cytochrome P450 reductase in membranes. *Pharmacol. Ther.* 98, 221–233. doi: 10.1016/S0163-7258(03)00031-7

Bruce, A., and Rybak, A. P. (2014). CYB5D2 requires heme-binding to regulate heLa cell growth and confer survival from chemotherapeutic agents. *PLoS ONE* 9:e86435. doi: 10.1371/journal.pone.0086435

Cahill, M. A. (2007). Progesterone receptor membrane component 1: an integrative review. *J. Steroid Biochem. Mol. Biol.* 105, 16–36. doi: 10.1016/j.jsbmb.2007.02.002

Cahill, M. A., Jazayeri, J. A., Catalano, S. M., Toyokuni, S., Kovacevic, Z., and Des Richardson, R. (2016). The emerging role of progesterone receptor membrane component 1 (PGRMC1) in cancer biology. *Biochim. Biophys. Acta* 1866, 339–349. doi: 10.1016/j.bbcan.2016.07.004

Cai, H. L., Tan, Q. Y., Jiang, P., Dang, R. L., Xue, Y., Tang, M. M., et al. (2015). A potential mechanism underlying atypical antipsychotics-induced lipid disturbances. *Transl. Psychiatry* 5:e661. doi: 10.1038/tp.2015.161

Chen, C., Sargent, C., Quilter, C., Yang, Z., Ren, J., Affara, N., et al. (2010). Cloning, mapping and molecular characterization of porcine progesterone receptor membrane component 2 (PGRMC2) gene. *Genet. Mol. Biol.* 33, 471–474. doi: 10.1590/S1415-47572010005000057

Craven, R. J., Mallory, J. C., and Hand, R. A. (2007). Regulation of iron homeostasis mediated by the heme-binding protein Dap1 (damage resistance protein 1) via the P450 rotein Erg11/Cyp51. *J. Biol. Chem.* 282, 36543–36551. doi: 10.1074/jbc.M706770200

Friel, A. M., Zhang, L., Pru, C. A., Clark, N. C., McCallum, M. L., Blok, L. J., et al. (2015). Progesterone receptor membrane component 1 deficiency attenuates growth while promoting chemosensitivity of human endometrial xenograft tumors. *Cancer Lett.* 356, 434–442. doi: 10.1016/j.canlet.2014.09.036

Gerdes, D., Wehling, M., Leube, B., and Falkenstein, E. (1998). Cloning and tissue expression of two putative steroid membrane receptors. *Biol. Chem.* 379, 907–911.

Habano, W., Gamo, T., Terashima, J., Sugai, T., Otsuka, K., Wakabayashi, G., et al. (2011). Involvement of promoter methylation in the regulation of Pregnane X receptor in colon cancer cells. *BMC Cancer* 11:81. doi: 10.1186/1471-2407-11-81

Han, K. H., Lee, S. H., Ha, S. A., Kim, H. K., Lee, C., Kim, D. H., et al. (2012). The functional and structural characterization of a novel oncogene GIG47 involved in the breast tumorigenesis. *BMC Cancer* 12:274. doi: 10.1186/1471-2407-12-274

Hand, R. A., Jia, N., Bard, M., and Craven, R. J. (2003). *Saccharomyces cerevisiae* Dap1p, a novel DNA damage response protein related to the mammalian membrane-associated progesterone receptor. *Eukaryot. Cell* 2, 306–317. doi: 10.1128/EC.2.2.306-317.2003

Hasegawa, S., Kasubuchi, M., Terasawa, K., and Kimura, I. (2016). Perspectives on membrane-associated progesterone receptors as prospective therapeutic targets. *Curr. Drug Targets* 17, 1189–1197. doi: 10.2174/1389450116666150518102651

Henderson, C. J., McLaughlin, L. A., Scheer, N., Stanley, L. A., and Wolf, C. R. (2015). Cytochrome b5 is a major determinant of human cytochrome P450 CYP2D6 and CYP3A4 activity in vivo. *Mol. Pharmacol.* 87, 733–739. doi: 10.1124/mol.114.097394

Hughes, A. L., Powell, D. W., Bard, M., Eckstein, J., Barbuch, R., Link, A. J., et al. (2007). Dap1/PGRMC1 binds and regulates cytochrome P450 enzymes. *Cell Metab.* 5, 143–149. doi: 10.1016/j.cmet.2006.12.009

Intlekofer, K. A., and Petersen, S. L. (2011). Distribution of mRNAs encoding classical progestin receptor, progesterone membrane components 1 and 2, serpine mRNA binding protein 1, and progestin and adipoQ receptor family members 7 and 8 in rat forebrain. *Neuroscience* 172, 55–65. doi: 10.1016/j.neuroscience.2010.10.051

Izzo, N. J., Xu, J., Zeng, C., Kirk, M. J., Mozzoni, K., Silky, C., et al. (2014). Alzheimer's therapeutics targeting amyloid beta 1–42 oligomers II: Sigma-2/PGRMC1 receptors mediate abeta 42 oligomer binding and synaptotoxicity. *PLoS ONE* 9:e111899. doi: 10.1371/journal.pone.0111899

Kabe, Y., Nakane, T., Koike, I., Yamamoto, T., Sugiura, Y., Harada, E., et al. (2016). Haem-dependent dimerization of PGRMC1/Sigma-2 receptor facilitates cancer proliferation and chemoresistance. *Nat. Commun.* 7:11030. doi: 10.1038/ncomms11030

Kaluka, D., Batabyal, D., Chiang, B.-Y., Poulos, T. L., and Yeh, S. R. (2015). Spectroscopic and mutagenesis studies of human PGRMC1. *Biochemistry* 54, 1638–1647. doi: 10.1021/bi501177e

Kandel, S. E., and Lampe, J. N. (2014). Role of protein–protein interactions in cytochrome P450-mediated drug metabolism and toxicity. *Chem. Res. Toxicol.* 27, 1474–1486. doi: 10.1021/tx500203s

Kassner, N., Huse, K., Martin, H. J., Gödtel-Armbrust, U., Metzger, A., Meineke, I., et al. (2008). Carbonyl reductase 1 is a predominant doxorubicin reductase in the human liver. *Drug Metab. Dispos.* 36, 2113–2120. doi: 10.1124/dmd.108.022251

Kimura, I., Nakayama, Y., Konishi, M., Kobayashi, T., Mori, M., Ito, M., et al. (2010). Neuferricin, a novel extracellular heme-binding protein, promotes neurogenesis. *J. Neurochem.* 112, 1156–1167. doi: 10.1111/j.1471-4159.2009.06522.x

Kimura, I., Nakayama, Y., Konishi, M., Terasawa, K., Ohta, M., Itoh, N., et al. (2012). Functions of MAPR (membrane-associated progesterone receptor) family members as heme/steroid-binding proteins. *Curr. Protein Pept. Sci.* 13, 687–696. doi: 10.2174/138920312804142110

Kimura, I., Yoshioka, M., Konishi, M., Miyake, A., and Itoh, N. (2005). Neudesin, a novel secreted protein with a unique primary structure and neurotrophic activity. *J. Neurosci. Res.* 79, 287–294. doi: 10.1002/jnr.20356

Klein, K., Thomas, M., Winter, S., Nussler, A. K., Niemi, M., Schwab, M., et al. (2012). PPARA: a novel genetic determinant of CYP3A4 in vitro and in vivo. *Clin. Pharmacol. Ther.* 91, 1044–1052. doi: 10.1038/clpt.2011.336

Laird, S. M., Vinson, G. P., and Whitehouse, B. J. (1988). Monoclonal antibodies against rat adrenocortical cell antigens. *Acta Endocrinol.* 119, 420–426. doi: 10.1530/acta.0.1190420

Lauschke, V. M., and Ingelman-Sundberg, M. (2015). Precision medicine and rare genetic variants. *Trends Pharmacol. Sci.* 37, 85–86. doi: 10.1016/j.tips.2015.10.006

Li, X., Rhee, D. K., Malhotra, R., Mayeur, C., Hurst, L. A., Ager, E., et al. (2016). Progesterone receptor membrane component-1 regulates hepcidin biosynthesis. *J. Clin. Invest.* 126, 389–401. doi: 10.1172/JCI83831

Lin, S.-T., May, E. W. S., Chang, J.-F., Hu, R.-Y., Wang, L. H.-C., and Chan, H.-L. (2015). PGRMC1 contributes to doxorubicin-induced chemoresistance in MES-SA uterine sarcoma. *Cell. Mol. Life Sci.* 72, 2395–2409. doi: 10.1007/s00018-014-1831-9

Losel, R., Besong, D., Peluso, J., and Wehling, M. (2008). Progesterone receptor membrane component 1—Many tasks for a versatile protein. *Steroids* 73, 929–934. doi: 10.1016/j.steroids.2007.12.017

Mallory, J. C., Crudden, G., Johnson, B. L., Mo, C., Pierson, C. A., Bard, M., et al. (2005). Dap1p, a heme-binding protein that regulates the cytochrome P450 protein Erg11p/Cyp51p in *Saccharomyces cerevisiae*. *Mol. Cell. Biol.* 25, 1669–1679. doi: 10.1128/MCB.25.5.1669-1679.2005

McCallum, M. L., Pru, C. A., Niikura, Y., Yee, S.-P., Lydon, J. P., Peluso, J. J., et al. (2016). Conditional ablation of progesterone receptor membrane component 1 results in subfertility in the female and development of endometrial cysts. *Endocrinology* 157, 3309–3319. doi: 10.1210/en.2016-1081

Meyer, C., Schmid, R., Scriba, P. C., and Wehling, M. (1996). Purification and partial sequencing of high-affinity progesterone-binding site(s) from porcine liver membranes. *Eur. J. Biochem.* 239, 726–731. doi: /10.1111/j.1432-1033.1996.0726u.x

Meyer, U. A. (2004). Pharmacogenetics – five decades of therapeutic lessons from genetic diversity. *Nat. Rev. Genet.* 5, 669–676. doi: 10.1038/nrg1428

Mifsud, W., and Bateman, A. (2002). Membrane-bound progesterone receptors contain a cytochrome b5-like ligand-binding domain. *Genome Biol.* 3, research0068.1–research0068.5. doi: 10.1186/gb-2002-3-12-research0068

Min, L., Strushkevich, N. V., Harnastai, I. N., Iwamoto, H., Gilep, A. A., Takemori, H., et al. (2005). Molecular identification of adrenal inner zone antigen as a heme-binding protein. *FEBS J.* 272, 5832–5843. doi: 10.1111/j.1742-4658.2005.04977.x

Min, L., Takemori, H., Nonaka, Y., Katoh, Y., Doi, J., Horike, N., et al. (2004). Characterization of the adrenal-specific antigen IZA (inner zone antigen) and its role in the steroidogenesis. *Mol. Cell. Endocrinol.* 215, 143–148. doi: 10.1016/j.mce.2003.11.025

Mir, S. U. R., Schwarze, S. R., Jin, L., Zhang, J., Friend, W., Miriyala, S., et al. (2013). Progesterone receptor membrane component 1/Sigma-2 receptor associates with MAP1LC3B and promotes autophagy. *Autophagy* 9, 1566–1578. doi: 10.4161/auto.25889

Neubauer, H., Clare, S. E., Wozny, W., Schwall, G. P., Poznanoviæ, S., Stegmann, W., et al. (2008). Breast cancer proteomics reveals correlation between estrogen receptor status and differential phosphorylation of PGRMC1. *Breast Cancer Res.* 10:R85. doi: 10.1186/bcr2155

Neubauer, H., Ma, Q., Zhou, J., Yu, Q., Ruan, X., Seeger, H., et al. (2013). Possible role of PGRMC1 in breast cancer development. *Climacteric* 16, 509–513. doi: 10.3109/13697137.2013.800038

Oda, S., Nakajima, M., Toyoda, Y., Fukami, T., and Yokoi, T. (2011). Progesterone receptor membrane component 1 modulates human cytochrome P450 activities in an isoform-dependent manner. *Drug Metab. Dispos.* 39, 2057–2065. doi: 10.1124/dmd.111.040907

Ohta, H., Kimura, I., Konishi, M., and Itoh, N. (2015). Neudesin as a unique secreted protein with multi-functional roles in neural functions, energy metabolism, and tumorigenesis. *Front. Mol. Biosci.* 2:24. doi: 10.3389/fmolb.2015.00024

Pandey, A. V., and Fluck, C. E. (2013). NADPH P450 oxidoreductase: structure, function, and pathology of diseases. *Pharmacol.Ther.* 138, 229–254. doi: 10.1016/j.pharmthera.2013.01.010

Peluso, J. J., Griffin, D., Liu, X., and Horne, M. (2014). Progesterone receptor membrane component-1 (PGRMC1) and PGRMC-2 interact to suppress entry into the cell cycle in spontaneously immortalized rat granulosa cells. *Biol. Reprod.* 91:104. doi: 10.1095/biolreprod.114.122986

Piel, R. B., Shiferaw, M. T., Vashisht, A. A., Marcero, J. R., Praissman, J. L., Phillips, J. D., et al. (2016). A novel role for progesterone receptor membrane component 1 (PGRMC1): a partner and regulator of ferrochelatase. *Biochemistry* 55, 5204–5217. doi: 10.1021/acs.biochem.6b00756

Raza, F. S., Takemori, H., Tojo, H., Okamoto, M., and Vinson, G. P. (2001). Identification of the rat adrenal zona fasciculata/reticularis specific protein, inner zone antigen (IZAg), as the putative membrane progesterone receptor. *Eur. J. Biochem.* 268, 2141–2147. doi: 10.1046/j.1432-1327.2001.02096.x

Ruan, X., Zhang, Y., Mueck, A. O., Willibald, M., Seeger, H., Fehm, T., et al. (2017). Increased expression of progesterone receptor membrane component 1 is associated with aggressive phenotype and poor prognosis in ER-positive and negative breast cancer. *Menopause* 24, 203–209. doi: 10.1097/GME.0000000000000739

Selmin, O., Lucier, G. W., Clark, G. C., Tritscher, A. M., Vanden Heuvel, J. P., Gastel, J. A., et al. (1996). Isolation and characterization of a novel gene induced by 2,3,7,8-tetrachlorodibenzo-p-dioxin in rat liver. *Carcinogenesis* 17, 2609–2615. doi: 10.1093/carcin/17.12.2609

Sueldo, C., Liu, X., and Peluso, J. J. (2015). Progestin and adipoQ receptor 7, progesterone membrane receptor component 1 (PGRMC1) and PGRMC2 and their role in regulating progesterone'sability to suppress human granulosa/luteal cells from entering into the cell cycle. *Biol. Reprod.* 93:63. doi: 10.1095/biolreprod.115.131508

Szczesna-Skorupa, E., and Kemper, B. (2011). Progesterone receptor membrane component 1 inhibits the activity of drug-metabolizing cytochromes P450 and binds to cytochrome P450 reductase. *Mol. Pharmacol.* 79, 340–350. doi: 10.1124/mol.110.068478

Wehling, M. (1997). Specific, nongenomic actions of steroid hormones. *Annu. Rev. Physiol.* 59, 365–393. doi: 10.1146/annurev.physiol.59.1.365

Wendler, A., and Wehling, M. (2013). PGRMC2, a yet uncharacterized protein with potential as tumor suppressor, migration inhibitor, and regulator of cytochrome P450 enzyme activity. *Steroids* 78, 555–558. doi: 10.1016/j.steroids.2012.12.002

Xie, Y., Bruce, A., He, L., Wei, F., Tao, L., and Tang, D. (2011). CYB5D2 enhances HeLa cells survival of etoposide-induced cytotoxicity. *Biochem. Cell Biol.* 89, 341–350. doi: 10.1139/o11-004

Xu, J., Zeng, C., Chu, W., Pan, F., Rothfuss, J. M., Zhang, F., et al. (2011). Identification of the PGRMC1 protein complex as the putative sigma-2 receptor binding site. *Nat. Commun.* 2:380. doi: 10.1038/ncomms1386

Zanger, U. M., and Schwab, M. (2013). Cytochrome P450 enzymes in drug metabolism: regulation of gene expression, enzyme activities, and impact of genetic variation. *Pharmacol. Ther.* 138, 103–141. doi: 10.1016/j.pharmthera.2012.12.007

Conflict of Interest Statement: The authors declare that the research was conducted in the absence of any commercial or financial relationships that could be construed as a potential conflict of interest.

frontiers in Pharmacology

ORIGINAL RESEARCH
published: 25 August 2017
doi: 10.3389/fphar.2017.00580

Altered CYP19A1 and CYP3A4 Activities Due to Mutations A115V, T142A, Q153R and P284L in the Human P450 Oxidoreductase

*Sameer S. Udhane[1,2†], Shaheena Parween[1,2], Norio Kagawa[3] and Amit V. Pandey[1,2]**

[1] Department of Pediatric Endocrinology, Diabetology and Metabolism, University Children's Hospital Bern, Bern, Switzerland, [2] Department of Clinical Research, University of Bern, Bern, Switzerland, [3] School of Medicine, Nagoya University, Nagoya, Japan

OPEN ACCESS

Edited by:
Kathrin Klein,
Dr. Margarete Fischer-Bosch Institut für Klinische Pharmakologie (IKP), Germany

Reviewed by:
Vangelis G. Manolopoulos,
Democritus University of Thrace, Greece
Claes Von Wachenfeldt,
Lund University, Sweden
Todd D. Porter,
University of Kentucky, United States

***Correspondence:**
Amit V. Pandey
amit@pandeylab.org

†Present address:
Sameer S. Udhane,
Department of Pathology, Medical College of Wisconsin Cancer Center, Milwaukee, WI, United States

Specialty section:
This article was submitted to Pharmacogenetics and Pharmacogenomics, a section of the journal Frontiers in Pharmacology

Received: 02 October 2016
Accepted: 10 August 2017
Published: 25 August 2017

Citation:
Udhane SS, Parween S, Kagawa N and Pandey AV (2017) Altered CYP19A1 and CYP3A4 Activities Due to Mutations A115V, T142A, Q153R and P284L in the Human P450 Oxidoreductase. Front. Pharmacol. 8:580. doi: 10.3389/fphar.2017.00580

All cytochromes P450s in the endoplasmic reticulum rely on P450 oxidoreductase (POR) for their catalytic activities. Mutations in POR cause metabolic disorders of steroid hormone biosynthesis and affect certain drug metabolizing P450 activities. We studied mutations A115V, T142A, Q153R identified in the flavin mononucleotide (FMN) binding domain of POR that interacts with partner proteins and P284L located in the hinge region that is required for flexibility and domain movements in POR. Human wild-type (WT) and mutant POR as well as CYP3A4 and CYP19A1 proteins in recombinant form were expressed in bacteria, and purified proteins were reconstituted in liposomes for enzyme kinetic assays. Quality of POR protein was checked by cytochrome c reduction assay as well as flavin content measurements. We found that proteins carrying mutations A115V, T142A located close to the FMN binding site had reduced flavin content compared to WT POR and lost almost all activity to metabolize androstenedione via CYP19A1 and showed reduced CYP3A4 activity. The variant P284L identified from apparently normal subjects also had severe loss of both CYP19A1 and CYP3A4 activities, indicating this to be a potentially disease causing mutation. The mutation Q153R initially identified in a patient with disordered steroidogenesis showed remarkably increased activities of both CYP19A1 and CYP3A4 without any significant change in flavin content, indicating improved protein–protein interactions between POR Q153R and some P450 proteins. These results indicate that effects of mutations on activities of individual cytochromes P450 can be variable and a detailed analysis of each variant with different partner proteins is necessary to accurately determine the genotype-phenotype correlations of POR variants.

Keywords: POR, P450 oxidoreductase, CYP19A1, CYP3A4, polymorphisms, protein–protein interaction, cytochrome P450

INTRODUCTION

Cytochrome P450 proteins metabolize a wide range of drugs, steroids and xenobiotics (Schuster and Bernhardt, 2007; Omura, 2010; Zanger and Schwab, 2013). There are two distinct types of cytochrome P450 proteins in humans (Omura, 2010). Type 1 P450s, that are located in the mitochondria, are primarily involved in the metabolism of steroids and use

adrenodoxin/adrenodoxin reductase proteins as redox partners (Omura, 2006; Zalewski et al., 2016). The type 2 P450s, located in the endoplasmic reticulum, rely on a single redox partner, the cytochrome P450 oxidoreductase (POR, NCBI# NP_000932, UniProt# P16435), for supply of electrons (Lu et al., 1969). POR is a flavoprotein that contains both the flavin mononucleotide (FMN) and the flavin adenine dinucleotide (FAD) and supplies electrons to cytochromes P450 and other proteins (Matsubara et al., 1976; Nagao et al., 1983; Guengerich, 2005). The structure of the FMN binding domain of human POR has been determined by x-ray crystallography (Zhao et al., 1999) and a more recent open conformation structure of POR shows potential interaction possibilities for redox partners (Aigrain et al., 2009).

P450 oxidoreductase deficiency (PORD, OMIM: 613537 and 201750) is a form of congenital adrenal hyperplasia, initially described in patients with altered steroidogenesis (Flück et al., 2004) followed by several reports with a broad spectrum of disorders (Adachi et al., 2004; Arlt et al., 2004; Pandey and Flück, 2013; Flück and Pandey, 2014; Pandey and Sproll, 2014; Burkhard et al., 2017). Sequencing of the POR gene revealed mutations in patients with disorders of steroid biosynthesis (Flück et al., 2004; Miller et al., 2004; Pandey et al., 2004). Afterward, many other laboratories reported mutations in POR in patients with steroidogenic disorders and/or bone malformation syndromes (Adachi et al., 2004; Arlt et al., 2004; Fukami et al., 2005; Pandey and Flück, 2013; Riddick et al., 2013). While initial studies on POR mutations focused on steroid metabolism, effects on other partner proteins like heme oxygenase and drug metabolizing P450s have also been studied (Agrawal et al., 2008, 2010; Flück et al., 2010; Nicolo et al., 2010; Pandey et al., 2010). Large scale sequencing projects have identified many variations in the POR gene, in several different human sub-populations, and multiple variants have been implicated in altered drug metabolism (Gomes et al., 2008, 2009; Huang et al., 2008; Agrawal et al., 2010; Nicolo et al., 2010; Pandey et al., 2010). Since POR is involved in multiple steroid biosynthesis reactions catalyzed by cytochrome P450 proteins, a complex disorder of steroidogenesis is expected from mutations in POR (**Figure 1**). Many POR variants found in patients as well as normal population have been tested for enzymatic activities (Adachi et al., 2004; Arlt et al., 2004; Fukami et al., 2005, 2006; Homma et al., 2006; Pandey, 2006; Huang et al., 2008; Sim et al., 2009). While mutations in POR can be found in all regions of the protein, based on analysis of previously identified mutations, some general observations can be made. Mutations found in the co-factor binding sites (FMN, FAD and NADPH) generally result in a severe form of the disease with the mutations causing loss of FMN or FAD showing most severe effects on activities of all supported redox partners. We have previously shown that aromatase (CYP19A1) activity responsible for conversion of androgens to estrogens (**Figure 1**) is more susceptible to changes in NADPH binding site mutations in POR (Pandey et al., 2007; Flück et al., 2011; Flück and Pandey, 2017). The studies described in this report were conducted by embedding POR and P450 proteins in liposomes followed by removal of detergents. In the current study, we have investigated effects of some mutations in the FMN binding domain and the hinge region of POR that facilitate interactions with redox partner proteins, including P450s, to transfer electrons from NADPH.

MATERIALS AND METHODS

Recombinant Expression of POR and Membrane Purification

The WT and variant POR (NCBI# NP_000932, Uniprot# P16435) proteins were expressed in bacteria using the expression constructs described previously (Huang et al., 2005, 2008; Pandey et al., 2007; Nicolo et al., 2010). The protocol for expression of N-27 form of POR variants and subsequent membrane purification is described and adopted from our previous publications (Huang et al., 2005; Pandey et al., 2007, 2010; Parween et al., 2016; Flück and Pandey, 2017). The cDNAs for WT or mutant POR in pET22b were transformed into *Escherichia coli* BL21(DE3), single colonies were selected for growth on ampicillin and grown in terrific broth pH 7.4 supplemented with 40 mM $FeCl_3$, 4 mM $ZnCl_2$, 2 mM $CoCl_2$, 2 mM Na_2MoO_4, 2 mM $CaCl_2$, 2 mM $CuCl_2$, 2 mM H_3BO_3, 0.5 mg/ml riboflavin, 100 μg/ml carbenicillin at 37°C to an optical density (OD) 600 nm of 0.6 and temperature was reduced to 25°C for 16 h. The bacterial cells were collected by centrifugation, washed with PBS and suspended in 100 mM Tris–acetate (pH 7.6), 0.5 M sucrose, and 1 mM EDTA and treated with lysozyme (0.5 mg/ml) and EDTA (0.1 mM [pH 8.0]) at 4°C for 1 h with slow stirring to generate spheroplasts. The spheroplasts were pelleted by centrifugation at 5000 × *g* for 15 min; and suspended in 100 mM potassium phosphate (pH 7.6), 6 mM MgOAc, 0.1 mM DTT, 20% (v/v) glycerol, 0.2 mM PMSF, and 0.1 mM DNase I; and disrupted by sonication. A clear lysate devoid of cellular debris was obtained by centrifugation at 12,000 × *g* for 10 min, and then the membranes were collected by centrifugation at 100,000 × *g* for 60 min at 4°C. Membranes were suspended in 50 mM Potassium phosphate buffer (pH 7.8) and 20% (v/v) glycerol and stored at −70°C. Protein concentration was measured by RC-DC protein assay (Protein Assay Dye Reagent, Bio-Rad, Hercules, CA, United States) and POR content in membrane proteins was quantitated by western blot analysis.

Quantification of POR Content in the Bacterial Membranes by Western Blot Analysis

For Western blots, 1 μg of WT and POR bacterial membrane proteins were separated on SDS–PAGE gel and blotted on to polyvinyldifluoride (PVDF) membranes. Blots were probed with a rabbit polyclonal antibody against wild-type human POR from Genscript (Genscript, Piscataway, NJ, United States) at a dilution of 1:1000. We used a secondary goat anti-rabbit antibody that was labeled with a phthalocyanine infrared dye (IRDye 700DX, LI-COR Bioscience Inc., Lincoln, NE, United States) at a dilution of 1:10000. Signals were detected with the green fluorescent channel (700 nm) on an Odyssey Infrared Imaging System (LI-COR Bioscience Inc., Lincoln, NE, United States), and

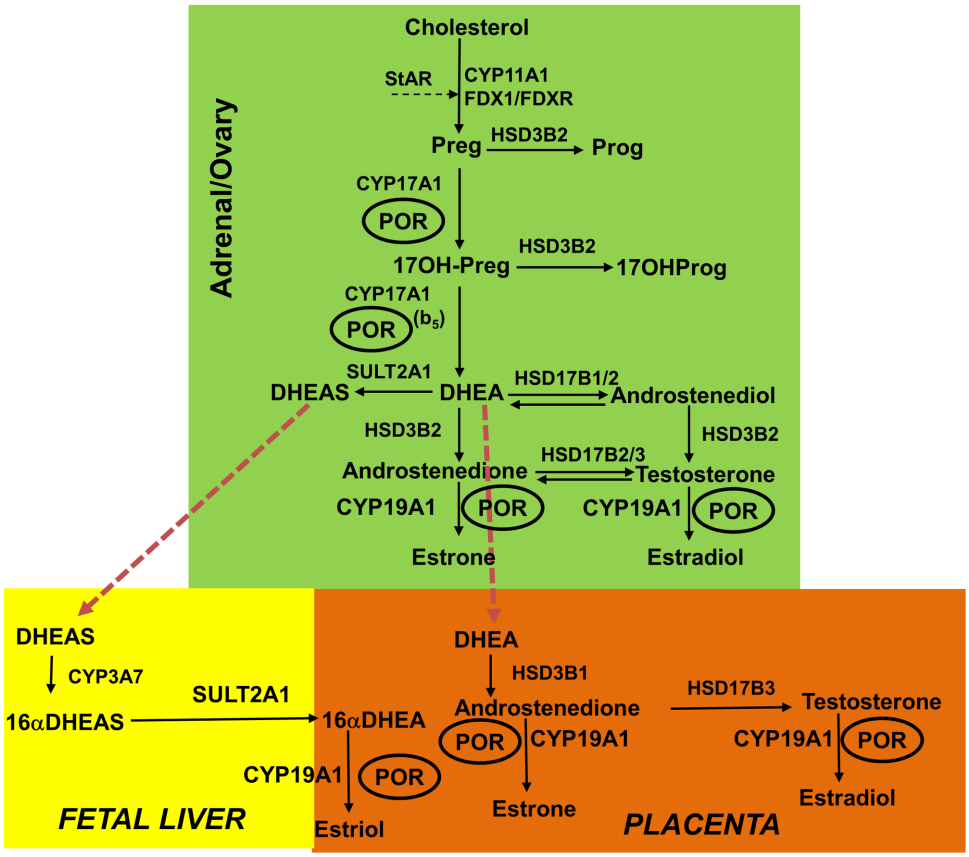

FIGURE 1 | Role of POR in the steroid hormone biosynthesis. In the first steps of steroid biosynthesis, cholesterol is transported to mitochondrion by steroidogenic acute regulatory protein (StAR). Then, inside the mitochondria, the cholesterol is metabolized by CYP11A1 to pregnenolone, and adrenodoxin and adrenodoxin reductase act as the redox mediators in this reaction. The pregnenolone produced in the mitochondria is further metabolized in the endoplasmic reticulum to downstream products 17OHPreg, DHEA, androstenedione or androstenediol; and then this process continues toward the production of testosterone in the Leydig cells of the testes. Testosterone is further metabolized to dihydrotestosterone (DHT) in the genital skin. In the placenta, DHEA is converted to androstenedione and then to testosterone, which is further metabolized to estrogens. In fetal liver, inactive precursor DHEAS is converted to 16αDHEAS, which gets converted to 16αDHEA in placenta to produce estrogens. The estrogen biosynthesis process requires CYP19A1 activity that is dependent on POR. The deficiency in POR can alter the enzymatic reactions of many cytochrome P450 enzymes and these changes can be variable based on structural properties of the mutation and nature of the redox partner. CYP11A1, P450scc, cholesterol side-chain cleavage enzyme; StAR, steroidogenic acute regulatory protein; FDX1, Adrenodoxin; FDXR, NADPH adrenodoxin oxidoreductase; CYP17A1, P450c17, 17α-hydroxylase/17,20-lyase; HSD3B2, 3βHSD2, 3β-hydroxysteroid dehydrogenase, type 2; CYB5, cytochrome b_5; POR, P450 oxidoreductase; HSD17B3, 17βHSD3, 17β-hydroxysteroid dehydrogenase, type 3. Full steroid names: 17OHPreg, 17-hydroxypregnenolone; 17OHProg, 17-hydroxyprogesterone; 17OH-DHP, 17-hydroxydihydroprogesterone (5α-pregnan-3α,17α-ol-20-one); DHEA, dehydroepiandrosterone.

bands were quantitated using Odyssey software. POR content of each membrane preparation was measured, and all samples were normalized against purified wild-type POR used as standard. In all experiments the normalized amount of POR content was used in each experiment for all mutants as well as WT protein.

Cytochrome c Reduction Assay by WT and Mutant POR

The cytochrome c reduction by bacterially expressed WT or mutant POR was assayed as described previously by measuring the change in absorbance at 550 nm ($\varepsilon = 21.1\ cm^{-1}\ mM^{-1}$) (Guengerich et al., 2009). Briefly, the reaction was performed in 96-well plates, in triplicate, with 5 μg of POR membrane preparation in each well, using a microplate reader (Spectramax M2e, Molecular Devices, Sunnyvale, CA, United States). The NADPH concentration was fixed at 100 μM and different concentrations of cytochrome c (0.6–80 μM) were used. The change in absorbance at 550 nm was monitored against time. Data were fitted based on Michaelis–Menten kinetics (Michaelis and Menten, 1913) using GraphPad Prism (GraphPad Software, La Jolla, CA, United States) to determine the Vmax and Km.

Flavin Content Analysis of WT and Mutant POR

To differentiate the conformational changes and effects of co-factor binding, we evaluated the relative flavin content in POR variants as the activity of POR is affected by the binding of cofactors FMN and FAD. Protein bound flavin molecules were

released by thermal denaturation of POR proteins (Faeder and Siegel, 1973). Flavin content of WT and mutant POR proteins (100 μg/ml) was determined by heating protein samples at 95°C for 10 min in the dark, followed by centrifugation at 14000 × *g* for 10 min to remove the coagulated protein. The FMN and FAD ratio was determined by measurement of fluorescence of the supernatant at pH 7.7 and pH 2.6 (excitation at 450 nm, emission at 535 nm) (Faeder and Siegel, 1973) using commercially available FMN and FAD as standards (Sigma–Aldrich, Basel, Switzerland).

CYP19A1 Expression and Purification

The CYP19A1 vector for bacterial expression was transformed in *E. coli* BL21(DE3) cells and the recombinant protein was expressed and purified following previously published protocols (Kagawa et al., 2003; Kagawa, 2011), with slight modifications. Briefly, a single transformed colony was selected for protein expression at 25°C. After 4 h of incubation, 1 mM δ-aminolevulinic acid (a heme precursor) and 4 mg/ml arabinose (for induction of molecular chaperones GroEL/GroES) were added to the culture and further incubated for 20 h. Cells were harvested and spheroplasts were prepared with 0.2 mg/ml lysozyme in 50 mM Tris–Acetate (pH 7.6), 250 mM sucrose and 0.5 mM EDTA and stored at −80°C. For protein purification, spheroplasts were lysed using 10XCellLytic B (Sigma–Aldrich) in buffer containing 100 mM potassium phosphate (pH 7.4), 500 mM sodium acetate, 0.1 mM EDTA, 0.1 mM DTT, 20% glycerol, and 1 mM PMSF. The cell lysate was centrifuged and the supernatants were pooled for purification by Ni^{2+} affinity chromatography. Purification was performed at 4°C and protein concentration after the dialysis was determined by DC protein assay (Protein Assay Dye Reagent, Bio-Rad, Hercules, CA, United States) using BSA as standard.

Aromatase Activity Measurement in Reconstituted Liposome System

Purified recombinant CYP19A1 using the bacterial expression system was used to test the effect of POR variants to support the aromatase activity of CYP19A1. Standard tritiated water release assay for the CYP19A1 activity was performed in a reconstituted liposome system using androstenedione as substrate. Bacterial membranes containing POR and purified CYP19A1 were reconstituted into DLPC-DLPG liposomes. The liposomes were prepared as described in **Figure 2**. Aromatase activity was measured by the tritiated water release assay originally described by Lephart and Simpson (1991) with modifications as described by us previously (Pandey et al., 2007; Flück and Pandey, 2017) using a reconstituted lipid-CYP19A1-POR system and androstenedione as the substrate. Reaction mixture consisted of 100 pmol of CYP19A1, 400 pmol of POR, 100 mM NaCl and ^3H labeled androstenedione ([1β-^{3}H(N)]-andros-tene-3,17-dione; ∼20,000 cpm) in 100 mM potassium-phosphate buffer (pH 7.4). Different concentrations (10–1000 nM) of androstenedione were used for kinetic analysis. The catalytic reaction was initiated by the addition of 1 mM NADPH and the reaction tube was incubated for 1 h under shaking. Data were fitted based on Michaelis–Menten kinetics using GraphPad Prism (GraphPad Software, La Jolla, CA, United States).

CYP3A4 Activity Measurement in Reconstituted Liposome System

To compare the activities of CYP19A1 with another steroid binding cytochrome P450, we tested the effect of POR mutations to support the enzyme activity of CYP3A4. The activity of the major drug metabolizing enzyme CYP3A4 supported by WT or mutant POR was tested using the fluorogenic substrates [BOMCC (7-Benzyloxy-4-trifluoromethylcoumarin) and DBOMF dibenzylmethylfluorescein] (Invitrogen Corp, Carlsbad, CA, United States) as described earlier (Flück et al., 2010). The purified CYP3A4 (CYPEX, Dundee, Scotland, United Kingdom) was used to test the activities of the POR variants using 20 μM BOMCC or 5 μM DBOMF as substrate (the apparent Km value of CYP3A4 for BOMCC, 10 μM, DBOMF 2.5 μM were derived from pilot experiments using WT POR and CYP3A4). *In vitro* CYP3A4 assays were performed using a reconstituted liposome system consisting of WT/mutant POR, CYP3A4 and cytochrome b_5 at a ratio of 4:1:1 (POR:CYP3A4:b_5). Reconstitution of liposomes was carried out similarly as described before. The final assay mixture consisted of liposomes and proteins (80 pmol POR: 20 pmol CYP3A4: 20 pmol b_5), 2.5 mM $MgCl_2$, 2.5 μM GSH and 20 μM BOMCC or 5 μM DBOMF in 50 mM HEPES buffer and the reaction volume was 200 μl. The catalytic reaction was initiated by addition of NADPH to 1 mM final concentration and fluorescence was monitored on a Spectramax M2e plate reader (Molecular Devices, Sunnyvale, CA, United States) at an excitation wavelength of 415 nm and emission wavelength of 460 nm for BOMCC and at an excitation wavelength of 490 nm and emission wavelength of 520 nm for DBOMF.

Statistical Analysis

Data are presented as mean standard errors of mean (SEM) in each group or replicates. Differences within the subsets of experiments were analyzed using Student's *t*-test with GraphPad Prism (GraphPad Software Inc., CA, United States). *P*-values less than 0.05 were considered statistically significant.

3D Protein Models

Three dimensional structural models of POR (NCBI# NP_000932) proteins were obtained from protein structure database[1]. We used the structures of the FMN binding domain of human POR (PDB # 1B1C) as well as an open structure of POR protein (PDB# 3FJO) to analyze the location of amino acids described in this report (Zhao et al., 1999; Aigrain et al., 2009). Structure models were drawn using the software Pymol[2] and rendering of images was performed with POVRAY[3].

[1]www.rcsb.org

[2]www.pymol.org

[3]www.povray.org

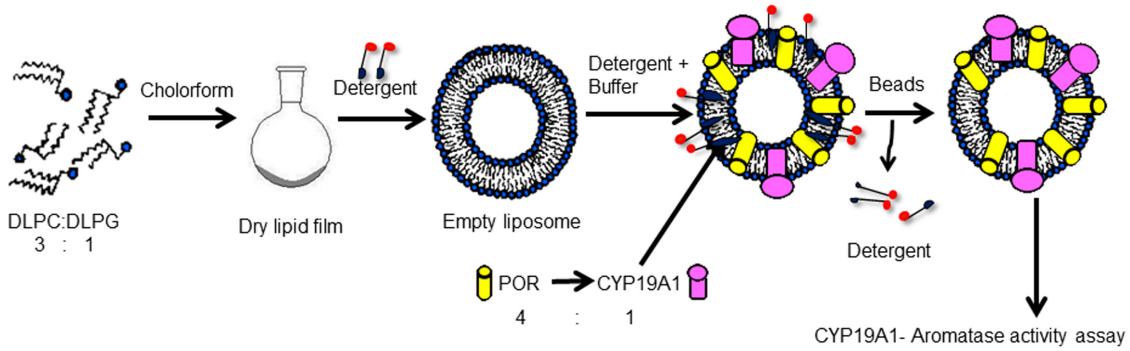

FIGURE 2 | Reconstitution of POR and CYP19A1 proteins into liposomes. Lipids (DLPC: DLPG) were dissolved in chloroform and kept overnight for drying in a fume hood. Next day, dried lipids were solubilized in detergent to prepare liposomes. The CYP19A1 and POR membranes were added to the liposomes and the protein-liposome mixture was incubated for 1 h with shaking to incorporate the proteins into the liposomes. After 1 h, biobeads were added to remove the detergent, and samples were incubated for another 1 h. After incubation, the mixture was cleared by centrifugation and the supernatant was used for assay of CYP19A1 activity.

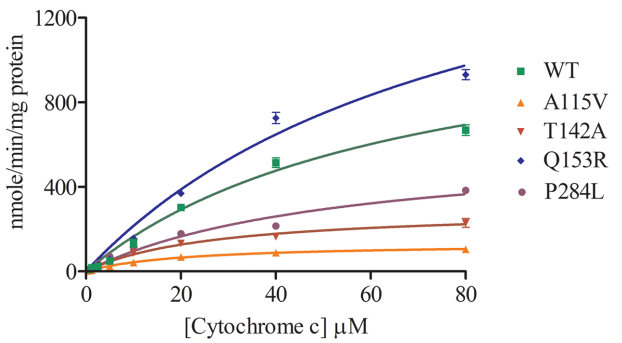

FIGURE 3 | Cytochrome c reduction assay with WT and mutant POR. Cytochrome c reduction assays was performed with the WT and variant forms of POR. Kinetic assay relied on the changes in absorbance at 550 nm when oxidized cytochrome c is converted into reduced cytochrome c. Data were fitted as Michaelis–Menten kinetics model using GraphPad Prism. The calculated Km and Vmax values are summarized in **Table 1**.

RESULTS

Cytochrome c Reduction Assay

Cytochrome c reduction assay with WT and POR variants was performed to assess the basic quality and general catalytic efficiency of POR as well as internal electron transfer in POR. As compared to WT POR, 40–70% loss of activity in reducing cytochrome c was observed with POR variants A115V, T142A and P284L (**Figure 3** and **Table 1**). This loss of activity indicates that these mutations affect electron transport in POR through flavins to cytochrome c since reduction of cytochrome c requires the participation of both FAD and FMN as do the cytochromes P450. Interestingly, Q153R showed 25% higher cytochrome c reduction activity than WT POR (**Table 1**).

Flavin Content

As compared to WT POR, a 40–50% decrease in flavin content of A115V mutant was observed (0.52 mol FMN/mol of POR and 0.59 mol FAD/mol of POR). Both the FMN as well as the FAD binding was severely affected due to T142A mutation with approximately 80% loss of relative flavin content as compared to WT (0.19 mol FMN/mol of POR and 0.22 mol FAD/mol of POR) (**Figure 4**). The total flavin content of the gain of function mutation Q153R (1 mol FMN/mol of POR and 0.99 mol FAD/mol of POR) was comparable to WT and for the loss of function mutation P284L the FMN content was similar to WT (0.91 mol FMN/mol of POR) while the FAD content was reduced by 25% (0.75 mol FAD/mol of POR) suggesting that these mutations do not severely affect either the FMN or the FAD binding to POR (**Figure 4**).

CYP19A1-Aromatase Activity

The POR variants A115V, T142A and P284L showed almost complete loss of CYP19A1 activity (**Figure 5** and **Table 1**). For the T142A variant, the apparent Km for androstenedione was increased fourfold as compared to WT POR suggesting that T142A mutation affects either substrate interaction of CYP19A1 or the CYP19A1-POR interaction. The apparent Km with P284L variant was comparable to that of WT POR but the apparent Vmax was reduced by 85%. Interestingly, POR variant Q153R showed 47% higher value of Vmax/Km compared to WT POR.

CYP3A4 Enzyme Activity

The A115 V and T142A variants of POR showed 2–10% activity compared to WT (**Figure 6**). In human POR residues A115V and T142A are directly involved in FMN binding. The POR variant P284L resulted in 12–15% of CYP3A4 activity (**Figure 6**). The CYP3A4 activity of POR variant

TABLE 1 | Kinetic parameters for activities of cytochrome c reduction and CYP19A1 activity supported by WT and mutant POR.

	Km, cytochrome c (μM)	Vmax nmol/min/mg	Vmax/Km	% WT
Cytochrome c reduction assay				
	67.4 ± 11.2	1279 ± 123.7	19	100
A115V	20.9 ± 11.1*	133.4 ± 2.8*	6.4	34
T142A	27.0 ± 13.4*	298.1 ± 15.4*	11	58
Q153R	81.5 ± 18.2*	1968 ± 270.2*	24.2	127
P284L	53.7 ± 10.5*	610 ± 63.5*	11.4	60
	Km androstenedione (nM)	**Vmax pmol/min/nmol**	**Vmax/Km**	**% WT**
CYP19A1; aromatase (androstenedione to estrone)				
WT	80 ± 14.5	0.72 ± 0.03	0.0090	100
A115V	nd	nd	nd	–
T142A	308.4 ± 121.5*	0.11 ± 0.01*	0.0004	5
Q153R	65.62 ± 11.38*	0.86 ± 0.03*	0.0132	147
P284L	82.4 ± 62.5*	0.039 ± 0.008*	0.0005	5

*For the cytochrome c reduction assay, the NADPH concentration was fixed at 100 μM and different concentrations of cytochrome c (0.6–80 μM) were used. For the conversion of androstenedione to estrone, variable concentrations (10–1000 nM) of androstenedione were used for kinetic analysis in presence of 1 mM NADPH. Data are presented as mean ± SEM of independent replicates. *Indicates p-values < 0.05. nd: not detectable.*

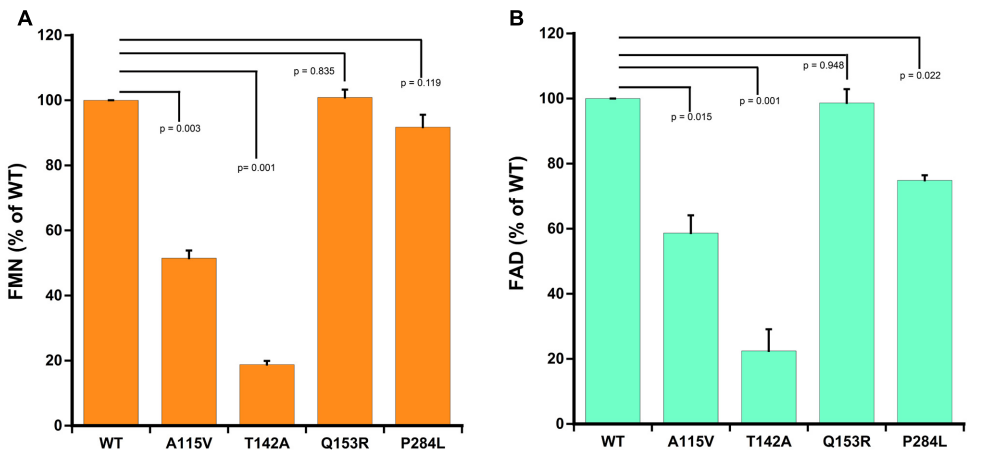

FIGURE 4 | Flavin content of WT and mutant POR proteins. Flavin content was measured by boiling protein samples under different buffer conditions. Relative fluorescence unit (RFU) of the flavins released from POR variants obtained at pH 7.7 ($F_{7.7}$) and pH 2.6 ($F_{2.6}$) were plotted. RFU of WT was set as hundred percent. **(A)** Shows FMN measurements and **(B)** shows FAD measurements. *p*-values for significance analysis compared to wild-type sample are indicated above the bars. Data are presented as mean ± SEM of three replicates.

Q153R was nearly three times more than wild-type (WT) POR (**Figure 6**).

DISCUSSION

P450 oxidoreductase is a membrane associated protein that binds NADPH, causing a conformation change that brings NADPH and FAD close together to transfer electrons. Afterward, further conformation changes cause a closing of the POR structure and brings FAD and FMN closer for electron transfer from FAD to FMN. The FMN binding domain of POR interacts with P450s and other partner proteins through charge pair interactions involving arginine and lysine residues on P450s and aspartate and glutamate residues on POR. Considering the importance of FMN binding domain of POR in protein–protein interactions we investigated the effects of mutations in this region of POR for enzymatic activities on partner proteins. The mutations studied in this report are either located close to the FMN binding site of POR (A115V, T142A and Q153R) or in the putative hinge region (P284L) required for flexibility of POR to interact with redox partners. Using WT and variant POR and P450 proteins expressed in bacteria, we determined the enzymatic activities for metabolism of androstenedione by CYP19A1 and compared them with CYP3A4 activities which can bind and metabolize testosterone. Some very interesting and surprising findings were made from this study, including the severe effect of POR variant A115V which was previously suspected as a polymorphism (rs 199634961, *POR*11*) and shows variable activities (Huang et al., 2005; Agrawal et al., 2008, 2010; Pandey et al., 2010; Pandey and

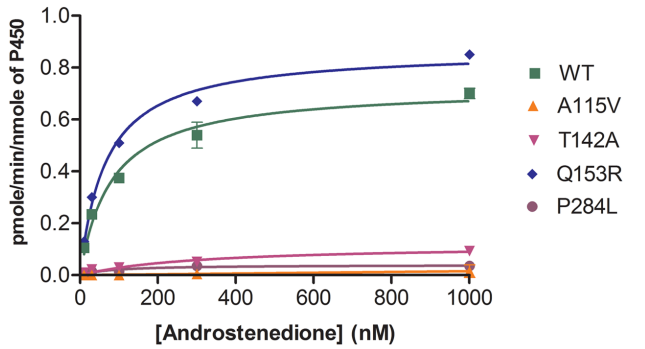

FIGURE 5 | Aromatase activity supported by WT and mutant POR proteins. Bacterially expressed purified recombinant CYP19A1 and POR membranes were incorporated into liposomes and their activity to convert [^{3}H] labeled androstenedione to estrone was tested by the tritiated water release assay. Data were fitted with Michaelis–Menten kinetics model using GraphPad Prism. The calculated Km and Vmax values are summarized in **Table 1**.

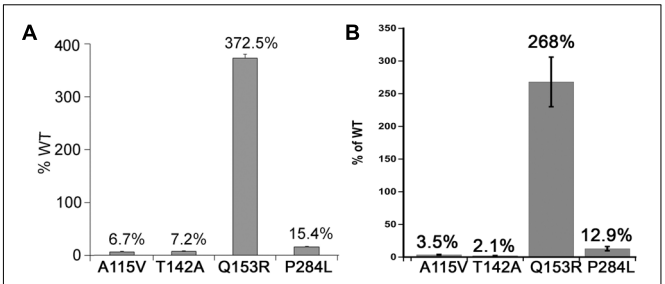

FIGURE 6 | CYP3A4 activity supported by WT and mutant POR proteins. CYP3A4 enzyme activity assays were performed to compare WT and mutant POR using either **(A)** 20 μM BOMCC or **(B)** 5 μM DBOMF as substrate. Activity with the WT POR was set as hundred percent and results are shown as percentage of WT activity. Data are presented as mean ± SEM of three independent replicates.

Flück, 2013; Burkhard et al., 2017). The POR variants P284L was found to result in severe loss of activities while mutation Q153R showed an activating effect. These results provide further insights into the interactions of POR with its redox partner proteins and help in establishing the genotype-phenotype correlations of POR variants and their metabolic effects. Loss of flavins could explain differences in activities for some mutations. Since the A115 and T142 residues are near the FMN binding site, a loss of FMN binding could be expected. However, both these mutants also showed loss of FAD binding indicating that binding of FMN may influence FAD binding. A similar relationship of FAD binding to FMN binding has been observed by Shen et al. (1989) in experiments with rat POR. Several different proposals could be made to explain this observation. It is likely that binding of FMN is required for recognition of FAD by POR. An FMN dependent change if affinity of POR for FAD is possible (Shen et al., 1989). The observation of Kurzban and Strobel (1986) that FAD comes of more readily from POR compared to FMN seems to support the hypothesis that affinity of POR for FMN is higher. Mutations in the FAD binding domain of POR result in complete loss of activities (Flück et al., 2004; Pandey et al., 2004; Huang et al., 2005; Pandey and Flück, 2013). For some POR mutations a rescue of activities may be possible by flavin supplementation (Marohnic et al., 2010; Nicolo et al., 2010).

Aromatase catalyzes the conversion of androstenedione to estrone (E1), testosterone to estradiol (E2) and 16-hydroxytestosterone to estriol (E3) (Simpson et al., 1994) (**Figure 1**). The CYP19A1 reaction requires multiple interactions with POR, and therefore, changes in redox partner binding sites on either CYP19A1 or POR may alter enzymatic activities. To test this hypothesis, we selected several mutations located in the FMN binding domain and the hinge region of POR, which facilitate interactions with partner proteins. One of the variants studied here, the A115V was first identified in a patient (Huang et al., 2005). The patient harboring A115V mutation was from Caucasian background and had Beare–Stevenson syndrome, which results in skeletal as well as genital abnormalities (Przylepa et al., 1996; Huang et al., 2005). A rugated labia majora and anteriorly placed anus had been reported but no steroid or biochemical analysis were available (Huang et al., 2005). Structure analysis of A115V mutation revealed hydrogen bonding interaction between A115 and V85 and Y87 residues located on the neighboring beta sheet, implicating its role in structural stability (**Figure 7A**). Previously Agrawal et al. (2008) have shown that A115V mutation caused complete loss of CYP1A2 and CYP2C19 activities, while only a 20–30% loss of 17-hydroxylase and 17,20 lyase activities was observed in CYP17A1 assays (Huang et al., 2005). Our results indicate the severe loss of CYP19A1 aromatization activity could lead to abnormal steroid metabolism in patients with A115V mutation in POR gene. A detailed steroid analysis of such patients would be necessary to confirm this linkage.

The patient with T142A mutation was from Iraqi/Yemeni parents and did not have bone malformation but showed abnormal genitalia (Augarten et al., 1992). The ACTH stimulation test for the adrenal function indicated combined CYP17A1 and CYP21A2 deficiencies, but no genetic defects in these genes were found. Augarten et al. (1992) had hypothesized that a deficiency in another enzyme, likely a flavoprotein may be the cause but this was not pursued further, and only in 2005 the T142A mutation in the POR from this patient was identified (Huang et al., 2005). In previous reports a 97% loss of CYP1A2 activity and complete loss of CYP2C19 activity has been reported by Agrawal et al. (2008) for the T142A mutation, while a 40–50% loss of CYP17A1 activity was observed by Huang et al. (2005). The patient with T142A mutation of POR had low serum levels of testosterone; and androstenedione and dehydroepiandrosterone sulfate were low (but present) and did not improve upon ACTH stimulation, consistent with loss of CYP17A1 activities (Augarten et al., 1992). This is consistent with crucial physiological role of androgen regulating enzyme CYP17A1, where complete loss of activities is lethal. The mutation T142A (*POR*12*) is located next to the Y143 residue which is crucial for the FMN binding

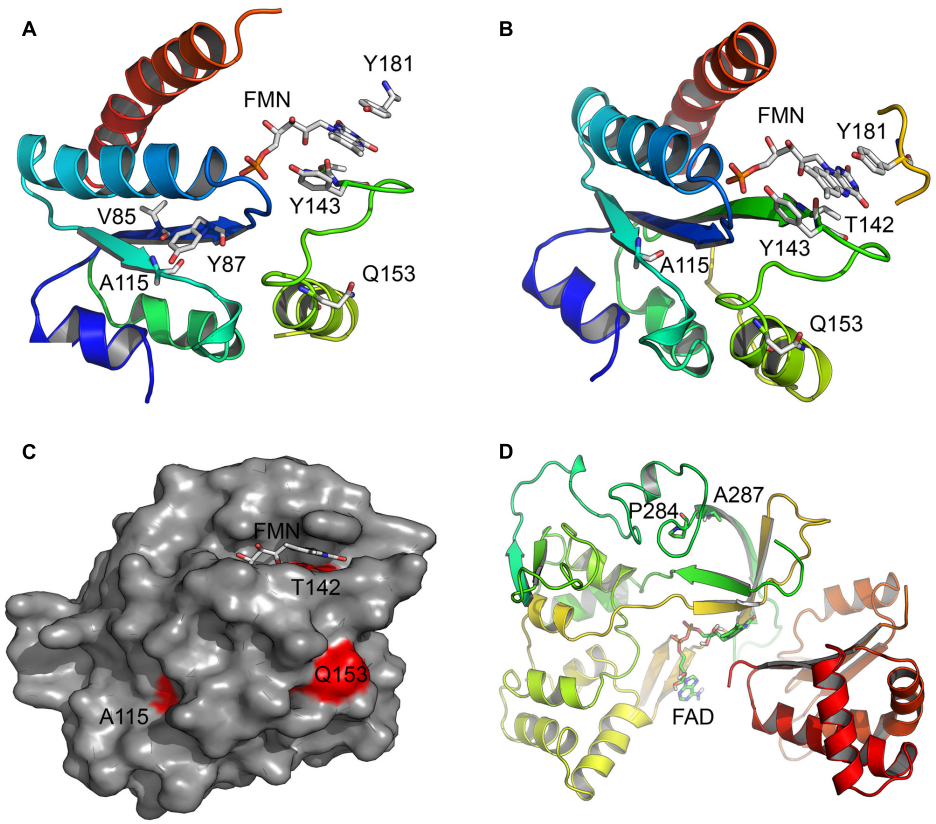

FIGURE 7 | Location of amino acid changes in POR described in current study. The x-ray crystal structures of the human POR (NCBI# NP_000932) protein; the FMN binding domain (**PDB#** 1B1C) and the flexible hinge region (**PDB#** 3FJO) showing the location of mutations studied in this report. **(A)** Location of residue A115. Structure analysis revealed hydrogen bonding interaction between A115 and V85 and Y87 residues located on a neighboring beta sheet in the FMN binding domain of POR, implicating its role in structural stability. The models are colored in rainbow colors with violet at the N-terminus and red at the C-terminus. The co-factors FMN and FAD are shown as sticks. **(B)** Location of residues T142 and Q153. The mutation T142A is located next to Y143 residue crucial for FMN binding to POR and its mutation affected FMN binding. The Q153 residue is located at the surface of POR and predicted to have a role in the interactions with the redox partners. **(C)** A surface representation of the POR FMN binding domain showing mutated residues in red. The Q153 residue is exposed to surface, while residues A115 and T142 are also partially exposed. **(D)** Location of P284 residue in the hinge region of the POR. Hinge region is required for conformational flexibility and mutations in this region are predicted to cause conformational changes that would alter both the electron transport and the interaction with redox partners.

to POR, and its mutation may affect FMN binding (**Figure 7B**). Consistent with this we found a severe loss of flavins in the T142A variant of POR (**Figure 4**). Loss of flavins could also make subtle conformation changes in POR and as these changes would be in the FMN binding domain of POR which interacts with redox partners via shape as well as charge-based protein–protein interactions, a change in activities of redox partners is expected. Severe loss of both CYP19A1 as well as CYP3A4 activities due to T142A mutation indicates a major impact on both steroid and drug metabolism in the patients carrying this mutation.

The mutation Q153R was first described from an Algerian family and was the product of an abortion carried out at 22 weeks of gestation due to information from an ultrasonographic examination which showed craniosynostosis with bilateral radiohumeral synostosis, bowing of long bones, and arachnodactyly (Huang et al., 2005). The karyotype of the fetus was 46,XY, and no abnormalities in external genitalia were detected. Steroids were not measured, but, since ABS was suspected, a GC-MS analysis of liver tissue was performed which indicated "substantially increased" lanosterol and dihydrolanosterol. In previous studies, the Q153R (*POR*13*) variant of POR was found to retain only 25–30% of WT activity in assays with CYP17A1 (Huang et al., 2005) but has shown higher activities in other assays (Agrawal et al., 2008). A higher level of activity with CYP19A1 observed with this mutation would not indicate any damaging effect on a 46,XY fetus, but GC-MS analysis indicates this mutation may affect CYP51A1 activity. The Q153 residue is located at the surface of POR and may have a direct role in the interactions with the redox partners (**Figure 7C**). However, higher levels of activities observed in both the CYP19A1, as well as the CYP3A4 assays indicate that the impact of Q153R variant may be selective for individual P450 enzymes with some being adversely affected while others would be activated due to potentially better protein–protein interactions. The activating effect of Q153R variant of POR can be useful for potential biotechnological applications where commercial production of

expensive chemicals through P450 mediated biotransformation is the preferred method of manufacturing.

The last mutation studied in this report, the P284L (rs 72557938), is located in the hinge region of POR, that is important for domain movements and efficient interactions between FMN and FAD binding regions and for the transfer of electrons from FAD to FMN (**Figure 7D**). In the sequencing study by Huang et al. (2008) the P284L mutation was present at an allele frequency of 0.003 in Chinese American population and in the currently available ExAc dataset containing 121000 samples it is present at an allele frequency of 0.00004132. A 54% loss of 17-hydroxylase activity was reported by Huang et al but the 17,20 lyase activity of CYP17A1 was 82% of the WT POR (Huang et al., 2008). No loss of flavin content was observed in the P284L variant which indicates altered inter as well as intra molecular protein–protein interactions may be responsible for the loss of activities in both the CYP19A1 as well as the CYP3A4 assays. Since the hinge region of POR is important for the domain motions to bring the FMN closer to the FAD for the transfer of electrons, a change in this region may affect the efficiency of electron transport process in POR, and therefore, affect the activities of partner proteins. It is possible that some redox partners of POR may experience greater impact on their catalytic activities while others may retain close to WT activities depending on their mode of interaction with POR.

In these studies, we have used POR and P450 proteins embedded in liposomes and removed the detergents used for solubilization of POR and P450s by treatment with biobeads (Bio-Rad Corp., Hercules, CA, United States) which provided a robust assay system. These results also emphasize the need for assay of POR variants with different partner proteins and substrates to accurately determine the impact of individual variations. The major polymorphism observed in POR is A503V (rs 1057868, *POR*28*), which is present in about 27% of all alleles and shows wide variability across different populations (Caucasian and Hispanic populations: 31%; Pacific Islanders: 48%; Asian populations 35%; Japanese, 40%; African Americans 16%) (Burkhard et al., 2017). There is some evidence of *POR*28* allele influencing the activities of drug metabolizing enzymes but more direct evidence is needed before any firm conclusions can be drawn (Pandey and Flück, 2013; Pandey and Sproll, 2014). As seen with the P284L mutation, there may be variations of POR in apparently normal populations with potentially disease causing effects. Since POR variations have now been linked to the metabolism of several drugs and steroids, it may be prudent to include the sequencing of POR gene while looking for genetic causes of altered drug or steroid metabolism. A detailed examination of the polymorphic variants of POR would be required to estimate their damaging effects.

AUTHOR CONTRIBUTIONS

Participated in research design: SU, SP, and AP. Conducted experiments: SU and SP. Contributed new reagents or analytical tools: NK. Performed data analysis: SU, SP, and AP. Overall supervision of the project: AP. Wrote or contributed the writing of the manuscript: SU, SP, NK, and AP.

FUNDING

This research was funded by grants to AP by the Swiss National Science Foundation (31003A-134926) and Bern University Research Foundation and Department of Clinical Research, University of Bern.

ACKNOWLEDGMENT

We thank Prof. Walter L. Miller (UCSF, San Francisco, CA, United States) for providing several POR expression constructs.

REFERENCES

Adachi, M., Tachibana, K., Asakura, Y., Yamamoto, T., Hanaki, K., and Oka, A. (2004). Compound heterozygous mutations of cytochrome P450 oxidoreductase gene (POR) in two patients with Antley-Bixler syndrome. *Am. J. Med. Genet. A* 128A, 333–339. doi: 10.1002/ajmg.a.30169

Agrawal, V., Choi, J. H., Giacomini, K. M., and Miller, W. L. (2010). Substrate-specific modulation of CYP3A4 activity by genetic variants of cytochrome P450 oxidoreductase. *Pharmacogenet. Genomics* 20, 611–618. doi: 10.1097/FPC.0b013e32833e0cb5

Agrawal, V., Huang, N., and Miller, W. L. (2008). Pharmacogenetics of P450 oxidoreductase: effect of sequence variants on activities of CYP1A2 and CYP2C19. *Pharmacogenet. Genomics* 18, 569–576. doi: 10.1097/FPC.0b013e32830054ac

Aigrain, L., Pompon, D., Morera, S., and Truan, G. (2009). Structure of the open conformation of a functional chimeric NADPH cytochrome P450 reductase. *EMBO Rep.* 10, 742–747. doi: 10.1038/embor.2009.82

Arlt, W., Walker, E. A., Draper, N., Ivison, H. E., Ride, J. P., Hammer, F., et al. (2004). Congenital adrenal hyperplasia caused by mutant P450 oxidoreductase and human androgen synthesis: analytical study. *Lancet* 363, 2128–2135. doi: 10.1016/S0140-6736(04)16503-3

Augarten, A., Pariente, C., Gazit, E., Chayen, R., Goldfarb, H., and Sack, J. (1992). Ambiguous genitalia due to partial activity of cytochromes P450c17 and P450c21. *J. Steroid Biochem. Mol. Biol.* 41, 37–41. doi: 10.1016/0960-0760(92)90222-5

Burkhard, F. Z., Parween, S., Udhane, S. S., Flück, C. E., and Pandey, A. V. (2017). P450 Oxidoreductase deficiency: analysis of mutations and polymorphisms. *J. Steroid Biochem. Mol. Biol.* 165(Pt A), 38–50. doi: 10.1016/j.jsbmb.2016.04.003

Faeder, E. J., and Siegel, L. M. (1973). A rapid micromethod for determination of FMN and FAD in mixtures. *Anal. Biochem.* 53, 332–336. doi: 10.1016/0003-2697(73)90442-9

Flück, C. E., Mallet, D., Hofer, G., Samara-Boustani, D., Leger, J., Polak, M., et al. (2011). Deletion of P399_E401 in NADPH cytochrome P450 oxidoreductase results in partial mixed oxidase deficiency. *Biochem. Biophys. Res. Commun.* 412, 572–577. doi: 10.1016/j.bbrc.2011.08.001

Flück, C. E., Mullis, P. E., and Pandey, A. V. (2010). Reduction in hepatic drug metabolizing CYP3A4 activities caused by P450 oxidoreductase mutations identified in patients with disordered steroid metabolism. *Biochem. Biophys. Res. Commun.* 401, 149–153. doi: 10.1016/j.bbrc.2010.09.035

Flück, C. E., and Pandey, A. V. (2014). Steroidogenesis of the testis – new genes and pathways. *Ann. Endocrinol. (Paris)* 75, 40–47. doi: 10.1016/j.ando.2014.03.002

Flück, C. E., and Pandey, A. V. (2017). Impact on CYP19A1 activity by mutations in NADPH cytochrome P450 oxidoreductase. *J. Steroid Biochem. Mol. Biol.* 165(Pt A), 64–70. doi: 10.1016/j.jsbmb.2016.03.031

Flück, C. E., Tajima, T., Pandey, A. V., Arlt, W., Okuhara, K., Verge, C. F., et al. (2004). Mutant P450 oxidoreductase causes disordered steroidogenesis with and without Antley-Bixler syndrome. *Nat. Genet.* 36, 228–230. doi: 10.1038/ng1300

Fukami, M., Hasegawa, T., Horikawa, R., Ohashi, T., Nishimura, G., Homma, K., et al. (2006). Cytochrome P450 oxidoreductase deficiency in three patients initially regarded as having 21-hydroxylase deficiency and/or aromatase deficiency: diagnostic value of urine steroid hormone analysis. *Pediatr. Res.* 59, 276–280. doi: 10.1203/01.pdr.0000195825.31504.28

Fukami, M., Horikawa, R., Nagai, T., Tanaka, T., Naiki, Y., Sato, N., et al. (2005). Cytochrome P450 oxidoreductase gene mutations and Antley-Bixler syndrome with abnormal genitalia and/or impaired steroidogenesis: molecular and clinical studies in 10 patients. *J. Clin. Endocrinol. Metab.* 90, 414–426. doi: 10.1210/jc.2004-0810

Gomes, A. M., Winter, S., Klein, K., Turpeinen, M., Schaeffeler, E., Schwab, M., et al. (2009). Pharmacogenomics of human liver cytochrome P450 oxidoreductase: multifactorial analysis and impact on microsomal drug oxidation. *Pharmacogenomics* 10, 579–599. doi: 10.2217/pgs.09.7

Gomes, L. G., Huang, N., Agrawal, V., Mendonca, B. B., Bachega, T. A., and Miller, W. L. (2008). The common P450 oxidoreductase variant A503V is not a modifier gene for 21-hydroxylase deficiency. *J. Clin. Endocrinol. Metab.* 93, 2913–2916. doi: 10.1210/jc.2008-0304

Guengerich, F. P. (2005). Reduction of cytochrome b5 by NADPH-cytochrome P450 reductase. *Arch. Biochem. Biophys.* 440, 204–211. doi: 10.1016/j.abb.2005.06.019

Guengerich, F. P., Martin, M. V., Sohl, C. D., and Cheng, Q. (2009). Measurement of cytochrome P450 and NADPH-cytochrome P450 reductase. *Nat. Protoc.* 4, 1245–1251. doi: 10.1038/nprot.2009.121

Homma, K., Hasegawa, T., Nagai, T., Adachi, M., Horikawa, R., Fujiwara, I., et al. (2006). Urine steroid hormone profile analysis in cytochrome P450 oxidoreductase deficiency: implication for the backdoor pathway to dihydrotestosterone. *J. Clin. Endocrinol. Metab.* 91, 2643–2649. doi: 10.1210/jc.2005-2460

Huang, N., Agrawal, V., Giacomini, K. M., and Miller, W. L. (2008). Genetics of P450 oxidoreductase: sequence variation in 842 individuals of four ethnicities and activities of 15 missense mutations. *Proc. Natl. Acad. Sci. U.S.A.* 105, 1733–1738. doi: 10.1073/pnas.0711621105

Huang, N., Pandey, A. V., Agrawal, V., Reardon, W., Lapunzina, P. D., Mowat, D., et al. (2005). Diversity and function of mutations in p450 oxidoreductase in patients with Antley-Bixler syndrome and disordered steroidogenesis. *Am. J. Hum. Genet.* 76, 729–749. doi: 10.1086/429417

Kagawa, N. (2011). Efficient expression of human aromatase (CYP19) in E. *coli*. *Methods Mol. Biol.* 705, 109–122. doi: 10.1007/978-1-61737-967-3-7

Kagawa, N., Cao, Q., and Kusano, K. (2003). Expression of human aromatase (CYP19) in *Escherichia coli* by N-terminal replacement and induction of cold stress response. *Steroids* 68, 205–209. doi: 10.1016/S0039-128X(02)00168-X

Kurzban, G. P., and Strobel, H. W. (1986). Preparation and characterization of FAD-dependent NADPH-cytochrome P-450 reductase. *J. Biol. Chem.* 261, 7824–7830.

Lephart, E. D., and Simpson, E. R. (1991). Assay of aromatase activity. *Methods Enzymol.* 206, 477–483. doi: 10.1016/0076-6879(91)06116-K

Lu, A. Y., Junk, K. W., and Coon, M. J. (1969). Resolution of the cytochrome P-450-containing w-hydroxylation system of liver microsomes into three components. *J. Biol. Chem.* 244, 3714–3721.

Marohnic, C. C., Panda, S. P., McCammon, K., Rueff, J., Masters, B. S., and Kranendonk, M. (2010). Human cytochrome P450 oxidoreductase deficiency caused by the Y181D mutation: molecular consequences and rescue of defect. *Drug Metab. Dispos.* 38, 332–340. doi: 10.1124/dmd.109.030445

Matsubara, T., Baron, J., Peterson, L. L., and Peterson, J. A. (1976). NADPH-cytochrome P450 reductase. *Arch. Biochem. Biophys.* 172, 463–469. doi: 10.1016/0003-9861(76)90099-0

Michaelis, L., and Menten, M. L. (1913). Die Kinetik der Invertinwirkung. *Biochem. Z.* 49, 333–369.

Miller, W. L., Huang, N., Flück, C. E., and Pandey, A. V. (2004). P450 oxidoreductase deficiency. *Lancet* 364, 1663. doi: 10.1016/S0140-6736(04)17344-3

Nagao, M., Ishibashi, T., Okayasu, T., and Imai, Y. (1983). Possible involvement of NADPH-cytochrome P450 reductase and cytochrome b5 on beta-ketostearoyl-CoA reduction in microsomal fatty acid chain elongation supported by NADPH. *FEBS Lett.* 155, 11–14. doi: 10.1016/0014-5793(83)80198-7

Nicolo, C., Flück, C. E., Mullis, P. E., and Pandey, A. V. (2010). Restoration of mutant cytochrome P450 reductase activity by external flavin. *Mol. Cell. Endocrinol.* 321, 245–252. doi: 10.1016/j.mce.2010.02.024

Omura, T. (2006). Mitochondrial P450s. *Chem. Biol. Interact.* 163, 86–93. doi: 10.1016/j.cbi.2006.06.008

Omura, T. (2010). Structural diversity of cytochrome P450 enzyme system. *J. Biochem.* 147, 297–306. doi: 10.1093/jb/mvq001

Pandey, A. V. (2006). Biochemical analysis of mutations in P450 oxidoreductase. *Biochem. Soc. Trans.* 34(Pt 6), 1186–1191. doi: 10.1042/BST0341186

Pandey, A. V., and Flück, C. E. (2013). NADPH P450 oxidoreductase: structure, function, and pathology of diseases. *Pharmacol. Ther.* 138, 229–254. doi: 10.1016/j.pharmthera.2013.01.010

Pandey, A. V., Fluck, C. E., Huang, N., Tajima, T., Fujieda, K., and Miller, W. L. (2004). P450 oxidoreductase deficiency: a new disorder of steroidogenesis affecting all microsomal P450 enzymes. *Endocr. Res.* 30, 881–888. doi: 10.1081/ERC-200044134

Pandey, A. V., Flück, C. E., and Mullis, P. E. (2010). Altered heme catabolism by heme oxygenase-1 caused by mutations in human NADPH cytochrome P450 reductase. *Biochem. Biophys. Res. Commun.* 400, 374–378. doi: 10.1016/j.bbrc.2010.08.072

Pandey, A. V., Kempna, P., Hofer, G., Mullis, P. E., and Flück, C. E. (2007). Modulation of human CYP19A1 activity by mutant NADPH P450 oxidoreductase. *Mol. Endocrinol.* 21, 2579–2595. doi: 10.1210/me.2007-0245

Pandey, A. V., and Sproll, P. (2014). Pharmacogenomics of human P450 oxidoreductase. *Front. Pharmacol.* 5:103. doi: 10.3389/fphar.2014.00103

Parween, S., Roucher-Boulez, F., Flück, C. E., Lienhardt-Roussie, A., Mallet, D., Morel, Y., et al. (2016). P450 oxidoreductase deficiency: loss of activity caused by protein instability from a novel L374H mutation. *J. Clin. Endocrinol. Metab.* 101, 4789–4798. doi: 10.1210/jc.2016-1928

Przylepa, K. A., Paznekas, W., Zhang, M., Golabi, M., Bias, W., Bamshad, M. J., et al. (1996). Fibroblast growth factor receptor 2 mutations in Beare-Stevenson cutis gyrata syndrome. *Nat. Genet.* 13, 492–494. doi: 10.1038/ng0896-492

Riddick, D. S., Ding, X., Wolf, C. R., Porter, T. D., Pandey, A. V., Zhang, Q. Y., et al. (2013). NADPH-cytochrome P450 oxidoreductase: roles in physiology, pharmacology, and toxicology. *Drug Metab. Dispos.* 41, 12–23. doi: 10.1124/dmd.112.048991

Schuster, I., and Bernhardt, R. (2007). Inhibition of cytochromes p450: existing and new promising therapeutic targets. *Drug Metab. Rev.* 39, 481–499. doi: 10.1080/03602530701498455

Shen, A. L., Porter, T. D., Wilson, T. E., and Kasper, C. B. (1989). Structural analysis of the FMN binding domain of NADPH-cytochrome P-450 oxidoreductase by site-directed mutagenesis. *J. Biol. Chem.* 264, 7584–7589.

Sim, S. C., Miller, W. L., Zhong, X. B., Arlt, W., Ogata, T., Ding, X., et al. (2009). Nomenclature for alleles of the cytochrome P450 oxidoreductase gene. *Pharmacogenet. Genomics* 19, 565–566. doi: 10.1097/FPC.0b013e32832af5b7

Simpson, E. R., Mahendroo, M. S., Means, G. D., Kilgore, M. W., Hinshelwood, M. M., Graham-Lorence, S., et al. (1994). Aromatase cytochrome P450, the enzyme responsible for estrogen biosynthesis. *Endocr. Rev.* 15, 342–355.

Zalewski, A., Ma, N. S., Legeza, B., Renthal, N., Flück, C. E., and Pandey, A. V. (2016). Vitamin D-dependent rickets type 1 caused by mutations in CYP27B1 affecting protein interactions with adrenodoxin. *J. Clin. Endocrinol. Metab.* 101, 3409–3418. doi: 10.1210/jc.2016-2124

Zanger, U. M., and Schwab, M. (2013). Cytochrome P450 enzymes in drug metabolism: regulation of gene expression, enzyme activities, and impact of genetic variation. *Pharmacol. Ther.* 138, 103–141. doi: 10.1016/j.pharmthera.2012.12.007

Zhao, Q., Modi, S., Smith, G., Paine, M., McDonagh, P. D., Wolf, C. R., et al. (1999). Crystal structure of the FMN-binding domain of human cytochrome P450 reductase at 1.93 A resolution. *Protein Sci.* 8, 298–306. doi: 10.1110/ps.8.2.298

Conflict of Interest Statement: The authors declare that the research was conducted in the absence of any commercial or financial relationships that could be construed as a potential conflict of interest.

frontiers in Pharmacology

ORIGINAL RESEARCH
published: 30 June 2017
doi: 10.3389/fphar.2017.00417

Evaluation of Selected CYP51A1 Polymorphisms in View of Interactions with Substrate and Redox Partner

*Tadeja Režen[1], Iza Ogris[1], Marko Sever[2], Franci Merzel[2], Simona Golic Grdadolnik[2] and Damjana Rozman[1]**

[1] Faculty of Medicine, Centre for Functional Genomics and Bio-Chips, Institute of Biochemistry, University of Ljubljana, Ljubljana, Slovenia, [2] Department of Biomolecular Structure, National Institute of Chemistry, Ljubljana, Slovenia

Cholesterol is essential for development, growth, and maintenance of organisms. Mutations in cholesterol biosynthetic genes are embryonic lethal and few polymorphisms have been so far associated with pathologies in humans. Previous analyses show that lanosterol 14α-demethylase (CYP51A1) from the late part of cholesterol biosynthesis has only a few missense mutations with low minor allele frequencies and low association with pathologies in humans. The aim of this study is to evaluate the role of amino acid changes in the natural missense mutations of the hCYP51A1 protein. We searched SNP databases for existing polymorphisms of *CYP51A1* and evaluated their effect on protein function. We found rare variants causing detrimental missense mutations of CYP51A1. Some missense variants were also associated with a phenotype in humans. Two missense variants have been prepared for testing enzymatic activity *in vitro* but failed to produce a P450 spectrum. We performed molecular modeling of three selected missense variants to evaluate the effect of the amino acid substitution on potential interaction with its substrate and the obligatory redox partner POR. We show that two of the variants, R277L and especially D152G, have possibly lower binding potential toward obligatory redox partner POR. D152G and R431H have also potentially lower affinity toward the substrate lanosterol. We evaluated the potential effect of damaging variants also using data from other *in vitro* CYP51A1 mutants. In conclusion, we propose to include damaging *CYP51A1* variants into personalized diagnostics to improve genetic counseling for certain rare disease phenotypes.

Keywords: CYP51A1, SNP, polymorphism, molecular dynamics simulations, POR

OPEN ACCESS

Edited by:
Ulrich M. Zanger, Dr. Margarete Fischer-Bosch Institut für Klinische Pharmakologie (IKP), Germany

Reviewed by:
Luis Abel Quiñones, Universidad de Chile, Chile
Su-Jun Lee, Inje University, South Korea

****Correspondence:***
Damjana Rozman
damjana.rozman@mf.uni-lj.si

Specialty section:
This article was submitted to Pharmacogenetics and Pharmacogenomics, a section of the journal Frontiers in Pharmacology

Received: *15 April 2017*
Accepted: *13 June 2017*
Published: *30 June 2017*

Citation:
Režen T, Ogris I, Sever M, Merzel F, Golic Grdadolnik S and Rozman D (2017) Evaluation of Selected CYP51A1 Polymorphisms in View of Interactions with Substrate and Redox Partner. Front. Pharmacol. 8:417. doi: 10.3389/fphar.2017.00417

INTRODUCTION

CYP51A1, lanosterol 14α-demethylase, is a cytochrome P450 involved in cholesterol biosynthesis and is present in all biological kingdoms. It was proposed to be one of the oldest cytochromes P450 and is evolutionary highly conserved. Amino acid sequence identity is 95% among mammals and about 23–34% among biological kingdoms (Lepesheva and Waterman, 2007). CYP51A1 is catalytically strict and all forms catalyze oxidative removal of the 14α-group from the sterol intermediates. The reaction occurs in three steps and requires a NADPH type reducing agent and

the presence of POR (cytochrome P450 oxidoreductase). Lanosterol and 24,25-dihydrolanosterol are CYP51A1 substrates in mammals. Since the reaction catalyzed by CYP51A1 is substrate specific, there are certain amino acids conserved through biological kingdoms (Lepesheva and Waterman, 2007). These are clustered in six substrate recognition sites (SRS1-6), which are CYP51A1 specific. There are also conserved signature structures of the CYP450 superfamily, such as surroundings of heme-Cys pocket and helices B, F, G, and I (Lepesheva et al., 2003).

Cholesterol biosynthesis is an essential housekeeping pathway and knockouts of genes involved in this pathway are embryonic lethal except for a few enzymes toward the end of the synthesis pathway (Horvat et al., 2011). Mouse *Cyp51a1* knockout is lethal at day 15 *post coitum* (Keber et al., 2011). This suggests that also in humans two mutated *CYP51A1* alleles rendering no active protein would be embryonic lethal. Heterozygous knockout $Cyp51a1^{+/-}$ mice are developmentally and morphologically normal and fertile; however, when challenged with high lipid diet, the response revealed a hidden susceptibility to detrimental effects of the diet (Lewinska et al., 2014). Studies in mice also revealed gender biased consequences of mutations in *Cyp51a1* (Lorbek et al., 2013; Lewinska et al., 2014; Urlep et al., 2017). Consequences of *CYP51A1* heterozygosity in humans need yet to be studied.

We have searched all available GWAS and other databases connecting SNPs with phenotype in humans. Only few phenotypes were so far associated with *CYP51A1* polymorphisms (**Table 1**). Several are associated with a rare variant rs2229188 causing a change of Val19 to Ala. This SNP was found associated with HDL-C level, hypertension, and lifespan (Charlesworth et al., 2009; Han et al., 2013; Yashin et al., 2015). This missense mutation lies at the N-terminal part of the protein and is responsible for interaction with the membrane; therefore, it is not directly involved in enzymatic activity (Pikuleva and Waterman, 2013). Also, Polyphen-2 or SIFT do not predict a detrimental effect of this variant. It is thus unclear how this missense variant affects the observed phenotypes. *CYP51A1* mutations were also associated with the incidence of pediatric cataracts. A mutation of Arg277 to Cys resulted in neurologically and systemically normal children with pediatric cataract (Aldahmesh et al., 2012; Khan et al., 2015). However, three other rare variants were clearly pathogenic in causing not only cataract but global developmental delay and hepatic failure (Gillespie et al., 2014, 2016; Patel et al., 2016). These are termination of protein at Trp421, change of Ile312 to Thr and Leu232 to Pro. All these mutations were labeled as damaging by Polyphen-2 or SIFT. Additionally, common *CYP51A1* SNPs in noncoding regions were associated with spontaneous premature labor, and lower LDL-C and TC in second trimester of pregnancy (Lewinska et al., 2013). Another common variant in 3′UTR region was reported

TABLE 1 | *CYP51A1* polymorphisms associated with phenotypes in humans and population frequency from 1,000 genomes.

cDNA NM_000786.3	Protein NP_000777.1	Phenotype	References	SNP ID (population frequency)
c.1263G>A	p.W421Ter	Infantile onset central and lamellar cataract, developmental delay, brain white-matter abnormality, cryptogenic neonatal liver cirrhosis, spastic diplegia, increased lanosterol	Gillespie et al., 2014, 2016	rs141654764 (0.00001647) /
c.935T>C	p.I312T			
c.829C>T	p.R277C	Congenital cataract, neurologically and systemically normal	Aldahmesh et al., 2012; Khan et al., 2015	rs944015648 (NA)
c.695T>C	p.L232P (SRS2)	Congenital cataract, neonatal fulminant hepatic, failure, and global developmental delay	Patel et al., 2016	/
c.56T>C	p.V19A	Significant association with HDL-C level	Charlesworth et al., 2009	rs2229188 (0.00000825)
c.56T>C	p.V19A	Significant association with hypertension	Han et al., 2013	rs2229188 (0.00000825)
c.56T>C	p.V19A	Negative association with lifespan	Yashin et al., 2015	rs2229188 (0.00000825)
c.56T>C	p.V19A	Association with hypertension	Wang and Lin, 2014	rs2229188 (0.00000825)
c.595+66A>G	/	Association with spontaneous premature labor	Lewinska et al., 2013	rs57218044 (0.0363)
c.1359T>C				rs7797834 (0.3596)
c.*251G>C				rs7793861 (0.3644)
c.*377T>C				rs6465348 (0.3576)
c.*1016C>T				rs12673910 (0.1697)
c.*377T>C	/	Association with lower LDL-C and TC in second trimester	Lewinska et al., 2013	rs6465348 (0.3576)
c.251G>C	3′UTR	Associated with glycemic HbA1c Association with expression of genes in pancreas	Ren et al., 2016	rs7793861 (0.3644)

NA, non-available.

to be associated with HbA1c and expression of genes in pancreas (Ren et al., 2016).

The aim of this study was to analyse natural *CYP51A1* missense SNPs *in vitro* and by molecular dynamics modeling in relation to the substrate lanosterol and obligatory redox partner POR (cytochrome P450 oxidoreductase). We selected three missense SNPs for *in silico* prediction and two for *in vitro* testing of the effect of the polymorphism on enzymatic activity. All these amino acids are highly conserved and were identified by SIFT and Polyphen-2 as damaging. We also searched the conserved regions of the protein for missense SNPs and evaluated their effect on the enzymatic activity. We show that up to date, there are only few potentially damaging SNPs of *CYP51A1* present in the human population. Although, we could not produce an active protein with the two SNPs, we *in silico* showed a potential effect of D152G and R431H mutation on enzymatic activity by increased distance between the heme and lanosterol and a less favorable binding of lanosterol in comparison to the wild type. Calculations also predicted D152G and R277L variants to have less favorable binding to the redox partner POR.

MATERIALS AND METHODS

Search of Human *CYP51A1* Polymorphisms and Associated Phenotypes

We have searched different GWAS databases for *CYP51A1* SNPs associated with any kind of phenotype in humans. We used NHGRI-EBI GWAS Catalog (Welter et al., 2014), GRASP, and FSNP etc. We also searched all available literature by PubMed. Results of this search are shown in **Table 1**. We also searched and evaluated *CYP51A1* SNPs using databases: dbSNP (https://www.ncbi.nlm.nih.gov/SNP/); COSMIC (Catalog of somatic mutations in cancer) (Forbes et al., 2016); and Exome Variant Server (http://evs.gs.washington.edu/EVS/, NHLBI GO Exome Sequencing Project). We used PolyPhen-2 and SIFT for prediction of variant effect (Ng and Henikoff, 2003; Adzhubei et al., 2010). We used NP_000777.1 as a reference for designating amino acid position.

Preparation of Mutant Proteins

Two mutant CYP51A1 proteins were prepared by site-directed mutagenesis of wild type human *CYP51A1* cloned in pCWori+ plasmid. The mutants were Arg431His and Arg277Leu. Site-directed mutagenesis was performed using QuikChange™ Site-Directed Mutagenesis kit (Stratagene, La Jolla, CA, USA) and primers R277L (forward primer: 5′-GCAATCCAGAAACTCAGACAGTCTCAAG-3′ and reverse primer: 5′-CTTGAGACTGTCTGAGTTTCTGGATTGC-3′), R431H (forward primer: 5′-GGACTTTAATCCTGATCACTACTTACAGGATAACC-3′ and reverse primer: 5′-GGTTATCCTGTAAGTAGTGATCAGGATTAAAGTCC-3′) (Sigma-Aldrich, Munich, Germany) according to manufacturer recommendations with some changes in PCR run (longer elongation time and higher concentration of primers). Plasmids were transformed in the *E. coli* strain HMS174 (DE3) (Novagen, Darmstadt, Germany) and isolated using GenElute HP Plasmid Miniprep Kit (Sigma Aldrich, Munich, Germany). Plasmids were linearized using HindIII (Roche, Basel, Switzerland) and size was checked using 0.7% agarose gel. Successful change in code and the *CYP51A1* insert in the plasmid was confirmed by sequencing. Expression was carried out at 26°C after induction with IPTG (Isopropyl β-D-1-thiogalactopyranoside) and addition of δ-aminolevulinic acid for 45 h. The cells were pelleted and resuspended in 50 mM potassium phosphate, pH 7.4 (containing 10% glycerol, 0.1% Triton X-100, 200 mM NaCl, 0.5 mM phenylmethylsulfonyl fluoride, and protease inhibitor cocktail). After sonification on ice for 4 × 15 s, Triton X-100 was added to final 0.4% concentration followed with ultracentrifugation at 100,000 × g for 1 h. Proteins were purified with Ni-nitriloacetic-acid agarose column (Qiagen, Valencia, CA, USA) as described before (Lepesheva et al., 2003). Concentration and reduced CO difference spectra was determined as described before (Zelenko et al., 2014). We used 200 μl of 3 μM protein extract for measurement of CO spectrum. Western blot analysis was done as described before (Lorbek et al., 2015).

Molecular Dynamics Simulations (MD) of CYP51A1 Mutants

In addition to the wild type structure of CYP51A1 protein, we modeled its three mutants: Asp152Gly, Arg431His, and Arg277Leu, in two different environments, aqueous solution and in complex with cytochrome P450 reductase (POR). For CYP51A1 we have chosen 3LD6 structure and for POR 3ES9 structure from RCSB Protein Data Bank (Berman et al., 2000). The point mutations were prepared using "residue mutagenesis" procedure in Pymol [2]. Appropriate rotamers were chosen, taking into account neighboring amino acids, as not to significantly perturb the structure of the protein. Following our previous work (Lewinska et al., 2013) we have generated appropriate structural models of CYP51A1-heme-lanosterol complexes and performed all-atom molecular dynamics (MD) simulations of all systems using the software package CHARMM (Brooks et al., 1983) and the available force field (MacKerell et al., 1998). The force-field parameterization for lanosterol was taken from work of Cournia et al. (2005). In addition, the proper connection between the heme (Fe) and Cys449 (S) atom was achieved by the correct protonation state of Cys449 and an additional harmonic restraint. Each protein was embedded in a tetragonal simulation cell with dimensions of 75 × 80 × 80 Å in explicit water environment modeled by the TIP3P water model (Jorgensen et al., 1983). Initially we performed 100 steps of steepest descent minimization followed by 500 steps of adopted-basis Newton-Raphson minimization. Subsequent MD simulations were run at constant pressure of 1 bar and temperature 300 K with a time-step of 1 fs for 10 ns to enable thermodynamic equilibration of the each system.

Protein structures obtained at the end of each all-atom simulation was taken further as the starting structures for docking of proteins. Docking was achieved using the server-side docking software Zdock (Pierce et al., 2014). According to the work (Sündermann and Oostenbrink, 2013) the POR should occupy an elongated conformation when forming contact

with CYP51A1. Therefore, we used weak harmonic constraints on extended-parts of the POR through CHARMM module MMFP GEO to smoothly stretch the protein to a structure resembling the one shown in the reference (Sündermann and Oostenbrink, 2013) during short term MD simulations. While for the CYP51A1 it is not known explicitly which residues take part in the interaction with POR, such information is available for other members in the CYP family, namely for CYP2D6 and CYPB24. In addition the similarity of electrostatic surfaces between proteins of the CYP family can be used as an indication of the interaction surface. We performed a sequence alignment followed by a structural superposition with refinement of different CYP proteins in Pymol. This method is known to be reliable if sequence homology is around 30%. Our proteins have 26–28% sequence identity based on the output of the BLAST algorithm, thus satisfying this criterion (Altschul et al., 1990). In addition we also found favorable electrostatic complementarity of protein contact surfaces.

Based on clustering of residues in the wild type and mutants around key interacting residues of CYP2D6 and CYPB24, we choose the following residues as key interacting residues in CYP51A1: K127, A172, K175, K364, K442, R452, N459, and corresponding residues of POR: E92, 93, 142. The isolated protein structures were subsequently docked using an online protein-protein docking software Zdock (Pierce et al., 2014) producing between 2 and 10 different poses of the complex. The three poses with the best result regarding the scoring function were taken for further evaluation. Based on the position of key homologous interacting residues with known favorable interactions for between CYP and POR the best-scored pose was chosen. For the final production run of the docked complexes, we used the implicit solvent method FACTS (Haberthür and Caflisch, 2008) to perform a more efficient sampling of the conformational space. The reliability of the FACTS method for the present system, was demonstrated by high level agreement between averages over FACTS and explicit solvent trajectories. FACTS parameters were set as follows: Tfps 3, dielectric constant 1.0, and gamma constant 0.015. The MD simulations were run at a temperature of 300 K with a time step of 1 fs. The non-bonded interactions were treated using a set of cut-offs. The distance cut off in generating the list of pairs was set to 20 Å. At 16 Å the switching function eliminated all contributions to the overall energy from pairwise interactions. At 14 Å the smoothing function began to reduce a pair's contribution. Last 20 ns of overall 40 ns of performed FACTS MD simulations were used for analysis. Simulated systems were visualized using Pymol. Analysis of results was done by in-house developed tools in addition to those available in CHARMM.

RESULTS

CYP51A1 Variants in Human Population

We searched the databases for SNPs in the human population causing missense mutations in any of the known regions important for substrate recognition, enzymatic activity, POR interaction and azole binding (Nitahara et al., 2001; Lepesheva et al., 2003; Strushkevich et al., 2010). We also compared existing SNPs to previously published *in vitro* mutations of human and rat *CYP51A1* and proposed a potential effect of such mutation in humans (**Table 2**). For some variants we can conclude that they probably affect enzymatic activity of CYP51A1, for example Y137C, D152G, Y233*, and H320P, while for other variants *in vitro* mutants do not confirm any effect on enzymatic activity.

Search of the dbSNP database revealed less than 200 SNPs causing a missense mutation in *CYP51A1*. Majority are labeled benign or tolerated by Polyphen-2 or SIFT. Looking at the regions not previously connected to any aspects of the protein activity we found 12 rare variants predicted deleterious and damaging by both softwares (**Table 3**). Next, we searched only for SNPs existing in SRS regions or any other region predicted to be involved in any aspect of enzymatic activity (**Table 4**). In total, we found 33 missense mutations. In SRS1 there are 8 missense mutations and majority of them were predicted damaging by SIFT and Polyphen-2. Both variants in SRS2 region are pathogenic. One was found only once in carcinoma tissue (Y233*), and second (L232P) in only one family causing congenital cataract, neonatal hepatic failure and global developmental delay. In SRS3 three variants of the same amino acid exists with different predicted effect. In SRS4 there are only two variants with predicted damaging effect on the protein. SRS5

TABLE 2 | Human SNP and rat/human *in vitro* mutant pairs.

Human SNP	Rat/human mutant	Mutant effect	Predicted human SNP effect
Y137C	ratY131F/S,	No protein, no activity	No activity
	humanY137F	55% expr, no activity, spectr. ok	
	humanY137A	Decrease in binding of substrate	
R139H	ratR133G	Normal activity	Unknown
D152G/N	ratD146A	Normal express, 106% activity	Decreased activity
	humanD152A	70% expression, 54% activity, 4 times decrease in turnover number	
Y233*	ratY227F	55% activity	Lower activity
H242R	humanH242A	Destabilization of the protein	Unknown effect
H320P	ratH314F/A/K/D	Lower activity (42.6, 34.9, 20.2, 14)	Lower activity of the enzyme
	humanH320A	Destabilization of protein, higher affinity for products	
T325A	ratT319A	Normal activity	Normal activity
R383V/L	humanR383A	Decrease in binding of substrate	Unknown
R388Ter	ratR382A	No protein	No protein
T492A	ratT486A	Normal activity	Normal activity
T496I	ratT490A	Normal activity	Normal activity
E375*	ratE369A	No protein	No protein

Rat and humans in vitro mutants were published previously (Nitahara et al., 2001; Lepesheva et al., 2003; Bellamine et al., 2004; Mukha et al., 2011).

TABLE 3 | *CYP51A1* SNPs predicted as deleterious or damaging by SIFT and PolyPhen-2 in regions not connected to enzymatic activity.

dbSNP	SIFT (score)	PolyPhen-2 (score)	SNP position	Amino-acid location
rs372875744	Damaging (0.03)	Probably damaging (0.993)	N125H	Helix B
rs535433995	Damaging (0.01)	Probably damaging (0.975)	H177R	Helix D
rs151249652	Damaging (0.01)	Probably damaging (0.984)	E194C	Beta sheet 3-1
rs536125410	Damaging (0)	Probably damaging (0.982)	L253S	Loop between helix F″/G, surface
rs141009880	Damaging (0.01)	Possibly damaging (0.892)	I274T	Helix G
rs140702410	Damaging (0)	Probably damaging (0.969)	**R277L**	Helix G
rs140118347	Damaging (0.02)	Possibly damaging (0.799)	A334S	Helix I
rs554366054	Damaging (0.02)	Probably damaging (1)	L417R	Loop between helix K′ and meander, surface
rs138109473	Damaging (0)	Probably damaging (0.974)	**R431H**	Meander ηk
rs542915180	Damaging (0)	Probably damaging (0.999)	R454H	Cys pocket
rs563098505	Damaging (0)	Probably damaging (0.98)	Y462D	Helix L, next to cys pocket
rs553164028	damaging (0)	Probably damaging (0.997)	R507K	C-terminal of the protein

Bold are SNP used for molecular dynamical modeling and in vitro protein expression. Amino acid location according to Lepesheva et al. (2003).

TABLE 4 | Reported missense SNPs in *CYP51A1* conserved regions (source: exome variant server, cosmic, dbSNP).

SNP ID	Protein	PolyPhen-2/SIFT	Location
rs368261783	Y137C	Possibly damaging (0.497)/damaging (0)	SRS1
rs750743669	S138N	Benign (0.262)/ damaging (0.04)	SRS1
rs758553106	R139C	Probably damaging (0.946)/damaging (0.03)	SRS1
rs140356336	R139H	Benign (0.029)/tolerated (0.65)	SRS1
COSM5500428	V144A	Probably damaging (0.994)/tolerated (0.29)	SRS1
rs312262912	Y151D	Probably damaging (0.962)/damaging (0)	SRS1
rs371492794	**D152G**	Probably damaging (0.988)/damaging (0.01)	SRS1
COSM1202901 rs755026542	D152N	Probably damaging (0.985)/damaging (0.01)	SRS1
rs776271983	A172V	Benign (0.101) /tolerated (0.22)	POR interaction
/	L232P	Probably damaging (0.995)/damaging (0)	SRS2
COSM353554	Y233*	Unknown	SRS2
COSM2863985	W245S	Probably damaging (0.981)/damaging (0.01)	Azole interaction
rs753673809	W245Ter	No protein	Azole interaction
COSM1579448	W250S	Probably damaging (0.999)/damaging (0.02)	Azole interaction
rs200921006 COSM3663398	R258C	Probably damaging (0.999)/ damaging (0)	SRS3
rs765961879 COSM1202902	R258H	Benign (0.93)/ damaging (0)	SRS3
rs765961879	R258L	Benign (0.168)/ damaging (0.01)	SRS3
rs745413412	H320P	Possibly damaging (0.899)/ damaging (0)	SRS4
rs377725460	T325A	Benign (0.359)/ damaging (0.01)	SRS4
rs760669078	P381T	Probably damaging (0.990)/tolerated (0.08)	SRS5
rs150090274	I383V	Benign (0.024)/damaging (0.05)	SRS5
rs150090274	I383L	Benign (0.143)/tolerated (0.14)	SRS5
COSM3698597	M384I	Probably damaging (0.930)/tolerated (0.34)	SRS5
rs759341868	I385F	Benign (0.075)/damaging (0.01)	SRS5
rs773893086	M386V	Benign (0.376)/tolerated (0.12)	SRS5
rs532896478	M386I	Benign (0.044)/tolerated (1)	SRS5
rs765119371	M387I	Possibly damaging (0.758)/damaging (0.05)	SRS5
COSM5986705	M387delM	Unknown	SRS5
rs748782320	R388Ter	No protein	SRS5
rs528934873	R452H	Benign (0.082)/ damaging (0.04)	POR interaction
rs779786966	R452C	Benign (0.166)/ damaging (0)	
rs768113032	T492A	Benign (0.117)/tolerated (0.15)	SRS6
rs749633381	M493V	Possibly damaging (0.545)/damaging (0.02)	SRS6

Bold is SNP used for molecular dynamical modeling. SRS, substrate recognition site.

has many variants, but majority are predicted as tolerated or benign as nonpolar amino acids are replaced by other nonpolar amino acids. SRS6 has also only two SNPs. Based on clustering of residues in the wild type and mutants around key interacting residues of CYP2D6 and CYPB24, the following residues were chosen as POR key interacting residues in CYP51A1: K127, A172, K175, K364, K442, R452, and N459. Among these only three SNPs at two positions exist in human population and are labeled deleterious by SIFT and benign by Polyphen-2. Additional conserved regions were also searched; however, only few have missense mutations with potentially deleterious effect existing in human population. Very interesting are also variants at positions predicted to interact with azoles (Strushkevich et al., 2010). There are two variants where large aromatic tryptophan is changed to a small polar serine. This change could potentially affect binding affinity toward azoles.

Next, we selected three variants for further analyses. All three were predicted as deleterious or damaging by Polyphen-2 and SIFT (**Tables 3, 4**, bold). First variant, D512G lies in SRS1 region, important for enzymatic activity, where a change of small negative aspartate to small non-polar glycine is potentially pathogenic. Second variant, R431H is in meander region with unknown function. A change from positively charged aliphatic arginine to positively charged aromatic histidine has an unknown effect on enzymatic activity. Third variant, R277L lies in SRS3 region and changes large positive arginine to small non-polar leucine. As a SNP at this position was associated with pediatric cataracts, we can postulate that the mutation affects the enzymatic activity of the protein.

Molecular Dynamics Simulations of Natural SNPs

Molecular simulations were done simulating wild type and three natural variants present in human population (**Table 3**, bold). Lanosterol has apart from a single hydroxyl group mainly a nonpolar surface and therefore, interacts through hydrophobic interactions with nonpolar residues of the CYP51A1. In order to quantify the position of lanosterol in each of the simulated proteins (mutants and wild type) we have determined all CYP51A1 residues taking part in hydrogen bonding with lanosterol hydroxyl group during a production run. Hydrogen bonds (HB) were determined according to the distance criterion for donor-acceptor atoms that fit the cut-off of 2.4 Å. The relative occupation times for hydrogen bonds (HB) formed mainly with the backbone amide groups of individual residues are shown in **Table 5**. While the lanosterol HB distribution of the mutant R277L resembles that found for the native protein, distributions of R431H and D152G indicate clear deviation from the relative position the lanosterol has in the native protein.

Another measure for the lanosterol position is the distance between the heme iron atom and the methyl carbon C30 of lanosterol. This distance is important because lanosterol is axially coordinated to the heme iron with the methyl carbon C30, which is the lanosterol's center of oxidation. Distances between the aforementioned atoms were calculated as a function of simulation time across entire trajectories. It was found that the characteristic distance between the heme's iron and lanosterol's C30 atoms of the R277L mutant most closely resembles the wild type, while the R431H and D152G mutants distance are on average around 4 Å further away. The distances were also found to be quite stable during the production run of the simulations. The iron-C30 distances are plotted in **Figure 1A** for isolated CYP51A1 and its mutants in aqueous solution, while **Figure 1B** shows the situation for the CYP51A1 proteins in also contact with POR.

TABLE 5 | Relative occupation times of lanosterol's hydroxyl group and its hydrogen bond formed with a given residue (amide group of the protein backbone) during production run (20 ns).

CYP51A1	Amino acid	τ_{HB}/τ_0 [%]
WT	M384	24.5
	I385	65.9
	I383	1.5
R277L	M384	12.7
	I385	30.1
	I383	0.8
R431H	M493	6.3
	I494	1.2
D152G	W245	10.8
	M493	1.6
	F240	0.8

Comparison between native CYP51A1 and its three mutants.

Next, we calculated binding energies of individual complex by subtracting the thermodynamic averages of internal energies of individual components from the complex:

$$E_b = \langle U_{cmplx} \rangle - \langle U_{m1} \rangle - \langle U_{m2} \rangle, \quad (1)$$

where $\langle\ \rangle$ stands for the average over the entire trajectory of individual component. Each term in the above formula is calculated in a separate simulation. Here, $\langle U_{m1} \rangle$ was the average internal energy of isolated lanosterol molecule in aqueous environment, $\langle U_{m2} \rangle$ average internal energy of CYP protein without lanosterol and $\langle U_{cmplx} \rangle$ average internal energy of CYP-lanosterol complex. Calculations of total energy of the complex's between the CYP's and POR showed that the wild type protein in complex with POR had the most favorable total energy while the others had significantly less favorable calculated total energies (**Figure 2A**). Especially, mutant D152G has almost zero binding enthalpy between CYP51A1 and POR. Calculations of binding energy between lanosterol in the various CYP proteins had shown that on average lanosterol is most favorably bound in the wild type, followed by the R277L mutant, while in the R431H and D152G mutants lanosterol is bound significantly less to the interacting molecules (**Figures 2B,C**). This was shown for calculations in aqueous solution and in complex with POR. **Figure 3** show interactions between CYP51A1 (wild type and three mutants) and POR amino acid residues including FMN and heme.

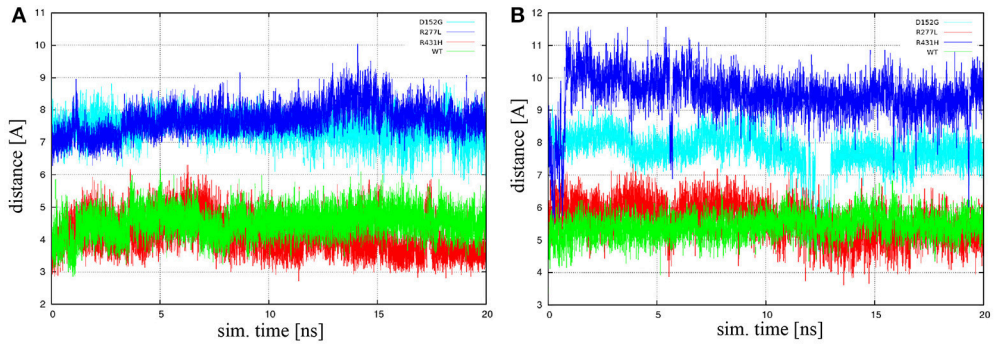

FIGURE 1 | The heme iron-C30 distances as a function of simulation time (sim. time) for isolated CYP51A1 and its mutants in **(A)** aqueous solution and **(B)** complex with POR. Green line is wild type hCYP51A1, dark blue is variant R431H, red is R277L, and light blue is D152G.

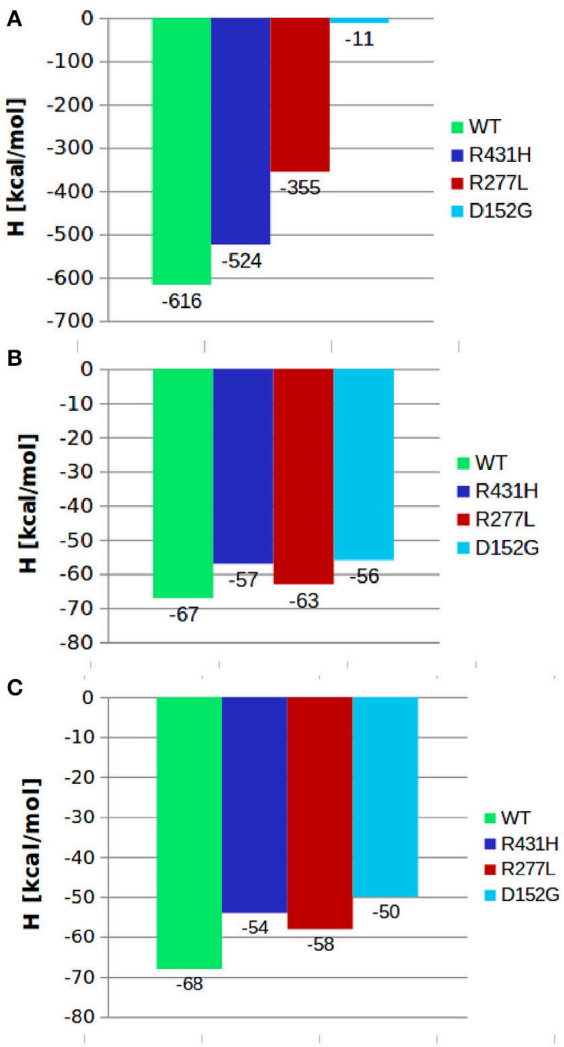

FIGURE 2 | Comparison between the binding enthalpies of various mutants and the wild type CYP51A1 and **(A)** POR; **(B)** lanosterol; **(C)** lanosterol in complex with POR.

CO-Difference Spectra of Mutants

We prepared two mutant CYP51A1 proteins R277L and R431H (**Table 3**). We used site directed mutagenesis and mutated a *CYP51A1* insert in expression vector. Expression level determined from absolute spectra (420 nm) was 2 times reduced for mutant R277L and 3 times for mutant R431H. Western blot analyses using CYP51A1 specific antibody confirmed the presence of CYP51A1 protein in the extracts (Supplementary Figure 1). Wild type hCYP51A1 spectrum shows a typical CO-difference spectrum, with a peak at 417 nm representing catalytically inactive form of hCYP51 and a peak at 447 nm representing the active form of wild type hCYP51A1 as a result of coordinated CO in the active site (**Figure 4**). Mutants with amino acid changes R431H and R277L were unable to produce a peak at 447 nm and were therefore inactive. The preparation of the hCYP51A1 mutant protein was performed several times and in two different laboratories always yielding a protein with no P450 spectrum.

DISCUSSION

CYP51A1 is an essential housekeeping enzyme with only few known associations with diseases in humans. We searched human natural *CYP51A1* SNPs to find the damaging variants, performed molecular dynamic modeling for wild type, three selected variants, and measured CO-difference spectra of proteins. Reported damaging variants are rare variants often reported only once, which is in agreement with the requirement of this protein for normal embryonal development and adult life. In addition, only few variants have been connected to any phenotype in humans. This indicates that damaging missense variants are highly unfavorable and have not been preserved in the human populations. Clinically, *CYP51A1* variants have been proposed to be included in genetic testing in certain clinical conditions, such as pediatric cataract, to enable a more accurate genetic counseling (Gillespie et al., 2014). On the other hand, *Cyp51a1*$^{+/-}$ heterozygous mice indicate that this genotype renders subjects potentially more susceptible to detrimental effects of unhealthy life style. Therefore, we propose to include

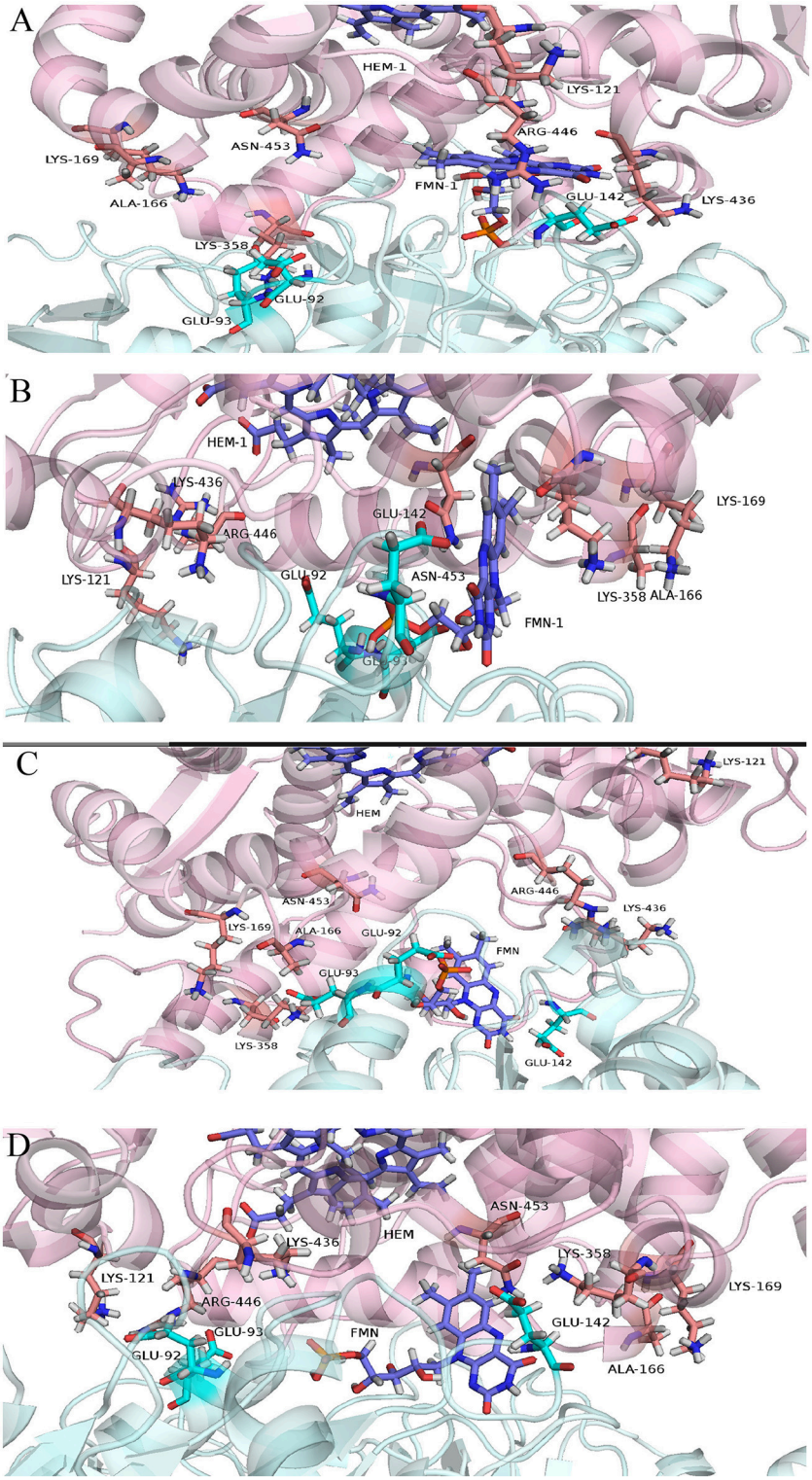

FIGURE 3 | Cartoon representing predicted CYP51A1 residues interacting with POR (depicted in cyan color) in **(A)** wild type, **(B)** R277L variant, **(C)** R431H variant, and **(D)** D152G variant. (**A–D** are depicted in pink color).

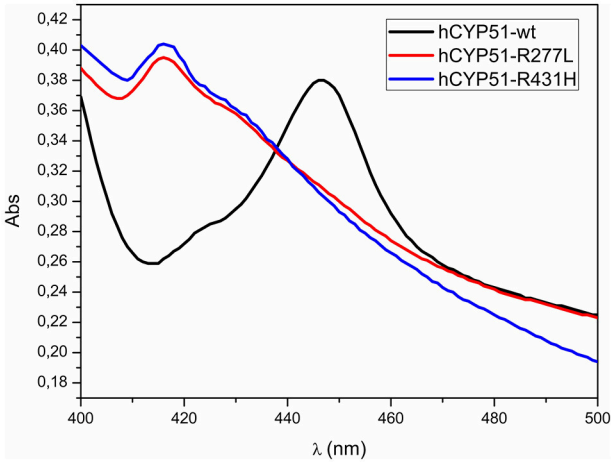

FIGURE 4 | CO-difference spectra for wild type hCYP51-wt (black line), hCYP51-R277L (red line), and hCYP51-R431H (blue line) protein.

selected *CYP51A1* variants into personalized diagnostics panel for evaluating risks for pediatric cataract, neonatal hepatic failure, global developmental delay, azole susceptibility, and cardiovascular and metabolic diseases.

We selected three mutants with predicted deleterious effects on protein activity, prepared mutant proteins *in vitro*, and compared them with wild type protein using molecular dynamic simulations. Aspartate at position 152 lies within SRS1 region and is part of a highly conserved CYP51A1 signature present among all kingdoms (Lepesheva et al., 2003). Exception are *T. brucei* and *L. major* where alanine is at this position. *In vitro* mutants of aspartate to alanine had no effect in rat Cyp51a1, but significantly decreased activity of human CYP51A1 (Nitahara et al., 2001; Lepesheva et al., 2003). In human SNP database, two substitutions of aspartic acid are reported, to glycine and to asparagine. Both are predicted to be pathogenic and we selected D152G mutant to test the effect of this mutation using molecular modeling. Results indicate that this amino acid change dramatically affected different CYP51A1 interactions with its substrate lanosterol and obligatory redox partner POR. Therefore, we can propose that this variant is highly pathogenic and results in a less active or even in inactive protein.

Interestingly, among SNPs associated with any phenotype in humans almost all are outside parts of the CYP51A1 known to be critical for enzymatic activity. Exception is leucine change to proline at position 232 lying within SRS2. Missense variants associated with any phenotype in humans are all rare variants and are predicted to be damaging by Polyphen-2 and SIFT. One of these variants is termination of protein at 421, which very likely results in no active protein. Another rare variant associated with a mild phenotype is R277C (Aldahmesh et al., 2012), which is at the end of helix G and changes a large positively charged arginine to smaller uncharged but polar cysteine. We selected a similar variant where large positively charged arginine is changed to small non-polar leucine (R277L). We were not successful in *in vitro* preparation of this mutant, but molecular modeling gave us some hints about the potential effect of this variant. Calculations of binding enthalpies indicated that this variant has lower binding properties toward redox partner POR compared to the wild type; however, binding of lanosterol is not affected. Therefore, we could predict that poorer interactions with POR would indicate that R277L variant would have a potentially lower enzymatic activity. Since the change to cysteine has been shown to be associated with pediatric cataracts, we can confirm that protein activity is affected also *in vivo* in humans.

Another mutant we selected to test was arginine change to histidine at position 431. This variant lies in a region with unknown function; however, it is highly conserved among CYP51A1 members from all kingdoms. Again, we were not successful in preparing *in vitro* the mutant protein; however, molecular dynamic modeling gave us some hints about the nature if this variant. R431H variant has unfavorable interactions with lanosterol but the variant does not affect interactions with POR. We could speculate that this variant could have potentially lower enzymatic activity but additional evidence to support this conclusion would be required.

It is not known how human CYP51A1 actually interacts with POR, therefore, we predicted amino acid residues (K127, A172, K175, K364, K442, R452, N459) to be involved in interaction with POR using CYP2D6 and CYP2B4 as a model. Only three rare variants exist at these positions. One is at position 172 where an alanine is changed to valine, both are nonpolar but valine is larger the alanine. However, both Polyphen-2 and SIFT predicted this variant as benign/tolerated. Two variants are at position 452 where arginine is changed to cysteine or histidine. These two variants are predicted by Polphen-2 as benign but deleterious by SIFT. Additional data would be needed to fully evaluate the consequences of these variants on interaction with POR.

Other interesting variants are at the positions predicted to be involved in azole interactions with CYP51A1 (Strushkevich et al., 2010). As large tryptophan at position 245 and 250 is changed to smaller serine this could affect the interaction with azoles, affecting individual susceptibility to azole treatments. Another amino acid potentially involved in azole interaction is Y151, where hydroxyl group of tyrosine is sterically interfering with fluconazole. A mutation of human Y151 to histidine increased affinity for fluconazole (Bellamine et al., 2004). Therefore, variant Y151D could also have a different affinity for azoles, affecting individual susceptibility to azoles. Y151 is part of the CYP51A1 signature at SRS1 and a change from tyrosine to aspartic acid was predicted to be damaging (Lewinska et al., 2013). This tyrosine was shown before to form an H-bond with heme and molecular modeling predicted that the change to smaller aspartic acid would make the distance to heme too large to form an H-bond. This position was also predicted to interact with POR and a change of polar uncharged amino acid to negatively charged amino acid could affect interactions with POR.

Y137 is proposed to interact with heme and is important for enzymatic activity. Interestingly, although tyrosine can be substituted by phenylalanine, this change at position 137 resulted in no protein and activity (Lepesheva et al., 2003). This indicates that OH-group is essential for catalytic activity. A mutation of rat CYP51A1 tyrosine to serine, which has an OH-group

but no aromatic group, also resulted in no expressed protein (Nitahara et al., 2001). Mutation of tyrosine to cysteine, present in human population, brings in a nonaromatic amino acid with SH group. However, according to *in vitro* mutants it seems that any amino acid change at this position is highly unfavorable and we can postulate that this mutation results in a defective protein in humans. The RRR (257–259) motif in SRS3 is proposed to interact with the membrane phosphates through salt-bridges (Strushkevich et al., 2010). Three missense mutations exist at position 258 in the middle of RRR motif. Mutation of arginine is to cysteine, leucine, or histidine. The change to leucine and histidine was predicted to be benign, and change to cysteine was predicted pathogenic. As these amino acids do not form readily salt bridges, we could predict a weakening of the interaction with the membrane. Another CYP51A1 signature is HTS region in SRS4 where only one SNP exists (Lepesheva and Waterman, 2007). This is histidine 320 replaced by proline. Mutating the histidine to phenylalanine, alanine, lysine or aspartate lowered activity of rat Cyp5a11 and replacement of histidine to aspartate or asparagine also dramatically affected activity of *M. tuberculosis* CYP51A1 (Nitahara et al., 2001). H320 is necessary for proton transfer for the formation of activated oxygen. These results indicate that at this position an aromatic amino acid is necessary, for substitution with an aliphatic side chain proline, we could expect a lower activity of such protein.

In conclusion, CYP51A1 is an essential enzyme and only rare variants affecting enzymatic activity exist in the human population. Using molecular dynamic modeling we showed that two missense variants, D152G and R277L, probably affect enzymatic activity also through lowered interaction with obligatory redox partner POR. We propose to include damaging *CYP51A1* variants in genetic testing to increase the discovery of underlying causes for diseases such as pediatric cataract neonatal hepatic failure, global developmental delay, azole susceptibility, and cardiovascular and metabolic diseases.

AUTHOR CONTRIBUTIONS

TR and IO searched for *CYP51A1* SNPs. TR, IO, and SG prepared *in vitro* CYP51A1 mutants. MS and FM performed molecular dynamical simulations. DR, TR, SG, and FM designed the study. All authors contributed to drafting of the paper.

FUNDING

The work was funded by Slovenian Research Agency project J1-7441 and programme P1-0390 and P1-0010. MS was funded by young researcher scholarship.

ACKNOWLEDGMENTS

We wish to thank Dr. Galina I. Lepesheva (Vanderbilt University School of Medicine, Nashville, Tennessee, U.S.A.) for the generous gift of plasmid pCWOri+/hCYP51. We would especially like to thank Dr. Frederick Peter Guengerich and Dr. Jeannette Zinggeler Berg (Vanderbilt University School of Medicine, Nashville, Tennessee, U.S.A.) for performing additional expressions of the *in vitro* CYP51A1 mutants.

SUPPLEMENTARY MATERIAL

The Supplementary Material for this article can be found online at: http://journal.frontiersin.org/article/10.3389/fphar.2017.00417/full#supplementary-material

REFERENCES

Adzhubei, I. A., Schmidt, S., Peshkin, L., Ramensky, V. E., Gerasimova, A., Bork, P., et al. (2010). A method and server for predicting damaging missense mutations. *Nat. Methods* 7, 248–249. doi: 10.1038/nmeth0410-248

Aldahmesh, M., Khan, A., and Mohamed, J. (2012). Genomic analysis of pediatric cataract in Saudi Arabia reveals novel candidate disease genes. *Genet. Med.* 14, 955–962. doi: 10.1038/gim.2012.86

Altschul, S. F., Gish, W., Miller, W., Myers, E. W., and Lipman, D. J. (1990). Basic local alignment search tool. *J. Mol. Biol.* 215, 403–410. doi: 10.1016/S0022-2836(05)80360-2

Bellamine, A., Lepesheva, G. I., and Waterman, M. R. (2004). Fluconazole binding and sterol demethylation in three CYP51 isoforms indicate differences in active site topology. *J. Lipid Res.* 45, 2000–2007. doi: 10.1194/jlr.M400239-JLR200

Berman, H. M., Westbrook, J., Feng, Z., Gilliland, G., Bhat, T. N., Weissig, H., et al. (2000). The protein data bank. *Nucleic Acids Res.* 28, 235–242. doi: 10.1093/nar/28.1.235

Brooks, B. R., Bruccoleri, R. E., Olafson, B. D., States, D. J., Swaminathan, S., and Karplus, M. (1983). CHARMM: a program for macromolecular energy, minimization, and dynamics calculations. *J. Comput. Chem.* 4, 187–217. doi: 10.1002/jcc.540040211

Charlesworth, J. C., Peralta, J. M., Drigalenko, E., Göring, H. H., Almasy, L., Dyer, T. D., et al. (2009). Toward the identification of causal genes in complex diseases: a gene-centric joint test of significance combining genomic and transcriptomic data. *BMC Proc.* 3(Suppl. 7):S92. doi: 10.1186/1753-6561-3-s7-s92

Cournia, Z., Smith, J. C., and Ullmann, G. M. (2005). A molecular mechanics force field for biologically important sterols. *J. Comput. Chem.* 26, 1383–1399. doi: 10.1002/jcc.20277

Forbes, S. A., Beare, D., Boutselakis, H., Bamford, S., Bindal, N., Tate, J., et al. (2016). COSMIC: somatic cancer genetics at high-resolution. *Nucleic Acids Res.* 45, D777–D783. doi: 10.1093/nar/gkw1121

Gillespie, R. L., O'Sullivan, J., Ashworth, J., Bhaskar, S., Williams, S., Biswas, S., et al. (2014). Personalized diagnosis and management of congenital cataract by next-generation sequencing. *Ophthalmology* 121, 2124.e2–2137.e2. doi: 10.1016/j.ophtha.2014.06.006

Gillespie, R. L., Urquhart, J., Anderson, B., Williams, S., Waller, S., Ashworth, J., et al. (2016). Next-generation sequencing in the diagnosis of metabolic disease marked by pediatric cataract. *Ophthalmology* 123, 217–220. doi: 10.1016/j.ophtha.2015.06.035

Haberthür, U., and Caflisch, A. (2008). FACTS: fast analytical continuum treatment of solvation. *J. Comput. Chem.* 29, 701–715. doi: 10.1002/jcc.20832

Han, M., Hu, Y. Q., and Lin, S. (2013). Joint detection of association, imprinting and maternal effects using all children and their parents. *Eur. J. Hum. Genet.* 21, 1449–1456. doi: 10.1038/ejhg.2013.49

Horvat, S., McWhir, J., and Rozman, D. (2011). Defects in cholesterol synthesis genes in mouse and in humans: lessons for drug development and safer treatments. *Drug Metab. Rev.* 43, 69–90. doi: 10.3109/03602532.2010.540580

Jorgensen, W. L., Chandrasekhar, J., Madura, J. D., Impey, R. W., and Klein, M. L. (1983). Comparison of simple potential functions for simulating liquid water. *J. Chem. Phys.* 79, 926–935. doi: 10.1063/1.445869

Keber, R., Motaln, H., Wagner, K. D., Debeljak, N., Rassoulzadegan, M., Ačimovič, J., et al. (2011). Mouse knockout of the cholesterogenic cytochrome p450 lanosterol 14α-demethylase (Cyp51) resembles antley-bixler syndrome. *J. Biol. Chem.* 286, 29086–29097. doi: 10.1074/jbc.M111.253245

Khan, A. O., Aldahmesh, M. A., and Alkuraya, F. S. (2015). Phenotypes of recessive pediatric cataract in a cohort of children with identified homozygous gene mutations (An american ophthalmological society thesis). *Trans. Am. Ophthalmol. Soc.* 113, 1–15.

Lepesheva, G. I., Virus, C., and Waterman, M. R. (2003). Conservation in the CYP51 family. Role of the B' helix/BC loop and helices F and G in enzymatic function. *Biochemistry* 42, 9091–9101. doi: 10.1021/bi034663f

Lepesheva, G. I., and Waterman, M. R. (2007). Sterol 14α-demethylase cytochrome P450 (CYP51), a P450 in all biological kingdoms. *Biochim. Biophys. Acta* 1770, 467–477. doi: 10.1016/j.bbagen.2006.07.018

Lewinska, M., Juvan, P., Perse, M., Jeruc, J., Kos, S., Lorbek, G., et al. (2014). Hidden disease susceptibility and sexual dimorphism in the heterozygous knockout of Cyp51 from cholesterol synthesis. *PLoS ONE* 9:e112787. doi: 10.1371/journal.pone.0112787

Lewinska, M., Zelenko, U., Merzel, F., Grdadolnik, S. G., Murray, J. C., and Rozman, D. (2013). Polymorphisms of CYP51A1 from cholesterol synthesis: associations with birth weight and maternal lipid levels and impact on CYP51 protein structure. *PLoS ONE* 8:e82554. doi: 10.1371/journal.pone.0082554

Lorbek, G., Perše, M., Horvat, S., Björkhem, I., and Rozman, D. (2013). Sex differences in the hepatic cholesterol sensing mechanisms in mice. *Molecules* 18, 11067–11085. doi: 10.3390/molecules180911067

Lorbek, G., Perše, M., Jeruc, J., Juvan, P., Gutierrez-mariscal, F. M., Lewinska, M., et al. (2015). Lessons from hepatocyte-specific Cyp51 knockout mice : impaired cholesterol synthesis leads to oval cell-driven liver. *Sci. Rep.* 5:8777. doi: 10.1038/srep08777

MacKerell, A. D., Bashford, D., Bellott, M., Dunbrack, R. L., Evanseck, J. D., Field, M. J., et al. (1998). All-atom empirical potential for molecular modeling and dynamics studies of proteins. *J. Phys. Chem. B* 102, 3586–3616. doi: 10.1021/jp973084f

Mukha, D. V., Feranchuk, S. I., Gilep, A. A., and Usanov, S. A. (2011). Molecular modeling of human lanosterol 14α-demethylase complexes with substrates and their derivatives. *Biochemistry* 76, 175–185. doi: 10.1134/S0006297911020039

Ng, P. C., and Henikoff, S. (2003). SIFT: predicting amino acid changes that affect protein function. *Nucleic Acids Res.* 31, 3812–3814. doi: 10.1093/nar/gkg509

Nitahara, Y., Kishimoto, K., Yabusaki, Y., Gotoh, O., Yoshida, Y., Horiuchi, T., et al. (2001). The amino acid residues affecting the activity and azole susceptibility of rat CYP51 (sterol 14-demethylase P450). *J. Biochem.* 129, 761–768. doi: 10.1093/oxfordjournals.jbchem.a002917

Patel, N., Anand, D., Monies, D., Maddirevula, S., Khan, A. O., Algoufi, T., et al. (2016). Novel phenotypes and loci identified through clinical genomics approaches to pediatric cataract. *Hum. Genet.* 136, 205–225. doi: 10.1007/s00439-016-1747-6

Pierce, B. G., Wiehe, K., Hwang, H., Kim, B.-H., Vreven, T., and Weng, Z. (2014). ZDOCK server: interactive docking prediction of protein-protein complexes and symmetric multimers. *Bioinformatics* 30, 1771–1773. doi: 10.1093/bioinformatics/btu097

Pikuleva, I. A., and Waterman, M. R. (2013). Cytochromes P450: roles in diseases. *J. Biol. Chem.* 288, 17091–17098. doi: 10.1074/jbc.R112.431916

Ren, Q., Xiao, D., Han, X., Edwards, S. L., Wang, H., Tang, Y., et al. (2016). Genetic and clinical predictive factors of sulfonylurea failure in patients with type 2 diabetes. *Diabetes Technol. Ther.* 18, 1–8. doi: 10.1089/dia.2015.0427

Strushkevich, N., Usanov, S. A., and Park, H. W. (2010). Structural basis of human CYP51 inhibition by antifungal azoles. *J. Mol. Biol.* 397, 1067–1078. doi: 10.1016/j.jmb.2010.01.075

Sündermann, A., and Oostenbrink, C. (2013). Molecular dynamics simulations give insight into the conformational change, complex formation, and electron transfer pathway for cytochrome P450 reductase. *Protein Sci.* 22, 1183–1195. doi: 10.1002/pro.2307

Urlep, Ž., Lorbek, G., Perše, M., Jeruc, J., Juvan, P., Matz-Soja, M., et al. (2017). Disrupting hepatocyte Cyp51 from cholesterol synthesis leads to progressive liver Injury in the developing mouse and decreases RORC signalling. *Sci. Rep.* 7:40775. doi: 10.1038/srep40775

Wang, M., and Lin, S. (2014). FamLBL: detecting rare haplotype disease association based on common SNPs using case-parent triads. *Bioinformatics* 30, 2611–2618. doi: 10.1093/bioinformatics/btu347

Welter, D., MacArthur, J., Morales, J., Burdett, T., Hall, P., Junkins, H., et al. (2014). The NHGRI GWAS Catalog, a curated resource of SNP-trait associations. *Nucleic Acids Res.* 42, 1001–1006. doi: 10.1093/nar/gkt1229

Yashin, A. I., Wu, D., Arbeeva, L. S., Arbeev, K. G., Kulminski, A., Akushevich, I., et al. (2015). Genetics of aging, health and survival: dynamic regulation of human longevity related traits. *Front. Genet.* 6:122. doi: 10.3389/fgene.2015.00122

Zelenko, U., Hodošček, M., Rozman, D., and Golič Grdadolnik, S. (2014). Structural insight into the unique binding properties of pyridylethanol(phenylethyl)amine inhibitor in human CYP51. *J. Chem. Inf. Model.* 54, 3384–3395. doi: 10.1021/ci500556k

Conflict of Interest Statement: The authors declare that the research was conducted in the absence of any commercial or financial relationships that could be construed as a potential conflict of interest.

frontiers in Pharmacology

REVIEW
published: 08 August 2017
doi: 10.3389/fphar.2017.00521

Advances in the Understanding of Protein-Protein Interactions in Drug Metabolizing Enzymes through the Use of Biophysical Techniques

Jed N. Lampe *

Department of Pharmacology, Toxicology, and Therapeutics, University of Kansas Medical Center, Kansas City, MO, United States

In recent years, a growing appreciation has developed for the importance of protein-protein interactions to modulate the function of drug metabolizing enzymes. Accompanied with this appreciation, new methods and technologies have been designed for analyzing protein-protein interactions both *in vitro* and *in vivo*. These technologies have been applied to several classes of drug metabolizing enzymes, including: cytochrome P450's (CYPs), monoamine oxidases (MAOs), UDP-glucuronosyltransferases (UGTs), glutathione S-transferases (GSTs), and sulfotransferases (SULTs). In this review, we offer a brief description and assessment of the impact of many of these technologies to the study of protein-protein interactions in drug disposition. The still expanding list of these techniques and assays has the potential to revolutionize our understanding of how these enzymes carry out their important functions *in vivo*.

Keywords: cytochrome P450, protein-protein interaction, cytochrome P450 reductase, cytochrome b5, homodimer, heterodimer, allosterism, PGRMC

OPEN ACCESS

Edited by:
Wayne Louis Backes, LSU Health Sciences Center New Orleans, United States

Reviewed by:
Todd D. Porter, University of Kentucky, United States
Dmitri R. Davydov, Washington State University, United States

***Correspondence:**
Jed N. Lampe
jlampe@kumc.edu

Specialty section:
This article was submitted to Pharmacogenetics and Pharmacogenomics, a section of the journal Frontiers in Pharmacology

Received: *08 April 2017*
Accepted: *24 July 2017*
Published: *08 August 2017*

Citation:
Lampe JN (2017) Advances in the Understanding of Protein-Protein Interactions in Drug Metabolizing Enzymes through the Use of Biophysical Techniques. Front. Pharmacol. 8:521. doi: 10.3389/fphar.2017.00521

INTRODUCTION

Drug metabolism and disposition continues to be an important part of the drug discovery and development process in the pharmaceutical industry (Wienkers and Heath, 2005; Evers et al., 2013). While our knowledge of the structure-function relationships of the various drug metabolizing enzymes involved with metabolism and disposition has improved dramatically in the past 50 years (Ortiz de Montellano, 2005; Guengerich, 2006), there is still much that is unknown regarding their functioning *in vivo*. One particular aspect of this is how their structure and function may be modulated by protein-protein interactions.

Abbreviations: CYP, cytochrome P450; CPR, cytochrome P450 reductase; b5, cytochrome b5; SULT, sulfotransferase; GST, glutathione-S-transferase; HLM, human liver microsomes; HO, heme oxygenase; UGT, uridine 5′-diphospho-glucuronosyltransferase; UDPGA, uridine 5′-diphospho-glucuronic acid; MAO, monoamine oxidase; sEH, soluble epoxide hydrolase; 2D NMR, two dimensional nuclear magnetic resonance; Pdx, putidaredoxin; SLF, separated local field; 2D PELF, two dimensional proton evolved local field; INEPT, insensitive nuclei enhanced by polarization transfer; DREPT, dipolar enhanced polarization transfer; FRET, fluorescence resonance energy transfer; NHS, *N*-Hydroxysuccinimide; ER, endoplasmic reticulum; SER, smooth endoplasmic reticulum; PGRMC1, progesterone receptor membrane component 1; PAPS, 3′-phosphoadenosine-5′-phosphosulfate.

Protein-protein interactions are a hallmark of biological systems. They mediate a vast number of critical cellular processes, including: cell division, hormone-receptor binding, signal transduction, enzyme allostery, molecular transport, and electron transfer (Murakami et al., 2017). Additionally, protein-protein interactions are essential to the function of many, if not all, of the enzymes involved in drug metabolism and disposition (Kandel and Lampe, 2014). These types of interactions may take the form of interactions with electron transfer partners, such as the case with cytochrome P450 (CYP) enzymes, or homo and hetero dimerization as observed with sulfotransferase (SULT; Yoshinari et al., 2001) and glutathione-*S*-transferase (GST; Balogh et al., 2009) enzymes. Protein-protein interactions between enzymes and proteins that are not directly required for enzymatic function may also be important for modulating specific activity of drug metabolizing enzymes in different contexts, such as the interaction of progesterone receptor membrane component 1 (PGRMC1) with CYP enzymes in the endoplasmic reticulum (ER) membrane (Rohe et al., 2009; also see the excellent recent review by Ryu et al., 2017). Unfortunately for the experimentalist, most protein-protein interactions are of a transient nature; i.e., short lifetime, low affinity, and low stability; which makes them difficult to analyze, since typically a large amount of stable complex is required for traditional biophysical techniques (Henzler-Wildman and Kern, 2007). This has hindered our basic understanding of the functional impact of many protein-protein interactions in drug metabolizing enzymes. Despite this, there have been numerous efforts made to apply biophysical methodologies and techniques to examine protein-protein interactions in proteins involved in metabolism and disposition. These range from traditional types of analysis, such as X-ray crystallography, NMR, and fluorescence, to more exotic techniques, such as luminescence resonance energy transfer (LRET) and conductometric monitoring. Each of these have their strengths and limitations in regards to the amount of sample needed, tolerance for lipid, cost, time commitment, and the type of observable information retrieved (**Table 1**). The reward for the experimentalist bold enough to apply these biophysical techniques is a richer understanding of protein-protein interactions in these important enzymes.

In this review, we offer an overview of many of the biophysical techniques that have been applied over the years to understand protein-protein interactions in drug metabolizing enzymes, with a focus on the techniques themselves and the salient information that has been obtained from each. Additionally, we will provide a perspective on the future of the field and some newly emerging techniques of interest to the active researcher.

X-RAY CRYSTALLOGRAPHY

Over the course of the previous two decades, X-ray crystallography has provided us with an enormous amount of information regarding protein structure in drug metabolizing enzymes (Cupp-Vickery et al., 2000; Podust et al., 2001; Yoshinari et al., 2001; Williams et al., 2003; Yano et al., 2004; Nagano and Poulos, 2005; Nagano et al., 2005; Grahn et al., 2006; He et al., 2006; Wilderman et al., 2012; Basudhar et al., 2015), for a recent review in this area, see (Reed and Backes, 2017). Despite this, structures of multi-protein complexes involved in drug metabolism and disposition are exceedingly rare. While direct examples of crystal structures of protein complexes are uncommon, there have been many clues provided as to how proteins might interact with one another in their native state. One such case is the interaction of CYPs with their endogenous electron transfer partners, cytochrome P450 reductase (CPR) and cytochrome b_5 (b_5). In order to oxidize the various drugs that serve as their substrates, CYPs must receive electron reducing equivalents from CPR and/or b_5 (Ortiz de Montellano, 2005; Henderson et al., 2013). This involves formation of a protein complex that allows electrons to be directly shuttled from CPR/b_5 to the CYP. Despite more than 50 years of study, the exact molecular process by which this occurs still remains somewhat of a mystery. X-ray crystal structures utilizing traditional techniques have demonstrated that the interaction is predominantly mediated by electrostatics (Hiruma et al., 2013; Tripathi et al., 2013). However, the question has remained as to the role of conformational dynamics in the electron transfer process, as the CPR enzyme has previously been crystalized in a "closed" conformation (Vincent et al., 2012) that limits access to the flavin mononucleotide (FMN) domain. In order to determine the distinct conformational state of CPR that interacts with the CYP enzyme, a co-crystal structure of the two proteins in complex was needed. A breakthrough came in this regard when Sevriukova and colleagues were able to determine the crystal structure between the heme and FMN-containing domains of the model cytochrome P450BM-3 (Sevrioukova et al., 1999). This was facilitated by a novel strategy of individual expression and purification of the heme, FMN, and FAD containing domains of the enzyme (Sevrioukova et al., 1997) and then carefully reconstituting both the heme containing domain with the FMN domain (Sevrioukova et al., 1997, 1999). The structure itself indicated that the proximal side of the heme was the primary site of interaction with the FMN domain and, furthermore, identified a pathway for electron transfer from the FMN domain to the heme iron (Sevrioukova et al., 1999). This led to the hypothesis, developed somewhat later, that a "hinging" motion opens the protein and allows the FMN domain to directly interact with the CYP heme (Hall et al., 2001; Hamdane et al., 2009; Sugishima et al., 2014).

A clever strategy involving crystallization of a four amino acid deletion mutant demonstrated that the CPR protein can pivot along the C terminus of the hinge region and thereby undergo a conformational rearrangement that allows sufficient opening of the protein to expose the FMN domain to the CYP interface (Hamdane et al., 2009). Interestingly, this hypothesis of a conformational rearrangement being necessary for an effective route of electron transfer to be formed between the CPR and CYP proteins was later confirmed when CPR was co-crystalized with heme oxygenase (HO; Sugishima et al., 2014). In this complex, it became clear that shortening the CPR hinge region leads to a protein that favors the open conformation and promotes association with HO (Sugishima et al., 2014). These studies demonstrate the utility of combining the power of

TABLE 1 | A summary of the biophysical techniques discussed in this review and their application to monitoring protein-protein interactions in DMEs.

Technique	Biophysical basis	Physical observables	Pros	Cons	Drug metabolizing enzyme (DME)	References
X-ray crystallography	Electron diffraction by protein crystal lattice	Atomic bond position and length	Definitive structural assignment of all the residues in a polypeptide	Requires a large amount of protein and limited to a "snapshot" in time	CYP, CPR, GST, SULT, MAO, UGT, and others	Sevrioukova et al., 1997, 1999; Cupp-Vickery et al., 2000; Hall et al., 2001; Podust et al., 2001; Yoshinari et al., 2001; Williams et al., 2003; Scott et al., 2004; Yano et al., 2004; Nagano and Poulos, 2005; Nagano et al., 2005; Grahn et al., 2006; He et al., 2006; Hamdane et al., 2009; Deng et al., 2010; Vincent et al., 2012; Wilderman et al., 2012; Hiruma et al., 2013; Tripathi et al., 2013; Peng et al., 2014; Sugishima et al., 2014; Basudhar et al., 2015; Reed and Backes, 2017; Gill, 1983; Kakuta et al., 1997; Meech and Mackenzie, 1997; Argiriadi et al., 1999; Binda et al., 2001, 2011; Petrotchenko et al., 2001; Polekhina et al., 2001; Abdalla et al., 2002; Miley et al., 2007; Wang and Edmondson, 2007; Schoch et al., 2008; Lewis et al., 2011; Nelson et al., 2013; Matsumoto et al., 2014; Suzuki et al., 2014; Fujiwara et al., 2016; Audet-Delage et al., 2017; Chenge et al., 2017
NMR	Measures changes in magnetic resonance of atomic nuclei (typically ^{1}H)	Provides detailed information about the structure, dynamics, reaction state, and chemical environment of macromolecules	Potential for complete structural assignment of the entire protein; also captures protein dynamics	Large amount of protein required; must be soluble	CYP, CPR (domains only), GST, and SULT	Lian, 1998; McCallum et al., 1999; Mahajan et al., 2006; Kijac et al., 2007; Lampe et al., 2008, 2010; Vallurupalli et al., 2008; Gluck et al., 2009; Raman et al., 2010; Ahuja et al., 2013; Estrada et al., 2013, 2014, 2016; Hiruma et al., 2013; Basudhar et al., 2015; Cook et al., 2016; Zhang et al., 2016
Fluorescence: FRET/BRET	Energy transfer from a donor fluorophore to an acceptor fluorophore through non-radiative dipole–dipole coupling	Intermolecular distance, detection of direct molecular interaction between two proteins	Unique information regarding protein dynamics and specific residues involved in the interaction	(Usually) requires the addition of an exogenous fluorophore	CYP, CPR, GST, UGT	Nisimoto et al., 1983; Schwarze et al., 1983; Wang et al., 1993, 2001; Davydov et al., 1996, 2000, 2010, 2013a,b, 2015; Dietze et al., 1996; Lakowicz, 1999; Lu and Atkins, 2004; Wen et al., 2006; Praporski et al., 2009; Li et al., 2011; Yuan et al., 2015, 2016; Fujiwara et al., 2016
Fluorescence: fluorescence anisotropy	Measurement of the photon emission of a fluorophore along different axis of polarization	Measurement of intermolecular binding constants and reaction kinetics	Allows monitoring of direct interaction in real time	Requires exogenous fluorophore with high quantum yield	CYP, GST	Greinert et al., 1979, 1982; Gut et al., 1985; Schwarz et al., 1993; Gorovits and Horowitz, 1995; Lim et al., 1995; Lakowicz, 1999; Szczesna-Skorupa et al., 2003
Photoaffinity labels/peptide MS	Covalent alkylation of a protein with a photo-reactive group, such as an azide, a diazirine, or benzophenone	Identification of specific sites of protein-protein interaction and distances	Provides direct information on specific sites of interaction	Requires introduction of an exogenous photolabile probe on the protein	CYP	Hodek and Smrcek, 1999; Wen et al., 2005; Gao et al., 2006a; Sulc et al., 2008

(Continued)

TABLE 1 | Continued

Technique	Biophysical basis	Physical observables	Pros	Cons	Drug metabolizing enzyme (DME)	References
Chemical crosslinking/peptide MS	Covalent modification of a protein with a chemically reactive group, such as a malimide, iodoacetamide, or isothiocyanates	Identification of specific sites of protein-protein interaction and distances	Provides direct information on specific sites of interaction	Requires introduction of an exogenous chemically labile probe on the protein	CYP, GST	Cooper, 2002; Gao et al., 2006b; Losel et al., 2008; Reed et al., 2010
SPR/Surface immobilization	Determines the change in refractive index of incident light on a surface bilayer due to resonant oscillation of conduction electrons at the interface	Determination of binding constant (Kd) of interaction, thermodynamic analysis, epitope mapping	Allows for determination of binding constants and mode of interaction	Requires that one protein partner be immobilized on a chip surface	CYP	Ivanov et al., 1997, 1999, 2001; Kuznetsov et al., 2004; Shimada et al., 2005; Pearson et al., 2006; Archakov and Ivanov, 2011; Martin et al., 2015; Bostick et al., 2016; Yablokov et al., 2017
Quartz crystal microbalance conductometric monitoring	Conductometric biosensor coupled with *in vitro* transcription/translation system for monitoring protein-protein interactions using a quartz crystal microbalance with dissipation monitoring	Disassociation constants (Kd), thermodynamic parameters, complex size	Allows for determination of binding and thermodynamic constants	Requires efficient combined transcription and translation of protein	CYP	Davydov et al., 2013b; Spera et al., 2013

X-ray crystallography with traditional site-directed mutagenesis techniques to obtain answers to structural questions that might not be readily available by either technique alone.

X-ray crystallography has also been useful for dissecting the protein-protein interactions of another CYP electron transfer partner, b_5. Using a combination of chemical crosslinking and protein crystal structures, Peng et al. were able to propose a model for the b_5 mediated stimulation of the 17,20-lyase activity of cytochrome P450c17 (Peng et al., 2014), suggesting that electrostatic interactions predominate in the CYP-b5 interaction, as they do with the CYP-CPR complex. In another example, X-ray crystal structures of b_5 have informed our understanding of electron transfer from b_5 to individual CYPs, such as CYP2B4, where ligand-induced structural changes were found to be coupled to b_5 effector binding (Scott et al., 2004).

It has also been useful in defining novel interactions with CYP proteins, as well as those currently known. In an X-ray crystallography study comparing the b_5-like protein, Ncb5or, with b_5, Deng et al. determined that the positioning of the second histidine heme ligand (His 112) in b_5 is critical for efficient electron transfer, both from b_5 reductase and to the (CYP) electron transfer partner (**Figure 1**; Deng et al., 2010). These are just a few of the many examples available where X-ray crystallography has been used to interrogate CYP and electron transfer partner interactions.

However, CYPs are also known to form both hetero and homo oligomers which can influence their functional activity (Davydov, 2011, 2016; Reed and Backes, 2016, 2017). In this aspect, X-ray crystallography has contributed to our structural understanding of the factors involved in dimer formation. For example, the *M. tuberculosis* CYP126A1 protein was recently demonstrated to form homodimers under crystallization conditions (Chenge et al., 2017). The dimer interface is composed of interactions along the hydrophobic B/C and F/G loop regions of the protein, which are known substrate recognition regions. Interestingly, the CYP126A1 protein forms a dimer both in the ligand-free state and also with substrate bound. However, the dimer is disrupted when the inhibitor ketoconazole is bound to the protein, leading to conversion to the monomer (Chenge et al., 2017). Similarly, CYP2C8 has been shown to crystalize as a dimer (Schoch et al., 2008). As observed with CYP126A1, the CYP2C8 homodimer was formed around interactions at the hydrophobic F/G loop interface. The presence of the dimer was also confirmed in solution as well as under the original crystallization conditions used (Schoch et al., 2008). Remarkably, two molecules of the substrate palmitic acid were found to be bound in the dimer interface, illustrating the potential physiological relevance of dimer formation. In contrast to CYP126A1, the presence of ligand did not prevent dimer formation, suggesting that homodimeric protein-protein interaction modes may vary between different CYPs. Despite this, the peripheral ligand binding site identified in CYP2C8 has been proposed to be important in modulating the cooperative effects observed with multiple ligand binding in certain CYPs (Davydov et al., 2013a, 2015; Reed and Backes, 2017), and may also serve as a "hot spot" for protein-protein interaction.

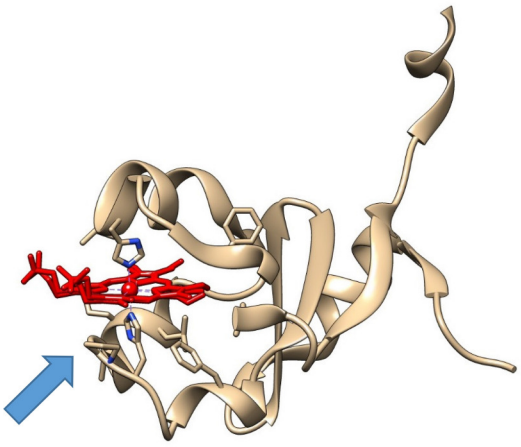

FIGURE 1 | The crystal structure of the b_5-like protein, Ncb5or (PDB: 3LF5), showing the heme (in red), with the Fe atom coordinated between the two active site histidine residues.

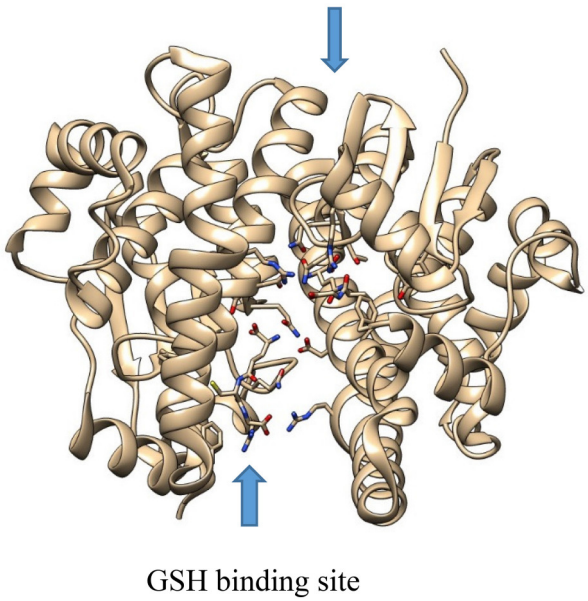

FIGURE 2 | The crystal structure of GST A1-1 (PDB: 3I6A), showing the "ball-and-socket" dimer interface and the GSH binding site.

X-ray crystallography has also been useful in informing our understanding of the function of protein dimers of other drug metabolizing enzymes as well. Both cytosolic GST (Balogh et al., 2009) and SULT (Yoshinari et al., 2001) enzymes have been crystalized as dimers. Moreover, dimerization seems to be important to function in both classes of enzymes (Kakuta et al., 1997; Petrotchenko et al., 2001; Abdalla et al., 2002). In the case of GST enzymes, the dimer is composed of a two-fold axis between each monomer with multiple hydrophobic, so called "ball-and-socket", interactions between the different domains of each monomer (**Figure 2**) (Balogh et al., 2009). The crystal structure of maleylacetoacetate isomerase/glutathione transferase zeta revealed that residues M51 and F52 from a loop between helix α2 and strand β3, where the residues are wedged into a hydrophobic pocket formed between the α4 and α5 helices, thereby vividly illustrating the ball-and-socket type structure (Polekhina et al., 2001).

In SULT enzymes, the dimerization domain (**Figure 3**) consists of ten residues near the C-terminus of the protein, represented by the consensus sequence KXXXTVXXXE, also known as the KTVE motif (Petrotchenko et al., 2001). In contrast to the interaction interface observed with GST enzymes, this region forms a hydrophilic loop that creates multiple contacts between the two individual monomers. This is reinforced by multiple hydrophobic contacts internal to the KTVE motif, resulting in a "dumbbell"-like structure (Petrotchenko et al., 2001; Yoshinari et al., 2001). While the exact role dimerization plays in catalysis is not totally understood in these enzyme families, it is likely that future X-ray crystal structures will help elucidate it.

Unfortunately, our structural understanding of UGT enzymes is much more limited. While there is ample biophysical evidence to support the existence of UGT dimers (Meech and Mackenzie, 1997; Lewis et al., 2011; Suzuki et al., 2014), the lack of structural data has hampered protein-protein interaction research with this enzyme class. Interestingly, the structural data that does exist for human UGT enzymes, that of a partial UGT2B7 structure, does provide an indication for the presence of homo dimers (Miley et al., 2007; Fujiwara et al., 2016; Audet-Delage et al., 2017). In the asymmetric unit, the C terminus of one monomer packs into the predicted UDPGA binding site of the other monomer (Miley et al., 2007). At first glance, this may seem somewhat counter intuitive, as the UDPGA co-factor is needed for enzymatic activity. However, the UDPGA binding site of the other UGT2B7 monomer in the asymmetric unit is not occluded, indicating that this monomer may be active while the other subunit is blocked. As Miley and co-workers demonstrated, removal of the C-terminal residues, in an effort to eliminate blockage of the UDPGA binding site, produced protein samples that were highly unstable and could not be crystallized (Miley et al., 2007). This may suggest that the blockage of the UDPGA co-factor binding site serves as a form of regulatory control of enzymatic activity, although this has not yet been established.

The situation with the MAO enzymes is a bit more complex, with MAO-A being represented as a monomer, while MAO-B is a functional homodimer (Binda et al., 2001, 2011). Comparison studies between the human and rat MAO-A enzymes, with the latter also being a dimer, have suggested that dimerization increases structural stability and may directly influence the kinetic properties of the individual enzymes (Wang and Edmondson, 2007). Others have hypothesized that dimerization may be essential to orient the protein dipole-dipole moment toward the anionic membrane surface in order to promote catalysis (Binda et al., 2011). While human MAO-A crystalized as a monomer, it is not entirely clear if this is an artifact of the

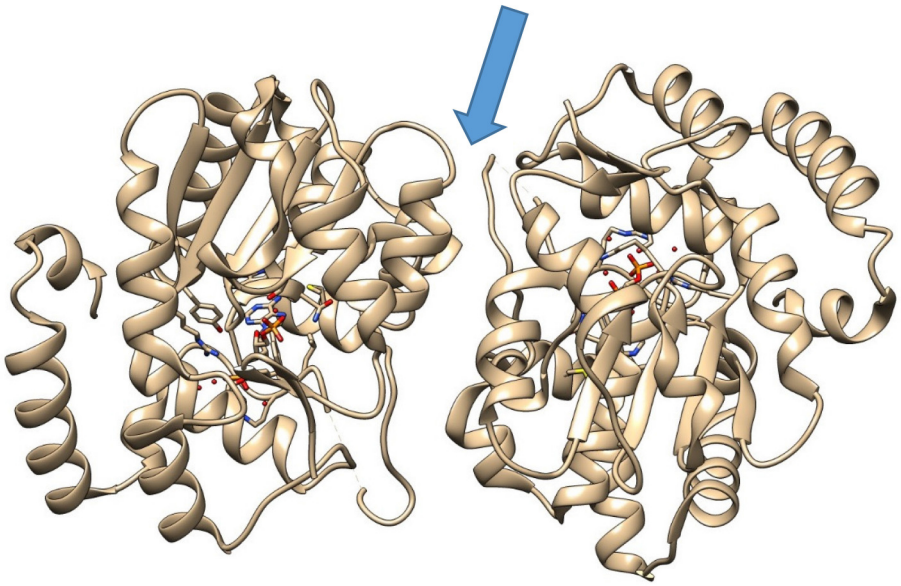

FIGURE 3 | The crystal structure of SULT2A3 (PDB: 1EFH), demonstrating the dimer interaction motif (center).

crystallization conditions, or has direct functional relevance, as MAO-A is thought to be a dimer in the membrane bound form of the enzyme (Binda et al., 2011). This illustrates a critical point in examining protein-protein interactions with membrane bound proteins: protein-protein interactions are highly dependent on local conditions, particularly the presence/absence of lipid.

Soluble EH (sEH) has also been observed to form dimers upon crystallization (Argiriadi et al., 1999). The sEH dimer structure itself is stabilized by "domain-swapped" or "handshake" architecture, whereby the vestigial and catalytic domains adopt unrelated α/β folds and are connected by a 16-residue, proline-rich linker (Thr-219–Asp-234). A "domain-swapped" architecture occurs when the domain of one monomer is displaced by the same domain of the other monomer in the asymmetric unit thereby forming a stable dimer interface (Gill, 1983). While the vestigial active site does not participate in epoxide hydrolysis, the vestigial domain plays a critical structural role by stabilizing the dimer. More recent studies have confirmed the importance of dimerization for enzymatic activity (Nelson et al., 2013). Moreover, it has been suggested that the dimer interface may make an attractive target for small molecule therapeutics designed against sEH (Nelson et al., 2013; Matsumoto et al., 2014).

NUCLEAR MAGNETIC RESONANCE (NMR)

A powerful and complementary technique to X-ray crystallography is protein NMR (Lampe et al., 2008, 2010; Vallurupalli et al., 2008; Raman et al., 2010; Ahuja et al., 2013; Hiruma et al., 2013; Basudhar et al., 2015). In particular, solution NMR can report not only on protein tertiary structure, but also on conformational dynamics which are important to the interaction with protein partners (Lampe et al., 2008, 2010). An additional advantage is that protein NMR can be performed in the presence of lipid bilayer mimetics, such as bicells (Ahuja et al., 2013) or nanodiscs (Kijac et al., 2007; Gluck et al., 2009), allowing the investigator to examine the effect of lipid on protein-protein interactions. Protein NMR has been most widely used to examine interactions between CYP enzymes and their electron transfer partners (Ahuja et al., 2013; Estrada et al., 2013, 2014, 2016). The Scott lab has been a leader in this area, examining the interactions of CYP17A1 with b_5 (Estrada et al., 2013, 2014) and the FMN domain of reductase (Estrada et al., 2016). This system has a particular advantage in that multiple types of interaction can be monitored through titrations involving substrate, CYP, b_5, reductase FMN domain, or any combination thereof. One important result to come out of these studies is that the strength of the CYP17A1- b_5 interaction is dependent on the identity of the substrate, with the CYP17A1-b_5 interaction being stronger when the hydroxylase substrate pregnenolone is present in the CYP17A1 active site than when the lyase substrate 17α-hydroxypregnenolone is bound (Estrada et al., 2013). In these titration experiments, only the b_5 protein was isotopically labeled with ^{15}N. When the "reverse" titration experiment was conducted (i.e., where the CYP17A1 molecule is ^{15}N labeled and the b_5 protein was isotopically "silent"), the results were similar (Estrada et al., 2014). Additionally, titration of b_5 into the ^{15}N-labeled CYP17A1-pregnenolone complex induced a set of conformational substates closely resembling those of CYP17A1-17α-hydroxypregnenolone complex without b_5, suggesting that b_5 may also be able to allosterically induce enzymatically productive conformations in CYP17A1, even in the absence of the lyase substrate (Estrada et al., 2013, 2014).

While these data have yet to be replicated with any other drug metabolizing CYP enzymes, it is intriguing to postulate that the results may be extrapolated to b_5 interactions with other CYPs.

As noted above, a particular advantage of using NMR to examine protein-protein interactions is that it can tolerate the presence of lipid. This fact was exploited by Ramamoorthy et al. to determine the structure of full-length, membrane bound b_5 in the presence of CYP2B4 (Ahuja et al., 2013). This was the very first time that a structure of b_5 had been determined in the presence of a phospholipid bilayer. The structure confirmed the electrostatic nature of the CYP-b_5 interaction, revealing a large number of charge-charge interactions between surface residues on CYP2B4 and b_5 enabling complex formation between the two proteins (Ahuja et al., 2013). Interestingly, it also hinted at the importance of hydrophobic interactions between the complex and the phospholipid bilayer. Confirming the result observed by Estrada et al. when examining the CYP17A1- b_5 interaction, Ramamoorthy et al. also observed increased affinity between the CYP and b_5 in the presence of a small molecule substrate or inhibitor. Finally, their data suggested a pathway for electron transfer between b_5 and CYP2B4, mediated through a salt bridge from the heme propionates of b_5 with Arg125 of CYP2B4. More recently, Ramamoorthy et al. have extended their original studies to examine the interactions of the CYP-b_5 complex using phospholipid bilayer nanodiscs (Zhang et al., 2016). The advantage of this versatile phospholipid bilayer memetic is that it permits exquisite control over the composition of lipid, allowing researchers to examine the effects of various lipid components on structure and catalysis. The examples above illustrate the advantages of 2D protein NMR to obtain detailed structural data for protein-protein interactions in the CYP enzyme family.

Almost 20 years ago, Lian pioneered a novel approach combining both X-ray crystallography and NMR to study homo- and hetero-dimeric interactions in the GST A1-1 isoform (Lian, 1998). In the crystal structure of GST A1-1, the hydrophobic C-terminal region of the protein is highly disordered and absent from the structure, as is often the case with dynamic regions of proteins. Lian's group was able to resolve this region of the protein in the 2D HSQC spectrum and identify residues that might be involved in ligand binding and/or protein-protein interactions. Since that time, a number of studies relying on protein NMR have been conducted using GST enzymes (McCallum et al., 1999; Mahajan et al., 2006).

While fewer structural NMR studies have been carried out with the SULT family of enzymes, a recent novel example of NMR, combined with the use of a nitrox spin label positioned in dynamic regions of the enzyme, gave information regarding dimer interaction and the structure of the catechin ligand binding site on the protein (Cook et al., 2016). This was accomplished by replacing each cysteine residue in the protein with an unreactive residue, then selectively reincorporating a cysteine at each position of interest and reacting the protein with a nitroxyl-oxygen spin label (3-maleimido-PROXYL). The label was attached to the protein at six individual cysteine positions in the protein in order to saturate the dimer in a paramagnetic field of sufficient strength to detect its effects on the solution NMR spectrum, without compromising the catalytic integrity of the enzyme. The design allowed the entire surface of the enzyme to be covered in a detectible paramagnetic field and allowed ligands to be positioned within the active site by triangulating their protons from multiple spin labels attached at various positions within the active site (Cook et al., 2016). After obtaining the NMR spectrum for each mutant, the spectrum was overlaid on the previously determined crystal structure and the final structure was obtained using distance-constrained molecular dynamics docking. This approach was advantageous, and preferred over others, in that: (1) it is applicable over a wide range of ligand affinities, (2) does not require much protein, (3) does not require an isotopic label, and (4) has essentially no molecular weight limitations. Moreover, the same strategy may apply to other drug metabolizing enzyme protein-protein complexes that have limiting cysteine residues.

Progress in applying NMR to the study of UGT enzymes has been slower due to the integral attachment to cellular membranes but, as in the case of the CYP enzymes, it is likely that newly emerging technologies, such as nanodiscs and membrane bicells will be useful in defining their interaction with protein partners.

FLUORESCENCE TECHNOLOGIES

The use of both endogenous and exogenous fluorescence labels for conducting protein-protein interaction studies has a long history (Lakowicz, 1999). Indeed, they have been used very effectively in defining the structural determinants and dynamics required for interaction among drug metabolizing enzymes (Nisimoto et al., 1983; Schwarze et al., 1983; Wu and Yang, 1984; Centeno and Gutierrez-Merino, 1992; Davydov et al., 1996, 2001). Most studies to date have preferred to use exogenous fluorophores due to the fact that they typically exhibit much higher quantum yields than the endogenous fluorophores; tryptophan, tyrosine, phenylalanine, and the fluorescent prosthetic groups.

Unarguablely, the greatest use of fluorescence to monitor protein-protein interactions has been with the CYP enzymes. A key early study, suggesting the presence of CYP homodimers in the ER membrane, involved monitoring the fluorescence anisotropy of the substrate diphenylhexatriene as a proxy for membrane rigidity (Gut et al., 1985). Fluorescence anisotropy is the phenomena by which fluorophore containing molecules emit polarized light when the exciting light source is also polarized. The degree of the polarization of the emitted light is proportional to the anisotropy (r), or rotational motion, of the molecule (Lakowicz, 1999). This can be a powerful technique to determine the relative size of molecules or macromolecular complexes, and has been exploited as such in antibody-based assays, among others (Gorovits and Horowitz, 1995; Lim et al., 1995). In a similar fashion, fluorescence depolarization has also been extensively used to monitor CYP-CYP interactions as well (Greinert et al., 1979, 1982; Schwarz et al., 1993).

Other aspects of fluorescence have also been exploited in studying CYP protein-protein interactions. The technique of fluorescence resonance energy transfer (FRET), whereby an excited donor molecule is able to quantitatively transfer energy

to an acceptor molecule that then emits in another region of the spectrum, has been used successfully in several studies of protein-protein interactions among drug metabolizing enzymes (Nisimoto et al., 1983; Schwarze et al., 1983; Davydov et al., 1996, 2000, 2010, 2013a, 2015; Szczesna-Skorupa et al., 2003; Praporski et al., 2009). A singular advantage of this fluorescence technique is that it allows for an indirect measurement of distance between the two fluorophores due to the phenomena of Förster energy transfer (Lakowicz, 1999). In an elegant FRET study conducted in 2003, Kemper et al. were able to observe a direct physical interaction between individual CYPs in a live cell membrane utilizing CYP2E1 and CYP2C2 which were labeled with donor and acceptor fluorophores in cells transfected with murine CYP cDNA (Szczesna-Skorupa et al., 2003). They discovered that, while FRET occurred between individual CYP2C2 molecules in a membrane, it could not be detected between CYP2E1 monomers, representing a homomeric self-association with CYP2C2, but not CYP2E1. Later work confirmed the existence of the CYP2C2 dimers in murine hepatocyte endoplasmic reticulum membranes, demonstrating the potential *in vivo* relevance of these types of protein-protein interactions (Li et al., 2011).

Sligar's group at the University of Illinois was an early adopter of fluorescence technologies to monitor CYP interactions with effector proteins, such as b_5 (Stayton et al., 1988). By selectively replacing threonine residues with cysteine in b_5, they were able to site-specifically introduce the sulfhydryl selective fluorescent reagent, acrylodan, at different positions in the protein. Acrylodan generally reacts with accessible thiol groups more slowly than maleimides or iodoacetamides, but tends to form highly stable thioether bonds (Weber and Farris, 1979). Additionally, in the excited state there is a substantial charge separation between the amino and carbonyl groups, which produces large spectral shifts in a hydrophobic environment, making it an ideal spectral probe for monitoring protein-protein interactions. When the labeled b_5 protein was allowed to interact with CYP P-450cam, a model bacterial isoform, a significant fluorescence enhancement and blue shift was observed, indicating the fluorophore's transition to a more hydrophobic binding site and an increased binding free energy for the two proteins.

More recently, Usanov et al. expanded on the Sligar lab's early work by using a chimeric b_5-GFP to examine protein-protein interactions between b_5 and CYP3A4 (Yantsevich et al., 2009). Utilizing this chimeric construct, the authors were able to determine binding affinities between various b_5 and CYP3A4 complexes. An interesting result from this report was that the hydrophobic domain of b_5 was observed to participate both in hemeprotein interaction and electron transfer directly from b_5 to the CYP enzyme. Simonov et al. used a CYP17A1 with eCFP fused to the C-terminus and eYFP fused to the N-terminus of b_5 to examine CYP17A1- b_5 protein-protein interactions using FRET (Simonov et al., 2015). They combined this technique with structural modeling and molecular dynamics simulations to show that b_5 interacts directly with CYP17A1 in the ER membrane to stimulate the lyase reaction.

Fluorescence tools have also proven useful to examine CYP-CPR interactions. A unique approach by Davydov et al. to study the effect of substrate binding on CYP protein-protein interactions involved substituting the ferric-protoprophyrin IX heme with an aluminum-protoporphyrin IX (Nisimoto et al., 1983). While previous studies had used zinc substituted protoporphyrins, the replacement of the iron atom with aluminum resulted in an isosteric displacement, since both transition metals have approximately the same interatomic radius. Therefore, the aluminum substitution was unlikely to have a major effect on the overall structure of the active site. Additionally, while the aluminum atom is not able to donate or accept electrons, it imparts a high degree of fluorescence to the protoprophyrin, thereby introducing an internal probe which allowed the authors to monitor the interactions between CYP P450 BM-3 and its substrates and protein partners using fluorescence energy transfer (Davydov et al., 2013b). The CYP P450 BM-3 retained its ability to interact with the reductase domain despite the substitution in the protoprophyrin and the newly imparted fluorescence from the aluminum-protoporphyrin IX allowed the authors to determine affinity between the CYP domain and the reductase domain.

Fluorescence studies have also been useful in the study of the human UGT enzymes (Operana and Tukey, 2007; Fujiwara et al., 2016; Yuan et al., 2016). Turkey et al. used FRET to examine UGT1A oligomerization *in vivo* (Operana and Tukey, 2007). Using this technique, they were able to show that UGT1A1, 1A3, 1A4, 1A6, 1A7, 1A8, 1A9, and UGT1A10 all form homodimers in live cells. Additionally, the authors confirmed heterodimer interactions between UGT1A1 and the UGT1A3, 1A4, 1A6, 1A7, 1A8, 1A9, and UGT1A10 isoforms. More recently, Yuan et al. used FRET to demonstrate that UGT2B7 was able to form homo oligomers with both wild-type and mutant forms of the enzyme, which had the possibility of affecting zidovudine glucuronidation (Yuan et al., 2015). Yuan further went on to demonstrate that the UGT isoforms UGT1A1, 1A9, and 2B7 were all able to form heterodimeric complexes, expanding on their previous work that examined homodimerization in this enzyme class (Yuan et al., 2016).

Beckman et al took a unique approach to studying intersubunit communication in dimeric complexes of SULT enzymes, by examining fluorescence quenching of the enzyme's intrinsic fluorophores upon binding of the inhibitors, 2,6-dichloro-4-nitrophenol (DCNP) and pentachlorophenol (PCP; Beckmann et al., 1998). Using this technique, the authors were able to determine that binding of the co-factor 3′-phosphoadenosine-5′-phosphosulfate (PAPS) facilitated positive cooperative binding between the individual subunits. This illustrates the use of a powerful fluorescence technique that does not rely on introduction of an extrinsic fluorophore to obtain information on protein-protein interactions, allowing for an examination of protein-protein interactions in the native state of the enzyme.

Another seminal FRET study, this time involving GST P1-1, demonstrated that the C-terminus of c-Jun N-terminal kinase could interact directly with this GST enzyme (Wang et al., 2001). This was an early study that identified a role for GST P1-1 in regulating certain kinase pathways. The Atkins group has used both intrinsic fluorescence of proteins (Wang et al., 1993; Dietze

et al., 1996) and of ligands (Lu and Atkins, 2004) to examine the interaction of GST dimers and their substrates.

PHOTO-AFFINITY LABELS AND CROSSLINKING STUDIES

Photoaffinity labels and chemical crosslinking agents have long been recognized as useful tools to understand protein-protein interactions. Photoaffinity labels are particularly useful if they are also enzyme substrates, as they are typically localized at the CYP active site until activated with irradiation (Wen et al., 2005, 2006). Wen and Lampe utilized the photoaffinity label lapachenole in combination with cysteine-scanning mutagenesis to identify specific residues of CYP3A4 that interact with CPR, including cysteine 98, using LC-MS (Wen et al., 2006). Similarly, Sulc et al. employed the photoaffinity ligand 3-azidiamantane to label CYP2B1 (Hodek and Smrcek, 1999) and CYP2B4 (Sulc et al., 2008). While, in this case, the diamantoid probe did not function specifically as a probe of protein-protein interactions, it has the potential to report on specific conformational changes in the CYP enzyme that may accompany interaction with protein partners.

In general, crosslinking agents are more versatile and have been used more extensively in assessing protein-protein interactions. In particular, LC-MS combined with crosslinking, can be powerful in detecting specific interactions between two proteins that are known to interact. However, the non-specificity of most chemical crosslinking agents make the large datasets generated from such experiments difficult to analyze. Gao et al. developed a software tool called Pro-CrossLink to address this specific issue (Gao et al., 2006a). Using this tool, combined with a site-directed mutagenesis approach and the standard crosslinking agent, 1-ethyl-3-[3-dimethylaminopropyl]carbodiimide hydrochloride (EDC), they were able to identify relevant protein-protein interactions that occurred between CYP2E1 and b_5 (Gao et al., 2006b). Their strategy relied on an ^{18}O-labeling method that incorporated twice as many ^{18}O atoms in cross-linked peptides as non-cross-linked peptides when proteolysis was conducted in ^{18}O-labeled water. Subsequent tandem mass spectrometric (MS/MS) analysis of the selected cross-linked peptide candidates led to the identification of two intermolecular cross-links, one at K428-CYP2E1 to D53-b5 and K434-CYP2E1 to the E56 residue of b_5. These results provided some of the first direct biophysical evidence for the interacting orientations of a microsomal CYP and b_5.

More recently, investigators have used chemical crosslinkers to identify CYP interaction with other, non-canonical proteins. Using the amine-reactive EGS crosslinker, Losel et al. was able to demonstrate that PGRMC1, a known CYP modulator, interacts with a yet-to-be-identified 52 kDa protein, presumably a CYP enzyme, in pig liver microsomes (Losel et al., 2008). Additionally, substantial progress has been made examining the homodimeric interactions of other CYPs, such as CYP3A4 (Davydov et al., 2015) and others (Reed et al., 2010) using crosslinking technology.

SPR AND SURFACE IMMOBILIZATION

Surface Plasmon Resonance (SPR) and related surface biolayer technologies have been mainstay technologies for examining protein-protein interactions in a variety of systems for many years (Cooper, 2002). These technologies rely on immobilization of the target, or "receptor," protein onto the solid surface of a chip (usually Au), then a (potential) protein partner, the "ligand," is allowed to flow over the surface of the chip and, if binding occurs, this results in a cascading plasmon wave in the gold layer that causes a detectable change in the refractive index of an incident light source (usually a laser) that is directly proportional to the binding interaction (Cooper, 2002). Early studies with CYP enzymes demonstrated the sensitivity of this technology in monitoring ligand binding directly to CYP enzymes, paving the way for more sophisticated protein-protein interaction studies (Pearson et al., 2006). More recently, this technology has been applied to examining CYP interactions with electron transfer partners (Ivanov et al., 1997, 1999, 2001; Kuznetsov et al., 2004; Archakov and Ivanov, 2011; Yablokov et al., 2017).

Yablokov et al. used a modified construct of b_5 covalently attached through an NHS linkage to a gold SPR chip to directly monitor the interactions between b_5 and various human CYP isoforms, including both CYP's whose activity was allosterically regulated by b_5 and those whose activity was unchanged in the presence of b_5 (Yablokov et al., 2017). Interestingly, they determined that the CYP-b_5 interactions fell into two classes: those that were enthalpy driven and those that were entropy driven. The CYP-b_5 interactions that were enthalpy driven tended to belong to CYPs that were allosterically regulated by b_5 (i.e., whose activity could be modulated by b_5), whereas the CYP-b_5 interactions that were entropy driven tended to represent the CYP's whose activity was unaffected by b_5. The authors attributed the differences in these effects to positive ΔH values corresponding to displacement of the solvation shells of proteins upon clustering (Yablokov et al., 2017).

Gannett and his team applied SPR to examine CYP-CYP interactions between CYP2C9, CYP3A4, CYP2D6, and other isoforms (Bostick et al., 2016). Somewhat surprisingly, they found that the highest affinity complex was formed between CYP2C9 and CYP2D6, a heterodimeric complex, with the affinity between CYP2C9 and CPR being lower than that of heterodimers and CYP2C9 homodimers. Additionally, they observed that the affinities of specific complexes were highly dependent on the order of addition of the individual proteins involved.

Previously, in a clever application combining two technologies, Shimada and Guengerich used immobilized CYP proteins, coupled with an enzyme-linked affinity approach, to measure relative affinities between the CYP-CPR complexes and CYP-b_5 complexes (Shimada et al., 2005). Individual CYP proteins were purified and bound to separate wells of a polystyrene plate, after which the biotinylated partner enzymes were added. Finally, a streptavidin-peroxidase complex was added to each well and protein-protein interaction was monitored by measuring peroxidase activity of the bound biotinylated proteins. This allowed for an indirect calculation of K_d's for the individual CYPs to CPR and b_5.

The ever-expanding and versatile nature of the SPR platform(s) indicate that this technology will continue to be useful for monitoring protein-protein interactions in the immediate future and beyond.

EMERGING BIOPHYSICAL TECHNOLOGIES TO EXAMINE PROTEIN-PROTEIN INTERACTIONS AND FUTURE PERSPECTIVE

Today is an exciting time to study protein-protein interactions in drug metabolizing enzymes. A number of new technologies are beginning to emerge that have the power to revolutionize our understanding of how protein-protein interactions modulate the activity of these important proteins. Quartz crystal microbalance studies have helped define the protein-protein interactions between CYP17A1 and b_5, in part explaining enzymatic product distribution ratios (Simonov et al., 2015). Additionally, these types of studies have also been useful in identifying sites of protein-protein interaction in CYP19 (aromatase; Martin et al., 2015). Along with quartz crystal microbalance studies, conductometric monitoring is another emerging technology that has the potential to provide information on protein-protein interaction in drug metabolizing enzymes (Spera et al., 2013).

In conclusion, the future use of traditional and emerging biophysical technologies to monitor protein-protein interactions is likely to provide us with further insight to the function and regulation of these enzymes critically important for drug metabolism and disposition.

AUTHOR CONTRIBUTIONS

The author confirms being the sole contributor of this work and approved it for publication.

FUNDING

This work was supported in part by grants from the National Center for Research Resources [Grant P20-RR021940-07], the National Institute of General Medical Sciences [Grant P20-GM103549-07], and the Kansas IDeA Network of Biomedical Research Excellence [Grant QH846868-K-INBRE] (JNL) from the National Institutes of Health.

REFERENCES

Abdalla, A. M., Bruns, C. M., Tainer, J. A., Mannervik, B., and Stenberg, G. (2002). Design of a monomeric human glutathione transferase GSTP1, a structurally stable but catalytically inactive protein. *Protein Eng.* 15, 827–834. doi: 10.1093/protein/15.10.827

Ahuja, S., Jahr, N., Im, S. C., Vivekanandan, S., Popovych, N., Le Clair, S. V., et al. (2013). A model of the membrane-bound cytochrome b5-cytochrome P450 complex from NMR and mutagenesis data. *J. Biol. Chem.* 288, 22080–22095. doi: 10.1074/jbc.M112.448225

Archakov, A. I., and Ivanov, Y. D. (2011). Application of AFM and optical biosensor for investigation of complexes formed in P450-containing monooxygenase systems. *Biochim. Biophys. Acta* 1814, 102–110. doi: 10.1016/j.bbapap.2010.08.013

Argiriadi, M. A., Morisseau, C., Hammock, B. D., and Christianson, D. W. (1999). Detoxification of environmental mutagens and carcinogens: structure, mechanism, and evolution of liver epoxide hydrolase. *Proc. Natl. Acad. Sci. U.S.A.* 96, 10637–10642. doi: 10.1073/pnas.96.19.10637

Audet-Delage, Y., Rouleau, M., Rouleau, M., Roberge, J., Miard, S., Picard, F., et al. (2017). Cross-Talk between alternatively spliced UGT1A Isoforms and Colon Cancer Cell Metabolism. *Mol. Pharmacol.* 91, 167–177. doi: 10.1124/mol.116.106161

Balogh, L. M., Le Trong, I., Kripps, K. A., Tars, K., Stenkamp, R. E., Mannervik, B., et al. (2009). Structural analysis of a glutathione transferase A1-1 mutant tailored for high catalytic efficiency with toxic alkenals. *Biochemistry* 48, 7698–7704. doi: 10.1021/bi900895b

Basudhar, D., Madrona, Y., Kandel, S., Lampe, J. N., Nishida, C. R., and de Montellano, P. R. (2015). Analysis of cytochrome P450 CYP119 ligand-dependent conformational dynamics by two-dimensional NMR and X-ray crystallography. *J. Biol. Chem.* 290, 10000–10017. doi: 10.1074/jbc.M114.627935

Beckmann, J. D., Henry, T., Ulphani, J., and Lee, P. (1998). Cooperative ligand binding by bovine phenol sulfotransferase. *Chem. Biol. Interact.* 109, 93–105. doi: 10.1016/S0009-2797(97)00123-3

Binda, C., Angelini, R., Federico, R., Ascenzi, P., and Mattevi, A. (2001). Structural bases for inhibitor binding and catalysis in polyamine oxidase. *Biochemistry* 40, 2766–2776. doi: 10.1021/bi002751j

Binda, C., Mattevi, A., and Edmondson, D. E. (2011). Structural properties of human monoamine oxidases A and B. *Int. Rev. Neurobiol.* 100, 1–11. doi: 10.1016/B978-0-12-386467-3.00001-7

Bostick, C. D., Hickey, K. M., Wollenberg, L. A., Flora, D. R., Tracy, T. S., and Gannett, P. M. (2016). Immobilized Cytochrome P450 for Monitoring of P450-P450 interactions and metabolism. *Drug Metab. Dispos.* 44, 741–749. doi: 10.1124/dmd.115.067637

Centeno, F., and Gutierrez-Merino, C. (1992). Location of functional centers in the microsomal cytochrome P450 system. *Biochemistry* 31, 8473–8481. doi: 10.1021/bi00151a013

Chenge, J. T., Duyet, L. V., Swami, S., McLean, K. J., Kavanagh, M. E., Coyne, A. G., et al. (2017). Structural characterization and Ligand/Inhibitor identification provide functional insights into the *Mycobacterium tuberculosis* Cytochrome P450 CYP126A1. *J. Biol. Chem.* 292, 1310–1329. doi: 10.1074/jbc.M116.748822

Cook, I., Wang, T., Girvin, M., and Leyh, T. S. (2016). The structure of the catechin-binding site of human sulfotransferase 1A1. *Proc. Natl. Acad. Sci. U.S.A.* 113, 14312–14317. doi: 10.1073/pnas.1613913113

Cooper, M. A. (2002). Optical biosensors in drug discovery. *Nat. Rev. Drug Discov.* 1, 515–528. doi: 10.1038/nrd838

Cupp-Vickery, J., Anderson, R., and Hatziris, Z. (2000). Crystal structures of ligand complexes of $P450_{eryF}$ exhibiting homotropic cooperativity. *Proc. Natl. Acad. Sci. U.S.A.* 97, 3050–3055. doi: 10.1073/pnas.97.7.3050

Davydov, D. R. (2011). Microsomal monooxygenase as a multienzyme system: the role of P450-P450 interactions. *Expert Opin. Drug Metab. Toxicol.* 7, 543–558. doi: 10.1517/17425255.2011.562194

Davydov, D. R. (2016). Molecular organization of the microsomal oxidative system: a new connotation for an old term. *Biochem. Suppl. Ser. B* 10, 10–21. doi: 10.1134/S1990750816010042

Davydov, D. R., Davydova, N. Y., Sineva, E. V., and Halpert, J. R. (2015). Interactions among cytochromes P450 in microsomal membranes: oligomerization of cytochromes P450 3A4, 3A5, and 2E1 and its functional consequences. *J. Biol. Chem.* 290, 3850–3864. doi: 10.1074/jbc.M114.615443

Davydov, D. R., Davydova, N. Y., Sineva, E. V., Kufareva, I., and Halpert, J. R. (2013a). Pivotal role of P450-P450 interactions in CYP3A4 allostery: the case of alpha-naphthoflavone. *Biochem. J.* 453, 219–230. doi: 10.1042/BJ20130398

Davydov, D. R., Kariakin, A. A., Petushkova, N. A., and Peterson, J. A. (2000). Association of cytochromes P450 with their reductases: opposite sign of the

electrostatic interactions in P450BM-3 as compared with the microsomal 2B4 system. *Biochemistry* 39, 6489–6497. doi: 10.1021/bi992936u

Davydov, D. R., Knyushko, T. V., Kanaeva, I. P., Koen, Y. M., Samenkova, N. F., Archakov, A. I., et al. (1996). Interactions of cytochrome P450 2B4 with NADPH-cytochrome P450 reductase studied by fluorescent probe. *Biochimie* 78, 734–743. doi: 10.1016/S0300-9084(97)82531-X

Davydov, D. R., Petushkova, N. A., Bobrovnikova, E. V., Knyushko, T. V., and Dansette, P. (2001). Association of cytochromes P450 1A2 and 2B4: are the interactions between different P450 species involved in the control of the monooxygenase activity and coupling? *Adv. Exp. Med. Biol.* 500, 335–338. doi: 10.1007/978-1-4615-0667-6_53

Davydov, D. R., Ponomarev, G. V., Bobrovnikova-Marjon, E., Haines, D. C., and Peterson, J. A. (2013b). Aluminum-substituted heme domain of P450BM-3 (BMP): introducing a heme-derived fluorescent probe for studies of substrate binding and protein-protein interactions in cytochromes P450. *Biotechnol. Appl. Biochem.* 60, 41–51. doi: 10.1002/bab.1085

Davydov, D. R., Sineva, E. V., Sistla, S., Davydova, N. Y., Frank, D. J., Sligar, S. G., et al. (2010). Electron transfer in the complex of membrane-bound human cytochrome P450 3A4 with the flavin domain of P450BM-3: the effect of oligomerization of the heme protein and intermittent modulation of the spin equilibrium. *Biochim. Biophys. Acta* 1797, 378–390. doi: 10.1016/j.bbabio.2009.12.008

Deng, B., Parthasarathy, S., Wang, W., Gibney, B. R., Battaile, K. P., Lovell, S., et al. (2010). Study of the individual cytochrome b5 and cytochrome b5 reductase domains of Ncb5or reveals a unique heme pocket and a possible role of the CS domain. *J. Biol. Chem.* 285, 30181–30191. doi: 10.1074/jbc.M110.120329

Dietze, E. C., Wang, R. W., Lu, A. Y., and Atkins, W. M. (1996). Ligand effects on the fluorescence properties of tyrosine-9 in alpha 1-1 glutathione S-transferase. *Biochemistry* 35, 6745–6753. doi: 10.1021/bi9530346

Estrada, D. F., Laurence, J. S., and Scott, E. E. (2013). Substrate-modulated cytochrome P450 17A1 and cytochrome b5 interactions revealed by NMR. *J. Biol. Chem.* 288, 17008–17018. doi: 10.1074/jbc.M113.468926

Estrada, D. F., Laurence, J. S., and Scott, E. E. (2016). Cytochrome P450 17A1 Interactions with the FMN Domain of Its Reductase as Characterized by NMR. *J. Biol. Chem.* 291, 3990–4003. doi: 10.1074/jbc.M115.677294

Estrada, D. F., Skinner, A. L., Laurence, J. S., and Scott, E. E. (2014). Human cytochrome P450 17A1 conformational selection: modulation by ligand and cytochrome b5. *J. Biol. Chem.* 289, 14310–14320. doi: 10.1074/jbc.M114.560144

Evers, R., Dallas, S., Dickmann, L. J., Fahmi, O. A., Kenny, J. R., Kraynov, E., et al. (2013). Critical review of preclinical approaches to investigate cytochrome p450-mediated therapeutic protein drug-drug interactions and recommendations for best practices: a white paper. *Drug Metab. Dispos.* 41, 1598–1609. doi: 10.1124/dmd.113.052225

Fujiwara, R., Yokoi, T., and Nakajima, M. (2016). Structure and Protein-Protein Interactions of Human UDP-Glucuronosyltransferases. *Front. Pharmacol.* 7:388. doi: 10.3389/fphar.2016.00388

Gao, Q., Doneanu, C. E., Shaffer, S. A., Adman, E. T., Goodlett, D. R., and Nelson, S. D. (2006b). Identification of the interactions between cytochrome P450 2E1 and cytochrome b5 by mass spectrometry and site-directed mutagenesis. *J. Biol. Chem.* 281, 20404–20417. doi: 10.1074/jbc.M601785200

Gao, Q., Xue, S., Doneanu, C. E., Shaffer, S. A., Goodlett, D. R., and Nelson, S. D. (2006a). Pro-CrossLink. Software tool for protein cross-linking and mass spectrometry. *Anal. Chem.* 78, 2145–2149. doi: 10.1021/ac051339c

Gill, S. S. (1983). Purification of mouse liver cytosolic epoxide hydrolase. *Biochem. Biophys. Res. Commun.* 112, 763–769. doi: 10.1016/0006-291X(83)91527-9

Gluck, J. M., Wittlich, M., Feuerstein, S., Hoffmann, S., Willbold, D., and Koenig, B. W. (2009). Integral membrane proteins in nanodiscs can be studied by solution NMR spectroscopy. *J. Am. Chem. Soc.* 131, 12060–12061. doi: 10.1021/ja904897p

Gorovits, B. M., and Horowitz, P. M. (1995). The molecular chaperonin cpn60 displays local flexibility that is reduced after binding with an unfolded protein. *J. Biol. Chem.* 270, 13057–13062. doi: 10.1074/jbc.270.22.13057

Grahn, E., Novotny, M., Jakobsson, E., Gustafsson, A., Grehn, L., Olin, B., et al. (2006). New crystal structures of human glutathione transferase A1-1 shed light on glutathione binding and the conformation of the C-terminal helix. *Acta Cryst.* 62(Pt. 2), 197–207. doi: 10.1107/S0907444905039296

Greinert, R., Finch, S. A., and Stier, A. (1982). Cytochrome P-450 rotamers control mixed-function oxygenation in reconstituted membranes. Rotational diffusion studied by delayed fluorescence depolarization. *Xenobiotica* 12, 717–726. doi: 10.3109/00498258209038946

Greinert, R., Staerk, H., Stier, A., and Weller, A. (1979). E-type delayed fluorescence depolarization, technique to probe rotational motion in the microsecond range. *J. Biochem. Biophys. Methods* 1, 77–83. doi: 10.1016/0165-022X(79)90014-9

Guengerich, F. P. (2006). Cytochrome P450s and other enzymes in drug metabolism and toxicity. *AAPS J.* 8, E101–E111. doi: 10.1208/aapsj080112

Gut, J., Kawato, S., Cherry, R. J., Winterhalter, K. H., and Richter, C. (1985). Lipid peroxidation decreases the rotational mobility of cytochrome P-450 in rat liver microsomes. *Biochim. Biophys. Acta* 817, 217–228. doi: 10.1016/0005-2736(85)90023-9

Hall, D. A., Vander Kooi, C. W., Stasik, C. N., Stevens, S. Y., Zuiderweg, E. R., and Matthews, R. G. (2001). Mapping the interactions between flavodoxin and its physiological partners flavodoxin reductase and cobalamin-dependent methionine synthase. *Proc. Natl. Acad. Sci. U.S.A.* 98, 9521–9526. doi: 10.1073/pnas.171168898

Hamdane, D., Xia, C., Im, S. C., Zhang, H., Kim, J. J., and Waskell, L. (2009). Structure and function of an NADPH-cytochrome P450 oxidoreductase in an open conformation capable of reducing cytochrome P450. *J. Biol. Chem.* 284, 11374–11384. doi: 10.1074/jbc.M807868200

He, Y. A., Gajiwala, K. S., Wu, M., Parge, H., Burke, B., Lee, C. A., et al. (Eds.) (2006). The crystal structure of human CYP3A4 in complex with testosterone. [Abstracts]. in *16th Int Smpos Microsomal Drug Oxidations (MDO 2006). Budapest, Hungary: Diamond Congress, Ltd. (Budapest).*

Henderson, C. J., McLaughlin, L. A., and Wolf, C. R. (2013). Evidence that cytochrome b5 and cytochrome b5 reductase can act as sole electron donors to the hepatic cytochrome P450 system. *Mol. Pharmacol.* 83, 1209–1217. doi: 10.1124/mol.112.084616

Henzler-Wildman, K., and Kern, D. (2007). Dynamic personalities of proteins. *Nature* 450, 964–972. doi: 10.1038/nature06522

Hiruma, Y., Hass, M. A., Kikui, Y., Liu, W. M., Olmez, B., Skinner, S. P., et al. (2013). The structure of the cytochrome p450cam-putidaredoxin complex determined by paramagnetic NMR spectroscopy and crystallography. *J. Mol. Biol.* 425, 4353–4365. doi: 10.1016/j.jmb.2013.07.006

Hodek, P., and Smrcek, S. (1999). Evaluation of 3-azidiamantane as photoaffinity probe of cytochrome P450. *Gen. Physiol. Biophys.* 18, 181–198.

Ivanov, Y. D., Kanaeva, I. P., Eldarov, M. A., Sklyabin, K. G., Lehnerer, M., Schulze, J., et al. (1997). An optical biosensor study of the interaction parameters and role of hydrophobic tails of cytochrome P450 2B4, b5 and NADPH-flavoprotein in complex formation. *Biochem. Mol. Biol. Int.* 42, 731–737. doi: 10.1080/15216549700203161

Ivanov, Y. D., Kanaeva, I. P., Karuzina, I. I., Usanov, S. A., Hui Bon Hoa, G., Sligar, S. G., et al. (2001). Revelation of ternary complexes between redox partners in cytochrome P450-containing monooxygenase systems by the optical biosensor method. *J. Inorg. Biochem.* 87, 175–184. doi: 10.1016/S0162-0134(01)00332-4

Ivanov, Y. D., Kanaeva, I. P., Kuznetsov, V. Y., Lehnerer, M., Schulze, J., Hlavica, P., et al. (1999). The optical biosensor studies on the role of hydrophobic tails of NADPH-cytochrome P450 reductase and cytochromes P450 2B4 and b5 upon productive complex formation within a monomeric reconstituted system. *Arch. Biochem. Biophys.* 362, 87–93. doi: 10.1006/abbi.1998.0981

Kakuta, Y., Pedersen, L. G., Carter, C. W., Negishi, M., and Pedersen, L. C. (1997). Crystal structure of estrogen sulphotransferase. *Nat. Struct. Biol.* 4, 904–908. doi: 10.1038/nsb1197-904

Kandel, S. E., and Lampe, J. N. (2014). Role of protein-protein interactions in cytochrome P450-mediated drug metabolism and toxicity. *Chem. Res. Toxicol.* 27, 1474–1486. doi: 10.1021/tx500203s

Kijac, A. Z., Li, Y., Sligar, S. G., and Rienstra, C. M. (2007). Magic-angle spinning solid-state NMR spectroscopy of nanodisc-embedded human CYP3A4. *Biochemistry* 46, 13696–13703. doi: 10.1021/bi701411g

Kuznetsov, V. Y., Ivanov, Y. D., and Archakov, A. I. (2004). Atomic force microscopy revelation of molecular complexes in the multiprotein cytochrome P450 2B4-containing system. *Proteomics* 4, 2390–2396. doi: 10.1002/pmic.200300751

Lakowicz, J. R. (1999). *Principles of Fluorescence Spectroscopy. 2nd. ed.* New York, NY: Kluwer Academic/Plenum Publishers.

Lampe, J. N., Brandman, R., Sivaramakrishnan, S., and de Montellano, P. R. (2010). Two-dimensional NMR and all-atom molecular dynamics of cytochrome P450

CYP119 reveal hidden conformational substates. *J. Biol. Chem.* 285, 9594–9603. doi: 10.1074/jbc.M109.087593

Lampe, J. N., Floor, S. N., Gross, J. D., Nishida, C. R., Jiang, Y., Trnka, M. J., et al. (2008). Ligand-induced conformational heterogeneity of cytochrome P450 CYP119 identified by 2D NMR spectroscopy with the unnatural amino acid (13)C-p-methoxyphenylalanine. *J. Am. Chem. Soc.* 130, 16168–16169. doi: 10.1021/ja8071463

Lewis, B. C., Mackenzie, P. I., and Miners, J. O. (2011). Homodimerization of UDP-glucuronosyltransferase 2B7 (UGT2B7) and identification of a putative dimerization domain by protein homology modeling. *Biochem. Pharmacol.* 82, 2016–2023. doi: 10.1016/j.bcp.2011.09.007

Li, B., Yau, P., and Kemper, B. (2011). Identification of cytochrome P450 2C2 protein complexes in mouse liver. *Proteomics* 11, 3359–3368. doi: 10.1002/pmic.201100001

Lian, L. Y. (1998). NMR structural studies of glutathione S-transferase. *Cell. Mol. Life Sci.* 54, 359–362. doi: 10.1007/s000180050164

Lim, K., Jameson, D. M., Gentry, C. A., and Herron, J. N. (1995). Molecular dynamics of the anti-fluorescein 4-4-20 antigen-binding fragment. 2. Time-resolved fluorescence spectroscopy. *Biochemistry* 34, 6975–6984. doi: 10.1021/bi00021a009

Losel, R. M., Besong, D., Peluso, J. J., and Wehling, M. (2008). Progesterone receptor membrane component 1–many tasks for a versatile protein. *Steroids* 73, 929–934. doi: 10.1016/j.steroids.2007.12.017

Lu, W. D., and Atkins, W. M. (2004). A novel antioxidant role for ligandin behavior of glutathione S-transferases: attenuation of the photodynamic effects of hypericin. *Biochemistry* 43, 12761–12769. doi: 10.1021/bi049217m

Mahajan, S. S., Hou, L., Doneanu, C., Paranji, R., Maeda, D., Zebala, J., et al. (2006). Optimization of bivalent glutathione S-transferase inhibitors by combinatorial linker design. *J. Am. Chem. Soc.* 128, 8615–8625. doi: 10.1021/ja061766n

Martin, L. L., Holien, J. K., Mizrachi, D., Corbin, C. J., Conley, A. J., Parker, M. W., et al. (2015). Evolutionary comparisons predict that dimerization of human cytochrome P450 aromatase increases its enzymatic activity and efficiency. *J. Steroid Biochem. Mol. Biol.* 154, 294–301. doi: 10.1016/j.jsbmb.2015.09.006

Matsumoto, N., Suzuki, E., Ishikawa, M., Shirafuji, T., and Hasumi, K. (2014). Soluble Epoxide Hydrolase as an Anti-inflammatory Target of the Thrombolytic Stroke Drug SMTP-7. *J. Biol. Chem.* 289, 35826–35838. doi: 10.1074/jbc.M114.588087

McCallum, S. A., Hitchens, T. K., and Rule, G. S. (1999). Solution structure of the carboxyl terminus of a human class Mu glutathione S-transferase: NMR assignment strategies in large proteins. *J. Mol. Biol.* 285, 2119–2132. doi: 10.1006/jmbi.1998.2428

Meech, R., and Mackenzie, P. I. (1997). UDP-glucuronosyltransferase, the role of the amino terminus in dimerization. *J. Biol. Chem.* 272, 26913–26917. doi: 10.1074/jbc.272.43.26913

Miley, M. J., Zielinska, A. K., Keenan, J. E., Bratton, S. M., Radominska-Pandya, A., and Redinbo, M. R. (2007). Crystal structure of the cofactor-binding domain of the human phase II drug-metabolism enzyme UDP-glucuronosyltransferase 2B7. *J. Mol. Biol.* 369, 498–511. doi: 10.1016/j.jmb.2007.03.066

Murakami, Y., Tripathi, L. P., Prathipati, P., and Mizuguchi, K. (2017). Network analysis and *in silico* prediction of protein-protein interactions with applications in drug discovery. *Curr. Opin. Struct. Biol.* 44, 134–142. doi: 10.1016/j.sbi.2017.02.005

Nagano, S., and Poulos, T. L. (2005). Crystallographic study on the dioxygen complex of wild-type and mutant cytochrome P450cam:Implications for the dioxygen activation mechanism. *J. Biol. Chem.* 22102–22107. doi: 10.1074/jbc.M501732200

Nagano, S., Cupp-Vickery, J. R., and Poulos, T. L. (2005). Crystal structures of the ferrous dioxygen complex of wild-type cytochrome P450eryF and its mutants, A245S and A245T: investigation of the proton transfer system in P450eryF. *J. Biol. Chem.* 280, 22102–22107. doi: 10.1074/jbc.M501732200

Nelson, J. W., Subrahmanyan, R. M., Summers, S. A., Xiao, X. S., and Alkayed, N. J. (2013). Soluble epoxide hydrolase dimerization is required for hydrolase activity. *J. Biol. Chem.* 288, 7697–7703. doi: 10.1074/jbc.M112.429258

Nisimoto, Y., Kinosita, K. Jr., Ikegami, A., Kawai, N., Ichihara, I., and Shibata, Y. (1983). Possible association of NADPH-cytochrome P-450 reductase and cytochrome P-450 in reconstituted phospholipid vesicles. *Biochemistry* 22, 3586–3594. doi: 10.1021/bi00284a008

Operana, T. N., and Tukey, R. H. (2007). Oligomerization of the UDP-glucuronosyltransferase 1A proteins: homo- and heterodimerization analysis by fluorescence resonance energy transfer and co-immunoprecipitation. *J. Biol. Chem.* 282, 4821–4829. doi: 10.1074/jbc.M609417200

Ortiz de Montellano, P. R. (2005). *Cytochrome P450: Structure, Mechanism, and Biochemistry. 3rd. Edn*. New York, NY: Kluwer Academic/Plenum Publishers.

Pearson, J. T., Hill, J. J., Swank, J., Isoherranen, N., Kunze, K. L., and Atkins, W. M. (2006). Surface plasmon resonance analysis of antifungal azoles binding to CYP3A4 with kinetic resolution of multiple binding orientations. *Biochemistry* 45, 6341–6353. doi: 10.1021/bi0600042

Peng, H. M., Liu, J., Forsberg, S. E., Tran, H. T., Anderson, S. M., and Auchus, R. J. (2014). Catalytically relevant electrostatic interactions of cytochrome P450c17 (CYP17A1) and cytochrome b5. *J. Biol. Chem.* 289, 33838–33849. doi: 10.1074/jbc.M114.608919

Petrotchenko, E. V., Pedersen, L. C., Borchers, C. H., Tomer, K. B., and Negishi, M. (2001). The dimerization motif of cytosolic sulfotransferases. *FEBS Lett.* 490, 39–43. doi: 10.1016/S0014-5793(01)02129-9

Podust, L. M., Poulos, T. L., and Waterman, M. R. (2001). Crystal structure of cytochrome P450 14alpha -sterol demethylase (CYP51) from *Mycobacterium tuberculosis* in complex with azole inhibitors. *Proc. Natl. Acad. Sci. U.S.A.* 98, 3068–3073. doi: 10.1073/pnas.061562898

Polekhina, G., Board, P. G., Blackburn, A. C., and Parker, M. W. (2001). Crystal structure of maleylacetoacetate isomerase/glutathione transferase zeta reveals the molecular basis for its remarkable catalytic promiscuity. *Biochemistry* 40, 1567–1576. doi: 10.1021/bi002249z

Praporski, S., Ng, S. M., Nguyen, A. D., Corbin, C. J., Mechler, A., Zheng, J., et al. (2009). Organization of cytochrome P450 enzymes involved in sex steroid synthesis: PROTEIN-PROTEIN INTERACTIONS IN LIPID MEMBRANES. *J. Biol. Chem.* 284, 33224–33232. doi: 10.1074/jbc.M109.006064

Raman, S., Lange, O. F., Rossi, P., Tyka, M., Wang, X., Aramini, J., et al. (2010). NMR structure determination for larger proteins using backbone-only data. *Science* 327, 1014–1018. doi: 10.1126/science.1183649

Reed, J. R., and Backes, W. L. (2016). The functional effects of physical interactions involving cytochromes P450: putative mechanisms of action and the extent of these effects in biological membranes. *Drug Metab. Rev.* 48, 453–469. doi: 10.1080/03602532.2016.1221961

Reed, J. R., and Backes, W. L. (2017). Physical Studies of P450-P450 Interactions: Predicting Quaternary Structures of P450 complexes in membranes from their X-ray crystal structures. *Front. Pharmacol.* 8:28. doi: 10.3389/fphar.2017.00028

Reed, J. R., Eyer, M., and Backes, W. L. (2010). Functional interactions between cytochromes P450 1A2 and 2B4 require both enzymes to reside in the same phospholipid vesicle: evidence for physical complex formation. *J. Biol. Chem.* 285, 8942–8952. doi: 10.1074/jbc.M109.076885

Rohe, H. J., Ahmed, I. S., Twist, K. E., and Craven, R. J. (2009). PGRMC1 (progesterone receptor membrane component 1): a targetable protein with multiple functions in steroid signaling, P450 activation and drug binding. *Pharmacol. Ther.* 121, 14–19. doi: 10.1016/j.pharmthera.2008.09.006

Ryu, C. S., Klein, K., and Zanger, U. M. (2017). Membrane associated progesterone receptors: promiscuous proteins with Pleiotropic Functions - Focus on Interactions with Cytochromes P450. *Front. Pharmacol.* 8:159. doi: 10.3389/fphar.2017.00159

Schoch, G. A., Yano, J. K., Sansen, S., Dansette, P. M., Stout, C. D., and Johnson, E. F. (2008). Determinants of cytochrome P450 2C8 substrate binding: structures of complexes with montelukast, troglitazone, felodipine, and 9-cis-retinoic acid. *J. Biol. Chem.* 283, 17227–17237. doi: 10.1074/jbc.M802180200

Schwarz, D., Kruger, V., Chernogolov, A. A., Usanov, S. A., and Stier, A. (1993). Rotation of cytochrome P450SCC (CYP11A1) in proteoliposomes studied by delayed fluorescence depolarization. *Biochem. Biophys. Res. Commun.* 195, 889–896. doi: 10.1006/bbrc.1993.2128

Schwarze, W., Bernhardt, R., Janig, G. R., and Ruckpaul, K. (1983). Fluorescent energy transfer measurements on fluorescein isothiocyanate modified cytochrome P-450 LM2. *Biochem. Biophys. Res. Commun.* 113, 353–360. doi: 10.1016/0006-291X(83)90473-4

Scott, E. E., White, M. A., He, Y. A., Johnson, E. F., Stout, C. D., and Halpert, J. R. (2004). Structure of mammalian cytochrome P450 2B4 complexed with 4-(4-chlorophenyl)imidazole at 1.9 {angstrom} resolution: insight into the range of P450 conformations and coordination of redox partner binding. *J. Biol. Chem.* 279, 27294–27301. doi: 10.1074/jbc.M403349200

Sevrioukova, I. F., Li, H., Zhang, H., Peterson, J. A., and Poulos, T. L. (1999). Structure of a cytochrome P450-redox partner electron-transfer complex. *Proc. Natl. Acad. Sci. U.S.A.* 96, 1863–1868. doi: 10.1073/pnas.96.5.1863

Sevrioukova, I., Truan, G., and Peterson, J. A. (1997). Reconstitution of the fatty acid hydroxylase activity of cytochrome P450BM-3 utilizing its functional domains. *Arch. Biochem. Biophys.* 340, 231–238. doi: 10.1006/abbi.1997.9895

Shimada, T., Mernaugh, R. L., and Guengerich, F. P. (2005). Interactions of mammalian cytochrome P450, NADPH-cytochrome P450 reductase, and cytochrome b(5) enzymes. *Arch. Biochem. Biophys.* 435, 207–216. doi: 10.1016/j.abb.2004.12.008

Simonov, A. N., Holien, J. K., Yeung, J. C., Nguyen, A. D., Corbin, C. J., Zheng, J., et al. (2015). Mechanistic Scrutiny Identifies a Kinetic Role for Cytochrome b5 Regulation of Human Cytochrome P450c17 (CYP17A1, P450 17A1). *PLoS ONE* 10:e0141252. doi: 10.1371/journal.pone.0141252

Spera, R., Festa, F., Bragazzi, N. L., Pechkova, E., LaBaer, J., and Nicolini, C. (2013). Conductometric monitoring of protein-protein interactions. *J. Proteome Res.* 12, 5535–5547. doi: 10.1021/pr400445v

Stayton, P. S., Fisher, M. T., and Sligar, S. G. (1988). Determination of cytochrome b5 association reactions. characterization of metmyoglobin and cytochrome P-450cam binding to genetically engineered cytochromeb5. *J. Biol. Chem.* 263, 13544–13548.

Sugishima, M., Sato, H., Higashimoto, Y., Harada, J., Wada, K., Fukuyama, K., et al. (2014). Structural basis for the electron transfer from an open form of NADPH-cytochrome P450 oxidoreductase to heme oxygenase. *Proc. Natl. Acad. Sci. U.S.A.* 111, 2524–2529. doi: 10.1073/pnas.1322034111

Sulc, M., Hudecek, J., Stiborova, M., and Hodek, P. (2008). Structural analysis of binding of a diamantoid substrate to cytochrome P450 2B4: possible role of Arg 133 in modulation of function and activity of this enzyme. *Neuro Endocrinol. Lett.* 29, 722–727.

Suzuki, M., Hirata, M., Takagi, M., Watanabe, T., Iguchi, T., Koiwai, K., et al. (2014). Truncated UDP-glucuronosyltransferase (UGT) from a Crigler-Najjar syndrome type II patient colocalizes with intact UGT in the endoplasmic reticulum. *J. Hum. Genet.* 59, 158–162. doi: 10.1038/jhg.2013.138

Szczesna-Skorupa, E., Mallah, B., and Kemper, B. (2003). Fluorescence resonance energy transfer analysis of cytochromes P450 2C2 and 2E1 molecular interactions in living cells. *J. Biol. Chem.* 278, 31269–31276. doi: 10.1074/jbc.M301489200

Tripathi, S., Li, H., and Poulos, T. L. (2013). Structural basis for effector control and redox partner recognition in cytochrome P450. *Science* 340, 1227–1230. doi: 10.1126/science.1235797

Vallurupalli, P., Hansen, D. F., and Kay, L. E. (2008). Structures of invisible, excited protein states by relaxation dispersion NMR spectroscopy. *Proc. Natl. Acad. Sci. U.S.A.* 105, 11766–11771. doi: 10.1073/pnas.0804221105

Vincent, B., Morellet, N., Fatemi, F., Aigrain, L., Truan, G., Guittet, E., et al. (2012). The closed and compact domain organization of the 70-kDa human cytochrome P450 reductase in its oxidized state as revealed by NMR. *J. Mol. Biol.* 420, 296–309. doi: 10.1016/j.jmb.2012.03.022

Wang, J., and Edmondson, D. E. (2007). Do monomeric vs dimeric forms of MAO-A make a difference? A direct comparison of the catalytic properties of rat and human MAO-A's. *J. Neural. Transm.* 114, 721–724. doi: 10.1007/s00702-007-0678-8

Wang, R. W., Bird, A. W., Newton, D. J., Lu, A. Y., and Atkins, W. M. (1993). Fluorescence characterization of Trp 21 in rat glutathione S-transferase 1-1: microconformational changes induced by S-hexyl glutathione. *Protein Sci.* 2, 2085–2094. doi: 10.1002/pro.5560021209

Wang, T., Arifoglu, P., Ronai, Z., and Tew, K. D. (2001). Glutathione S-transferase P1-1 (GSTP1-1) inhibits c-Jun N-terminal kinase (JNK1) signaling through interaction with the C terminus. *J. Biol. Chem.* 276, 20999–21003. doi: 10.1074/jbc.M101355200

Weber, G., and Farris, F. J. (1979). Synthesis and spectral properties of a hydrophobic fluorescent probe: 6-propionyl-2-(dimethylamino)naphthalene. *Biochemistry* 18, 3075–3078. doi: 10.1021/bi00581a025

Wen, B., Doneanu, C. E., Lampe, J. N., Roberts, A. G., Atkins, W. M., and Nelson, S. D. (2005). Probing the CYP3A4 active site by cysteine scanning mutagenesis and photoaffinity labeling. *Arch. Biochem. Biophys.* 444, 100–111. doi: 10.1016/j.abb.2005.09.010

Wen, B., Lampe, J. N., Roberts, A. G., Atkins, W. M., David Rodrigues, A., and Nelson, S. D. (2006). Cysteine 98 in CYP3A4 contributes to conformational integrity required for P450 interaction with CYP reductase. *Arch. Biochem. Biophys.* 454, 42–54. doi: 10.1016/j.abb.2006.08.003

Wienkers, L. C., and Heath, T. G. (2005). Predicting *in vivo* drug interactions from *in vitro* drug discovery data. *Nat. Rev. Drug Discov.* 4, 825–833. doi: 10.1038/nrd1851

Wilderman, P. R., Gay, S. C., Jang, H. H., Zhang, Q., Stout, C. D., and Halpert, J. R. (2012). Investigation by site-directed mutagenesis of the role of cytochrome P450 2B4 non-active-site residues in protein-ligand interactions based on crystal structures of the ligand-bound enzyme. *FEBS J.* 279, 1607–1620. doi: 10.1111/j.1742-4658.2011.08411.x

Williams, P. A., Cosme, J., Ward, A., Angove, H. C., Matak Vinkovic, D., and Jhoti, H. (2003). Crystal structure of human cytochrome P450 2C9 with bound warfarin. *Nature.* 424, 464–468 doi: 10.1038/nature01862

Wu, E. S., and Yang, C. S. (1984). Lateral diffusion of cytochrome P-450 in phospholipid bilayers. *Biochemistry* 23, 28–33. doi: 10.1021/bi00296a005

Yablokov, E., Florinskaya, A., Medvedev, A., Sergeev, G., Strushkevich, N., Luschik, A., et al. (2017). Thermodynamics of interactions between mammalian cytochromes P450 and b5. *Arch. Biochem. Biophys.* 619, 10–15. doi: 10.1016/j.abb.2017.02.006

Yano, J. K., Wester, M. R., Schoch, G. A., Griffin, K. J., Stout, C. D., and Johnson, E. F. (2004). The structure of human microsomal cytochrome P450 3A4 determined by X-ray crystallography to 2.05 Å resolution. *J. Biol. Chem.* 279, 38091–38094. doi: 10.1074/jbc.C400293200

Yantsevich, A. V., Gilep, A. A., and Usanov, S. A. (2009). Conformational stability of cytochrome b5, enhanced green fluorescent protein, and their fusion protein Hmwb5-EGFP. *Biochem. Mosc.* 74, 518–527. doi: 10.1134/S000629790905006X

Yoshinari, K., Petrotchenko, E. V., Pedersen, L. C., and Negishi, M. (2001). Crystal structure-based studies of cytosolic sulfotransferase. *J. Biochem. Mol. Toxicol.* 15, 67–75. doi: 10.1002/jbt.1

Yuan, L. M., Gao, Z. Z., Sun, H. Y., Qian, S. N., Xiao, Y. S., Sun, L. L., et al. (2016). Inter-isoform Hetero-dimerization of Human UDP-Glucuronosyltransferases (UGTs) 1A1, 1A9, and 2B7 and Impacts on Glucuronidation Activity. *Sci. Rep.* 6:34450. doi: 10.1038/srep34450

Yuan, L., Qian, S., Xiao, Y., Sun, H., and Zeng, S. (2015). Homo- and hetero-dimerization of human UDP-glucuronosyltransferase 2B7 (UGT2B7) wild type and its allelic variants affect zidovudine glucuronidation activity. *Biochem. Pharmacol.* 95, 58–70. doi: 10.1016/j.bcp.2015.03.002

Zhang, M., Huang, R., Ackermann, R., Im, S. C., Waskell, L., Schwendeman, A., et al. (2016). Reconstitution of the Cytb5-CytP450 Complex in Nanodiscs for Structural Studies using NMR Spectroscopy. *Angew. Chem. Int. Ed Engl.* 55, 4497–4499. doi: 10.1002/anie.201600073

Conflict of Interest Statement: The author declares that the research was conducted in the absence of any commercial or financial relationships that could be construed as a potential conflict of interest.

frontiers in Pharmacology

REVIEW
published: 30 January 2017
doi: 10.3389/fphar.2017.00028

Physical Studies of P450–P450 Interactions: Predicting Quaternary Structures of P450 Complexes in Membranes from Their X-ray Crystal Structures

James R. Reed and Wayne L. Backes*

Department of Pharmacology and Experimental Therapeutics, Louisiana State University Health Sciences Center New Orleans, LA, USA

Cytochrome P450 enzymes, which catalyze oxygenation reactions of both exogenous and endogenous chemicals, are membrane bound proteins that require interaction with their redox partners in order to function. Those responsible for drug and foreign compound metabolism are localized primarily in the endoplasmic reticulum of liver, lung, intestine, and other tissues. More recently, the potential for P450 enzymes to exist as supramolecular complexes has been shown by the demonstration of both homomeric and heteromeric complexes. The P450 units in these complexes are heterogeneous with respect to their distribution and function, and the interaction of different P450s can influence P450-specific metabolism. The goal of this review is to examine the evidence supporting the existence of physical complexes among P450 enzymes. Additionally, the review examines the crystal lattices of different P450 enzymes derived from X-ray diffraction data to make assumptions regarding possible quaternary structures in membranes and in turn, to predict how the quaternary structures could influence metabolism and explain the functional effects of specific P450–P450 interactions.

Keywords: P450 cytochrome, protein–protein interaction (PPI), crystal structure, drug metabolism, microsomes, liver

OPEN ACCESS

Edited by:
Marcelo Rizzatti Luizon, Universidade Federal de Minas Gerais, Brazil

Reviewed by:
Ryoichi Fujiwara, Kitasato University, Japan
Eric F. Johnson, The Scripps Research Institute, USA

****Correspondence:***
James R. Reed
rreed@lsuhsc.edu

Specialty section:
This article was submitted to Pharmacogenetics and Pharmacogenomics, a section of the journal Frontiers in Pharmacology

Received: *01 December 2016*
Accepted: *16 January 2017*
Published: *30 January 2017*

Citation:
Reed JR and Backes WL (2017) Physical Studies of P450–P450 Interactions: Predicting Quaternary Structures of P450 Complexes in Membranes from Their X-ray Crystal Structures. Front. Pharmacol. 8:28. doi: 10.3389/fphar.2017.00028

INTRODUCTION

The mammalian cytochromes P450 (P450 or CYP) that are primarily housed in the endoplasmic reticulum are versatile catalysts that metabolize 75–90% of marketed drugs (Guengerich, 2006; Lynch and Price, 2007). These enzymes use a heme group, coordinated in one of the axial positions with a critical thiolate residue, to catalyze a diverse set of reactions through the mixed-function oxygenation of substrate carbons and heteroatoms (Guengerich, 2001). In addition to catalyzing a variety of reactions, the mammalian P450s also recognize a wide range of exogenous substrates due to a variety of closely related enzymes, representing three to four gene families, that have differing but overlapping substrate specificities (Nelson, 2006). Humans contain 57 P450 genes expressed in a tissue-specific fashion (Zanger and Schwab, 2013), with approximately 13 P450s being responsible for the majority of *in vivo* drug metabolism.

The P450 catalytic cycle relies on molecular oxygen and electrons supplied by the redox partners, cytochrome P450 reductase (CPR) and/or cytochrome b_5. In this process, two distinct electron-transfer steps occur (White and Coon, 1980), each one following a protein-protein interaction with one of the potential redox partners (Miwa et al., 1979). Thus, protein-protein interactions are essential for optimal catalytic activities of the P450s. In addition to the interactions with redox partners, P450s also interact with each other. There is now considerable evidence that these P450–P450 interactions influence P450-mediated catalytic activities in form- and substrate-specific manners. In fact, studies now demonstrate that the function of a given P450 also can be altered by its own homomeric interaction (Davydov et al., 2010; Reed et al., 2012). Our recent review on this topic (Reed and Backes, 2016), in addition to several other excellent reviews (Davydov, 2011; Reed and Backes, 2012; Kandel and Lampe, 2014), have summarized the studies that demonstrated the effects of specific P450–P450 interactions on enzyme function and have categorized the effects mechanistically.

Although significant progress has been made to demonstrate that the interaction of specific P450s can influence enzyme function in membrane systems, very little is known about the specific quaternary structures of the P450 complexes in membranes and more importantly, into the ways in which different types of physical interactions between P450s influence function. Although many biophysical techniques have been employed to detect multimeric P450 in membranes, these studies, for the most part, are not conclusive with regards to specific protein-protein interactions within the P450 complexes or to the exact sizes of the multimeric complexes.

In contrast to the limits associated with the biophysical techniques used to analyze membrane systems, X-ray crystal structures provide clear images of protein conformation and intermolecular arrangement. In addition, these structures clearly elucidate the ways in which protein conformations change upon the binding of different substrates. The crystallographic analysis of human P450 forms has exploded this century. Numerous structures of mammalian P450s with a variety of substrates have been reported [reviewed in (Johnson and Stout, 2013)]. Because of limitations related to determining both the specific sizes of P450 complexes and the relative orientations of the P450 units contained in these heteromeric complexes, detailed information about the ways in which P450s may interact *in vivo* might be inferred from X-ray crystal structures and crystallographic lattices of the individual, purified forms. This approach was used previously (Hazai et al., 2005); however, when the study was published, there were only a limited number of available structures of the mammalian P450s to analyze. Thus, in the current review, the X-ray structures and the corresponding lattice arrangements of human CYP1A2 (PDB: 2HI4); rabbit CYP2B4 (PDB: 1SUO and 1PO5); human CYP2C8 (PDB: 1PQ2); human CYP2C9 (PDB: 1OG5); human CYP2C19 (PDB: 4GQS); human CYP2D6 (PDB: 2F9Q);; human CYP3A4 (PDB: 2V0M, 2J0D, 1TQN, and 1W0F) have been interpreted with respect to the reported effects of specific P450-P450 interactions on enzymatic function.

Unlike our previous reviews that emphasized the functional effects of P450–P450 interactions, this review will focus on the physical studies that have been used to elucidate the nature of P450 multimers and summarize the current state of knowledge derived from these studies regarding the physical characteristics of these oligomers. The crystal structures and crystallographic arrays of different P450s will then be analyzed for their possible relationships to protein–protein interactions in membranes and to the possible ways that these interactions may explain some of the functional effects associated with these interactions. Initially, we will discuss instances of homomeric P450–P450 interactions in membrane systems that appear to correspond very nicely with available crystal structures of these P450s. Various types of homomeric interactions identified in the crystal structures will then be used to propose explanations for the functional effects that are associated with specific heteromeric P450–P450 interactions. The possible role of protein conformational changes in the functional effects of P450–P450 interactions will also be addressed. Hopefully, the comparison of crystal structures will provide a framework for future studies to determine whether these functional effects can indeed be attributable to the 450–P450 interactions deduced from the crystallographic analyses.

PHYSICAL STUDIES OF MEMBRANE SYSTEMS CONTAINING P450s

Determination of P450–P450 Binding Affinities

Purified P450s have a remarkable tendency to aggregate in aqueous solutions (Guengerich and Holladay, 1979; French et al., 1980; Dean and Gray, 1982; Myasoedova and Berndt, 1990; Myasoedova and Tsuprun, 1993). The arrangement of purified, detergent-free homomeric CYP1A2 (as well as CYP2B4) in solution was defined by electron microscopy as being hexameric with two layers of P450 trimers that are comprised of two types of distinct P450–P450 interactions (Tsuprun et al., 1986; Myasoedova and Tsuprun, 1993). Because of this characteristic of P450s, it is expected that the enzymes would have a very low K_D for homomeric interactions in membranes. Using a new approach to study P450–P450 interactions both physically and functionally, CYP2C9 was covalently immobilized to a self-assembled monolayer on gold film and its homomeric and heteromeric interactions with CYP2D6, CYP3A4, and CPR were monitored by surface plasmon resonance (Bostick et al., 2016). This technique allowed interactions between immobilized CYP2C9 and its binding partners in real time. From the data, the K_D constants for the various dimeric interactions were calculated and ranged from 1 to 18 nM. Similarly, in a global analysis of data derived from a thorough kinetic study involving CYP2E1-mediated metabolism of para-nitrophenol over a range of CYP2E1 and CPR concentrations, a K_D of 38 nM was approximated for the homomeric association of the CYP2E1 within a lipid milieu (Jamakhandi et al., 2007).

It should be pointed out that measurements of K_D which are based on volumetric concentrations, while providing a

relative number that is more easily appreciated, are actually not relevant to P450–P450 binding affinities that occur in the two-dimensional lipid membrane (the interactions detected by surface plasmon resonance actually did occur with the enzymes in solution). Davydov et al. (2015) measured the two-dimensional binding affinities for both the homomeric and heteromeric interactions of CYP2E1, CYP3A4, and CYP3A5 by luminescence resonance energy transfer (LRET) after each of the pair of enzymes were variably labeled at cysteine residues with LRET molecular partners. The binding constants [defined as the P450 concentrations at which the fluorescence resonance energy transfer (FRET) level reached 50% of the maximum] for the various homomeric and heteromeric interactions ranged from 0.07 to 0.56 pmol/cm^2, and the corresponding two-dimensional binding constant for homomeric CYP2E1 binding was 0.16 pmol/cm^2 [as compared to a K_D of 38 nM (Jamakhandi et al., 2007)]. In many cases, the heteromeric P450 associations detected in these studies had higher binding affinities than the homomeric interactions. Because the surface density of P450 in the endoplasmic reticulum of mouse hepatocytes is estimated to be in the range of 0.6–2.8 pmol/cm^2 (Watanabe et al., 1993), P450s are likely highly oligomerized *in vivo*.

Studies Measuring Rotational Mobility of P450s

As summarized in our previous reviews (Reed and Backes, 2012; Brignac-Huber et al., 2016; Reed and Backes, 2016), the literature provides many different lines of evidence that P450s physically interact in lipid membranes by the application of a variety of techniques that studied the rotational mobility of P450s such as the following: (1) optical rotary diffusion (ORD) following photolysis of the ferrous P450-CO complex with plane polarized light (McIntosh et al., 1980; Gut et al., 1982, 1983; Kawato et al., 1982; Iwase et al., 1991); (2) electron paramagnetic resonance (EPR) of P450s containing cysteine groups that were labeled with a maleimide containing a spin probe (Schwarz et al., 1982); and (3) time-resolved polarized fluorescence of cysteine residues in P450 that were labeled with diiodofluorescein iodoacetamide (Greinert et al., 1982). Specifically, in these studies, the mobility and rotation of P450s incorporated in lipid bilayers of a given viscosity were compared with the theoretical mobility and rotation for a monomeric sphere with the approximate dimensions of the P450. These studies provided useful information regarding certain characteristics of the P450 complexes in the lipid environment. These parameters were also measured under conditions that would favor dissociation of P450 aggregates such as high lipid:P450 ratios (Kawato et al., 1982) or high salt (Iwase et al., 1991).

When microsomes were studied or when P450s were incorporated in artificial membranes at lipid:P450 ratios that are comparable to those in the endoplasmic reticulum at 37°C, there was a high proportion (approximately 50% or higher) of aggregated P450 in the membrane as indicated by immobilized protein over the time course of the experiments (Gut et al., 1982; Iwase et al., 1991). Lower temperatures favored higher proportions of immobilized P450s (Kawato et al., 1982). Although these data did not provide specific determinations of the sizes of the P450 aggregates, rotational relaxation/correlation times suggest that the mobile fraction of P450 in these microsomes and lipid bilayers is at least dimeric in size (and probably larger) (Kawato et al., 1982), which in turn, indicates that the immobilized fraction is represented by higher degrees of aggregation, and the fluorescent study generated data consistent with a rotating hexameric aggregate (Schwarz et al., 1982). Interestingly, the fluorescent study indicated that changes in the angle between orientation of the fluorescent label on CYP2B4 and the plane normal to the membrane occurred upon substrate binding and reduction by CPR. This was indicative of functional changes in protein conformation (and not protein aggregation) that could correspond to the change from the open to the closed conformation of CYP2B4 [as determined in X-ray crystal structures (Scott et al., 2003; Scott et al., 2004)].

The interaction of rabbit CYP1A2 and CYP2B4 is the most studied P450–P450 interaction. For many substrates, the functional effects of this interaction are stimulation of CYP1A2-mediated activity and inhibition of that by CYP2B4 (Backes et al., 1998; Reed et al., 2010). There is also evidence that CYP1A2 (and other P450s) can form homomeric complexes (Reed et al., 2012). Although rotational studies show that an excess concentration of either lipid or CPR can disperse homomeric aggregates of CYP1A (Iwase et al., 1991) and CYP2B4 (Gut et al., 1982) within membranes, this does not diminish the significance of the high-affinity heteromeric CYP1A2-CYP2B4 interaction *in vivo* (Backes et al., 1998; Cawley et al., 2001).

Many P450–P450 hetero-interactions have been shown to be resistant to disruption by CPR. The interaction of CYP2C9 with both CYP2D6 and CYP3A4 (which both result in inhibition of CYP2C9-mediated activity) was evidenced in the presence of equimolar or excess CPR (if the P450s were mixed before CPR was added) (Subramanian et al., 2009, 2010). The effect of CYP2E1 on the apparent K_m of CYP2B4 for metabolism of benzphetamine also was observed when CPR concentrations were in excess (Kenaan et al., 2013). Thus, some mixed P450 complexes are clearly refractory to dissociation upon the binding of CPR. Taking into account these findings and the fact that many heteromeric P450 interactions tend to display higher binding affinities (discussed above), these interactions may occur preferentially in biological membranes.

Cross-Linking Studies with P450s

Another method that has been used to demonstrate P450 complex formation in membranes and to estimate the size(s) of P450 multimers is chemical cross-linking. There is some evidence to suggest that the hexameric level of aggregation for P450s in solution (Tsuprun et al., 1986; Myasoedova and Tsuprun, 1993) (discussed above) may also exist when the P450s are incorporated in membranes. Covalent crosslinking of CYP2B4, either in detergent-free solution or when incorporated into lipid vesicles of varying composition, generated virtually identical cross-linked protein bands in terms of mass distribution and densities (Myasoedova and Berndt, 1990). This suggests that the levels of aggregation were similar for CYP2B4 under either condition. This conclusion also was drawn from gel filtration studies with

CYP2B1 showing that the aggregation state of the enzyme was unaffected by its association with dilauroylphosphatidylcholine (DLPC) (Rietjens et al., 1989).

Chemical cross-linking studies have shown that amine-reactive cross-linkers generate high levels of cross-linked P450s in incubations with purified, reconstituted systems (Reed et al., 2010) (Myasoedova and Berndt, 1990). The cross-linked proteins are characterized by a range of bands (dimeric to at least tetrameric) with tight grouping of three or more closely migrating bands for each size of oligomer when the samples are separated by PAGE indicating that multiple amine groups are in close proximity at the interface of the interacting P450s.

In contrast, studies of P450–P450 interactions using cysteine-reactive cross linkers have generated only a limited sized range of P450 multimers showing primarily dimeric (and in some cases trimeric) associations without significant evidence of higher levels of associations (McIntosh and Freedman, 1980; McIntosh et al., 1980; Davydov et al., 2015). Thus, cysteine–cysteine interactions between P450s may be more representative of specific, evolutionarily conserved interactions between the P450s. Certainly, this would seem to be the case for the homomeric interaction of CYP2C8 as disulfide bonds between the cysteines of adjacent protein units in CYP2C8 dimers helped stabilize the interaction when the enzyme was expressed in cells (discussed below).

Tsalkova et al. (2007) and Davydov et al. (2015) have designed a number of studies regarding protein interactions involving CYP3A4 that used site-directed mutagenesis to generate CYP3A4 mutants in which various cysteine residues in the enzyme were substituted for serine or alanine. In one study examining cysteine cross-linking with these mutants, the interaction of CYP3A4 was suggested to be dominantly trimeric both in solution and in membranes. Furthermore, the interaction apparently involved two different types of contact between the trimer units as indicated by the disappearance of the trimeric cross-linked band in gel electrophoresis (leaving the cross-linked dimer as the prevalent band) when one of the conserved cysteines was mutated to a serine (Davydov et al., 2015). The cross-linking experiment in this study also provided support for predictions of the arrangement of units in CYP3A4 oligomers that were based on examination of the X-ray crystal structure of the P450. Cysteine-reactive cross-linking was also used effectively with site-directed mutagenesis to demonstrate the dimerization of CYP2C8 and to elucidate details regarding the quaternary structure of the dimer (Hu et al., 2010). The details regarding the cross-linking studies involving CYP3A4 and CYP2C8 are discussed below in the section regarding the crystal structures of the P450s and their relationship to the homomeric P450–P450 interactions in membranes.

Fluorescent Studies with P450s

Studies with fluorescently labeled [or P450s labeled with probes capable of fluorescence or luminescence resonance energy transfer (LRET)] P450s have also revealed aspects of P450–P450 interactions. Originally, Davydov et al. (2001) used different thiol-reactive fluorescent compounds to label the cysteine residues in P450s and CPR. FRET involving the variably labeled enzymes provided physical evidence for the interactions of CYP1A2 and CYP2B4 in addition to their interactions with CPR. This study provided physical evidence that the binding of CYP1A2 and CPR was enhanced when the P450 was in a mixed complex with CYP2B4, a finding that was predicted previously by kinetic analyses of CYP1A2- and CYP2B4-mediated metabolism as a function of the CPR concentration (Backes et al., 1998).

Luminescence resonance energy transfer and FRET experiments have been useful in demonstrating the homomeric interactions of CYP3A4 (Fernando et al., 2007; Davydov et al., 2013, 2015). FRET caused by the binding of 1-pyrenebutanol to the active site and its resulting interaction with the heme group of a CYP3A4 mutant (that did not display cooperative binding of the compound like the wild type enzyme) indicated a simple binding equilibrium (Fernando et al., 2007). However, spectral experiments using constant variation of substrate and enzyme concentrations (Job's titration) indicated enzyme oligomerization influenced substrate binding. It was then shown that the binding of apo form of the mutant CYP3A4 to the holo-enzyme resulted in a loss of cooperative binding typically associated with the wild type enzyme, and removal of the apo form restored cooperativity.

Luminescence resonance energy transfer of appropriately labeled CYP3A4 CYS-depleted mutants (discussed above) was also used to demonstrate that homomeric interaction of the P450 possibly explained the heterotropic activation of CYP3A4-mediated metabolism by α-naphthoflavone (ANF) (Davydov et al., 2013). Interestingly, the effects of ANF and the oligomerization of the P450s were coincident with high surface density of the P450 in the proteoliposomes. The homomeric oligomerization of the enzyme was cooperative as shown by the LRET. Furthermore, using FRET to measure the interaction of a fluorescent substrate with pyrene-labeled CYP3A4 at different positions (in addition to the LRET technique), it was shown that ANF (and other substrates) could affect the degree of oligomerization of the enzyme at low protein concentrations by binding to a peripheral, allosteric site on the enzyme that was far removed from the active site (Tsalkova et al., 2007; Davydov et al., 2012, 2013; Sineva et al., 2013). The effects of ANF on enzyme oligomerization occurred over the same enzyme concentration range that resulted in cooperative metabolism of 7-benzyloxy-4-trifluoromethylcoumarin by CYP3A4. Thus, the heterotropic effects of ANF on CYP3A4-mediated metabolism may relate to its ability to influence the oligomerization of the P450 and may not be caused solely by altering substrate binding through interactions within the active site as proposed previously (Korzekwa et al., 1998; Shou et al., 2001; Houston and Galetin, 2005).

Luminescence resonance energy transfer was also used to characterize the nature of P450–P450 interactions involving CYP3A4, CYP3A5, and CYP2E1, and, as mentioned above, the two-dimensional binding dissociation constants for each binary combination were generated from these data (Davydov et al., 2015). These data also demonstrated that the CYP3A protein–protein interactions (but not those involving CYP2E1) were cooperative with Hill coefficients ranging from 2 to 3.7. As in the study with ANF, the cooperative homomeric interaction of the LRET-labeled CYP3A was associated with cooperative

metabolism of 7-benzyloxyquinoline by CYP3A. The study also showed that the interaction of CYP2E1 with CYP3A resulted in both stimulation of the k_{cat} of CYP2E1-mediated metabolism of 7-methoxy-trifluoromethylcoumarin and a decrease in the 7-methoxy-trifluoromethylcoumarin binding affinity of CYP2E1. This LRET study also implicated the likely quaternary structure of the CYP3A4 multimer which is discussed in the section below regarding P450 crystal structures.

Fluorescence resonance energy transfer and bimolecular fluorescence complementation (BiFC) studies have been invaluable in demonstrating specific homo- and hetero-interactions of the enzymes of the P450 monooxygenase system in natural membranes and in discerning the relative tendencies of these labeled proteins to interact after co-expression in COS1 cells and HEK293 T cells (Szczesna-Skorupa et al., 2003; Ozalp et al., 2005). Briefly, FRET or BiFC pairs were co-expressed as fusion proteins by linking the cDNAs of complimentary fluorescent probes to the cDNA of the P450 system proteins. These studies showed the homomeric interaction of CYP2C2 as well as its interaction with the CPR. Although the interaction with CPR could also be detected for CYP2E1, the homomeric interaction of CYP2E1 was not detected in the cellular membranes. However, the heteromeric interaction of CYP2E1 and CYP2C2 was detected. The studies also were significant in showing the roles of specific protein domains in mediating the protein-protein interactions. The *N*-terminal, membrane-spanning domain was critical for CYP2C2 self-oligomerization, whereas the cytosolic domain (N-truncated form of the enzyme) was implicated in the interactions of CYP2C2 with both the CPR and CYP2E1. These findings again support the assumption that heteromeric P450–P450 interactions occur more readily than homomeric interactions.

Positional Heterogeneity of P450–P450 Complexes

One of the most striking attributes of P450–P450 complexes is their stability over time. This trait is ultimately responsible for the functional effects of P450–P450 interactions and has been demonstrated by many studies. A k_{off} for the dissociation of CYP2B4 oligomers was calculated in the FRET study by Davydov et al. (2001) (discussed above) by measuring the rate of change in FRET after mixing two populations of CYP2B4 in which the sulfhydryl groups were labeled with different fluorescent probes. The very low value for k_{off} calculated in this experiment was 0.44 h^{-1}. Interestingly, the quasi-irreversible nature of the heteromeric interactions of CYP2D6 and CYP2C9 also were demonstrated functionally by showing that the changes in metabolism caused by the interaction of the enzymes could be influenced by the order that P450s and CPR were added to the reconstituted system (Subramanian et al., 2009). Excess CPR could only attenuate inhibition of CYP2C9-mediated activity, caused by its interaction with CYP2D6, when CPR was added concurrently or before addition of the second P450 and not when the two P450s were added before the CPR.

"Positional heterogeneity" (or "persistent conformational heterogeneity") of P450–P450 complexes are synonymous terms that have been used to describe the quasi-irreversible nature of P450–P450 complexes (Davydov, 2011; Davydov et al., 2015). Davydov, working with various researchers, has clearly demonstrated the significance of this trait using a variety of approaches. Initially, heterogeneity in the CYP2B4 homomeric complex was demonstrated by hyperbaric studies of the ferrous CYP2B4-CO complex (Davydov et al., 1995). This study indicated that a specific population of the CYP2B4 subunits in P450 multimers was susceptible to a pressure-induced conversion to P420. The different populations of CYP2B4 also could be distinguished by the equilibrium between low and high spin forms of the enzymes, a transition that occurs very rapidly unless the spin state of the enzyme is "frozen" through the quasi-irreversible interaction with other P450s. Evidence that these traits were associated with multimeric enzyme complexes was demonstrated by loss of enzyme heterogeneity when the P450 was treated with detergent. Given that P450 half-lives range from 4 to 37 h (Zhukov and Ingelman-Sundberg, 1999), quasi-irreversible P450–P450 interactions could have a profound influence on drug metabolism.

The interaction of CYP1A2 and CYP2B4 was initially inferred by its functional effects by Backes in the mid to late 1990s (Cawley et al., 1995; Backes et al., 1998). These studies showed that upon interaction of the two P450s, CYP2B4-mediated activity was inhibited, whereas that of CYP1A2 was dramatically activated. Davydov provided physical evidence for the formation of this complex using the hyperbaric technique (Davydov et al., 2000b). In this study, P450 stability as a function of pressure was compared for CYP1A2 and CYP2B4. Unlike CYP2B4, the ferrous CYP1A2-CO complex did not demonstrate a susceptibility to convert to P420 under increasing pressure. More importantly, when CYP1A2 and CYP2B4 were pre-incubated for 9 h (but not when measurements were made immediately after mixing the P450s), the barotropic instability of CYP2B4 disappeared and the peak absorption of the Soret band of the CYP2B4-CO complex shifted from 450 to 448 nm, similar to that of CYP1A2. Furthermore, there was a "steeper" dependence of spin state change to the change in pressure when the CYP2B4 was in a complex with CYP1A2 indicating greater hydration of the CYP2B4 active site as a result of its interaction with CYP1A2.

More recently, Davydov et al. (2016) conducted a hyperbaric study to demonstrate a pressure-induced conformation change in CYP3A4 that was either dual-labeled with a LRET donor/acceptor pair or an electron spin probe. It was determined that only approximately 15% of the CYP3A4 population adopted the "high pressure" conformation at ambient pressure. Furthermore, the allosteric activator, testosterone, caused a shift to this "high pressure" conformation when bound to the enzyme. By selective modification of the protein with fluorescent and nitroxide side-chain spin probes, the region of the CYP3A most affected by the conformation changes was defined as the regions involving the α-helices, A/A′, and the meander loop and was shown to correspond to open and closed states of the enzymes. The pressure-induced conformation change was consistent with the putative change in the oligomeric state of the enzyme associated with ANF and other allosteric activators (discussed

above) indicating that the conformational state of the protein is intimately related to its state of aggregation.

Conformational heterogeneity of many P450s has also been explored by using CO-flash photolysis of the ferrous CO-P450 complex (Koley et al., 1994, 1995, 1996, 1997). Because the CO-complex that absorbs maximally at 450 nm is photo-sensitive, the kinetics of CO-rebinding to a P450 can be monitored on a rapid time scale by stopped flow spectrophotometry after subjecting the complex to a flash of white light. In the study with CYP3A4 (Koley et al., 1995), the experiments clearly demonstrated three populations of enzymes corresponding to three conformations of the enzyme. Furthermore, the equilibrium between the conformers was influenced by the substrate bound to the enzyme. These results are quite consistent with the findings regarding CYP3A4 oligomerization and heterogeneity by Davydov and co-workers (discussed above). Specifically, a trimer of the P450 was implicated in which there was a conformational equilibrium that was influenced by substrate/effector binding.

Positional heterogeneity of P450 multimers has also been demonstrated by the multiphasic, time-dependent chemical reduction of populations of CYP2B4 (Davydov et al., 1985) and of CYP3A4 (Davydov et al., 2005) by dithionite. Subsequent to measuring the chemical reduction of CYP3A4, heterogeneity in the CYP3A4 multimer was demonstrated by its time-dependent, enzymatic reduction using the soluble reductase domain of the bacterial P450, BM3 (Fernando et al., 2008). These studies showed the rate of reduction was related to the spin state of the enzyme. The low spin form was chemically reduced most rapidly; whereas, high spin form was more rapidly reduced enzymatically indicating this form preferentially interacted with the redox partner. These studies showed that the differences in reduction due to spin state were related to heterogeneity within the enzyme oligomer by using detergents to disperse the P450 multimers whereupon the reduction of P450 became monophasic with respect to time. The solubilized P450 was refractory to a substrate-induced spin state change. However, the study examining chemical reduction of CYP3A4 by dithionite also utilized nanodiscs to disperse the CYP3A4. Nanodiscs utilize phospholipid and a membrane scaffolding protein that allows for the stabilization of small, discoidal lipid-bilayer particles that are reported to contain monomeric enzyme when mixed at appropriate relative concentrations (Baas et al., 2004). This was significant because nanodisc-incorporated CYP3A4 was capable of a substrate-induced spin state change (Baas et al., 2004). More recent studies have indicated that CYP3A4 incorporated into nanodiscs with CPR also was catalytically active (Grinkova et al., 2010; Denisov et al., 2015). Thus, the monomeric state of the P450 was not necessarily inactive as might be concluded from the studies using detergents to disperse the P450.

THE RELEVANCE OF P450 CRYSTAL STRUCTURES TO P450–P450 INTERACTIONS IN MEMBRANES

Because of the lack of detail concerning the arrangement of P450s in their multimeric form, the crystal structures and lattices have been interpreted for their potential relevance to the functional effects of P450–P450 interactions. This approach also has been used in a previous study (Hazai et al., 2005). Of the four types of P450–P450 interactions that were evaluated in the prior study, it was concluded that none of the regions involved in binding for a given P450 dimer overlapped with the regions involved in other types of dimers. Thus, there was the potential for large aggregates to be built from the different types of dimers, and any given aggregate could be characterized by a variety of P450–P450 contacts.

The assumption in drawing inferences from P450 crystal structures is that each type of P450 has a tendency to arrange itself in characteristic associations that also may be observed in solution and in lipid membranes. As the crystal structures are generated from soluble P450 mutants that lack the *N*-terminal, membrane-spanning sequence and thus, are favorable to the formation of crystals, there is some uncertainty about the relevance of these structures to P450–P450 interactions within a lipid milieu. Speculation about the quaternary structure of mixed P450 complexes is even more problematic given that crystal structures for mixed P450 complexes do not exist. Despite the limitations of the approach, P450 crystal structures reveal some intriguing interactions that could explain some of the functional effects related to the physical interactions of different P450s.

In order to discuss the potential significance of arrangements in P450 crystal lattices, it is necessary to provide a basic description of the prominent structural features of the P450 protein. The enzymes are comprised of approximately 460 amino acids making up a series of α-helices, β-sheets, and interconnecting regions that are organized around a central heme prosthetic group. The drug-metabolizing P450s are tethered to the membrane by the insertion of a hydrophobic, N-terminal tail. The N-terminal region is connected to the structural core of the protein, known as the catalytic domain, via the polar linking region that contains several cationic amino acids and protrudes out the cytosolic side of the membrane.

It has been postulated that the polar linking region would be positioned to interact with the anionic charges of the phosphate groups in membrane lipids as a means to modulate membrane positioning of the P450s (Ozalp et al., 2006) and presumably, the interaction with redox partners and other P450s. Both the membrane penetration and α-helical content of CYP1A2 were increased in the presence of anionic phospholipids (Ahn et al., 1998), and these changes may be attributable to stronger electrostatic interactions between the negatively charged phospholipids and the positively charged, polar linking regions of this P450. Furthermore, these protein-lipid interactions may allow for tighter packing of the polar linking regions between adjacent P450s as they might minimize the repulsion between the like-charged, cationic amino acids in the polar linker regions of adjacent enzymes. The cross-linking results with amine-reactive cross-linkers (discussed above) would be consistent with covalent bonds involving this region in adjacent protein units of P450 multimers. Interactions involving this region also have been implicated in a membrane-bound, dimeric CYP2C8 complex (discussed below). Interestingly, electrostatic interactions have been implicated in the homomeric interaction of CYP1A2 that

causes inhibition of the enzyme (Reed et al., 2012) and have been shown to be involved in both the heteromeric CYP1A2-CYP2B4 (Kelley et al., 2005) and CYP1A2-CYP2E1 (Kelley et al., 2006) interactions. Future work is needed to show whether the electrostatic interactions between lipids and the polar linking regions are those responsible for these P450–P450 interactions.

P450s are wedge-shaped with two prominent sides that have important functional roles and are identified by their relative orientation with respect to the heme group. The distal side (relative to the heme group) protrudes out from the heme and contains the F and G helices that form the outer wall of the substrate binding cavity. For many P450s, the B-C loop and F-G loop/minor helices region between the F and G helices has been shown to play a role in substrate recognition (Ibeanu et al., 1996; Williams et al., 2004; Pochapsky et al., 2010). Studies examining P450s in nanodiscs indicate that the monomeric enzyme is tilted at an angle with respect to the membrane surface with the distal region partially buried in the membrane along with the hydrophobic, N-terminal tail of the P450 (Baylon et al., 2013). Indeed, truncated P450s lacking the N-terminal tails interact with membranes by virtue of the F-G region (Pernecky et al., 1993; Pernecky and Coon, 1996; Williams et al., 2000a; Scott et al., 2001). P450s demonstrate conformational flexibility, and dramatically different open and closed structures involving primarily changes in the positions of the B-C loop and the F-G helices have been identified for some P450s (Scott et al., 2003; Ekroos and Sjogren, 2006; Roberts et al., 2010).

The other prominent face of the P450 is the proximal side of the enzyme. This surface constitutes a broad, flat area with multiple, positively charged residues that facilitate interaction with and electron transfer from the redox partners, CPR and cytochrome b_5 (Tamburini et al., 1986; Bridges et al., 1998; Sevrioukova et al., 1999; Davydov et al., 2000a). The results with amine-reactive cross-linkers may also implicate this region as the interface of P450 multimers. In the section below regarding P450 crystal structures, proximal-to-proximal interactions are observable in the crystal lattices of some P450s and may explain some of the functional effects attributable to P450–P450 interactions.

When considering the potential functional consequences of a protein–protein interaction using the crystal structure as a model, it is important to only consider crystal structure interactions in which the N-terminal ends of the interacting P450s can be contained in a single plane (representative of the surface of the membrane lipid bilayer) that does not intersect the center of the interface of the interacting units or have the two (or more) proteins projecting outward from opposite sides of the imaginary plane. Structures not meeting these criteria would not likely be plausible *in vivo* (unless P450s could interact on the opposing folds of the endoplasmic reticulum membrane) given the physical constraint that the P450s are known to be tethered to the membrane by the N-terminal tails.

Quaternary structures that have been elucidated from the crystal structures in this study have also been evaluated using the program, PDBePISA (Proteins, Interfaces, Structures, and Assemblies) (European Bioinformatics Institute, Hinxton, England). This algorithm evaluates the interfaces of protein–protein contacts within the crystal to assess their potential stability within the membrane and also predicts the sizes of complexes that would be formed from these intermolecular interactions. The strength of the interaction is evaluated based on the number of potential hydrogen bonds, salt bridges, and disulfide bonds that can be detected within the interaction and is quantified by a Complex Significance Score (CSS) that ranges from 0 to 1 (with 1 being a strong interaction). The analysis can also determine the interface area of the contact and the number of interacting residues between protein units for any given arrangement in the crystal.

Interestingly, evaluations of P450–P450 interactions using this program generally predict that the proteins exist as monomers (CSS scores close to 0) despite the preponderance of evidence for multimeric P450s in membranes (as described above). In conjunction with this trend, none of the P450–P450 complexes we evaluated in this study were predicted to be stable in the membrane (shown in **Table 1**) even though the direct evidence suggests that quaternary structures very similar to those identified from the CYP2C8 (**Figure 1**) and CYP3A4 (**Figure 2**) crystal structures have been demonstrated in membranes (as discussed below). The uncertainties regarding the *in silico* interpretation of intermolecular interactions may reflect the importance of the N-terminal, hydrophobic tails (which are absent in x-ray crystal structures of P450s) in stabilizing P450–P450 complexes in the membrane.

Examination of the available crystal lattices of P450s shows many different types of plausible interactions that could exist in the membrane including distal-to-distal, proximal-to-proximal, and those involving the sides between the proximal and distal faces of the enzymes. Interactions involving the sides between distal and proximal faces of a P450 will be referred to as side-on or side-to-side interactions. These side-on interactions also can involve contacts between the proximal and distal regions of the interacting partner. Direct interactions between the proximal and distal sides are not commonly observed in the crystal structures for mammalian P450s. However, this arrangement has been identified in the crystal structure of the bacterial reductase-P450 fusion protein, BM3 (Ravichandran et al., 1993). Our analysis will start with examples of crystal structures that have been demonstrated to be likely representations of the homomeric interactions of certain P450s in membranes.

Homomeric Crystal Structures That have been Supported by Data in Cellular Systems

Homomeric CYP2C8

Computer modeling and hydropathy analyses indicate that lipophilic P450 substrates presumably enter the active site via the B-C loop and F-G helices region in the membrane, and the P450-generated products exit through a solvent access channel often found between the F and I helices (Petrek et al., 2006, 2007; Cojocaru et al., 2011). Thus, the distal region plays an important role in substrate binding to most mammalian P450s. A distal-to-distal arrangement in P450 crystal structures has been observed

TABLE 1 | Binding characteristics of the different homomeric complexes of P450 shown in the figures as determined from PISA analysis.

Complex Figure #	Nature of complex	N_{res}[a]	Interface area (Å^2)	Δ^iG[b] kcal/mol	N_{HB}[c]	N_{SB}[d]	N_{DS}[e]	CSS[f]
CYP2C8 **Figure 1**	Distal-to-distal	11	265.6	−2.2	4	2	0	0.000
CYP3A4 **Figure 2**	Distal-to-distal	17	444.9	−6.4	0	0	0	0.000
CYP1A2 **Figure 3**	Proximal-to-proximal	17	523.6	1.3	0	0	0	0.000
CYP2B4 (closed form) **Figure 4** Interface 1[g]	Side-to-side	26	644	0.4	4	2	0	0.000
CYP2B4 (closed form) **Figure 4** Interface 2[g]	Side-to-side	25	789	−4.5	1	0	0	0.000
CYP2B4 (open form) **Figure 5**		18	290	2.6	4	2	0	0.000
CYP3A4 (open form) **Figure 6**	Proximal-to-proximal	20	469	−1.1	4	0	0	0.000
CYP2C9 **Figure 7**	Proximal-to-side	21	553.1	3.8	5	6	0	0.000
CYP2C19 **Figure 8**	Side-to-side	11	359.7	−4.4	3	0	0	0.047
CYP2C9 **Figure 9**[h]	Hexameric	17	398.3	−1.2	4	1	0	0.000

*The binding characteristics of P450 homomeric complexes shown in **Figures 1–9** were determined by using the program PDBePISA (EMBL-EBI, Hinxton, England).* [a]N_{res} *– The number of interacting residues in the complex.* [b]Δ^iG *– the solvation free energy gain upon formation of the interface of the P450–P450 complex.* [c]N_{HB} *– The number of hydrogen bonds detected.* [d]N_{SB} *– The number of salt bridges detected.* [e]N_{DS} *– The number of disulfide bonds detected.* [f]*CSS – Complexation significance score.* [g]***Figure 4** depicts a trimer of CYP2B4. Interface 1 corresponds to the interaction of the center unit with the left-most unit of CYP2B4, whereas interaction 2 corresponds to the right-most interaction.* [h]*The figure represents a hexamer of CYP2C9. The interactions comprising the "arms" of the hexamer are those depicted in **Figure 7**. Thus, the values shown for **Figure 9** represent those for the central interacting units of the hexamer.*

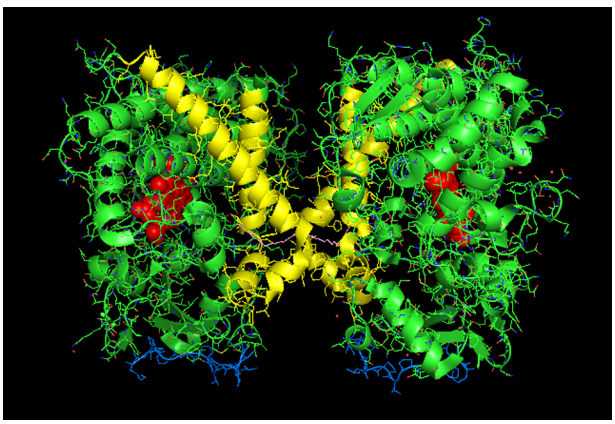

FIGURE 1 | Crystal structure of dimeric form of CYP2C8 bound to palmitate (PDB: 1PQ2). The units of the dimer are oriented with the N-terminal region (shown in blue) at the base of the dimers in a "membrane plane" running perpendicular to the plane of the image. The heme groups are shown as red spheres with α-helices drawn as cylindrical features. The dimers are joined at F-G loop region. The F-G helices on the surface of the distal faces of the dimer are shown in yellow. Two molecules of palmitate bound on the periphery of the active site at the junction of the dimer are shown in pink. All molecular structures in this study were generated in PyMOL v. 1.8.4.1 (Schrödinger, Cambridge, MA, USA).

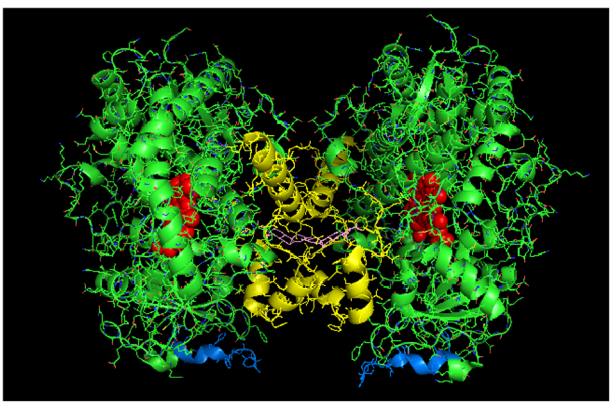

FIGURE 2 | Crystal structure of distal-to-distal dimeric form of CYP3A4 bound to progesterone (PDB: 1W0F). The units of the dimer are oriented with the N-terminal region (shown in blue) at the base of the dimers in a "membrane plane" running perpendicular to the plane of the image. The heme groups are shown as red spheres with α-helices drawn as cylindrical features. The F-G helices region indicating the distal surface is shown in yellow. The peripheral effector site for binding of two molecules of progesterone are shown in pink.

with many different drug-metabolizing P450s including CYP3A4 (1W0F), CYP1A2 (PDB: 2HI4), CYP2D6 (PDB: 2F9Q), CYP2A6 (PDB: 2FDV), and the open form of CYP2B4 (PDB: 1PO5). Recent studies involving CYP2C8 (PDB:1PQ2) (Hu et al., 2010) and CYP3A4 (Davydov et al., 2013, 2015) have provided evidence that this type of dimer is also formed from the homomeric interactions of these P450s when they are membrane-bound.

Studies with purified CYP2C8 in which Trp residues were introduced by mutagenesis in order to examine the interaction (by Trp fluorescence quenching) of the mutated P450 with spin-labeled lipids in artificial membranes (Ozalp et al., 2006) suggested that the F-G loop did not interact with the membrane as predicted from similar studies with human CYP2J2 (McDougle et al., 2015) and hydropathy analysis of a similar CYP2C enzyme (Williams et al., 2000b). Interestingly, this region also was the major point of interaction in the dimeric X-ray crystal structure of CYP2C8 (PDB:1PQ2; **Figure 1**; **Table 1**). It was predicted from the crystal structure that the dimerization would be facilitated by adjacent sulfhydryl groups in cysteine residues of the interacting CYP2C8 units. Dimerization was then demonstrated on electrophoretic gels after either oxidation or cross-linking of the cysteine residues on CYP2C8 that was transiently expressed in bacterial membranes and in AD-293 cells (Hu et al., 2010). Subsequent mutagenesis experiments indicated that dimerization through the sulfhydryls was dependent on

having cysteine residues within either the polar linker sequence (between the N-terminal, membrane-spanning region and the catalytic domain) or the F-G loop. Thus, these regions were implicated as the points of contact in the membrane-bound CYP2C8 dimer.

Dimerization through the sulfhydryls was not observed in the cell membranes when the hydrophobic N-terminal membrane anchor was deleted or substituted with a hydrophilic N-terminal sequence. This is consistent with BiFC (Ozalp et al., 2005) and FRET (Szczesna-Skorupa et al., 2003) studies of the closely related CYP2C2 in COS1 cells (discussed above) showing that homomeric P450–P450 interactions required the N-terminal membrane domain. Similarly, N-terminal truncation prevented the interaction of CYP3A4 and CYP2C9 (Subramanian et al., 2010). Thus, the N-terminal region is very important in stabilizing some P450–P450 interactions in the membrane.

Interestingly, the arrangement of subunits in the crystal structure of CYP2C8 were such that the cysteines in the polar linker regions of adjacent units did not align in close enough proximity to allow for disulfides and/or cross linking to occur between the units. In fact, for the polar-linking regions of the dimer units to be in close proximity, the F-G loop would have to be pulled out of the membrane. Thus, dimers with similar features were apparently formed with both full-length CYP2C8 in membranes and with truncated CYP2C8 in solution. However, the membrane interaction that is stabilized by the N-terminal sequence of the full-length form imparts a slight change in alignment within the dimer that allows for cross-linking through adjacent sulfhydryls in the polar linker region. It was speculated that the high enzyme concentrations needed to form CYP2C8 crystals facilitated dimerization even without the N-terminal sequences. However, the N-terminal segment was needed for stabilization of the dimer after transient expression of the enzyme in cellular membranes. Unfortunately, the functional effects of the CYP2C8 homomeric interaction were not assessed. However, as discussed above, movement of the F-G loops, which form part of the substrate access channel from out of the membrane bilayer upon the formation of the dimer, would undoubtedly influence the binding of substrate by the enzyme.

Homomeric CYP3A4 and Its Functional Effects

CYP3A4 is quantitatively the most important P450 in drug metabolism (Anzenbacher and Anzenbacherová, 2001; Guengerich, 2003). As a result, considerable effort has been devoted to resolving crystal structures for this enzyme, and a number of conformations have been identified for the P450 when bound to different compounds (Williams et al., 2004; Yano et al., 2004; Ekroos and Sjogren, 2006). Several lines of evidence have suggested that a dimeric arrangement of CYP3A4 in the crystal lattice has functional relevance to the multimeric state of the membrane-bound enzyme. The quaternary structure is unusual because it has two molecules of progesterone bound to a peripheral "cleft" formed in the interface of a homomeric dimer [PDB: 1W0F; **Figure 2**)]. Interestingly, the CYP2C8 crystal dimer (PDB: 1PQ2) also displayed a peripheral binding site for two palmitate molecules in a similar location to that of the CYP3A4 dimer, but its functional significance was not explored.

Davydov et al. (2016) have now provided evidence from studies using LRET/FRET and chemical cross-linking that the CYP3A4 crystal dimer is a reasonable analog to a quaternary structure adopted in the membrane. First, it was described above how FRET/LRET studies indicated that the binding of ANF to CYP3A4 could change the oligomeric state of the enzyme. FRET was also measured after mixing different combinations of specific cysteine-depleted mutants that were variably labeled with donor/acceptor FRET pairs (Tsalkova et al., 2007; Sineva et al., 2013). From dramatic FRET changes upon the binding of the effector, ANF, it was possible to prove a change in conformation that was not elicited when a prototypical substrate bound to the heme active site. These findings are consistent with the hyperbaric study (described above) monitoring a pressure-dependent conformation change in CYP3A4 that was facilitated by the allosteric effector, testosterone (Davydov et al., 2016).

Using another approach, the FRET/LRET efficiencies and the Förster radius of the donor/acceptor pair, it was possible to approximate the separation distance between adjacent cysteines on an interacting pair of variably labeled CYP3A4 cysteine mutants (Davydov et al., 2015). For each pair of mutants, the calculated distances between the cysteine locations were within the range of error of the distances that would be expected in the progesterone-bound crystal. Similarly, by using cysteine-reactive cross-linkers of different lengths with the CYS-depleted CYP3A4 mutants in order to explore the distance between adjacent cysteines in CYP3A4 multimers, it was possible to demonstrate that the results were also consistent with the progesterone-bound CYP3A4 structure. From these studies, it was proposed that ANF and other effectors bound to the same peripheral site bound by progesterone in the implicated crystal structure, and that its binding changed the oligomerization state of the enzyme and in turn, its catalytic activity. From the crystal structure, it was proposed that the progesterone-binding site could play a role in initial substrate recognition because it lines up with a suitable route (through the F-G helices region) from the membrane to the active site (Williams et al., 2004). Thus, in light of the other biophysical data, the conformation change required to open up this putative channel may be facilitated by interactions with the peripheral ligand. Interestingly, the less catalytically active form of CYP3A4 in the absence of effector binding may also be a distal-to-distal dimer (from crystal structure PDB:1W0G). Thus, the change in oligomerization caused by effector binding to the peripheral binding may only be a subtle repositioning of the dimer that opens up a putative substrate access channel through the F-G helices region and not necessarily a change from the monomeric state to a multimeric enzyme complex.

Metabolism by CYP3A4 is often characterized by sigmoidal, homo-, and heterotropic cooperativity (Korzekwa et al., 1998; Shou et al., 2001; Houston and Galetin, 2005). One of the best examples of heterotropic cooperativity involves the effects of ANF on CYP3A4-mediated metabolism. This compound often activates metabolism by eliminating sigmoidal enzyme kinetics. Until recently, cooperativity was attributed to a large active site that is capable of binding multiple substrates. Effector compounds could thus influence positioning of a substrate (and in turn its metabolism) by simultaneous binding to the active

site. It has also been postulated that effector binding may elicit a change in CYP3A4 conformation that is more catalytically active. In support of these ideas are crystal structures of CYP3A4 (Ekroos and Sjogren, 2006) showing multiple compounds within the active site (PDB: 2V0M) as well as variations in conformation upon binding to different substrates (PDB: 2J0D). Various biophysical techniques also indicate a ligand-influenced equilibrium between multiple conformations of the enzyme (Koley et al., 1995; Sineva et al., 2013; Davydov et al., 2016). In addition, studies with CYP3A4, reconstituted in nanodiscs with excess CPR, observed both homotropically cooperative substrate binding (Baas et al., 2004) and heterotropically cooperative substrate metabolism (Denisov et al., 2015).

In contrast, the LRET/FRET studies with CYP3A4 described above suggest that effector-induced changes in protein conformation lead to changes in protein oligomerization, and it may in fact be the latter changes that directly relate to cooperative metabolism by CYP3A4. The relative roles that effector-mediated substrate re-positioning in the active site and effector-mediated changes in protein conformation/oligomerization play in causing cooperative CYP3A4-mediated metabolism have not yet been determined. However, one of the objectives of this review is to entertain the possibility that many functional changes of P450–P450 interactions could simply be explained by positional changes of enzyme units in P450 multimers and not solely by changes in enzyme conformation and substrate-positioning within the active site.

Using Positional Re-arrangement within P450 Multimers to Explain the Functional Effects of P450–P450 Interactions

The reported functional effects involving a given P450 that are caused by its interaction with another P450 will be considered with respect to any distinctive features observed in the crystal lattice arrangement of the P450 that may impart functional properties to the homomeric complex. The validity of this approach lies in the fact that any discussion about the functional effects of P450–P450 interactions is relative to the frame of reference. As discussed in detail above, the P450 units in homomeric multimers are not identically distributed within the aggregate but are characterized by different spin states and different abilities to be reduced/bind substrates. Furthermore, the transition between subunit positions within the aggregate is extremely limited or hindered as indicated by removal of a segment of the P450 population from the rapid spin state equilibrium. Thus, any aggregate of P450 is inhibitory by nature of the fact that some of the units in the aggregate may not be fully functional. With this in mind, any heteromeric P450–P450 interaction that causes activation of a P450 could be due to the homomeric interactions of the affected P450 being relatively inhibitory. Conversely, inhibitory P450–P450 interactions would be related to subunit arrangements in the hetero-complex that contrast with those associated with higher functionality in the homomeric complex. Studies that have elucidated the kinetic mechanisms by which P450–P450 interactions influence metabolism will be used to explain how specific homomeric interactions may be more or less functional.

P450–P450 Interactions That Influence CPR Binding

CYP1A2 Interactions

Several studies have demonstrated that the ability of a P450 to bind CPR is altered when it forms a mixed complex with another P450. For the P450–P450 interactions of CYP1A2-CYP2B4 (Backes et al., 1998), CYP1A2-CYP2E1 (Kelley et al., 2006), CYP2C9-CYP2C19 (Hazai and Kupfer, 2005), and CYP2E1-CYP2B4 (Kenaan et al., 2013), CYP1A2 and CYP2C9 (and CYP2E1 in its interaction with CYP2B4) were able to bind CPR more readily (and thus be more catalytically active) when bound to the indicated P450s; whereas the ability of the interacting P450 to bind CPR was either inhibited or unaffected. If one only considers the relative positions of the protein "units" in a P450 multimer (and not necessarily the conformation of the enzyme as a determinant in its activity), CPR binding could most logically be affected by interactions involving the proximal side of the P450 enzyme sterically disturbing formation of the CPR·P450 complex and consequently electron transfer.

Thus, taking the CYP1A2-CYP2B4 interaction as the most well-studied example of this effect and the line of reasoning used in the introductory paragraph to this section, the activation of CYP1A2 via enhanced CPR binding in mixed P450–P450 complexes would imply that its homomeric complex is limited in its ability to bind CPR. In support of this conclusion, research from our lab has clearly demonstrated that the homomeric interaction of CYP1A2 inhibits its activity by a mechanism that involves a lower CPR-binding affinity (Reed et al., 2012). In these studies, CYP1A2 activities showed a sigmoidal response as a function of CPR concentration, which is consistent with a CYP1A2·CYP1A2 dimer that is inactive (Reed et al., 2012).

Interestingly, a proximal-to-proximal interaction is very prevalent in the crystal lattice for CYP1A2 (PDB: 2HI4, **Figure 3**). With this proximal-to-proximal arrangement, the units in the CYP1A2 dimer directly overlay the proximal face of the identical binding partner in a manner that would completely prevent access for CPR binding. Thus, the stimulation of CYP1A2 caused by heteromeric P450 interactions (with either CYP2B4 or CYP2E1) may stem from the CYP1A2 having a different arrangement with its proximal face exposed in the presence of these other P450s. This in turn, would cause a higher proportion of the CYP1A2 to be available to functionally interact with CPR.

Proximal-to-Proximal Interactions with Open Conformations of P450s

The proximal-to-proximal interaction is very unusual in closed forms of P450s. For instance, the closed conformation of CYP2B4 (PDB: 1SUO) is predominated by side-to-side interactions (**Figure 4**). However, a proximal-to-proximal interaction is observed in the crystal lattice of an open form of CYP2B4 (PDB:1PO5; **Figure 5A**). The open form of this P450 was crystallized as a distal-to-distal dimer (**Figure 5B**). This conformation of CYP2B4 adopts many different arrangements

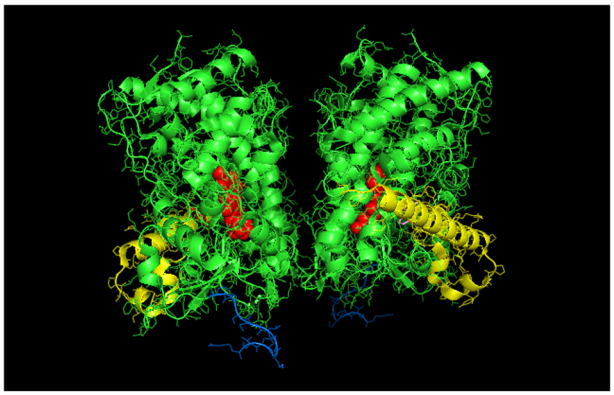

FIGURE 3 | Crystal structure showing lattice arrangement of proximal-to-proximal dimer of CYP1A2 bound to the inhibitor, ANF (PDB:2HI4). The units of the dimer are oriented with the N-terminal region (shown in blue) at the base of the dimers in a "membrane plane" running perpendicular to the plane of the image. The heme groups are shown as red spheres with α-helices drawn as cylindrical features. The bound ligand, ANF is shown in the active site in a pink color. The F-G helices region on the distal face of the enzyme is shown in yellow.

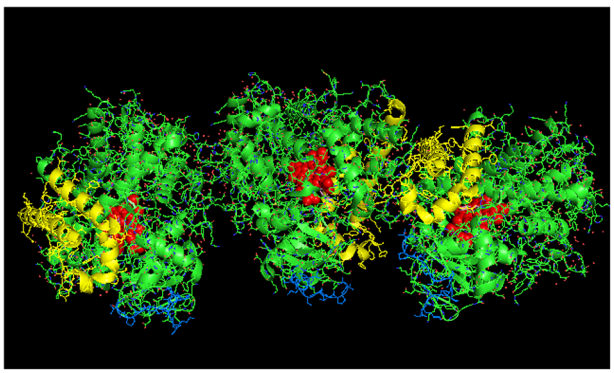

FIGURE 4 | Crystal structure showing side-to-side lattice arrangement of a CYP2B4 trimer of closed form CYP2B4 with 4-(4-chlorophenyl)imidazole (shown in pink) bound to the active site (PDB:1SUO). The units of the trimer are arranged with the N-terminal ends (shown in blue) at the base of the units in a "membrane plane" running perpendicular to the plane of the page. Regions involved in the interactions include the G-, H-, J-, C-, and D-helices. The heme groups are shown as red spheres with α-helices drawn as cylindrical features. The F-G helices region on the distal face of the enzyme are shown in yellow.

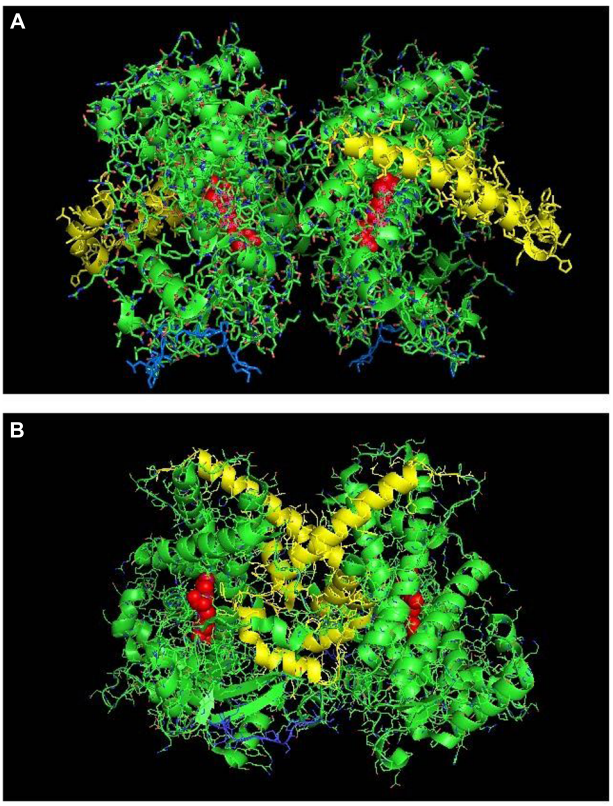

FIGURE 5 | The crystal structure of open-formed, ligand-free CYP2B4 (PDB:1PO5) showing lattice arrangements of a proximal-to-proximal dimer (A) and an intercalated, distal-to-distal dimer **(B)**. The units of the dimers are oriented with the N-terminal region (shown in blue) at the base of the dimers in a "membrane plane" running perpendicular to the plane of the image. The heme groups are shown as red spheres with α-helices drawn as cylindrical features. The F-G helices regions on the surface of the distal faces of the enzyme units are shown in yellow.

in its crystal structure including two types of side-to-side interactions in addition to the distal-to-distal and proximal-to-proximal orientations. The open-form, intercalated, distal-to-distal dimer represents an inactive complex having a His in the F-helix of one open unit coordinating with the active site heme of the other open CYP2B4 unit. An evaluation of the open conformation of the CYP2B4 crystal structure led to the conclusion that this form of CYP2B4 also would be deficient in functionally interacting with CPR because of repositioning of the C helix (Scott et al., 2003). Thus, whether or not the open CYP2B4 is in a proximal-to-proximal interaction, it is probably not reducible by CPR. In the inhibition of CYP2B4 caused by its interaction with CYP1A2, it seems conceivable that the effect could be due in part, to a proximal-to-proximal association of open form CYP2B4 with CYP1A2 in which the CYP2B4-binding site for CPR is blocked. The hyperbaric studies of the CYP1A2-CYP2B4 complex (Davydov et al., 2000b) showed that there was increased hydration of the active site of CYP2B4 as a result of its interaction with CYP1A2 which is consistent with the interaction involving the open form of CYP2B4.

A proximal-to-proximal interaction can also be observed in the crystal lattice of an open form of CYP3A4 bound to ketoconazole (PDB: 2V0M; **Figure 6**) (Ekroos and Sjogren, 2006). Furthermore, the crystal structure of the open CYP3A4 dimer associated with the binding of erythromycin is arranged in an offset proximal-to-proximal orientation (PDB: 2J0D). As is the case with CYP2B4, proximal-to-proximal interactions of the open CYP3A4 are not observed in crystal lattices of closed CYP3A4 forms (discussed above). CYP3A4 metabolizes very large substrates, and the open form apparently is adopted when large substrates are metabolized by the P450. Thus, unlike

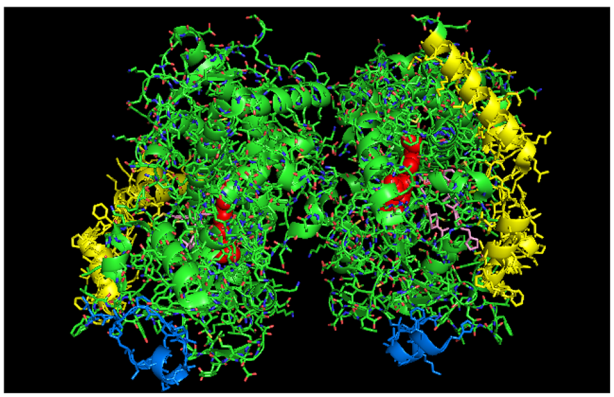

FIGURE 6 | Crystal structure showing lattice arrangement of proximal-to-proximal dimer of open-formed CYP3A4 with two molecules of ketoconazole bound to each active site (shown in pink) (PDB:2V0M). The units of the dimer are oriented with the N-terminal region at the base of the dimers in a "membrane plane" running perpendicular to the plane of the image. The heme groups are shown as red spheres with α-helices drawn as cylindrical features. The two ketoconazole molecules bound to each active site are shown in pink.

CYP2B4, the open CYP3A4 form is likely to be catalytically active. Similar to the crystal lattice of open CYP2B4, the open form of CYP3A4 also displays a variety of arrangements including distal-to-distal (not intercalated) and side-to-side. Thus, these open forms may be versatile in the types of associations they can adopt.

The open conformation has also been implicated for a R108H mutant of CYP2C9 through the use of size exclusion chromatography, UV-visible spectrophotometry, pulsed electron paramagnetic resonance, and molecular dynamics simulations (Roberts et al., 2010). The mutant was isolated in a conformation in which the substituted His in the B-C loop coordinated *intramolecularly* with the heme group. Thus, this form is a monomer, but the mobility of the B-C loop in coordinating with the heme is similar to the conformational mobility needed to form the open conformation of CYP2B4. Because this conformation was ascertained by physical techniques other than X-ray crystallography, the tendency of this form to associate in a proximal-to-proximal orientation cannot be determined.

Any open form in which inter- or intramolecular rearrangement blocks substrate access to the active site would be inhibitory. Thus, it seems open conformations of P450s may in general, be a means to limit the activities of the P450s by favoring the formation of proximal-to-proximal arrangements that are deficient in binding to CPR. Unfortunately, very few P450 crystal structures have been isolated in the open conformation to confirm that this form consistently adopts these arrangements. Thus, this hypothesis needs further testing. However, it should be pointed out that the arrangement is observed in all of the available open-form crystal structures.

It is clear that the crystal structure of CYP1A2 is unusual in adopting a proximal-to-proximal arrangement in the closed conformation. Furthermore, it can also be argued that CYP1A2 would be incapable of adopting the open conformation given its narrow active site that is conducive for metabolism of planar, aromatic substrates (Sansen et al., 2007). If the conformation of CYP1A2 did open up, the P450 would be expected to metabolize a wider range of substrates. Thus, the proximal-to-proximal interaction may have an important regulatory role in P450-mediated catalysis, and CYP1A2 may utilize its ability to adopt this arrangement in the closed form to influence the conformation and quaternary structure of interacting P450s.

CYP2C9 Interactions

Stimulation of CYP2C9-mediated activity through a mechanism involving higher CPR binding affinity was also reported for the interaction of the P450 with CYP2C19 (Hazai and Kupfer, 2005). An explanation for this effect was proposed through an examination of CYP2C9 crystal structure in a subsequent study (Hazai et al., 2005). At the time of this study, the number of available crystal structures for mammalian P450s was limited, and the functional effects of P450–P450 interactions were interpreted solely by the potential effects on CPR binding as this was the only identified mechanism.

To explain the activation of CYP2C9 metabolism by its interaction with CYP2C19, the previous study examined a side-to-proximal dimer (PDB: 1OG5; **Figure 7**) which has the proximal face of one unit being occluded by the side of the protein containing the C-terminal end of the I-helix and the J-helix. In the previous study, it was postulated that the CYP2C9 dimer would bind CPR with greater affinity than a CYP2C9 monomer because the exposed J and K helices of the obstructed proximal face would contribute to CPR binding by the exposed proximal face of the self-interacting CYP2C9 unit. Although this is an intriguing conclusion to be drawn from this crystal structure arrangement, it must also be considered that this complex instead represents an inhibitory, homomeric CYP2C9 complex because

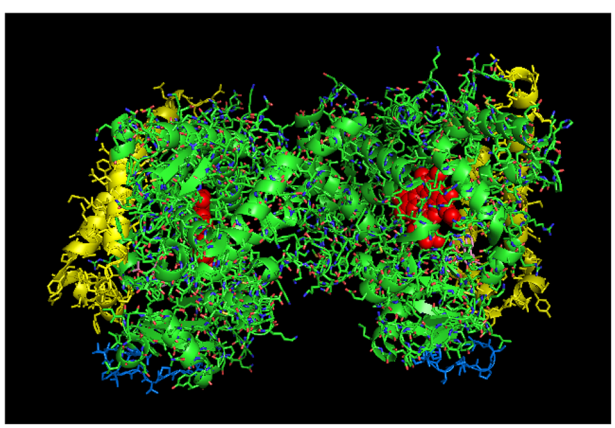

FIGURE 7 | Crystal structure of side-to-proximal dimer of CYP2C9 bound to warfarin (PDB: 1OG5). The units of the dimer are oriented with the N-terminal region (shown in blue) at the base of the dimers in a "membrane plane" running perpendicular to the plane of the image. The heme groups are shown as red spheres with α-helices drawn as cylindrical features. The F-G helices region on the distal surfaces of the dimer are shown in yellow. Warfarin molecules (pink) are bound in the active sites.

one of the two proximal faces is sterically hindered in its ability to bind CPR. Thus, at least one of the two CYP2C9 units in the dimer would be catalytically limited. Furthermore, it is possible that CPR binding to the "exposed" proximal side of the alternate unit also would be limited because it is partially obstructed in the crystal structure.

Because positional heterogeneity implies that any heteromeric P450–P450 interaction stimulating a P450 catalytic activity can also be interpreted as the homomeric interactions being inhibitory, the side-to-proximal interaction of CYP2C9 may instead be inhibitory and not one that is characterized by increased CPR-binding affinity. As a result, the stimulation of CYP2C9 through its interaction with CYP2C19 may be mediated through a quaternary structure that fully exposes the CYP2C9 proximal face, possibly doubling the amount of catalytically active CYP2C9 relative to what would be observed with the homomeric CYP2C9 dimer (PDB: 1OG5). The CYP2C19 crystal lattice (PDB:4GQS; **Figure 8**) shows one arrangement that would be a credible membrane alignment in which the N-terminal ends of a symmetrical dimer interact in a manner that would expose the proximal faces at a rather flat angle to the membrane normal with the distal faces buried below the membrane surface. In conjunction with this arrangement, many hydrophobic residues on the distal side project below what would be the membrane surface in this orientation. Thus, the functional effects reported for this interaction could be explained if a greater proportion of CYP2C9 adopted the "CYP2C19-like" arrangement at the expense of the side-to-proximal dimer associated with the CYP2C9 crystal lattice, and more of the CYP2C19 adopted the CYP2C9 homodimer arrangement.

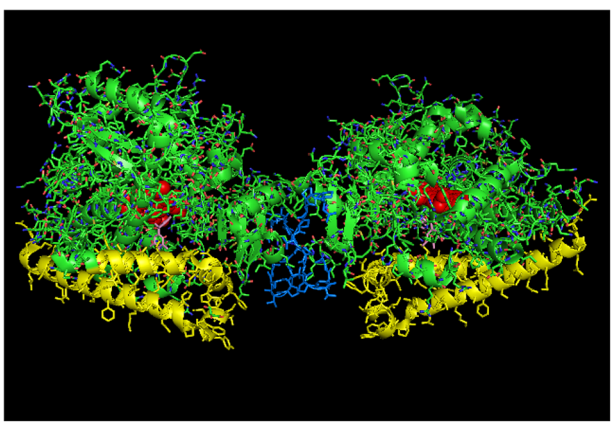

FIGURE 8 | Crystal structure of side-to-side dimer of CYP2C19 bound to (2-methyl-1-benzofuran-3-yl)-(4-hydroxy-3,5-dimethylphenyl) methanon (PDB: 4GQS). This arrangement typifies the interactions that can be observed in the CYP2C9 crystal lattice. The units of the dimer are oriented with the N-terminal region at the base of the dimers in a "membrane plane" running perpendicular to the plane of the image. The crystal is predominated by many side-on interactions, many of which do not orient in a manner consistent with being incorporated in a single membrane bilayer. The heme groups are shown as red spheres with α-helices drawn as cylindrical features. The molecules of (2-methyl-1-benzofuran-3-yl)-(4-hydroxy-3, 5-dimethylphenyl) methanon bound to the active site are shown in pink.

The distinction between a conformational mechanism and the one involving a change in the arrangement of a P450 complex that exposes the proximal face of the P450 is significant. In the second case, the amount of a specific P450 participating in the metabolism of a substrate would increase because a higher proportion of the P450 would have the ability to interact with CPR. It is important to note that this effect could mistakenly be attributed to a change in the rate of a catalytic step of the reaction cycle. To take the effects of the CYP2C9-CYP2C19 interaction as an example (Hazai and Kupfer, 2005), stimulation of the CYP2C9-mediated metabolism of methoxychlor was observed in the presence of CYP2C19 when CPR was at a saturating concentration. This would not happen if the change was caused by a conformation-related increase in the binding affinity of CPR and CYP2C9 because the CPR level was saturating both in the presence and absence of CYP2C19. However, the effect could be explained if the interaction of CYP2C9 with CYP2C19 causes more of the proximal face of CYP2C9 to be exposed for binding to CPR. Thus, any P450–P450 interaction that has been attributed to a change in the rate of a catalytic step, other than substrate binding, may in fact be caused by this mechanism instead. In other words, any apparent change in the k_{cat} of a reaction associated with a P450–P450 interaction could instead be attributable to an alteration in the amount of available active enzyme through a ***re***-rearrangement within a P450 multimer that exposes or hides more of the proximal face of the affected P450 (*i.e., an effective increase it total active enzyme would present as an increase in* k_{cat}).

Another important kinetic distinction in the formation of the proximal-to-proximal dimer is that the P450 in this arrangement would be effectively removed from the population of P450 capable of binding CPR. Thus, if there is a net exchange of one P450 form for another in this arrangement, the effective CPR:P450 ratio would increase for the P450 that is activated through this mechanism. This would be another potential mechanism for enzymatic stimulation in the mixed system.

P450–P450 Interactions That Influence Substrate Binding

As reviewed previously (Reed and Backes, 2016), the interactions of CYP2C9 with CYP2D6 (Subramanian et al., 2009) (and possibly with CYP3A4) (Subramanian et al., 2010) and CYP2B4 with CYP2E1 (Kenaan et al., 2013) have been shown to cause inhibition of CYP2C9 and CYP2B4, respectively, by increasing the dissociation constants for substrate binding. Changes in substrate binding could be plausibly explained through P450–P450 interactions that involve the distal side of the affected P450. A distal-to-distal P450 quaternary structure is commonly observed in P450 crystal lattices. A membrane-bound analog of this type of dimer is typified by the crystal structure of CYP2C8 (Hu et al., 2010). In these types of dimers, the P450s can assume either closed or open conformations around the active site, and the F and G helices of the interacting P450s form the dimerization interface. Interestingly, the dimerization of CYP2C8 probably causes the F/G loops to be pulled out of the membrane bilayer (Schoch et al., 2004; Ozalp et al., 2006).

This effect in turn, would likely affect substrate binding to the enzyme and would probably inhibit metabolism of hydrophobic substrates that partition largely to the membrane. Perhaps, in its interaction with CYP2C9, CYP2D6 may favor a rearrangement of the CYP2C9 that obstructs its distal face and in turn, causes its substrate to bind less tightly to its active site and inhibits CYP2C9-mediated metabolism in the process. Similarly, by consideration of positional heterogeneity as the primary determinant of P450–P450 effects, it would be presumed that CYP3A4 binds to the distal side of CYP2C9 to disrupt binding of S-naproxen and *S*-flurbiprofen, and in a similar manner, CYP2E1 (at high enzyme concentrations) distorts the distal side of CYP2B4 and negatively influences binding of benzphetamine to its active site (Kenaan et al., 2013).

A more recent study (Bostick et al., 2016) has reported that the interaction of CYP2D6 and CYP2C9 resulted in stimulation of the CYP2C9-mediated metabolism of *S*-flurbiprofen [the same substrate in the study reporting inhibition of CYP2C9 (Subramanian et al., 2009)]. There were several distinctions in the methods used in the two studies that could explain the discrepancy in the findings. Most importantly, the reaction went for 16 h in the later study, and it was reported that the rates were not linear over this time period. Thus, "stimulation" could merely reflect longer enzymatic stability when CYP2C9 was in the mixed complex, and the earlier study probably describes the effects of the CYP2C9-CYP2D6 interaction more accurately.

Putative Hexameric Quaternary Structure of Membrane-Bound CYP2C9

In examining crystal lattices of purified P450s for the putative hexameric aggregate that has been implicated by electron microscopy (Tsuprun et al., 1986; Myasoedova and Tsuprun, 1993) and saturation transfer electron paramagnetic resonance (Schwarz et al., 1982), an interesting arrangement can be observed in the crystal lattice of CYP2C9 (PDB: 1OG5; **Figures 9A,B**) in which a large-scale pattern that includes a trimer of asymmetric dimers can be observed. The dimers referred to are the side-to-proximal dimers described above. The arrangement is intriguing in that it is consistent with functional membrane binding and has similar features to the hexameric structures of CYP1A2 (Myasoedova and Tsuprun, 1993) and CYP2B4 (Tsuprun et al., 1986) observed by electron microscopy as it is comprised of two types of contacts between the CYP2C9 units of the hexamer. In addition to the side-to-proximal interaction, the three sets of dimers are joined together with threefold symmetry along the distal faces and the side between the proximal and distal faces that contains the regions between the B/C helices and the H/I helices in addition to the C-terminus of the enzyme. Future research should consider this hexamer as a possible quaternary structure when metabolism by CYP2C9 is assessed in the context of P450–P450 interactions.

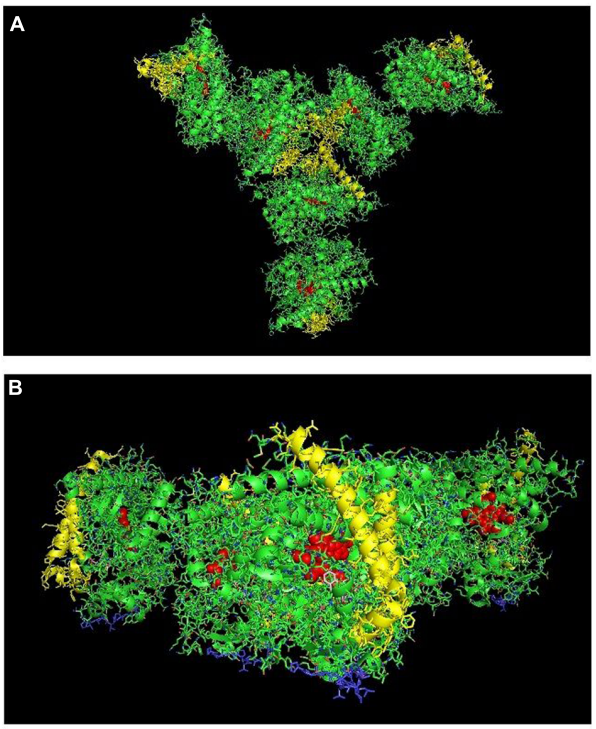

FIGURE 9 | Crystal lattice of side-to-proximal dimer of CYP2C9 (PDB: 1OG5) (shown in Figure 7) showing conceivable hexameric association within a membrane. The crystal lattice of the side-to-proximal dimer shown in **Figure 7** was examined for higher ordered quaternary structure. **(A)** Shows a trimeric association of the dimers in threefold symmetry formed from a side abutting in an angle against a neighboring distal region of an adjacent CYP2C9 unit. The N-terminal, membrane-binding region for each unit is at the bottom of the hexamer in the plane of the page. **(B)** Shows the same hexamer with the blue N-terminal ends arranged at the bottom of the hexamer in a common plane that runs perpendicular to the plane of the image. The heme groups are shown as red spheres with α-helices drawn as cylindrical features. The F-G helices region on the distal faces of the hexamer units are shown in yellow.

DISCUSSION

Physical studies have convincingly shown that P450s have a propensity to form complexes in membranes. Studies measuring FRET/LRET and surface plasmon resonance now allow for determinations of the dynamics of P450–P450 association. Measurements indicate dissociation constants ranging from 1 to 50 nM (0.05–0.6 pmol/m^2 for calculations based on the two-dimensional lipid bilayer). Thus, P450s bind with affinities that are higher than those measured for some signaling complexes within the plasma membrane where the dissociation constants of various G_α subunits for the $G_{\beta\gamma}$ subunit, coupled to the *N*-formyl peptide receptor, ranged from 1 to 3 μM (Bennett et al., 2001).

Studies with cross-linkers and those designed to monitor the rotational mobility of P450s indicate the presence of dimeric to hexameric (and larger?) P450 multimers in membranes with some P450–P450 interactions being governed by electrostatic forces possibly involving amine groups in the polar linker region and/or the proximal faces of the enzymes. In natural membranes, P450s form complexes of varying sizes with higher ordered aggregates containing essentially rotationally immobilized P450 units.

These P450–P450 interactions would not be of particular interest if they did not impart functional changes that affect drug metabolism. However, the P450 units in these multimers display positional heterogeneity with respect to chemical/enzymatic reduction, spin state, and access to substrate. The heterogeneity of P450 multimers with respect to these properties is a testament to the quasi-irreversible nature of P450–P450 associations and is the underlying source of the functional effects of P450–P450 interactions with regards to drug metabolism.

An integral question concerning the functional effects of P450–P450 interactions involves the physiologic rationale for their existence. Given their important role in the elimination of hydrophobic xenobiotics, it may seem counter-intuitive that their activities could be selectively inhibited by oligomerization. Enzymatic regulation through oligomerization also provides a means for the P450 system to respond immediately to the presence of a given substrate through quaternary re-arrangements that "unmask" otherwise latent P450-mediated activities. If this were not the case, the P450 system might be ineffective at removing the compound until delayed induction of the relevant P450s. In addition, the P450 catalytic cycle depends on the activation of molecular oxygen through the transfer of electrons to the heme group. This process can result in uncoupling and the generation of destructive reactive oxygen species. Thus, the regulation of P450-mediated activities through oligomerization may provide a mechanism to limit deleterious uncoupling reactions. This topic has been addressed more fully in other reviews (Zangar et al., 2004; Davydov, 2011). It is also possible that P450 oligomerization has a more complex role with the expression of specific P450s serving to silence or enhance the activities of P450s with which they tend to interact.

Despite the fact that general mechanisms involving altered CPR and/or substrate binding have been identified for the functional effects of P450–P450 interactions, the specific ways that the interactions cause these changes have been difficult to interpret. Typically, general explanations attribute the phenomena to protein conformation changes. Undoubtedly, undefined conformation changes are the underlying causes given that the effects of P450–P450 interactions are substrate-specific. For instance, all interactions involving CYP2E1 and CYP2B4 do not cause activation of the former and inhibition of the latter (Kelley et al., 2006). However, *p*-nitrophenol and benzphetamine trigger specific conformation changes in CYP2E1 and CYP2B4, respectively, that lead to those effects when the two P450s interact (Kenaan et al., 2013).

While the underlying protein conformational changes that affect oligomerization are important to elucidate, the actual changes in oligomerization affecting positional heterogeneity are possibly the ultimate source of functional changes. In fact, it can be reasoned that certain arrangements of P450s would have very predictable consequences on drug metabolism. Thus, for this review, we have examined the crystal lattices of several P450 structures to identify arrangements that may be analogous to their organization in membranes, with the ultimate objective of identifying potential changes in oligomerization that would explain the alterations in function observed with specific P450–P450 interactions.

To explain the role of oligomerization in affecting the enzymatic function of drug-metabolizing P450s, it is proposed that the degree and the variability of P450 oligomerization represents a P450-specific equilibrium that is influenced by the conformational state of the protein. The conformational variability of most P450s (except CYP1A) is proposed to be distinguished by the open and closed states represented by CYP2B4 crystal structures (PDB: 1PO5 and PDB: 1SUO, respectively), with ligand-free CYP2B4 existing in the membrane in both states. In most cases, substrate binds to or triggers formation of the closed state. The exception to this trend would be cases such as that with CYP3A4 when large substrates are bound to the active site which in itself induces the open conformation of the enzyme.

The model maintains that each P450 displays a specific tendency to distribute to different proportions of P450–P450 associations that can be categorized as distal-to-distal, proximal-to-proximal, side-to-side, and side to either proximal or distal faces. Thus, interactions between different P450s cause a redistribution of each P450 to different proportions of each arrangement which is influenced by the tendency of the binding partner to adopt a specific arrangement. It is proposed that a functional effect is associated with a P450–P450 interaction when the interaction causes changes in the relative proportions (as compared to the proportions observed in homomeric reconstituted systems) of side-on; distal-to-distal; and proximal-to-proximal P450 arrangements. More specifically, an interaction with a P450 that favors distal-to-distal (e.g., CYP2D6, PDB: 2F9Q) or proximal-to-proximal (e.g., CYP1A2) arrangements would be expected to result in inhibition of P450s that participate in predominantly side-on interactions [e.g., CYP2B4 (**Figure 4**) and CYP2C19 (**Figure 8**)]. In conjunction, this has been shown to be the case for several P450–P450 interactions involving these P450s (Hazai and Kupfer, 2005; Reed et al., 2010; Kenaan et al., 2013).

This is not meant to imply that CYP2B4 and CYP2C19 only arrange in side-on interactions in the membrane. Clearly, the functional heterogeneity of CYP2B4 has been demonstrated (Davydov et al., 1985, 1995; Backes and Eyer, 1989) and may represent a mixture of distal-to-distal (and possibly proximal-to-proximal of the open form) in addition to the side-on interactions. Conformational changes caused by substrate binding would be predicted to alter the proportions of the P450 in each characteristic state of oligomerization. Interestingly, distal-to-proximal interactions were not observed in any of the mammalian structures although they have been reported for bacterial P450s (Ravichandran et al., 1993). This leads to the possibility that the arrangement of P450 units in multimers is not random. Thus, distal-to-distal and proximal-to-proximal interactions may be specific mechanisms that have evolved to regulate the activities of membrane-bound P450s.

For most P450s except CYP1A2, the open conformation of P450 appears to be uniquely associated with both proximal-to-proximal and the distal-to-distal dimeric interaction in which the F-helix of one binding partner intercalates with the active site of the interacting P450 (for simplicity, this will be referred to as the intercalated open-form dimer). As described above,

both of these open arrangements are inactive. CYP1A2 presents an unusual situation for the drug-metabolizing P450s because it is not thought to be able to adopt the open conformation. However, unlike most of the drug-metabolizing P450s, CYP1A2 can adopt the proximal-to-proximal arrangement when it is in the closed, substrate-binding conformation. For other drug metabolizing P450s, the proximal-to-proximal interaction has only been associated with crystal lattices of open form P450s. Thus, rearrangement of CYP1A2 from its proximal-to-proximal orientation to one associated with optimal catalytic activity upon its interaction with another P450 would stimulate CYP1A2 by increasing the total amount of "enzymatically active CYP1A2" and also by increasing the effective CPR:CYP1A2 ratio. Conversely, the P450 interacting with CYP1A2 may be inhibited because of the increased accessibility of CYP1A2 to the limiting concentrations of CPR. Inhibition may also occur if the affected P450 interacts as an open form in a proximal-to-proximal manner with CYP1A2.

Distal-to-distal interactions commonly observed in many P450 crystal structures in which the units of the P450 multimer interact on the periphery of the distal regions of P450s in the *closed* conformation are proposed to be impaired in substrate binding. The analogous membrane-bound CYP2C8 dimer has been proposed to be deficient in lipophilic substrate binding from the membrane (Hu et al., 2010). Changes in the relative amounts of this type of dimer may explain the functional interactions of CYP2C9-CYP2D6 (Subramanian et al., 2009); CYP2C9-CYP3A4 (Subramanian et al., 2010); and possibly CYP2E1-CYP2B4 (when a high concentration of CYP2E1 interacts with CYP2B4) (Kenaan et al., 2013). CYP inhibition in these instances is caused by an increase in the proportion of the affected P450 in the closed-form, distal-to-distal arrangement and a corresponding decrease in the proportion of enzyme involved in side-on interactions. Homotropic and heterotropic cooperation in metabolism by CYP3A4 have been related to this type of distal-to-distal dimer (Davydov et al., 2013) indicating a limitation in the ability of it to bind substrate until a putative access channel is opened by effector binding to a peripheral site on the adjoining distal regions of the dimer (Williams et al., 2004; Davydov et al., 2015).

The proposed equilibria actually can explain all of the reported functional effects of these interactions. For instance, changes in the proportion of a P450 in a quasi-irreversible proximal-to-proximal arrangement which are caused by interactions with another P450 can explain the functional effects involving modifications in CPR-binding capability. This also includes mechanisms implicating a change in the apparent k_{cat} as the positional change of the affected P450 would present more or less of the total enzyme population for interactions with CPR. Note, the heterocomplex would need to be stable in the presence of excess CPR like the CYP2C9-CYP2C19 complex in order for rigorous kinetic analysis to detect an apparent change in k_{cat}. The purported effects for the proximal-to-proximal interaction are believed to explain the reported functional interactions for homomeric CYP1A2 (Reed et al., 2012) and for those between CYP2C9-CYP2C19 (Hazai and Kupfer, 2005); CYP1A2-CYP2B4 (Backes et al., 1998); and CYP2E1-CYP2B4 (Kenaan et al., 2013).

In Fernando et al. (2008) three functional populations were identified in the study of the positional heterogeneity of P450–P450 complexes. One population responded to substrate by shifting rapidly to the high spin form and subsequently being reduced enzymatically to form the ferrous-CO complex. This could represent closed-form, side-on P450–P450 interactions fully capable of substrate and reductase binding ("HS+" in the Fernando study).

Another population did not shift to high spin upon addition of substrate and could not be reduced ("HS−" in previous study). This characteristic could actually be representative of the intercalated, open-formed P450 dimer and/or the open-form proximal-to-proximal dimer. Clearly, the proximal-to-proximal dimer would not be reducible given the fact that the dimer is physically unable to interact with CPR. Furthermore, if the dimerization limited conversion to the closed conformation, the proximal-to-proximal CYP2B4 dimer also would be expected to be intransigent to a substrate-induced spin state transition. The "HS−" population also could represent the open-form, intercalated dimer of CYP2B4 given the fact that it was thought to be incapable of *functionally* interacting with CPR (note, a putative opened-form dimer of CYP3A4 must be able to interact with CPR in order to metabolize large substrates) and substrate would not bind to the intercalated P450 dimer since the active site is blocked by the F-helix of the binding partner. In support of the possibility that the HS− population is represented (at least in part) by the intercalated dimer, the biphasicity of the pre-steady state reduction of CYP2B4 by CPR was explained by a model involving a slow equilibrium between two conformations that bind to CPR, but only one of which could be reduced (Backes and Eyer, 1989). Thus, these two groups of CYP2B4 would be consistent with P450 in side-on interactions and the open intercalated dimer of CYP2B4. It is important to note that both types of open-form dimerization may be a means to regulate P450 activities and may be related by a dynamic equilibrium. However, because of the constraints of the lipid membrane and the limitation imposed by the P450s being tethered by the amino terminal tail, trimeric quaternary structures comprised of both proximal-to-proximal and distal-to-distal arrangements do not appear to be possible. Thus, the two types of dimers are exclusive of one another.

The final population in the previous study consisted of low spin CYP3A4 that was slowly converted to high spin prior to enzymatic reduction ("HS_0"). Substrate binding was proposed to slowly shift the enzyme to the high spin/reducible form. This is fully consistent with our predicted properties of the closed-form distal-to-distal P450 complex as substrate binding is proposed to be limited for this population which would in turn, cause a slower spin state transition and subsequent reduction by the reductase. The Fernando study indicated that ANF (the allosteric activator of CYP3A4 that is believed to facilitate substrate binding by interaction at the peripheral effector site of the dimer) was shown to dramatically decrease the proportion of the HS_0 population. This would be expected if the peripheral binding by ANF facilitates substrate access to the active sites of these closed form CYP3A4 distal-to-distal dimers.

Although there has been significant progress on the topic of the functional effects of P450–P450 interactions, there is still

much more that is unknown than known about how these interactions influence catalytic activities and drug metabolism *in vivo*. For instance, of the roughly 40 possible binary P450–P450 interactions in liver that involve the major P450s in drug metabolism and of the approximately 1500 drugs that have been approved by the FDA (Kinch et al., 2014), only about 12 specific P450–P450 interactions related to the metabolism of approximately 30 substrates (many of which are not even drugs) have been studied (Reed and Backes, 2016). Another topic of relevance that needs to be explored is the study of tissue-specific P450–P450 interactions involving the unique assemblages of P450s expressed in each tissue and the consequent functional effects of these interactions.

In total, these findings suggest that heteromeric P450 association serves as a means to regulate specific P450-mediated drug metabolism *in vivo*. Only rigorous comparative studies will determine whether specific P450s preferentially interact. It is possible that all P450s have similar tendencies to interact with one another. If this is the case, identification of the P450s involved in the metabolism of specific drugs (information that is routinely obtained before phase I drug studies) will allow for the determination of specific P450–P450 interactions that influence metabolism of the given drug by the implicated P450. This information will be invaluable in pharmaceutical risk assessment and in pharmacokinetic evaluations of drug metabolism and disposition.

AUTHOR CONTRIBUTIONS

Substantial contributions to the conception or design of the work; or the acquisition, analysis, or interpretation of data for the work – JR and WB. Drafting the work or revising it critically for important intellectual content – JR and WB. Final approval of the version to be published – JR and WB. Agreement to be accountable for all aspects of the work in ensuring that questions related to the accuracy or integrity of any part of the work are appropriately investigated and resolved – JR and WB.

FUNDING

This work was supported by the National Institutes of Health Grants ES004344 and ES013648 from NIEHS, USPHS.

REFERENCES

Ahn, T., Guengerich, F. P., and Yun, C. H. (1998). Membrane insertion of cytochrome P450 1A2 promoted by anionic phospholipids. *Biochemistry* 37, 12860–12866. doi: 10.1021/bi980804f

Anzenbacher, P., and Anzenbacherová, E. (2001). Cytochromes P450 and metabolism of xenobiotics. *Cell Mol. Life Sci.* 58, 737–747. doi: 10.1007/PL00000897

Baas, B. J., Denisov, I. G., and Sligar, S. G. (2004). Homotropic cooperativity of monomeric cytochrome P450 3A4 in a nanoscale native bilayer environment. *Arch. Biochem. Biophys.* 430, 218–228. doi: 10.1016/j.abb.2004.07.003

Backes, W. L., Batie, C. J., and Cawley, G. F. (1998). Interactions among P450 enzymes when combined in reconstituted systems: formation of a 2B4-1A2 complex with a high affinity for NADPH-cytochrome P450 reductase. *Biochemistry* 37, 12852–12859. doi: 10.1021/bi980674a

Backes, W. L., and Eyer, C. S. (1989). Cytochrome P-450 LM2 reduction. Substrate effects on the rate of reductase-LM2 association. *J. Biol. Chem.* 264, 6252–6259.

Baylon, J. L., Lenov, I. L., Sligar, S. G., and Tajkhorshid, E. (2013). Characterizing the membrane-bound state of cytochrome P450 3A4: structure, depth of insertion, and orientation. *J. Am. Chem. Soc.* 135, 8542–8551. doi: 10.1021/ja4003525

Bennett, T. A., Key, T. A., Gurevich, V. V., Neubig, R., Prossnitz, E. R., and Sklar, L. A. (2001). Real-time analysis of G protein-coupled receptor reconstitution in a solubilized system. *J. Biol. Chem.* 276, 22453–22460. doi: 10.1074/jbc.M009679200

Bostick, C. D., Hickey, K. M., Wollenberg, L. A., Flora, D. R., Tracy, T. S., and Gannett, P. M. (2016). Immobilized cytochrome P450 for monitoring of P450-P450 interactions and metabolism. *Drug Metab. Dispos.* 44, 741–749. doi: 10.1124/dmd.115.067637

Bridges, A., Gruenke, L., Chang, Y. T., Vakser, I. A., Loew, G., and Waskell, L. (1998). Identification of the binding site on cytochrome P450 2B4 for cytochrome b5 and cytochrome P450 reductase. *J. Biol. Chem.* 273, 17036–17049. doi: 10.1074/jbc.273.27.17036

Brignac-Huber, L. M., Park, J. W., Reed, J. R., and Backes, W. L. (2016). Cytochrome P450 Organization and function are modulated by endoplasmic reticulum phospholipid heterogeneity. *Drug Metab. Dispos.* 44, 1859–1866. doi: 10.1124/dmd.115.068981

Cawley, G. F., Batie, C. J., and Backes, W. L. (1995). Substrate-dependent competition of different P450 isozymes for limiting NADPH-cytochrome P450 reductase. *Biochemistry* 34, 1244–1247. doi: 10.1021/bi00004a018

Cawley, G. F., Zhang, S., Kelley, R. W., and Backes, W. L. (2001). Evidence supporting the interaction of CYP2B4 and CYP1A2 in microsomal preparations. *Drug Metab. Dispos.* 29, 1529–1534.

Cojocaru, V., Balali-Mood, K., Sansom, M. S., and Wade, R. C. (2011). Structure and dynamics of the membrane-bound cytochrome P450 2C9. *PLoS Comput. Biol.* 7:e1002152. doi: 10.1371/journal.pcbi.1002152

Davydov, D. R. (2011). Microsomal monooxygenase as a multienzyme system: the role of P450-P450 interactions. *Exp. Opin. Drug Metab. Toxicol.* 7, 543–558. doi: 10.1517/17425255.2011.562194

Davydov, D. R., Davydova, N. Y., Sineva, E. V., and Halpert, J. R. (2015). Interactions among cytochromes P450 in microsomal membranes: oligomerization of cytochromes P450 2E1, 3A5, and 2E1 and its functional consequences. *J. Biol. Chem.* 290, 3850–3864. doi: 10.1074/jbc.M114.615443

Davydov, D. R., Davydova, N. Y., Sineva, E. V., Kufareva, I., and Halpert, J. R. (2013). Pivotal role of P450-P450 interactions in CYP3A4 allostery: the case of alpha-naphthoflavone. *Biochem. J.* 453, 219–230. doi: 10.1042/BJ20130398

Davydov, D. R., Deprez, E., Hoa, G. H., Knyushko, T. V., Kuznetsova, G. P., Koen, Y. M., et al. (1995). High-pressure-induced transitions in microsomal cytochrome P450 2B4 in solution: evidence for conformational inhomogeneity in the oligomers. *Arch. Biochem. Biophys.* 320, 330–344. doi: 10.1016/0003-9861(95)90017-9

Davydov, D. R., Fernando, H., Baas, B. J., Sligar, S. G., and Halpert, J. R. (2005). Kinetics of dithionite-dependent reduction of cytochrome P450 3A4: heterogeneity of the enzyme caused by its oligomerization. *Biochemistry* 44, 13902–13913. doi: 10.1021/bi0509346

Davydov, D. R., Kariakin, A. A., Petushkova, N. A., and Peterson, J. A. (2000a). Association of cytochromes P450 with their reductases: opposite sign of the electrostatic interactions in P450BM-3 as compared with the microsomal 2B4 system. *Biochemistry* 39, 6489–6497. doi: 10.1021/bi992936u

Davydov, D. R., Karyakin, A. V., Binas, B., Kurganov, B. I., and Archakov, A. I. (1985). Kinetic studies on reduction of cytochromes P-450 and b5 by dithionite. *Eur. J. Biochem.* 150, 155–159. doi: 10.1111/j.1432-1033.1985.tb09001.x

Davydov, D. R., Petushkova, N. A., Archakov, A. I., and Hoa, G. H. (2000b). Stabilization of P450 2B4 by its association with P450 1A2 revealed by high-pressure spectroscopy. *Biochem. Biophys. Res. Commun.* 276, 1005–1012. doi: 10.1006/bbrc.2000.3596

Davydov, D. R., Petushkova, N. A., Bobrovnikova, E. V., Knyushko, T. V., and Dansette, P. (2001). Association of cytochromes P450 1A2 and 2B4: are the interactions between different P450 species involved in the control of the

monooxygenase activity and coupling? *Adv. Exp. Med. Biol.* 500, 335–338. doi: 10.1007/978-1-4615-0667-6_53

Davydov, D. R., Rumfeldt, J. A., Sineva, E. V., Fernando, H., Davydova, N. Y., and Halpert, J. R. (2012). Peripheral ligand-binding site in cytochrome P450 3A4 located with fluorescence resonance energy transfer (FRET). *J. Biol. Chem.* 287, 6797–6809. doi: 10.1074/jbc.M111.325654

Davydov, D. R., Sineva, E. V., Sistla, S., Davydova, N. Y., Frank, D. J., Sligar, S. G., et al. (2010). Electron transfer in the complex of membrane-bound human cytochrome P450 3A4 with the flavin domain of P450BM-3: the effect of oligomerization of the heme protein and intermittent modulation of the spin equilibrium. *Biochim. Biophys. Acta* 1797, 378–390. doi: 10.1016/j.bbabio.2009.12.008

Davydov, D. R., Yang, Z., Davydova, N., Halpert, J. R., and Hubbell, W. L. (2016). Conformational mobility in cytochrome P450 3A4 explored by pressure-perturbation EPR spectroscopy. *Biophys. J.* 110, 1485–1498. doi: 10.1016/j.bpj.2016.02.026

Dean, W. L., and Gray, R. D. (1982). Hydrodynamic properties of monomeric cytochromes P-450LM2 and P-450LM4 in n-octylglucoside solution. *Biochem. Biophys. Res. Commun.* 107, 265–271. doi: 10.1016/0006-291X(82)91699-0

Denisov, I. G., Grinkova, Y. V., Baylon, J. L., Tajkhorshid, E., and Sligar, S. G. (2015). Mechanism of drug-drug interactions mediated by human cytochrome P450 CYP3A4 monomer. *Biochemistry* 54, 2227–2239. doi: 10.1021/acs.biochem.5b00079

Ekroos, M., and Sjogren, T. (2006). Structural basis for ligand promiscuity in cytochrome P450 3A4. *Proc. Natl. Acad. Sci. U.S.A.* 103, 13682–13687. doi: 10.1073/pnas.0603236103

Fernando, H., Davydov, D. R., Chin, C. C., and Halpert, J. R. (2007). Role of subunit interactions in P450 oligomers in the loss of homotropic cooperativity in the cytochrome P450 3A4 mutant L211F/D214E/F304W. *Arch. Biochem. Biophys.* 460, 129–140. doi: 10.1016/j.abb.2006.12.025

Fernando, H., Halpert, J. R., and Davydov, D. R. (2008). Kinetics of electron transfer in the complex of cytochrome P450 3A4 with the flavin domain of cytochrome P450BM-3 as evidence of functional heterogeneity of the heme protein. *Arch. Biochem. Biophys.* 471, 20–31. doi: 10.1016/j.abb.2007.11.020

French, J. S., Guengerich, F. P., and Coon, M. J. (1980). Interactions of cytochrome P-450, NADPH-cytochrome P-450 reductase, phospholipid, and substrate in the reconstituted liver microsomal enzyme system. *J. Biol. Chem.* 255, 4112–4119.

Greinert, R., Finch, S. A., and Stier, A. (1982). Cytochrome P-450 rotamers control mixed-function oxygenation in reconstituted membranes. Rotational diffusion studied by delayed fluorescence depolarization. *Xenobiotica* 12, 717–726. doi: 10.3109/00498258209038946

Grinkova, Y. V., Denisov, I. G., and Sligar, S. G. (2010). Functional reconstitution of monomeric CYP3A4 with multiple cytochrome P450 reductase molecules in Nanodiscs. *Biochem. Biophys. Res. Commun.* 398, 194–198. doi: 10.1016/j.bbrc.2010.06.058

Guengerich, F. P. (2001). Common and uncommon cytochrome P450 reactions related to metabolism and chemical toxicity. *Chem. Res. Toxicol.* 14, 611–650. doi: 10.1021/tx0002583

Guengerich, F. P. (2003). Cytochromes P450, drugs, and diseases. *Mol. Interv.* 3, 194–204. doi: 10.1124/mi.3.4.194

Guengerich, F. P. (2006). A malleable catalyst dominates the metabolism of drugs. *Proc. Natl. Acad. Sci. U.S.A.* 103, 13565–13566. doi: 10.1073/pnas.0606333103

Guengerich, F. P., and Holladay, L. A. (1979). Hydrodynamic characterization of highly purified and functionally active liver microsomal cytochrome P-450. *Biochemistry* 18, 5442–5449. doi: 10.1021/bi00591a029

Gut, J., Richter, C., Cherry, R. J., Winterhalter, K. H., and Kawato, S. (1982). Rotation of cytochrome P-450. II. Specific interactions of cytochrome P-450 with NADPH-cytochrome P-450 reductase in phospholipid vesicles. *J. Biol. Chem.* 257, 7030–7036.

Gut, J., Richter, C., Cherry, R. J., Winterhalter, K. H., and Kawato, S. (1983). Rotation of cytochrome P-450. Complex formation of cytochrome P-450 with NADPH-cytochrome P-450 reductase in liposomes demonstrated by combining protein rotation with antibody-induced cross-linking. *J. Biol. Chem.* 258, 8588–8594.

Hazai, E., Bikadi, Z., Simonyi, M., and Kupfer, D. (2005). Association of cytochrome P450 enzymes is a determining factor in their catalytic activity. *J. Comput. Aided Mol. Des.* 19, 271–285. doi: 10.1007/s10822-005-4995-4

Hazai, E., and Kupfer, D. (2005). Interactions between CYP2C9 and CYP2C19 in reconstituted binary systems influence their catalytic activity: possible rationale for the inability of CYP2C19 to catalyze methoxychlor demethylation in human liver microsomes. *Drug Metab. Dispos.* 33, 157–164. doi: 10.1124/dmd.104.001578

Houston, J. B., and Galetin, A. (2005). Modelling atypical CYP3A4 kinetics: principles and pragmatism. *Arch. Biochem. Biophys.* 433, 351–360. doi: 10.1016/j.abb.2004.09.010

Hu, G., Johnson, E. F., and Kemper, B. (2010). CYP2C8 exists as a dimer in natural membranes. *Drug Metab. Dispos.* 38, 1976–1983. doi: 10.1124/dmd.110.034942

Ibeanu, G. C., Ghanayem, B. I., Linko, P., Li, L., Pederson, L. G., and Goldstein, J. A. (1996). Identification of residues 99, 220, and 221 of human cytochrome P450 2C19 as key determinants of omeprazole activity. *J. Biol. Chem.* 271, 12496–12501. doi: 10.1074/jbc.271.21.12496

Iwase, T., Sakaki, T., Yabusaki, Y., Ohkawa, H., Ohta, Y., and Kawato, S. (1991). Rotation and interactions of genetically expressed cytochrome P-450IA1 and NADPH-cytochrome P-450 reductase in yeast microsomes. *Biochemistry* 30, 8347–8351. doi: 10.1021/bi00098a010

Jamakhandi, A. P., Kuzmic, P., Sanders, D. E., and Miller, G. P. (2007). Global analysis of protein-protein interactions reveals multiple CYP2E1-reductase complexes. *Biochemistry* 46, 10192–10201. doi: 10.1021/bi7003476

Johnson, E. F., and Stout, C. D. (2013). Structural diversity of eukaryotic membrane cytochrome p450s. *J. Biol. Chem.* 288, 17082–17090. doi: 10.1074/jbc.R113.452805

Kandel, S. E., and Lampe, J. N. (2014). Role of protein-protein interactions in cytochrome P450-mediated drug metabolism and toxicity. *Chem. Res. Toxicol.* 27, 1474–1486. doi: 10.1021/tx500203s

Kawato, S., Gut, J., Cherry, R. J., Winterhalter, K. H., and Richter, C. (1982). Rotation of cytochrome P-450. I. Investigations of protein-protein interactions of cytochrome P-450 in phospholipid vesicles and liver microsomes. *J. Biol. Chem.* 257, 7023–7029.

Kelley, R. W., Cheng, D., and Backes, W. L. (2006). Heteromeric complex formation between CYP2E1 and CYP1A2: evidence for the involvement of electrostatic interactions. *Biochemistry* 45, 15807–15816. doi: 10.1021/bi061803n

Kelley, R. W., Reed, J. R., and Backes, W. L. (2005). Effects of ionic strength on the functional interactions between CYP2B4 and CYP1A2. *Biochemistry* 44, 2632–2641. doi: 10.1021/bi0477900

Kenaan, C., Shea, E. V., Lin, H. L., Zhang, H., Pratt-Hyatt, M. J., and Hollenberg, P. F. (2013). Interactions between CYP2E1 and CYP2B4: effects on affinity for NADPH-cytochrome P450 reductase and substrate metabolism. *Drug Metab. Dispos.* 41, 101–110. doi: 10.1124/dmd.112.046094

Kinch, M. S., Haynesworth, A., Kinch, S. L., and Hoyer, D. (2014). An overview of FDA-approved new molecular entities: 1827-2013. *Drug Discov. Today* 19, 1033–1039. doi: 10.1016/j.drudis.2014.03.018

Koley, A. P., Buters, J. T., Robinson, R. C., Markowitz, A., and Friedman, F. K. (1995). CO binding kinetics of human cytochrome P450 3A4. Specific interaction of substrates with kinetically distinguishable conformers. *J. Biol. Chem.* 270, 5014–5018. doi: 10.1074/jbc.270.10.5014

Koley, A. P., Dai, R. K., Robinson, R. C., Markowitz, A., and Friedman, F. K. (1997). Differential interaction of erythromycin with cytochromes P450 3A1/2 in the endoplasmic reticulum: a CO flash photolysis study. *Biochemistry* 36, 3237–3241. doi: 10.1021/bi962110h

Koley, A. P., Robinson, R. C., and Friedman, F. K. (1996). Cytochrome P450 conformation and substrate interactions as probed by CO binding kinetics. *Biochimie* 78, 706–713. doi: 10.1016/S0300-9084(97)82528-X

Koley, A. P., Robinson, R. C., Markowitz, A., and Friedman, F. K. (1994). Kinetics of CO binding to cytochromes P450 in the endoplasmic reticulum. *Biochemistry* 33, 2484–2489. doi: 10.1021/bi00175a017

Korzekwa, K. R., Krishnamachary, N., Shou, M., Ogai, A., Parise, R. A., Rettie, A. E., et al. (1998). Evaluation of atypical cytochrome P450 kinetics with two-substrate models: evidence that multiple substrates can simultaneously bind to cytochrome P450 active sites. *Biochemistry* 37, 4137–4147. doi: 10.1021/bi9715627

Lynch, T., and Price, A. (2007). The effect of cytochrome P450 metabolism on drug response, interactions, and adverse effects. *Am. Fam. Physician* 76, 391–396.

McDougle, D. R., Baylon, J. L., Meling, D. D., Kambalyal, A., Grinkova, Y. V., Hammernik, J., et al. (2015). Incorporation of charged residues in the CYP2J2

F-G loop disrupts CYP2J2-lipid bilayer interactions. *Biochim. Biophys. Acta* 1848, 2460–2470. doi: 10.1016/j.bbamem.2015.07.015

McIntosh, P. R., and Freedman, R. B. (1980). Characteristics of a copper-dependent cross-linking reaction between two forms of cytochrome P-450 in rabbit-liver microsomal membranes. *Biochem. J.* 187, 227–237. doi: 10.1042/bj1870227

McIntosh, P. R., Kawato, S., Freedman, R. B., and Cherry, R. J. (1980). Evidence from cross-linking and rotational diffusion studies that cytochrome P450 can from molecular aggregates in rabbit-liver microsomal membranes. *FEBS Lett.* 122, 54–58. doi: 10.1016/0014-5793(80)80400-5

Miwa, G. T., West, S. B., Huang, M. T., and Lu, A. Y. H. (1979). Studies on the association of cytochrome P-450 and NADPH- cytochrome c reductase during catalysis in a reconstituted hydroxylating system. *J. Biol. Chem.* 254, 5695–5700.

Myasoedova, K. N., and Berndt, P. (1990). Cytochrome P-450LM2 oligomers in proteoliposomes. *FEBS Lett.* 275, 235–238. doi: 10.1016/0014-5793(90)81479-8

Myasoedova, K. N., and Tsuprun, V. L. (1993). Cytochrome P-450: hexameric structure of the purified LM4 form. *FEBS Lett.* 325, 251–254. doi: 10.1016/0014-5793(93)81083-C

Nelson, D. R. (2006). Cytochrome P450 nomenclature. *Methods Mol. Biol.* 320, 1–10.

Ozalp, C., Szczesna-Skorupa, E., and Kemper, B. (2005). Bimolecular fluorescence complementation analysis of cytochrome p450 2c2, 2e1, and NADPH-cytochrome p450 reductase molecular interactions in living cells. *Drug Metab. Dispos.* 33, 1382–1390. doi: 10.1124/dmd.105.005538

Ozalp, C., Szczesna-Skorupa, E., and Kemper, B. (2006). Identification of membrane-contacting loops of the catalytic domain of cytochrome P450 2C2 by tryptophan fluorescence scanning. *Biochemistry* 45, 4629–4637. doi: 10.1021/bi051372t

Pernecky, S. J., and Coon, M. J. (1996). N-terminal modifications that alter P450 membrane targeting and function. *Methods Enzymol.* 272, 25–34. doi: 10.1016/S0076-6879(96)72005-0

Pernecky, S. J., Larson, J. R., Philpot, R. M., and Coon, M. J. (1993). Expression of truncated forms of liver microsomal P450 cytochromes 2B4 and 2E1 in *Escherichia coli*: influence of NH2-terminal region on localization in cytosol and membranes. *Proc. Natl. Acad. Sci. U.S.A.* 90, 2651–2655. doi: 10.1073/pnas.90.7.2651

Petrek, M., Kosinova, P., Koca, J., and Otyepka, M. (2007). MOLE: a Voronoi diagram-based explorer of molecular channels, pores, and tunnels. *Structure* 15, 1357–1363. doi: 10.1016/j.str.2007.10.007

Petrek, M., Otyepka, M., Banas, P., Kosinova, P., Koca, J., and Damborsky, J. (2006). CAVER: a new tool to explore routes from protein clefts, pockets and cavities. *BMC Bioinformatics* 7:316. doi: 10.1186/1471-2105-7-316

Pochapsky, T. C., Kazanis, S., and Dang, M. (2010). Conformational plasticity and structure/function relationships in cytochromes P450. *Antioxid. Redox. Signal.* 13, 1273–1296. doi: 10.1089/ars.2010.3109

Ravichandran, K. G., Boddupalli, S. S., Hasermann, C. A., Peterson, J. A., and Deisenhofer, J. (1993). Crystal structure of hemoprotein domain of P450BM-3, a prototype for microsomal P450's. *Science* 261, 731–736. doi: 10.1126/science.8342039

Reed, J. R., and Backes, W. L. (2012). Formation of P450.*P450* complexes and their effect on P450 function. *Pharmacol. Ther.* 133, 299–310. doi: 10.1016/j.pharmthera.2011.11.009

Reed, J. R., and Backes, W. L. (2016). The functional effects of physical interactions involving cytochromes P450: putative mechanisms of action and the extent of these effects in biological membranes. *Drug Metab. Rev.* 48, 453–469. doi: 10.1080/03602532.2016.1221961

Reed, J. R., Connick, J. P., Cheng, D., Cawley, G. F., and Backes, W. L. (2012). Effect of Homomeric P450·P450 Complexes on P450 Function. *Biochem. J.* 446, 489–497. doi: 10.1042/BJ20120636

Reed, J. R., Eyer, M., and Backes, W. L. (2010). Functional interactions between cytochromes P450 1A2 and 2B4 require both enzymes to reside in the same phospholipid vesicle: evidence for physical complex formation. *J. Biol. Chem.* 285, 8942–8952. doi: 10.1074/jbc.M109.076885

Rietjens, I. M., Ancher, L. J., and Veeger, C. (1989). On the role of phospholipids in the reconstituted cytochrome P-450 system. A model study using dilauroyl and distearoyl glycerophosphocholine. *Eur. J. Biochem.* 181, 309–316. doi: 10.1111/j.1432-1033.1989.tb14725.x

Roberts, A. G., Cheesman, M. J., Primak, A., Bowman, M. K., Atkins, W. M., and Rettie, A. E. (2010). Intramolecular heme ligation of the cytochrome P450 2C9 R108H mutant demonstrates pronounced conformational flexibility of the B-C loop region: implications for substrate binding. *Biochemistry* 49, 8700–8708. doi: 10.1021/bi100911q

Sansen, S., Yano, J. K., Reynald, R. L., Schoch, G. A., Griffin, K. J., Stout, C. D., et al. (2007). Adaptations for the oxidation of polycyclic aromatic hydrocarbons exhibited by the structure of human P450 1A2. *J. Biol. Chem.* 282, 14348–14355. doi: 10.1074/jbc.M611692200

Schoch, G. A., Yano, J. K., Wester, M. R., Griffin, K. J., Stout, D., and Johnson, E. F. (2004). Structure of human microsomal cytochrome P450 2C8: evidence for a peripheral fatty acid binding site. *J. Biol. Chem.* 279, 9497–9503. doi: 10.1074/jbc.M312516200

Schwarz, D., Pirrwitz, J., and Ruckpaul, K. (1982). Rotational diffusion of cytochrome P-450 in the microsomal membrane-evidence for a clusterlike organization from saturation transfer electron paramagnetic resonance spectroscopy. *Arch. Biochem. Biophys.* 216, 322–328. doi: 10.1016/0003-9861(82)90217-X

Scott, E. E., He, Y. A., Wester, M. R., White, M. A., Chin, C. C., Halpert, J. R., et al. (2003). An open conformation of mammalian cytochrome P450 2B4 at 1.6-A resolution. *Proc. Natl. Acad. Sci. U.S.A.* 100, 13196–13201. doi: 10.1073/pnas.2133986100

Scott, E. E., Spatzenegger, M., and Halpert, J. R. (2001). A truncation of 2B subfamily cytochromes P450 yields increased expression levels, increased solubility, and decreased aggregation while retaining function. *Arch. Biochem. Biophys.* 395, 57–68. doi: 10.1006/abbi.2001.2574

Scott, E. E., White, M. A., He, Y. A., Johnson, E. F., Stout, C. D., and Halpert, J. R. (2004). Structure of mammalian cytochrome P450 2B4 complexed with 4-(4-chlorophenyl)imidazole at 1.9-A resolution: insight into the range of P450 conformations and the coordination of redox partner binding. *J. Biol. Chem.* 279, 27294–27301. doi: 10.1074/jbc.M403349200

Sevrioukova, I. F., Li, H., Zhang, H., Peterson, J. A., and Poulos, T. L. (1999). Structure of a cytochrome P450-redox partner electron-transfer complex. *Proc. Natl. Acad. Sci. U.S.A.* 96, 1863–1868. doi: 10.1073/pnas.96.5.1863

Shou, M., Dai, R., Cui, D., Korzekwa, K. R., Baillie, T. A., and Rushmore, T. H. (2001). A kinetic model for the metabolic interaction of two substrates at the active site of cytochrome P450 3A4. *J. Biol. Chem.* 276, 2256–2262. doi: 10.1074/jbc.M008799200

Sineva, E. V., Rumfeldt, J. A., Halpert, J. R., and Davydov, D. R. (2013). A large-scale allosteric transition in cytochrome P450 3A4 revealed by luminescence resonance energy transfer (LRET). *PLoS ONE* 8:e83898. doi: 10.1371/journal.pone.0083898

Subramanian, M., Low, M., Locuson, C. W., and Tracy, T. S. (2009). CYP2D6-CYP2C9 protein-protein interactions and isoform-selective effects on substrate binding and catalysis. *Drug Metab. Dispos.* 37, 1682–1689. doi: 10.1124/dmd.109.026500

Subramanian, M., Zhang, H., and Tracy, T. S. (2010). CYP2C9-CYP3A4 protein-protein interactions in a reconstituted expressed enzyme system. *Drug Metab. Dispos.* 38, 1003–1009. doi: 10.1124/dmd.109.030155

Szczesna-Skorupa, E., Mallah, B., and Kemper, B. (2003). Fluorescence resonance energy transfer analysis of cytochromes P450 2C2 and 2E1 molecular interactions in living cells. *J. Biol. Chem.* 278, 31269–31276. doi: 10.1074/jbc.M301489200

Tamburini, P. P., MacFarquhar, S., and Schenkman, J. B. (1986). Evidence of binary complex formations between cytochrome P-450, cytochrome b5, and NADPH-cytochrome P-450 reductase of hepatic microsomes. *Biochem. Biophys. Res. Commun.* 134, 519–526. doi: 10.1016/S0006-291X(86)80451-X

Tsalkova, T. N., Davydova, N. Y., Halpert, J. R., and Davydov, D. R. (2007). Mechanism of interactions of alpha-naphthoflavone with cytochrome P450 3A4 explored with an engineered enzyme bearing a fluorescent probe. *Biochemistry* 46, 106–119. doi: 10.1021/bi061944p

Tsuprun, V. L., Myasoedova, K. N., Berndt, P., Sograf, O. N., Orlova, E. V., Chernyak, V. Y., et al. (1986). Quaternary structure of the liver microsomal cytochrome P-450. *FEBS Lett.* 205, 35–40. doi: 10.1016/0014-5793(86)80861-4

Watanabe, J., Asaka, Y., Fujimoto, S., and Kanamura, S. (1993). Densities of NADPH-ferrihemoprotein reductase and cytochrome P-450 molecules in the endoplasmic reticulum membrane of rat hepatocytes. *J. Histochem. Cytochem.* 41, 43–49. doi: 10.1177/41.1.8417111

White, R. E., and Coon, M. J. (1980). Oxygen activation by cytochrome P-450. *Annu. Rev. Biochem.* 49, 315–356. doi: 10.1146/annurev.bi.49.070180.001531

Williams, P. A., Cosme, J., Sridhar, V., Johnson, E. F., and McRee, D. E. (2000a). Mammalian microsomal cytochrome P450 monooxygenase: structural adaptations for membrane binding and functional diversity. *Mol. Cell.* 5, 121–131. doi: 10.1016/S1097-2765(00)80408-6

Williams, P. A., Cosme, J., Sridhar, V., Johnson, E. F., and McRee, D. E. (2000b). Microsomal cytochrome P450 2C5: comparison to microbial P450s and unique features. *J. Inorg. Biochem.* 81, 183–190. doi: 10.1016/S0162-0134(00)00102-1

Williams, P. A., Cosme, J., Vinkovic, D. M., Ward, A., Angove, H. C., Day, P. J., et al. (2004). Crystal structures of human cytochrome P450 3A4 bound to metyrapone and progesterone. *Science* 305, 683–686. doi: 10.1126/science.1099736

Yano, J. K., Wester, M. R., Schoch, G. A., Griffin, K. J., Stout, C. D., and Johnson, E. F. (2004). The structure of human microsomal cytochrome P450 3A4 determined by X-ray crystallography to 2.05-A resolution. *J. Biol. Chem.* 279, 38091–38094. doi: 10.1074/jbc.C400293200

Zangar, R. C., Davydov, D. R., and Verma, S. (2004). Mechanisms that regulate production of reactive oxygen species by cytochrome P450. *Toxicol. Appl. Pharmacol.* 199, 316–331. doi: 10.1016/j.taap.2004.01.018

Zanger, U. M., and Schwab, M. (2013). Cytochrome P450 enzymes in drug metabolism: regulation of gene expression, enzyme activities, and impact of genetic variation. *Pharmacol. Ther.* 138, 103–141. doi: 10.1016/j.pharmthera.2012.12.007

Zhukov, A., and Ingelman-Sundberg, M. (1999). Relationship between cytochrome P450 catalytic cycling and stability: fast degradation of ethanol-inducible cytochrome P450 2E1 (CYP2E1) in hepatoma cells is abolished by inactivation of its electron donor NADPH-cytochrome P450 reductase. *Biochem. J.* 340 (Pt 2), 453–458. doi: 10.1042/0264-6021:3400453

Conflict of Interest Statement: The authors declare that the research was conducted in the absence of any commercial or financial relationships that could be construed as a potential conflict of interest.

frontiers in Pharmacology

ORIGINAL RESEARCH
published: 30 October 2017
doi: 10.3389/fphar.2017.00755

The Hinge Segment of Human NADPH-Cytochrome P450 Reductase in Conformational Switching: The Critical Role of Ionic Strength

Diana Campelo[1†], Thomas Lautier[2†], Philippe Urban[2], Francisco Esteves[1], Sophie Bozonnet[2], Gilles Truan[2] and Michel Kranendonk[1*]*

[1] Center for Toxicogenomics and Human Health (ToxOmics), Genetics, Oncology and Human Toxicology, NOVA Medical School, Faculdade de Ciências Médicas, Universidade Nova de Lisboa, Lisboa, Portugal, [2] LISBP, Université de Toulouse, CNRS, INRA, INSA, Toulouse, France

NADPH-cytochrome P450 reductase (CPR) is a redox partner of microsomal cytochromes P450 and is a prototype of the diflavin reductase family. CPR contains 3 distinct functional domains: a FMN-binding domain (acceptor reduction), a linker (hinge), and a connecting/FAD domain (NADPH oxidation). It has been demonstrated that the mechanism of CPR exhibits an important step in which it switches from a compact, closed conformation (locked state) to an ensemble of open conformations (unlocked state), the latter enabling electron transfer to redox partners. The conformational equilibrium between the locked and unlocked states has been shown to be highly dependent on ionic strength, reinforcing the hypothesis of the presence of critical salt interactions at the interface between the FMN and connecting FAD domains. Here we show that specific residues of the hinge segment are important in the control of the conformational equilibrium of CPR. We constructed six single mutants and two double mutants of the human CPR, targeting residues G240, S243, I245 and R246 of the hinge segment, with the aim of modifying the flexibility or the potential ionic interactions of the hinge segment. We measured the reduction of cytochrome *c* at various salt concentrations of these 8 mutants, either in the soluble or membrane-bound form of human CPR. All mutants were found capable of reducing cytochrome *c* yet with different efficiency and their maximal rates of cytochrome *c* reduction were shifted to lower salt concentration. In particular, residue R246 seems to play a key role in a salt bridge network present at the interface of the hinge and the connecting domain. Interestingly, the effects of mutations, although similar, demonstrated specific differences when present in the soluble or membrane-bound context. Our results demonstrate that the electrostatic and flexibility properties of the hinge segment are critical for electron transfer from CPR to its redox partners.

Keywords: diflavin reductase, protein dynamics, multidomain proteins, conformational exchange, electron transfer, protein–protein interaction

OPEN ACCESS

Edited by:
Ulrich M. Zanger,
Dr. Margarete Fischer-Bosch Institut für Klinische Pharmakologie (IKP), Germany

Reviewed by:
Rheem Totah,
University of Washington, United States
Dmitri R. Davydov,
Washington State University, United States
Gianfranco Gilardi,
Università degli Studi di Torino, Italy

****Correspondence:***
Gilles Truan
gilles.truan@insa-toulouse.fr
Michel Kranendonk
michel.kranendonk@nms.unl.pt

† These authors have contributed equally to this work.

Specialty section:
This article was submitted to Pharmacogenetics and Pharmacogenomics, a section of the journal Frontiers in Pharmacology

Received: *11 May 2017*
Accepted: *04 October 2017*
Published: *30 October 2017*

Citation:
Campelo D, Lautier T, Urban P, Esteves F, Bozonnet S, Truan G and Kranendonk M (2017) The Hinge Segment of Human NADPH-Cytochrome P450 Reductase in Conformational Switching: The Critical Role of Ionic Strength. Front. Pharmacol. 8:755. doi: 10.3389/fphar.2017.00755

INTRODUCTION

Monooxygenase enzymes occur in all kingdoms of life and cytochromes P450 (P450s) represent the largest superfamily of them (Lamb and Waterman, 2013; Munro et al., 2013). In mammals, microsomal P450s catalyze the oxidation of a wide variety of essential endogenous and xenobiotic compounds (Coon, 2005; Rendic and Guengerich, 2015) by a two-electron activation of molecular oxygen, whereby one atom of oxygen is inserted into the organic substrate and the other is reduced to water (Guengerich, 2007). The catalytic cycle of P450 enzymes depends on redox partners for electron delivery. The NADPH-cytochrome P450 reductase (CPR) is strictly required for the activity of microsomal P450s, while cytochrome b_5 can potentially be a donor molecule, albeit only for the second electron transfer step (Scott et al., 2016).

Human CPR, encoded by the *POR* gene, is a 78-kDa multidomain diflavin reductase that binds both FMN and FAD and is attached to the cytoplasmic side of the endoplasmic reticulum via a transmembrane segment at its N-terminus. The domains that bear the two cofactors are: a flavodoxin-like FMN-binding domain and a ferredoxin-$NADP^+$ reductase like FAD-binding domain. The third domain, called the hinge segment, links the FMN and the connecting/FAD domain. Electrons flow through CPR from NADPH to oxidized FAD as a hydride ion transfer to the FAD N5 atom, then, one by one, from the FAD to the FMN, then from the FMN hydroquinone to external acceptors, with the FMN cycling mainly between the hydroquinone and the blue semiquinone states (Murataliev et al., 1999).

Although studies of CPR have predominantly focused on its role in P450 catalysis, CPR also support electron transfer to other enzymes like heme oxygenase (Schacter et al., 1972), squalene epoxidase (Ono and Bloch, 1975), dehydrocholesterol reductase (Nishino and Ishibashi, 2000), and though not uniquely, cytochrome b_5, involved also in fatty acid desaturation and elongation reactions (Oshino et al., 1971). The determinants of this promiscuity in physiological acceptors are not yet known, however, they might indicate that the mechanisms of recognition of this heterogenic group of redox partners by CPR are probably not highly stringent.

The first X-ray diffraction studies on soluble rat CPR showed a surprising compact structure in which the distance of FAD to FMN was about 4 Å, the two isoalloxazine rings almost coplanar and some parts of the FMN domain tightly packed against the rest of the CPR protein (Wang et al., 1997). This conformation, referred thereafter as part of a locked state, was easily ascribed to the conformation allowing electron transfer from FAD to FMN. Several other X-ray structures of CPR displaying the same spatial organization were subsequently obtained (Lamb et al., 2006; Xia et al., 2011b; McCammon et al., 2016). This conformational state as obtained in crystals, also occurs in solution (Vincent et al., 2012). Furthermore, a CPR mutant in which the FMN domain was linked to the FAD domain via a disulfide bridge was competent for electron transfer to the FMN moiety, ultimately proving that the locked state is fit for the internal flavin electron transfer but is unable to reduce external cytochrome acceptors unless the disulfide bridge is reduced (Xia et al., 2011a). This led to the hypothesis that interdomain motions have to take place to render the FMN domain accessible to electron acceptors.

The crystal structure of a mutant CPR in which the hinge segment was shortened by deletion of four residues (ΔTGEE) shows three different molecules per asymmetric unit. In each of them, the FMN domain is in a different position, more and more distant from the rest of the protein, whereas their connecting and FAD-binding domains are strictly superimposable, demonstrating a marked reorientation of the FMN domain relative to the FAD domain (Hamdane et al., 2009). Another evidence for domain mobility has come from the structural study of a chimeric enzyme consisting of the FMN-binding domain of yeast CPR and the remainder of the molecule, including the hinge segment, from human CPR (Aigrain et al., 2009). This chimeric enzyme, which is active in NADPH reduction of cytochromes *c* and P450, displays a single, well-defined, molecule in the asymmetric unit. In this structure, the FMN domain is no longer making any interface with the connecting and FAD domains. Hence, large domain movements can happen in CPR (∼86 Å distance between the two flavins). Furthermore, the redox potential of the flavins exhibit changes that maybe attributed to this large conformational change (Aigrain et al., 2011). The various conformations in which the FMN domain is no longer making an interface with the FAD domain represent an ensemble of structures that can be designated as the unlocked state. SAXS studies on human CPR have also been crucial in demonstrating that, in solution, human CPR is in equilibrium between a closed, compact and a series of open, extended conformations (Ellis et al., 2009; Huang et al., 2013; Frances et al., 2015). The abovementioned mutant CPR containing a disulfide bond, though capable of NADPH-mediated ferricyanide reduction, is essentially incapable of supporting P450 activity unless the disulfide bond is reduced (Xia et al., 2011a). The ability of both flavin domains to move relatively back and forth from each other is thus a prerequisite for the FMN domain to interact with its physiological acceptors. However, the structural determinants that guide this conformational transition between open and closed forms, a process demonstrated to be essential for gating the interflavin electron transfer in CPR and thus to its redox partners, are still not fully identified.

It has long been known that electron transfer from CPR to cytochromes P450 displays a strong ionic strength dependency which demonstrated that the electron transfer complex between the CPR and a P450 is, beside hydrophobic interactions, strongly based on charge pair interactions (Tamburini and Schenkman, 1986; Nadler and Strobel, 1988, 1991; Davydov et al., 1996, 2000; Bridges et al., 1998). Most of these studies evidenced that ionic interactions between CPR and its redox partners were the major determinants of the salt effects on P450s activities and are reviewed in (Hlavica et al., 2003). However, we also demonstrated that the ionic strength effect on cytochrome *c* reduction by the soluble form of human CPR depends on the

Abbreviations: CPR, NADPH cytochrome P450 reductase; DCPIP, 2,6-dichlorophenolindophenol; FMN, flavin mononucleotide; FAD, flavin adenine dinucleotide; k_{obs}, observed rate constant; NOS, nitric oxide synthase; P450, cytochrome P450; WT, wild-type.

conformational equilibrium between the locked and unlocked states (Frances et al., 2015). From the comparative studies of the open conformation seen in the chimeric yeast-human CPR, two residues in the hinge, G240 and S243, were proposed to be important molecular determinants for the large conformational changes (Aigrain et al., 2009). Beside these two residues, I245 and R246 were also recently identified, in a molecular dynamics simulation study, as two essential residues of the hinge segment, forming a part of the conformational axis and involved in a rotational movement of the FMN domain relative to the rest of the protein (Sündermann and Oostenbrink, 2013). S243 and R246 were also found to display large chemical shifts during the change in the conformational equilibrium between the locked and unlocked states (Frances et al., 2015). Additionally, the hinge segment was also found to be directly controlling electron transfer to cytochrome *c* from the reductase domain of nNOS (Haque et al., 2007, 2012) as well as in CPR (Grunau et al., 2007).

In this work we have targeted four specific residues of the hinge segment indicated above, for site-directed mutagenesis to test their potential role in the conformational equilibrium of human CPR. By analyzing the salt-dependent changes of the cytochrome *c* reductase activity in the context of both soluble and membrane-bound forms of CPR, we propose several hypotheses on the role played by these residues on the transition between the locked to the unlocked state, and thus in the electron transfer mechanism of CPR.

MATERIALS AND METHODS

Reagents

Dichlorophenolindophenol (DCPIP) and potassium ferricyanide were from Fluka (Buchs, Switzerland). L-Arginine, ampicillin, kanamycin sulfate, chloramphenicol, cytochrome *c* (horse heart), isopropyl β-D-1-thiogalactopyranoside (dioxane-free), thiamine, glucose 6-phosphate, glucose 6-phosphate dehydrogenase, $NADP^+$ and NADPH were obtained from Sigma–Aldrich (St. Louis, MO, United States). Phenylmethanesulfonyl fluoride was purchased from Gerbu Biotechnik GmbH (Heidelberg, Germany). Bacto agar, Bacto peptone and Bacto tryptone were obtained from BD Biosciences (San Jose, CA, United States). Bacto yeast extract was obtained from Formedium (Norwich, England). A polyclonal antibody from rabbit serum raised against recombinant human CPR obtained from Genetex (Irvine, CA, United States) was used for immunodetection of the membrane-bound CPR, while the respective antibody used the in the case of the soluble form of the enzyme was obtained from Thermofisher Scientific (Waltham, MA, United States).

Construction and Cloning of the Different Mutants

Soluble Forms of Human CPR

Soluble CPR mutants, deleted of their first 44 N-terminal amino acids, were cloned by the Gibson method using a synthetic DNA fragment containing the desired mutation, with a compatible divergent PCR amplification of the plasmid pET15b expressing the soluble form of the human CPR, containing a N-terminal 6xHis tag. DNA sequencing confirmed the absence of any undesired mutations. The constructed plasmids were transformed into competent *Escherichia coli* BL21 (DE3) cells for expression.

Membrane-Bound Forms of Human CPR

Plasmid pLCM_POR (Kranendonk et al., 2008) was used for the expression of the membrane-bound, full-length forms of human CPR. Mutants containing alanine substitutions of residues I245 and R246 were initially obtained through standard site-directed mutagenesis, using the sub-cloning vector pUC_POR, containing the initial segment (1–1269 bp) of human POR cDNA comprising the FMN and hinge domains (based on National Center for Biotechnology Information sequence NM_000941, encoding the CPR consensus protein sequence (NP_000932)). The mutated segments were obtained from the different mutated pUC_POR plasmids, using *Eco*RI + *Aat*II restriction enzymes and cloned back into full-length CPR expression vector pLCM_POR. CPR mutants containing proline substitutions of residues G240, S243, I245 and R246 were obtained by the Gibson method using a synthetic DNA fragment containing the desired mutation and a compatible divergent PCR amplification of the plasmid pET15b expressing the soluble form of human CPR. The mutated gene fragments were sub-cloned in vector pUC_POR using Megaprimer PCR of whole plasmid (MegaWhop) (Miyazaki and Takenouchi, 2002), followed by *Dpn*I treatment. The mutated segments were obtained using *Eco*81I + *Sac*I restriction enzymes and cloned back into the CPR expression vector pLCM_POR. The different constructed pLCM_POR plasmids were transformed into DH5α *E. coli* cells for plasmid propagation. POR cDNA of plasmids was fully sequenced to confirm the introductions of the designed mutations and the absence of any undesired mutations. CPR mutants were expressed in *E. coli* BTC, using the specialized bi-plasmid system for co-expression of CPR with human CYPs (Duarte et al., 2005). The pLCM_POR and the CYP-void plasmid pCWΔ (Kranendonk et al., 2008) were transfected through standard electroporation procedures.

Protein Expression and Isolation

Soluble Forms of CPR

Protein expression in BL21 (DE3) cells was carried out at 29°C in Terrific Broth medium complemented with 1 $mg.l^{-1}$ riboflavin and 100 $\mu g.ml^{-1}$ ampicillin during 36 h (Frances et al., 2015). Cultures were spun down for 10 min at 7,200 *g* and suspended in 20 mM Na/K phosphate buffer pH 7.4 (buffer A). Cell lysis was achieved by 4 cycles of sonication (30 s of burst followed by intervals of 2 min for cooling) in buffer A containing a protease inhibitor cocktail (aprotinin 0.3 μM, leupeptin 1 μM, pepstatin A 1.5 μM, benzamidine 100 μM, metabisulfite 100 μM). Cell debris were removed by centrifugation at 8,200 *g* for 1 h at 4°C. His-tagged proteins were bound on a TALON polyhistidine-TAG Purification Resin (Clontech, Mountain View, CA, United States), equilibrated with buffer A, containing 0.25 M NaCl and 0.25 M KCl, washed with this equilibrium buffer and eluted with a 0.25 M imidazole step gradient. Imidazole was eliminated from the eluted fraction by sequential washes in

buffer A using a Vivaspin-15 centrifugal concentrator (Sartorius, Goettingen, Germany). The protein solution was stored at 4°C in buffer A, containing 1 μM of both FMN and FAD. Purity of the sample was determined by SDS–PAGE and examination of the 280/450 nm ratio measured by optical spectroscopy.

Membrane-Bound Forms of CPR

Expression of the full-length membrane bound CPR mutants was obtained in BTC bacteria and membrane fractions of the different strains were prepared and characterized for protein content as described previously (Marohnic et al., 2010; Palma et al., 2013). CPR content of membrane fractions was quantified by immunodetection against a standard curve of purified human, full-length WT CPR, using polyclonal rabbit anti-CPR primary antibody and biotin-goat anti-rabbit antibody in combination with the fluorescent streptavidin conjugate (WesternDot 625 Western Blot Kit; Invitrogen). Densitometry of CPR signals was performed using LabWorks 4.6 software (UVP, Cambridge, United Kingdom).

DCPIP and Ferricyanide Reduction Assay and Cytochrome *c* Reduction Microplate Assay

DCPIP and Ferricyanide Reduction

With DCPIP, assays were performed in 20 mM Tris-HCl buffer containing 1 mM EDTA, and various NaCl concentrations (from 50 mM up to 1.4 M), pH 7.4 at 25°C in the presence of 70 μM DCPIP. Initial rates were monitored at 600 nm using $\Delta\varepsilon_M = 21{,}000\ M^{-1}.cm^{-1}$. With ferricyanide, assays were performed in the same conditions as described above, but in the presence of 1 mM ferricyanide. Initial rates were monitored at 420 nm using $\Delta\varepsilon_M = 1{,}020\ M^{-1}cm^{-1}$.

Cytochrome *c* Reduction Activities

Initial experiments were performed with soluble CPR. Cytochrome *c* reductase activity was followed at 550 nm ($\Delta\varepsilon_M = 21{,}000\ M^{-1}.cm^{-1}$) with CPR concentrations ranging from 2 to 20 nM. In cuvette assays, cytochrome *c* (100 μM final) and NADPH (200 μM final) were mixed in 20 mM Tris-HCl buffer containing 1 mM EDTA, and various NaCl concentrations (from 50 mM up to 1.4 M), pH 7.4 at 25°C. The reaction was initiated by adding CPR. A set of preliminary rate assays were performed in a microtiter plate format to optimize linearity of the reaction traces for the mutants, with conditions close to the traditional cuvette approach. In particular, the concentrations of CPR, cytochrome *c* and NADPH were varied in several control experiments to ensure linearity. In these assays, CPR and NADPH (200 μM final) were mixed and the reaction was started by diluting directly this mix in microplate wells containing 20 mM Tris-HCl buffer pH 7.4, supplemented with cytochrome *c* (100 or 200 μM) and the *ad hoc* NaCl final concentration (from 50 mM to 1.25 M) at 37°C. The reaction was monitored at 550 nm for 5 min in a PowerWave X select microplate reader (Biotek Instruments, Winooski, VT, United States).

A first set of kinetic measurements was performed in triplicate using the two cytochrome *c* concentrations indicated above. A second set of triplicate experiments was repeated with another batch of purified CPR. Reduction velocities were found virtually equal when using cytochrome *c* at 100 or 200 μM (data not shown). Cytochrome *c* was subsequently used in the microplate format at 200 μM (final concentration) for all kinetic measurements. CPR samples (soluble forms) were diluted up to concentrations giving linear velocity traces to compensate for lower or increased velocities, see Supplementary Table S1. Each k_{obs} value is the average of six measurements: one triplicate using a first batch of enzyme and a second triplicate, using a second batch of purified CPR.

The conditions of the microplate rate assay were then verified for the membrane-bound CPRs, to ensure linearity of the reaction traces. Reactions were followed for 4 min in a multi-mode microtiter plate reader (SpectraMax®i3x, Molecular Devices) and each sample was assayed at least in triplicate. The optimal dilution of the membrane bound WT CPR was determined (0.5 pmol/ml), using 200 μM of cytochrome *c*, NADPH regenerating system (NADPH 200 μM, glucose 6-phosphate 500 μM and glucose 6-phosphate dehydrogenase 0.04 U/mL, final concentrations) and 372 mM NaCl in a 100 mM Tris buffer (pH 7.4). The same CPR dilution was applied in the cuvette assay under the same conditions except for cytochrome *c* (50 μM) and NADPH (200 μM, without regeneration) and was measured during 60 s, which resulted in virtually the same k_{obs} as with the microtiter plate format assay. Finally, the membrane bound mutants were assayed with CPR well-concentrations, proportionally diluted as those determined for the soluble forms (see Supplementary Table S1). Control experiments with *E. coli* (BTC) membranes without CPR expression demonstrated no cytochrome *c* reduction upon dilution.

RESULTS

Ionic Strength Dependency of the Electron Transfer of the Soluble Form of Human CPR to Three Artificial Acceptors

In order to further understand the role of the ionic strength in electron transfer from CPR to acceptors such as cytochrome *c* and discriminate between the two major hypotheses (salt-dependent conformational equilibrium or electrostatic interactions with the substrates), we analyzed and compared the ionic strength dependency of CPR toward DCPIP and ferricyanide with that of cytochrome *c*. DCPIP and ferricyanide have unique characteristics in term of charge and electron receiving capabilities (redox potential). **Figure 1** shows the activity profiles of the soluble, WT form of human CPR in function of the ionic strength for cytochrome *c*-, DCPIP- and ferricyanide-reduction.

Cytochrome *c* and DCPIP related graphs share the same bell-shaped curve. For cytochrome *c*, the concentration of NaCl giving the maximal k_{obs} is around 400 mM, a value quite comparable to the one measured in our previous study (Frances et al., 2015). However, the maximum of k_{obs} is different for DCPIP (575 mM). This difference might be attributed to the fact that DCPIP is an obligate two electrons (hydride) acceptor, which may have a different overall electron transfer scheme compared

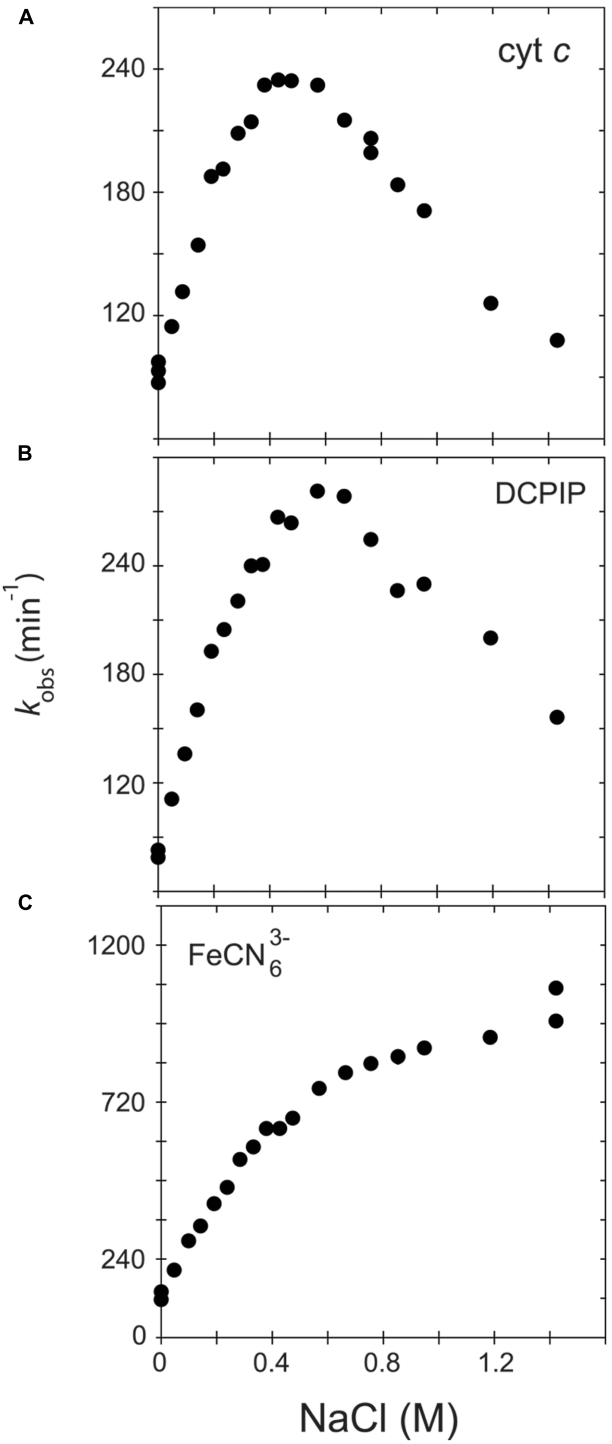

FIGURE 1 | Variation of k_{obs} in function of the ionic strength. The activity of the soluble, WT form of human CPR was assayed with various acceptors, namely cytochrome *c* **(A)**, DCPIP **(B)** or ferricyanide **(C)**.

to cytochrome *c*. The ionic strength dependent variation of k_{obs} measured for the reduction of DCPIP and cytochrome *c* by soluble human CPR display both a bell-shaped profile. However, these substrates are different in term of net charge (cytochrome *c* contains + 9.5 charges at pH 7.0 while DCPIP is neutral). This result thus strengthens the hypothesis that the ionic strength dependency of electron flow from CPR to acceptors is mainly determined by the conformational equilibrium between the locked and unlocked states of CPR and only in a minor manner by electrostatic interactions between the FMN domain and the acceptor.

We also analyzed the reduction of ferricyanide, another non-natural substrate. Interestingly, the salt-dependent k_{obs} profile is totally different from the ones seen with cytochrome *c* or DCPIP, being composed of two straight lines crossing at a NaCl concentration of around 450 mM. The constant rise of the k_{obs} might be attributed to a gradual increase of the redox potential of ferricyanide due to the increase of ionic strength in Tris-based buffers (O'Reilly, 1973). Therefore, the ferricyanide reduction, which mainly occurs at the FAD cofactor (Vermilion et al., 1981), may be relatively independent from the salt concentration and hence from the conformational equilibrium, a result that was previously observed with the ΔTGEE mutant (Hamdane et al., 2009). Interestingly, the inflection occurs around a salt concentration quite similar to the one yielding the maximum k_{obs} with cytochrome *c*. However, we do not have any coherent explanation for the peculiar salt profile observed with this substrate.

Based on these latter results, we decided to use cytochrome *c* reduction as an appropriate reporter to probe salt-mediated conformational equilibrium changes in electron transfer of specific CPR mutants.

Design of the Different Mutants

The hinge segment is defined by a stretch of 14–15 amino acids that does not display any particularly defined secondary structure. It is also the only part of the CPR structure where evident structural changes can be seen when comparing the two open conformations of CPR (crystallographic structures of the ΔTGEE mutant and the yeast/human chimera) and the other closed conformations of CPR (yeast, human, rat). Residues G240 and S243 (numbering according to the human CPR consensus amino acid sequence NP_000932) correspond to positions with strongly modified phi and psi angles between the closed and open forms (Aigrain et al., 2009). These two residues were therefore mutated into prolines in order to test if and how geometrical constraints modify the conformational equilibrium of CPR. Residues I245 and R246 were selected based on the observation that the backbone atoms of both residues were rotated in the ΔTGEE mutant or in the closed to open transition visualized by molecular modeling (Hamdane et al., 2009; Sündermann and Oostenbrink, 2013). For this last residue, we evidently switched the cationic Arg residue into a non-charged one (either Ala or Pro) while for the previous Ile residue, we preferred mutations affecting either the mobility/rigidity (Ile to Ala or Pro). Two double mutants, cumulating charge and flexibility changes were also designed for residues 245/246. Finally, as the physiological form of CPR is membrane-bound and the membrane anchoring segment may have a profound influence on the equilibrium between locked and unlocked states or the open-closed exchange

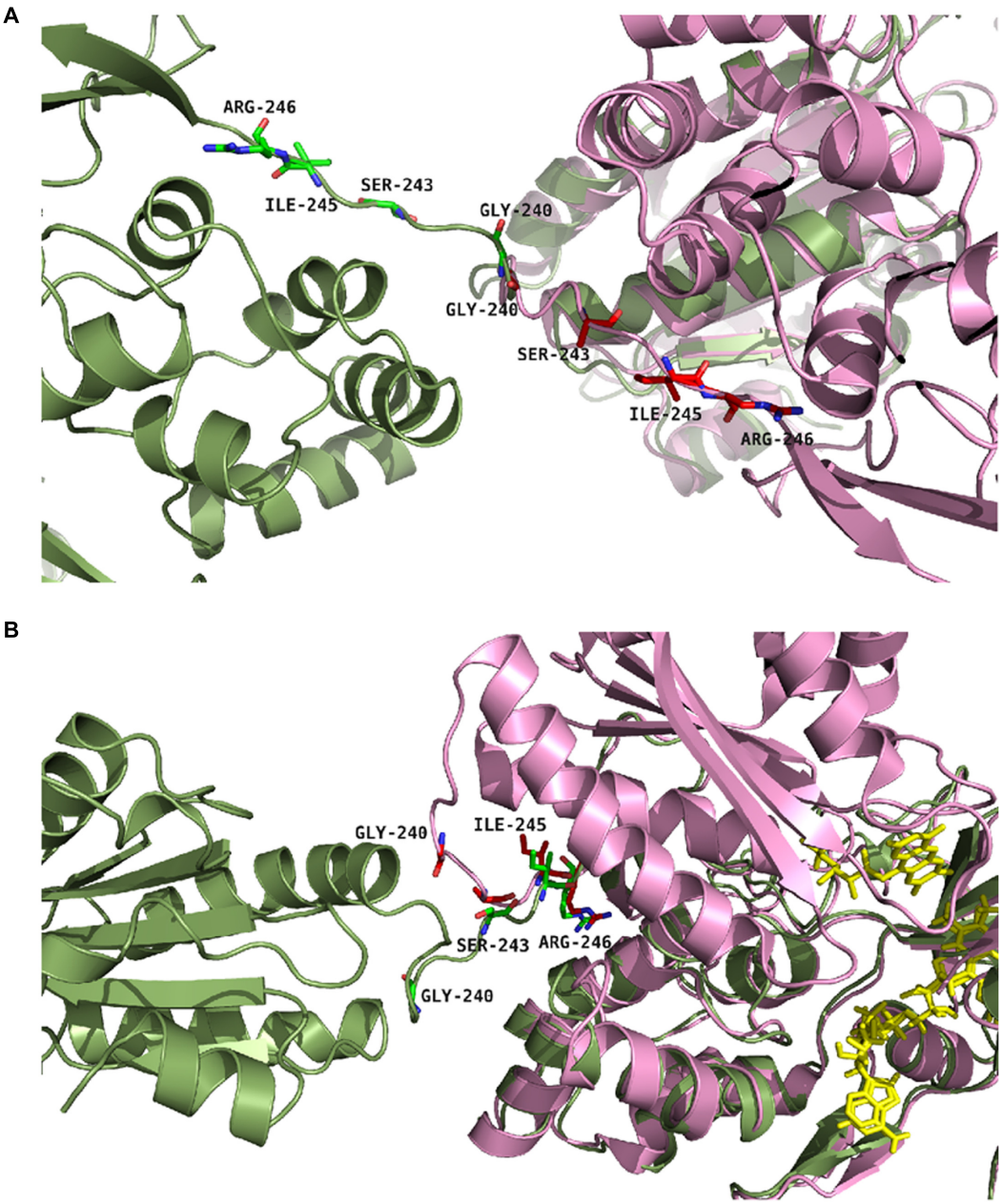

FIGURE 2 | Positions of the studied mutations in CPR. The structure of the yeast-human open form CPR chimera (3FJO, in dark green) and the WT soluble human closed form CPR (5FA6, chain A, in pink) were used to analyze the variations in the hinge segment between the closed and open form of CPR. Mutated residues are displayed as sticks of either green or magenta colors according to the structures. **(A)** Both structures were aligned onto their FMN domains. **(B)** Both structures were aligned onto their connecting/FAD domains. The figure was prepared using the PyMol software (Schrödinger, 2015).

rates, we analyzed the effects of these mutations in both the soluble and membrane bound context.

Based on these rationales, six single mutants (G240P, S243P, I245A, I245P, R246A and R246P) and two double mutants (I245A/R246A and I245R/R246I) were produced both in the soluble and membrane-bound (full-length) forms of CPR. **Figure 2** provides a representation of the positions of the four targeted amino acids in the structure of the closed conformation of human CPR (5FA6, chain A) and on the structure of the open conformation of the yeast/human chimeric CPR (3FJO). The two structures (5FA6, chain A and 3FJO) were aligned onto the FAD domain (**Figure 2A**) or the FMN domain (**Figure 2B**). Both views provide the rationale for the design of our mutants: G240 corresponds to the position where the hinge is tilted in the open conformation compared to the closed conformation (**Figure 2A**); S243 side chain orientation is different between the two forms

(**Figure 2A**); I245 and R246 show an interesting proximity and potential interaction with the connecting domain (**Figures 2A,B**).

Production of the Various Mutants of Human CPR

Soluble Forms

Eight different plasmids encoding the soluble CPR mutants G240P, S243P, I245A, I245P, R246A, R246P, I245A/R246A and I245R/R246I were introduced into *E. coli* and the various proteins expressed and purified as described in Section "Material and Methods." SDS−PAGE gel analysis shows that the different mutant proteins present the same profile than the wild type, with a major band just below 70 kDa which corresponds to the soluble form of the CPR (69 kDa). Biological duplication of the entire expression and purification stages was performed to ensure repeatability. Some discrete bands, at lower molecular weights compared to WT CPR were detected either with Coomassie staining or by western blot analysis (see Supplementary Figure S1), indicating some minor degradation of the purified enzymes. However, these represent less than 5% of the full-length soluble CPR and hence would have a minor impact on the kinetic assays. All CPR mutants presented the same absorbance spectra as the WT soluble enzyme, with a maximum of absorption at 450 nm, indicating no or minor changes in the chemical surrounding of both flavins. Last, all mutants were obtained in the semiquinone form, like the WT CPR, indicating no major changes in the absolute redox potential values of the flavins in the mutant forms. These results emphasize that the introduced mutations did not apparently modify the surroundings of the flavins.

Membrane-Bound Forms

The eight different mutants were introduced in the *E. coli* BTC strain, expressed and bacterial microsomes were isolated, as described previously (Kranendonk et al., 2008). No expression problems were encountered, except for mutant G240P for which the level of expression was substantially lower than for the other mutants. Immunodetection of CPR in isolated microsomes showed only trace amounts of the G240P mutant protein, not sufficient for subsequent analysis. Other CPR mutants demonstrated expression levels comparable with the WT form (see Supplementary Figure S1).

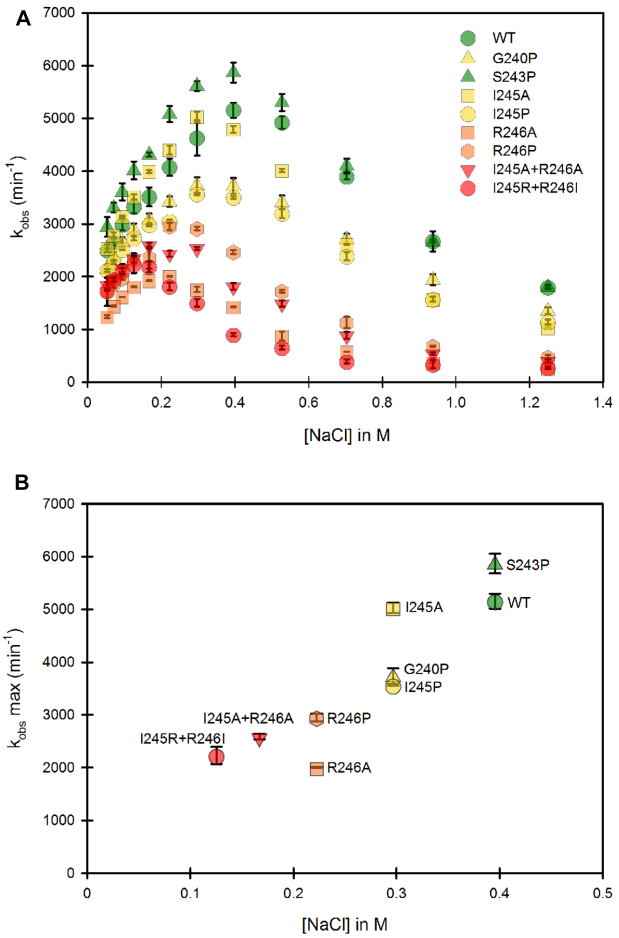

FIGURE 3 | Variation of the k_{obs} for cytochrome *c* reduction in function of the ionic strength for the WT and mutants of the soluble forms of human CPR. Cytochrome *c* reduction assays were performed in triplicate in 96 well microtiter plates as described in the Material and Methods section. **(A)** Salt dependent profile of the k_{obs} with the WT and the mutants. Symbols depicting the different mutants are included in the panel. **(B)** Maximal k_{obs} values were extracted from panel A and plotted as a function of the salt concentration. Symbols depicting the different mutants are identical as the ones in **(A)**. k_{obs} values represent the average of three replicates and the error bars depict the standard deviation.

Mutations Affect Differently the Soluble and Membrane-Bound Forms of CPR

Assay Conditions

Our study was designed to test the variation of cytochrome *c* reduction in various salt concentration conditions for nine CPR enzymes variants (WT + eight mutants) in the context of the soluble or membrane bound forms. We therefore developed and optimized a 96-well plate format assay to follow cytochrome *c* reduction. These experiments were performed at 37°C, contrarily to the primary test realized at room temperature in cuvette with the WT, soluble form of human CPR (**Figure 1**). Optimal conditions of the microplate rate assay were determined to ensure the linearity of the reaction traces. Initially, assays were performed at two cytochrome c concentrations (100 and 200 μM) in order to ensure that saturation was reached at all salt concentrations, which virtually gave the same velocities (data not shown). Subsequently cytochrome *c* was used at 200 μM. CPR concentrations in the tests were also optimized to obtain linear traces for each mutant (both for the soluble and membrane bound forms) in order to compensate for lower or higher activities (see Supplementary Table S1). We verified that salt profiles were equivalent between the tests performed in the cuvette and in the 96-well plate format (data not shown). **Figure 3A** displays the salt profile of the WT as well as mutants in the context of their soluble form at 37°C. Clearly the WT profile is superimposable to the one in **Figure 1**, although minor differences can be seen, notably for the concentration of salt that

gives the maximal value of k_{obs} (425 mM at 25°C instead of 395 mM at 37°C). This minor variation could be explained by the temperature shift from 25°C to 37°C, probably favoring the opening mechanism and therefore the unlocked state. Apart from this difference, no other changes were noted and the comparison of the salt profiles of the mutants either in their soluble or membrane bound forms was pursued at 37°C, with the 96 well plate assay format.

The Hinge Partly Controls the Conformational Equilibrium of the Soluble CPR Form

As mentioned earlier, the ionic strength dependency of cytochrome *c* reduction by CPR can be partly considered as a direct measure of the proportion of the locked *vs*. unlocked states (Frances et al., 2015) and the bell shaped curve of this ionic strength dependence has been also reported in the electron transfer from the flavodoxin of *Desulfovibrio vulgaris* to cytochrome b_{553} (Sadeghi et al., 2000). We therefore performed a full analysis of the ionic strength dependency of cytochrome *c* reduction for all single and double mutants (**Figure 3**). **Figure 3A** depicts the 8 different ionic strength profiles obtained with the various mutants compared with the WT one. All curves of the k_{obs} vs. ionic strength display the same typical bell shaped curve seen with the WT CPR. With the exception of the S243P mutant, all ionic strength profiles are shifted to the left (lower NaCl concentrations). Moreover, nearly all of them (except S243P and I245A) have lower maximal k_{obs} values. This result indicates that the various introduced mutations have pronounced effects either on the conformational equilibrium or the electron transfer efficiency, yet all of them are still active (lowest k_{obs} is 30% of the one observed with WT CPR). The redox potentials of both flavins and cytochrome *c* are known to depend to some extent on the ionic strength. While for cytochrome *c* these changes are known and relatively small (Gopal et al., 1988), it is difficult to predict the changes that would occur for the flavins. Based on our observation that the microenvironment of flavins is probably not significantly altered between mutants and WT CPR (equal absorption spectra) we have based our working hypotheses on the assumption that the redox potential of the flavins are not functionally different between the mutants and the WT soluble or membrane-bound forms of CPR.

From **Figure 3A**, maximal k_{obs} values were extracted and used to generate a graph comparing the salt concentration at which the maximum k_{obs} occur and the maximal k_{obs} value itself (**Figure 3B**). The case of S243P and I245A is interesting. Both have approximately the same k_{obs} (slightly higher than the WT for S243P). However, I245A denotes a clear difference in term of optimal ionic strength contrarily to S243P and WT. Another example is the situation for I245A, G240P and I245P, for which the optimal ionic strengths are identical yet the three mutants have different maximal k_{obs} values. Hence these data seem to indicate a separation between the efficiency of cytochrome *c* reduction and the conformational equilibrium of CPR (represented by the salt concentration at which the maximal k_{obs} occurs). However, globally, when the profiles are shifted to lower ionic strength the maximal k_{obs} values are lower.

The effects on the conformational equilibrium are interesting and merit further analysis. With the exception of S243P, all mutants either favored the unlocked state or destabilized the locked state. The introduction of a proline residue (G240P, I245P and R246P) probably imposes strong constraints on the hinge and may therefore stabilize discrete conformations of the unlocked state. The removal of the positive charge of the arginine residue at position 246 (R246A) may loosen the potential interactions between the hinge and the connecting domain and also destabilize the locked state. It should also be noted that the double mutants present the maximal displacements in term of salt profile and that the charge suppression at position 246 cannot be compensated by the introduction of an arginine at position 245 (see the double mutant I245R/R246I).

Lower maximal k_{obs} values are probably associated to some decrease in the rate constants of one or several electron transfer steps. We already demonstrated that conformational exchange occurs at a much faster rate than electron transfer (Frances et al., 2015). Hence, during the course of steady state activity, CPR opens and closes several times before electrons are transferred from FAD to FMN. This also means that the locked state might actually have several closed conformations, not all of them productive for inter-flavin electron transfer, a feature that has already been described (Hay et al., 2010). Therefore, the mutants might disfavor the occurrence of productive conformations in the locked state, hereby reducing the maximal k_{obs} value. Hence, although there would not be a direct relationship between conformational equilibrium and maximal k_{obs}, the effects of some of the mutations on the destabilization of the locked state could also change the rate limiting step.

The Hinge Controls the Conformational Equilibrium of the Membrane Bound CPR

The same mutants, when present in the full-length, membrane-anchored form, were subsequently studied. **Figure 4** presents the same analysis of both the variation of k_{obs} and the optimal ionic strength value for each of the mutants in the context of the membrane bound form. Our first striking result is that the ionic strength giving the maximum k_{obs} for the WT membrane bound form is shifted to higher salt concentrations compared to the WT soluble form, indicating a stronger interaction between the two domains (**Figure 4A**). Various hypotheses can be formulated to account for this fact. First, the presence of the negatively charged phospholipid heads of the membrane probably modifies the electrostatic potential around the FMN domain, potentially strengthening the interactions between the two flavin domains and thus favoring the equilibrium toward the locked state. Second, the presence of the membrane close to the FMN domain might impeach movements of the FAD domain compared to those attainable with the soluble form. This restriction of movement could favor the closing mechanism, hereby stabilizing the locked state.

Despite the above peculiarity of membranous CPR, **Figure 4A** shows that, as seen with the majority of the soluble forms, all mutants have their salt profiles shifted to lower ionic strengths when compared to the WT. This result confirms that

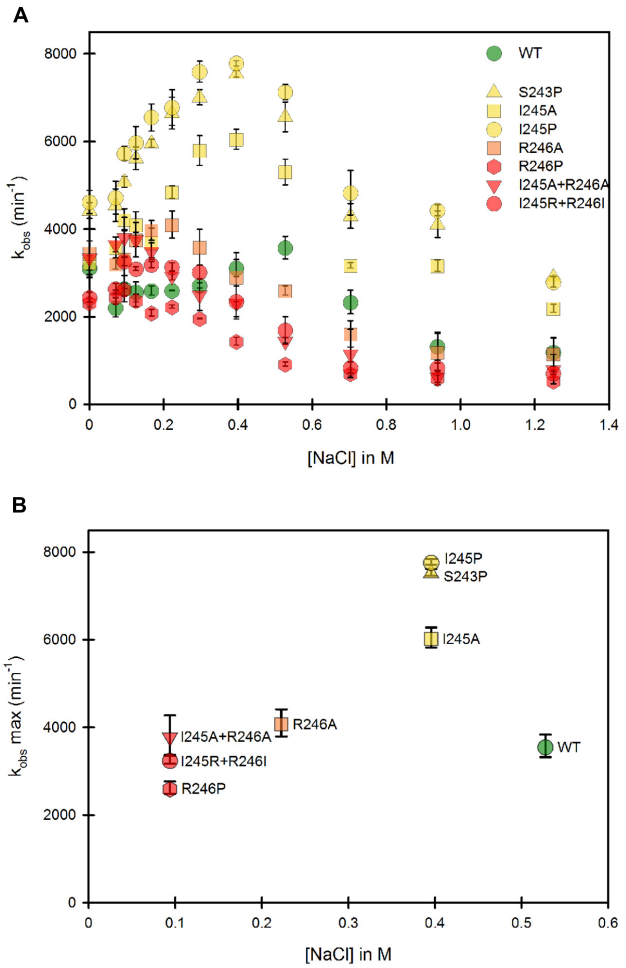

FIGURE 4 | Variation of the k_{obs} for cytochrome *c* reduction in function of the ionic strength for the WT and mutants of the membrane bound forms of human CPR. Cytochrome *c* reduction assays were performed in triplicate in 96 well microtiter plates as described in the Material and Methods section. **(A)** Salt dependent profile of the k_{obs} with the WT and the mutants. Symbols depicting the different mutants are included in the panel. **(B)** Maximal k_{obs} values were extracted from panel A and plotted as a function of the salt concentration. Symbols depicting the different mutants are identical as the ones in **(A)**. k_{obs} values represent the average of three replicates and the error bars depict the standard deviation.

the generated mutants have a greater tendency to favor the unlocked state, independently of the presence or absence of the membrane. Although differences exist between individual mutants depending on the context (soluble or membrane bound forms), again the maximal effects are seen with the R246 mutations and the double mutants containing mutations at the positions 246 and 245.

Maximal k_{obs} values were also extracted and plotted against the corresponding salt concentration (**Figure 4B**). Overall, the salt concentration at which k_{obs} is maximal covers a larger range with the membrane bound forms compared to the soluble forms. This indicates that the influence of salt on the conformational equilibrium is greater when CPR is attached to the membrane than when the various domains have more degree of liberty, i.e., when in the soluble form.

Interestingly, **Figure 4B** shows marked differences in the clustering of mutants compared to **Figure 3B**. This suggests again that the salt concentration giving the highest possible k_{obs} (1:1 proportion of locked/unlocked states) does not correlate with the value of the k_{obs} itself. This is particularly evident with the membrane-bound forms of the S243 and I245 mutants.

Some parallels can be drawn between mutants in the soluble and the membrane bound forms from comparison of **Figures 3B**, **4B**: (i) the group which had lower cytochrome *c* reduction rates in the soluble form (R246A, R246P, I245R/R246I and I245A/R246A) have almost the same k_{obs} than the WT in the membrane bound form and, (ii) the group that had similar cytochrome *c* reduction rates than the wild type in the soluble form (S243P, I245A and I245P), display a greater efficiency of electron transfer to cytochrome *c* in the membrane bound form.

DISCUSSION

The role of the hinge segment in diflavin reductase enzymes was studied both in NOS enzymes (Haque et al., 2007, 2012) and in CPR (Hamdane et al., 2009), using either lengthening or shortening of the primary sequence. Our study was designed to address the role of specific residues of the hinge segment of CPR (G240, S243, I245 and R246) without modifying its length. We have analyzed the salt-induced changes in the conformational equilibrium between the locked and unlocked states, via cytochrome *c* reduction, in the context of both the soluble and membrane-bound forms of CPR. In our first set of experiments using the soluble form of WT CPR, we compared the ionic strength profiles of the k_{obs} with three artificial substrates. Our results confirmed that the well-known salt dependency of either cytochrome *c* or P450 reductions (Voznesensky and Schenkman, 1992) can be mostly attributed to a change in the conformational equilibrium of CPR, between the locked state, non-competent in electron transfer to cytochrome *c* and the unlocked state capable of transferring electrons from the reduced FMN to acceptors. However, as explained in Section "The Hinge Partly Controls the Conformational Equilibrium of the Soluble CPR Form," we cannot rule out that the redox potentials of the flavins in the mutants forms of CPR are equivalent. Still, as mentioned before, the fact that the absorption spectra of the different WT and mutant CPRs are indistinguishable indicates that the chemical environment of the flavins is similar in all studied proteins. In the rest of the discussion, we therefore assumed that these redox potentials are equal between all CPR forms studied, bearing in mind that the various properties of the mutants (especially the rate constants) might, to some extent, be attributed to these putative redox potentials changes.

In the membrane bound form of WT CPR, the k_{obs} is lower than the one measured with the soluble form, a feature already seen upon solubilization of CPR (Phillips and Langdon, 1962). A possible explanation is a potential restrictive access of cytochrome *c* to the FMN domain caused by the membrane, giving rise to the observed differences between the effects of

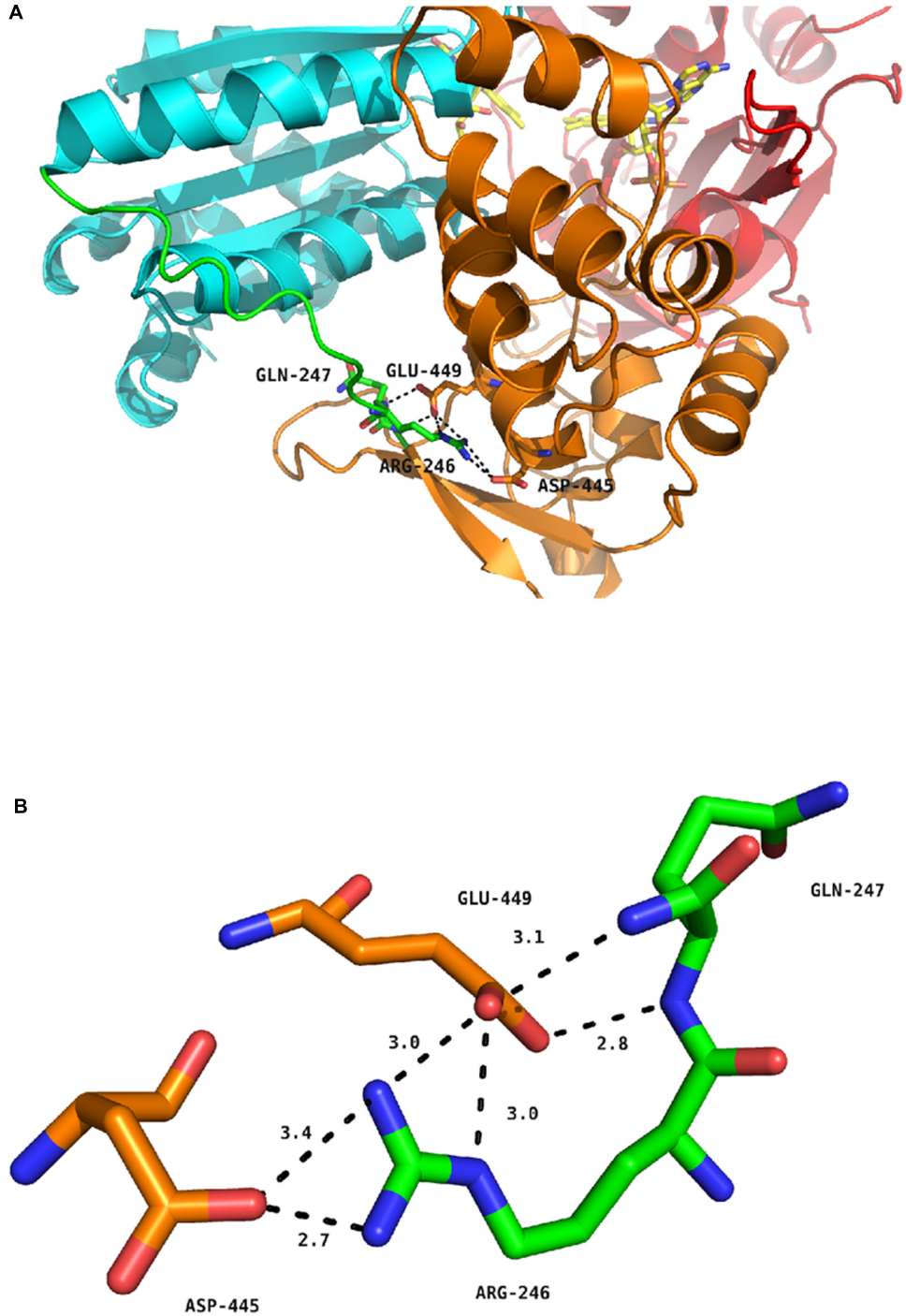

FIGURE 5 | Hydrogen bond network around residue R246 of human CPR. **(A)** Position of R246, Q247, D445 and E449 in the structure of the soluble form of WT human CPR. The color coding is as follows: FMN domain, cyan; hinge segment, green; connecting domain, orange; FAD domain, red. Flavins are depicted in yellow sticks, the various positions as stick in the same color code of the domain to which they belong. **(B)** Detailed view of the hydrogen bonding network. The color coding is the same as in **(A)**.

mutations when present in the soluble or membrane bound forms. Interestingly, none of the introduced mutations were capable of completely abolishing the CPR electron transfer to cytochrome *c* but rather displayed several intermediate features, either changing the salt profile or the efficiency of electron transfer, or both. We thus hypothesize that the targeted positions, although important, are only a part of the structural determinants promoting the conformational exchange between the locked and

unlocked states. It is also worth noting that the ionic strength profiles obtained with all mutant forms (soluble and membrane-bound, except for the soluble form of the S243P mutant) were shifted to lower salt concentrations compared to that of the WT CPR. This clearly indicates that the majority of changes that were introduced displaced the equilibrium toward the unlocked state. This is not completely surprising for the mutations that potentially enhance the flexibility (I245A) or removed salt bridges between the hinge and the connecting domain (R246A). However, for the mutations introducing proline residues in the hinge (G240P, S243P, I245P, R246P) the shift in the ionic strength profile might indicate that rigidifying these positions could result either in the destabilization of the locked state or the stabilization of the unlocked state. Still, the maintenance of a rather effective cytochrome *c* reduction in all cases might indicate that the loss of flexibility in the mutants bearing a proline residue may also be partly compensated by the hinge flexibility involving residues at other positions.

The second interesting feature of our mutants is that we can separate the ionic strength profile from the efficiency of the electron transfer to cytochrome *c*, i.e., there is no evident direct relationship between the salt concentration at which k_{obs} is maximal and the value of k_{obs} itself (**Figures 3B**, **4B**). Thus, in our conditions, the rate limiting steps remain independent of the conformational equilibrium. The conformational exchange frequency between the locked and unlocked states is at minimum 600 s^{-1} (Frances et al., 2015), a value 10 times greater than the k_{obs} observed with cytochrome *c* and coherent with the one determined by Haque et al. (2014). This also means that the locked state might actually have several closed conformations, not all of them productive for inter-flavin electron transfer, a feature that has already been described (Hay et al., 2010). Hence, there would not be a direct relationship between conformational equilibrium and maximal k_{obs} and the effects of our introduced mutations, destabilization of the locked state, could also affect the rate limiting step giving rise to either equal, lower or higher k_{obs} values compared to the WT forms.

In the soluble form of human CPR, only the S243P and possibly the I245A mutations have no effect on the rate of cytochrome *c* reduction. However, in the membrane bound form, these two mutants, along with I245P, present cytochrome *c* reduction rates higher than the WT form, and higher than the soluble counterparts. To our knowledge, this is the first report of k_{obs} values up to 8,000 min^{-1} for electron transfer to cytochrome *c* with CPR. However, these features were already observed in some mutants affecting the charge pairing between the FMN and FAD domains of nNOS (Haque et al., 2013) and in a C-terminal-truncated version of murine iNOS in which cytochrome *c* reduction attained 31,467 min^{-1} (Roman et al., 2000). In the nNOS mutants, the increase of k_{obs} for cytochrome *c* reduction was attributed to a change of the conformational behavior. However, in our case, the maximal k_{obs} was determined at a salt concentration where the conformational equilibrium corresponds to a 1:1 ratio of locked/unlocked states, as we demonstrated before (Frances et al., 2015). Therefore, the high maximal k_{obs} values observed in the mutants may be attributed to a change in the FAD to FMN electron transfer rate limiting step, because, in the case of cytochrome *c* reduction by CPR, this step is considered the slowest. Still, it should be reminded here that natural redox partners of CPR such as microsomal P450, may have specific structural requisites to bind CPR and form productive electron-transfer complexes with its membrane anchored redox partners, a situation evidently different with soluble partners such as cytochrome *c*. The differences in our results for the soluble and membrane-bound forms seem to indicate that residues S243 and I245 of human CPR are playing a role in this specific aspect.

Figure 5 depicts the position of the R246 amino acid in the structure of the WT, soluble form of human CPR (McCammon et al., 2016). The R246 is in close contact with two acidic residues (D445 and E449) present in the connecting domain (**Figure 5A**). Mutations at position 246 abolish a charge pairing with these two acidic residues. The distances of the three nitrogen atoms of R246 (NE, NH1 and NH2) with both terminal oxygens of D445 and E449 and the carbonyl oxygen of D445 are compatible with hydrogen bonds (**Figure 5B**). Furthermore, one terminal oxygen atom of E449 is also in a distance compatible to form a hydrogen bond with the amide nitrogen atom of Q247. This relatively strong hydrogen bonding network is evidently disrupted in the mutants changing R246 into any non-charged residue. The addition of a charge at the previous residue (in the double mutant I245R/R246I) does not restore the WT phenotype because I245 side-chain is clearly not oriented favorably in order to substitute for R246 in the complex hydrogen bonding network. This result is reminiscent of the mutations analyzed by Shen and coworkers demonstrating a similar shift in the salt profile when removing potential ionic interactions between the FMN and the connecting domains by mutating E216 into a glutamine residue (Shen and Kasper, 1995). Our results thus demonstrate that the hinge segment also actively participates in the construction of the FMN/FAD interface. When the loss of critical ionic interactions modifies the equilibrium between the locked and unlocked states, the ionic strength at which the maximal value of k_{obs} occurs is evidently lower, yet the maximum k_{obs} value may remain roughly constant, as demonstrated by several of the mutant CPRs.

A final remark should be made concerning the salt concentration at which the maximal k_{obs} was observed for the WT, membrane bound form of CPR, which is around 500 mM NaCl. It is clear that the ionic strength at this salt concentration is much higher than the physiological one, 154 mM KCl (physiological serum). As such it seems that the conformational equilibrium of CPR, *in vivo*, is probably in favor of the locked state, thereby reinforcing the idea of an external trigger for opening CPR (Grunau et al., 2006, 2007), such as the presence of membrane-bound P450s which are physiologically outnumbering CPR molecules by a factor of 5–10 in the liver. How this competition for CPR is affected by the conformational equilibrium is still an open and intriguing question.

AUTHOR CONTRIBUTIONS

Experimental design: all authors; experimental work: DC, TL, PU, FE, and SB; data analysis and interpretation: all authors; writing,

reviewing and editing of the manuscript: all authors; funding acquisition: GT and MK.

FUNDING

This work was in part funded by a joint ANR/FCT program; France: ANR-13-ISV5-0001 (DODYCOEL), and Portuguese national funds, through the *Fundação para a Ciência e a Tecnologia* (Project FCT-ANR/BEX-BCM/0002/2013).

ACKNOWLEDGMENT

We are grateful to Solène Galinier for technical assistance on the CPR soluble form enzymatic assays.

SUPPLEMENTARY MATERIAL

The Supplementary Material for this article can be found online at: https://www.frontiersin.org/articles/10.3389/fphar.2017.00755/full#supplementary-material

REFERENCES

Aigrain, L., Pompon, D., Moréra, S., and Truan, G. (2009). Structure of the open conformation of a functional chimeric NADPH cytochrome P450 reductase. *EMBO Rep.* 10, 742–747. doi: 10.1038/embor.2009.82

Aigrain, L., Pompon, D., and Truan, G. (2011). Role of the interface between the FMN and FAD domains in the control of redox potential and electronic transfer of NADPH–cytochrome P450 reductase. *Biochem. J.* 435, 197–206. doi: 10.1042/BJ20101984

Bridges, A., Gruenke, L., Chang, Y.-T., Vakser, I. A., Loew, G., and Waskell, L. (1998). Identification of the binding site on cytochrome P450 2B4 for cytochrome b 5 and cytochrome P450 reductase. *J. Biol. Chem.* 273, 17036–17049. doi: 10.1074/jbc.273.27.17036

Coon, M. J. (2005). Cytochrome P450: nature's most versatile biological catalyst. *Annu. Rev. Pharmacol. Toxicol.* 45, 1–25. doi: 10.1146/annurev.pharmtox.45.120403.100030

Davydov, D. R., Kariakin, A. A., Petushkova, N. A., and Peterson, J. A. (2000). Association of cytochromes P450 with their reductases: opposite sign of the electrostatic interactions in P450BM-3 as compared with the microsomal 2B4 system. *Biochemistry* 39, 6489–6497. doi: 10.1021/bi992936u

Davydov, D. R., Knyushko, T. V., Kanaeva, I. P., Koen, Y. M., Samenkova, N. F., Archakov, A. I., et al. (1996). Interactions of cytochrome P450 2B4 with NADPH-cytochrome P450 reductase studied by fluorescent probe. *Biochimie* 78, 734–743. doi: 10.1016/S0300-9084(97)82531-X

Duarte, M. P., Palma, B. B., Laires, A., Oliveira, J. S., Rueff, J., and Kranendonk, M. (2005). *Escherichia coli* BTC, a human cytochrome P450 competent tester strain with a high sensitivity towards alkylating agents: involvement of alkyltransferases in the repair of DNA damage induced by aromatic amines. *Mutagenesis* 20, 199–208. doi: 10.1093/mutage/gei028

Ellis, J., Gutierrez, A., Barsukov, I. L., Huang, W.-C., Grossmann, J. G., and Roberts, G. C. K. (2009). Domain motion in cytochrome P450 reductase: conformational equilibria revealed by NMR and small-angle x-ray scattering. *J. Biol. Chem.* 284, 36628–36637. doi: 10.1074/jbc.M109.054304

Frances, O., Fatemi, F., Pompon, D., Guittet, E., Sizun, C., Pérez, J., et al. (2015). A well-balanced preexisting equilibrium governs electron flux efficiency of a multi-domain diflavin reductase. *Biophys. J.* 108, 1527–1536. doi: 10.1016/j.bpj.2015.01.032

Gopal, D., Wilson, G. S., Earl, R. A., and Cusanovich, M. A. (1988). Cytochrome c: ion binding and redox properties. Studies on ferri and ferro forms of horse, bovine, and tuna cytochrome c. *J. Biol. Chem.* 263, 11652–11656.

Grunau, A., Geraki, K., Grossmann, J. G., and Gutierrez, A. (2007). Conformational dynamics and the energetics of protein-ligand interactions: role of interdomain loop in human cytochrome P450 reductase†. *Biochemistry* 46, 8244–8255. doi: 10.1021/bi700596s

Grunau, A., Paine, M. J., Ladbury, J. E., and Gutierrez, A. (2006). Global effects of the energetics of coenzyme binding: NADPH controls the protein interaction properties of human cytochrome P450 reductase†. *Biochemistry* 45, 1421–1434. doi: 10.1021/bi052115r

Guengerich, F. P. (2007). Mechanisms of cytochrome P450 substrate oxidation: MiniReview. *J. Biochem. Mol. Toxicol.* 21, 163–168. doi: 10.1002/jbt.20174

Hamdane, D., Xia, C., Im, S.-C., Zhang, H., Kim, J.-J. P., and Waskell, L. (2009). Structure and function of an NADPH-cytochrome P450 oxidoreductase in an open conformation capable of reducing cytochrome P450. *J. Biol. Chem.* 284, 11374–11384. doi: 10.1074/jbc.M807868200

Haque, M. M., Bayachou, M., Tejero, J., Kenney, C. T., Pearl, N. M., Im, S.-C., et al. (2014). Distinct conformational behaviors of four mammalian dual-flavin reductases (cytochrome P450 reductase, methionine synthase reductase, neuronal nitric oxide synthase, endothelial nitric oxide synthase) determine their unique catalytic profiles. *FEBS J.* 281, 5325–5340. doi: 10.1111/febs.13073

Haque, M. M., Fadlalla, M. A., Aulak, K. S., Ghosh, A., Durra, D., and Stuehr, D. J. (2012). Control of electron transfer and catalysis in neuronal nitric-oxide synthase (nNOS) by a hinge connecting its FMN and FAD-NADPH domains. *J. Biol. Chem.* 287, 30105–30116. doi: 10.1074/jbc.M112.339697

Haque, M. M., Panda, K., Tejero, J., Aulak, K. S., Fadlalla, M. A., Mustovich, A. T., et al. (2007). A connecting hinge represses the activity of endothelial nitric oxide synthase. *Proc. Natl. Acad. Sci. U.S.A.* 104, 9254–9259. doi: 10.1073/pnas.0700332104

Haque, M. M., Tejero, J., Bayachou, M., Wang, Z.-Q., Fadlalla, M., and Stuehr, D. J. (2013). Thermodynamic characterization of five key kinetic parameters that define neuronal nitric oxide synthase catalysis. *FEBS J.* 280, 4439–4453. doi: 10.1111/febs.12404

Hay, S., Brenner, S., Khara, B., Quinn, A. M., Rigby, S. E. J., and Scrutton, N. S. (2010). Nature of the energy landscape for gated electron transfer in a dynamic redox protein. *J. Am. Chem. Soc.* 132, 9738–9745. doi: 10.1021/ja1016206

Hlavica, P., Schulze, J., and Lewis, D. F. V. (2003). Functional interaction of cytochrome P450 with its redox partners: a critical assessment and update of the topology of predicted contact regions. *J. Inorg. Biochem.* 96, 279–297. doi: 10.1016/S0162-0134(03)00152-1

Huang, W.-C., Ellis, J., Moody, P. C. E., Raven, E. L., and Roberts, G. C. K. (2013). Redox-linked domain movements in the catalytic cycle of cytochrome P450 reductase. *Structure* 21, 1581–1589. doi: 10.1016/j.str.2013.06.022

Kranendonk, M., Marohnic, C. C., Panda, S. P., Duarte, M. P., Oliveira, J. S., Masters, B. S. S., et al. (2008). Impairment of human CYP1A2-mediated xenobiotic metabolism by Antley-Bixler syndrome variants of cytochrome P450 oxidoreductase. *Arch. Biochem. Biophys.* 475, 93–99. doi: 10.1016/j.abb.2008.04.014

Lamb, D. C., Kim, Y., Yermalitskaya, L. V., Yermalitsky, V. N., Lepesheva, G. I., Kelly, S. L., et al. (2006). A second FMN binding site in yeast NADPH-cytochrome P450 reductase suggests a mechanism of electron transfer by diflavin reductases. *Structure* 14, 51–61. doi: 10.1016/j.str.2005.09.015

Lamb, D. C., and Waterman, M. R. (2013). Unusual properties of the cytochrome P450 superfamily. *Philos. Trans. R. Soc. Lond. B. Biol. Sci.* 368:20120434. doi: 10.1098/rstb.2012.0434

Marohnic, C. C., Panda, S. P., McCammon, K., Rueff, J., Masters, B. S. S., and Kranendonk, M. (2010). Human cytochrome P450 oxidoreductase deficiency caused by the Y181D mutation: molecular consequences and rescue of defect. *Drug Metab. Dispos.* 38, 332–340. doi: 10.1124/dmd.109.030445

McCammon, K. M., Panda, S. P., Xia, C., Kim, J.-J. P., Moutinho, D., Kranendonk, M., et al. (2016). Instability of the human cytochrome P450 reductase A287P variant is the major contributor to its antley-bixler syndrome-like phenotype. *J. Biol. Chem.* 291, 20487–20502. doi: 10.1074/jbc.M116.716019

Miyazaki, K., and Takenouchi, M. (2002). Creating random mutagenesis libraries using megaprimer PCR of whole plasmid. *BioTechniques* 33, 1036–1038.

Munro, A. W., Girvan, H. M., Mason, A. E., Dunford, A. J., and McLean, K. J. (2013). What makes a P450 tick? *Trends Biochem. Sci.* 38, 140–150. doi: 10.1016/j.tibs.2012.11.006

Murataliev, M. B., Ariño, A., Guzov, V. M., and Feyereisen, R. (1999). Kinetic mechanism of cytochrome P450 reductase from the house fly (*Musca domestica*). *Insect. Biochem. Mol. Biol.* 29, 233–242. doi: 10.1016/S0965-1748(98)00131-3

Nadler, S. G., and Strobel, H. W. (1988). Role of electrostatic interactions in the reaction of NADPH-cytochrome P-450 reductase with cytochromes P-450. *Arch. Biochem. Biophys.* 261, 418–429. doi: 10.1016/0003-9861(88)90358-X

Nadler, S. G., and Strobel, H. W. (1991). Identification and characterization of an NADPH-cytochrome P450 reductase derived peptide involved in binding to cytochrome P450. *Arch. Biochem. Biophys.* 290, 277–284. doi: 10.1016/0003-9861(91)90542-Q

Nishino, H., and Ishibashi, T. (2000). Evidence for requirement of NADPH-cytochrome P450 oxidoreductase in the microsomal NADPH-sterol Delta7-reductase system. *Arch. Biochem. Biophys.* 374, 293–298. doi: 10.1006/abbi.1999.1602

Ono, T., and Bloch, K. (1975). Solubilization and partial characterization of rat liver squalene epoxidase. *J. Biol. Chem.* 250, 1571–1579.

O'Reilly, J. E. (1973). Oxidation-reduction potential of the ferro-ferricyanide system in buffer solutions. *Biochim. Biophys. Acta* 292, 509–515. doi: 10.1016/0005-2728(73)90001-7

Oshino, N., Imai, Y., and Sato, R. (1971). A function of cytochrome b5 in fatty acid desaturation by rat liver microsomes. *J. Biochem.* 69, 155–167. doi: 10.1093/oxfordjournals.jbchem.a129444

Palma, B. B., Silva, E., Sousa, M., Urban, P., Rueff, J., and Kranendonk, M. (2013). Functional characterization of eight human CYP1A2 variants: the role of cytochrome b5. *Pharmacogenet. Genomics* 23, 41–52. doi: 10.1097/FPC.0b013e32835c2ddf

Phillips, A. H., and Langdon, R. G. (1962). Hepatic triphosphopyridine nucleotide-cytochrome c reductase: isolation, characterization, and kinetic studies. *J. Biol. Chem.* 237, 2652–2660.

Rendic, S., and Guengerich, F. P. (2015). Survey of human oxidoreductases and cytochrome P450 enzymes involved in the metabolism of xenobiotic and natural chemicals. *Chem. Res. Toxicol.* 28, 38–42. doi: 10.1021/tx500444e

Roman, L. J., Miller, R. T., de la Garza, M. A., Kim, J.-J. P., and Masters, B. S. S. (2000). The C terminus of mouse macrophage inducible nitric-oxide synthase attenuates electron flow through the flavin domain. *J. Biol. Chem.* 275, 21914–21919. doi: 10.1074/jbc.M002449200

Sadeghi, S. J., Valetti, F., Cunha, C. A., Romão, M. J., Soares, C. M., and Gilardi, G. (2000). Ionic strength dependence of the non-physiological electron transfer between flavodoxin and cytochrome c553 from *D. vulgaris*. *J. Biol. Inorg. Chem.* 5, 730–737. doi: 10.1007/s007750000162

Schacter, B. A., Nelson, E. B., Marver, H. S., and Masters, B. S. (1972). Immunochemical evidence for an association of heme oxygenase with the microsomal electron transport system. *J. Biol. Chem.* 247, 3601–3607.

Schrödinger (2015). *The PyMOL Molecular Graphics System, Version 1.8*. New York, NY: Schrödinger.

Scott, E. E., Wolf, C. R., Otyepka, M., Humphreys, S. C., Reed, J. R., Henderson, C. J., et al. (2016). The role of protein-protein and protein-membrane interactions on P450 function. *Drug Metab. Dispos.* 44, 576–590. doi: 10.1124/dmd.115.068569

Shen, A. L., and Kasper, C. B. (1995). Role of acidic residues in the interaction of NADPH-cytochrome P450 oxidoreductase with cytochrome P450 and cytochrome c. *J. Biol. Chem.* 270, 27475–27480. doi: 10.1074/jbc.270.46.27475

Sündermann, A., and Oostenbrink, C. (2013). Molecular dynamics simulations give insight into the conformational change, complex formation, and electron transfer pathway for cytochrome P450 reductase. *Protein Sci.* 22, 1183–1195. doi: 10.1002/pro.2307

Tamburini, P. P., and Schenkman, J. B. (1986). Differences in the mechanism of functional interaction between NADPH-cytochrome P-450 reductase and its redox partners. *Mol. Pharmacol.* 30, 178–185.

Vermilion, J. L., Ballou, D. P., Massey, V., and Coon, M. J. (1981). Separate roles for FMN and FAD in catalysis by liver microsomal NADPH-cytochrome P-450 reductase. *J. Biol. Chem.* 256, 266–277.

Vincent, B., Morellet, N., Fatemi, F., Aigrain, L., Truan, G., Guittet, E., et al. (2012). The closed and compact domain organization of the 70-kDa human cytochrome P450 reductase in its oxidized state as revealed by NMR. *J. Mol. Biol.* 420, 296–309. doi: 10.1016/j.jmb.2012.03.022

Voznesensky, A. I., and Schenkman, J. B. (1992). The cytochrome P450 2B4-NADPH cytochrome P450 reductase electron transfer complex is not formed by charge-pairing. *J. Biol. Chem.* 267, 14669–14676.

Wang, M., Roberts, D. L., Paschke, R., Shea, T. M., Masters, B. S. S., and Kim, J.-J. P. (1997). Three-dimensional structure of NADPH–cytochrome P450 reductase: prototype for FMN- and FAD-containing enzymes. *Proc. Natl. Acad. Sci. U.S.A.* 94, 8411–8416. doi: 10.1073/pnas.94.16.8411

Xia, C., Hamdane, D., Shen, A. L., Choi, V., Kasper, C. B., Pearl, N. M., et al. (2011a). Conformational changes of NADPH-cytochrome P450 oxidoreductase are essential for catalysis and cofactor binding. *J. Biol. Chem.* 286, 16246–16260. doi: 10.1074/jbc.M111.230532

Xia, C., Panda, S. P., Marohnic, C. C., Martásek, P., Masters, B. S., and Kim, J.-J. P. (2011b). Structural basis for human NADPH-cytochrome P450 oxidoreductase deficiency. *Proc. Natl. Acad. Sci. U.S.A.* 108, 13486–13491. doi: 10.1073/pnas.1106632108

Conflict of Interest Statement: The authors declare that the research was conducted in the absence of any commercial or financial relationships that could be construed as a potential conflict of interest.

The handling Editor is currently co-organizing a Research Topic with one of the authors MK, and confirms the absence of any other collaboration.

frontiers in Pharmacology

ORIGINAL RESEARCH
published: 21 March 2017
doi: 10.3389/fphar.2017.00121

Human Cytochrome P450 3A4 as a Biocatalyst: Effects of the Engineered Linker in Modulation of Coupling Efficiency in 3A4-BMR Chimeras

*Danilo Degregorio †, Serena D'Avino †, Silvia Castrignanò, Giovanna Di Nardo, Sheila J. Sadeghi, Gianluca Catucci and Gianfranco Gilardi **

Department of Life Sciences and Systems Biology, University of Turin, Turin, Italy

Human liver cytochrome P450 3A4 is the main enzyme involved in drug metabolism. This makes it an attractive target for biocatalytic applications, such as the synthesis of pharmaceuticals and drug metabolites. However, its poor solubility, stability and low coupling have limited its application in the biotechnological context. We previously demonstrated that the solubility of P450 3A4 can be increased by creating fusion proteins between the reductase from *Bacillus megaterium* BM3 (BMR) and the N-terminally modified P450 3A4 (3A4-BMR). In this work, we aim at increasing stability and coupling efficiency by varying the length of the loop connecting the two domains to allow higher inter-domain flexibility, optimizing the interaction between the domains. Starting from the construct 3A4-BMR containing the short linker Pro-Ser-Arg, two constructs were generated by introducing a 3 and 5 glycine hinge (3A4-3GLY-BMR and 3A4-5GLY-BMR). The three fusion proteins show the typical absorbance at 450 nm of the reduced heme-CO adduct as well as the correct incorporation of the FAD and FMN cofactors. Each of the three chimeric proteins were more stable than P450 3A4 alone. Moreover, the 3A4-BMR-3-GLY enzyme showed the highest NADPH oxidation rate in line with the most positive reduction potential. On the other hand, the 3A4-BMR-5-GLY fusion protein showed a V_{max} increased by 2-fold as well as a higher coupling efficiency when compared to 3A4-BMR in the hydroxylation of the marker substrate testosterone. This protein also showed the highest rate value of cytochrome *c* reduction when this external electron acceptor is used to intercept electrons from BMR to P450. The data suggest that the flexibility and the interaction between domains in the chimeric proteins is a key parameter to improve turnover and coupling efficiency. These findings provide important guidelines in engineering catalytically self-sufficient human P450 for applications in biocatalysis.

Keywords: P450 biocatalysis, domain interaction, glycine linker, stability, uncoupling, electron transfer

OPEN ACCESS

Edited by:
Amit V. Pandey,
University of Bern, Switzerland

Reviewed by:
Yuji Ishii,
Kyushu University, Japan
Rita Bernhardt,
Saarland University, Germany

****Correspondence:***
Gianfranco Gilardi
gianfranco.gilardi@unito.it

† These authors have contributed equally to the work.

Specialty section:
This article was submitted to Pharmacogenetics and Pharmacogenomics, a section of the journal Frontiers in Pharmacology

Received: *30 November 2016*
Accepted: *27 February 2017*
Published: *21 March 2017*

Citation:
Degregorio D, D'Avino S, Castrignanò S, Di Nardo G, Sadeghi SJ, Catucci G and Gilardi G (2017) Human Cytochrome P450 3A4 as a Biocatalyst: Effects of the Engineered Linker in Modulation of Coupling Efficiency in 3A4-BMR Chimeras. Front. Pharmacol. 8:121. doi: 10.3389/fphar.2017.00121

INTRODUCTION

Cytochromes P450 are heme-thiolate monooxygenases found in all domains of life (Coon, 2005; Bernhardt, 2006) able to metabolize several endogenous molecules and xenobiotics, including drugs (Nelson et al., 1996; Ortiz de Montellano, 2005; Isin and Guengerich, 2007).

They catalyze many chemical reactions such as hydroxylation of non-activated carbon atoms, epoxidation of double bonds and dealkylation on C-, N-, and S- atoms (Isin and Guengerich, 2007).

Electrons for these reactions are provided by NADPH and transferred to the heme cofactor via different redox partners classified by Hannemann et al. (2007). Thus, NADPH is used as electron source and in the presence of molecular oxygen, reaction product(s) can be generated in single or multistep reactions.

Although the human liver enzymes are an attractive biotechnological target in their use as biocatalysts for their ability to produce pharmaceuticals and drug metabolites, limitations are given by poor stability and by the so-called "uncoupling," the formation of reactive oxygen species at the heme site leading to the release of intermediates such as superoxide and peroxide during the reaction cycle (Guengerich, 2002; Meunier et al., 2004; Zangar et al., 2004; Denisov et al., 2005). The uncoupling process can lead to a loss of NADPH redox equivalents as high as 99% in human cytochrome P450 1A2 (Mayuzumi et al., 1993) or 16% for 3A4 (Perret and Pompon, 1998) and it can be seen as a wasteful process. These high uncoupling levels, together with the need of a reductase, are a considerable disadvantage in the use of human enzymes as biocatalysts.

On the other hand, bacterial P450 enzymes are known to be well coupled and as in the case of P450 BM3 from *Bacillus megaterium*, have been shown to be able to produce drug metabolites typical of the human enzymes with a high coupling efficiency (Di Nardo et al., 2007; Di Nardo and Gilardi, 2012). This has led to a wide range of protein engineering studies on this enzyme to widen its catalytic abilities (Tsotsou et al., 2012, 2013; Ryu et al., 2014; Di Nardo et al., 2015; Ren et al., 2015; Capoferri et al., 2016).

One factor that makes P450 BM3 a well-coupled biocatalyst resides in the productive interaction between the heme catalytic domain (BMP) and its flavin-containing reductase domain (BMR) that, unlike in other cytochromes P450, are all part of the same polypetide chain. For this reason we already reported the construction of different fusion human P450 enzymes, engineered by connecting the reductase domain BMR with human cytochromes P450 2E1(Fairhead et al., 2005), 3A4, 2C9, 2C19 (Dodhia et al., 2006), 2A6, CYP2C6, and CYP4F11 (Ortolani, 2012; Rua, 2012a; Castrignanò et al., 2014), monkey 2C20 (Rua et al., 2012b) and dog CYP2D15 (Sadeghi and Gilardi, 2013; Rua et al., 2015).

As human cytochrome P450 3A4 is responsible for the metabolism of the majority of commercial drugs and it is at the origin of many drug-drug interactions of clinical concern (Evans and Relling, 1999), we further characterized the parameters influencing uncoupling in the reconstituted fusion protein P450 3A4-apo-BMR, such as flavin content, substrate, and NADPH concentration, pH and ionic strength (Degregorio et al., 2011). Among P450 systems, P450 BM3 is considered as a model for self-sufficiency and high coupling efficiency (Munro et al., 1996; Noble et al., 1999). In 2005, Neeli and colleagues suggested that BM3 fatty acid hydroxylation activity can be related to a dimeric form of the enzyme and for this protein electron transfer is achieved through an "inter subunits" interaction between protomers rather than direct flow between the di-flavin and the heme held by the same polypeptide chain (Neeli et al., 2005).

In the present work we consider another parameter that can influence the coupling efficiency in the fusion protein P450 3A4-BMR: the length of the loop linking the oxygenase domain with the reductase one. In 1995, Govindaraj and Poulos demonstrated that the length of the linker is the critical feature that controls flavin-to-heme electron transfer in cytochrome P450 BM3 (Govindaraj and Poulos, 1995). Moreover, the role of the linker sequence in facilitating the ability of cyt b_5 to reduce P450 2B4 was explored by altering the length and sequence of the flexible linker region between the heme domain and membrane anchor of cyt b_5 (Clarke et al., 2004). Clarke and co-workers demonstrated that, although the sequence of the linker region can be varied without significant effects on the properties of cyt b_5, the linker region has a critical minimum length of 6–8 residues.

Here we aim at elucidating first if then how the length of the linker connecting the reductase and catalytic domain in the 3A4-BMR fusion protein has an effect in modulating the activity and the uncoupling process.

Flexibility between protein domains is a critical parameter in modulating the uncoupling process via the formation of an active complex and by tuning the electron flow to the heme. The ability of the reductase of P450 BM3 from *B. megaterium* (BMR) to transfer electrons in the redox chain from NADPH to the heme is evaluated by varying the length of the linker region between BMR and the N-terminally modified 3A4 heme domain. As shown in **Figure 1**, the BMR and P450 3A4 domains possess the surface charges complementarity that is known to be more crucial for the complex formation than when the physiological redox partner, cytochrome P450 reductase (hCPR) was used instead. In order for catalysis to occur, this active complex should form with high propensity. Thus, starting from the 3A4-BMR chimera in which the BMR domain is linked to the 3A4 *via* the short linker Pro-Ser-Arg, two new constructs are engineered to include 3- or 5-Gly inserted after the Pro-Ser-Arg loop leading to 3A4-3GLY-BMR and 3A4-5GLY-BMR chimeric proteins. This glycine rich region close to the C-terminal of P450 3A4 has been proposed to function as a flexible hinge that can provide the enzyme the degrees of freedom required to achieve a functional complex. The effect of the linker length on the electron transfer between the reductase and the catalytic domains in the presence of NADPH as electron supplier is studied for the three chimeras.

The electrons delivery from NADPH to the flavins of the reductase domainis is evaluated in the three complexes by anaerobic stopped flow spectroscopy measurement of NADPH consumption rate in the absence of substrate. The electron transfer capability of reducing equivalents by flavins of the reductase domain is investigated using cyt *c* as an artificial electron acceptor (Guengerich et al., 2009) and the effect of the linker length is examined. Finally, the ability of the BMR to sustain catalysis at the 3A4 catalytic domain is explored in relation to the length of the linker by investigating enzyme activity and coupling efficiency during erythromycin N-demethylation and testosterone 6β-hydroxylation.

MATERIALS AND METHODS

Chemicals and Reagents

The pCW-3A4-BMR plasmid containing the gene of human P450 3A4 fused to the reductase of cytochrome P450 BM3

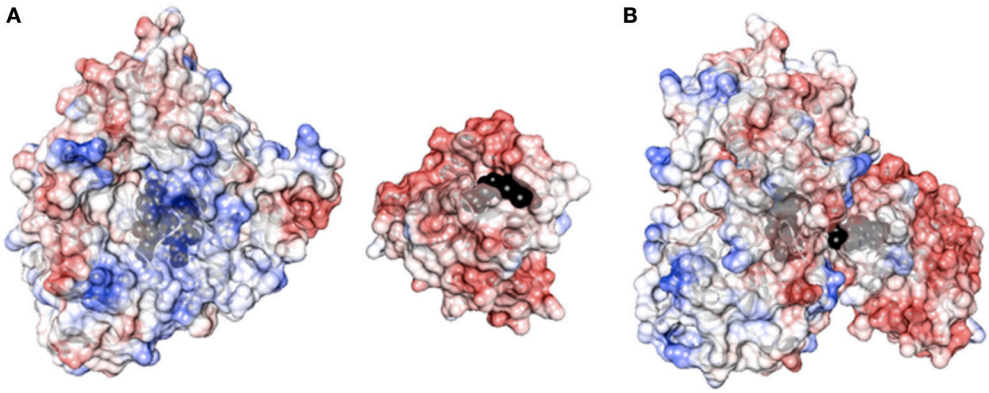

FIGURE 1 | (A) Surface charge distribution of P450 3A4 (left, PDB ID 1TQN) and the FMN binding domain of P450 BM3 (right, PDB ID 1BVY). Heme and FMN are shown in black. **(B)** Complex between P450 3A4 and the FMN binding domain of BMR. The complex was created by super-imposition of the crystal structure of P450 3A4 with the heme domain of P450 BM3 in the complex crystal structure.

from *B. megaterium* (BMR) linked via a Pro-Ser-Arg linker was available in our laboratory (Dodhia et al., 2006). GenElute plasmid miniprep kit was obtained from Sigma (Italy). PCR purification kit and gel extraction kit were purchased from Macherey-Nagel (Germany).

The primers for PCR and oligonucleotides for the linker region between P450 3A4 and BMR reductase were prepared by MWG (Germany). DNA Ladder, restriction endonucleases enzymes *Avr II* and *Hind III*, Vent polymerase, T4 DNA ligase enzyme and buffers used in sub-cloning were from New England Biolabs (UK) and Promega (Italy). Horse heart cytochrome *c*, erythromycin, testosterone, 6β-hydroxytestosterone, horseradish peroxidase type X, superoxide dismutase from bovine erythrocytes, catalase, N,N-dimethylaniline, and 4-amino-2,3-dimethyl-1-phenyl-3-pyrazolin-5-one were purchased from Sigma (Italy). NADPH (tetrasodium salt) was acquired from Calbiochem (Germany). Human CPR was purchased from Life Technologies. All other chemicals, biochemicals used in this study were purchased from Sigma (Italy) at the highest available grade and used as recommended by the manufacturer.

Engineering the Linkers in the 3A4-BMR Chimeras

The strategy used in the construction of the fusion proteins is based upon introduction of 3 or 5 glycines in the pre-existent Pro-Ser-Arg linker connecting P450 CYP 3A4 domain and BMR one domain via 3 amino acids (Pro-Ser-Arg) by using as a starting template the vector pCW-3A4-BMR available in our laboratory (**Figure 2A**; Dodhia et al., 2006). Glycine was chosen to allow the highest flexibility of the loop to support conformational rearrangements between the two domains as much as possible.

All PCR reactions were performed in a DNA thermal cycler (PerkinElmer Life Sciences, Italy) and employed Vent polymerase under conditions recommended by the manufacturer (Promega, Italy).

The 3A4-3GLY-BMR chimera was engineered to contain the N-terminally modified human P450 CYP 3A4 (aa 13-503), the linker Pro-Ser-Arg-Gly-Gly-Gly and the C-terminal reductase (aa 472-1049) of P450 BM3 from *B. megaterium*. The 3A4-5GLY-BMR chimera contains the N-terminally modified human P450 3A4 (aa 13-503), the linker Pro-Ser-Arg-Gly-Gly-Gly-Gly-Gly and the C-terminal reductase domain (aa 472-1049) of *B. megaterium*. The gene coding for the BMR reductase was amplified using the forward 5-AGTGGAGCCCCTAGG TCAGGCGGTGGCAAAAAGGCAGAAAACGCTCATAAT-3′ and reverse 5′-GCTCATGTTTGACAGCTTATCATCGAT AAGCTTTTACCC-3′ primers for the chimera with 3 glycines. The forward 5′-AGTGGAGCCCCTAGGTCAGGCGGT GGCGGTGGCAAAAAGGCAGAAAACGCTCATAAT-3′ and reverse 5′-GCTCATGTTTGACAGCTTATCATCGATAAGCTT TTACCC-3′ primers were used for the 5-glycine chimera. The forward primers were synthesized with an overhanging *Hind III* restriction site upstream of the BMR start codon, whereas the reverse primers contained an *Avr II* site downstream of the stop codon. The underlined letters represent the endonuclease restriction sites. DNA was melted for 2 min at 94°C, followed by 30 cycles of 1 min at 94°C, 1 min and 45 s at 60°C, 1 min at 72°C. The polymerase chain reaction products obtained were digested with *Hind III* and *Avr II* endonucleases and purified by the GeneClean II method as described by the manufacturer. The pCW-3A4-BMR vector was digested for 1 h at 37°C with *Hind III* and *Avr II* and genomic DNA corresponding to pCW-3A4 was isolated by NAGEL KIT extraction and then ligated using T4 DNA ligase with the sticky sites of the digest PCR products. The ligation mix was transformed into *E. coli* DH5α cells and plated on LB agar containing 100 μg/ml ampicillin. The positive clones were chosen and the plasmid DNA was purified using a Mini-prep plasmid extraction kit (Sigma, Italy). The correct insertion of the glycine codons was verified by DNA sequencing.

Expression, Purification, and Characterization

Heterologous expression of 3A4-BMR, 3A4-3GLY-BMR, and 3A4-5GLY-BMR was performed by transforming competent

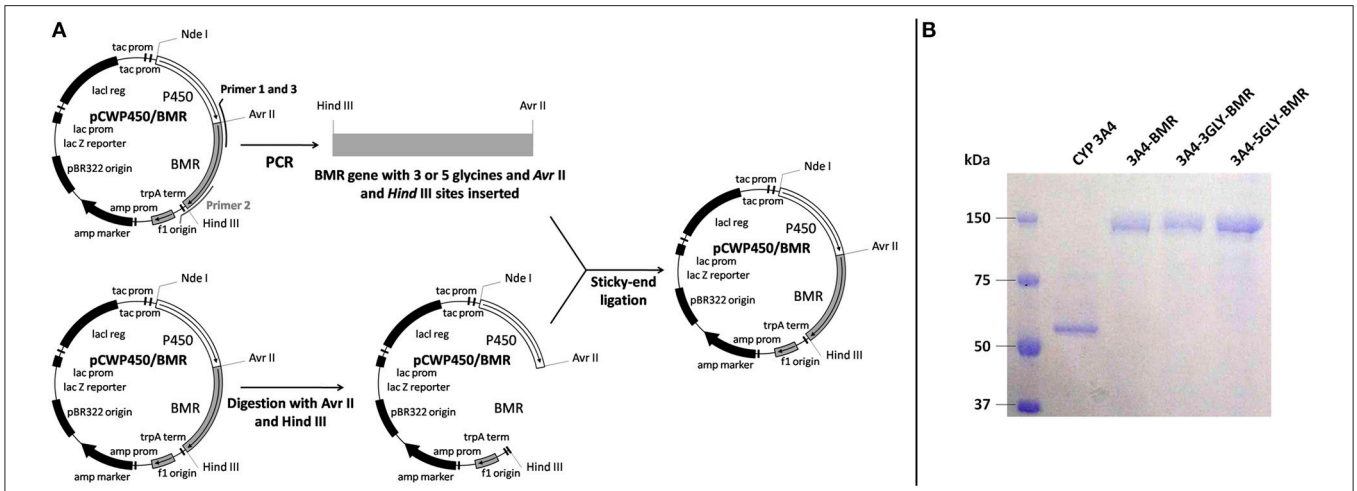

FIGURE 2 | (A) Schematic illustration of the chimeras construction strategy. **(B)** SDS-PAGE of the purified chimeric proteins.

E. Coli DH5α cells with the corresponding plasmid vectors. The proteins were purified using diethylaminoethyl and hydroxylapatite columns as described before (Dodhia et al., 2006). The purity of the enzymes was checked by sodium dodecyl sulfate polyacrylamide gel electrophoresis on 7.5% gel using a Mini-Protean apparatus (Bio-Rad, USA) with Coomassie blue staining.

Protein concentrations were determined from the absorption at 450 nm of the carbon monoxide-bound reduced form by using the Omura and Sato method (Omura and Sato, 1964) using an extinction coefficient of 91 mM^{-1} cm^{-1}. Protein reduction was achieved by addition of saturating sodium dithionite, and formation of the carbon monoxy-adduct of the heme was obtained by bubbling the reduced enzyme with carbon monoxide.

Determination of the Heme and Flavin Contents

The ratio protein:heme:FMN:FAD were calculated using different spectroscopic methods. Protein concentration was estimated using Bradford assay (Bradford, 1976), while the heme concentration was obtained from the CO-binding assay described above (Omura and Sato, 1964). FAD and FMN contents were calculated using fluorescence emission spectroscopy in each purified enzymes (Faeder and Siegel, 1973). Excitation at 450 nm produced fluorescence emission spectra with an emission maximum at 535 nm as expected for flavin-containing proteins. Quantification of FAD and FMN present in the protein is based on the different behavior of the two cofactors at different pH-values (Aliverti et al., 1999). The samples were boiled for 3 min to release the flavins, then rapidly cooled on ice and centrifuged at 14,000 g for 10 min. An aliquot of the clear supernatant was diluted with standard buffer (0.1 M potassium phosphate buffer pH 7.7, containing 0.1 mM EDTA) so that the final volume was 1.5 mL and the mixture was transferred to a 1 cm path-length fluorimeter cuvette.

Fluorescence emission was recorded at 535 nm; the excitation wavelength was set at 450 nm. After the initial fluorescence measurement at pH 7.7, the pH of the solution was adjusted to 2.6 by the addition of 0.1 mL of 1 N HCl (final concentration 62.5 mM) and the fluorescence was determined again. The concentrations of FAD and FMN in the supernatant were determined from the fluorescence intensity compared to those obtained for standard solutions of flavins by using as extinction coefficients 11.3 and 12.2 $mM^{-1}cm^{-1}$, respectively (Aliverti et al., 1999).

Time Dependent Loss of CO-Binding

The stability of 3A4-BMR fusion proteins was compared with that of CYP 3A4 by following the loss of CO-binding at a temperature of 37°C. Recombinant CYP3A4 was expressed and purified as described by Dodhia et al. (2006). CO-binding spectral assay was performed at 37°C both in the presence of CYP3A4 and 3A4-BMR chimeric proteins as described in the Section Determination of the Heme and Flavin Contents by using 1.6 μM protein solutions. The absorbance at 450 nm was followed for 60 min by collecting one spectrum every 5 min at 37°C. All the collected spectra were corrected by subtraction of the spectrum of the reduced protein and the loss of CO-binding was measured as a percentage loss in absorbance of the peak at 450 nm.

Anaerobic Stopped Flow Spectrophotometric Evaluation of NADPH Consumption

Rates of NADPH oxidation were measured using a Hi-Tech scientific SF-61 single mixing stopped-flow system (TgK Scientific, UK) at 25°C in a glovebox (Belle Technology, UK) with an oxygen concentration below 10 ppm. NADPH consumption was monitored at 340 nm ($\varepsilon = 6.22$ mM^{-1} cm^{-1}) for 750 sunder anaerobic conditions. Proteins and reducing agent solutions (in the absence and presence of saturating amounts of substrate) were prepared in syringes in an anaerobic glove box and

transferred to the sample handling unit of the stopped-flow instrument. The experiment was performed by mixing the NADPH (syringe A, 200 μM NADPH in 50 mM potassium phosphate buffer pH 8.0) and the enzyme or enzyme plus substrate solutions (syringe B, 1 μM enzyme in 50 mM potassium phosphate buffer pH 8.0+150 μM erythromycin or testosterone). Analysis of the resulting kinetic data was performed with Kinetic studio V3 software (TgK Scientific, UK). In order to calculate the NADPH consumption rate, the plot of absorbance at 340 nm vs. time was fitted to a single exponential decay function.

Determination of the Reduction Potentials of the Chimeras

Potentiometric titrations were performed in an anaerobic glovebox (Belle Technology, UK) with an oxygen concentration below 10 ppm using a cuvette equipped with a gold laminar working electrode and an Ag/AgCl reference electrode connected to a potentiostat controlled by GPES3 software (Ecochemie, The Netherlands). Ambient reduction potentials were adjusted by addition of aliquots (2–5 μL) of anaerobically freshly prepared sodium dithionite solution. Titrations were performed in 50 mM potassium phosphate, pH 8. Electrode-solution mediation was facilitated by adding the following mediators at 5 μM concentration: methyl viologen ($E_m = -440$ mV), benzyl viologen ($E_m = -359$ mV), safranine O ($E_m = -280$ mV), anthraquinone-2,6-di sulfonic acid ($E_m = -185$ mV), phenazinemethosulfate ($E_m = +80$ mV), methylene blue ($E_m = +11$ mV). The modified cuvette was flushed with oxygen-free nitrogen before and during the measurements. After equilibration at each potential, the optical spectrum was recorded. Reduction of the heme in 3A4-BMR fusion proteins was followed by the increase in the absorption at 550 nm related to the merging of Q-bands, using a diode array spectrophotometer (TgK Scientific, UK). The fraction of reduced heme, proportional to the measured spectral transition, was plotted against potential, and the data were fitted to the Nernst equation:

$$E = E_m + (RT/nF)ln([ox]/[red])$$

where [*ox*] and [*red*] are the concentrations of oxidized and reduced heme, respectively, *E* is the solution reduction potential at equilibrium, *n* is the number of electrons, E_m is the midpoint potential, *F* is the Faraday constant, *R* is the gas constant, and *T* is the absolute temperature.

Determination of the Catalytic Activity and Coupling Efficiency

The enzymatic activity of chimeras was determined toward erythromycin N-demethylation and testosterone 6β-hydroxylation.

Erythromycin N-demethylation was investigated under aerobic conditions by quantification of the formaldehyde arising from the N-demethylation of erythromycin using the Nash method (Nash, 1953), using a concentration range of this substrate under 120 μM where this molecule still acts as a substrate. Uncoupling reactions leading to hydrogen peroxide were determined and quantified using the N,N-dimethylaniline/4-amino-2,3-dimethyl-1-phenyl-3-pyrazolin-5-one/crude horseradish peroxidase colorimetric assay as described by Sugiura et al. (1977). Reactions were carried out at 37°C in a 1 cm path length quartz cuvette and consisted of the following mixture: 0.1 M potassium phosphate buffer pH 8.0, 2% glycerol, 5 mM $MgCl_2$, 100 mM KCl, 1 μM of the chimeric protein and different concentrations of erythromycin in the range 0–120 μM. For each protein preparation, some preliminary experiments were performed in order to assess linearity of reaction rates with respect to time. After blanking the absorbance at 412 nm with the erythromycin incubated at 37°C for 5 min with 1 μM of the enzymes, catalysis was initiated by addition of 150 μM NADPH. The reactions were then stopped after 30 min by addition of HCl. The samples were centrifuged at 13,000 rpm for 5 min and 0.5 mL of the supernatant were transferred to another tube and mixed with 0.5 mL of a concentrated Nash reagent (3 g ammonium acetate, 40 μL acetylacetone, 60 μL acetic acid in 10 mL of water) as described before (Dodhia et al., 2006).

The reaction linearity was assessed over a 40 min time. Thus, the mixture was incubated at 50°C for 30 min and the samples were analyzed by measuring absorbance at 412 nm to determine the formation of formaldehyde. The amount of formaldehyde produced during the reaction was quantified by using a calibration curve constructed in the same reaction condition with a range of concentration between 0 and 30 μM. Zero-time controls were performed in the absence of erythromycin.

Coupling efficiency was calculated as the ratio of formaldehyde produced during erythromycin N-demethylation and the total amount of NADPH consumed by the chimeras.

Testosterone 6β-hydroxylation was investigated at 37°C by incubating 1 μM protein in the presence of testosterone in a concentration range between 1 and 150 μM for 5 min. Catalysis was initiated by addition of 200 μM NADPH. The reaction linearity was assessed over a 40 min time. The reactions were then stopped after 30 min by addition of HCl. The samples were centrifuged at 13,000 rpm for 5 min. The amount of 6β-hydroxytestosterone formed was evaluated by HPLC coupled with a diode array UV detector (Agilent-1200, Agilent technologies, USA) equipped with a 4.6 × 250 mm, 5 μm C18 column. Testosterone and 6β-hydroxytestosterone were separated using a gradient elution programmed as follows: isocratic elution of 20% acetonitrile and 80% water, 0–2 min; linear gradient elution from 20 to 90% acetonitrile and from 80 to 10% water, 2–20 min; linear gradient elution from 90 to 20% acetonitrile and from 10 to 80% water, 20–22 min; isocratic elution of 20% acetonitrile and 80% water 22 min-end of the run. The flow rate was set at 1 mL/min and detection wavelength was 244 nm. Retention times were 9.2 min and 13.1 min for 6β-testosterone and testosterone, respectively. Coupling efficiency was calculated as the ratio of 6β-hydroxytestosterone produced and the total amount of NADPH consumed by the chimeras.

Measurement of Cytochrome *c* Reduction by the BMR of the Chimeras

Cytochrome *c* reduction activity spectrophotometric assay was performed as described by Guengerich et al. (2009) with slight modification. In particular, 10 μM of cyt *c* (in 0.1 M potassium

phosphate buffer pH 8.0) were pipetted into a 0.5 mL quartz cuvette (1 cm path-length). Then, 0.1 μM of chimeric proteins were added and gently mixed. The assay was started by adding NADPH to a final concentration of 75 μM. Using the kinetic mode of the spectrophotometer, the absorbance increase at 550 nm upon cytochrome *c* reduction was monitored for 5 min. The rate of cytochrome *c* reduction was calculated using reduced cyt *c* extinction coefficient at 550 nm,7.04 $mM^{-1}cm^{-1}$, as nmol of reduced cyt *c* per min. The experiment was carried out both in the absence and in the presence of 20% glycerol.

Statistical Analysis

All collected data were recorded at least in triplicate and expressed as mean ± standard deviation. The comparison of the results obtained was performed by one way ANOVA and two way ANOVA followed by Student-Newman-Keuls *post hoc* test using SigmaPlot software.

RESULTS

Protein Purification and UV-Visible Properties of the P450 3A4-BMR Chimeras

After expression and purification (**Figure 2B**), the UV-visible spectral properties of the purified chimeras were analyzed between 300 and 600 nm for the oxidized, reduced and carbon monoxide bound forms. The spectra show the typical features of both heme and flavin cofactors (**Figures 3A–D**). These comprise the characteristic Soret peak at 418 nm corresponding to the oxidized heme iron, the β and α bands at 535 and 570 nm, the shoulder around 455–485 nm belonging to the oxidized FAD and FMN of the BMR domain.

Full reduction of the chimeras was achieved by addition of excess sodium dithionite leading to the hydroquinone forms with a concomitant decrease in the intensity in the visible region spectra (**Figures 3A–D**, dashed lines). In all cases a clear shift to 450 nm upon CO bubbling indicates the presence of a properly folded P450 domain (**Figures 3A–D**, dark gray lines).

The correct stoichiometry of the heme and flavin incorporation in the chimeras was also investigated by absorption and fluorescence spectroscopy. The heme content was determined from the absorbance value at 450 nm of the CO-adduct and the amount of the total protein was obtained by Bradford method. In all chimeras the ratio heme:protein resulted to be close to 1:1 (**Table 1**). This indicates that the proteins have a full complement of bound heme cofactor. The FAD and FMN content was determined by fluorescence emission spectroscopy as detailed in the materials and methods section, resulting in a FAD-to-protein and FMN-to-protein ratio of 0.81 and 0.82 for 3A4-BMR, 0.83, and 0.87 for 3A4-3GLY-BMR and 0.83 and 0.83 for P450 3A4-5GLY-BMR (**Table 1**). The ratios in flavins:heme content suggest that there is a minimal amount of apoenzyme with a nearly-stoichiometric amount of each cofactor and indicating that the domains are independently able to uptake the cofactor while folding.

NADPH Consumption and Reduction Potentials of the Heme

Since the inter-domain interactions modulated by the loops are crucial in determining both the electron transfer rates and reduction potentials, these parameters were evaluated on the three chimeras.

Rates of NADPH oxidation by the chimeras were measured by rapid scanning stopped flow spectrophotometry by following the decrease in absorbance at 340 nm for 750 s in anaerobic condition (Sevrioukova et al., 1996; Davydov et al., 2010), as this is the first essential step in the electron transfer chain involving the FAD and FMN cofactors of BMR to sustain the 3A4 catalysis (Guengerich, 1983). The NADPH consumption rates were estimated by fitting the absorbance decrease with single exponential decay equation both for 3A4-BMR chimeras and for CYP3A4 in the presence of hCPR as reference system. Moreover, NADPH oxidation rates were calculated also in the presence of substrate, erythromycin and testosterone, in saturating conditions. The results are summarized in the **Figure 4**. As reported, compared to CYP3A4/hCPR system, 3A4-BMR chimeric proteins were found significantly faster both in absence and in presence of substrate, resulting more efficient in the transfer of reducing equivalents from NADPH. In addition, 3A4-3GLY-BMR protein resulted significantly faster in NADPH consumption with respect to the other two constructs ($P < 0.05$), both in the presence and in the absence of substrate. Moreover, the presence of both erythromycin and testosterone significantly enhances NADPH consumption rate in all the examined fusion proteins. This effect is probably due to the fact that the substrate-bound complex has a higher reduction potential and is capable to accept electrons from the redox partner more easily leading to a faster reduction of the heme-Fe^{3+} to heme-Fe^{2+} (Sligar et al., 1979; Guengerich, 1983).

Reduction potentials of the heme were determined with anaerobic spectro-potentiometric titrations of the chimeras using the method described by Dutton (1978). The change in population from the oxidized (Fe^{3+}) to the reduced (Fe^{2+}) state upon addition of sodium dithionite reducing agent was monitored by observing the spectral transition related to the merging of the Q-bands in a single band at 550 nm. Reduction potential values were calculated by plotting the calculated 3A4-BMR reduced fraction vs. the recorded potential using the Nernst's equation. Midpoint potential values were calculated to be -367 ± 3 mV, -327 ± 8 mV, and -397 ± 8 mV for 3A4-BMR, 3A4-3GLY-BMR and 3A4-5GLY-BMR, respectively.

The differences observed in NADPH oxidation and reduction potentials indicate that the loops indeed have an impact on these parameters and therefore also different functional performace in catalysis are expected.

Stability of the Chimeras

In order to study if and how the length of the loop has an impact on the stability of the P450 catalytic module, the time dependent decrease of the absorbance at 450 nm upon reduction and CO binding was used to compare the relative stability of P450 proteins (Lin et al., 2005; Foti et al., 2011; Amunugama et al., 2012). This assay is based on the assumption that the loss

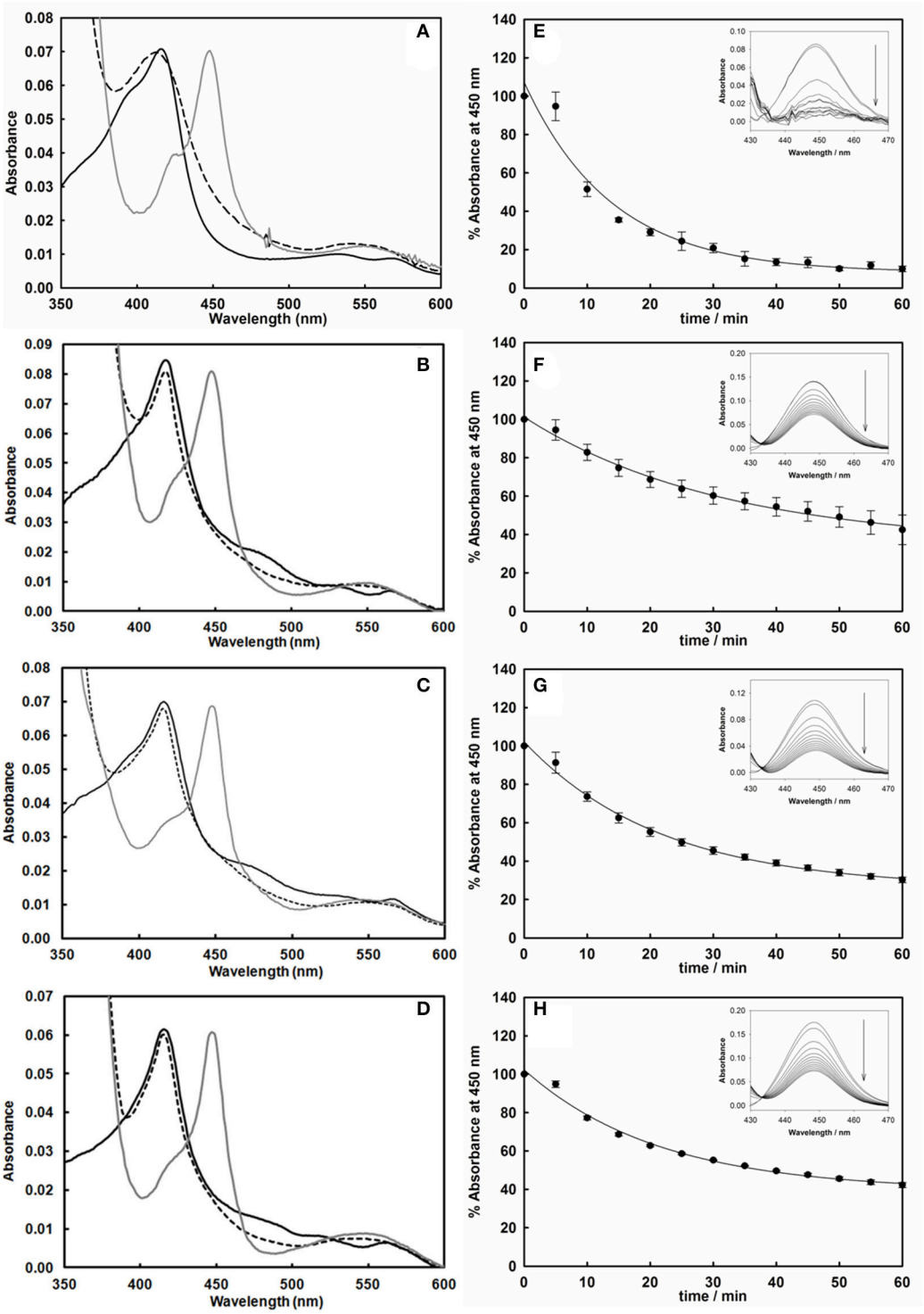

FIGURE 3 | Left: UV-vis spectra of the purified cytochrome P450 3A4 (A), 3A4-BMR **(B)**, 3A4-3GLY-BMR **(C),** and 3A4-5GLY-BMR **(D)** in their oxidized (black line), reduced (dashed line), and reduced/carbon monoxide-bound (dark gray line) forms. Sodium dithionite completely reduces the flavin cofactors in all enzymes, leading to spectral bleaching. Binding of carbon monoxide results in the formation of Fe^{2+}-CO complex with heme Soret absorption maxima shifted to 450 nm in all cases. Right: Time-dependent decrease of the absorbance at 450 nm of the CO-bound cytochrome P450 3A4 **(E)**, 3A4-BMR **(F)**, 3A4-3GLY-BMR **(G)**, and 3A4-5GLY-BMR **(H)**. CO binding loss is significantly higher, in terms of both rate and total absorbance decrease, for CYP 3A4 compared to the three BMR linked chimeras. Insets: difference spectra generated by subtraction of the reduced P450 spectrum to each Fe^{2+}-CO complex spectrum.

TABLE 1 | Heme and flavin contents obtained for 3A4-BMR, 3A4-3GLY-BMR, and 3A4-5GLY-BMR.

	3A4-BMR	3A4-3GLY-BMR	3A4-5GLY-BMR
Heme content (nmolheme/nmol protein)	0.97 ± 0.03	0.98 ± 0.01	0.98 ± 0.02
FMN content (nmol FMN/nmol protein)	0.82 ± 0.01	0.87 ± 0.03	0.83 ± 0.05
FAD content (nmol FAD/nmol protein)	0.81 ± 0.04	0.83 ± 0.02	0.83 ± 0.02

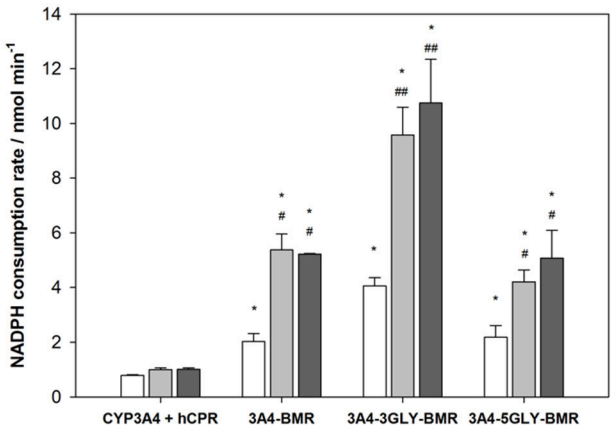

FIGURE 4 | Anaerobic NADPH oxidation rates for cytochrome P450 3A4-BMR, 3A4-3GLY-BMRand 3A4-5GLY-BMR compared to those obtained for CYP 3A4 + hCPR system, obtained both in absence (white bars) and in presence of substrate erythromycin (light gray) and testosterone (dark gray). Data are mean ± SD for 3 to 6 replicates. $^{*}P < 0.001$ compared to CYP 3A4 + hCPR system; $^{\#}P < 0.05$, $^{\#\#}P < 0.001$ compared to the protein in absence of substrate; two way ANOVA.

of the band at 450 nm is associated with a loss of activity of P450 enzymes (Omura and Sato, 1964). Thus, the absorbance at 450 nm was followed for 60 min at 37°C after the CO-binding assay for CYP 3A4 as well as the three 3A4-BMR fusion proteins. The results are shown as percentage residual absorbance in the **Figures 3E–H**. **Figure 3E** shows that 3A4 domain when alone retains only 10 ± 1% of the initial absorbance at 450 nm with a loss of 450 nm peak rate of 0.072 ± 0.011 min^{-1}, whereas 3A4-BMR (**Figure 2F**), 3A4-3GLY-BMR (**Figure 2G**), and 3A4-5GLY-BMR (**Figure 2H**) show a higher stability with a residual absorbance at 450 nm of 42 ± 7, 30 ± 1, and 42 ± 1% respectively and a loss of 450 nm peak rate of 0.032 ± 0.003 min^{-1}, 0.046 ± 0.004 min^{-1}, and 0.047 ± 0.005 min^{-1} respectively. These values show that, in these experimental conditions, the stability is significantly higher for the 3A4-BMR chimeras ($P < 0.001$, one way ANOVA) when compared to the 3A4 alone.

Catalytic Properties and Coupling Efficiency of the Chimeras

Turnover of the different chimeras was studied in the presence of the substrates erythromycin and testosterone using NADPH as electron source, and the results are reported in **Table 2**. Quantification of both the amount of product formed in the N-demethylation of erythromycin and coupling efficiency, determined from the ratio product formed/NADPH oxidized, were performed for the three chimeras. Erythromycin N-demethylation rates were calculated at increasing concentration of the substrate in the presence of all the 3A4-BMR constructs, and the experimental data were fitted to the Michaelis-Menten model in order to calculate kinetic parameters (**Figure 5A**). The K_M-values of 3A4-BMR, 3A4-3GLY-BMR, and 3A4-5GLY-BMR were 20.8 ± 3.6, 27.4 ± 4.0, and 21.3 ± 4.4 μM respectively. In this case no statistically relevant differences were found. These results show that the glycine linker length does not influence 3A4-BMR affinity for erythromycin substrate, indicating that the binding pockets of the heme domain of the chimeras are not perturbed.

Further analysis in terms of turnover rate led to V_{max}-values of 0.0515 ±.0004, 0.1177 ± 0.0006, and 0.1387 ± 0.0009 nmol min^{-1} for 3A4-BMR, 3A4-3GLY-BMR, and 3A4-5GLY-BMR (**Figure 4B**), respectively. In this case, a statistically significant increase in V_{max} for 3A4-3GLY-BMR and 3A4-5GLY-BMR with respect to the 3A4-BMR construct was observed. This shows that the glycine linker increases the enzyme turnover rate in the presence of erythromycin substrate. Moreover, a significant increase in V_{max}-value was found for 3A4-5GLY-BMR compared to 3A4-3GLY-BMR.

Also the testosterone 6β-hydroxylation rates were calculated at increasing concentrations of the substrate in the presence of all the 3A4-BMR constructs, and the results were fitted to the Michaelis-Menten model in order to calculate kinetic parameters (**Figure 5D**). The K_M-values obtained from fitting the Michaelis-Menten curves of 3A4-BMR, 3A4-3GLY-BMR, and 3A4-5GLY-BMR were 19.6 ± 2.6, 21.3 ± 2.7, and 19.8 ± 2.2 μM respectively, indicating again no statistically relevant differences in the binding pocket. The V_{max}-values were 0.0066 ± 0.0002, 0.0089 ± 0.0002, and 0.0113 ± 0.0003 nmol min^{-1} respectively for 3A4-BMR, 3A4-3GLY-BMR, and 3A4-5GLY-BMR enzymes (**Figure 5E**). As observed in the presence of erythromycin, when comparing V_{max} results, a statistically significant increase was found for 3A4-3GLY-BMR and 3A4-5GLY-BMR with respect to the 3A4-BMR construct. Also in this case the glycine linker increases the enzyme turnover rates, with a significant higher V_{max}-value for 3A4-5GLY-BMR compared to 3A4-3GLY-BMR.

The coupling efficiency percentage during erythromycin N-demethylation, calculated as ratio of HCHO formed and NADPH consumed, were found to be 9.4 ± 0.5, 10.0 ± 0.8, and 12.5 ± 0.9% for 3A4-BMR, 3A4-3GLY-BMR, and 3A4-5GLY-BMR, respectively (**Figure 5C**). When performing statistical analysis of these results, the 3A4-5GLY-BMR fusion protein was found more coupled than the other two constructs, whereas no significant difference was found when comparing 3A4-BMR and 3A4-3GLY-BMR. A similar comparison was also performed for testosterone catalysis by calculating coupling efficiency as the ratio of the amount of 6β-hydroxytestosterone formed and NADPH consumed. The calculated coupling efficiency percentage ratios were found to be 3.4 ± 0.1, 4.6 ± 0.1, and 5.8 ± 0.2% for 3A4-BMR, 3A4-3GLY-BMR, and 3A4-5GLY-BMR, respectively (**Figure 5F**).

TABLE 2 | Catalysis and uncoupling parameters for erythromycin N-demethylation and testosterone 6β-hydroxylation for 3A4-BMR, 3A4-3GLY-BMR, and 3A4-5GLY-BMR.

	Erythromycin N-demethylation			Testosterone 6β-hydroxylation		
	K_M(μM)	V_{max}(nmol min^{-1})	Coupling efficiency%[(a)]	K_M(μM)	V_{max} (nmol min^{-1})	Coupling efficiency%[(b)]
3A4-BMR	20.8 ± 3.6	0.0515 ± 0.0004	9.4 ± 0.5	19.6 ± 2.6	0.0066 ± 0.0002	3.4 ± 0.1
3A4-3GLY-BMR	27.4 ± 4.0	0.1177 ± 0.0006	10.0 ± 0.8	21.3 ± 2.7	0.0089 ± 0.0002	4.6 ± 0.1
3A4-5GLY-BMR	21.3 ± 4.4	0.1387 ± 0.0009	12.5 ± 0.9	19.8 ± 2.2	0.0113 ± 0.0003	5.8 ± 0.2

Coupling parameters are determined at saturating erythromycin (120 μM) and testosterone(150 μM) concentrations. Values are means ± standard deviation of four experiments.
[(a)] The coupling efficiency is calculated as: HCHO × 100/NADPH consumed.
[(b)] The coupling efficiency is calculated as 6β-hydroxytestosterone × 100/NADPH consumed.

NADPH–Cytochrome *c* Reduction by 3A4-BMR Chimeras

The results from enzymatic activity, coupling and reduction potentials indicate that the different loops affect the interaction between the BMR and 3A4 domains of the chimeras, probably due to the different degrees of length and flexibility associated with them. Cytochrome *c* was therefore used as external probe to check its ability to intercept the electrons of NADPH delivered by the BMR when this is exposed and hence available to interact with proteins other than the 3A4 domain. The ability of cytochrome *c* to be reduced by NADPH *via* free cytochrome P450 reductase has already been described in the literature (Guengerich et al., 2009).

The capability of 3A4-BMR chimeras to use NADPH electrons to reduce cytochrome *c* is strictly related to cytochrome *c* ability to interact directly with the BMR domain when this is exposed. In order to explore the effect of viscosity on the interaction of cytochrome *c* with the chimera BMR domain, we performed the experiments both in the absence and in the presence of 20% glycerol. The reduction rates were calculated as nmoles of reduced cytochrome *c* per min and the results are summarized in the **Figure 5**.

The 3A4-5GLY-BMR chimera shows the highest cytochrome *c* reduction rate compared to the other two proteins. Moreover, the presence of 20% glycerol significantly impaired cytochrome *c* reduction ability of all the three constructs, with the 3A4-5GLY-BMR being the most affected one.

DISCUSSION

Cytochromes P450 have been extensively used in our laboratories to investigate their potential for applications in biocatalysis as electron transfer domains in chimeric constructs (Cunha et al., 1999; Sadeghi et al., 2011; Sadeghi and Gilardi, 2013). This work investigates how the stability and activity of self-sufficient chimeric human enzymes can be optimized not only by creating fusion proteins but also with the correct choice of loop connecting the reductase and the catalytic domains.

The stability of the P450 catalytic domain is significantly improved in the presence of the BMR domain since all the three fusion proteins showed a 1.5–2 fold lower rate of P450 loss compared to P450 3A4. In this case, the presence of an extra domain rather than the length of the loop is essential for stability as no significant differences are observed among the three proteins. However, the length of the loop has an impact on other parameters, such as NADPH oxidation rates and reduction potential. In particular, the chimeric proteins show a higer NADPH consumption rate compared to the CYP3A4-hCPR system at a 1:1 molar ratio. Moreover, the 3A4-3GLY-BMR protein shows a 2-folds faster rate in NADPH consumption with respect to the other two constructs. This effect suggests that the 3GLY construct is more prone to accept electrons from the redox partner with respect to no GLY and 5GLY leading to a faster reduction of the heme-Fe^{3+} to heme-Fe^{2+} (Sligar et al., 1979). These data show that there is a critical length of the linker between the domains that can modulate the inter-domain interactions that determine the rate of the electron transfer.

The fastest oxidation rate in the 3GLY protein is explained by its more positive reduction potential compared to the other two fusion proteins. It is known that in redox proteins, the interaction with the redox partner can influence the conformation, the reduction potential and in general, the dielectric environment of the redox cofactor (Bendall, 1996). Here, the three fusion proteins show a different, although negative, reduction potential that can reflect a different dielectric heme environment triggered by a different domain arrangement and interaction.

When investigating the catalytic domain ability to use reducing equivalents for erythromycin N-demethylation and testosterone 6β-hydroxylation during the catalytic event, the 5GLY construct resulted the best for both turnover rate and coupling efficiency. Thus, the increase in turnover number and coupling efficiency is neither directly related to an improvement in electron transfer rate nor to a more positive heme iron reduction potential. Differences in substrate binding can also be excluded as the K_M-values measured for both erythromycin and testosterone substrates are similar for the three proteins and within the range of previously published data (Riley and Howbrook, 1998; Yuan et al., 2002). Moreover, these data are consistent with previously published results in which it was demonstrated that the use of artificial redox chains allows the regulation of the electron flow to the P450 catalytic domain through the mediation of the non-physiological reductase domain by lowering the electron transfer rate and improving the correct electrochemical inter-domain tuning thus enhancing coupling efficiency and catalytic activity (Dodhia et al., 2008; Degregorio et al., 2011; Castrignanò et al., 2014).

In order to investigate if there is a correlation between the observed improved turnover/coupling efficiency and an increased inter-domain flexibility in the 5GLY protein, cytochrome *c* was used as external probe to check its ability to

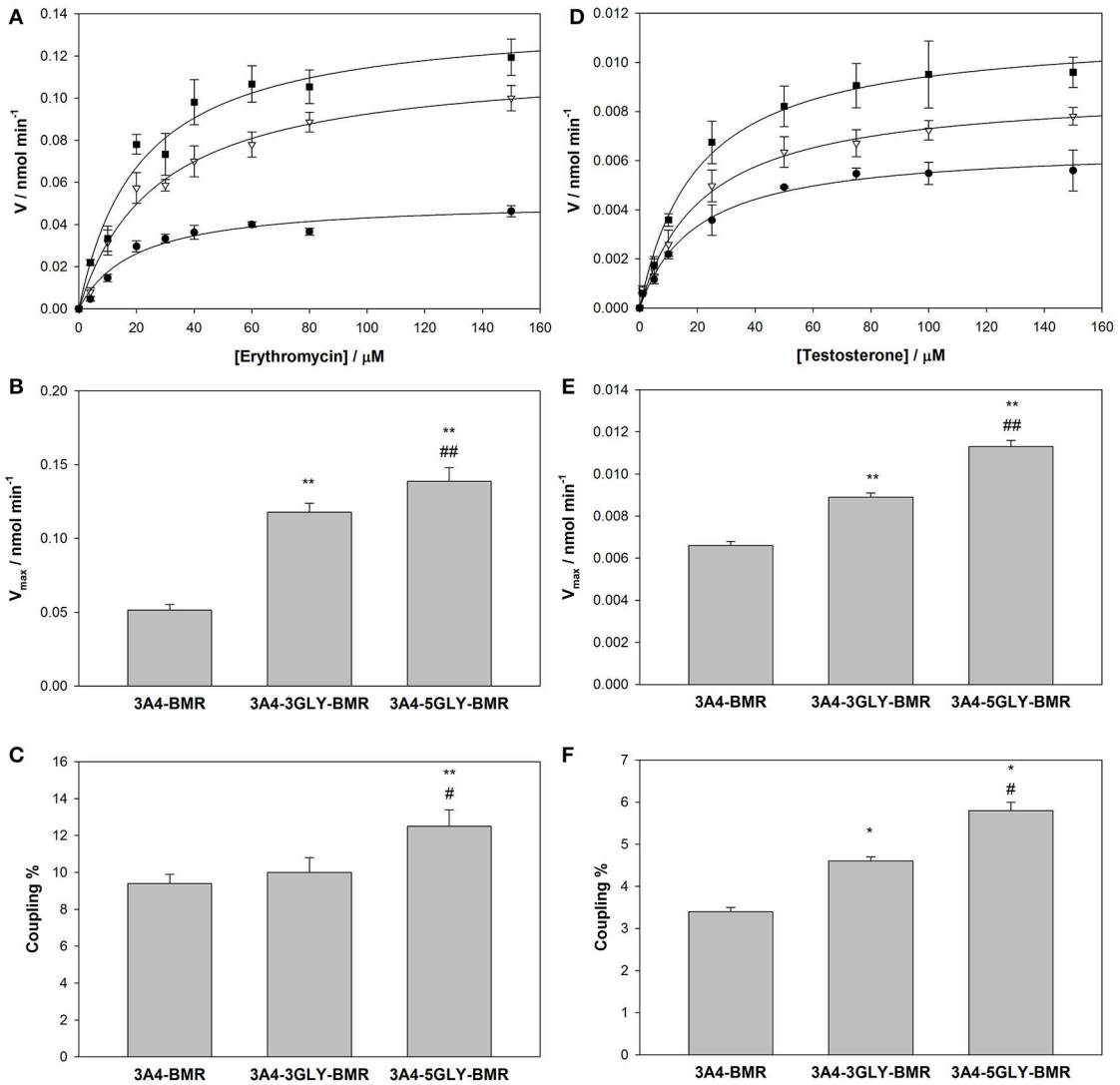

FIGURE 5 | Activity and coupling of the 3A4-BMR, 3A4-3GLY-BMR and 3A4-5GLY-BMR chimeras toward erythromycin N-demethylation. (A) Catalytic activity measured as HCHO production rate in the presence of 3A4-BMR (circles), 3A4-3GLY-BMR (triangles) and 3A4-5GLY-BMR (squares) as function of erythromycin concentration fitted with MichaelisMenten curves. **(B)** Summary of V_{max}-values calculated during erythromycin N-demethylation in the presence of cytochrome P450 3A4-BMR, 3A4-3GLY-BMR and 3A4-5GLY-BMR. **(C)** Summary of coupling percentage values calculated during erythromycin N-demethylation in the presence of cytochrome P450 3A4-BMR, 3A4-3GLY-BMR and 3A4-5GLY-BMR. **(D)** Catalytic activity measured as 6β-hydroxytestosterone production rate in the presence of 3A4-BMR (circles), 3A4-3GLY-BMR (triangles) and 3A4-5GLY-BMR (squares) as function of testosterone concentration fitted with Michaelis Menten curves. **(E)** Summary of V_{max}-values calculated during testosterone 6β-hydroxylation in the presence of cytochrome P450 3A4-BMR, 3A4-3GLY-BMR and 3A4-5GLY-BMR. **(F)** Summary of coupling percentage values calculated during testosterone6β-hydroxylation in the presence of cytochrome P450 3A4-BMR, 3A4-3GLY-BMR and 3A4-5GLY-BMR. All reactions were carried out at 37°C for 30 min. Data are mean ± SD of at least 3 replicates. $R^2 > 0.99$. $^*P < 0.01$, $^{**}P < 0.001$ compared to 3A4-BMR, $^{\#}P < 0.05$, $^{\#\#}P < 0.001$ compared to 3A4-3GLY-BMR, one way ANOVA.

intercept the electrons of NADPH delivered by the BMR when this is exposed and hence available to interact with proteins other than the 3A4 domain. The 5GLY resulted in the fastest in cytochrome *c* reduction and this result can be explained by the highest flexibility between the reductase and catalytic domain of the chimera allowing a better interaction with cytochrome *c* and an easier electron delivery from BMR reductase domain (**Figure 6**). This interpretation is further confirmed by the fact that the impairment of inter-domain flexibility upon glycerol addition that increases the medium viscosity, causes a significant decrease in the cytochrome *c* reduction rate in all the three constructs, with a more marked effect on the more flexible for 5GLY loop.

Taken together, the erythromycin N-demethylation and testosterone 6β-hydroxylation activity and the coupling results show that the 3A4-5GLY-BMR chimera is the more catalytically efficient and the more coupled. This result suggests that the higher linker flexibility allows a more proficient arrangement of

catalytic and reductase domains and improves the tuning of the electron transfer to the active site leading to a more accurate electrons delivery from the NADPH electron source during the catalytic event (**Figure 7**).

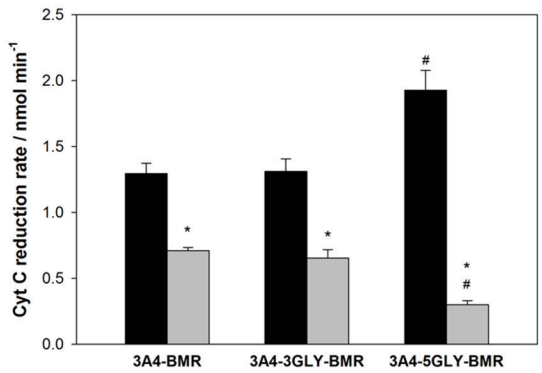

FIGURE 6 | Summary of NADPH-cytochrome *c* reduction rates by 3A4-BMR, 3A4-3GLY-BMR and 3A4-5GLY-BMR chimeras. Data obtained in the presence of 0% glycerol (black bars) and 20% glycerol (gray bars) are shown. They are mean ± SD of at least 3 replicates. *$P < 0.001$ vs. 0% glycerol; #$P < 0.001$ vs. 3A4 BMR and 3GLY(two way ANOVA followed by Student-Newman-Keuls *post hoc* test).

CONCLUSIONS

The creation of chimeric proteins was shown before to improve the solubility of P450 3A4 and to generate catalytically self-sufficient enzymes (Degregorio et al., 2011). Here, the P450 3A4-BMR catalytic performance is improved in terms of coupling efficiency and enzyme turnover by engineering the loop connecting the P450 3A4 and the BMR modules. The glycine linker acts as a flexible hinge that can control electron flow rate, catalytic activity and coupling efficiency of the 3A4-BMR chimeras. Data in this work highlight that the modulation of the length of the linker connecting the modules of a multi-domain protein has an impact on electron transfer, catalytic ability and coupling efficiency of the system that can be ascribed to the modulation of inter-domain flexibility and interactivity rather than to a different tuning of the electron transfer process. These parameters can be considered as the major requirement for an optimization of the electron delivery to the heme iron center showing that the design of the linker hinge between the interacting domains plays a crucial role in the optimization of reductase domain improvement of P450 catalytic efficiency. Our results suggest that for the 3A4-BMR fusion proteins studied here, the electron transfer may be achieved through the direct flow between the reductase and the heme domain rather than through "inter subunits" interaction between

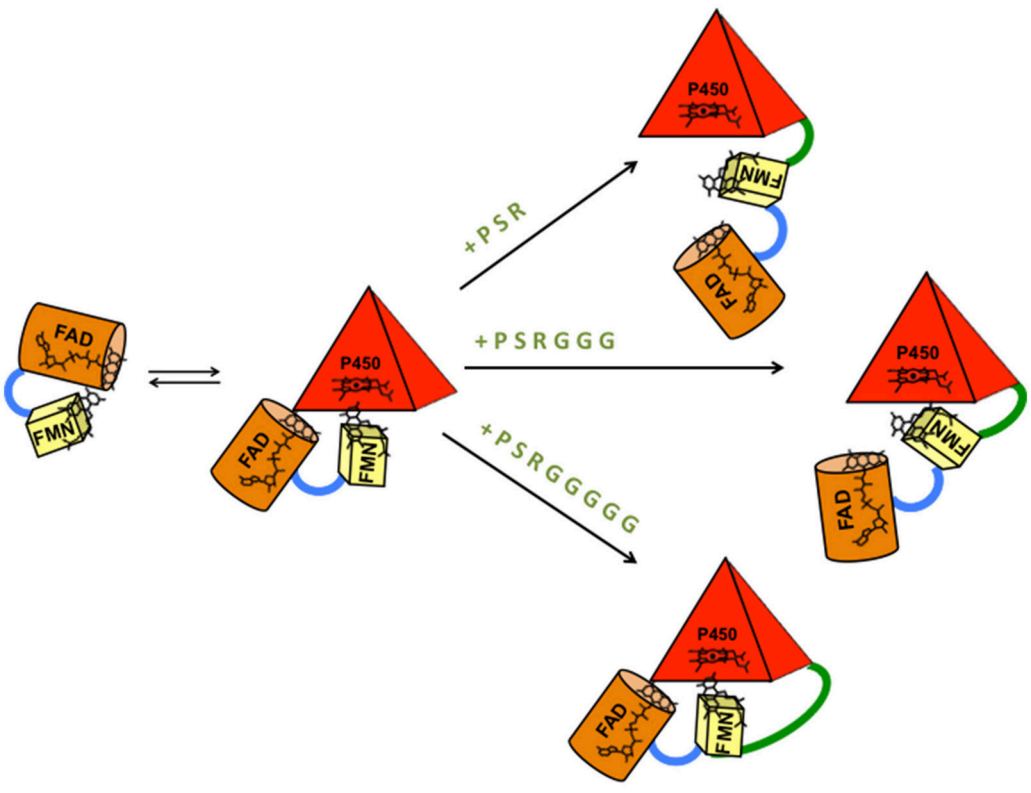

FIGURE 7 | Model of BMR-P450 active complex formation and interaction in the three different chimeric proteins. The length of the inter-domains loop favors the formation of different types of complexes that can justify different electron transfer rates, turnover and coupling efficiency. P (proline), S (serine), and R (arginine) are the three amino acids common to the three chimeras. G is glycine.

protomers in a dimeric system as suggested for the P450 BM3 system.

This molecular design approach can be successfully developed for the obtainment of performing enzymatic paradigms suitable for biotechnological applications. The next step is the introduction of such catalysts in bacterial cells for the large-scale production of drug metabolites using whole cells as a less expensive system.

AUTHOR CONTRIBUTIONS

DD performed the catalysis experiments on Erythromycin. SD performed the catalysis experiments on Testosterone. SC performed the uncoupling experiments, redox potential determination and cyt c interaction. GDN and GC performed the modeling of the chimeras. SS and GG interpreted the data and wrote the manuscript.

REFERENCES

Aliverti, A., Curti, B., and Vanoni, M. A. (1999). "Identifying and quantitating FAD and FMN in simple and in iron-sulfur-containing flavoproteins," in *Methods in Molecular Biology, Vol. 131*, eds S. K. Champman and G. A. Reid (Totowa, NJ: Humana Press Inc), 9–23.

Amunugama, H. T., Zhang, H., and Hollenberg, P. F. (2012). Mechanism-based inactivation of cytochrome P450 2B6 by methadone through destruction of prosthetic heme. *Drug Metab. Dispos.* 40, 1765–1770. doi: 10.1124/dmd.112.045971

Bendall, D. (1996). *Protein Electron Transfer.* Oxford: BIOS Scientific Publishers Ltd.

Bernhardt, R. (2006). Cytochromes P450 as versatile biocatalysts. *J. Biotechnol.* 124, 128–145. doi: 10.1016/j.jbiotec.2006.01.026

Bradford, M. M. (1976). A rapid and sensitive method for the quantitation of microgram quantities of protein utilizing the principle of protein-dye binding. *Anal. Biochem.* 72, 248–254. doi: 10.1016/0003-2697(76)90527-3

Capoferri, L., Leth, R., TerHaar, E., Mohanty, A. K., Grootenhuis, P. D., Vottero, E., et al. (2016). Insights into regioselective metabolism of mefenamic acid by cytochrome P450 BM3 mutants through crystallography, docking, molecular dynamics, and free energy calculations. *Proteins* 84, 383–396. doi: 10.1002/prot.24985

Castrignanò, S., Ortolani, A., Sadeghi, S. J., Di Nardo, G., Allegra, P., and Gilardi, G. (2014). Electrochemical detection of human Cytochrome P450 2A6 inhibition: a step towards reducing dependence from smoking. *Anal. Chem.* 86, 2760–2766. doi: 10.1021/ac4041839

Clarke, T. A., Im, S. C., Bidwai, A., and Waskell, L. (2004). The role of the length and sequence of the linker domain of cytochrome b5 in stimulating cytochrome P450 2B4 catalysis. *J. Biol. Chem.* 279, 36809–36818. doi: 10.1074/jbc.M406055200

Coon, M. J. (2005). Cytochrome P450: nature's most versatile biological catalyst. *Ann. Rev. Pharmacol. Toxicol.* 45, 1–25. doi: 10.1146/annurev.pharmtox.45.120403.100030

Cunha, C. A., Romao, M. J., Sadeghi, S. J., Valetti, F., Gilardi, G., and Soares, C. M. (1999). Effects of protein-protein interactions on electron transfer: docking and electron transfer calculations for complexes between flavodoxin and c-type cytochromes, *J. Biol. Inorg. Chem*. 4, 360–337. doi: 10.1007/s007750050323

Davydov, D. R., Sineva, E. V., Sistla, S., Davydova, N. Y., Frank, D. J., Sligar, S. G., et al. (2010). Electron transfer in the complex of membrane-bound human cytochrome P450 3A4 with the flavin domain of P450BM-3: the effect of oligomerization of the heme protein and intermittent modulation of the spin equilibrium. *Biochim. Biophys. Acta* 1797, 378–390. doi: 10.1016/j.bbabio.2009.12.008

Degregorio, D., Sadeghi, J. S., Di Nardo, G., Gilardi, G., and Solinas, S. P. (2011). Understanding uncoupling in the multiredox centre P450 3A4-BMR model system, *J. Biol. Inorg. Chem.* 16, 109–116. doi: 10.1007/s00775-010-0708-0

Denisov, G., Makris, T. M., Sligar, S. G., and Schlichting, I. (2005). Structure and chemistry of cytochrome P450. *Chem. Rev.* 105, 2253–2278. doi: 10.1021/cr0307143

Di Nardo, G., Dell'Angelo, V., Catucci, G., Sadeghi, S. J., and Gilardi, G. (2015). Subtle structural changes in the Asp251Gly/Gln307His P450 BM3 mutant responsible for new activity toward diclofenac, tolbutamide and ibuprofen. *Arch. Biochem. Biophys.* S0003–S9861, 30116–30118. doi: 10.1016/j.abb.2015.12.005

Di Nardo, G., Fantuzzi, A., Sideri, A., Panicco, P., Sassone, C., Giunta, C., et al. (2007). Wild type CYP102A1 as biocatalyst: turnover of drugs usually metabolized by human liver enzymes. *J. Biol. Inorg. Chem.* 12, 313–323. doi: 10.1007/s00775-006-0188-4

Di Nardo, G., and Gilardi, G. (2012). Optimization of the Bacterial Cytochrome P450 BM3 System for the Production of Human Drug Metabolites. *Int. J. Mol. Sci.* 13, 15901–15924. doi: 10.3390/ijms131215901

Dodhia, V. R., Fantuzzi, A., and Gilardi, G. (2006). Engineering human cytochrome P450 enzymes into catalytically self-sufficient chimeras using molecular Lego. *J. Biol. Inorg. Chem.* 11, 903–916. doi: 10.1007/s00775-006-0144-3

Dodhia, V. R., Sassone, C., Fantuzzi, A., Di Nardo, G., Sadeghi, S. J., and Gilardi, G. (2008). Modulating the coupling efficiency of human cytochrome P450 CYP3A4 At electrode surfaces through protein engineering. *Electrochem. Commun.* 10, 1744–1747. doi: 10.1016/j.elecom.2008.09.007

Dutton, P. L. (1978). Redox potentiometry: determination of midpoint potentials of oxidation-reduction components of biological electron-transfer systems. *Methods Enzymol.* 54, 411–435. doi: 10.1016/S0076-6879(78)54026-3

Evans, W. E., and Relling, M. V. (1999). Pharmacogenomics: translating functional genomics into rational therapeutics. *Science* 286, 487–491. doi: 10.1126/science.286.5439.487

Faeder, E. J., and Siegel, L. M. (1973). A rapid micromethod for determination of FMN and FAD in mixtures. *Anal. Biochem.* 53, 332–336. doi: 10.1016/0003-2697(73)90442-9

Fairhead, M., Giannini, S., Gillam, E. M. J., and Gilardi, G. (2005). Functional characterisation of an engineered multidomain human P450 2E1 by molecular Lego. *J. Biol. Inorg. Chem.* 10, 842–953. doi: 10.1007/s00775-005-0033-1

Foti, R. S., Rock, D. A., Pearson, J. T., Wahlstrom, J. L., and Wienkers, L. C. (2011). Mechanism-based inactivation of cytochrome P450 3A4 by mibefradil through heme destruction. *Drug Metab. Dispos.* 39, 1188–1195. doi: 10.1124/dmd.111.038505

Govindaraj, S., and Poulos, T. L. (1995). Role of the linker region connecting the reductase and heme domains in cytochrome P450BM-3 *Biochemtry* 34, 11221–11226. doi: 10.1021/bi00035a031

Guengerich, F. (2002). Rate-limiting steps in cytochrome P450 catalysis. *J. Biol. Chem.* 383, 1553–1564. doi: 10.1515/BC.2002.175

Guengerich, F. P. (1983). Oxidation-reduction properties of rat liver cytochromes P-450 and NADPH-cytochrome p-450 reductase related to catalysis in reconstituted systems. *Biochemistry* 22, 2811–2820. doi: 10.1021/bi00281a007

Guengerich, F. P., Martin, M. V., Sohl, C. D., and Cheng, Q. (2009). Measurement of cytochrome P450 and NADPH-cytochrome P450 reductase. *Nat. Protoc.* 4, 1245–1251. doi: 10.1038/nprot.2009.121

Hannemann, F., Bichet, A., Ewen, K. M., and Bernhardt, R. (2007). Cytochrome P450 systems – biological variations of electron transport chain. *Biochim. Biophys. Acta* 1770, 330–344. doi: 10.1016/j.bbagen.2006.07.017

Isin, E. M., and Guengerich, F. P. (2007). Complex reactions catalyzed by cytochrome P450 enzymes. *Biochim. Biophys. Acta* 1770, 314–329. doi: 10.1016/j.bbagen.2006.07.003

Lin, H. L., Kent, U. M., and Hollenberg, P. F. (2005). Thr302 is the site for the covalent modification of human cytochrome P450 2B6 leading to mechanism-based inactivation by tert-butylphenylacetylene. *Pharmacol. J. Exp. Ther.* 313, 154–164. doi: 10.1124/dmd.111.042176

Mayuzumi, H., Sambongi, C., Hiroya, K., Shimizu, T., Tateishi, T., and Hatano, M. (1993). Effect of mutations of ionic amino acids of cytochrome P450 1A2 on catalytic activities toward 7-ethoxycoumarin and methanol. *Biochemtry* 32, 5622–5628. doi: 10.1021/bi00072a018

Meunier, B., de Visser, S. P., and Shaik, S. (2004). Mechanism of oxidation reactions catalyzed by cytochrome p450 enzymes. *Chem. Rev.* 104, 3947–3980. doi: 10.1021/cr020443g

Munro, A. W., Daff, S., Coggins, J. R., Lindsay, J. G., and Chapman, S. K. (1996). Probing electron transfer in flavocytochrome P-450 BM3 and its component domains, *Eur. J. Biochem.* 239, 403–409. doi: 10.1111/j.1432-1033.1996.0403u.x

Nash, T. (1953). The colorimetric estimation of formaldehyde by means of the Hantzsch reaction. *Biochem. J.* 55, 416–442. doi: 10.1042/bj0550416

Neeli, R., Girvan, H. M., Lawrence, A., Warren, M. J., Leys, D., Scrutton, N. S., et al. (2005). The dimeric form of flavocytochrome P450 BM3 is catalytically functional as a fatty acid hydroxylase. *FEBS Lett.* 579, 5582–5588. doi: 10.1016/j.febslet.2005.09.023

Nelson, D. R., Koymans, L., Kamataki, T., Stegeman, J. J., Feyereisen, R., Waxman, D. J., et al. (1996). P450 superfamily: update on new sequences, gene mapping, accession numbers and nomenclature. *Pharmacogenetics* 6, 1–42. doi: 10.1097/00008571-199602000-00002

Noble, M. A., Miles, C. S., Chapman, S. K., Lysek, D. A., Mackay, A. C., Reid, G. A., et al. (1999). Roles of key active-site residues in flavocytochrome P450 BM3. *Biochem. J.* 339, 371–379. doi: 10.1042/bj3390371

Omura, T., and Sato, R. (1964). The carbon monoxide-binding pigment of liver microsomes. *II.* Solubilization, purification, and properties. *J. Biol. Chem.* 239, 2379–2385.

Ortiz de Montellano, P. R. (2005). *Cytochrome P450: Structure, Mechanism and Biochemistry*. New York, NY: Plenum Press.

Ortolani, A. (2012). *Engineering CYP2C8 and CYP2A6 for Drug Screening*. PhD Dissertation, University of Torino, Italy.

Perret, A., and Pompon, D. (1998). Electron shuttle between membrane-bound cytochrome P450 3A4 and b5 rules uncoupling mechanisms. *Biochemistry* 37, 11412–11424. doi: 10.1021/bi980908q

Ren, X., Yorke, J. A., Taylor, E., Zhang, T., Zhou, W., and Wong, L. L. (2015). Drug oxidation by cytochrome P450BM3: metabolite synthesis and discovering new P450 Reaction types. *Chemistry* 21, 15039–15047. doi: 10.1002/chem.201502020

Riley, R. J., and Howbrook, D. (1998). *In vitro* analysis of the activity of the major human hepatic CYP Enzyme (CYP3A4) using [lV-Methyl-14C] –Erythromycin. *J. Pharmacol. Toxicol. Meth.* 38, 189–193. doi: 10.1016/S1056-8719(97)00103-2

Rua, F. (2012a). *Engineering Platforms for Drug Metabolism as Alternative to P450 Testing in Animals*. PhD Dissertation. University of Torino, Italy.

Rua, F., Sadeghi, S. J., Castrignanò, S., Di Nardo, G., and Gilardi, G. (2012b). Engineering *Macaca fascicularis* cytochrome P450 2C20 to reduce animal testing for new drugs. *J. Inorg. Biochem.* 117, 277–284. doi: 10.1016/j.jinorgbio.2012.05.01

Rua, F., Sadeghi, S. J., Silvia Castrignanò, S., Valetti, F., and Gilardi, G. (2015). Electrochemistry of *Canis familiaris* cytochrome P450 2D15 with gold nanoparticles: an alternative to animal testing in drug discovery. *Bioelectrochemtry* 105, 110–116. doi: 10.1016/j.bioelechem.2015.03.012

Ryu, S. H., Park, B. Y., Kim, S. Y., Park, S. H., Jung, H. J., Park, M., et al. (2014). Regioselective hydroxylation of omeprazole enantiomers by bacterial CYP102A1 mutants, *Drug Metab. Dispos.* 42, 1493–1497. doi: 10.1124/dmd.114.058636

Sadeghi, S. J., Fantuzzi, A., and Gilardi, G. (2011). Breakthrough in P450 bioelectrochemistry and future perspectives. *Biochim. Biophys. Acta* 1814, 237–248. doi: 10.1016/j.bbapap.2010.07.010

Sadeghi, S. J., and Gilardi, G. (2013). Chimeric P450 Enzymes: activity of artificial redox fusions driven by different reductases for biotechnological applications. *Biotechnol. Appl. Biochem.* 60, 102–110. doi: 10.1002/bab.1086

Sevrioukova, I., Shaffer, C., Ballou, D. P., and Peterson, J. A. (1996). Electron transfer in the complex of membrane-bound human cytochrome P450 3A4 with the flavin domain of P450BM-3: the effect of oligomerization of the heme protein and intermittent modulation of the spin equilibrium. *Biochemistry* 35, 7058–7068. doi: 10.1016/j.bbabio.2009.12.008

Sligar, S. G., Cinti, D. L., Gibson, G. G., and Schenkman, J. B. (1979). Spin state control of the hepatic cytochrome P450 redox potential. *Biochem. Biophys. Res. Commun.* 90, 925–932. doi: 10.1016/0006-291X(79)91916-8

Sugiura, M., Ito, Y., Hirano, K., Sasaki, M., and Sawakj, S. (1977). A new method for peptidase activity measurement in serum and tissues, using L-Leu-L-Leu as substrate, *Clin. Chim. Acta* 78, 381–389. doi: 10.1016/0009-8981(77)90071-7

Tsotsou, G. E., Di Nardo, G., Sadeghi, S. J., Fruttero, R., Lazzarato, L., Bertinaria, M., et al. (2013). A rapid screening for cytochrome P450 catalysis on new chemical entities: cytochrome P450 BM3 and 1,2,5-oxadiazole derivatives, *J. Biomol. Screen.* 18, 211–218. doi: 10.1177/1087057112459351

Tsotsou, G. E., Sideri, A., Goyal, A., Di Nardo, G., and Gilardi, G. (2012). Identification of mutant Asp251Gly Gln307His of cytochrome P450 BM3 for the generation of metabolites of diclofenac, ibuprofen and tolbutamide. *Chemistry* 18, 3582–3588. doi: 10.1002/chem.201102470

Yuan, R., Madani, S., Wei, X. X., Reynolds, K., and Huang, S. M. (2002). Evaluation of cytochrome P450 probe substrates commonly used by the pharmaceutical industry to study *in vitro* drug interactions. *Drug Metab. Dispos.* 30, 1311–1319. doi: 10.1124/dmd.30.12.1311

Zangar, R. C., Davydov, D. R., and Verma, S. (2004). Mechanisms that regulate production of reactive oxygen species by cytochrome P450. *Toxicol. Appl. Pharmacol.* 199, 316–331. doi: 10.1016/j.taap.2004.01.018

Conflict of Interest Statement: The authors declare that the research was conducted in the absence of any commercial or financial relationships that could be construed as a potential conflict of interest.

Advantages of publishing in Frontiers

OPEN ACCESS
Articles are free to read, for greatest visibility

COLLABORATIVE PEER-REVIEW
Designed to be rigorous – yet also collaborative, fair and constructive

FAST PUBLICATION
Average 85 days from submission to publication (across all journals)

COPYRIGHT TO AUTHORS
No limit to article distribution and re-use

TRANSPARENT
Editors and reviewers acknowledged by name on published articles

SUPPORT
By our Swiss-based editorial team

IMPACT METRICS
Advanced metrics track your article's impact

GLOBAL SPREAD
5'100'000+ monthly article views and downloads

LOOP RESEARCH NETWORK
Our network increases readership for your article

Frontiers
EPFL Innovation Park, Building I • 1015 Lausanne • Switzerland
Tel +41 21 510 17 00 • Fax +41 21 510 17 01 • info@frontiersin.org
www.frontiersin.org

Find us on